

**PHASE TRANSITIONS IN BINARY  
MIXTURES OF CALAMITIC AND BENT-  
CORE MESOGENS**

**A Thesis submitted to the University of North Bengal**

**For the Award of**

**Doctor of Philosophy**

**in**

**Physics**

**BY**

**SUSANTA CHAKRABORTY**

**GUIDE**

**Prof. Malay Kumar Das**

Department of Physics  
University of North Bengal  
Raja Rammohunpur,  
Siliguri, Darjeeling-734 013,  
West Bengal, India  
January 2019

*To my loving parents and sweet sister*

## Declaration

I declare that the thesis entitled "*Phase Transitions in Binary Mixtures of Calamitic and Bent-Core Mesogens*" has been prepared by me under the guidance of Dr. Malay Kumar Das, Professor, Department of Physics, University of North Bengal. No part of this thesis has formed the basis for the award of any degree or fellowship previously.

Susanta Chakraborty

(Susanta Chakraborty)

Department of Physics,  
University of North Bengal,  
Raja Rammohunpur, Siliguri  
Darjeeling-734013  
West Bengal, India

Date: 31.01.2019

**DEPARTMENT OF PHYSICS  
UNIVERSITY OF NORTH BENGAL**

P.O. North Bengal University, Siliguri, Dist. Darjeeling, West Bengal, Pin - 734013, India

Website: [www.nbu.ac.in](http://www.nbu.ac.in)



Phone: +91-(0) 353-2776338, Fax: +91-(0) 353-2699001

ENLIGHTENMENT TO PERFECTION

**CERTIFICATE**

I certify that Mr. Susanta Chakraborty has prepared the thesis entitled "*Phase Transitions in Binary Mixtures of Calamitic and Bent-Core Mesogens*", for the award of Ph.D. degree of the University of North Bengal, under my guidance. He has carried out the work at the Department of Physics, University of North Bengal.

*M. K. Das*

(Dr. Malay Kumar Das)

Professor,  
Department of Physics,  
University of North Bengal,  
Raja Rammohunpur, Siliguri  
Darjeeling-734013  
West Bengal, India

Date: *30.01.2019*

## Urkund Analysis Result

Analysed Document: Susanta Chakraborty\_Physics.pdf (D46897703)  
Submitted: 1/17/2019 10:47:00 AM  
Submitted By: nbuplg@gmail.com  
Significance: 1 %

### Sources included in the report:

<http://samo.kralj.fnm.uni-mb.si/clanki/a7c1.pdf>  
<https://www.mdpi.com/1422-0067/10/9/3971/htm>  
[https://prism.ucalgary.ca/bitstream/handle/11023/189/ucalgary\\_2012\\_Ward\\_Sandra.pdf?sequence=2](https://prism.ucalgary.ca/bitstream/handle/11023/189/ucalgary_2012_Ward_Sandra.pdf?sequence=2)  
<https://core.ac.uk/download/pdf/16175728.pdf>  
<https://pdfs.semanticscholar.org/7a29/dca14457607c609d16d24fd80f15d1d4870c.pdf>  
[http://eprints.utar.edu.my/1868/1/Final\\_thesis\\_\(Draft\\_9\)\\_Foo\\_Kok\\_Leei.pdf](http://eprints.utar.edu.my/1868/1/Final_thesis_(Draft_9)_Foo_Kok_Leei.pdf)  
[http://www.ijarset.com/upload/2017/march/12\\_IJARSET\\_PURNACHANDRA.pdf](http://www.ijarset.com/upload/2017/march/12_IJARSET_PURNACHANDRA.pdf)  
[http://softmat.upatras.gr/wp-content/uploads/2011/05/11-TiltInv\\_PRE2002.pdf](http://softmat.upatras.gr/wp-content/uploads/2011/05/11-TiltInv_PRE2002.pdf)  
<https://hal.archives-ouvertes.fr/hal-00467925/document>  
[https://tel.archives-ouvertes.fr/tel-01543637/file/these\\_archivage\\_3573094o.pdf](https://tel.archives-ouvertes.fr/tel-01543637/file/these_archivage_3573094o.pdf)

### Instances where selected sources appear:

35

M. K. Das

31.01.2019

Susanta Chakraborty .  
31.01.2019

# Abstract

Investigations of phase transitions and critical phenomena in liquid crystals (LCs) are the focus of great attention in soft condensed matter research. The characteristic behavior of different mesophases impart a significant role in determining the phase transitional nature in liquid crystal system. Several extensive experimental attempts have been made so far to characterize a wide variety of phase transition in pure calamitic samples and binary mixtures of homologous compounds. Apart from the calamitic compounds, the divergent shaped bent-core liquid crystals exhibit a number of exotic mesomorphic behaviors and have been observed to influence the molecular interaction and hence the mesophase transitions in binary mixtures with calamitic compounds. This dissertation deals with systematic experimental investigations on the critical phenomena and phase transitional behavior of the isotropic–nematic ( $I-N$ ), nematic–smectic- $A$  ( $N-Sm-A$ ) and smectic- $A$ –smectic- $C$  ( $Sm-A-Sm-C$ ) phase transitions in binary mixtures comprising of calamitic and bent-core compounds. Additionally, investigation of different physical properties in some pure and binary liquid crystal systems has been measured to probe the molecular interactions in several mesophases. Concise overviews of the entire dissertation along with salient features of the outcome are described below.

**Chapter 1** describes the basic concept of liquid crystal materials along with their classifications. The molecular arrangements and general behavior of different mesophases for both of the calamitic and bent-core liquid crystal systems have been discussed. Besides, a brief discussion about the phase transitions along with the critical phenomena and related critical exponents has been explored.

**Chapter 2** provides the detailed description about different experimental setups and relevant investigation procedures employed to study different LC compounds and mesogenic binary mixtures. Additionally, the supporting

theories of various mesophase transitions related to this dissertation have been discussed.

**Chapter 3** illustrates the effect of hockey stick-shaped mesogen 4-(3-decyloxyphenyliminomethyl)phenyl-4-decyloxy-cinnamate (SF7) on the critical behavior at the isotropic–nematic ( $I-N$ ) and nematic–smectic- $A$  ( $N-Sm-A$ ) phase transitions in some binary mixtures with the calamitic 4'-octyloxy-4-cyanobiphenyl (8OCB), by analyzing the temperature dependent optical birefringence ( $\Delta n$ ) data.

- i. Introduction of the molecular bend of the angular mesogenic dopant significantly destabilizes the temperature range of the nematic phase of the calamitic compound.
- ii. The extracted order parameter critical coefficient  $\beta$  related to the  $I-N$  phase transition has found to reveal a good conformity with the tricritical hypothesis for all of the studied mixtures.
- iii. The obtained critical exponent ( $\alpha'$ ,  $\beta'$ ) values describing the critical fluctuations at the  $N-Sm-A$  phase transition reveals a non-universal nature and demonstrates a strong dependency on the width of the nematic phase.
- iv. Shrinkage of nematic phase range demonstrates a strong tendency to drive the  $N-Sm-A$  phase transition towards a first-order nature.

**Chapter 4** includes the dielectric and visco-elastic properties of the binary system as discussed in chapter 3.

- i. All the investigated mixtures possess a large positive dielectric anisotropy ( $\Delta\epsilon$ ), although a noticeable reduction has been found by increasing the diverse-shaped dopant concentration due to strong polar interaction of anti-parallel aligned dipoles.
- ii. Investigation on the pretransitional phenomena in the vicinity of  $I-N$  phase transition suggesting a tricritical character for all the investigated mixtures.

- iii. Parameterization of dielectric permittivity close to the  $N$ -Sm-A phase transition reveals a quite good consistency about the nature of the transition obtained from the high-resolution optical birefringence measurements for the present binary system.
- iv. The splay elastic constant ( $K_{11}$ ) and the rotational viscosity ( $\gamma_1$ ) are found to exhibit a systematic temperature and concentration dependency along with the magnitude in between typical bent-core and calamitic compounds.
- v. Effect of the induced molecular clusters within the mixtures successively deteriorates the nematic phase range and exhibit a crossover character from second order to first order in nature for the  $N$ -Sm-A phase transition.

In **Chapter 5**, investigation on critical behavior has been explored at the Sm-A-Sm-C phase transition of a homologous calamitic binary system (5-*n*-ethyloxy-2-(4-nonyloxy-phenyl)pyrimidine (PhP1) and 5-*n*-heptyloxy-2-(4-*n*-nonyloxy-phenyl)pyrimidine (PhP2) by studying the temperature dependent optical birefringence data. The  $N$ -Sm-A and  $I$ - $N$  phase transitions have also been studied for the same binary system.

- i. Analysis of  $\Delta n$  value in close vicinity of both the  $N$ -Sm-A and Sm-A-Sm-C phase transitions explored the difference between the order natures of these transitions that solely depends upon the temperature range of the  $N$  and Sm-A phases respectively.
- ii. An approximate range of the Sm-A phase has found to be  $\sim 10.5$  K to demonstrate a tricritical point of the Sm-A-Sm-C phase transition which is somewhat greater than that of the  $N$  phase range ( $\sim 2.5$  K) for the  $N$ -Sm-A phase transition.
- iii. The transitional behavior of the Sm-A-Sm-C phase transition has found to be really critical over the range  $3 \times 10^{-3}$  and follows a unique curve against temperature ratio ( $T_{AC}/T_{NA}$ ) in comparison to

the similar curve obtained for the  $N$ -Sm- $A$  phase transition against McMillan ratio ( $T_{NA}/T_{IN}$ ).

- iv. The critical exponent ( $\beta$ ), characterizing the critical anomaly at the  $I$ - $N$  phase transition reveals a good consistency with the tricritical hypothesis.

**Chapter 6** focuses on the extensive analysis of the critical behavior in the vicinity of Sm- $A$ -Sm- $C$  phase transition in some binary mixtures consisting of a hockey stick-shaped compound 4-(3- $n$ -decyloxy-2-methylphenyliminomethyl) phenyl 4- $n$ -dodecyloxy cinnamate (H-22.5) and a calamitic mesogen 4-cyano-4'-heptyloxybiphenyl (7OCB).

- i. The yielded values of the effective critical exponent ( $\alpha'$ ) have found to be non-universal in nature and exhibit a linear dependence against the Sm- $A$  phase range.
- ii. The values of  $\alpha'$  follow the same curve in between 3D-XY and tricritical (TCP) limit as observed in previous work (chapter5).
- iii. The present system characterizes a broad tricritical range for the Sm- $A$ -Sm- $C$  phase transition.

**Chapter 7** deals with the study of the influence of an achiral hockey stick-shaped compound (H-22.5) on the optical, dielectric and electro-optical properties in some binary mixtures with chiral ferroelectric compound (S)-(+)-4'-( $\omega$ -alkanoyloxy)alkoxybiphenyl-4-yl-4-(1-methylheptyloxy)benzoates (2H6R).

- i. Addition of hockey stick-shaped compound completely suppress the Sm- $C^*$  phase of the pure chiral compound and induces two broad ranged frustrated TGB phases (TGBA and TGBC\*) in between cholesteric ( $N^*$ ) and Sm- $B^*_{\text{hex}}$  phases for all of the investigated mixtures.
- ii. The dielectric anisotropy ( $\Delta\epsilon$ ) value reveals an inversion from positive to negative and the temperature range of the positive

dielectric anisotropy region has found to increase by increasing the amount of H-22.5 mesogen.

- iii. The temperature dependent spontaneous polarization ( $P_s$ ) value in the TGBC\* phase significantly decreases with increasing hockey stick-shaped molecular concentration, while the response time ( $\tau$ ) and effective torsional bulk viscosity ( $\eta$ ) exhibit a higher value than that of the Sm-C\* phase of the pure compound.
- iv. The investigation on the frequency-dependent dielectric spectroscopy demonstrates the signature of the soft and Goldstone modes in the  $N^*$  and TGBC\* phases respectively. However, the intermediate TGBA phase represents a transition from soft mode in  $N^*$  phase to a Goldstone mode in TGBC\* phase with a greater value of activation energy.

All the physical properties in those mixtures have been discussed by considering the perturbation introduced by the achiral hockey stick-shaped compound.

**Chapter 8** is devoted to a comparative study of three pure homologous bent-core compounds (**1/7**, **1/9** and **1/10**) derived from 4-cyanoresorcinol bisbenzoates based on the dielectric spectroscopy and the electro-optical investigation.

- i. Compounds **1/7** and **1/9**, exhibit a high-frequency molecular relaxation mode ( $P_1$ ) and a low-frequency molecular mode ( $H_1$ ) in the  $N_{CybC}$  phase of the planar (HG) and homeotropically (HT) aligned samples. Additionally another distinct high-frequency molecular mode ( $H_2$ ) appears in HT cell for both the compounds which is further influenced by the effect of anti-ferroelectric ordering of molecular dipoles in adjacent layers of Sm-C<sub>(1)</sub> phase for compound **1/9**.
- ii. The higher homologue (**1/10**) exhibits a longitudinal relaxation mode ( $H_2$ ) and a transverse mode ( $P_1$ ) throughout the mesomorphic

region along with another relaxation mode ( $P_2$ ) in planar aligned Sm- $C_{(1)}$  phase.

- iii. The field reversal polarization technique and the simultaneous observation of optical textures in polarizing optical microscope confirm the polar nature of these mesophases.

These outcomes have been explained by considering the structural changes of the molecules by increasing the chain length and effect of their association in dielectric parameters.

## PREFACE

This thesis entitled “*Phase transitions in binary mixtures of calamitic and bent-core mesogens*” is an outcome of the experimental investigation in liquid crystal system carried out from 2014, at the Department of Physics, University of North Bengal as a Research Fellow in the DST-SERB funded research project, under the supervision of Prof. Malay Kumar Das. These five years imparted me a lot of acquirements on in-depth understanding on the subject matter as well as hands-on experience on the operation of different sophisticated instruments through several endure. This dissertation covers the experimental findings regarding the order character of a number of mesophase transitions associated with binary liquid crystal systems and the investigation has been extended to obtain different mesophase properties that certainly help me to understand the molecular interactions in several mesophases. During this research period, my perception over the phase transition and critical phenomena has been grown up over time all the way through the theoretical interpretation and experimental activities. In order to achieve the high-resolution experimental data, precise modifications have been carried out by me in the experimental set-ups. Best on my ability, I have reached a few steps to solve the problems related to phase transitions in liquid crystal compounds. I have compiled all those problems in this dissertation combined with theoretical knowledge. Although the innumerable research activities are going on in the field of phase transitional behavior, still some problems yet not have been resolved. The outcomes of this dissertation may contribute a significant dimension for the attention of scientists towards an easy framework.

All these scientific activities and achievements make my life full of joy and happiness. With regards, the support and inspiration of a number of people obviously make it possible to accomplish in realizing this wonderful journey. Therefore, I would like to avail this opportunity to convey my indebtedness one and all of them for their role throughout the journey.

It is my privilege to express the deepest gratitude to my supervisor Prof. Malay Kumar Das, whose contribution to this whole journey made me devoted and supportive. In each and every situation he encouraged me a lot, not only in my research life but also in my personal life. I feel very auspicious to come and remain in touch with such a brilliant and elegant minded person, who persistently keeps me on the track with astute ideas and observations in every up and down. It is my pleasure to express my overwhelmed thanks to Dr. Banani Adhikari (Das) for her fruitful discussion, support, encouragement and sustained helps to perform the research work.

I am deeply grateful to Prof. Wolfgang Weissflog and Prof. Carsten Tschierske of Martin-Luther-University Halle-Wittenberg, Germany, Prof. Roman Dabrowski of Institute of Chemistry, Military University of Technology, Warsaw, Poland for providing the liquid crystal samples used in this work.

My heartfelt thank to my seniors and co-workers, Dr. Akhileshwar Prasad, Mr. Gautam Sarkar, Dr. Prajnamita Dasgupta, Dr. Anish Chakraborty, Dr. Sudipta Kumar Sarkar, Dr. Anamika Pramanik, Miss. Barnali Barman, Mr. Shantiram Nepal and Miss. Smriti Mitra for their kind cooperation and support.

I would like to convey my thank to all the respected faculty members and other staff of the Department of Physics, University of North Bengal, for their needful help in the entire period of my research work. I am also grateful to all the staff of the University Science and Instrumentation Centre (USIC).

Finally, I would like to acknowledge the Department of Science and Technology, New Delhi for the financial support.

Last but not the least special thanks to my family members, relatives, friends and well-wishers especially my mother Niva Chakraborty and younger sister Priyanka Chakraborty, brother-in-law Souvik Chatterjee and my all-time friend Gargi Banerjee for their unconditional love, support and sacrifices all throughout the tenure. It's a pleasure to express my indebtedness to my

maternal uncle Dr. Subhasis Chattopadhyay, for his invaluable care and support. He gives me the opportunity to express myself and mold me into the person who I am now. He has always illumined the path of my journey up till now and will continue to do so in the rest of my life. Finally, my father Mr. Ramjiban Chakraborty, helps me to get out of every bad situation and teaches me about etiquette, humanity and ethics. He always acts as the pillar of strength and support for me. No words can ever be strong enough to owe a deep sense of gratitude to him for his unconditional love. God bless him for being there for me and my family.

Susanta Chakraborty  
Susanta Chakraborty

Date: 31.01.2019

Place: Raja Rammohunpur

# CONTENTS

<b>Contents</b> .....	xiii
<b>List of Tables</b> .....	xviii
<b>List of Figures</b> .....	xx
<b>Chapter 1. Introduction</b>	<b>1</b>
1.1. Liquid crystals .....	2
1.2. Classification of liquid crystals .....	3
1.2.1. Lyotropic liquid crystals.....	3
1.2.2. Thermotropic liquid crystals .....	4
1.2.3. Calamitic liquid crystals.....	5
1.2.3.1. Nematic ( <i>N</i> ) phase .....	5
1.2.3.2. Smectic ( <i>Sm</i> ) phase .....	7
a. Smectic <i>A</i> ( <i>Sm-A</i> ) phase.. ..	8
b. Smectic <i>C</i> ( <i>Sm-C</i> ) phase.....	9
c. Hexatic smectic ( <i>Sm-B</i> , <i>Sm-I</i> , <i>Sm-F</i> ) phases ....	10
d. Soft crystal ( <i>B</i> , <i>E</i> , <i>J</i> , <i>G</i> , <i>K</i> , <i>H</i> ) phases .....	11
1.2.3.3. Chiral phases.....	12
a. Cholesteric or chiral nematic ( <i>N*</i> ) phase.....	12
b. Chiral Smectic <i>A</i> ( <i>Sm-A*</i> ) phase .....	14
c. Chiral Smectic <i>C</i> ( <i>Sm-C*</i> ) phase.....	14
1.2.3.4. Liquid crystalline frustrated phases.. ..	16
a. Blue phases .....	16
b. Twist grain boundary (TGB) phase .....	17
1.2.4. Bent-core liquid crystals.....	19
1.2.4.1. Smectic phases of bent-core liquid crystals.....	22
a. <i>B</i> <sub>1</sub> phase.....	22
b. <i>B</i> <sub>2</sub> phase .....	23
c. <i>B</i> <sub>3</sub> phase.....	25
d. <i>B</i> <sub>4</sub> phase .....	25
e. <i>B</i> <sub>5</sub> phase.....	26
f. <i>B</i> <sub>6</sub> phase .....	27

g. $B_7$ phase .....	28
h. $B_8$ phase .....	28
1.2.4.2. Nematic phases of bent-core liquid crystals .....	29
1.2.5. Hockey stick-shaped liquid crystals .....	31
1.3. Liquid crystalline mixtures .....	32
1.4. Phase transitions .....	33
1.5. Critical exponents .....	34
References .....	37
<b>Chapter 2. Experimental techniques and theoretical background</b>	<b>51</b>
2.1. Introduction .....	52
2.2. Experimental techniques .....	52
2.2.1. Liquid crystal cells and sample preparation .....	52
2.2.2. Texture study .....	53
2.2.3. Differential scanning calorimetry (DSC) .....	54
2.2.4. Optical birefringence measurement .....	55
a. Thin prism technique .....	55
b. Optical transmission technique .....	57
2.2.5. Static dielectric permittivity measurement .....	59
2.2.6. Dielectric spectroscopy measurement .....	61
2.2.7. Splay elastic constant measurement .....	64
2.2.8. Rotational viscosity measurement .....	66
2.2.9. Electro-optical study .....	68
2.3. Theoretical background .....	71
2.3.1. Maier-Saupe theory .....	71
2.3.2. McMillan theory for the Sm-A phase .....	75
2.3.3. Landau de-Gennes theory for the $I-N$ and $N-Sm-A$ phase transition .....	78
2.3.4. Sm-A–Sm-C phase transition .....	85
References .....	95

<b>Chapter 3. Effect of the hockey stick-shaped mesogen as an additive on the critical behavior at the isotropic to nematic and nematic to smectic-A phase transitions in octyloxy-cyano-biphenyl</b>	<b>101</b>
3.1. Introduction .....	102
3.2. Materials .....	105
3.3. Phase diagram.....	105
3.4. Optical birefringence measurements .....	107
3.4.1. Optical transmission (OT) technique .....	107
3.4.2. Thin prism technique.....	108
3.5. Critical behavior at the $I-N$ phase transition .....	111
3.6. Critical behavior at the $N-Sm-A$ phase transition .....	115
3.7. Conclusion.....	125
References .....	127
<b>Chapter 4. Dielectric, elastic and viscous properties of some binary mixtures of hockey stick-shaped mesogen and octyloxy-cyano-biphenyl</b>	<b>132</b>
4.1. Introduction .....	133
4.2. Static dielectric parameters measurements.....	135
4.3. Critical behavior at the $N-Sm-A$ phase transition .....	143
4.4. Threshold voltage and splay elastic constant measurements. ...	147
4.5. Relaxation time and rotational viscosity measurements .....	152
4.6. Determination of activation energy .....	156
4.7. Conclusion.....	161
References .....	163
<b>Chapter 5. Critical behavior at the smectic-A to smectic-C, nematic to smectic-A and isotropic to nematic phase transitions in a binary pyrimidine liquid crystal mixtures from high-resolution optical birefringence measurement</b>	<b>169</b>
5.1. Introduction .....	170
5.2. Materials .....	173
5.3. Phase diagram.....	174
5.4. Optical birefringence measurements .....	175
5.5. Critical behavior at the $Sm-A-Sm-C$ phase transition.....	178
5.6. Critical behavior at the $N-Sm-A$ phase transition .....	185

5.7. Critical behavior at the $I-N$ phase transition .....	190
5.8. Conclusion.....	193
References .....	195
<b>Chapter 6. Evidence of broad tricritical range for the smectic-A to smectic-C phase transition</b>	<b>199</b>
6.1. Introduction .....	200
6.2. Materials .....	202
6.3. Texture observation.....	203
6.4. Phase diagram.....	205
6.5. Optical birefringence measurements .....	207
6.6. Critical behavior at the Sm-A–Sm-C phase transition.....	209
6.7. Tricritical fitting .....	215
6.8. Conclusion.....	221
References .....	223
<b>Chapter 7. Induced TGB phases in binary mixtures of achiral hockey stick-shaped and chiral rod-like mesogen</b>	<b>227</b>
7.1. Introduction .....	228
7.2. Materials .....	230
7.3. Optical textures and DSC studies .....	231
7.4. Phase diagram.....	239
7.5. Optical transmission intensity study.....	241
7.6. Static dielectric parameters measurement.....	244
7.7. Spontaneous polarization study.....	249
7.8. Response time and effective torsional bulk viscosity measurement.....	252
7.9. Dielectric spectroscopy measurement.....	255
7.10. Conclusion.....	260
References .....	263
<b>Chapter 8. Dielectric spectroscopy and electro-optical studies of three homologous bent-core mesogens</b>	<b>270</b>
8.1. Introduction .....	271
8.2. Materials .....	273

8.3. Dielectric spectroscopy study.....	274
8.4. Electro-optical investigation.....	287
8.5. Conclusion.....	294
References .....	297
<b>Chapter 9. Summary and conclusions</b>	<b>303</b>
<b>List of publications</b>	<b>313</b>
<b>Index</b>	<b>315</b>

## List of Tables:

<b>Table 3.1.</b> Values of the fit parameters obtained from the four-parameter fit of the temperature dependence of $\Delta n$ to Eq. (3.3).....	114
<b>Table 3.2.</b> Results corresponding to the best fit for $Q(T)$ near the $N$ – $Sm$ - $A$ phase transition obtained in accordance with Eq. (3.7) and related $\chi_v^2$ values associated with the fits. $ \tau _{\max}$ presents the upper limit of reduced temperature considered for these fits.....	117
<b>Table 3.3.</b> Values of the fit parameters obtained from the fit of the temperature dependence of $\Delta n$ to Eq. (3.8).....	121
<b>Table 4.1.</b> Results corresponding to the best fit for permittivity above and below the isotropic-nematic ( $T_{IN}$ ) phase transition temperatures obtained in accordance with Eq. (4.1) and Eq. (4.2).....	142
<b>Table 4.2.</b> Results corresponding to the best fit for $E(T)$ near $N$ – $Sm$ - $A$ phase transition obtained in accordance with Eq. (4.4) and related $\chi_v^2$ values associated with the fits. $ \tau _{\max}$ presents the upper limit of reduced temperature considered for these fits.....	145
<b>Table 4.3.</b> Fit parameters obtained from the fitting of the temperature dependence of $\gamma_1$ to Eq. (4.7) for different molar concentrations.....	156
<b>Table 4.4.</b> Values of the fitting parameters $\Delta n_0$ and $\beta$ obtained from Haller’s fit .....	158
<b>Table 4.5.</b> Activation energies for all the mixtures in the nematic phase .....	160
<b>Table 5.1.</b> Results corresponding to the best fit for $Q(T)$ of pure PhP2 compound near the $Sm$ - $A$ – $Sm$ - $C$ phase transition obtained in accordance with Eq. (5.2) and related $\chi_v^2$ values associated with the fits. The $Sm$ - $A$ – $Sm$ - $C$ phase transition temperature $T_{AC} = 352.45$ K was kept fixed in the fits. $ \tau _{\max}$ represents the upper limit of reduced temperature considered for these fits.....	180
<b>Table 5.2.</b> Results corresponding to the best fit for $Q(T)$ near $Sm$ - $A$ – $Sm$ - $C$ phase transition of all the mixtures obtained in accordance with Eq. (5.2) and related $\chi_v^2$ values associated with the fits .....	183
<b>Table 5.3.</b> Results corresponding to the best fit for $Q(T)$ of pure PhP2 compound near the $N$ – $Sm$ - $A$ phase transition and related $\chi_v^2$ values associated with the fits. The $N$ – $Sm$ - $A$ phase transition temperature $T_{NA} = 363.5$ K was kept fixed in the fits. $ \tau _{\max}$ represents the upper limit of reduced temperature considered for these fits .....	186

<b>Table 5.4.</b> Results corresponding to the best fit for $Q(T)$ near $N$ – $Sm$ - $A$ phase transition of all the mixtures obtained in accordance with Eq. (5.2) and related $\chi_v^2$ values associated with the fits .....	188
<b>Table 5.5.</b> Values of the fit parameters obtained from the four-parameter fit of the temperature dependence of $\Delta n$ to Eq. (5.3).....	192
<b>Table 6.1.</b> Results corresponding to the best fit for $Q(T)$ near $Sm$ - $A$ – $Sm$ - $C$ phase transition obtained in accordance with Eq. (6.2) and related $\chi_v^2$ values associated with the fits. $ \tau _{\max}$ presents the upper limit of reduced temperature considered for these fits.....	212
<b>Table 6.2.</b> Results corresponding to the best fit for $Q(T)$ near $Sm$ - $A$ – $Sm$ - $C$ phase transition obtained in accordance with Eq. (6.4) and related $\chi_v^2$ values associated with the fits. $ \tau _{\max}$ presents the upper limit of reduced temperature considered for these fits.....	218
<b>Table 7.1.</b> Sequence of phases, temperature scheme ( $^{\circ}C$ ) and transition enthalpies [ $\Delta H$ (J/g)] during cooling cycle for the mixture $x_{H-22.5} = 0.202$ .....	238
<b>Table 7.2.</b> Obtained fit parameter values from the fit to experimental $P_s$ value with Eq. (7.2) for all of the mixtures including 2H6R compound .....	251

## List of Figures:

<b>Figure 1.1.</b> Schematic diagram of three different types of thermotropic liquid crystals: (a) calamitic, (b) discotic, and (c) bent-core .....	4
<b>Figure 1.2.</b> General representation of molecular ordering in (a) uniaxial and (b) biaxial nematic phase .....	6
<b>Figure 1.3.</b> Structural representation of molecular ordering in smectic <i>A</i> phase. The director $\hat{n}$ is parallel to the smectic layer normal ( $\hat{k}$ ) .....	8
<b>Figure 1.4.</b> Structural representation of molecular ordering in layers for smectic <i>C</i> phase. The director $\hat{n}$ is tilted with respect to the smectic layer normal $\hat{k}$ by a certain angle .....	9
<b>Figure 1.5.</b> Structural representation of molecular ordering in each layer for hexatic smectic <i>B</i> phase.....	10
<b>Figure 1.6.</b> Structural representation of molecular ordering in each layer for smectic <i>I</i> and smectic <i>F</i> phases .....	11
<b>Figure 1.7.</b> Molecular geometry of soft crystal <i>E</i> phase .....	12
<b>Figure 1.8.</b> (a) Molecular representation of cholesteric or chiral nematic phase, (b-c) Optical textures appeared in cholesteric phase at two different temperatures ...	13
<b>Figure 1.9.</b> (a) Helical superstructure of the chiral smectic <i>C</i> ( <i>Sm-C*</i> ) phase with the helix axis parallel to the smectic layer normal $\hat{k}$ , (b) Orientation of a single molecule in each layer. The polarization vector $\vec{P}_s$ is always perpendicular to the director $\hat{n}$ and the tilt plane .....	15
<b>Figure 1.10.</b> (a) Molecular representation in a double twist cylinder. Relative orientation of the double twist cylinders in case of the (b) <i>BPII*</i> and (c) <i>BPI*</i> phase.....	17
<b>Figure 1.11.</b> A structural representation of the molecular superstructure with screw dislocations for (a) <i>TGBA</i> and (b) <i>TGBC*</i> phases.....	18
<b>Figure 1.12.</b> Molecular structures of (a) a symmetrical and (b) an asymmetrical bent-core compound.....	21
<b>Figure 1.13.</b> Schematic illustration of molecular geometry in <i>B<sub>1</sub></i> mesophase. a and b give the measure of periodicities in the two perpendicular directions.....	23
<b>Figure 1.14.</b> Representations of molecular geometry in (a) three mutually orthogonal planes and (b) four fundamental variants of <i>Sm-CP</i> phase in the <i>B<sub>2</sub></i> phase .....	24
<b>Figure 1.15.</b> Schematic representation of the in-plane molecular packing in the <i>B<sub>5</sub></i> phase. Vectors a and b suggests the presence of in-plane order .....	26

<b>Figure 1.16.</b> Schematic illustration of molecular ordering in the $B_6$ phase.....	27
<b>Figure 1.17.</b> Sketch of the molecular arrangement in bent-core nematic liquid crystals comprising smectic-like cybotactic clusters .....	30
<b>Figure 1.18.</b> Structural representation of a hockey stick-shaped compound H-22.5 [details in Chapter 5].....	31
<b>Figure 2.1.</b> Orientations of the molecules in planar (HG) and homeotropic (HT) cells.....	53
<b>Figure 2.2.</b> Schematic diagram of the experimental set-up for refractive index measurement.....	56
<b>Figure 2.3.</b> Schematic diagram of the experimental set-up for optical transmission measurement.....	58
<b>Figure 2.4.</b> Schematic diagram of the experimental set-up for the dielectric study .....	60
<b>Figure 2.5.</b> Frequency-dependent variation of the real ( $\epsilon'$ ) and imaginary ( $\epsilon''$ ) parts of dielectric permittivity for a fixed temperature of a bent-core compound-1/7 (described in chapter 8).....	63
<b>Figure 2.6.</b> Voltage dependent variation of sample filled cell-capacitance due to electrically driven Fredericksz transition in the nematic phase of a binary mixture (described in chapter 4) at 345 K. Inset shows the closer view near the threshold voltage .....	65
<b>Figure 2.7.</b> Schematic diagram of the experimental set-up for electro-optical study using field reversal polarization technique .....	69
<b>Figure 2.8.</b> Input and output waveforms of the LC sample for (a) square wave and (b) triangular wave input voltages.....	69
<b>Figure 2.9.</b> Orientational order parameter predicted from Maier-Saupe mean field theory.....	74
<b>Figure 2.10.</b> (a) The free energy density ( $f$ ) as a function of scalar order parameter $S$ . (b) The nematic order parameter ( $S$ ) vs. temperature. $T^*$ and $T^{**}$ are the temperatures slightly lower and higher than $T_{IN}$ respectively .....	83
<b>Figure 2.11.</b> Schematic diagram of the heat capacity variation near the phase transition for the dimensions $d > 4$ and $d < 4$ . Red solid line is the mean field heat capacity and green dashed line corresponds to the same including the correction term appears due to the fluctuation of the correlation length.....	90
<b>Figure 3.1.</b> Chemical structure and phase behavior of (a) the hockey stick-shaped compound (SF7) and (b) the rod-like compound (8OCB).....	105

**Figure 3.2.** Phase diagram for the binary mixture consisting of SF7 and 8OCB.  $x_{\text{SF7}}$  denotes the mole fraction of SF7. *I* – isotropic phase, *N* – nematic phase and Sm-A – smectic-A phase. ■: *I*–*N* transition temperature; ●: *N*–Sm-A transition temperature; □: Melting temperatures measured during heating cycle. Inset depicts variation of nematic range with concentration for the present system. Solid lines are drawn for guidance to eye..... 106

**Figure 3.3.** Temperature dependence of optical birefringence ( $\Delta n$ ) data for all the mixtures along with that for pure 8OCB. Vertical arrows show the *N*–Sm-A phase transition for all the mixtures ..... 108

**Figure 3.4.** Refractive indices ( $n_e, n_o$ ) and birefringence ( $\Delta n = n_e - n_o$ ) as a function of temperature for (a)  $x_{\text{SF7}} = 0.012$ , (b)  $x_{\text{SF7}} = 0.03$ , (c)  $x_{\text{SF7}} = 0.05$  and (d)  $x_{\text{SF7}} = 0.065$ . Dashed arrow and solid arrows denote the isotropic–nematic ( $T_{IN}$ ) and nematic–smectic-A ( $T_{NA}$ ) transition temperatures respectively..... 109

**Figure 3.5.** Variation of the temperature-dependent optical birefringence data for all the mixtures including pure 8OCB. Dashed arrow denotes the nematic–smectic-A ( $T_{NA}$ ) transition temperature. The solid line is a fit to Eq. (3.3) ..... 113

**Figure 3.6.** Temperature dependent variation of the quotient  $Q(T)$  in the vicinity of *N*–Sm-A phase transition for different mole fractions of SF7. Data are arranged in sequence of increasing mole fraction of SF7 from left to right with 1: 8OCB; 2:  $x_{\text{SF7}} = 0.012$ ; 3:  $x_{\text{SF7}} = 0.03$ ; 4:  $x_{\text{SF7}} = 0.05$ ; 5:  $x_{\text{SF7}} = 0.065$ . The solid lines are fit to Eq. (3.7)..... 117

**Figure 3.7.** Concentration dependence of the effective critical exponent ( $\alpha'$ ) obtained by fitting  $Q(T)$  to Eq. (3.7). The vertical dashed line corresponds to the tricritical point (TCP). The solid line is a 2<sup>nd</sup> order polynomial fit to the data.... 119

**Figure 3.8.** Variation of effective critical exponent ( $\alpha'$ ) with McMillan ratio ( $T_{NA}/T_{IN}$ ). The vertical dashed line corresponds to the tricritical point (TCP). The solid line is a linear fit to the data ..... 119

**Figure 3.9.** Plot of optical birefringence as a function of reduced temperature  $|\tau| = |1 - T/T_{NA}|$  for different mixtures. The solid lines are fit to Eq. (3.8) ..... 121

**Figure 3.10.** Variation of order parameter critical exponent ( $\beta'$ ) value with McMillan ratio ( $T_{NA}/T_{IN}$ ). The solid line is a second-order polynomial fit to the data ..... 122

**Figure 3.11.** Optimized molecular structure of (a) H-22.5, (b) SF7 ..... 124

**Figure 4.1.** Temperature variation of the dielectric parameters for (a)  $x_{\text{SF7}} = 0.012$ , (b) 0.03, (c) 0.05 and (d) 0.065. Solid arrow and dashed vertical arrow indicate the *I*–*N* ( $T_{IN}$ ) and the *N*–Sm-A ( $T_{NA}$ ) phase transition temperatures respectively ..... 136

<b>Figure 4.2.</b> Temperature variation of the dielectric anisotropy ( $\Delta\epsilon$ ) for all the mixtures. Inset depicts the average permittivity ( $\epsilon_{\text{avg}}$ ) of the same. Solid arrow and dashed vertical arrow indicate the $I-N$ ( $T_{IN}$ ) and the $N\text{-Sm-A}$ ( $T_{NA}$ ) phase transition temperatures respectively .....	138
<b>Figure 4.3.</b> Variation of permittivities with temperature for the concentration $x_{\text{SF7}} = 0.012$ . Solid lines are fit to Eq. (4.1) and (4.2). The critical temperatures $T^*$ and $T^{**}$ are indicated with star symbols ( $\star$ ) and the dotted vertical line represents the nematic-isotropic phase transition temperature ( $T_{IN}$ ). .....	140
<b>Figure 4.4.</b> Variation of the isotropic permittivity ( $\epsilon_{\text{iso}}$ ) with temperature for all of the mixtures. Solid lines are the fit to Eq. (4.1) and the star symbols ( $\star$ ) are representing the critical temperatures ( $T^*$ ) .....	141
<b>Figure 4.5.</b> Temperature-dependent variation of the quotient $E(T)$ in the vicinity of $N\text{-Sm-A}$ phase transition at different mole fractions of SF7 in the binary mixtures. The solid lines are fit to Eq. (4.4).....	144
<b>Figure 4.6.</b> The variation of the effective critical exponent ( $\alpha'$ ) with (a) molar concentration and (b) McMillan ratio ( $T_{NA}/T_{IN}$ ), obtained by fitting $E(T)$ to Eq. (4.4). The vertical dashed line corresponds to the tricritical point (TCP). The solid lines are the polynomial fits to the data points.....	146
<b>Figure 4.7.</b> Variation of cell capacitance in planar configuration at different temperatures for $x_{\text{SF7}} = 0.012$ . Different temperatures are mentioned in the figure in unit of Kelvin (K).....	148
<b>Figure 4.8.</b> The variations of threshold voltage ( $V_{\text{th}}$ ) with temperature for all the mixtures only in nematic phase. The vertical dashed line and solid line corresponds to the $T_{IN}$ and $T_{NA}$ respectively for each of molar concentration.....	148
<b>Figure 4.9.</b> The variation of the splay elastic constant ( $K_{11}$ ) with reduced temperature for all the mixtures in the nematic phase. The vertical arrows correspond to $T_{NA}$ for each of molar concentration. ....	150
<b>Figure 4.10.</b> (a) Energy optimized molecular structure of SF7 and 8OCB. (b) Mutual alignment of both the hockey-stick shaped (SF7) and calamitic molecule (8OCB) in the nematic phase. ....	151
<b>Figure 4.11.</b> The variation of the relaxation time ( $\tau_0$ ) with reduced temperature for all the mixtures in the nematic phase. The vertical arrows correspond to $T_{NA}$ for each of molar concentration .....	152
<b>Figure 4.12.</b> The variation of rotational viscosity ( $\gamma_1$ ) with reduced temperature for all the mixtures only in nematic phase. The vertical arrows correspond to $T_{NA}$ for each of molar concentration. Solid lines are fit to Eq. (4.7). ....	154

<b>Figure 4.13.</b> Temperature dependence of optical birefringence data for $x_{SF7} = 0.012$ . Dashed arrow denotes the Nematic–Smectic-A transition temperature ( $T_{NA}$ ). The solid line is a fit to Eq. (4.9).....	157
<b>Figure 4.14.</b> The temperature dependence of orientational order parameter ( $\langle P_2 \rangle$ ) for all the mixtures. Dashed arrow denotes the nematic–smectic-A ( $T_{NA}$ ) transition temperatures respectively. Inset represents the value of $\langle P_2 \rangle$ at a particular temperature in both nematic and smectic phases for all the mixtures.....	159
<b>Figure 4.15.</b> The variations of $\ln(\gamma_1/\langle P_2 \rangle)$ with reciprocal of temperature ( $1/T$ ) for all the concentrations only in nematic phase. Solid lines represent a linear fit to the data points ...	160
<b>Figure 5.1.</b> Partial phase diagram of the binary system comprising of PhP2 and PhP1. $x_{PhP1}$ denotes the mole fraction of PhP1. <i>I</i> – isotropic phase, <i>N</i> – nematic phase, <i>Sm-A</i> –smectic-A phase, <i>Sm-C</i> –smectic-C phase, ○: isotropic to nematic transition temperature; ●: nematic to smectic-A transition temperature; ■: smectic-A to smectic-C transition temperature; Inset shows the concentration dependence of the <i>Sm-A</i> and nematic ranges for the present system. Solid lines are drawn for guidance to eye.....	174
<b>Figure 5.2.</b> Temperature dependence of birefringence ( $\Delta n$ ) data for the (a) Pure PhP2 compound and (b) mixture $x_{PhP1} = 0.1$ , (c) 0.2 and (d) 0.3. Vertical arrows show the <i>I</i> – <i>N</i> , <i>N</i> – <i>Sm-A</i> and <i>Sm-A</i> – <i>Sm-C</i> phase transitions for the mixtures. In the insets variation of birefringence in the vicinity of <i>Sm-A</i> – <i>Sm-C</i> transition [inset (a)] and <i>N</i> – <i>Sm-A</i> transition [inset (b)] has been presented.....	176
<b>Figure 5.3.</b> The temperature variation of the parameter $Q(T)$ near the <i>Sm-A</i> – <i>Sm-C</i> phase transition. Solid lines are fit to Eq. (5.2) near the <i>Sm-A</i> – <i>Sm-C</i> phase transition.....	180
<b>Figure 5.4.</b> The temperature dependence of $Q(T)$ in the vicinity of the <i>Sm-A</i> – <i>Sm-C</i> transition in mixtures of PhP1 and PhP2 for $ \tau _{\max} = 3 \times 10^{-3}$ . 1: $x_{PhP1} = 0.0$ ; 2: $x_{PhP1} = 0.05$ ; 3: $x_{PhP1} = 0.1$ ; 4: $x_{PhP1} = 0.15$ ; 5: $x_{PhP1} = 0.2$ ; 6: $x_{PhP1} = 0.3$ ; 7: $x_{PhP1} = 0.35$ ; 8: $x_{PhP1} = 0.4$ ; 9: $x_{PhP1} = 0.45$ .....	183
<b>Figure 5.5.</b> Variation of the effective critical exponent ( $\alpha'$ ) with $T_{AC}/T_{NA}$ for <i>Sm-A</i> – <i>Sm-C</i> phase transition. The vertical dashed line and solid line corresponds to the tricritical point (TCP) and 3D-XY limit respectively. The solid lines (red) are linear fit to the data points.....	184
<b>Figure 5.6.</b> Temperature variation of the parameter $Q(T)$ near the <i>N</i> – <i>Sm-A</i> phase transition for sample PhP2. Solid lines are fit to Eq. (5.2) near the <i>N</i> – <i>Sm-A</i> phase transition. ....	186

**Figure 5.7.** The temperature dependence of  $Q(T)$  in the vicinity of the  $N$ -Sm-A transition in mixtures of PhP1 and PhP2. 1:  $x_{\text{PhP1}} = 0.0$ ; 2:  $x_{\text{PhP1}} = 0.05$ ; 3:  $x_{\text{PhP1}} = 0.1$ ; 4:  $x_{\text{PhP1}} = 0.15$ ; 5:  $x_{\text{PhP1}} = 0.2$ ; 6:  $x_{\text{PhP1}} = 0.3$ ; 7:  $x_{\text{PhP1}} = 0.35$ ; 8:  $x_{\text{PhP1}} = 0.4$ ... 188

**Figure 5.8.** The variation of effective critical exponent ( $\alpha'$ ) with  $T_{NA}/T_{IN}$  for the  $N$ -Sm-A phase transition and  $T_{AC}/T_{NA}$  for the Sm-A-Sm-C phase transition. The vertical dashed lines and solid line corresponds to the tricritical point (TCP) and 3D-XY limit respectively. The solid lines (red) are linear fit to the data... 189

**Figure 5.9.** Experimental values of birefringence ( $\Delta n = n_e - n_o$ ) as a function of temperature for (a) PhP2, (b)  $x_{\text{PhP1}} = 0.05$ , (c)  $x_{\text{PhP1}} = 0.1$  and (d)  $x_{\text{PhP1}} = 0.3$ . Solid lines (Red) represent the fit to Eq. (5.3) and extrapolated to the Sm-A phase..... 191

**Figure 6.1.** Chemical structure and phase behavior of the hockey-stick-shaped compound (Compound 1: H-22.5) and the rod-like compound (Compound 2: 7OCB) ..... 202

**Figure 6.2.** Optical texture observed for a mixture with mol fraction  $x_{7\text{OCB}} = 0.184$  in homogeneous alignment (a-c) and homeotropic alignment (d-f). (a) Sm-A phase at 380 K, (b) Sm- $C_s$  phase at 369 K, (c) Sm- $C_a$  phase at 360 K, (d) Sm-A phase at 378 K, (e) Sm- $C_s$  phase at 371 K, (f) Sm- $C_a$  phase at 365 K. Arrows indicates the direction of the polarizers..... 204

**Figure 6.3.** Partial phase diagram of the binary system comprising of 7OCB and H-22.5.  $x_{7\text{OCB}}$  denotes the mole fraction of 7OCB.  $I$  – isotropic phase, Sm-A – smectic-A phase, Sm- $C_s$  – smectic- $C_s$  phase, Sm- $C_a$  – smectic- $C_a$  phase  $\square$ :  $N$ -Sm- $C_s$  phase transition;  $\blacksquare$ :  $I$ -Sm-A phase transition;  $\bullet$ : Sm-A-Sm- $C_s$  phase transition;  $\circ$ : Sm- $C_s$ -Sm- $C_a$  phase transition temperatures. The inset shows the concentration dependence of the Sm-A range for the present system. Solid lines are drawn for guidance to the eye. .... 206

**Figure 6.4.** Temperature dependence of birefringence ( $\Delta n$ ) data for (a)  $x_{7\text{OCB}} = 0.184$  and (b)  $x_{7\text{OCB}} = 0.167$ .  $\circ$ : Birefringence data from optical transmission method,  $\square$ : Birefringence data from thin prism technique. Blue solid arrows indicate isotropic to smectic-A ( $I$ -Sm-A) phase transition temperatures ( $T_{IA}$ ), black solid arrows indicate the smectic-A to smectic-C (Sm-A-Sm- $C_s$ ) phase transition temperatures ( $T_{AC}$ ) and dashed arrows indicate the smectic- $C_s$  to smectic- $C_a$  phase transition temperatures ( $T_{CC}$ ). Insets show the variation of birefringence in the vicinity of Sm-A-Sm- $C_s$  transition temperature ( $T_{AC}$ ) ..... 208

**Figure 6.5.** The temperature dependence of  $Q(T)$  in the vicinity of Sm-A-Sm- $C_s$  transition in mixtures of H-22.5 and 7OCB for  $|\tau|_{\text{max}} = 4 \times 10^{-3}$ . 8:  $x_{7\text{OCB}} = 0.211$ ; 7:  $x_{7\text{OCB}} = 0.2$ ; 6:  $x_{7\text{OCB}} = 0.184$ ; 5:  $x_{7\text{OCB}} = 0.174$ ; 4:  $x_{7\text{OCB}} = 0.167$ ; 3:  $x_{7\text{OCB}} = 0.158$ ; 2:  $x_{7\text{OCB}} = 0.15$ ; 1:  $x_{7\text{OCB}} = 0.1$ . All of these  $Q(T)$  data have been shifted in temperature axis for the guidance of eye as follows: curve 7 by +0.5 K, curve 6 by

+0.5 K, curve 4 by +1 K, curve 3 by +1.5 K, curve 2 by +1.5 K. Solid lines representing the fits to Eq. (6.2).....211

**Figure 6.6.** Variation of the effective critical exponent against (a) the temperature ratio  $T_{AC}/T_{IA}$  and (b) the temperature width of Sm-A phase at the Sm-A–Sm-C phase transition in the present investigated binary mixtures. The vertical dashed lines correspond to the tricritical point (TCP). The solid lines (red) are the 2<sup>nd</sup> order fit to the data points .....214

**Figure 6.7.** The temperature dependent variation of  $Q(T)$  in the vicinity of Sm-A–Sm-C transition in mixtures of H-22.5 and 7OCB for (a) fit range-B ( $|\tau|_{\max} = 4 \times 10^{-3}$ ), and (b) fit range-A ( $|\tau|_{\max} = 2 \times 10^{-3}$ ). 5:  $x_{7OCB} = 0.174$ ; 4:  $x_{7OCB} = 0.167$ ; 3:  $x_{7OCB} = 0.158$ ; 2:  $x_{7OCB} = 0.15$ ; 1:  $x_{7OCB} = 0.1$ . These  $Q(T)$  data has been shifted in temperature axis for the guidance of eye as follows: curve 7 by +0.5 K, curve 6 by +0.5 K, curve 4 by +1 K, curve 3 by +1.5 K, curve 2 by +1.5 K.....217

**Figure 6.8.** The representation of extracted  $z$  values with the variation of the amplitude ratio  $A^-/A^+$  over three fit ranges in the vicinity of Sm-A–Sm-C transition. Solid line is a 2<sup>nd</sup> order polynomial to the data points .....219

**Figure 6.9.** Variation of the effective critical exponent ( $\alpha'$ ) with the temperature ratio  $T_{AC}/T_{IA}$  for Sm-A–Sm-C<sub>s</sub> phase transitions of the present binary system. ○: Values of  $\alpha'$  for Sm-A–Sm-C transition from chapter 5; □: Values of  $\alpha'$  for N–Sm-A transition from chapter 5. The vertical dashed-dot lines are corresponding to the tricritical point (TCP). The solid lines (red) are the linear fit to the data points .....220

**Figure 7.1.** Chemical structure and phase behavior of the chiral ferroelectric compound (2H6R).....231

**Figure 7.2.** Optical textures of  $N^*$  phase by lowering the temperature as: (a) nematic droplets at 98.5 °C, (b) cholesteric Grandjean texture of 2H6R at 98.3 °C, (c) cholesteric fan-like texture at 98 °C, (d-e) oily streaks texture at 97.6 °C and 97.2 °C, (f-g) color domain texture of different twist and twist-inversion states at 96.8 °C and 96.6 °C, (h) texture with cholesteric finger at 96.2 °C, (i) oily streaks textures appears again at 95.5 °C, (j-k) texture with cholesteric finger in homeotropic cell at 96.5 °C, 96 °C respectively, (l) coexisting of fingerprint texture with cholesteric finger at 94.3 °C for  $x_{H-22.5} = 0.306$  .....233

**Figure 7.3.** Optical textures of TGBA phase by lowering the temperature as follows: (a-b) transition from  $N^*$  to TGBA phase in planar configuration at 93.3 °C and 93.25 °C, (c) Grandjean texture of TGBA phase at 92.1 °C, (d-e) filament texture at the transition from  $N^*$  to TGBA phase in homeotropic configuration at 93.25 °C and 93.2 °C, (f) appearance of black domain for TGBA phase at 93 °C .....235

<b>Figure 7.4.</b> Optical textures of TGBC* phase by lowering the temperature: (a) appearance of cross-grid pattern in planar aligned Grandjean texture of TGBA phase at 84.6 °C, (b) well-formed texture of TGBC* phase at 84.5 °C, (c) appearance of modulated texture of TGBC* phase at 80 °C for $x_{H-22.5} = 0.306$ , (d) transition to TGBA–TGBC* phase at 84.8 °C in homeotropic cell, (e) well-formed TGBC* phase texture at 82 °C in homeotropic cell .....	236
<b>Figure 7.5.</b> Optical textures of lower temperature Sm- $B^*_{hex}$ phase at (a) 50 °C for pure 2H6R compound in planar cell, (b) 48.6 °C for $x_{H-22.5} = 0.202$ in homeotropic alignment .....	237
<b>Figure 7.6.</b> DSC thermograms on both heating and cooling cycle for the mixture concentration $x_{H-22.5} = 0.202$ .....	238
<b>Figure 7.7.</b> (a) Phase diagram for the composite mixture consisting of H-22.5 and 2H6R. $x_{H-22.5}$ denotes the mole fraction of H-22.5. <i>I</i> - isotropic phase, $N^*$ - chiral nematic phase, Sm- $C^*$ - chiral Sm- <i>C</i> phase, TGBA- frustrated smectic- <i>A</i> phase and TGBC*- frustrated smectic- <i>C</i> phase. ○: <i>I</i> – $N^*$ transition temperature; ■: $N^*$ –TGBA transition temperature; □: TGBA–TGBC* transition temperature; ★: $N^*$ –Sm- $C^*$ transition temperature; ●: TGBC*–Sm- $B^*_{hex}$ phase transition temperature. (b) Variation of $N^*$ , TGBA and TGBC* phase range with concentration for the present system. Solid lines are drawn for guidance to the eye .....	240
<b>Figure 7.8.</b> Temperature-dependent measured optical transmission intensity for compound (a) 2H6R, (b) $x_{H-22.5} = 0.101$ , (c) $x_{H-22.5} = 0.202$ and (d) $x_{H-22.5} = 0.306$ respectively in planar (open circle) cell and also homeotropic (closed square) cell configuration. Vertical arrows represent the corresponding phase transition.....	242
<b>Figure 7.9.</b> Temperature-dependent dielectric parameters ( $\epsilon_{  }$ , $\epsilon_{\perp}$ , $\epsilon_{avg}$ ) for compound compound (a) 2H6R, (b) $x_{H-22.5} = 0.101$ , (c) $x_{H-22.5} = 0.202$ and (d) $x_{H-22.5} = 0.306$ in planar or HG (open circle) cell and also homeotropic or HT (open square) cell configuration. The dashed line represents the average permittivity ( $\epsilon_{avg}$ ). Inset depicts the magnified version of permittivity inversion region. Vertical arrows represent the corresponding phase transition .....	245
<b>Figure 7.10.</b> (a) Variation of dielectric anisotropy ( $\Delta\epsilon$ ) against the reduced temperature ( $T-T_{I-N^*}$ ). Vertical arrows represent the corresponding phase transition temperatures(b) The concentration variation of positive anisotropy ( $\Delta\epsilon$ ) range for all the mixture including the pure chiral 2H6R mesogen .....	248
<b>Figure 7.11.</b> Value of spontaneous polarization ( $P_s$ ) as a function of reduced temperature for pure compound (2H6R) and all the mixture components. The solid line is a fitting curve of Eq. (7.2).....	250

<b>Figure 7.12.</b> Reduced temperature dependent value of response time ( $\tau$ ) for pure compound (2H6R) including all the mixture components.....	252
<b>Figure 7.13.</b> (a) Reduced temperature dependent value of effective torsional bulk viscosity ( $\eta$ ) for all of the mixtures including the pure compound (2H6R). (b) Arrhenius plot of effective torsional bulk viscosity vs. ( $1000/T$ ). Inset represents the linear fit to Eq. (7.3) to experimental data of $x_{H-22.5} = 0.306$ .....	254
<b>Figure 7.14.</b> (a) Reduced temperature dependent value of effective torsional bulk viscosity ( $\eta$ ) for all of the mixtures including the pure compound (2H6R). (b) Arrhenius plot of effective torsional bulk viscosity vs. ( $1000/T$ ). Inset represents the linear fit to Eq. (7.3) to experimental data of $x_{H-22.5} = 0.306$ .....	256
<b>Figure 7.15.</b> (a) Arrhenius plot of the relaxation frequency ( $f_R$ ) and (b) the variation of dielectric strength ( $\delta\epsilon$ ) at different mesophases for the pure compound 2H6R .....	257
<b>Figure 7.16.</b> (a) Arrhenius plot of the relaxation frequency ( $f_R$ ) and (b) the variation of dielectric strength ( $\delta\epsilon$ ) at different mesophases for the mixture concentration $x_{H-22.5} = 0.202$ .....	258
<b>Figure 8.1.</b> Frequency dependence of the real ( $\epsilon'$ ) and imaginary ( $\epsilon''$ ) parts of the permittivity for compound <b>1/7</b> in (a) HG or planar and (b) HT or homeotropic cell configurations. Red solid lines represent the fitting curve to data points with Eq. (8.2).. .....	276
<b>Figure 8.2.</b> Temperature dependence of relaxation frequency ( $f_R$ ) and dielectric strength ( $\delta\epsilon$ ) for compound <b>1/7</b> in (a,c) planar and (b,d) homeotropic cells respectively. Vertical arrows define the corresponding phase transition temperatures .....	276
<b>Figure 8.3.</b> Frequency dependence of the imaginary ( $\epsilon''$ ) parts of the permittivity for compound <b>1/9</b> in (a) HG or planar and (b) HT or homeotropic cell configurations.....	279
<b>Figure 8.4.</b> Temperature dependence of relaxation frequency ( $f_R$ ) and dielectric strength ( $\delta\epsilon$ ) for compound <b>1/9</b> in (a,c) planar and (b,d) homeotropic cells respectively. Vertical arrows define the corresponding phase transition temperatures .....	280
<b>Figure 8.5.</b> The variation of frequency-dependent imaginary ( $\epsilon''$ ) part of permittivity with the bias voltage for compound <b>1/9</b> in (a) planar and (b) the homeotropic alignment cells .....	282
<b>Figure 8.6.</b> Frequency dependence of the imaginary ( $\epsilon''$ ) parts of the complex permittivity for compound <b>1/10</b> in (a) HG or planar and (b) HT or homeotropic configuration cells.....	284

**Figure 8.7.** Temperature dependence of relaxation frequency ( $f_R$ ) and dielectric strength ( $\delta\varepsilon$ ) for the compound **1/10** in (a,c) planar and (b,d) homeotropic cells respectively. Vertical arrows define the corresponding phase transition temperatures. .... 285

**Figure 8.8.** The variation of frequency-dependent imaginary ( $\varepsilon''$ ) part of the complex permittivity with the bias voltage for compound **1/10** in (a) planar and (b) the homeotropic alignment cells. .... 285

**Figure 8.9.** Switching current response curves of compound **1/9** and **1/10** for a triangular wave voltage (Red dashed line) at different temperatures; (a-c) Compound **1/9** in HG cell, (d) Compound **1/10** in HG cell, (e) Compound **1/10** in HT cell, (f-g) Temperature-dependent polarization value for the compound **1/9** and **1/10** respectively.. .... 289

**Figure 8.10.** Optical textures of the compound **1/9** and **1/10** for an applied square wave AC voltage at different mesophases; (a-c): compound **1/9** in HG cell, (d-f): compound **1/9** in HT cell, (g-j): compound **1/10** in HG cell, (k-n): compound **1/10** in HT cell. Corresponding insets are the textures before the application of the field, and arrows indicate the direction of the analyzer and polarizer... .... 290

# CHAPTER 1

---

## Introduction

## 1.1. Liquid crystals

Liquid crystals (LCs) or mesophases are fascinating state of matter, existing in between the three-dimensionally ordered crystals and completely disordered isotropic liquid [1,2]. Several compounds formed by organic molecules do not exhibit a direct transition from solid to liquid; rather it passes through a single or series of fluid like phases in between, known as the liquid crystalline phases. The self assembly of the molecules in LC compounds provides both the orientational order as in liquids as well as the positional order as in crystalline solids which may be of one or two dimensional. The combination of both these ordering promote the LC material to reveal the properties of both the crystalline (*i.e.*, anisotropy in optical, electrical and magnetic properties, periodic arrangement of molecules in one spatial direction etc.) and the liquid (*i.e.*, fluidity, viscosity, inability to support shear) states [3]. The main criterion for organic molecules to exhibit mesomorphic behavior is shape-anisotropy [1,2]. LCs are made up of molecules in various shapes such as the rod-like, bent-shaped or disc-like etc. In addition to this, the presence of flexible terminal chain in such molecules produces some molecular disorder, which also decides the type and temperature stability of the mesophases. It is interesting to investigate their physical properties systematically for better understanding about the nature of the mesophases which requires different tools and techniques. Moreover, due to the presence of optical and dielectric anisotropy in LCs, along with many other applications they are widely used in display technology. Therefore, a complete understanding of different LC systems can be helpful in modifying and improving their applications in display technology [4,5].

An Austrian botanist Friedrich Reinitzer was the first to discover the liquid crystalline phase in 1888 while working on Cholesteryl benzoate ( $C_6H_5COOC_{27}H_{45}$ ) [6]. During the heating cycle, he observed that Cholesteryl benzoate formed a cloudy fluid state in between 145.4 °C and 178.5 °C which

---

---

then completely turned into the isotropic liquid. Further confirmation was made by a German physicist Otto Lehmann [7] when investigating such type of material in polarizing optical microscope and he named it as “flüssige kristalle” (meaning liquid crystals) in 1890. Furthermore, in 1922, George Friedel [8,9], renamed “mesophase” to such a fascinating class of matter. Since then a number of different phases have been identified as liquid crystalline mesophases. In both theoretical and experimental research, with the focus of complete understanding and continuous development of these mesophases, lots of works have been devoted. Various researchers have been successful in accomplishing the structural modification by considering intermolecular interactions of the LC molecules which emphasized the liquid crystal material for the applications in liquid crystal display, optical switch, phase modulator, beam steering, holography, laser projection, temperature sensor etc. [10-19].

## **1.2. Classification of liquid crystals**

Based on the structural property of liquid crystal molecules, transition to different mesophases occurs mainly due to two distinct ways: one by purely thermal process and other under the influence of solvents. In the former process, the phase transitions among the intermediate phases occur by varying the temperature of the compound and are known as thermotropic liquid crystal. If the phase transition among the different mesophases are brought about by the change in concentration of solvent (influence of solvent) then such compounds are called as lyotropic liquid crystal. A brief introduction for both type of liquid crystals are discussed below.

### **1.2.1. Lyotropic liquid crystals**

Lyotropic liquid crystals are associated with the amphiphilic molecules (surfactant), which comprises a polar head that is attracted towards water or polar substances (hydrophilic) and also non-polar flexible terminal tails (hydrophobic) [20-23]. In an anisotropic solution of such molecules with an

appropriate solvent, small aggregates are formed with a particular shape in which hydrophobic tails are protected by polar head and these small aggregates are called micelles. Generally, micelles are spherical in shape; they may be lamellar, cubic and hexagonal in structure. It has been observed that by increasing the surfactant concentration, molecular ordering also increases. Most general example of a lyotropic liquid crystal is soap solution, although it is most familiar in biological system like in certain proteins, lipid, cell membrane etc. [24].

### 1.2.2. Thermotropic liquid crystals

In case of thermotropic liquid crystal, the transition between different mesophases is caused by varying the temperature externally. The organic molecules associated with these types of compounds have a specific architecture with a rigid core or aromatic ring in addition to flexible terminal chain linked with it. Depending upon such molecular structure, liquid crystal compounds are further classified as rod-like or calamitic liquid crystal, disc-shaped or discotic liquid crystal, banana-like or bent-core liquid crystal as depicted in Fig. 1.1. Based on the position of bent angle, the bent-core liquid crystals are also of several types: hockey stick-shaped, T-shaped, star-shaped, pyramid-shaped etc. A limited description of the LC compounds composed of

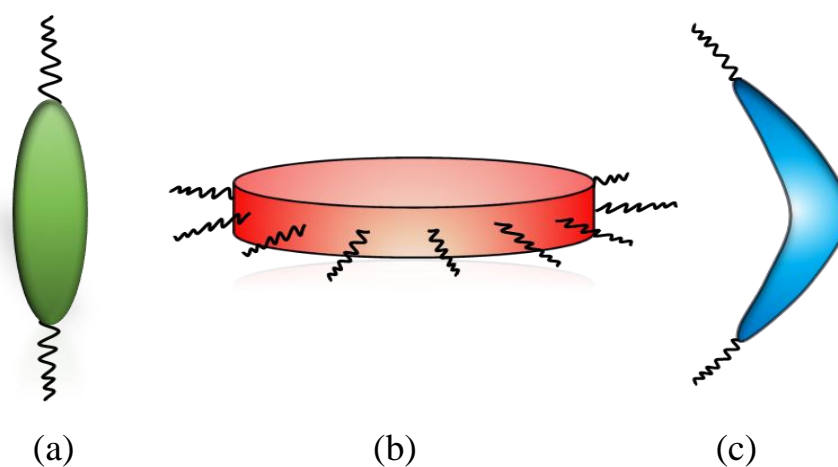


**Figure 1.1.** Schematic diagram of three different types of thermotropic liquid crystals: (a) calamitic, (b) discotic, and (c) bent-core.

calamitic and bent-core molecules has been demonstrated in the following sections which are relevant to the thesis work.

### 1.2.3. Calamitic liquid crystals

In general, the term “calamitic” or “rod-like” simply defines the macroscopic view of the structural unit. More precisely it can be stated that the molecules are constructed by a rigid straight aromatic core of phenyl rings, attached with one or more terminal alkyl or alkoxy chains at its end. Depending upon the chain length and number of phenyl rings in central core unit, such liquid crystal compounds possess distinct mesophase behavior and unusual mesomorphic properties, which are described in details further.

#### 1.2.3.1. Nematic (*N*) phase

Nematic phase is the simplest and least ordered phase with the highest symmetry among all the mesophases of thermotropic liquid crystal. In case of a nematic phase, there exists a high degree of long-range orientational ordering without any positional ordering of the molecules, *i.e.*, the organic molecules are on the average preferred to align their long axis along a particular direction, though the molecular center of mass is arbitrarily oriented within a finite volume [25-27]. Hence, the compound possesses a high degree of mobility as like as isotropic liquid. The preferred aligned direction is called the nematic director or simply director and symbolized as  $\hat{n}$  (See Fig. 1.2). The directional distribution is symmetric in case of nematic molecules due to the presence of molecular head-tail symmetry [3], *i.e.*, there is an indistinguishable property between  $\hat{n}$  and  $-\hat{n}$  with respect to the molecule. The preferred direction of molecules usually varied from point to point in the medium, but a homogeneously aligned domain is optically uniaxial and strongly birefringent. However, the biaxial nematic phase also exist [28-34], in which a second director  $\hat{m}$  is present and directed along molecular short axis, orthogonal to  $\hat{n}$  as illustrated in Fig. 1.2. The biaxial nematic phase is often found in case of

---

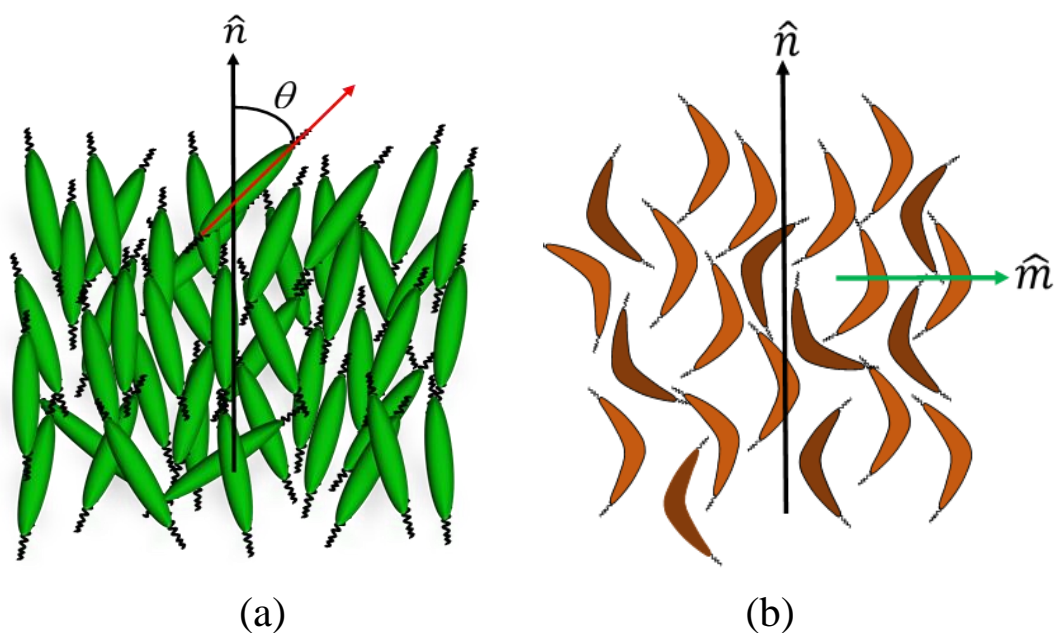


**Figure 1.2.** General representation of molecular ordering in (a) uniaxial and (b) biaxial nematic phase.

bent-core compounds. However, another type of nematic phase is also discovered, in which molecules are oriented in layers, called the cybotactic nematic phase [35-44]. Furthermore, due to the presence of polarity of the molecule, deformation of uniaxiality or biaxiality in nematic phase is also possible by the influence of the external field (electrical, magnetic or mechanical perturbation), which affects the optical and dielectric properties of the compound. This mechanism is most useful in display technological application.

The long-range orientational order of the molecules in the uniaxial nematic phase is defined by a scalar order parameter  $S$  and expressed as:

$$S = \langle P_2(\cos \theta) \rangle = \frac{1}{2} \langle 3 \cos^2 \theta - 1 \rangle \quad (1.1)$$

where,  $\theta$  is the angle between the molecular long axis and the nematic director  $\mathbf{n}$ , the bracket  $\langle \dots \rangle$  indicates an ensemble average over all the molecules. However, the value of  $S$  is equal to 0 in case of isotropic liquid, as because of random orientation of the molecules. Moreover, well within the nematic phase or a perfectly order phase,  $\theta$  is equal to 0, provides  $\langle \cos^2 \theta \rangle = 1$  and hence  $S =$

1. On other hand, if the molecules are oriented randomly in a plane perpendicular to the director, having the same director axis on the average, then  $\theta$  is equal to  $\pi/2$ , and  $\langle \cos^2\theta \rangle = 0$  which presented a value  $S = -1/2$ . Therefore, the theoretical prediction of this order parameter value varies from  $-1/2$  to  $+1$ , whereas experimental value provides a range between 0.3 and 0.8 well within the nematic phase.

In the planar geometrical arrangement of the nematic LC sample, a schlieren textures with curved four and two dark brushes and often thread like or marble texture are observed under polarizing optical microscope [45].

### 1.2.3.2. Smectic (Sm) phase

In addition to orientational ordering, molecules have some degrees of positional ordering within the smectic phase which is generally appeared at lower temperature than nematic phase. This phase is more ordered than the nematic phase, *i.e.*, the smectic phase is more “solid-like” than the usual nematic phase. In this phase, the centers of mass of the molecules are on the average arranged within equidistant layers with a well-defined interlayer separation. The molecular director in each layer is aligned either orthogonal or tilted relative to the layer normal. Moreover, due to lack of interlayer attraction, individual layers of smectic phase can slide over one another as like fluid phase even though with a viscosity much higher compared to that in the nematic phase. Although, smectic phases have one-dimensional long-range positional order as like one-dimensional crystal, some other smectic phases have three-dimensional long-range Bond-Orientational Order (BOO), but without any long-range positional ordering as in case of hexatic phases. Depending on the orientation and ordering of molecules within the layer, smectic phases can be classified into different sub-phases which are designated in accordance with increasing order: Smectic *A*, Smectic *B*, Smectic *C*, Smectic *E*, Smectic *G*, Smectic *H*, Smectic *I*, Smectic *F* and so on. In the following section, brief introductions to some of those smectic phases have been presented.

## a. Smectic A (Sm-A) phase

In case of smectic A (Sm-A) phase, molecules are aligned on average to a direction parallel to the layer normal ( $\hat{k}$ ) with their centre of mass oriented arbitrarily as depicted in Fig. 1.3. Such a configuration can be described by considering a one-dimensional mass density wave along the layer normal. However, this one dimensional ordering is not truly long-range rather it can be said as quasi long-range. Furthermore, as this phase is optically uniaxial with respect to optic axis, the homeotropically aligned optical texture is appeared to be black where a fan-shaped or focal conic type textures are visible for planar aligned sample. On the basis of the relation between the molecular length and the layer spacing, the Sm-A phase can be subdivided into several distinct phases, namely Smectic  $A_1$ , Smectic  $A_2$  and Smectic  $A_d$ . All have the same point group symmetry but differ by translational symmetry due to specific packing of the molecules within a layer. In smectic  $A_1$  the layer thickness is equal to the molecular length, whereas in smectic  $A_2$  phase, the layer thickness is equal to the twice of the molecular length and the smectic  $A_d$  phase has an intermediate

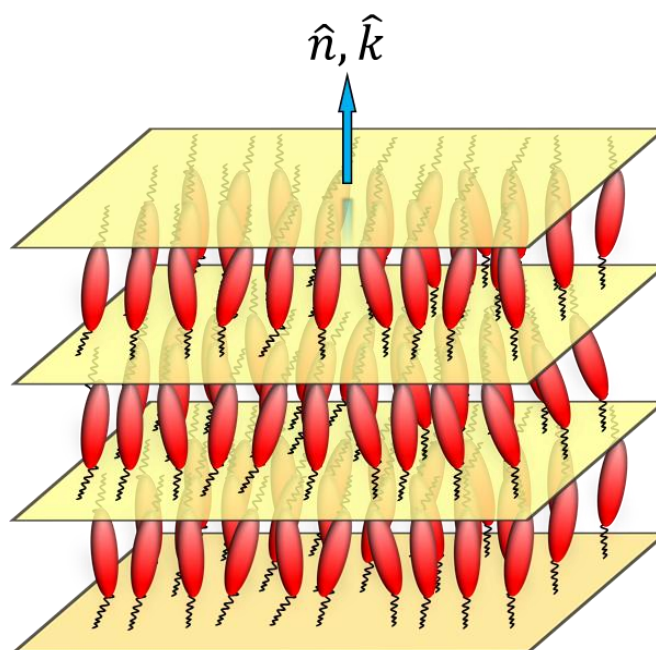


**Figure 1.3.** Structural representation of molecular ordering in smectic A phase. The director  $\hat{n}$  is parallel to the smectic layer normal ( $\hat{k}$ ).

---

---

layer structure in-between smectic  $A_1$  and smectic  $A_2$ , *i.e.*, the layer thickness ( $l$ ) is intermediate between the single molecular length ( $d$ ) and twice of that ( $2d$ ) [46-49].

## b. Smectic $C$ (Sm- $C$ ) phase

The molecular organization in the smectic  $C$  phase is quite similar to that of the smectic  $A$  phase, but the only difference is that the molecules are tilted by an angle  $\theta$  (temperature dependent tilt angle) with respect to the layer normal ( $\hat{k}$ ) as in Fig. 1.4. This tilt angle is more or less same for all molecules within a layer and also same for the adjacent layers. However, the smectic layers also have no positional correlation as like Sm- $A$  phase, and hence exhibit fluid-like sliding features in one over another. In this case the molecules have the freedom to rotate about their tilt direction. Hence, due to the introduction of such tilt the rotational symmetry breaks about the layer normal [50,51]. Thus the Sm- $C$  phase exhibits an optical biaxiality as well as a relatively greater

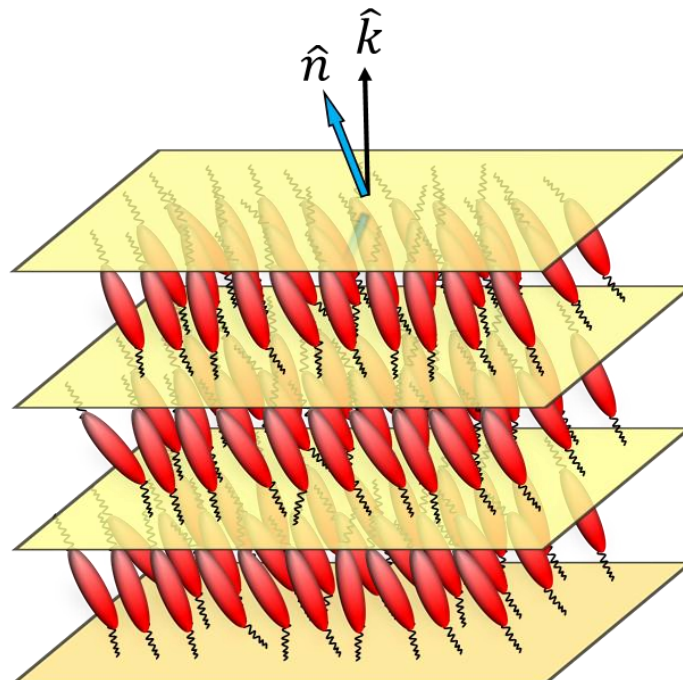


**Figure 1.4.** Structural representation of molecular ordering in layers for smectic  $C$  phase. The director  $\hat{n}$  is tilted with respect to the smectic layer normal  $\hat{k}$  by a certain angle.

viscosity than that of the Sm-A phase. Again, the Sm-C phase can also be subdivided into two distinct sub-phases, based on the relative tilt alignment of the molecules in adjacent layers – (a) the synclinic smectic C (Sm-C<sub>s</sub>) phase, where the tilt direction is the same in adjacent smectic C layers and (b) the anticlinic smectic C (Sm-C<sub>a</sub>) phase, where the tilt direction alternates in the adjacent smectic C layers. Moreover, the optical textures of the Sm-C phase can be visualized as fan-shaped and often as broken fan-shaped typed in planar alignment [45], while schlieren textures also visible in homeotropically aligned Sm-C<sub>s</sub> and Sm-C<sub>a</sub> phases [52].

### c. Hexatic smectic (Sm-B, Sm-I, Sm-F) phases

Like other smectic phases discussed above, molecules are arranged in layers in hexatic phase, but the molecular centre of mass are arranged in a shape of hexagonal grid with long-range Bond-Orientational Order (BOO) of the hexagons. A short-range positional order of the molecules is also present in each smectic layer [53-56], whereas no positional correlation is present in between the adjacent layers [57]. Moreover, on the basis of molecular long axis direction, hexatic smectic phases are also classified into sub-phases- Sm-B, Sm-I, Sm-F etc. In Sm-B phase, the direction of molecular long axis is parallel to the smectic layer normal as in Fig. 1.5, which defines that Sm-B<sub>hex</sub> is

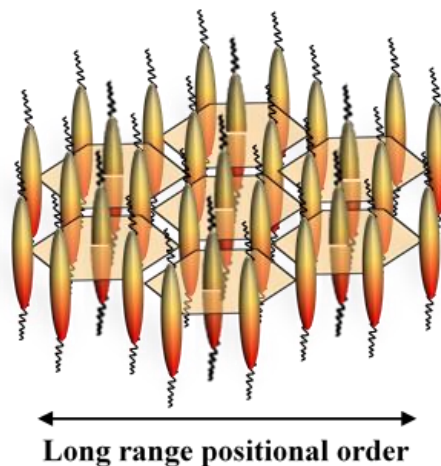


**Figure 1.5.** Structural representation of molecular ordering in each layer for hexatic smectic B phase.

uniaxial in nature as like Sm-A phase, while in case of Sm-*I* and Sm-*F* phases (Fig. 1.6) the molecular long axis is tilted with respect to layer normal. In case of Sm-*I* phase, tilt direction is perpendicular to the sides of hexagon, while the molecular tilt direction is towards the corner of hexagon for Sm-*F* phase [58].

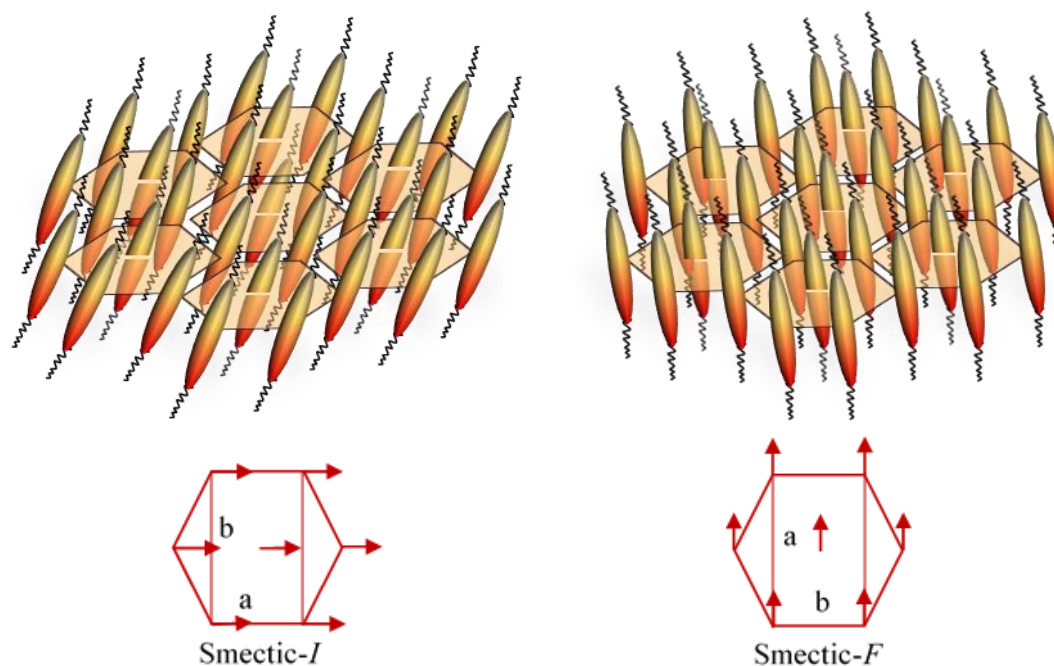


**Figure 1.6.** Structural representation of molecular ordering in each layer for smectic *I* and smectic *F* phases.

#### d. Soft crystal (*B*, *E*, *J*, *G*, *K*, *H*) phases

In case of soft crystal *B* phase, associated molecules are aligned perpendicular to the layers and having long-range translational order in the same way as like as hexatic Sm-*B* phase. However, in this case in addition to long-range bond orientational order, a long-range positional order is also present in three dimensions [57]. Alongside in crystal *E* phase, molecules are also arranged perpendicular to the smectic layers, but they have a tendency to arrange themselves in a herringbone pattern with orthorhombic symmetry in each layer [59] as illustrated in Fig. 1.7. This phase has no fluidity and supposed to form a most ordered crystal. Furthermore, there are some tilted soft crystal phases, such as crystal *J*, *G*, *K*, *H* etc. Soft crystal *J* and *G* are the three-dimensionally long-range ordered version of Sm-*I* and Sm-*F* phases

respectively [58,60,61]. The soft crystal  $H$  and  $K$  phases are tilted analogs of the crystal  $E$  phase. The molecules in the crystal  $H$  phase are tilted along the direction perpendicular to a side (towards a corner in case of crystal  $K$  phase) of the underlying hexagonal structure. In case of soft crystal  $B$ ,  $J$  and  $G$  phases, the molecular rotation around the long axis is totally independent and they feel free to rotate, while in the crystal  $E$ ,  $K$  and  $H$  phases the rotational hindrance is acting around the molecular long axes and such hindrance is so strong that only jumps between two favored positions are allowed [61,62]. All of the soft crystal phases exhibit mosaic type texture more or less similar to each other [45] under polarizing optical microscope.

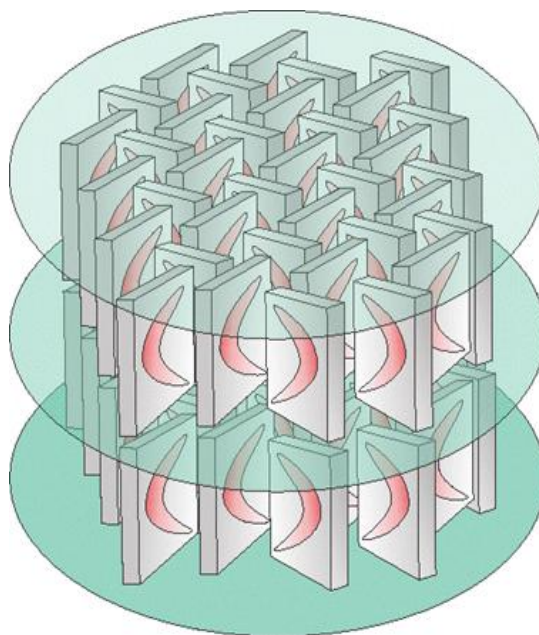


**Figure 1.7.** Molecular geometry of soft crystal  $E$  phase.

### 1.2.3.3. Chiral phases

#### a. Cholesteric or chiral nematic ( $N^*$ ) phase

Cholesteric or chiral nematic phase is more complex mesophase than usual nematic phase where the constituent molecules have chiral property, *i.e.*, the mirror symmetry is absent for the molecular structure. These chiral (optically active) molecules are similar to ordinary LC molecules, except one

or more chiral center which are generally introduced by substituting one or more carbon atoms asymmetrically as the linkage between aromatic core and associated terminal alkyl chain by four different ligands. The intermolecular interaction or force between the molecules precisely affected their effective orientations in such a way that they are separated by a very small angle with each other. Moreover, this orientation leads to the formation of a superstructure that can be visualized as a stack of two-dimensional very thin virtual layers without any positional ordering of the molecules within the layers. Additionally, the director axis of each layer rotated periodically about a perpendicular axis called helix axis [63]. Therefore, as a whole macroscopic helical superstructure is formed as like Fig. 1.8(a). In this molecular superstructure, the perpendicular distance for which the layer director rotates a full turn in helical axis is called pitch length ( $P$ ). During cooling or heating, several types of cholesteric textures are observed in planar aligned sample (see

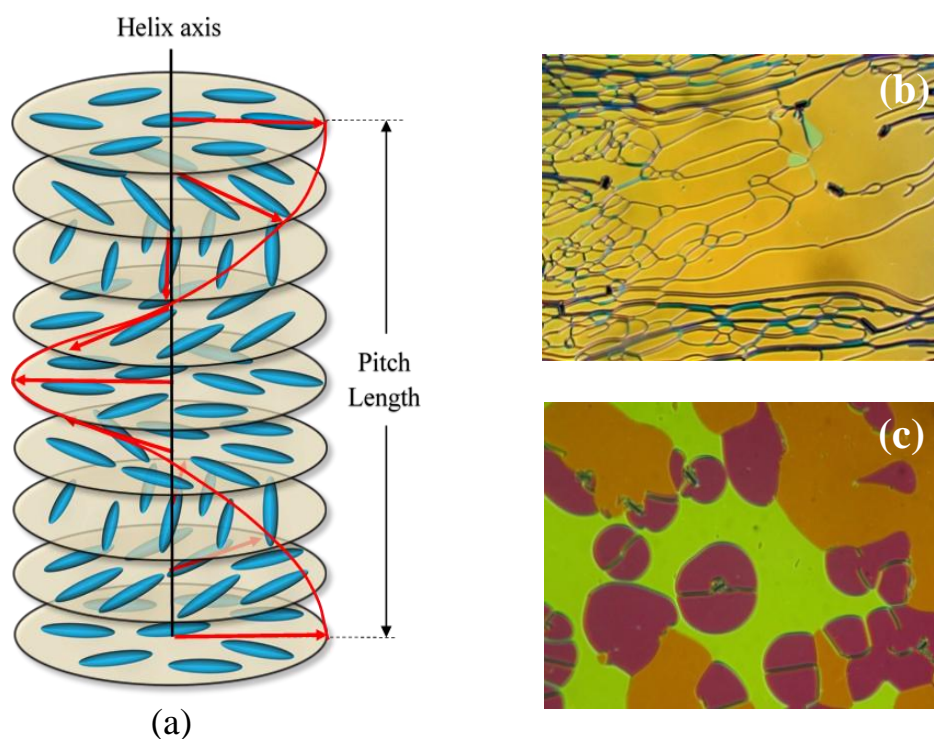


**Figure 1.8.** (a) Molecular representation of cholesteric or chiral nematic phase, (b-c) Optical textures appeared in cholesteric phase at two different temperatures.

Fig. 1.8(b-c)) as because the pitch length of helical rotation is temperature dependent. Hence, the cholesteric phase is nearly identical to usual nematic phase but having finite pitch length. Moreover, the advantages of this helical superstructure are - high optical rotatory power, reflection of lights (Bragg reflection) for wavelength equal to pitch length of the sample [64,65] etc. which are desirable for some electro-optic applications.

### **b. Chiral Smectic A (Sm-A\*) phase**

Chiral smectic A (Sm-A\*) phase is the chiral analogue of Sm-A phase, where the molecules are aligned orthogonally in layers and at the same time they also rotate in a liquid-like fashion around their long axis [66-68]. However, the symmetry of this phase is further reduced than that of the Sm-A phase. Due to the absence of symmetrical correlation among the molecules in the smectic layer, the net transverse polarization vanishes, *i.e.*, the Sm-A\* phase exhibits paraelectric behavior. Hence, in spite of being made up by chiral molecules, the Sm-A\* is apolar in nature. Furthermore, by applying external electric field, molecular tilt angle and hence an effective polarization can be induced with respect to smectic layer normal, which is an interesting feature in technological applications.

### **c. Chiral Smectic-C (Sm-C\*) phase**

Similar to the Sm-A\* phase, Sm-C\* phase is chiral analogue of the Sm-C phase, without any mirror symmetry. As the molecules are tilted in-layer, a precession of molecular tilt direction around the layer normal is present in a macroscopic helical form [69,70]. However, due to existence of molecular tilt in smectic layers, only the two-fold rotational symmetry along  $C_2$  axis is active in this phase and hence a non-zero polarization or ferroelectricity can be visualized in each layer directed perpendicular to the tilt plane of the Sm-C\* phase [71]. However, as the azimuthal tilt direction is rotating by small amount from layer to layer around the helix axis, the overall polarization cancels out

for a complete rotational cycle of tilt director (See Fig. 1.9(a)). Hence, this phase can be named as “helielectric”, rather than “ferroelectric” [72]. Although, a non-zero finite macroscopic polarization can be induced in a specific geometries if the helix of Sm-C\* phase unwinds by applying an external electric field or via elastic interactions with surface [73-76].

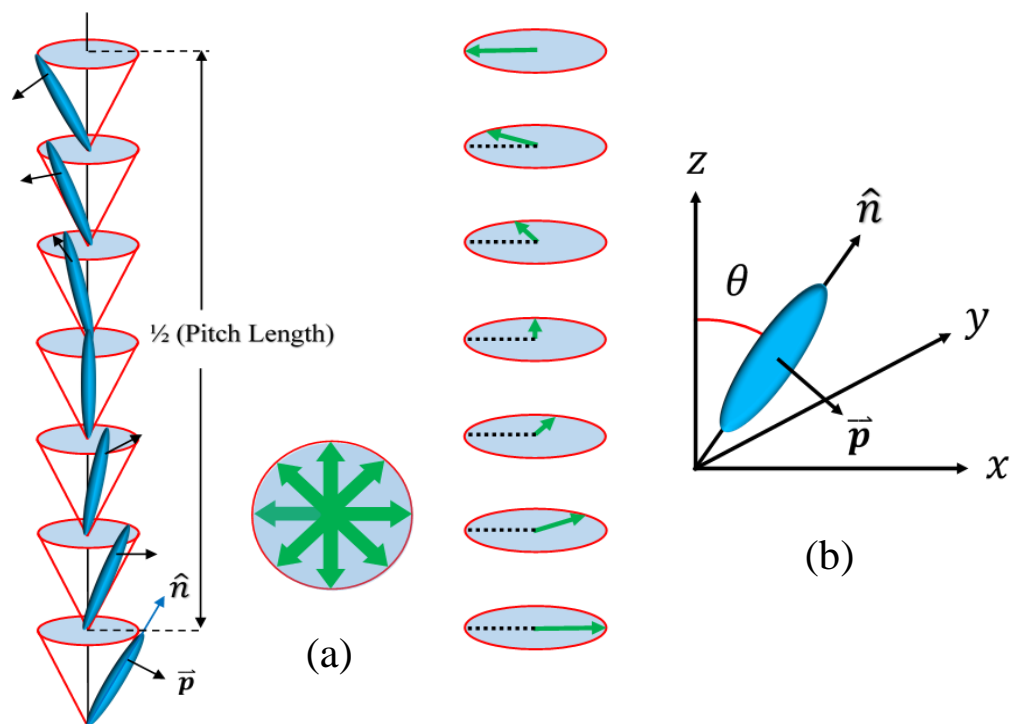


**Figure 1.9.** (a) Helical superstructure of the chiral smectic  $C$  (Sm- $C^*$ ) phase with the helix axis parallel to the smectic layer normal  $\hat{k}$ , (b) Orientation of a single molecule in each layer. The polarization vector  $\vec{P}_s$  is always perpendicular to the director  $\hat{n}$  and the tilt plane.

In contrast to this, an anti-ferroelectric chiral smectic  $C$  phase (Sm- $C_A^*$ ) has also been discovered, where the molecular orientations are same as like as Sm- $C^*$  phase but the direction of tilt alternates in adjacent layers and hence, the direction of polarization also alternates from one layer to the next, canceling out the total polarization [77-80]. The polarization can be aligned uniformly between the layers on applying a strong external field. However, the tri-state switching characteristic of anti-ferroelectric Sm- $C^*$  phase is potentially effective to achieve easy grayscale switching in display devices. Also the wide

viewing angle with a relatively large contrast ratio, inherent DC compensation and fast response time make anti-ferroelectric liquid crystals superior to ferroelectric liquid crystals. Nowadays high tilted or orthoconic anti-ferroelectric liquid crystals are used to remove its initial linear response and high-quality alignment problems [77-80].

### **1.2.3.4. Liquid crystalline frustrated phases**

Chirality is the self-assemble property of chiral molecules. However, in this case, the molecular symmetry significantly reduced than achiral molecules. Again due to existence of temperature variant tilt angle and the pitch length, it drastically modifies the mesomorphic behavior of the sample. Sometimes it is not so compatible for the chiral molecules to hold both layer structure and twisted helical orientation simultaneously due to molecular constraints. Such type of disturbance leads to the formation of some defected and quite complex type of frustrated phases [81,82]. Blue phase (BP) and twist grain boundary (TGB) phases are the examples of such superstructure frustrated phases, which are briefly described in the following sections.

#### **a. Blue phases**

A thermodynamically distinct mesophase, called blue phase (BP) generally appeared in between isotropic phase and the cholesteric ( $N^*$ ) phase for a narrow temperature scale in some highly chiral LC compounds. This type of frustrated phases can be regarded as self-assembled three-dimensional counterparts of the cholesteric phase, exhibiting cubic lattices (lattice period of several hundred nanometer) without any long-range positional order [81]. The blue phase is a cubic phase with regular lattice defect, *i.e.*, it consist of two double twist cylinders (Fig. 1.10(a)), arranged in two mutually perpendicular directions to form a continuous director field and a third double twist cylinder is placed mutually perpendicular with them to create a defect. Blue phases are the optically isotropic LC material which exhibit optical activity with a small

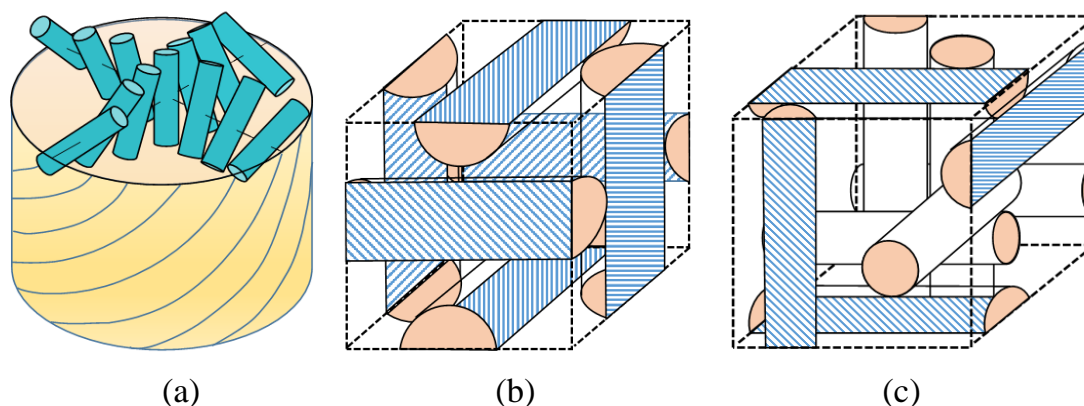


**Figure 1.10.** (a) Molecular representation in a double twist cylinder. Relative orientation of the double twist cylinders in case of the (b) BPII\* and (c) BPI\* phase.

value of birefringence. However, the naming of these phases as blue is due to their Bragg reflections in the blue wavelengths. Furthermore, blue phases have three distinct sub-phases – BPIII\*, BPII\* and BPI\* that emerges in order of decreasing temperature from isotropic phase [83]. BPIII\* (observed at highest temperature and appears foggy) is amorphous in nature and it has a local cubic lattice structure defect in the director field. Besides in BPII\* phase has a unit cell (simple cubic) of lattice defects and in BPI\* phase has a three-dimensional periodic structure in the director field with body-centered cubic symmetry which are shown in Figure 1.10(b-c). Due to presence of several advantageous property such as very fast switching times, non-zero elastic shear modulus etc., blue phases are potentially attractive for LCD devices and photonic applications.

## b. Twist grain boundary (TGB) phases

Another distinct and special type of frustrated mesophase, named Twist Grain Boundary (TGB) phase appears in between chiral nematic ( $N^*$ ) and higher ordered smectic phases [84,85] at relatively lower temperature than the blue phase. In general the molecules in cholesteric phase possess a helical structure around the helix axis and on the other side in smectic phases, the

molecules have a tendency to align themselves in layer structure. Therefore, a direct transition from cholesteric phase to smectic phase is not always favorable to the orientation of molecules. Hence such incompatibility to hold both rigid structural features at a same time is responsible for this type of frustrated phase. In those defected superstructures, some locally ordered defected or smectic slabs are formed which are again separated by the grain boundaries which in turn consists of a lattice with screw dislocations [84,85]. However, the successive layers are relatively twisted by a constant small angle to give a helical structure with the helix axis orthogonal to the layer normal direction. This phase is equivalent to the Abrikosov flux lattice phase of a type-II superconductor in an external magnetic field [84,86,87]. Moreover, the TGB phases can be classified further into distinct sub-phases- TGBA, TGBC and

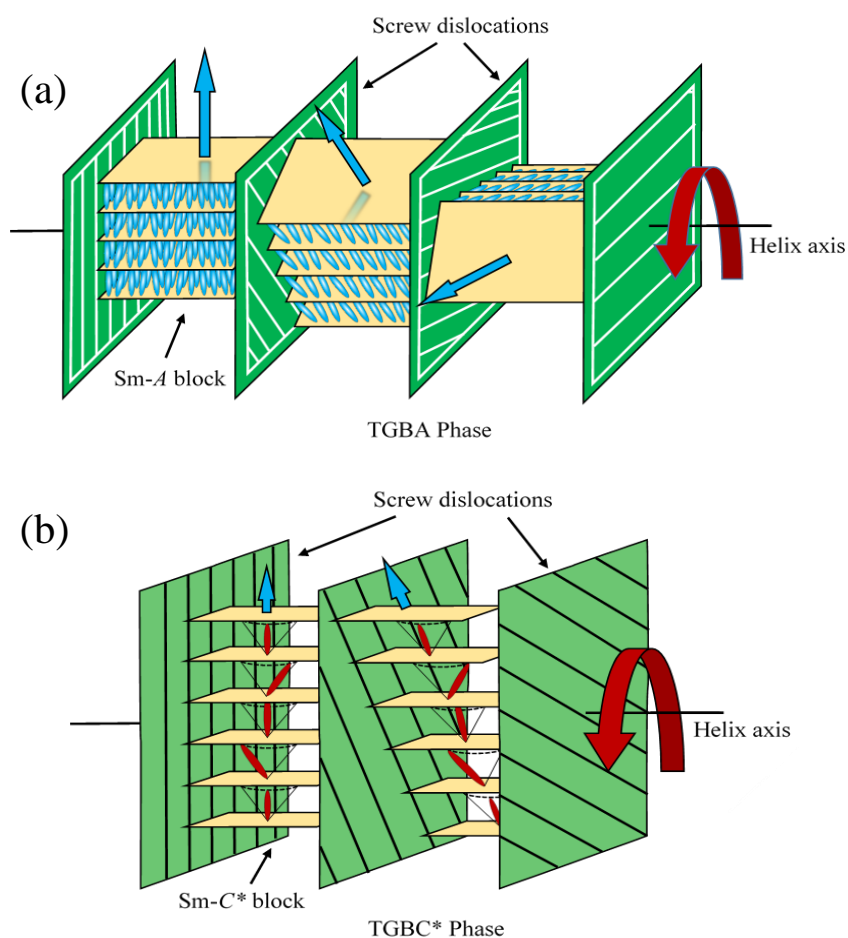


**Figure 1.11.** A structural representation of the molecular superstructure with screw dislocations for (a) TGBA and (b) TGBC\* phases.

TGBC\* phases, based on the layer structure within the slabs of TGB phase. If the molecules are aligned orthogonally with the layer plane, as like as Sm-A phase, modified phase is called TGBA phase (See Fig. 1.11(a)), whereas in case of TGBC phase, molecules are tilted within building blocks, as like as Sm-C phase [86-88]. Furthermore, if the smectic blocks are formed as helical Sm-C\* type, the obtained phase is designated as TGBC\* phase as illustrated in Fig. 1.11(b). TGBA phases are generally appears before the TGBC phase as being cooled from isotropic phase and also the pitch length is greater in TGBC phase. The planar oriented optical texture of TGBA phase exhibits a Grandjean type appearance with a temperature dependent pitch length, whereas the homeotropically aligned sample represents a fingerprint texture (equidistant line pattern) and often filament type textures, which is of the order of magnitude of the pitch length [45,89]. Besides in TGBC\* phase, square grid type optical textures were observed which are described further in Chapter 7.

#### **1.2.4. Bent-core liquid crystals**

Apart from calamitic liquid crystals with rod-like molecular shape, various fascinating mesogenic properties have also been revealed in the compounds having other molecular geometries. Among them, the banana-shaped or bent-core molecules unveil a new branch in the field of thermotropic liquid crystal as they exhibit several striking properties in different mesophases due to the modification in the core unit. Earlier the bent-core molecules were thought of as inadequate molecules to form liquid crystal mesophases because they excluded a large volume under rotation about their long molecular axis, leading to a destabilization of the liquid crystalline phase [90]. In 1929, D. Vorländer and his group synthesized several bent-core LC compounds [91,92] and reported that they are not as stable as the calamitic molecules in temperature range. Furthermore, in 1991, Matsunaga *et al.* synthesized few series of the bent-core liquid crystals [93-96] and reported that the nonlinear molecular structure of the bent-core molecules is not necessarily incompatible

---

---

---

for the formation of LC mesophases. Again in 1996, Niori *et al.* first discovered the polar switching behavior in achiral bent-core compounds in one of the smectic phases [97]. More surprisingly, Link *et al.* [98] discovered the chirality in layers in bent-core mesogens composed of achiral molecules [99]. Sekine *et al.* also discovered the spontaneous chiral character in non-tilted mesophase [100,101]. Hence, the occurrence of unpredictable exciting mesomorphic behavior of different unique mesophases in the bent-core compounds brought them at the focus of scientific attention, unveiling a fascinating new domain in the branch of thermotropic liquid crystals.

The structure of bent-core molecules can be described in general as a central bent-unit of aromatic rings comprising one or more alkyl or alkoxy terminal chains attached at both ends of the molecules. Bent-core molecules are also symmetric or asymmetric depending on the position of bending and terminal polar or non-polar chain length determining the basic mesogenic behavior of these compounds. Fig. 1.12(a-b) illustrates symmetrical and asymmetrical bent-core molecules. Due to the existence of kink shape in the molecular structure, each molecule has two distinct axis around which it can rotate, *i.e.*, the bent-core molecules have two different directors – (i) along the molecular long axis, as like as calamitic molecules ( $\hat{n}$ ), and (ii) along the molecular short axis or the bow axis ( $\hat{m}$ ). However, the bent-core molecules self-organize themselves in a number of exclusive ways due to their non-linear molecular conformation as well as the steric interaction between the molecular associations. They experience a periodic potential while translating through the neighboring molecules, causing a translational symmetry breaking of the molecules along the long axis. At the same time there also exists a rotational hindrance about the director  $\hat{n}$  to reduce the excluded volume effect. Consequently, the molecules organize themselves in a close packed smectic like layer structure with a common direction of molecular bow axis ( $\hat{m}$ ). Moreover, as the molecules comprised of two segments at a certain angle to

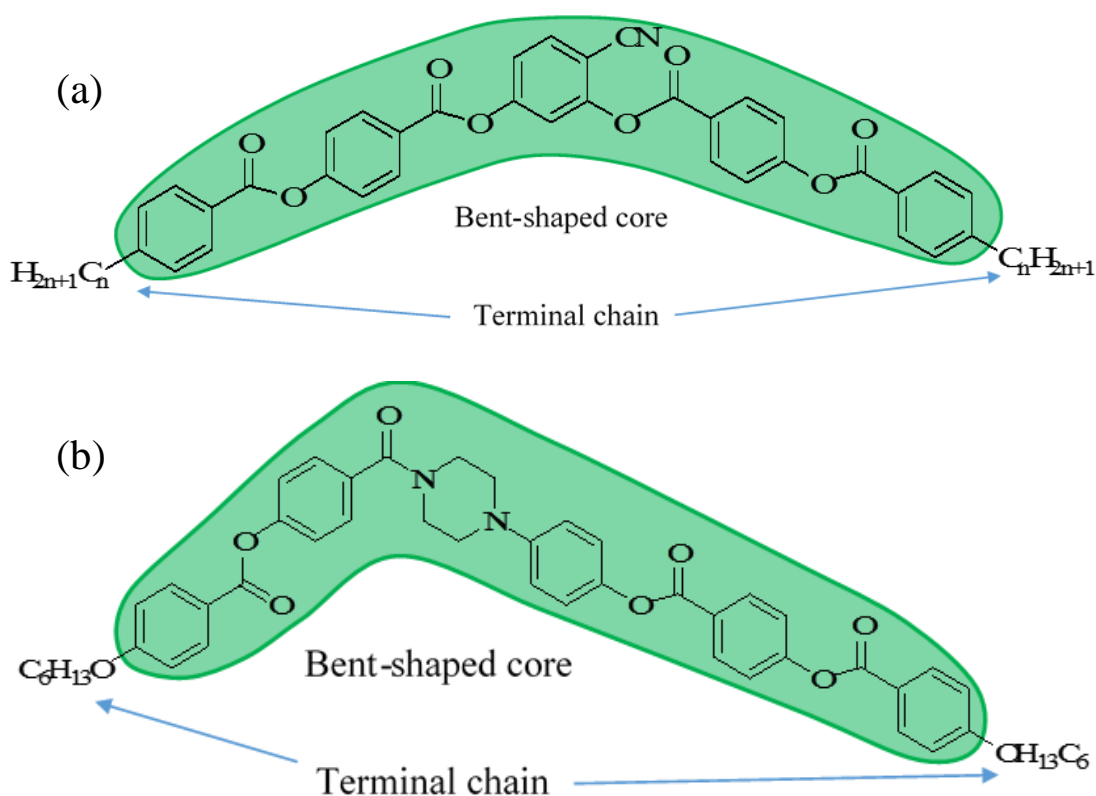


**Figure 1.12.** Molecular structures of (a) a symmetrical and (b) an asymmetrical bent-core compound.

each other and due to existence of polar linking groups, it produces a permanent dipole moment along the molecular transverse axis. The mutual correlations of those molecular dipoles packed in smectic-like layer structure reveals a small polar domain within the layer which can be switched by applying the external field. Hence, a macroscopic ferroelectric phase builds up within the system when the polarizations of adjacent layers are parallel [97] to each other and the anti-ferroelectric phase developed when they are aligned in anti-parallel way [102]. Furthermore, a combination of molecular tilt and polar vector produces the layer chirality effect, although the molecules are not optically active [90,98,99,103-105]. Thus the bent-core LC compounds represent a number of unusual modified smectic phases with ferroelectric, anti-ferroelectric nature as well as chirality in some mesophases.

Depending upon the mutual orientation of the molecules and associated mesophase behavior, the bent-core or banana-shaped compounds

can exhibit a group of columnar and smectic phases, named as  $B$  phases – the series  $B_1$  to  $B_8$  [90,99,106]. These types of phases have different mesomorphic characteristics than phases formed by usual calamitic mesogens. Moreover, the conventional mesophases such as Sm-A, Sm-C phases as well as nematic phases also been observed in some bent-core compounds, provided the bend angle is not too acute and the molecular length is sufficient to overcome the destructive nature of the bent-shape structure [32-34,38,107-116]. Conversely, some exotic mesophases with diverse molecular ordering like as dark conglomerate phase [117], polar Sm-A [118,119] and polar Sm-C phases with synclinic or anticlinic tilt ordering (Sm- $C_s$  or Sm- $C_a$ ) along with ferroelectric or anti-ferroelectric polar ordering (Sm- $CP_F$  or Sm- $CP_A$ ) and also biaxial nematic [34,97,98,120,121] phases has also been observed in several bent-core compounds. In the following section different mesophases formed by banana-shaped or bent-core compounds has been discussed.

### 1.2.4.1. Smectic phases of bent-core liquid crystals

#### a. $B_1$ phase

The  $B_1$  phase is assigned to a columnar mesophase and it consist of two-dimensional lattice structure with rectangular form [122] which are generally observed in the bent-core compounds having short terminal alkyl chains. According to Watanabe *et al.* the  $B_1$  phase is made up of columns formed by small fragments in layer structure [122]. However, the associated molecules in such fragments are oriented in parallel to each other to give rise a particular polarization direction in each layer, while the direction of polarization in adjacent layers are anti-parallel to each other [122] as shown in Fig. 1.13. However, the direction of polarization is orthogonal to the columnar axis. Hence, due to anti-parallel alignment of polarization vector in adjacent layers, the effective polarization in this phase vanishes. Again due to the mutual interactions between columnar boundaries, produces a steric hindrance for the rotational motion of the molecules which further restricts the field-induced

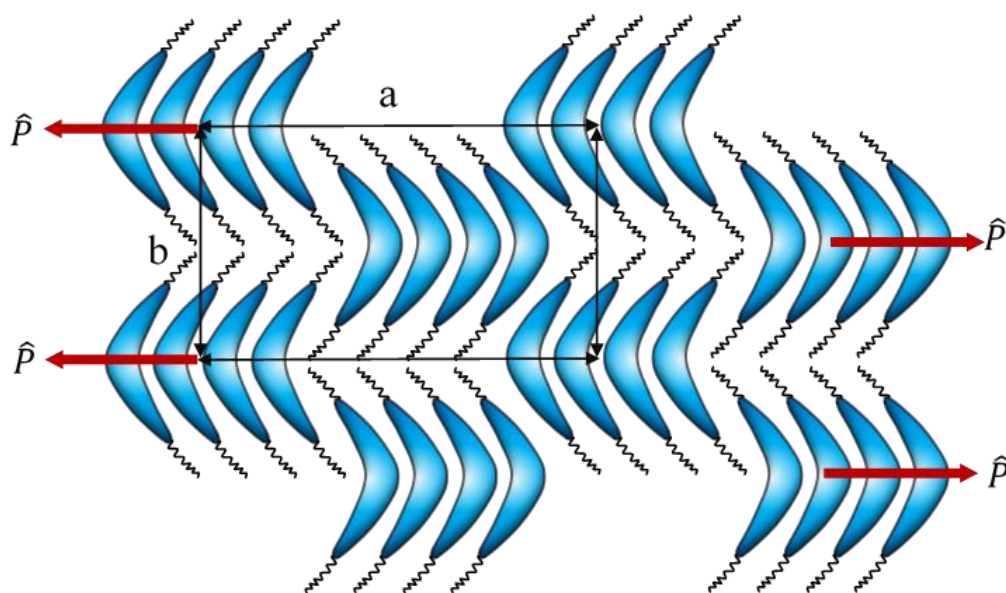


**Figure 1.13.** Schematic illustration of molecular geometry in  $B_1$  mesophase.  $a$  and  $b$  give the measure of periodicities in the two perpendicular directions.

polarization. The wide-angle scattering of X-ray diffraction pattern demonstrates this  $B_1$  phase as liquid-like in plane ordered phase, while the small angle pattern indicates an intercalation in the structure, *i.e.*, it reveals a two-dimensional frustrated layer structure [90,99]. In contrast to response of external field, the  $B_1$  phase can be further classified into two distinct classes –  $B_{1\text{rev}}$  and  $B_{1\text{revtilt}}$ . In  $B_{1\text{rev}}$  phase, the polarization direction is parallel to columnar axis whereas  $B_{1\text{revtilt}}$  phase is the tilted analogous of the  $B_{1\text{rev}}$  phase and both are switchable in response to applied field [123-125].

## b. $B_2$ phase

The  $B_2$  phase is the most common and widely popular mesophase among all the banana phases which are generally observed in some bent-core compounds with long terminal alkyl chain. In 1997, Link *et al.* represented that the molecular long axis in this mesophase is tilted with respect to layer normal in each layer which leads to a  $C_{2v}$  structural symmetry and the effective direction of polarization is orthogonal to the tilt direction [98]. The closed packed structure of parallel aligned molecules in each layer produces the layer polarization and it alternates the direction from one layer to adjacent another.

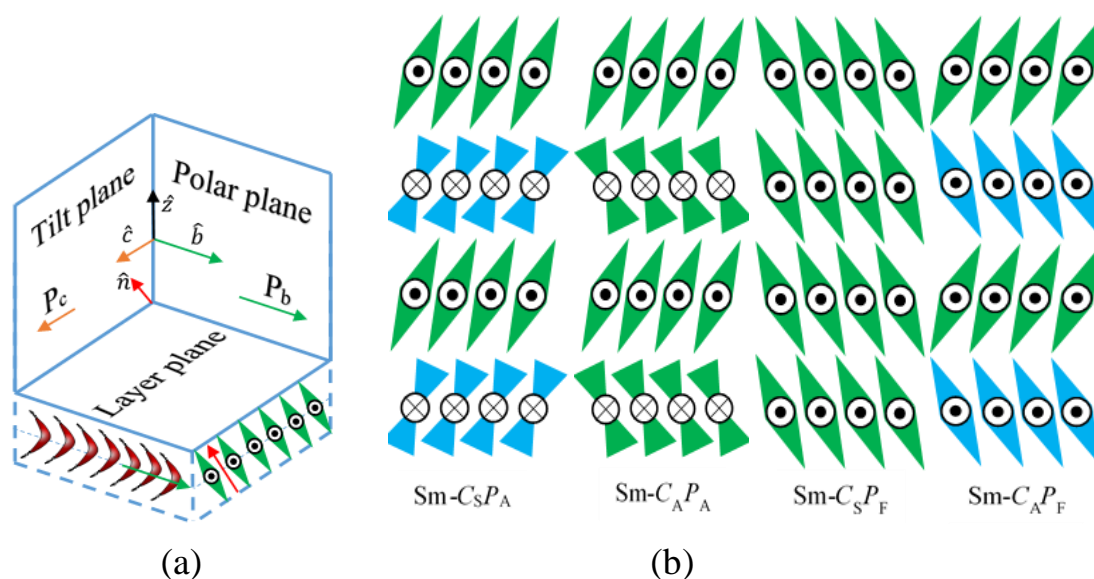


**Figure 1.14.** Representations of molecular geometry in (a) three mutually orthogonal planes and (b) four fundamental variants of Sm-CP phase in the  $B_2$  phase.

Therefore, the complete mesophase structure can be considered to be consisting of three distinct mutually orthogonal planes, a tilt plane, a polar plane and a layer plane in each layer, as shown in Fig. 1.14(a). The mirror image of such mutual orthogonal planes does not superimpose with the original one. Thus the layer chirality produces in this mesophase, although the individual banana molecules are achiral in nature. However, the associated mesophase can be designated as Sm-CP phase ( $P$  symbolizes as polar order). Furthermore depending upon the molecular tilt direction and the effective polarization direction in adjacent layers, this phase is also further classified into–  $Sm-C_S P_A$ ,  $Sm-C_A P_A$ ,  $Sm-C_S P_F$ , and  $Sm-C_A P_F$  phases [34-36,98] as illustrated in Fig. 1.14(b), where  $Sm-C_S$  and  $Sm-C_A$  represent the layer structure as in Sm-C type with synclinal and anticlinal arrangement of tilt direction in adjacent layers respectively. Conversely,  $P_F$  and  $P_A$  correspond to ferroelectric and anti-ferroelectric type of polarization in the adjacent layers respectively. Furthermore, on application of external electric field, a switching process by a collective rotation of the molecules around a cone from antiferroelectric to ferroelectric state is usually observed in such Sm-CP phases. At the time of

switching, the polar direction as well as the tilt direction gets reverses, but they preserve the layer chirality. Thus the anti-ferroelectric ground state of Sm- $CP$  or  $B_2$  phases of banana-shaped molecules switches to ferroelectric state by applying external electric field.

In general different types of optical textures are observed in this phase, among them the schlieren and the focal-conic textures and quite often fingerprint texture are also observed. Sometimes chiral domains of opposite handedness are also recognized during slow cooling from the isotropic phase.

### **c. $B_3$ phase**

During cooling from isotropic phase, another type of banana phase named as  $B_3$  phase generally appears in between  $B_2$  and  $B_4$  phases, where  $B_2$  phase is the higher temperature mesophase [99]. However, in a fast cooling process from  $B_2$  to  $B_3$  phase, the appearance of the optical textures is found to identical as that of  $B_2$  phase, while a broken fan-shaped texture appears on slow cooling. An inspection of X-ray diffraction pattern for this phase in non-oriented sample representing several diffraction peaks at wide angle as well as in small angle region which indicates a crystal-like ordered structure [101,126,127], whereas the 2-D X-ray diffraction pattern in planar oriented sample reveals that the layer thickness is smaller than the molecular length of all *trans*-conformation. Therefore, it has been predicted that the molecules are tilted within the layer [98,101,126] to accomplish such condition. Further study from the dielectric [128] and terahertz spectroscopy [129] in  $B_3$  phase also suggest the same molecular dynamics as in  $B_2$  phase, which indicates a higher-ordered smectic-like nature of this mesophase.

### **d. $B_4$ phase**

During cooling from the higher temperature  $B_3$  or  $B_2$  phase, a dark bluish type optical texture of another banana phase named as  $B_4$  phase appears in crossed polarizing microscope and hence this mesophase is designated as

smectic blue phase [101,126,130]. However, by rotating one of the polarizer in any direction, optical texture exhibits some tiny domains with different brightness and again they interchanges their brightness by rotating the polarizer further in clockwise or anticlockwise directions [131]. Such an appearance is identical to chiral phases which clearly suggesting the  $B_4$  phase as a chiral mesophase. Moreover, the XRD patterns in wide angle and small angle region in  $B_4$  phase implying the layer spacing comparable to length of the molecule, which is an indication of non-tilted smectic ordering of the molecules and packed as a crystalline phase. However, the low-frequency dielectric study reveals this mesophase as non-crystalline in nature. Although the FFTEM study demonstrates that this phase is fabricated by chiral nano-bundles associated with twisted layers of molecules [117], it does not possess any switchable property. Furthermore, in the absence of any external electric field, the simple harmonic generation (SHG) signal was observed in this mesophase, which indicates a spontaneous non-centrosymmetric ordering [132,133].

### e. $B_5$ phase

The  $B_5$  phase is rare among all the banana phases and it appears in few compounds just below the  $B_2$  phase with a small change in transition enthalpy [98,99,134]. Both the  $B_2$  and  $B_5$  phases appeared to be identical in textural appearance and also in the electro-optical response. However, the XRD pattern

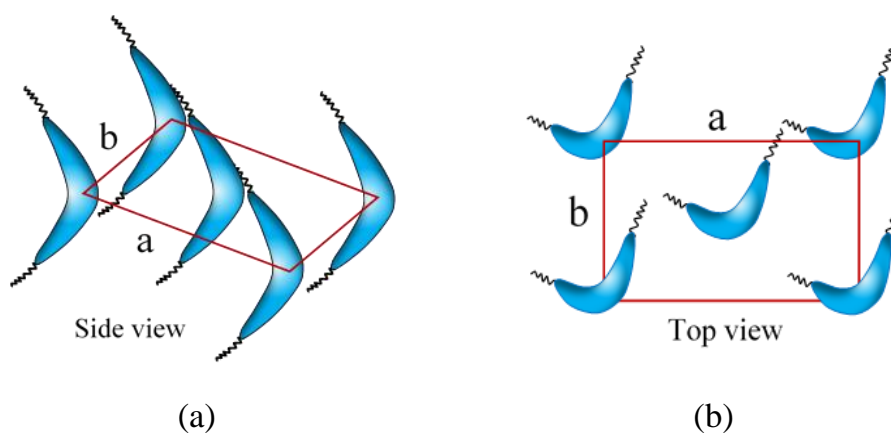


**Figure 1.15.** Schematic representation of the in-plane molecular packing in the  $B_5$  phase. Vectors **a** and **b** suggests the presence of in-plane order.

---

---

is quite different than  $B_2$  phases because additional reflection has been observed in wide angle region and perpendicular to the small-angle layer-reflection. This is due to the presence of in-plane positional ordering of the molecules within the smectic layers (Fig. 1.15), which again has been described by considering the existence of a 2D rectangular lattice within the layers [99,105,134].

### f. $B_6$ phase

The  $B_6$  phase is generally observed in some bent-core compounds having short alkyl chain. Although a typical fan-shaped optical texture similar to that of Sm-A phase formed by calamitic molecules is visible in the  $B_6$  phase for a homogenous aligned sample [111], it is difficult to obtain a homeotropically aligned texture. From the lamellar reflection of XRD pattern in small angle region reveals that a periodicity of the molecules is present in this phase which is less than half of the molecular length, *i.e.*, an intercalated smectic structure of the molecules [99,135] observed in this phase. However, the wide-angle reflection represents four broad diffuse peaks, specifying a liquid-like in-plane ordering of the molecules. The inclination between the neighboring diffuse peaks corresponds to a molecular tilt organization in this

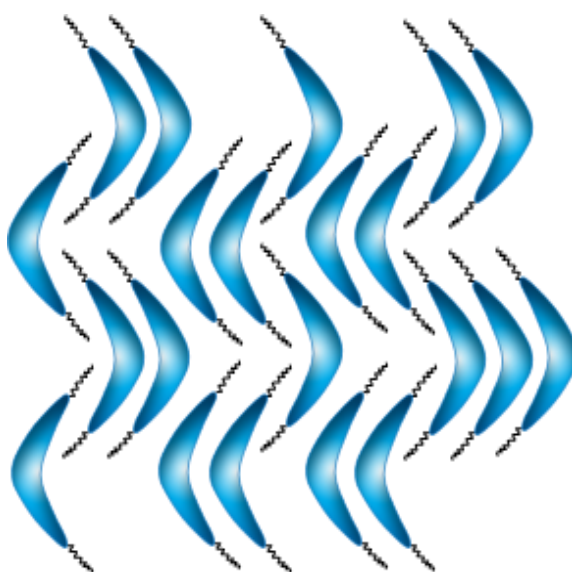


**Figure 1.16.** Schematic illustration of molecular ordering in the  $B_6$  phase.

---

---

phase [99,135] and the tilt angle varies from  $20^\circ$  to  $30^\circ$  in each layer [99]. Furthermore, by increasing the chain length, the  $B_6$  phase transform to  $B_1$  and  $B_2$  phases as observed in some homologous compounds [111,135,136]. The intercalated structure of  $B_6$  phase is shown in Fig. 1.16.

### **g. $B_7$ phase**

$B_7$  phase is the most unique mesophase among all the banana phases due to revelation of a number of distinct textural appearances much disparity than other phases. On cooling from isotropic phase the optical textures appear a number of unique pattern like – helical smectic filament, twisted helical filaments with single, double or triple coils, myelin-like, accordion-like, checkerboard-like, lancet-like or thread-like germs, banana-leaf-like, and circular domain textures etc. [99,106,137-141]. However, the spirals of smectic filaments are the most interesting texture among them and it has been assumed that such helical textures are the indication of chirality [137] for  $B_7$  phase. However, as a result of applying electric field on  $B_7$  phase, a ferroelectric-like switching is observed, which again transform to tristable switching state on lowering the temperature [142]. Investigation of X-ray diffraction pattern for  $B_7$  phase illustrates several sharp reflections in the small angle region as well as liquid-like diffuse broad scattering at wide-angle region [139,142,143]. Therefore, this phase supposed to be considered as two dimensional ordered modulated layer structures caused by the polarization splay modulation in the ferroelectric state [144] and this 2D structure is quite different from those found in  $B_1$  phases.

### **h. $B_8$ phase**

In 2001, Bedel *et al.* observed another banana phase named as  $B_8$  phase. He reported that a few bent-core compounds having  $n$ -alkyl carboxylate groups as a terminal chain exhibit a fan-shaped texture, in which the extinction direction is parallel to the layer normal. However, the X-ray diffraction study

proclaimed a bi-layer structure of the molecules in  $B_8$  phase [106]. Additionally, by applying external electric field in this phase, it possesses an anti-ferroelectric switching. Since limited information has been reported on  $B_8$  phase so far, further investigations are required to understand the actual molecular structure and associated mesophase behavior.

#### **1.2.4.2. Nematic phases of bent-core liquid crystals**

Due to the presence of bend angle in the molecular structure of bent-core molecules (absence of rotational symmetry around long axis), they try to form a layer structure to fill the available space in order to minimize the excluded volume in liquid crystal material. Therefore, it is easy for the molecules to form tilted or non-tilted layered structure of smectic mesophases, while such molecular structure is quite incompatible to form the nematic phase. Therefore, the nematic mesophase is quite rare than smectics for such bent-core molecules as they distorted the translational symmetry which resists to form  $N$  phase. Hence, to overcome this problem for the appearance of nematic phase, certain specific structural modification has been introduced to bent-core molecules. Subsequently, a number of distinct bent-core molecules have been synthesized to manifest the nematic phase by some particular techniques, such as by the extending aromatic core with shorter terminal chains as in different bent oligophenyleneethynylenes [145,146], *m*-terphenyls [111], and naphthalene derivatives [112-115]. Another technique is to reduce the molecular bend-angle as obtained in 5-membered heterocycles, like oxadiazoles [32-34,38,107] or some di-mesogens composed of rod-like and bent-units [147-149]. Due to the presence of such kink in the molecular structure and hence an inter-molecular lateral correlation, the bent-core molecules has an affinity to form certain small clusters within nematic phase even also in the isotropic phase [43]. Such domains are called “cybotactic cluster” and the molecules are arranged in smectic like layer within such short-range domains [37-44] as indicated in Fig. 1.17. Moreover, the cybotactic

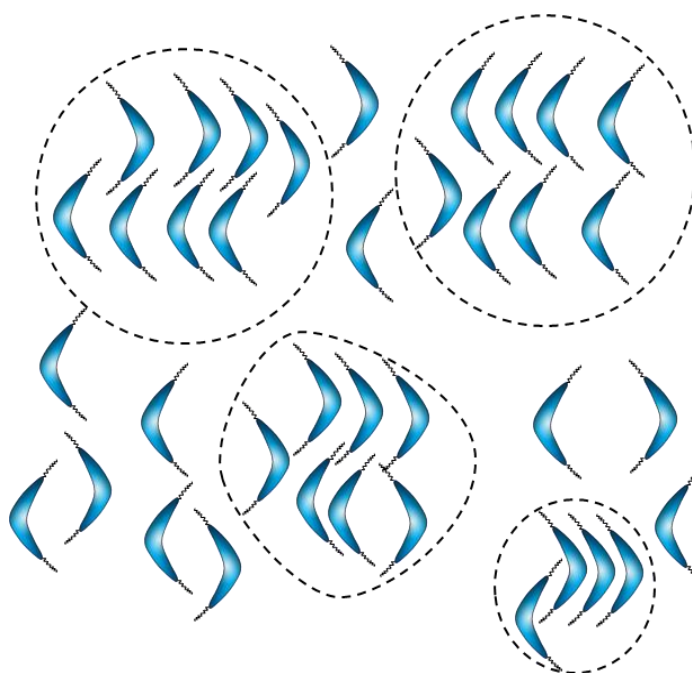


**Figure 1.17.** Sketch of the molecular arrangement in bent-core nematic liquid crystals comprising smectic-like cybotactic clusters.

clusters shows a microscopic polar order, effect of which makes the bent-core nematic phase an exclusive phase quite different from usual calamitic nematics. As the bent-core molecules in general are biaxial in nature, cybotactic clusters also exhibit biaxiality, although on the average the entire nematic phase is uniaxial in nature. Therefore, the existence of such unique features of cybotactic clusters in nematic phase, the bent-core nematic reveals a number of intriguing mesomorphic properties such as great flexo-electricity [150,151], extraordinary electro-convection patterns [152-154], a considerable Kerr effect [155], unique rheological properties [156,157] etc., which are absent in usual nematic phases formed by rod-like molecules. Moreover, in recent times, attention has grown up to understand some unusual characteristics like field induced biaxiality in nematic phase [158], twist-bend nematic phase [159,160], and ferroelectric switching in nematic phase [161] for bent-core liquid crystals to employ them in technological applications.

### 1.2.5. Hockey stick-shaped liquid crystals

The hockey stick-shaped LC compound is the unique variant of bent-core liquid crystal, in which the molecules are asymmetric in contrast to the position of structural bend-angle in aromatic core. Fig. 1.18, represents a hockey stick-shaped compound in which the bend-angle has been introduced by attaching an alkyl or alkyloxy chain at the *meta*-position of a terminal phenyl ring [162-169]. These types of mesogens are intermediate in shape between usual calamitic and the bent-core liquid crystals, and also exhibit some

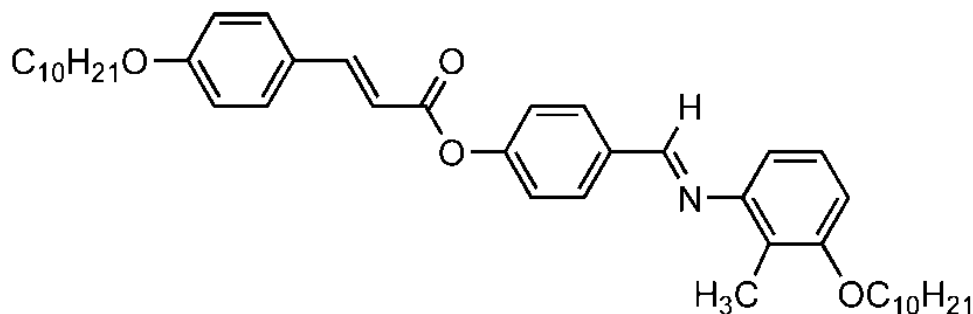


**Figure 1.18.** Structural representation of a hockey stick-shaped compound H-22.5 [details in Chapter 5].

unusual mesophases with greater temperature stability. Moreover, based on the terminal chain length, orientation of the linking groups and number of aromatic rings present in such asymmetrical bent-shaped molecules, they exhibit a number of exotic mesophases displaying both calamitic and bent-core like properties [170]. Recent discovery on some hockey stick-shaped liquid crystal reveals two polymorphic tilted smectic phases – the synclincic smectic *C* ( $Sm-C_s$ ) as well as the anticlinic smectic *C* ( $Sm-C_a$ ) phases [163,171]. Furthermore, some other characteristics such as the dark conglomerate phases [172], the co-occurrence of two different molecular tilts at the *N*–*Sm-C* transition [173], a transition having layer thinning [174] etc. also been discovered in hockey stick-shaped compound which bring them as a potential candidate for designing the future noble materials.

### 1.3. Liquid crystal mixtures

Although different liquid crystal compounds have its inherent unique mesophase characteristics, all the desired properties for practical applications cannot be fulfilled by a single mesogenic compound. Hence, by choosing the appropriate pure compounds, mixtures are prepared in certain specific concentrations to acquire the desired material for application purpose. As a result of mixing the individual LC components in particular proportion, the effective clearing temperature can be lowered as well as the thermal mesophase stability can be achieved higher than the pure compounds. At the same time different physical properties like dielectric permittivity and anisotropy, optical birefringence, elastic constant, rotational viscosity, threshold voltage etc. can be tuned so far [175-179]. Moreover, a proper understanding can be acquired about the mutual interactions of the constituent molecules having similar or dissimilar conformers such as calamitic-calamitic, calamitic-discotic, calamitic and bent-core along with some nano-doped systems with LC compounds [180-183]. The transitional phenomena at several mesophase transitions and associated critical behavior can be investigated more rigorously by the mixtures of LC compounds [184-188]. However, always it is not possible to interpolate the physical properties of the mesophases in mixtures by an assumption for that of the pure compounds. In certain cases several new mesophases developed in mixtures called “induced mesophase”, even they are not present in pure compounds [189,190]. Furthermore, some less ordered mesophases also reappears in the mesomorphic range at lower temperature region, called the “re-entrant mesophase” [191-194]. In order to improve the mesophase behavior and to study associated physical properties, in some cases the multi-component mixtures also been developed rather than binary mixtures [195-196]. Such mixtures are of great interest not only for application purpose but they also extract some important characteristics regarding phase transition behavior and molecular interaction in such soft condensed matter systems.

## 1.4. Phase transitions

Transition between different LC mesophases occurs due to the external influence of temperature, pressure, concentration, electric or magnetic field etc. Actually the phase transition is a transformation of a thermodynamic function from one mesophase to another. Typically this thermodynamic function is the free energy and this free energy does not change smoothly at the phase transition point, *i.e.*, a non-analytic property (critical phenomena) of the system which is present at that point (critical point). In order to understand the actual phenomena at this phase transition point, it is necessary to consider a physical quantity that distinguishes both the phases before and after the transition. Such an observable physical quantity is the order parameter which represents how the microscopic constituents organize the macroscopic mesophases that are ordered. Choosing of such order parameter varies from system to system like as the magnetization ( $M$ ) for ferromagnet to para-magnetic transition, density difference ( $\rho$ ) for liquid to gas transition, shear modulus ( $G$ ) for liquid to solid transition, pair wave function ( $\psi_S$ ) for superconductor to metal transition, the electrical polarization ( $P$ ) for a ferroelectric system etc. However, in liquid crystal system this order parameter is the degree of molecular ordering [1] which is associated with spontaneous symmetry breaking. The value of it is found to be identically zero in case of completely disordered state or more symmetric mesophases and found to be some non-zero value for relatively more ordered or less symmetric phases [197,198]. The order parameter is a physical observable parameter which is correlated to first derivative of the Gibbs free energy ( $G$ ). Hence, the behavior of order parameter may changes gradually or abruptly at the phase transition point. Thus it is quite significant to classify the possible types of phase transitions which are somewhat more complicated.

According to P. Ehrenfest, the first-order phase transition of the system possesses a discontinuity in the first order derivative of Gibb's free energy ( $G$ )

---

---

( $G(T, p) = U - TS + PV$ ,  $U$  is energy,  $T$  is temperature,  $S$  is entropy,  $P$  is pressure and  $V$  is volume) with respect to some thermodynamic variable, while in case of the second order transition the first order derivative of Gibb's free energy is continuous but second order derivative is discontinuous [199,200]. Mathematically,  $\left(\frac{\partial G}{\partial T}\right)_P = -S$ , and  $\left(\frac{\partial G}{\partial P}\right)_T = V$  are discontinuous at first order transition, but  $\left(\frac{\partial^2 G}{\partial T^2}\right)_P = -\frac{C_p}{T}$  and  $\left(\frac{\partial^2 G}{\partial P^2}\right)_T = -V\Delta K$ ,  $\left(\frac{\partial^2 G}{\partial T \partial P}\right) = V\Delta\alpha$  are discontinuous at second order transition. Hence, it is possible to obtain phase transitions above the second order in accordance with Ehrenfest classification. Moreover, the modern classification suggesting only two types of transition, the first order and the second order, associated with latent heat of the system [201]. The discontinuous transition or first-order phase transition involves a latent heat of the system, while continuous or second order transition does not involve any latent heat. The thermodynamic function  $G$  is correlated with order parameter in different systems. In this context, degree of molecular ordering, which is the order parameter of liquid crystal system changes continuously or abruptly at the transition points. However, most of the phase transitions in liquid crystal belong to either weakly first order or second order depending on the small enthalpy change ( $\Delta H$ ) and  $\Delta V/V$ . Hence, in accordance with the change in order parameter value, it is more interesting to take an insight into the critical anomaly at the transition point for different phase transitions in liquid crystal system.

## 1.5. Critical exponents

The asymptotic critical behavior (degree of singularity or diverging behavior) of any physical quantity for thermodynamical systems in the vicinity of the transition point can be classified into universality classes characterized by some critical indices or critical exponents like  $\alpha$ ,  $\beta$ ,  $\gamma$ ,  $\nu$  etc. [202-204]. They exhibit either branch point singularity or diverging singularity. The order parameter of any thermodynamical system approaches to zero at the critical

point and represents a branch point singularity. However, the physical quantities generally have power-law divergence as a function of the difference between the control parameter (say temperature,  $T$ ) and their critical values ( $T_c$ ). For example, the magnetization density ( $m$ ) as referred to as the order parameter of a magnetic system and can be expressed by,  $m = M/V$  ( $M$  = total magnetization,  $V$  = volume). The value of  $m$  is zero for paramagnet while it assumes a non-zero value for ferromagnetic sample without any external field, *i.e.*,  $m \propto 0$  at  $T > T_c$  and  $m \propto |\tau|^\beta$  at  $T < T_c$ , where  $\tau = (T - T_c)/T_c$ , is called the reduced temperature. Hence the singular behavior or non-analyticity of magnetization order parameter is characterized by the critical exponent  $\beta$ . Similarly, for liquid-gas phase transition, the isothermal susceptibility (divergence of compressibility) is governed by similar critical exponent  $\gamma$  and expressed as,  $\chi^\pm \propto |\tau|^{-\gamma^\pm}$  where  $\pm$  denotes both sides of phase transition point and in most of the cases  $\gamma^+$  and  $\gamma^-$  are equal. Moreover, the singularity for the thermal response function as heat capacity is governed by critical exponent  $\alpha$  and can be expressed as,  $C^\pm \propto |\tau|^{\alpha^\pm}$  where  $\alpha^+ = \alpha^-$ . Furthermore, the correlation length (characteristic distance over a local fluctuation in one part of the system affected by other) expressed as  $\xi$ , diverges as  $\xi^\pm \propto |\tau|^{-\nu^\pm}$  at the critical temperature and also again in this case  $\nu^+ = \nu^-$ . The experimental evidences reveal that these sets of critical exponents are independent of materials whether it is dependent on the range of interaction (it may be long-range or short-range), spatial dimensionality, spin dimensionality, symmetry of the ordered state, and the number of components of the order parameter [205]. Thus in general they are found to belong in the same universal class in nature because several system exhibits the same critical behavior [201,202]. Moreover, such exponents are also correlated to each other by some inequalities such as Rushbrooke inequality  $\alpha + 2\beta + \gamma \geq 2$ , the Griffiths inequality  $\gamma \geq \beta(\delta - 1)$ , the Fisher inequality  $(2 - \eta)\nu \geq \gamma$ , the Josephson inequality  $d\nu \geq 2 - \alpha$ , etc. [206-209], where  $\delta$  and  $\eta$  relates the order parameter to the source field and the size

of correlations respectively at the critical temperature. Study of the critical phenomena in liquid crystal systems has become a fundamental importance in soft condensed matter physics. In order to deal with the critical fluctuations of physical parameters at critical region, the theory of renormalization group has been introduced, which also becomes a plausible calculation tool to deal with the critical phenomena of the universal quantities. Therefore, by using renormalization group theory it is possible to investigate critical phenomena in detail for different mesophase transitions of liquid crystal systems.

---

---

**References:**

- [1] E.B. Priestley, P.J. Wojtowicz, and P. Sheng, (Eds.) in *Introduction to liquid crystals*, Plenum, New York (1974).
- [2] B. Bahadur (Ed.), in *Liquid crystals: Applications and uses*, World Scientific, Singapore (1992).
- [3] P.G. de Gennes, and J. Prost, in *The Physics of Liquid Crystal*, Clarendon Press, Oxford (1993).
- [4] S. Kumar, in *Experimental Study of Physical Properties and Phase Transitions*, Cambridge University Press, New York (2011).
- [5] P. Oswald, and P. Pieranski, in *Nematic and Cholesteric Liquid Crystals*, CRC Press, Taylor & Francis, Boca Raton (2005).
- [6] (a) F. Reinitzer, *Monatshefte fur Chemie*, **9**, 421 (1988); and (b) F. Reinitzer, *Liq. Cryst.*, **5**, 7 (1989).
- [7] O. Lehmann, Über fließende Krystalle. *Zeitschrift für Physik. Chemie.*, **4**, 462 (1889).
- [8] G. Friedel, *Ann. Physique.*, **18**, 273 (1922).
- [9] G. Friedel, in *Colloid chemistry*, The chemical catalogue company inc., New York (1926).
- [10] P. Kirsch, and M. Bremer, *Angew. Chem. Int. Ed.*, **39**, 4216 (2000).
- [11] J.P.F. Lagerwall, and G. Scalia, *Curr. Appl. Phys.*, **12**, 1387 (2012).
- [12] R. Stannarius, *Nat. Mater.*, **8**, 617 (2009).
- [13] Q. Li, in *Liquid crystals beyond displays: chemistry, physics, and applications*, John Wiley & Sons, USA (2012).
- [14] W.A. Crossland, T.D. Wilkinson, T.M. Coker, T.C.B. Yu, and M. Stanley, *OSA TOPS.*, **14**, 102 (1997).
- [15] C.J. Henderson, B. Robertson, D.G. Leyva, T. Wilkinson, D. O'Brien, and G. Faulkner, *Opt. Eng.*, **44**, 75401 (2005).
- [16] R.K. Komanduri, W.M. Jones, C. Oh, and M.J. Escuti, *J. Soc. Inform. Disp.*, **15**, 589 (2007).

- 
- 
- [17] W.A. Crossland, I.G. Manolis, M.M. Redmond, K.L. Tan, T.D. Wilkinson, M.J. Holmes, T.R. Parker, H.H. Chu, J. Croucher, V.A. Handerek, S.T. Warr, B. Robertson, I.G. Bonas, R. Franklin, C. Stace, H.J. White, R.A. Woolley, and G. Henshall, *J. Lightwave Technol.*, **18**, 1845 (2000).
- [18] S. Muto, T. Nagata, K. Asai, H. Ashizawa, and K. Ariei, *Jpn. J. Appl. Phys.*, **29**, 1724 (1990).
- [19] L.L. Lai, E. Wang, Y.H. Liu, and Y. Wang, *Liq. Cryst.*, **29**, 871 (2002).
- [20] F. Nilsson, O. Siderman, and I. Johansson, *Langmuir*, **12**, 902 (1996).
- [21] D.W. Bruce, D.A. Dunmur, E. Lalinde, P.M. Maitlis, and P. Styring, *Nature*, **323**, 791 (1986).
- [22] B.-G. Kim, E.J. Jeong, J.W. Chung, S. Seo, B. Koo, and J. Kim, *Nat. Mater.*, **12**, 659 (2013).
- [23] A.M.F. Neto, and S.R.A. Salinas, in *The physics of lyotropic liquid crystals*, Oxford University Press, Oxford (2005).
- [24] A.G. Petrov, in *The lyotropic state of matter: molecular physics and living matter physics*, Gordon and Breach Science, Amsterdam (1999).
- [25] G.W. Gray, in *Liquid crystals and plastic crystals*, Ellis Harwood, Chichester, England (1974).
- [26] W.H. de Jeu, in *Physical properties of liquid crystalline materials*, Gordon and Breach, New York (1980).
- [27] L.M. Blinov, and V.G. Chigrinov, in *Electro-optic effects in liquid crystal materials*, Springer-Verlag, New York (1994).
- [28] K. Merkel, A. Kocot, J.K. Vij, R. Korlacki, G.H. Mehl, and T. Meyer, *Phys. Rev. Lett.*, **93**, 237801 (2004).
- [29] K. Neupane, S.W. Kang, S. Sharma, D. Carney, T. Meyer, G.H. Mehl, D.W. Allender, S. Kumar, and S. Sprunt, *Phys. Rev. Lett.*, **97**, 207802 (2006).
- [30] F. Hessel, and H. Finkelmann, *Polym. Bull.*, **15**, 349 (1986).
- [31] K. Severing, and K. Saalwächter, *Phys. Rev. Lett.*, **92**, 125501 (2004).
- 
-

- 
- 
- [32] B.R. Acharya, A. Primak, T.J. Dingemans, E.T. Samulski, and S. Kumar, *Pramana*, **61**, 231 (2003).
- [33] L.A. Madsen, T.J. Dingemans, M. Nakata, and E.T. Samulski, *Phys. Rev. Lett.*, **92**, 145505 (2004).
- [34] B.R. Acharya, A. Primak, and S. Kumar, *Phys. Rev. Lett.*, **92**, 145506 (2004).
- [35] A. de Vries, *Mol. Cryst. Liq. Cryst.*, **10**, 31 (1970); *ibid*, **10**, 219 (1970); *ibid*, **11**, 36 (1970).
- [36] O. Francescangeli, M. Laus, and G. Galli, *Phys. Rev. E*, **55**, 481 (1997).
- [37] S. Stojadinovic, A. Adorjan, S. Sprunt, H. Sawade, and A. Jákli, *Phys. Rev. E*, **66**, 060701 (2002).
- [38] O. Francescangeli, V. Stanic, S.I. Torgova, A. Strigazzi, N. Scaramuzza, C. Ferrero, I.P. Dolbnya, T.M. Weiss, R. Berardi, L. Muccioli, S. Orlandi, and C. Zannoni, *Adv. Funct. Mater.*, **19**, 2592 (2009).
- [39] N. Vaupotic, J. Szydłowska, M. Salamonczyk, A. Kovarova, J. Svoboda, M. Osipov, D. Pocięcha, and E. Gorecka, *Phys. Rev. E*, **80**, 030701 (2009).
- [40] C. Bailey, K. Fodor-Csorba, J.T. Gleeson, S.N. Sprunt, and A. Jákli, *Soft Matter*, **5**, 3618 (2009).
- [41] C. Keith, A. Lehmann, U. Baumeister, M. Prehm, and C. Tschierske, *Soft Matter*, **6**, 1704 (2010).
- [42] O. Francescangeli, and E.T. Samulski, *Soft Matter*, **6**, 2413 (2010).
- [43] S.H. Hong, R. Verduzco, J. Williams, R.J. Twieg, E. DiMasi, R. Pindak, A. Jákli, J.T. Gleeson, and S.N. Sprunt, *Soft Matter*, **6**, 4819 (2010).
- [44] V. Domenici, *Soft Matter*, **7**, 1589 (2011).
- [45] I. Dierking, in *Textures of liquid crystals*, WILEY-VCH Verlag GmbH & Co.KGaA, Weinheim (2003).
- [46] C. Druon and J.M. Wacrenier, *Mol. Cryst. Liq. Cryst.*, **98**, 201 (1983).
- [47] I. Hatta, Y. Nagai, T. Nakayama, and S. Imaizumi, *J. Phys. Soc. Jpn.*, **52**, 47 (1983).
- 
-

- 
- 
- [48] C. Chiang, and C.W. Garland, *Proc. of 10<sup>th</sup> ILCC*, York, July, abstract E20 (1994).
- [49] F. Hardouin, A.M. Levelut, M.F. Achard, and G. Sigaud, *J. de Chemie Physique.*, **80**, 53 (1983).
- [50] R. Berardi, S. Orlandi, D.J. Photinos, A.G. Vanakaras, and C. Zannoni, *Phys. Chem. Chem. Phys.*, **4**, 770 (2002).
- [51] D. Apreutesei, and G.H. Mehl, *Chem. Commun.*, 0, 609 (2006).
- [52] A. Chakraborty, B. Das, M.K. Das, S. Findeisen-Tandel, M.-G. Tamba, U. Baumeister, H. Kresse, and W. Weissflog, *Liq. Cryst.*, **38**, 1085 (2011).
- [53] D. Demus, J.W. Goodby, G.W. Gray, H.W. Spiess, and V. Vill, (Eds.), in *Handbook of liquid crystals*, Wiley-VCH, Weinheim (1998).
- [54] D.R. Nelson, and B.I. Halperin, *Phys. Rev. B*, **19**, 2457 (1979).
- [55] B.I. Halperin, and D.R. Nelson, *Phys. Rev. Lett.*, **41**, 121 (1978).
- [56] P.J. Collings, and J.S. Patel (Eds.), in *Handbook of liquid crystal research*, Oxford University Press, Oxford (1997).
- [57] R.J. Birgeneau, and J.D. Lister, *J. Phys. Lett.*, **39**, 399 (1978).
- [58] J.J. Benattar, F. Moussa, M. Lambert, and C. Germain, *J de Phys. Lett.*, **42**, 67 (1981).
- [59] T. Miyazawa, Y. Yamamura, M. Hishida, S. Nagatomo, M. Massalska-Arodz, and K. Saito, *J. Phys. Chem. B*, **117**, 8293 (2013).
- [60] P.S. Pershan, in *Structure of liquid crystal phases*, World Scientific Lecture Note in Physics, Singapore (1988).
- [61] G.W. Gray, and J.W. Goodby, in *Smectic liquid crystals: textures and structures*, Leonard Hill, London (1984).
- [62] S. Singh, in *Liquid crystals: Fundamentals*, World Scientific, Singapore (2002).
- [63] I. Dierking, *Symmetry*, **6**, 444 (2014).
- [64] A.Y. Bobrovsky, N.I. Boiko, and V.P. Shibaev, *Liq. Cryst.*, **27**, 219 (2000).
- 
-

- 
- 
- [65] D.K. Yang, J.L. West, L.C. Chien, and J.W. Doane, *J. Appl. Phys.*, **76**, 1331 (1994).
- [66] Y. Takanishi, Y. Ouchi, H. Takezoe, A. Fukuda, A. Mochizuki, and M. Nakatsuka, *Jpn. J. Appl. Phys. Lett.*, **29**, L984 (1990).
- [67] J.P.F. Lagerwall, in *Phase characterization of polar liquid crystals using dielectric spectroscopy*, Licentiate thesis, Chalmers, Göteborg (2000).
- [68] J.V. Selinger, P.J. Collings, and R. Shashidhar, *Phys. Rev. E*, **64**, 61705 (2001).
- [69] J.P.F. Lagerwall, and F. Giesselmann, *Chem. Phys. Chem.*, **7**, 20 (2006).
- [70] P. Mach, R. Pindak, A.-M. Levelut, P. Barois, H.T. Nguyen, H. Baltes, M. Hird, K. Toyne, A. Seed, J.W. Goodby, C.C. Huang, and L. Furenlid, *Phys. Rev. E*, **60**, 6793 (1999).
- [71] R.B. Meyer, L. Liebert, L. Strzelecki, and P.J. Keller, *Phys. Lett. (Orsay, Fr.)*, **36**, L-69 (1975).
- [72] P. Collings, and M. Hird, in *Introduction to Liquid Crystals: Chemistry and Physics*, Taylor & Francis, London, (1997).
- [73] N.A. Clark, and S.T. Lagerwall, *Appl. Phys. Lett.*, **36**, 899 (1980).
- [74] J.W. Goodby, R. Blinc, N.A. Clark, S.T. Lagerwall, M.A. Osipov, S.A. Pikin, T. Sakurai, K. Yoshino, and B. Žekš, in *Ferroelectric liquid crystals: principles, properties and applications*, Gordon & Breach, Philadelphia (1991).
- [75] S.T. Lagerwall, in *Ferroelectric and antiferroelectric liquid crystals*, Wiley-VCH, Weinheim (1999).
- [76] I. Musevič, R. Blinc, and B. Žekš, in *The physics of ferroelectric and antiferroelectric liquid crystals*, World Scientific, Singapore (2000).
- [77] A.M. Levelut, C. Germain, P. Keller, and L. Liebert, *J. Phys. (Paris)*, **44**, 623 (1983).
- [78] Y. Galerne, and L. Liebert, in *Abstract Book of 2nd International Conf. Ferroelectric Liq. Cryst.*, **O27** (1989).
- 
-

- 
- 
- [79] A.D.L. Chandani, Y. Ouchi, H. Takezoe, A. Fukuda, K. Terashima, K. Furukawa, and A. Kishi, *Jpn. J. Appl. Phys.*, **28**, L 69 (1989).
- [80] H.S. Kitzerow, and C. Bahr, in *Chirality in Liquid crystals*, Springer-Verlag, New York, Inc., (2001).
- [81] P.P. Crooker, in *Chirality in Liquid Crystals*, Ed. H.S. Kitzerow, C. Bahr Springer-Verlag, New York (2001).
- [82] (a) P.P. Crooker, *Liq. cryst.*, **5**, 751 (1989); (b) D.C. Wright, and N.D. Mermin, *Review of Modern Physics.*, **61**, 385 (1989).
- [83] F. Castles, S.M. Morris, E.M. Terentjev, and H.J. Coles, *Phys. Rev. Lett.*, **104**, 157801 (2010).
- [84] T.C. Lubensky, *Physica A*, **220**, 99 (1995).
- [85] R. Dhar, *Phase Transit.*, **79**, 175 (2006).
- [86] S.R. Renn, and T.C. Lubensky, *Phys. Rev. A*, **38**, 2132 (1988).
- [87] S.R. Renn, and T.C. Lubensky, *Mol. Cryst. Liq. Cryst.*, **209**, 349 (1991).
- [88] J.W. Goodby, M.A. Waugh, S.M. Stein, E. Chin, R. Pindak, and J.S. Patel, *J. Am. Chem. Soc.*, **111**, 8119 (1989).
- [89] I. Dierking, *Symmetry*, **6**, 444 (2014).
- [90] H. Takezoe, and Y. Takanishi, *Jpn. J. Appl. Phys.*, **45(2A)**, 597 (2006).
- [91] D. Vorlander, *Ber. Dtsch. Chem. Ges.*, **62**, 2831 (1929).
- [92] D. Vorlander, and A. Apel, *Ber. Dtsch. Chem. Ges.*, **65**, 1101 (1932).
- [93] M. Kuboshita, Y. Matsunaga, and H. Matsuzaki, *Mol. Cryst. Liq. Cryst.*, **199**, 319 (1991).
- [94] T. Matsuda, and Y. Matsunaga, *Bull. Chem. Soc. Jpn.*, **64**, 2192 (1991).
- [95] H. Matsuzaki, and Y. Matsunaga, *Liq. Cryst.*, **14**, 105 (1993).
- [96] T. Akutagawa, Y. Matsunaga, and K. Yasuhara, *Liq. Cryst.*, **17**, 659 (1994).
- [97] T. Niori, T. Sekine, J. Watanabe, T. Furukawa, and H. Takezoe, *J. Mater. Chem.*, **6**, 1231 (1996).
- [98] D.R. Link, G. Natale, R. Shao, J.E. MacLennan, N.A. Clark, E. Körblova, and D.M. Walba, *Science*, **278**, 1924 (1997).
- 
-

- 
- 
- [99] G. Pelzl, S. Diele, and W. Weissflog, *Adv. Mater.*, **11**, 707 (1999).
- [100] T. Sekine, T. Niori, J. Watanabe, T. Furukawa, S.W. Choi, and H. Takezoe, *J. Mater. Chem.*, **7**, 1307 (1997).
- [101] T. Sekine, T. Niori, M. Sone, J. Watanabe, S.W. Choi, Y. Takanishi, and H. Takezoe, *Jpn. J. Appl. Phys.*, **36**, 6455 (1997).
- [102] R. Macdonald, F. Kentischer, P. Warnick, and G. Heppke, *Phys. Rev. Lett.*, **81**, 4408 (1998).
- [103] R.A. Reddy, and C. Tschierske, *J. Mater. Chem.*, **16**, 907 (2006).
- [104] D.M. Walba, D.J. Dyer, T. Sierra, P.L. Cobben, R. Shao, and N.A. Clark, *J. Am. Chem. Soc.*, **118**, 1211 (1996).
- [105] S. Diele, S. Grande, H. Kruth, Ch. Lischka, G. Pelzl, W. Weissflog, and I. Wirth, *Ferroelectrics*, **212**, 169 (1998).
- [106] J.P. Bedel, J.C. Rouillon, J.P. Marcerou, M. Laguerre, H.T. Nguyen, and M.F. Achard, *Liq. Cryst.*, **28**, 1285 (2001).
- [107] J.A. Olivares, S. Stojadinovic, T. Dingemans, S. Sprunt, and A. Jákli, *Phys. Rev. E*, **68**, 041704 (2003).
- [108] M.G. Tamba, B. Kosata, K. Pelz, S. Diele, G. Pelzl, Z. Vakhovskaya, H. Kresse, and W. Weissflog, *Soft Matter*, **2**, 60 (2006).
- [109] G. Shanker, M. Prehm, and C. Tschierske, *J. Mater. Chem.*, **22**, 168 (2012).
- [110] Y. Wang, H.G. Yoon, H.K. Bisoyi, S. Kumar, and Q. Li, *J. Mater. Chem.*, **22**, 20363 (2012).
- [111] D. Shen, S. Diele, G. Pelzl, I. Wirth, and C. Tschierske, *J. Mater. Chem.*, **9**, 661 (1999).
- [112] R.A. Reddy, and B.K. Sadashiva, *J. Mater. Chem.*, **14**, 1936 (2004).
- [113] R.A. Reddy, B.K. Sadashiva, and V.A. Raghunathan, *Chem. Mater.*, **16**, 4050 (2004).
- [114] N.S. Novikova, E. Gorecka, R.V. Kondratyeva, and E.D. Kilimenchuk, *Liq. Cryst.*, **35**, 743 (2008).
- 
-

- 
- 
- [115] S.K. Lee, X. Li, S. Kang, M. Tokita, and J. Watanabe, *J. Mater. Chem.*, **19**, 4517 (2009).
- [116] E.-J. Choi, X. Cui, C.-W. Ohk, W.-C. Zin, J.-H. Lee, T.-K. Lim, and W.-G. Jang, *J. Mater. Chem.*, **20**, 3743 (2010).
- [117] L.E. Hough, M. Spannuth, M. Nakata, D.A. Coleman, C.D. Jones, G. Dantlgraber, C. Tschierske, J. Watanabe, E. Körblova, D.M. Walba, J.E. MacLennan, M.A. Glaser, and N.A. Clark, *Science*, **325**, 452 (2009).
- [118] S.T. Wang, X.F. Han, A. Cady, Z.Q. Liu, A. Kamenev, L. Glazman, B.K. Sadashiva, R.A. Reddy, and C.C. Huang, *Phy. Rev. E*, **70**, 061705 (2004).
- [119] R.A. Reddy, C. Zhu, R. Shao, E. Körblova, T. Gong, Y. Shen, E. Garcia, M.A. Glaser, J.E. MacLennan, D.M. Walba, and N.A. Clark, *Science*, **332**, 72 (2011).
- [120] N. Chattham, M.-G. Tamba, R. Stannarius, E. Westphal, H. Gallardo, M. Prehm, C. Tschierske, H. Takezoe, and A. Eremin, *Phys. Rev. E*, **91**, 030502 (2015).
- [121] P. Grzybowski, and L. Longa, *Phys. Rev. Lett.*, **107**, 027802 (2011).
- [122] J. Watanabe, T. Niori, T. Sekine, and H. Takezoe, *Jpn. J. Appl. Phys.*, **37**, L139 (1998).
- [123] J. Szydłowska, J. Mieczkowski, J. Matraszek, D.W. Bruce, E. Gorecka, D. Pocięcha, and D. Guillon, *Phys. Rev. E*, **67**, 031702 (2003).
- [124] K. Pelzl, W. Weissflog, U. Baumeister, and S. Diele, *Liq. Cryst.*, **30**, 1151 (2003).
- [125] R.A. Reddy, V.A. Raghunathan, and B.K. Sadashiva, *Chem. Mater.*, **17**, 274 (2005).
- [126] J. Thisayukta, H. Takezoe and J. Watanabe, *Jpn. J. Appl. Phys.*, **40**, 3277 (2001).
- [127] H. Chan, and I. Dierking, *Phys. Rev. E*, **70**, 021703 (2004).
- [128] J. Salfetnikova, H. Schmalfuss, H. Nadası, W. Weissflog, and H. Kresse, *Liq. Cryst.*, **27**, 1663 (2000).
- 
-

- 
- 
- [129] Y. Takanishi, K. Ishikawa, J. Watanabe, H. Takezoe, M. Yamashita, and K. Kawase, *Phys. Rev. E*, **71**, 061701 (2005).
- [130] G. Heppke, D. Krueker, C. Lohning, D. Lotzsch, S. Rauch, and N.K. Sharma, in *Frieburger Arbeitstagung Flussige Kristalle*, Freiburg, Germany, P 70 (1997).
- [131] P. Collings *et al.*, Abtr. Workshop on *Banana-Shaped Liquid Crystals: Chirality by Achiral Molecules*, P-15, Berlin, Germany (1997).
- [132] F. Kentischer, R. Macdonald, P. Warnick, and G. Heppke, *Proc. SPIE*, **3143**, 128 (1997).
- [133] S.-W. Choi, Y. Kinoshita, B. Park, H. Takezoe, T. Niori, and J. Watanabe, *Jpn. J. Appl. Phys.*, **37**, 3408 (1998).
- [134] H. Nádasi, W. Weissflog, A. Eremin, G. Pelzl, S. Diele, B. Das, and S. Grande, *J. Mater. Chem.*, **12**, 1316 (2002).
- [135] W. Weissflog, I. Wirth, S. Diele, G. Pelzl, H. Schmalfuss, T. Schoss, and A. Würflinger, *Liq. Cryst.*, **28**, 1603 (2001).
- [136] H.N.S. Murthy, and B.K. Sadashiva, *Liq. Cryst.*, **29**, 1223 (2002).
- [137] A. Jákli, Ch. Lischka, W. Weissflog, G. Pelzl, and A. Saupe, *Liq. Cryst.*, **27**, 1405 (2000).
- [138] R.A. Reddy, and B.K. Sadashiva, *Liq. Cryst.*, **30**, 273 (2003).
- [139] H.N. Shreenivasa Murthy, and B.K. Sadashiva, *Liq. Cryst.*, **30**, 1051 (2003).
- [140] Y.A. Nastishin, M.F. Achard, H.T. Nguyen, and M. Kleman, *Eur. Phys. J. E*, **12**, 581 (2003).
- [141] A. Jákli, D. Krüerke, and G.G. Nair, *Phys. Rev. E*, **67**, 051702 (2003).
- [142] G. Pelzl, S. Diele, A. Jakli, Ch. Lischka, I. Wirth, and W. Weissflog, *Liq. Cryst.*, **26**, 135 (1999).
- [143] G. Pelzl, M.W. Schröder, U. Dunemann, S. Diele, W. Weissflog, C. Jones, D. Coleman, N.A. Clark, R. Stannarius, J. Li, B. Das, and S. Grande, *J. Mater. Chem.*, **14**, 2492 (2004).
- 
-

- 
- 
- [144] D.A. Coleman, J. Fernsler, N. Chattham, M. Nakata, Y. Takanishi, E. Körblova, D.R. Link, R.-F. Shao, W.G. Jang, J.E. Maclellan, O. Mondainn-Monval, C. Boyer, W. Weissflog, G. Pelzl, L.-C. Chien, J. Zasadzinski, J. Watanabe, D. M. Walba, H. Takezoe, and N. A. Clark, *Science*, **301**, 1204 (2003).
- [145] M. Lehmann, and J. Levin, *Mol. Cryst. Liq. Cryst.*, **411**, 273 (2004).
- [146] M. Lehmann, S.-W. Kang, C. Köhn, S. Haseloh, U. Kolb, D. Schollmeyer, Q. Wang, and S. Kumar, *J. Mater. Chem.*, **16**, 4326 (2006).
- [147] C.V. Yelamaggad, S. Shashikala, D.S. Shankar Rao, C.V. Lobo, and S. Chandrasekhar, *Angew. Chem., Int. Ed.*, **43**, 3429 (2004).
- [148] R. Stannarius, A. Eremin, M.-G. Tamba, G. Pelzl, and W. Weissflog, *Phys. Rev. E*, **76**, 061704 (2007).
- [149] P. Kumar, Y.G. Marinov, H.P. Hinov, U.S. Hiremath, C.V. Yelamaggad, K.S. Krishnamurthy, and A.G. Petrov, *J. Phys. Chem. B*, **113**, 9168 (2009).
- [150] J. Harden, B. Mbanga, N. Éber, K. Fodor-Csorba, S. Sprunt, J.T. Gleeson, and A. Jákli, *Phys. Rev. Lett.*, **97**, 157802 (2006).
- [151] J. Harden, R. Teeling, J.T. Gleeson, S. Sprunt, and A. Jákli, *Phys. Rev. E*, **78**, 031702 (2008).
- [152] D. Wiant, J.T. Gleeson, N. Éber, K. Fodor-Csorba, A. Jákli, and T. Tóth-Katona, *Phys. Rev. E*, **72**, 041712 (2005).
- [153] S. Tanaka, S. Dhara, B.K. Sadashiva, Y. Shimbo, Y. Takanishi, F. Araoka, K. Ishikawa, and H. Takezoe, *Phys. Rev. E*, **77**, 041708 (2008).
- [154] S. Tanaka, H. Takezoe, N. Éber, K. Fodor-Csorba, A. Vajda, and A. Buka, *Phys. Rev. E*, **80**, 021702 (2009).
- [155] S. Dhara, F. Araoka, M. Lee, K.V. Le, L. Guo, B.K. Sadashiva, K. Song, K. Ishikawa, and H. Takezoe, *Phys. Rev. E*, **78**, 050701 (2008).
- [156] E. Dorjgotov, K. Fodor-Csorba, J.T. Gleeson, S. Sprunt, and A. Jákli, *Liq. Cryst.*, **35**, 149 (2008).
- 
-

- 
- 
- [157] P. Tadapatri, U.S. Hiremath, C.V. Yelamaggad, and K.S. Krishnamurthy, *J. Phys. Chem. B*, **114**, 1745 (2010).
- [158] M. Nagaraj, Y.P. Panarin, U. Manna, J.K. Vij, C. Keith, and C. Tschierske, *Appl. Phys. Lett.*, **96**, 011106 (2010).
- [159] V.P. Panov, M. Nagaraj, J.K. Vij, Yu. P. Panarin, A. Kohlmeier, M.G. Tamba, R.A. Lewis, and G.H. Mehl, *Phys. Rev. Lett.*, **105**, 167801 (2010).
- [160] V.P. Panov, R. Balachandran, M. Nagaraj, J.K. Vij, M.G. Tamba, A. Kohlmeier, and G.H. Mehl, *Appl. Phys. Lett.*, **99**, 261903 (2011).
- [161] S. Ghosh, N. Begum, S. Turlapati, S.K. Roy, A.K. Das, and N.V.S. Rao, *J. Mater. Chem. C*, **2**, 425 (2014).
- [162] M. Hird, J.W. Goodby, N. Gough, and K.J. Toyne, *J. Mater Chem.*, **11**, 2732 (2001).
- [163] B. Das, S. Grande, W. Weissflog, A. Eremin, M.W. Schröder, G. Pelzl, S. Diele, and H. Kresse, *Liq. Cryst.*, **30**, 529 (2003).
- [164] H. Okamoto, Y. Morita, Y. Segawa, and S. Takenaka, *Mol. Cryst. Liq. Cryst.*, **439**, 221 (2005).
- [165] T. Kajitani, S. Kohmoto, M. Yamamoto, and K. Kishikawa, *Chem. Mater.*, **17**, 3812 (2005).
- [166] F.C. Yu, and L.J. Yu, *Chem. Mater.*, **18**, 5410 (2006).
- [167] C.D. Jones, R.-F. Shao, A.G. Rappaport, J.E. MacLennan, N.A. Clark, E. Körblova, and D.M. Walba, *Liq. Cryst.*, **33**, 25 (2006).
- [168] F.C. Yu and L.J. Yu, *Liq. Cryst.*, **35**, 799 (2008).
- [169] E. Enz, S. Findeisen-Tandel, R. Dabrowski, F. Giesselmann, W. Weissflog, U. Baumeister, and J. Lagerwall, *J. Mater. Chem.*, **19**, 2950 (2009).
- [170] A. Chakraborty, M.K. Das, B. Das, U. Baumeister, and W. Weissflog, *J. Mater. Chem. C*, **1**, 7418 (2013).
- [171] V. Novotná, J. Žurek, V. Kozmík, J. Svoboda, M. Glogarová, J. Kroupa, and D. Pocięcha, *Liq. Cryst.*, **35**, 1023 (2008).
- 
-

- 
- 
- [172] A. Belaïssaoui, S.J. Cowling, and J.W. Goodby, *Liq. Cryst.*, **40**, 822 (2013).
- [173] L. Chakraborty, N. Chakraborty, D.D. Sarkar, N.V.S. Rao, S. Aya, K.V. Le, F. Araoka, K. Ishikawa, D. Pocięcha, E. Gorecka, and H. Takezoe, *J. Mater. Chem. C*, **1**, 1562 (2013).
- [174] M.K. Paul, R.K. Nath, B. Moths, L. Pan, S. Wang, R. Deb, Y. Shen, N.V.S. Rao, and C.C. Huang, *Phase Transitions*, **85**, 1070 (2012).
- [175] S. DasGupta, S.K. Roy, *Phys. Lett. A*, **306**, 235 (2003).
- [176] A. Kubono, K. Yoshino, T. Ninomiya, R. Akiyama, K. Tanaka, *Liq. Cryst.*, **29**, 1089 (2002).
- [177] R. Dabrowski, *Mol. Cryst. Liq. Cryst.*, **191**, 17 (1990).
- [178] M.F. Grebyonkin, G.A. Beresnev, V.V. Belyaev, *Mol. Cryst. Liq. Cryst.*, **103**, 1 (1983).
- [179] H. Schad, *J. Appl. Phys.*, **54**, 4994 (1983).
- [180] S.K. Sarkar, and M.K. Das, *RSC Adv.*, **4**, 19861 (2014).
- [181] D. Venkata Sai, G. Mirri, I. Musevic, and S. Dhara, *Liq. Cryst.*, **43**, 1884 (2016).
- [182] P. Salamon, N. Éber, A. Buka, J.T. Gleeson, S. Sprunt, and A. Jákli, *Phys. Rev. E*, **81**, 031711 (2010).
- [183] M.K. Das, P.C. Barman, and S.K. Sarkar, *Eur. Phys. J. B*, **88**, 175 (2015).
- [184] M.B. Sied, S. Diez, J. Salud, D.O. Lopez, P. Cusmin, J.L. Tamarit, and M. Barrio, *J. Phys. Chem. B*, **109**, 16284 (2005).
- [185] Y. Sasaki, K. Ema, K.V. Le, H. Takezoe, S. Dhara, and B.K. Sadashiva, *Phys. Rev. E*, **82**, 011709 (2010).
- [186] M.B. Sied, J. Salud, D.O. Lopez, M. Barrio, and J.L. Tamarit, *Phys. Chem. Chem. Phys.*, **4**, 2587 (2002).
- [187] M.G. Lafouresse, M.B. Sied, H. Allouchi, D.O. Lopez, J. Salud, and J.L. Tamarit, *Chem. Phys. Lett.*, **376**, 188 (2003).
- 
-

- 
- 
- [188] M.A. Anisimov, in *Critical phenomena in liquids and liquid crystals*, Gordon and Breach, New York (1991).
- [189] A. Buka, (Ed.), in *Modern topics in liquid crystals*, World Scientific (1993).
- [190] C.S. Oh, *Mol. Cryst. Liq. Cryst.*, **42**, 1 (1977).
- [191] T. Narayanan, and A. Kumar, *Phys. Rep.*, **249**, 135 (1994).
- [192] G. Pelzl, C. Scholz, S. Diele, H.-J. Deutscher, D. Demus, H. Sackmann, *Mol. Cryst. Liq. Cryst.*, **168(1)**, 197 (1989).
- [193] F. Hardouin, G. Sigaud, M.F. Achard, and H. Gasparoux, *Phys. Lett. A*, **71**, 347 (1979).
- [194] K.W. Evans-Lutterodt, J.W. Chung, B.M. Ocko, R.J. Birgeneau, C. Chiang, C.W. Garland, E. Chin, J. Goodby, and N.H. Tinh, *Phys. Rev. A*, **36**, 1387 (1987).
- [195] A. Pramanik, B. Das, M.K. Das, K. Garbat, S. Urban, and R. Dabrowski, *Liq. Cryst.*, **40**, 149 (2013).
- [196] A. Chakraborty, S. Chakraborty, M.K. Das, and W. Weissflog, *J. Mol. Liq.*, **265**, 536 (2018).
- [197] J.M. Yeomans, in *Statistical mechanics of phase transitions*, Clarendon, Oxford (1992).
- [198] H.B. Callen, in *Thermodynamics*, J. Wiley and Sons, New York, 376 (1960).
- [199] G. Jaeger, *Arch. Hist. Exact Sci.*, **53**, 51 (1998).
- [200] P. Ehrenfest, *Proc. R. Acad. Sci. Amsterdam*, **36**, 153 (1933).
- [201] R.K. Pathria, in *Statistical mechanics*, Butterworth-Heinemann, Jordan Hill, Oxford (1996).
- [202] I. Herbut, in *A modern approach to critical phenomena*, Cambridge University Press, New York (2007).
- [203] H.E. Stanley, in *Introduction to phase transitions and critical phenomena*, Oxford University Press (1971).
- 
-

- [204] J.J. Binney, N.J. Dowrick, A.J. Fisher, and M.E.J. Newman, in *The theory of critical phenomena*, Clarendon Press, Oxford (1992).
- [205] J. Przystawa, *Physica A*, **114(1–3)**, 557 (1982).
- [206] H. Eugene Stanley, in *Introduction to Phase Transitions and Critical Phenomena*, Clarendon Press. Oxford (1971).
- [207] Robert B. Griffith, *Phys. Rev. Lett.*, **14**, 623-624 (1965).
- [208] M.E. Fisher, *Phys. Rev.*, **180**, 594 - 600 (1969).
- [209] B.D. Josephson, *Proc. Phys. Soc. (London)*, **92**, 276 (1967).

# **CHAPTER 2**

---

**Experimental techniques and theoretical  
background**

## 2.1. Introduction

This chapter deals with the detailed description of several experimental techniques employed, relevant operational principles, mathematical expressions and theories in connection with the study to perform the experiment. Theoretical discussions associated with mesophase transitions in liquid crystals those are related to the subject matter of this dissertation are also included in this chapter.

## 2.2. Experimental techniques

### 2.2.1. Liquid crystal cells and sample preparation

To investigate different physical properties of Liquid Crystal (LC) sample, it is necessary to prepare a proper alignment and uniform ordering. The crystalline property of the liquid crystal material is developed when it is considered as a smaller sized ordered domain. It is possible to obtain such small domains when the sample is taken sandwiched in between two glass slides, *i.e.*, when it becomes a thin layer. However, to investigate some higher order mesophases, the perfect alignment of molecules is required within the glass substrates. Such alignment can be achieved by using LC cells whose walls are treated with polyimide coating (for surface anchoring) and ITO coating (for application of external electric field) in a variety of ways to accomplish different molecular alignments. Examples of those alignment cells are – (i) homogeneous (HG) or planar cell where molecular long axes are directed parallel to the glass surface, (ii) homeotropic (HT) cell where molecular long axes are aligned perpendicular to the glass surface, (iii) tilted LC cell where the molecular long axis is tilted with respect to the surface normal, (iv) hybrid cell in which the molecules are parallel to one substrate and perpendicular to another substrate etc. Among them, only commercially available (AWAT PPW, Warsaw, Poland) HG and HT cells (Fig. 2.1) of

suitable thickness were used in different experiments related to this dissertation.

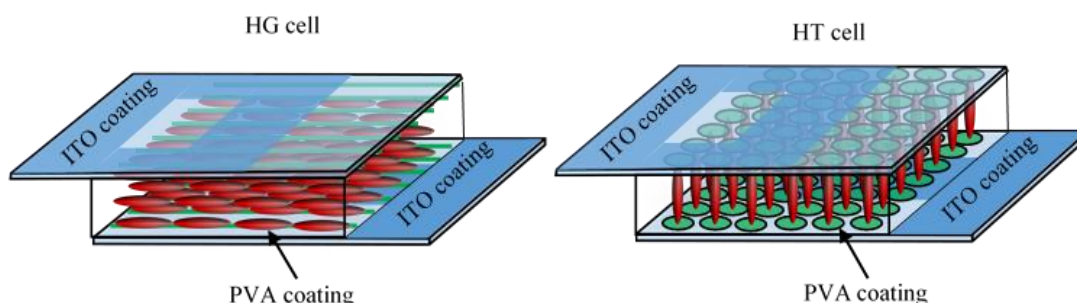


**Figure 2.1.** Orientations of the molecules in planar (HG) and homeotropic (HT) cells.

In order to improve different physical properties of LC materials for application purpose and also for the investigation of transitional phenomena at different mesophase transition, it is often required to formulate some binary or multi-component mixtures rather than investigating the pure compounds. Therefore, the two or more pure LC compounds were taken in a vial with particular proportion after carefully weighting it in a high precision digital balance (Mettler Toledo AB-265-S) and then mixed them by placing the vial in a continuous shaker machine or often placed in an ultrasonicator (SONAPROS PR 250-MP) for several hours at a fixed temperature close to their clearing temperatures. After preparation of homogenous mixture, samples were filled up in LC cells of suitable thickness and alignment by the capillary action and proceeds further for experimental studies.

### 2.2.2. Texture study

Optical textures of liquid crystal sample are the appearance of some characteristic visual pattern when viewed under a crossed polarizing microscope probed with a polarized light. Such appearance is due to the defect structure of long-range molecular ordering for liquid crystal samples. Visualization of these optical textures are different for different mesophases, details descriptions are available in the literature [1,2]. Therefore, the texture

observation is the preliminary tool to characterize different mesophases and their phase transition temperatures which helps further to construct a phase diagram of binary mixtures by varying the concentration of guest LC compound.

Texture observation were made by taking a small amount of sample in a glass slide and covered it by a small cover slip over the sample to make a thin layer and often filled the sample in commercially available LC cells. These slides/cells were kept in a hot/cooling stage (HCS302) made by INSTEC equipped with a programmable temperature controller mK1000 (INSTEC). The mesophase textures in the entire mesomorphic range were observed under polarizing optical microscope BANBROS BPL400 B attached with a CCD camera Moticam 580 (5.0 MP).

### **2.2.3. Differential scanning calorimetry (DSC)**

In order to detect the actual phase transition temperature of mesophases, the differential scanning calorimetry or DSC study is complementary technique to polarizing optical microscopy. DSC measurement reveals the presence of mesophases by detecting the enthalpy change associated with the phase transitions. It is also capable of identifying the order nature of phase transitions by variation of temperature [3-5]. Although this measurement cannot identify the type of phases, it provides some useful information about the conformational disorder [6], purity of the sample [7], order of the phase transitions [3-5] etc.

Investigation on DSC study for some LC samples related to this dissertation was carried out by Pyris Diamond Perkin-Elmer 7 [8], Institute of Physics, Academy of Sciences of the Czech Republic, 18221 Prague, Czech Republic. The sample of amount 4 mg was hermetically sealed in an aluminium pan and proceeds further to heat/cool in a nitrogen atmosphere at a heating/cooling rate of 10 °C per minute. The temperature and the enthalpy change [ $\Delta H$ ] were calibrated on the extrapolated onsets of melting points of

---

---

ice, indium and zinc. The details procedure to determine the transition temperature and corresponding enthalpy changes have been described by Ratna *et al.* [9].

#### 2.2.4. Optical birefringence measurement

The liquid crystal materials possess an optical anisotropy due to the existence of shape anisotropy of the constituent molecules and relative orientation of the molecular director with respect to the direction of light propagation. If the direction of the incident light beam (polarized) is perpendicular to the direction of the molecular optic axis, the refracted light beam splits into an ordinary refractive index ( $n_o$ ) along with an extraordinary refractive index ( $n_e$ ), directed perpendicular and parallel to the molecular optic axis respectively. Hence, it is well known as “doubled refraction”. Both the refracted light beam is plane polarized and orthogonal to each other. However, the birefringence ( $\Delta n$ ) is the difference of those refractive indices and can be defined as:

$$\Delta n = n_e - n_o \quad (2.1)$$

The optical birefringence of liquid crystal compounds have been determined in this dissertation by two different methods: (i) the thin prism method [10,11], where both  $n_o$  and  $n_e$  has been measured directly from sample filled thin prism by variation of temperature and (ii) the high-resolution optical transmission technique [12-16], where the birefringence has been measured by probing the temperature dependent phase retardation at different mesophases of liquid crystal materials filled in LC cells.

##### a. Thin prism technique

In the thin prism technique, the LC sample has been inserted within a lab-made hollow prism of prism angle less than  $2^\circ$ . This kind of prisms were constructed by two pieces of glass slide having dimension  $2 \times 3$  cm and  $2 \times 2$  cm and a thin glass spacer was introduced between them at one end of the vertical

edges to achieve the prism angle less than  $2^\circ$ . Glass slides were treated for one hour with an acid mixture (conc.  $\text{HNO}_3$  and conc.  $\text{H}_2\text{SO}_4$ ) at a temperature of about  $60^\circ\text{C}$ . After washing the glass slides with distilled water, treated further with 1 molar solution of  $\text{KOH}$  for several hours. They were the rinsed thoroughly with distilled water for several times and left in acetone for few hours to remove any residual impurity. Furthermore, to obtain a homogeneous molecular alignment, a thin layer of dilute polyvinyl alcohol was applied to contact surfaces of the glass slides and the dry surfaces were uniformly rubbed for several times with a filter paper. The glass plates were then sealed by using a high temperature adhesive. Next the prisms were baked in an oven at about  $100^\circ\text{C}$  for several hours. However, before introducing the LC samples, the refracting angle of the prisms were determined by filling with ultrapure water and measuring the deviation produced in LASER beam.

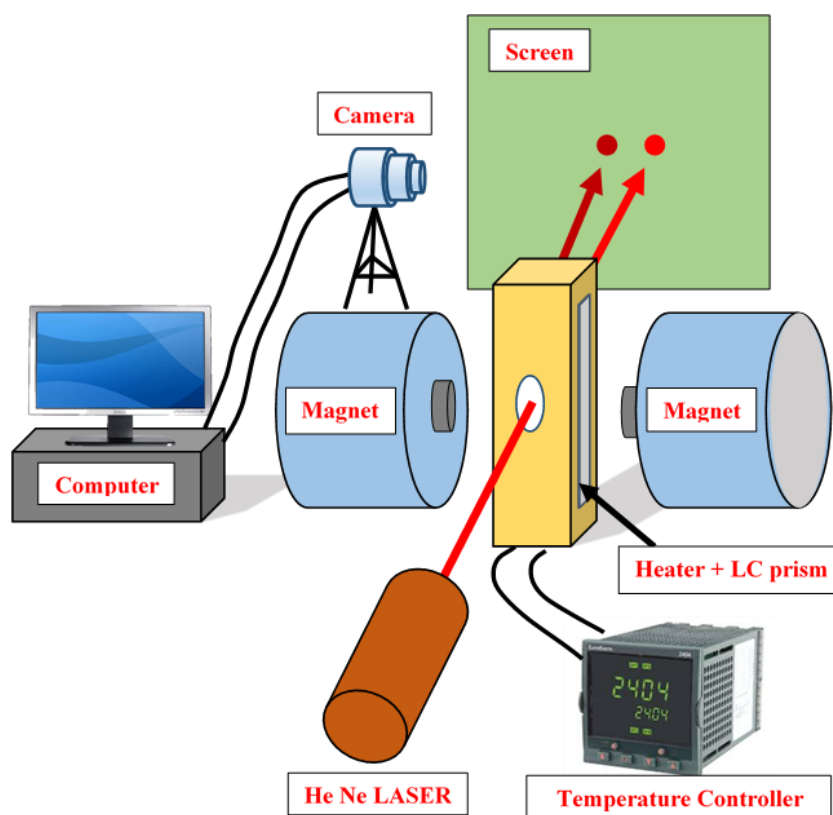


**Figure 2.2.** Schematic diagram of the experimental set-up for refractive index measurement.

An experimental set-up designed (Fig. 2.2) in such a way that a LASER beam of wavelength  $\lambda = 632.8$  nm (He-Ne laser made by Thorlab) can pass through the sample filled prism placed within a brass made heater, temperature of which was controlled by a temperature controller Eurotherm PID 2404 with an accuracy of  $\pm 0.1$  °C. The heater containing LC filled prism was placed in between two pole pieces of an electromagnet by which a magnetic field of about 1T can be applied to align the sample. After passing through the prism the incident light beam splits into the ordinary and extraordinary components and produces two spots on a white screen at a fixed distance (d). The images of such visual spots were recorded by a digital camera suitably interfaced with a computer. Moreover, by locating the center of the recorded spots, the temperature variation of ordinary ( $n_o$ ) and extraordinary ( $n_e$ ) refractive indices and hence the average refractive index  $n_{av} = \sqrt{\{(2n_o^2 + n_e^2)/3\}}$  along with birefringence ( $\Delta n$ ) has been determined by this technique with an accuracy of  $\pm 0.0006$ .

### **b. Optical transmission technique**

In order to obtain the precise value of optical birefringence ( $\Delta n$ ), the optical transmission (OT) technique [14-21] has been accomplished in which the intensity of a LASER beam transmitted through a liquid crystal filled cell and corresponding phase retardation ( $\Delta\phi$ ) has been measured. A high-intensity LASER beam of wavelength  $\lambda = 532$  nm (or 632.8 nm) was projected on a planar aligned sample filled LC cell, placed in between two crossed analyzer and polarizer (Glan-Thomson). The LC cell was placed in a brass made heater, the temperature of which was controlled and measured by a temperature controller Eurotherm PID 2404 with an accuracy of  $\pm 0.1$  °C. Additionally, to obtain better thermal stability in the experiment, a two stage heating arrangement was employed by placing the heater inside of a big heating/cooling oven which maintains a temperature difference of 3-5 K. The transmitted light intensity was acquired with the aid of a PMT module

(H10721-110, made by Hamamatsu) and stored in a computer via Keithley 2000 multimeter. During heating/cooling cycle at a rate of  $0.5\text{ }^{\circ}\text{C min}^{-1}$ , the measured data points were acquired in a computer with a programmable software at an interval of 2 or 3 seconds which leads to a temperature difference of about  $0.017\text{ }^{\circ}\text{C}$  or  $0.025\text{ }^{\circ}\text{C}$  between successive data points respectively. Furthermore, another PMT module was used to detect the fraction of incident light obtained by a beam splitter in order to monitor the stability of incident LASER beam during the experiment. Fig. 2.3 represents the experimental set-up used to measure temperature variation of the high-resolution optical birefringence for the investigated LC samples.

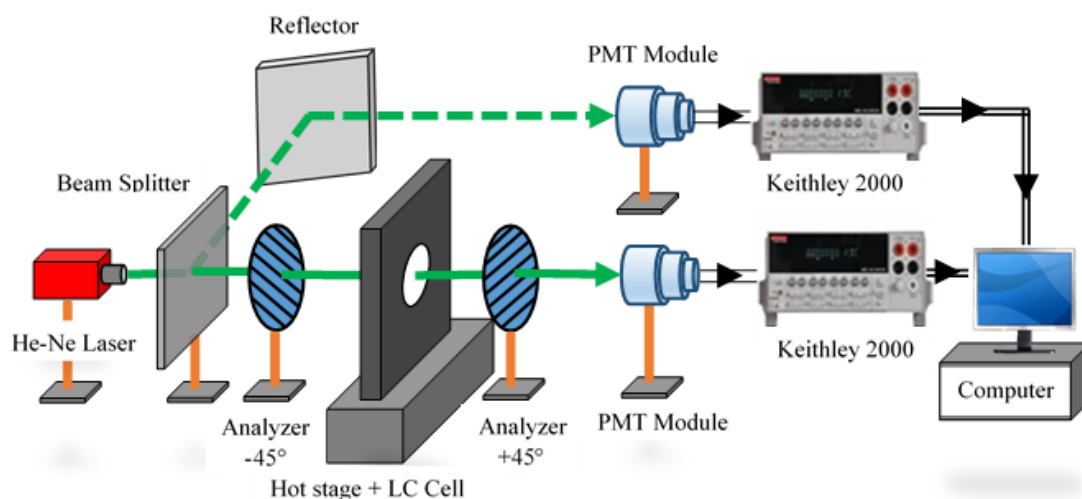


**Figure 2.3.** Schematic diagram of the experimental set-up for optical transmission measurement.

The normalized transmitted light intensity or transmittance of the LASER beam can be expressed in terms of phase retardation ( $\Delta\varphi$ ) and can be written as [22]

$$I_t = \frac{\sin^2 2\theta}{2} (1 - \cos \Delta\varphi) \quad (2.2)$$

where  $2\theta$  is the angle between the polarizer and analyzer and the corresponding phase retardation can be expressed as

---

---

$$\Delta\varphi = \frac{2\pi}{\lambda} \Delta n d \quad (2.3)$$

where  $\Delta n$  is the optical birefringence of the studied liquid crystal sample,  $d$  is the LC cell thickness and  $\lambda$  is the corresponding wavelength of LASER beam. For a precise measurement, each one of the polarizer and analyzer was held at an angle of  $45^\circ$  in clockwise and anti-clockwise directions respectively with respect to optic axis which effectively produces a total angle ( $2\theta$ ) about  $90^\circ$  or  $\pi/2$  between the analyzer and the polarizer. The oscillatory transmitted intensity of LASER beam possesses maxima and minima for  $\Delta\varphi = (2m+1)\pi$  and  $2m\pi$ , where  $m$  is an integer. Therefore, the optical birefringence value can be evaluated from the analysis of transmitted intensity data and the associated value of the phase retardation [17-21, 23].

Experimental works under this dissertation have been performed for studied liquid crystal samples filled in commercially available indium tin oxide (ITO) coated glass cells for different thickness ( $5-9 \mu\text{m}$ ) in planar as well as homeotropic alignments. As the liquid crystal samples gradually increase the molecular ordering from the isotropic state to lower temperature mesophases, all the experimental data for investigated compounds were taken during cooling cycle. The sensitivity in the measurement of  $\Delta n$  values was found to be better than  $10^{-5}$  for the  $5 \mu\text{m}$  thick sample.

### **2.2.5. Static dielectric permittivity measurement**

The liquid crystal sample act as a dielectric material and possesses dielectric anisotropy, *i.e.*, the anisotropy is present in between parallel and perpendicular (with respect to the molecular long axis or the director  $\mathbf{n}$ ) component of the dielectric permittivity. This is due to the presence of one or more polar groups or atoms attached with the organic molecules produces a dipole moment. Investigation of temperature dependent permittivities gives an idea about the intermolecular dipole-dipole interaction and relative orientation of the molecules in different mesophases. Such information about the dielectric

parameters of LC samples at different mesophases endows us to use in different application purposes.

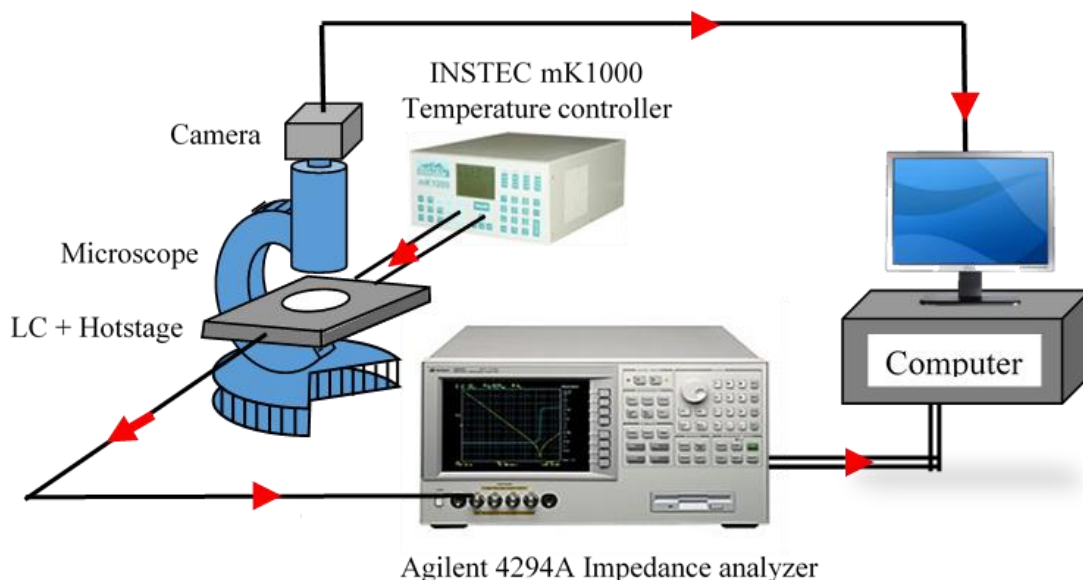


**Figure 2.4.** Schematic diagram of the experimental set-up for the dielectric study.

To obtain the temperature-dependent capacitance value, LC compounds were filled within the ITO coated cells in both planar and homeotropic alignments. The empty cell capacitance ( $C_0$ ) was measured prior to filling with samples. The LC cells were placed in a hot/cool stage (HCS 302) made by INSTEC with the aid of a programmable temperature controller mK1000 (INSTEC) having a maximum temperature resolution of  $0.001\text{ }^\circ\text{C}$ . The temperature variation of capacitance value was measured by using Agilent 4294A precision impedance analyzer (40 Hz –110 MHz) with a relative accuracy of  $\pm 0.08\%$ . Measured data points were collected in a computer suitably interfaced with the impedance analyzer [24-27]. The set-up for the measurement of dielectric study is shown in Fig. 2.4. Moreover, to determine the stray capacitance, the capacitance value of some standard materials was measured such as ultrapure water, pure benzene and *para*-xylene etc. If  $C_0$  is the capacitance of the air-filled cell and  $C_a$  is that of the empty cell excluding the stray capacitance  $C_s$ , then it can be expressed as:

$$C_0 = C_a + C_s \quad (2.4)$$

Now, for a standard material of dielectric permittivity  $\varepsilon$ , one can write it as:

$$C = \varepsilon C_a + C_s \quad (2.5)$$

where  $C$  presents the capacitance of the cell filled with the standard material. By solving the above equations it is possible to determine the related stray capacitance  $C_s$  and the dielectric permittivity of a fluid can be evaluated using the following relation:

$$\varepsilon = \frac{C - C_s}{C_0 - C_s} \quad (2.6)$$

The accuracy of the experimental setup had been validated by measuring the dielectric permittivities of the compounds 5CB and 7CB, which were found to be in close agreement with those reported in the literature [28].

In effect of applying an external voltage (fixed frequency), LC system consisting of polar molecules produces an orientational polarization in addition to their induced polarization. This orientational polarization along and perpendicular to the field direction is reflected by the measurement of dielectric permittivities. Therefore, the temperature dependent parallel ( $\varepsilon_{\parallel}$ ) and perpendicular ( $\varepsilon_{\perp}$ ) components of static dielectric permittivities for the investigated systems were determined throughout the entire mesomorphic range by using homeotropic and planar aligned cells respectively. Furthermore, the dielectric anisotropy  $\Delta\varepsilon (= \varepsilon_{\parallel} - \varepsilon_{\perp})$  and the average dielectric permittivity  $\{\varepsilon_{\text{avg}} = 1/3(2\varepsilon_{\perp} + \varepsilon_{\parallel})\}$  values were calculated with the help of the obtained parallel and perpendicular permittivity values [24-27].

### 2.2.6. Dielectric spectroscopy measurement

The dielectric spectroscopy measurement has been carried out by the computer controlled Agilent 4294A impedance analyzer (40 Hz-110 MHz) in ITO coated LC cell of different thickness both in the planar and homeotropic orientations. The sample filled cells were placed within a programmable hot stage HCS302 (INSTEC), the temperature of which was controlled and

measured by mK1000 thermo system designed by INSTRON (Fig. 2.4). Investigation of the dielectric parameters and molecular relaxations has been performed in order to obtain the real and imaginary parts of the impedance in the frequency range 40 Hz to 15 MHz with a maximum AC applied voltage of 0.5 V (RMS) to avoid nonlinear responses. The measurement was carried out at a fixed temperature and recorded in each temperature starting from the isotropic phase to the entire mesomorphic range at an interval of 1 °C. The frequency dependent complex dielectric permittivity is given by  $\varepsilon^*(f) = \varepsilon'(f) + i\varepsilon''(f)$ , where  $\varepsilon'(f)$  represents the real part of dielectric permittivity (representation spectrum is called the dispersion curve), and  $\varepsilon''(f)$  stands for the imaginary part of the complex permittivity (representation spectrum is called the absorption curve). Firstly, the capacitance ( $C_p$ ) and conductance ( $G$ ) values (in a parallel equivalent circuit) were accumulated from the instrument and then the real ( $\varepsilon'$ ) and imaginary ( $\varepsilon''$ ) parts of dielectric permittivity have been calculated from the measured  $C_p$  and  $G$  data points by using following relations [29,30]:

$$\varepsilon' = \frac{C_p - C_s}{C_0 - C_s} \quad (2.7)$$

$$\varepsilon'' = \frac{G}{2\pi f C_p} \quad (2.8)$$

where  $f$  is the frequency,  $C_0$  is the empty cell capacitance and  $C_s$  is the stray capacitance. The variation of frequency dependent  $\varepsilon'$  and  $\varepsilon''$  are displayed in Fig. 2.5 for an investigated sample.

In order to study the measured temperature dependence relaxation modes,  $\varepsilon^*(f)$  has been compared with the Havriliak-Negami (H-N) function [31,32] with the addition of a conductivity contribution (3<sup>rd</sup> term) term present at lower frequencies, which is expressed as:

$$\varepsilon^*(f) = \varepsilon_\infty + \sum_{k=1}^N \frac{\Delta\varepsilon_k}{[1 + (jf\tau_k)^{\alpha_k}]^{\beta_k}} - \frac{i\sigma_0}{\varepsilon_0(2\pi f)^n} \quad (2.9)$$

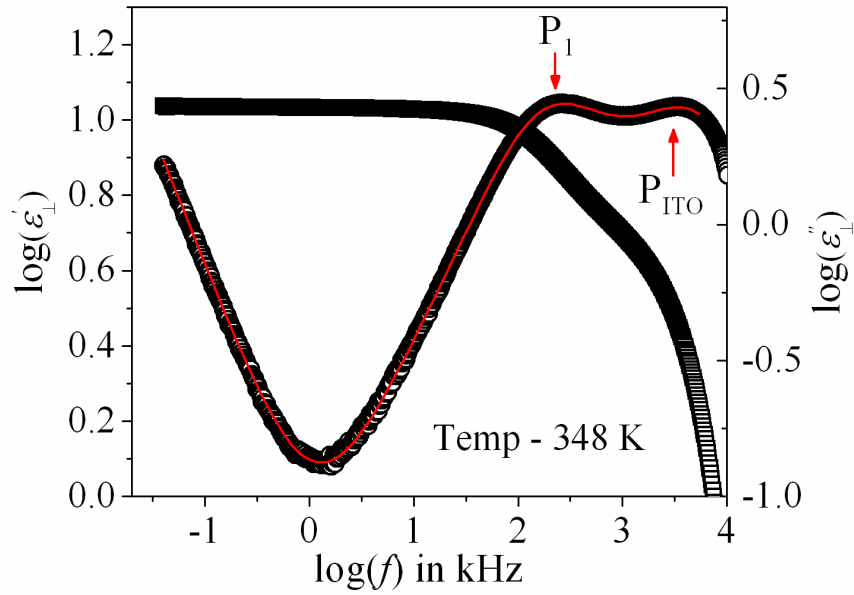


**Figure 2.5.** Frequency-dependent variation of the real ( $\epsilon'$ ) and imaginary ( $\epsilon''$ ) parts of dielectric permittivity for a fixed temperature of a bent-core compound-1/7 (described in chapter 8).

The real and imaginary parts of the complex dielectric permittivity were fitted with the Havriliak-Negami (H-N) fitting functions [33,34] given below:

$$\epsilon' = \epsilon_{\infty} + \sum_{k=1}^N \frac{\delta\epsilon_k [1 + (2\pi f\tau_k)^{\alpha_k} \cos(\alpha_k\pi/2)]}{[1 + (2\pi f\tau_k)^{2\alpha_k} + 2(2\pi f\tau_k)^{\alpha_k} \cos(\alpha_k\pi/2)]} \quad (2.10)$$

$$\epsilon'' = \frac{\sigma_0}{(2\pi f)^S} + \sum_{k=1}^N \frac{\delta\epsilon_k [1 + (2\pi f\tau_k)^{\alpha_k} \sin(\alpha_k\pi/2)]}{[1 + (2\pi f\tau_k)^{2\alpha_k} + 2(2\pi f\tau_k)^{\alpha_k} \cos(\alpha_k\pi/2)]} \quad (2.11)$$

where  $\delta\epsilon_k$  is the dielectric strength,  $\epsilon_{\infty}$  is the high-frequency limit of permittivity,  $\tau_k (=1/2\pi f_k)$  is the relaxation time,  $f$  is the corresponding relaxation frequency,  $\alpha_k$  and  $\beta_k$  are shape parameters describing the symmetric and non-symmetric broadness of the dielectric dispersion curve respectively, ranging between 0 and 1, and  $k$  is the number of relaxation processes. Here  $\sigma_0$  is related to the DC conductivity and  $S$  is a fitting parameter responsible for the slope of the conductivity. Corresponding fitting lines are also included in the representative figure (Fig. 2.5). The H-N response reduces to Cole-Davidson [35] response when  $\alpha = 1$  and to Cole-Cole [36] response when  $\beta = 1$ .

In addition to this, an external DC bias voltage was varied from 1 V to a maximum available 40 V to find the effect of applied voltage on the relaxation modes. The effect of bias voltage on the relaxation modes as well as on the optical textures at different mesophases has been studied in ITO coated cells placed between the two crossed polarizer of the optical microscope.

### 2.2.7. Splay elastic constant measurement

In case of uniaxial nematic phase, the molecular director is aligned on average in a particular direction which describes the entire phase alignment direction. However, the uniform nematic phase of the liquid crystal compounds can be deformed by applying external electric or magnetic field as well as by surface boundaries or particle inclusions. The free energy of this deformed state is evidently higher than that of the equilibrium state. Hence, due to the existence of such perturbed forces in the deformed state, some opposite elastic restoring torques of nematogens developed within the system those are always trying to restrict the deformation of the director field and known as restoring stresses [37]. In 1933, Oseen [38] and Zocher [39] proposed that such perturbations of molecular director (director curvature) can be well described by the elastic continuum theory which is analogous to the classical elastic theory of solids. Furthermore, in 1958, Frank [37] explored it again by presenting the theory of curvature elasticity. Basically, each of the deformation modes are described individually by an elastic constant [40-44] and expressed as follows: the splay ( $K_{11}$ ), twist ( $K_{22}$ ) and bend ( $K_{33}$ ) elastic constants which are also known as the Frank elastic moduli. According to the elastic continuum theory [44], the elastic free energy of deformed nematic phase is given by:

$$F_{def} = \frac{1}{2} \left[ K_{11} (\vec{\nabla} \cdot \hat{n})^2 + K_{22} (\hat{n} \cdot \vec{\nabla} \times \hat{n})^2 + K_{33} (\hat{n} \times \vec{\nabla} \times \hat{n})^2 \right] \quad (2.12)$$

where  $K_{11}$ ,  $K_{22}$  and  $K_{33}$  are the elastics constants known as Frank elastic constant whereas  $\hat{n}$  is the nematic director.

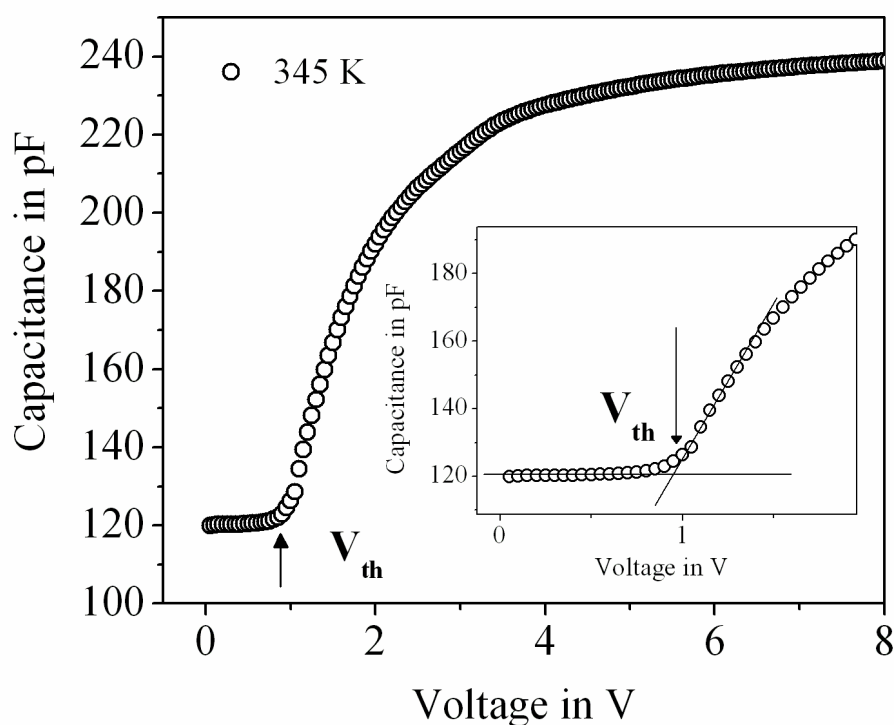


**Figure 2.6.** Voltage dependent variation of sample filled cell-capacitance due to electrically driven Fredericksz transition in the nematic phase of a binary mixture (described in chapter 4) at 345 K. Inset shows the closer view near the threshold voltage.

Out of them, this dissertation only deals with the measurement of splay elastic constant for the nematic liquid crystal sample by the method of field-induced Fredericksz transition [45-48]. Although the Fredericksz transition can be observed by an externally applied electric [49-51] or magnetic field [52-56], only the electric field has been applied in the experiments. Due to an application of sufficiently strong electric field to a planar aligned mesogenic medium in an orthogonal direction to the molecular long axis, the Fredericksz transition [49-51] develops within the system, resulting in a deformation of the molecular directors along the field direction. Beyond this Fredericksz threshold voltage ( $V_{th}$ ), the capacitance value ( $C_{\perp}$ ) for planar aligned sample sharply increases up to a saturation value ( $C_{\parallel}$ ) as shown in Fig. 2.6. However, these  $V_{th}$  and  $C_{\parallel}$  both depend upon the sample temperature.

Prior to determining the splay elastic constant ( $K_{11}$ ), at first the threshold voltage was evaluated in planar aligned ITO coated LC cell of suitable thickness by applying a sinusoidal voltage whose amplitude is maximum up to 20 Volt at a fixed frequency of 1 kHz. The capacitance value ( $C$ ) of the nematic liquid crystal was measured by the small variation of applied electric field voltage ( $V$ ) by using Agilent E4980A precession LCR-bridge with an accuracy of  $\pm 0.05\%$  [49,57-59]. This process has been performed at a fixed temperature and recorded it in a computer in each temperature starting from the isotropic phase to the entire nematic phase at a small temperature interval. Fig. 2.6 represents a voltage-dependent capacitance curve at a fixed temperature for a LC sample in the nematic phase. During this experiment, the temperature was controlled and measured by a temperature controller Eurotherm PID 2404 with an accuracy level  $\pm 0.1$  °C. The temperature dependent values of threshold voltage  $V_{th}$  (value of applied voltage where the deformation starts) were calculated from this  $C$ - $V$  curve and hence the splay elastic constant was determined by the following relation [60-62]:

$$K_{11} = \frac{\epsilon_0 \Delta \epsilon V_{th}^2}{\pi^2} \quad (2.13)$$

where  $\Delta \epsilon$  is the dielectric anisotropy value of that nematic LC sample and  $\epsilon_0$  is the free space permittivity, while  $V_{th}$  is the threshold voltage in r.m.s.

### 2.2.8. Rotational viscosity measurement

The rotational viscosity ( $\gamma_1$ ) of the nematic liquid crystal is the crucial parameter for the application purpose in display technology [63]. The rotational viscosity of the material defines the molecular dynamics of the molecules within the sample and it is correlated to the torque associated with the molecular rotation in response to an external perturbing field. Moreover, it is dependent upon the molecular structure and their association as well as the temperature of the compound. Due to the rotation of molecules, an internal

friction between the molecular directors is developed which is represented by the rotational viscosity of that material. Therefore, the higher value of rotational viscosity corresponds to a slower response to the external field and vice versa.

For the investigated LC systems, firstly the response time ( $\tau_0$ ) and consequently the rotational viscosity ( $\gamma_1$ ) values were determined by capacitive relaxation method [25,58,64] with the aid of Agilent 4980A digital impedance analyzer. An external AC voltage ( $V$ ) having a magnitude above the corresponding threshold voltage ( $V_{th}$ ) at a frequency 10 kHz has been applied in the nematic phase. The investigated sample was mounted in a planar aligned ITO coated cell of suitable thickness. After a certain time interval (in second), when the external field was suddenly removed, the molecular directors start to reorient to the equilibrium state (or energy-minimized state) and the time taken by the molecules to be relax back was characterized by the relaxation time ( $\tau_0$ ) of the nematic LC sample at a particular temperature. Hence, a voltage-dependent value of capacitance was accumulated through the impedance analyzer and stored in a computer with the help of programmable software. This process was repeatedly done in a certain temperature interval starting from the isotropic phase over the entire nematic phase. For a particular temperature, the difference between the instantaneous capacitance ( $C_t$ ) at a particular time  $t$  and the equilibrium state capacitance ( $C_{\perp}$ ) (for homogeneous alignment) in a small signal regime execute [64] a simple exponential decay curve which can be expressed as:

$$\Delta C_t = C_t - C_{\perp} = \Delta C_0(\exp(-2t/\tau_0)) \quad (2.14)$$

where  $\tau_0$  is the relaxation time and  $\Delta C_0 \approx C_{\perp}(\Delta\varepsilon/2\varepsilon_{\perp})\phi_m$  for planar alignment cell in which  $\Delta\varepsilon$  is the dielectric anisotropy,  $\varepsilon_{\perp}$  is the perpendicular component of the static dielectric permittivity,  $C_{\perp}$  is the capacitance of the cell when the molecules are aligned orthogonal to the substrate and  $\phi_m$  is the director tilt angle at the middle of the layer at time  $t = 0$ , *i.e.*, when the relaxation is being

---

initiated. Furthermore, several experimental results [64] reveal that Eq. (2.14) demonstrates a good approximation for  $\varphi_m < 1$ . Therefore, the relaxation time ( $\tau_0$ ) was measured from the slope of a logarithmic plot of the transient capacitance ( $\Delta C_t/C_\perp$ ) as a function of time at a particular temperature and hence the required rotational viscosity for a planar aligned LC sample of thickness  $d$  can be calculated by using the following relation [25,58,60,64]:

$$\gamma_1 = \frac{\tau_0 K_{11} \pi^2}{d^2} \quad (2.15)$$

where  $K_{11}$  is the splay elastic constant for that compound. By varying the temperature at a certain interval, the temperature dependent rotational viscosity has been measured throughout in the entire nematic mesophase.

### 2.2.9. Electro-optical study

The electro-optical study for the investigated LC compounds was carried out by the field reversal polarization technique [65-68]. The LC materials were filled in planar aligned LC cells of a suitable thickness having an active area of about  $0.25 \text{ cm}^2$  in between the ITO coated substrates. In this technique, an external electric field (square wave) having magnitude  $V_{pp} = 38 \text{ V}$  at frequency,  $f = 20 \text{ Hz}$  was applied to LC cells to drive a microscopic current through the material. For this purpose, a waveform generator Picotest G100A and the FLC (F20A) voltage amplifier (amplification factor 20 times) was used. The response current was measured from the value of voltage drop across the resistance connected in series to the sample filled cell as shown in Fig. 2.7. In some cases, triangular wave voltage has also been applied. Hence, an effective voltage  $\sim 8 \text{ Volt per } \mu\text{m}$  acts on each cell and often higher voltage was applied to acquire the polarization effect in some LC samples. As the polarization was inverted by the input voltage, the polarization current pulse thus obtained and fed to a Digital Storage Oscilloscope (Agilent DSO X2000A). The input and output waveforms were obtained in a computer suitably interfaced with the oscilloscope. This polarization current pulse

represents a hump in the spectrum while a sharp peak was observed in case of a triangular wave input voltage. Fig. 2.8(a) and Fig. 2.8(b) represent the input and output waveforms for both the square and triangular waves respectively.

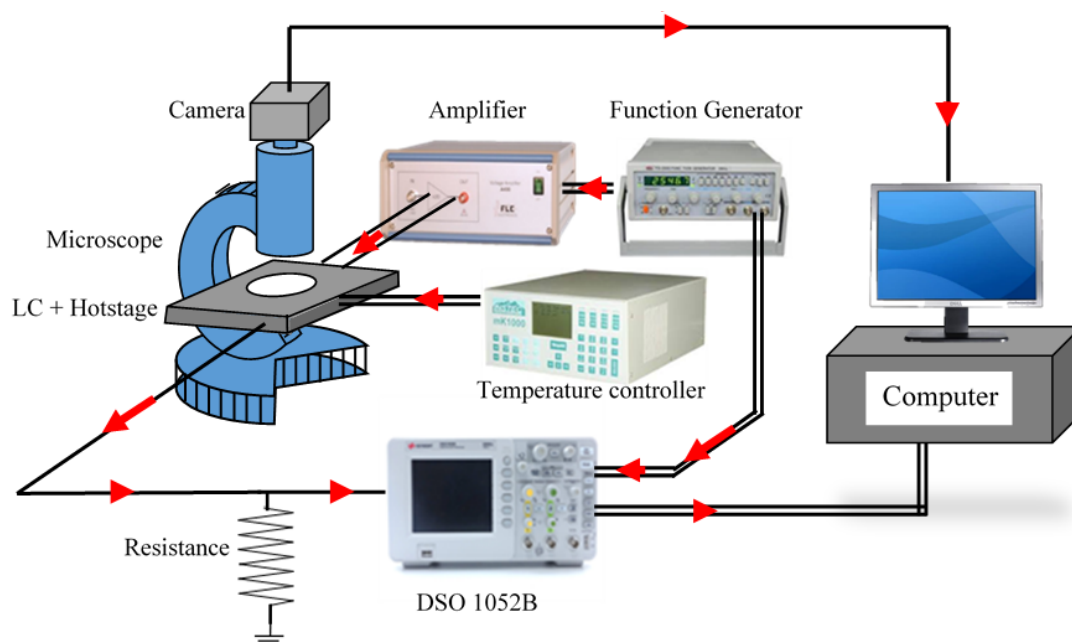


**Figure 2.7.** Schematic diagram of the experimental set-up for electro-optical study using field reversal polarization technique.

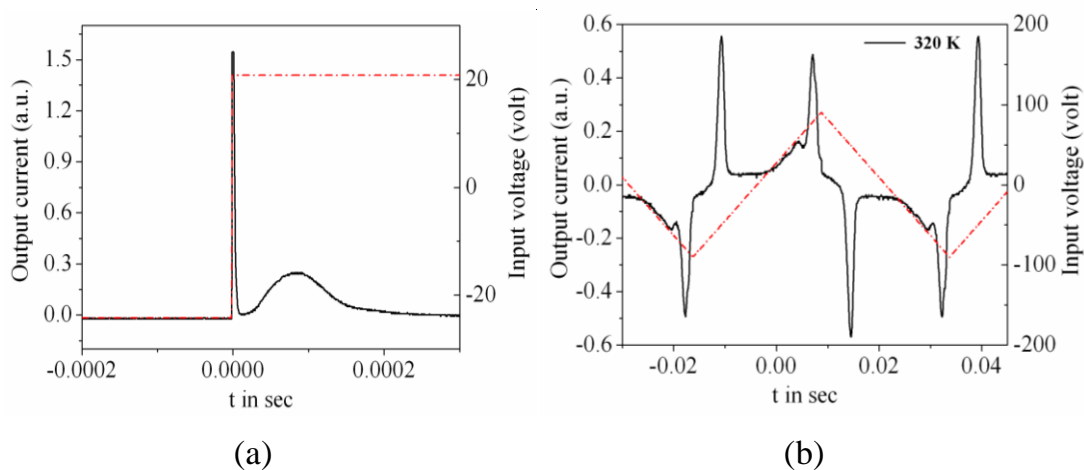


**Figure 2.8.** Input and output waveforms of the LC sample for (a) square wave and (b) triangular wave input voltages.

Moreover, the LC cell was placed in a hot/cool stage HCS 302 designed by INSTRON, USA, equipped with a programmable temperature controller mK1000, by which temperature was varied at a rate of 0.5 K per minute.

Additionally, the optical textures were also observed at the ON and OFF state of the external field to detect the polarization effect visually.

The liquid crystal material sandwiched between two electrode surfaces can be regarded as a parallel combination of a capacitor ( $C$ ) and a resistance ( $R$ ). Hence, for the given circuit arrangement, a polarization current ( $I_p$ ) is produced in the LC cell due to the reorientation of polarization ( $\vec{P}_s$ ) for the reversal effect of the input voltage. In addition to this, there exist two more current components, the current  $I_C$  for the charge accumulation in LC cell capacitor and the current  $I_I$  is produced due to the ionic contribution of liquid crystal sample. Therefore, an effective current ( $I$ ) pass through the LC cell [66] can be written as:

$$I = I_p + I_C + I_I = \frac{dP}{dt} + C \frac{dV}{dt} + \frac{V}{R} \quad (2.16)$$

where  $P$  represents the induced charge due to the polarization realignment, *i.e.*, the amount of induced charge at the time of sign reversal of spontaneous polarization ( $P_s$ ) in accordance with the input voltage.  $R$  is the effective resistance in the circuit where  $V$  is the voltage of input signal. In order to determine the polarization current ( $I_p$ ), neglecting the other contributions in output current, a proper baseline correction has to be performed by using mathematical software. However, the spontaneous polarization values were evaluated by integrating the hump/peak area ( $A$ ) of the output current spectrum by the following expression [68]:

$$P_s = \frac{1}{2A} \int I dt \quad (2.17)$$

In this study, the values of the spontaneous polarization have been measured with a precision of  $\pm 0.9$  nC/cm<sup>2</sup>.

Additionally, the relaxation time or response time ( $\tau$ ) has also been obtained by measuring the time taken by the output current to fall or rise from 10% to 90% of the peak value in response to the square wave input signal [69] and it can be expressed as [68,69]:

$$\tau = \frac{t_{10-90}}{1.8} \quad (2.18)$$

The effective torsional bulk viscosity ( $\eta$ ) was obtained using the following relation:

$$\eta = P_s E \tau \quad (2.19)$$

where  $E$  is the externally applied electric field. In this study, the free relaxation time and the effective torsional bulk viscosity were determined within an accuracy of  $\pm 1 \mu\text{s}$  and  $\pm 0.9 \text{ Pa s}$  respectively.

## 2.3. Theoretical background

### 2.3.1. Maier-Saupe Theory

There are several fundamental theories regarding the liquid crystal mesophases and associated phenomenological theories related to different mesophase transitions. Among them, the molecular mean-field approximation is the simplest theoretical approach to describe the thermodynamical behavior of the nematic phase as well as the qualitative discussion about the isotropic-nematic phase transition. According to mean field theory, molecules are assumed to be rod-like and possess cylindrical symmetry with a tendency to align their long axes in a particular direction (director,  $\hat{n}$ ). Again, a molecule orients under the action of a mean field due to interactions with the other molecules of the system. Maier-Saupe [70-72] proposed the most successful microscopic theory to explain the statistical behavior of the molecules in the nematic phase (many particle systems) by assuming some approximations as follows:

(i) An attractive interaction between the adjacent molecules acts in the nematic phase.

(ii) The anisotropic part of the dispersion interaction energy between the molecules is responsible for the nematic molecular ordering within the system.

(iii) Due to the presence of long-range nematic orientational ordering, LC molecules are assumed to be neutrally charged and thus the influence of

permanent dipoles can be totally ignored.

(iv) The effect of induced dipole-dipole interaction should be considered for sustaining the nematic phase. However, the momentary dipole moment of one molecule induces the same to another molecule which results in an attractive interaction between them.

(v) The LC molecules are supposed to be considered as cylindrically symmetric along the long axis and the mutual interaction between any two adjacent molecules depends upon their relative angle.

(vi) The distribution of the molecular center of mass for the adjacent molecules is spherically symmetric with respect to a particular molecule.

In case of nematic liquid crystal system, Maier and Saupe proposed the concept of orientational ordering for the constituent molecules. Here the molecules are averagely aligned towards a particular direction, but due to the presence of external mean field the molecular long axes are distributed with respect to the director ( $\hat{n}$ ) as a function of the angle ( $\theta$ ) between them. Thus each of the molecules are considered to experience an average attractive potential  $V(\cos\theta)$  which can be expressed as:

$$V(\cos\theta) = \sum_{L-even} U_L \langle P_L \rangle P_L(\cos\theta) \quad (L \neq 0) \quad (2.20)$$

where  $U_L$  is the function depends on the least distance between the central molecule and its adjacent neighbors only.  $\langle P_L \rangle$  are termed as the orientational order parameters.  $P_L(\cos\theta)$  is the  $L^{\text{th}}$  even order Legendre polynomial and the statistical average of  $P_L(\cos\theta)$  is given by

$$\langle P_L(\cos\theta) \rangle = \int_0^1 P_L(\cos\theta) f(\cos\theta) d(\cos\theta) \quad (2.21)$$

However, the orientational distribution function  $f(\cos\theta)$  in the nematic phase may be written as:

$$f(\cos\theta) = \sum_{L-even} \frac{(2L+1)}{2} \langle P_L(\cos\theta) \rangle P_L(\cos\theta) \quad (2.22)$$

Here the molecules in the nematic phase possess the head-tail symmetry, thus  $f(\cos\theta)$  is an even function of  $\cos\theta$ . Again, by assuming  $L = 2$ , Eq. (2.21) modified as:

$$\langle P_2(\cos\theta) \rangle = \int_0^1 P_2(\cos\theta) f(\cos\theta) d(\cos\theta) \quad (2.23)$$

Generally, this  $\langle P_2 \rangle$  is known as the order parameter for the liquid crystal system. The value of  $\langle P_2 \rangle$  is considered as zero for an isotropic liquid while  $\langle P_2 \rangle = 1$  for a perfectly ordered state or in crystal phase.

Consequently, the potential energy for a single molecule can be written by modifying Eq. (2.20) as follows:

$$V(\cos\theta) = -\nu P_2(\cos\theta) \langle P_2 \rangle \quad (2.24)$$

where  $\nu = -U_2$ . However, the single-molecule orientational distribution function takes the form

$$f(\cos\theta) = Z^{-1} \exp[-V(\cos\theta)/kT] \quad (2.25)$$

where  $k$  is the Boltzmann's constant and  $Z$  serves to normalize the function  $f(\cos\theta)$  which is the single molecule partition function that can be expressed as

$$Z = \int_0^1 \exp[-V(\cos\theta)/kT] d(\cos\theta) \quad (2.26)$$

Substituting all the values in Eq. (2.23), one can write

$$\langle P_2(\cos\theta) \rangle = \frac{\int_0^1 P_2(\cos\theta) \exp[P_2(\cos\theta) \langle P_2 \rangle / T^*] d(\cos\theta)}{\int_0^1 \exp[P_2(\cos\theta) \langle P_2 \rangle / T^*] d(\cos\theta)} \quad (2.27)$$

where,  $T^* = kT/\nu$ .

This is a self-consistent equation as it consists the term  $\langle P_2 \rangle$  on both sides of the equation and the solution of it can be easily obtained by an iterative method in which one can get a temperature ( $T^*$ ) dependent specific value of  $\langle P_2 \rangle$  or of the order parameter. Now, in this case, one solution appears as  $\langle P_2 \rangle = 0$  for all the temperatures in the isotropic or completely disordered phase.

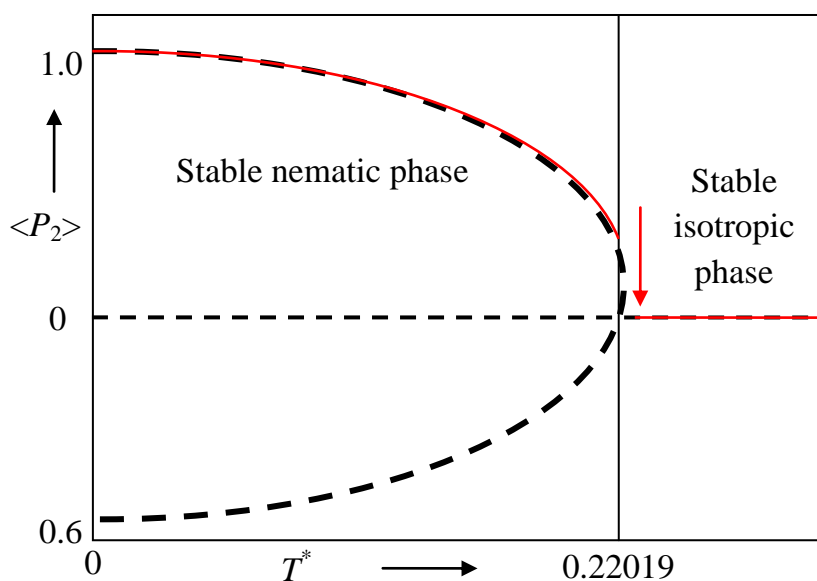


**Figure 2.9.** Orientational order parameter predicted from Maier-Saupe mean field theory.

Besides, two more solutions can be found for the temperatures  $T^* < 0.22284$ , as observed in Fig. 2.9. Eventually, a stable nematic phase exist with  $\langle P_2 \rangle$  greater than zero for a condition  $0 \leq T^* \leq 0.22019$  and for rest of the temperature range  $T^* > 0.22019$ , it reveals a thermodynamically stable isotropic phase having  $\langle P_2 \rangle = 0$ . However, by increasing temperature, the value of the order parameter  $\langle P_2 \rangle$  decreases from unity (for completely ordered phase) to a minimum value about 0.4289 at  $T^* = 0.22019$ . Therefore, the pronounced  $I-N$  phase transition occurs at that temperature following a discontinuous change of  $\langle P_2 \rangle$  from 0.4289 to 0 which reveals a first-order nature of the  $I-N$  phase transition. On the contrary, this transition is quite different than the solid to liquid first-order transition from the perspective issue of entropy change. The amount of entropy change is about  $25 \text{ cal K}^{-1} \text{ mole}^{-1}$  for usual solid-liquid transition while it is about  $0.83 \text{ cal K}^{-1} \text{ mole}^{-1}$  for the  $I-N$  phase transition which often known as weakly first-order transition. In several nematic LC compounds, the experimental data points of temperature dependent  $\langle P_2 \rangle$  represents a close

agreement with the  $\langle P_2 \rangle$  values obtained by solving self-consistent equation iteratively [43,73,74].

### 2.3.2. McMillan theory for the Sm-A phase

In order to characterize the macroscopical view-point of the Sm-A mesophase and also to reveal a satisfactory explanation about the N–Sm-A phase transition, McMillan [75,76] and Kobayashi [77-79] somewhat extended the mean field theory by considering an additional order character in the Sm-A phase. In general, the molecules in Sm-A phase possesses a one-dimensional positional ordering in addition to long-range orientational ordering of the nematic phase, *i.e.*, a periodic mass-density wave is present along the normal direction of smectic layers. Therefore, in order to sustain both the properties (parallel orientation of the molecular long axis along the director and the layer formation perpendicular to the director), a positional order parameter term is introduced in the expression of mean field potential energy function to describe the one-dimensional translational periodicity of the layered structure [75,76]. The effect of layering eventually leads to an enhancement of the orientational order parameter in the smectic phase relative to the nematic phase. However, in the Sm-A phase, the complete set of order parameters may be obtained by expanding the distribution function of a single molecule which depends on both spatial and angular coordinates. Hence, according to McMillan theory, the single molecule normalized distribution function for the Sm-A phase can be written as:

$$f(\cos \theta, z) = \sum_{L-even} \sum_n A_{L,n} P_L(\cos \theta) \cos\left(\frac{2\pi n z}{d}\right) \quad (2.28)$$

where  $d$  is the layer thickness and the expansion coefficients those are related to the Sm-A phase order parameters [80] can be expressed as:

$$A_{L,n} = \{(2L + 1)/d\} \langle P_L(\cos \theta) \cos\left(\frac{2\pi n z}{d}\right) \rangle \quad L \neq 0, n \neq 0 \quad (2.29)$$

and the normalization condition is given by

$$\int_{-1}^1 \int_0^d f(\cos \theta, z) dz d(\cos \theta) = 1 \quad (2.30)$$

Following Kobayashi [77-79], McMillan [75,76] has considered an anisotropic term in pair interaction energy function. Therefore, by averaging the pair interaction potential for a single molecule over the second molecule it can be written as:

$$V_M(\cos \theta, z) = \langle U(r) \rangle + \langle W(r) P_2(\cos \theta) \rangle P_2(\cos \theta) \quad (2.31)$$

where  $\langle U(r) \rangle$  and  $\langle W(r) P_2(\cos \theta) \rangle$  are the functions of  $z$ , the spatial coordinates of the molecular center of mass with respect to smectic layer, while  $\langle \dots \rangle$  denotes the statistical average of the quantities inside.  $\theta$  is the angle between the molecular long axis with respect to the director.

By expanding it in Fourier series and taking the suitable averages, the potential function becomes

$$V_M(\cos \theta, z) = U_0 + U_1 \tau \cos\left(\frac{2\pi z}{d}\right) + \dots + [W_0 \eta + W_1 \sigma \cos\left(\frac{2\pi z}{d}\right) + \dots] P_2(\cos \theta) \quad (2.32)$$

where  $U_0, U_1, W_0, W_1$  are the Fourier coefficients and  $\eta, \tau$  and  $\sigma$  are the leading order parameters those can be represented as :

$$\text{Orientational order parameter: } \eta = \langle P_2(\cos \theta) \rangle \quad (2.33)$$

$$\text{Translational order parameter: } \tau = \langle \cos(2\pi z/d) \rangle \quad (2.34)$$

$$\text{Mixed order parameter: } \sigma = \langle P_2(\cos \theta) \cos(2\pi z/d) \rangle \quad (2.35)$$

Moreover, due to the existence of short-range force, McMillan has considered the coefficients as  $W_0 = -v, W_1 = -v\alpha$  and  $U_1 = \delta W_1 = -\delta v\alpha$  where  $\alpha$  and  $\delta$  are the pair potential parameters.  $\alpha$  is related to the length of the molecules and  $\delta$  is associated with the ratio of the translational part of the potential to the orientational part of the same.

Consequently, the expression for effective pair potential of a single molecule in the Sm-A phase assumes the form

$$V_M(\cos \theta, z) = -v \left[ \delta \alpha \tau \cos \left( \frac{2\pi z}{d} \right) + \left\{ \eta + \alpha \sigma \cos \left( \frac{2\pi z}{d} \right) \right\} P_2(\cos \theta) \right] \quad (2.36)$$

Again, the distribution function for a single molecule can be expressed in terms of potential energy as follows:

$$f_M(\cos \theta, z) = Z^{-1} \exp[-V_M(\cos \theta, z)/kT] \quad (2.37)$$

where  $Z$  is the normalized partition function and can be written as:

$$Z = \int_0^1 \int_0^d \exp[-V_M(\cos \theta, z)/kT] d(\cos \theta) dz \quad (2.38)$$

Therefore, the self-consistency equations for the above-mentioned order parameters appear as:

$$\eta = \int_0^1 \int_0^d P_2(\cos \theta) f_M(\cos \theta, z) d(\cos \theta) dz \quad (2.39)$$

$$\tau = \int_0^1 \int_0^d \cos(2\pi z/d) f_M(\cos \theta, z) d(\cos \theta) dz \quad (2.40)$$

$$\sigma = \int_0^1 \int_0^d P_2(\cos \theta) \cos(2\pi z/d) f_M(\cos \theta, z) d(\cos \theta) dz \quad (2.41)$$

Depending on the values of different potential parameters, the following three cases can be obtained:

i) when  $\eta = \tau = \sigma = 0$ , corresponds to the isotropic or completely disordered phase;

ii) when  $\eta \neq 0$ ,  $\tau = \sigma = 0$ , corresponds to the nematic phase where only orientational ordering is present.

iii) when  $\eta \neq 0$ ,  $\tau \neq 0$ ,  $\sigma \neq 0$ , corresponds to smectic-A phase where both orientational and translational ordering is present.

All such significant solutions are obtained by solving the self-consistent Eqs. (2.39–2.41) by iteration method at several sets of values for  $\alpha$  and  $\delta$ . The major success of the McMillan theory is based on the prediction of the order nature of the nematic–smectic-A phase transition over the value of  $\alpha$  and  $\delta$ . If the value of  $\alpha > 0.98$ , there exhibit a direct transition from smectic-A to isotropic phase without stable nematic phase at any temperature. On the other

---



---

hand for  $\alpha < 0.98$ , it reveals two phase transition namely the isotropic–nematic ( $I-N$ ) phase transition followed by the nematic–smectic- $A$  ( $N-Sm-A$ ) phase transition at comparatively low temperature. Although, McMillan theory divulges the  $I-N$  phase transition is of first order in nature, but the  $N-Sm-A$  transition can be either first order or second order depending on the value of  $\alpha$  and a ratio (McMillan ratio) of the nematic–smectic- $A$  and the isotropic–nematic phase transition temperatures respectively, *i.e.*,  $T_{NA}/T_{IN}$ . When  $\alpha < 0.7$  and  $T_{NA}/T_{IN} < 0.87$ , it demonstrates a second order nature of the nematic–smectic- $A$  ( $N-Sm-A$ ) phase transition, whereas the value of  $T_{NA}/T_{IN}$  beyond 0.87, the  $N-Sm-A$  phase transition envisages a first-order transition in nature. Hence, this particular limiting point ( $\alpha = 0.7$  and  $T_{NA}/T_{IN} = 0.87$ ) where the  $N-Sm-A$  phase transition transforms its nature from second order to first order is referred to a tricritical point (TCP).

### 2.3.3. Landau-de Gennes theory for the $I-N$ and $N-Sm-A$ phase transitions

In LC system, Landau-de Gennes theory [80] is another qualitative endeavor as like mean-field theory which provides the semi-quantitative description about the isotropic–nematic transition. According to Landau, the free energy of the system is simply an analytic function of the order parameter and it is dependent upon the spatial derivatives at least near a second order phase transition [81,82]. To demonstrate a satisfactory explanation of the phase transitional phenomena in a macroscopic region, an extension of the Landau phenomenological theory [81,82] has been modified further by de Gennes [83], and again a brief review was given by Sheng and Priestly [84]. Thus, the Landau-de Gennes theory is a macroscopic manifestation of classical field theory, where the free energy function of the system can be expressed in terms of the order parameter in a power series in close vicinity to the transition. However, the order parameter is correlated with the symmetry of the thermodynamic system and further, a breaking of symmetry is associated with

a phase transition. Therefore, the order parameter of any thermodynamical system gathers the information about the change of symmetry as well as the change in different physical quantities in the neighborhood of phase transition.

According to Landau theory, the free energy density  $f$  (function of temperature  $T$ , pressure  $P$ , and order parameter  $S$ ) in the absence of any external field can be expanded in power series with a lower ordered polynomial in terms of scalar order parameter  $S$  and generally expressed as:

$$f(T, S) = f(T, 0) + \alpha S + \frac{1}{2}(AS^2) + \frac{1}{3}(BS^3) + \frac{1}{4}(CS^4) + \dots \quad (2.42)$$

where  $\alpha, A, B, C, \dots$  are the phenomenological coefficients as well as a function of temperature and pressure but having no inherent physical significance. The free energy density in the most disordered phase is denoted by  $f(T, 0)$ .

In order to characterize the order parameter  $S$  of a system at a certain temperature  $T$ , the minimization condition  $\left(\frac{df}{dS}\right) = 0$  is imposed on the free energy density function  $f$ , which results  $\alpha = 0$  and  $\frac{d^2f}{dS^2} = A$  for the disordered phase, *i.e.*,  $S = 0$ . Again from the symmetry consideration, the system has the reflection symmetry about  $xy$ -plane, which remains unchanged the free energy function for changing  $S(\hat{z}) \rightarrow S(-\hat{z})$ , *i.e.*,  $f(S) = f(-S)$ . Therefore, the free energy function takes the form as an even function of the order parameter  $S$  leading to vanish the odd terms in the power series and hence  $B = 0, D = 0$  etc. Thus, the remaining free energy density expression becomes

$$f(T, S) = f(T, 0) + \frac{1}{2}(AS^2) + \frac{1}{4}(CS^4) + \dots \quad (2.43)$$

However, the coefficients were previously assumed as phenomenological, but it is still undefined about their dependency on the temperature. For this reason, all the coefficients can be expressed in power series with respect to the transition temperature  $T_C$ .

$$A(T) = a_0 + a'(T - T_C) + \dots ,$$

$$C(T) = c_0 + c'(T - T_C) + \dots \quad \text{and so on.}$$

In this context, Landau has assumed that very close to the transition temperature ( $T \approx T_C$ ),  $a_0 = 0$  which again yields  $A(T) = a'(T - T_C)$ . Likewise, the second coefficient, the linear term can be neglected near the transition temperature which gives  $C(T) = c_0$ .

Now substituting all these values in Eq. (2.54), one can write:

$$f(T, S) = f(T, 0) + \frac{1}{2}a'(T - T_C)S^2 + \frac{1}{4}c_0S^4 + \dots \quad (2.44)$$

Furthermore, to determine the equilibrium value of  $S$ , the minimization condition is applied on the effective free energy density expression which gives  $a'(T - T_C)S + c_0S^3 = 0$ , and consequently the effective outcomes are represented as:

- (i) One real solution,  $S = 0$ , for  $T \geq T_C$  indicates a disordered phase.
- (ii) Three other real solutions  $S = 0, \pm \left(\frac{a'(T_C - T)}{c_0}\right)^{1/2}$ , for  $T < T_C$  in which first one ( $S = 0$ ) depicts a local maxima and the other two symbolizes the positive and negative minima in free energy density curve as a function of order parameter  $S$ .

These solutions signify that the behavior of the order parameter  $S$  follows a scaling relation in the vicinity of transition point which can be expressed as:

$$S \propto (T_C - T)^\beta \quad (2.45)$$

where  $\beta$  is the order parameter critical exponent which gives a value 1/2 in mean field theory for Ising model, while in more precise theoretical and experimental reviews demonstrated a value 1/8 for 2D Ising model and  $\approx 0.31$  for 3D Ising system.

Furthermore, the phenomenological Landau theory, discussed in the previous section has been extended by de Gennes [83] to elucidate the first order mesophase transition exhibited by nematogens by including two basic

assumptions [85] – (i) The free energy density expansion (Eq. (2.42)) must contain up to sixth order term in which the coefficient of the third order term  $B$  assumes a value equal to zero, while  $C < 0$  and the coefficient of the sixth term  $E > 0$  is required to preserve the stability of the ordered phase. (ii) On the other hand, the third order term  $BS^3$  is required in the free energy expansion as it is a tensorial quantity. Therefore, a first order mesophase transition can be obtained for a condition  $B \neq 0$ . The  $I-N$  phase transition defined so far in Landau theory as a second order nature because the molecules do not reveal any ordering in the isotropic phase and exhibit a continuous change in the order parameter value at the transition point [80,83-88]. Nevertheless, close investigation near the transition point suggests that the molecules are locally oriented in parallel to each other, results in a local molecular order which persists over a finite extent. de Gennes [83] named it as coherence length, which is dependent upon the temperature. Using this conceptual frame of reference and other thermodynamical assumptions, de Gennes [83] first successfully employed the power expansion series of the order parameter in a tensorial form in order to explain the first order nature of the isotropic-nematic ( $I-N$ ) phase transition in liquid crystal systems. Generally, the nematogens are portrayed by an order parameter in the form of a traceless symmetric tensor, called the order tensor ( $X$ ) *i.e.*,  $X_{ii} = 0$  [43]. Now, in this case, the free energy density can be expressed in a power series in terms of tensorial order parameter  $X$  as follows:

$$f_n = f_i + \frac{1}{2}A(X_{ij}X_{ji}) - \frac{1}{3}B(X_{ij}X_{jk}X_{ki}) + \frac{1}{4}C(X_{ij}X_{ji})^2 \quad (2.46)$$

where  $f_i$  and  $f_n$  represents the Helmholtz's free energy at the isotropic and nematic phases respectively and  $A, B, C$  are the free energy coefficients in the form of a tensor. Now being a scalar, the Helmholtz's free energy expansion in powers of  $X$  containing only the terms those have invariant combinations of  $X_{ij}$  of the order parameter [86]. However, the negative sign of  $B$  is chosen for convenience.

Now this free energy expansion emerges a mesophase transition near the transition point if the coefficient  $A$  vanishes, *i.e.*,  $A = 0$ , but has no dependency on  $B$  and  $C$ . Thus it can be concluded that this phase transition is always driven by the influence of the coefficient  $A$  and assumed to take a form as  $A = A'(T - T^*)$ . Here  $T^*$  is the super-cooling temperature which is close to the  $I-N$  transition temperature while  $B$  and  $C$  are taken to be constant. Furthermore, for a uniaxial liquid crystal system,  $X_{ij}$  can be written as  $X_{ij} = 1/2[S(3n_i n_j - \delta_{ij})]$ , where  $S$  is the scalar order parameter and  $\delta_{ij}$  is the identity tensor. Substituting all these values into Eq. (2.46), the free energy density assumes a form:

$$f_n = f_i + \frac{1}{3}A'(T - T^*)S^2 - \frac{2}{27}BS^3 + \frac{1}{9}CS^4 \quad (2.47)$$

In order to determine the value of order parameter in an equilibrium state, minimization condition is applied on the effective free energy density expression which provides the equilibrium order parameter values as follows:

(i)  $S = 0$ , for the isotropic phase, and

$$(ii) S_{\pm} = \left(\frac{B}{4C}\right) [1 \pm \{1 - 24\beta(T - T^*)\}^{1/2}] \text{ for the nematic phase} \quad (2.48)$$

where  $\beta = A'C/B^2$ . However, at the  $I-N$  phase transition temperature ( $T_{IN}$ ) the free energy density must be equal in both sides. Hence, the desired transition temperature obtained from Eq. (2.47) and (2.48) can be written as:

$$T_{IN} = T^* + 1/27(B^2/A'C) \quad \text{for } \beta = 1/27 \quad (2.49)$$

and the corresponding value of order parameter also can be represented by  $S_{IN} = \frac{B}{3C}$  at that temperature which depicts a stable nematic phase. On the other hand if  $T_{IN} = T^*$ , the order parameter value drops at  $S_{IN} = 0$  which represents the stable isotropic phase. From Eq. (2.49), it is observed that the temperature  $T^*$  is slightly lower than  $T_{IN}$ , where the isotropic phase is comparatively unstable. Similarly, there is an upper limit of  $T_{IN}$  where the nematic phase becomes unstable and it is possible when  $\beta = 1/24$ . This limiting

concept approaches another temperature  $T^{**} = T_{IN} + 1/24(B^2/A'C)$  which is the maximum temperature limit of the stable nematic phase during the heating cycle. The cubic term in the free energy density expression describes the first order mesophase transition. However, for  $B$  tends to zero,  $T_{IN}$  defines the second order phase transition at temperature  $T^*$ . The temperatures  $T^*$  and  $T^{**}$  also have the significance that they are the apparent “critical points” for the isotropic and orientationally ordered nematic phases respectively.  $T^*$  and  $T^{**}$  are also known as the spinodal temperatures. Therefore, four different temperature regions are observed in this situation- (i)  $T > T^{**}$ , stable isotropic phase with  $S = 0$ , (ii)  $T_{IN} < T < T^{**}$  corresponds to metastable nematic phase during heating, (iii)  $T^* < T < T_{IN}$ , represents a nematic phase and a possibility to occur super-cooled isotropic phase, (iv)  $T < T^*$ , signifies a thermodynamically stable nematic phase. An analogical representation of order parameter ( $S$ ) with the variation of temperature ( $T$ ) for a first-order isotropic–nematic phase transition is shown in Fig. 2.10(b). However, the order parameter value approaches to zero at the isotropic–nematic ( $I$ – $N$ ) phase transition temperature ( $T_{IN}$ ).

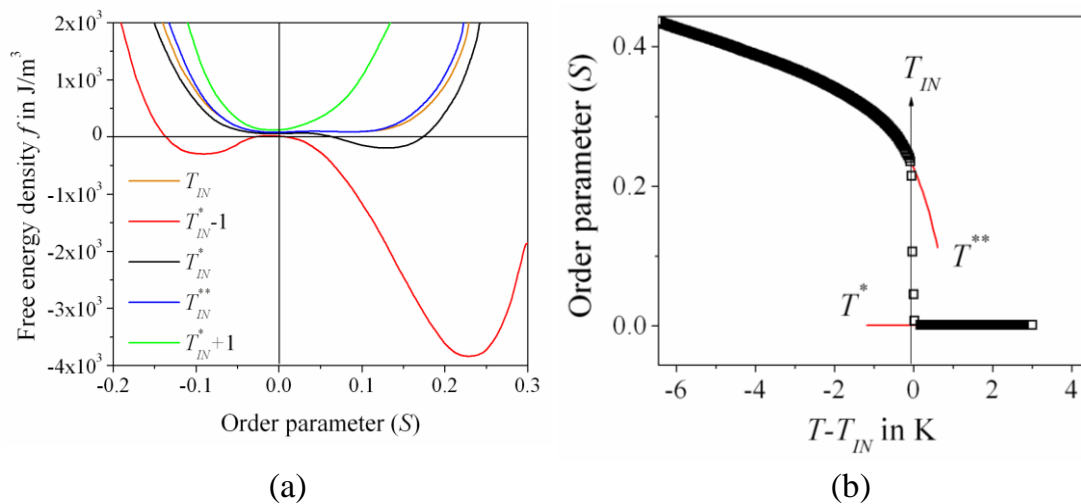


**Figure 2.10.** (a) The free energy density ( $f$ ) as a function of scalar order parameter  $S$ . (b) The nematic order parameter ( $S$ ) vs. temperature.  $T^*$  and  $T^{**}$  are the temperatures slightly lower and higher than  $T_{IN}$  respectively.

Furthermore, Landau-de Gennes theory of the isotropic–nematic ( $I-N$ ) phase transition has also been extended to the nematic–smectic- $A$  ( $N-Sm-A$ ) phase transition by considering an additional order parameter term of the Sm- $A$  phase in the free energy expansion. As the Sm- $A$  phase has a translational ordering in addition to orientational ordering of the LC molecules, they are supposed to be aligned perpendicularly within the equidistant layers. Hence, the Sm- $A$  phase is characterized by an effective one-dimensional periodic density wave along the perpendicular direction ( $\hat{z}$ ) with respect to the layer plane [75,87] and can be expressed as

$$\rho(r) = \rho(z) = \rho_0 + \sum_{i=1}^{\infty} \rho_i \cos(iq_s z - \varphi_i) \quad (2.50)$$

while in case of nematic phase the fundamental term  $\rho_1$  becomes zero but it provides a significant value for smectic- $A$  phase and  $\varphi_i$  is the arbitrary angle of the molecules with respect to the director. However, the free energy density expansion in the  $N-Sm-A$  phase transition contains only even power terms as because the density wave function is invariant under translation, *i.e.*,  $(\Psi) = -(\Psi)$ . Hence, the free energy expansion at the  $N-Sm-A$  phase transition is expressed as

$$\Delta f_1 = \frac{1}{2} r \rho_1^2 + u_0 \rho_1^4 + \dots \dots \quad (2.51)$$

Here the coefficient  $r$  is assumed as  $r = \alpha(T - T_0)$ , where  $T_0$  is the closest temperature to the  $N-Sm-A$  phase transition temperature ( $T_{NA}$ ). In this context when  $u_0$  is greater than zero and also  $T > T_0$ , the value of  $r$  leads to a positive value and when  $T < T_0$ , the value of  $r$  is seen as negative. By considering the above conditions, the  $N-Sm-A$  phase transition reveals a second order transition at the mean field temperature  $T_0 = T_{NA}$ . However, the situation became more complicated when the coupling with the nematic order parameter  $S_0 = \frac{1}{2} \langle 3 \cos^2 \theta - 1 \rangle$  has been taken into account. Again, if a small deviation ( $\delta S = S - S_0$ ) of the nematic order parameter occurs at the transition, the free energy density expansion becomes:

$$\Delta f_2 = \frac{1}{2} r \rho_1^2 + u_0 \rho_1^4 + \frac{1}{2\chi} \delta S^2 - C \rho_1^2 \delta S \quad (2.52)$$

where  $\chi$  is the response function (susceptibility) which assumes a smaller value at the  $N$ -Sm- $A$  phase transition and provides a greater value at the  $I$ - $N$  phase transition and  $C$  is a positive constant. Moreover, by imposing the minimization condition on free energy density expansion, it gives:

$$\delta S = \chi C \rho_1^2 \quad (2.53)$$

$$\text{with} \quad u = u_0 - 2C^2 \chi \quad (2.54)$$

So  $u$  is dependent on the values of  $\chi$  and  $C$ . The sign convention of the quantity  $u$  reveals the order nature of the  $N$ -Sm- $A$  phase transition. If  $\chi$  approaches a smaller value then  $u$  gives a positive sign which yields a second order nature of the  $N$ -Sm- $A$  phase transition at  $T_0 = T_{NA}$ , while  $u$  is negative for a higher value of  $\chi$ , it divulges a first-order transition at  $T_{NA} > T_0$  provided for a free energy expansion up to sixth order term. Furthermore, at  $u = 0$ ,  $\chi = \frac{u_0}{2C^2}$ ; it ensures a crossover from second order transition to first order transition through a tricritical point [TCP] on the  $N$ -Sm- $A$  transition line. Although a stronger coupling acts between the nematic and Smectic- $A$  order parameters which drives the transition from second order nature to the tricritical region [88], McMillan has considered this occurrence of tricritical point for a value of McMillan ratio ( $T_{NA}/T_{IN}$ ) equal to 0.87 which is somewhat lower than the experimentally obtained value 0.994 [16,20].

### 2.3.4. Sm- $A$ -Sm- $C$ phase transition

A well-defined Smectic- $C$  phase is illustrated by an inclined orientation of the molecular long axes at an angle  $\theta$  with respect to the layer normal, *i.e.*, the density wave of the smectic phase is tilted with respect to the orientational axis [87,89]. This phase may appear in the system of molecules which have the broken axial symmetry. Several experimental studies suggest that there exist a secondary axis which is associated with the molecular permanent electric dipoles and aligned in a direction different from the typical long axis of the

---



---

molecules. According to the mean-field theory, in absence of the broken axial symmetry, the LC system with smectic-*C* phase behaves like a usual smectic-*A* phase and at this circumstance, it is important to observe how the off-axis dipole may produce such a tilt angle  $\theta$ . These mean field theories [86], assumed the structure of a Landau theory with  $\theta$  or  $\sin \theta$  as order parameter and the molecular model is used to determine the sign of the coefficients in the expansion of the free energy in powers of the order parameter.

However, the order parameter of the Sm-*C* phase is more complicated because the complete description of the molecular orientation requires not only the tilt angle  $\theta$  with respect to the layer normal but also with an azimuthal angle  $\varphi$  of the axial direction for the molecules. Thus, the complex form of the order parameter can be written as [90,91]:

$$\omega = \theta \exp(i\varphi) = \omega_x + i\omega_y \quad (2.55)$$

According to Landau theory [81,82,86], the free energy density of the system can be expressed as a power series in terms of the relevant order parameter (in this case  $\omega$ ) in the vicinity of Sm-*A*–Sm-*C* phase transition. de Gennes [90-92] further modified this expression by including the concept of small fluctuation of  $\omega$  close to that transition and reconsidered the power series as follows [93]:

$$f_n = f_0 + a|\omega|^2 + \frac{1}{2}b|\omega|^4 \quad (2.56)$$

where  $f_n$  and  $f_0$  are the free energy density of the Sm-*C* and Sm-*A* phases respectively, while  $a$  and  $b$  are the temperature dependent constants. By using this free energy density expression, de Gennes [90-92] proposed a model that successfully describes a continuous or second order nature of the Sm-*A*–Sm-*C* phase transition analogous to the  $\lambda$  transition in superfluid helium ( $^4\text{He}$ ). From this analogy some results have been obtained:

(i) The Sm-*A*–Sm-*C* phase transition should belongs to a continuous transition if the specific heat capacity data exhibits a singularity at the Sm-*A*–

Sm-C phase transition temperature ( $T_{AC}$ ), *i.e.*, it follows the relation  $\delta C_p \cong A + B^\pm |\tau|^{-\alpha}$ , where  $A, B$  are constants,  $\tau = (T - T_{AC})/T_{AC}$  and  $\alpha \approx -0.007$ .

(ii) For the temperature below the transition temperature  $T_{AC}$ , the tilt angle  $\theta$  obey the relation  $\theta \sim \theta_0 |\tau|^\beta$ , with the exponent  $\beta = 1/3$ , susceptibility follows  $\chi \sim \chi_0 |\tau|^\gamma$  with the value  $\gamma = 1.33$  and correlation length also follows as  $\xi \sim \xi_0 |\tau|^\nu$  with  $\nu = 0.67$  where  $\theta_0, \chi_0$  and  $\xi_0$  are the parameters in the Sm-A phase.

(iii) For the temperatures above the transition temperature  $T_{AC}$ , an induced tilt angle appears by applying magnetic field  $H$  or electric field  $E$  to an oblique direction.

Additionally, Huang and Viner [94,95] proposed that the power series expansion contains the even ordered terms and at least up to sixth order term to explain the transitional behavior of the Sm-A–Sm-C phase transition and the free energy expression can be written as:

$$f_n = f_0 + a\tau|\omega|^2 + b|\omega|^4 + c|\omega|^6 \quad (2.57)$$

where  $a, b, c$  are the temperature dependent positive constants and  $\tau = (T - T_{AC})/T_{AC}$ .  $T_{AC}$  is the Sm-A–Sm-C phase transition temperature. Hence, by imposing the free energy minimization condition, one can get:

(i)  $\omega = 0$  for the Sm-A phase when  $T > T_{AC}$  or  $\tau > 0$ ,

(ii)  $\omega^2 = \frac{b}{3c} \left[ \left( 1 + \frac{3\tau}{\tau_0} \right)^{1/2} - 1 \right]$  for the Sm-C phase when  $T < T_{AC}$  or  $\tau < 0$

where  $\tau_0 = \frac{b^2}{ac}$ . Now, applying the obtained values into Eq. (2.57), the heat capacity expression can be written as:

$$C_p = -T \frac{\partial^2 f}{\partial T^2} \quad (2.58)$$

Corresponding heat capacity values in the Sm-A and Sm-C phases can be described as:

$$C_p = C_0, \quad \text{for } T > T_{AC} \text{ or } \tau > 0 \quad (2.59)$$

$$C_P = C_0 + A'T(T_m - T)^{-1/2}, \text{ for } T < T_{AC} \text{ or } \tau < 0 \quad (2.60)$$

where  $C_0$  is the background heat capacity obtained from  $f_0$  and  $A' = a^{3/2}/[2(3c)^{1/2}T_{AC}^{3/2}]$ , provided  $T_m = T_{AC}(1 + \tau_0/3)$ .

Now, in the vicinity of Sm-A–Sm-C phase transition point  $\tau = 0$  and thus the discontinuity in heat capacity value becomes:

$$\Delta C_P = C_P - C_0 = \frac{a^2}{2bT_{AC}} \quad \text{for } T = T_{AC} \quad (2.61)$$

when  $\tau = -\tau_0$ , Eq. (2.64) yields

$$\frac{C_P - C_0}{T} = \frac{a^2}{4bT_{AC}^2} = \frac{1}{2} \frac{\Delta C_P}{T_{AC}} \quad (2.62)$$

This  $\tau_0$  represents the full width at half maxima of the  $(C_P - C_0)/T$  vs.  $T$  curve in the reduced temperature scale.

However,  $\tau_0 = \frac{b^2}{ac}$ , it means that the order of the transition depends upon the values of coefficients  $a$ ,  $b$  and  $c$ . According to the prediction of deGennes, the sixth ordered term  $c$  in Eq. (2.57) must be positive, *i.e.*, greater than 0, but if the value of  $b$  is negative ( $b < 0$ ) the Sm-A–Sm-C phase transition demonstrates a first order nature, while if  $b > 0$  results in a second order transition and when  $b = 0$ , a tricritical point appears where the Sm-A–Sm-C phase transition exhibits a crossover from second order to first order in nature. Therefore, in case of second order transition the value of  $\tau_0$  is too large ( $|\tau| \ll \tau_0$ ) if  $b \gg c$  at the transition point and it reveals,  $\omega \propto \tau^{1/2}$  as seen from the solutions of Eq. (2.57). However, at the tricritical point,  $b \sim c > 0$  and  $\tau_0$  assumes a small value ( $|\tau| \gg \tau_0$ ) even for the temperatures close to the Sm-A–Sm-C phase transition. At the tricritical point, the solution approaches as  $\omega \propto \tau^{1/4}$ . Thus, this  $|\tau|$  or  $\tau_0$  value defines the crossover behavior from mean field to tricritical nature of the Sm-A–Sm-C phase transition.

Nevertheless, the phenomenological Ginzburg-Landau theory [96-99] imparts a significant influence in describing the true critical phenomena for both classical and quantum statistical mechanics. Landau theory is a

---



---

straightforward macroscopic theory in a framework of statistical mechanics which is based on the concept that an average field is experienced by the non-interacting molecules within the system and hence ignores the effect of fluctuations. These mean field approximations are satisfactorily acceptable to describe the phase transitional phenomena in different thermodynamical systems having dimension  $d \geq 4$ , but found to inadequate in low dimensional case ( $d < 4$ ), which is further explained by Ginzburg. For example, in case of  $d > 4$ , the critical exponent  $\beta$  represents a value 0.5 predicted by the mean field approximation, while it assumes a bit different value 1/8 and 0.315, for two-dimensional ( $d = 2$ ) and three-dimensions ( $d = 3$ ) respectively. It suggests that there must be a certain limit of microscopic length scale over which the fluctuations of degrees of freedom are correlated. This length is termed as correlation length ( $\xi$ ) which varies with temperature and serves as a scale for all distances. This  $\xi$  is connected to many particles of the system and the fluctuation of  $\xi$  near the transition point plays a role to determine the transitional phenomena. For a second-order phase transition, the correlation length becomes infinite, although it represents a finite value for a first-order transition. The parameter  $\xi$  is correlated over distances  $\xi \gg a$  ( $a$  is the intermolecular spacing) and diverges in close vicinity to the second order transition, *i.e.*, it follows the relation

$$\xi_{\pm} \propto |\tau|^{-\nu_{\pm}} \text{ or } \xi_{\pm} = \xi_0 |\tau|^{-\nu_{\pm}} \quad (2.63)$$

where  $\xi_0$  is the range of interaction or the bare correlation length that can be measured directly from scattering studies and  $\nu_+ = \nu_- = \nu = 1/2$ . Therefore, the influence of correlation length is a crucial parameter near critical points which is considered to develop an adequate understanding how close to the transition temperature, Landau theory can explain the true critical phenomena. By proposing the free energy functional expression in terms of a wave function ( $\psi$ ) as a complex order parameter, Ginzburg describes the fluctuation effect on the saddle point or mean field behavior for both the condition  $\tau < 0$  and  $\tau > 0$ . He

introduces a correction term to the free energy expression regarding the dependency of the correlation length in which the integral term [100,101] is proportional to  $(\text{length})^{4-d}$ . Mathematically, the fluctuation correlation term in heat capacity expression is expressed as:

$$C_{Fluct} \simeq \frac{1}{K^2} \begin{cases} a^{4-d} & \text{for } d > 4 \\ \xi^{4-d} & \text{for } d < 4 \end{cases} \quad (2.64)$$

where  $K$  is the Hook's constant ( $K \propto \xi_0^2$ ). The obtained results demonstrate that if  $d > 4$ , the correlation integral term diverges close to the transition temperature provided by an upper cutoff equal to  $1/a$  ( $a = \text{lattice spacing}$ ) as indicated in Fig. 2.11(a). However, the discontinuity in heat capacity value remains unchanged in the vicinity of the transition. Conversely, for  $d < 4$ , the correction term corresponds to the divergence of fluctuation ( $\xi = \xi_0 |\tau|^{-1/2}$ ) and then the correlation integral reveals a convergent behavior. Effectively, the heat capacity value diverges close to the transition, implying that the mean field approximation fails to explain the true critical phenomena for the dimension  $d \leq 4$ , which is called the upper critical dimension [101]. Now, imposing the condition  $\xi = \xi_0 |\tau|^{-1/2}$  and  $K \propto \xi_0^2$  into Eq. (2.64), the correction term modifies to  $\xi_0^{-d} |\tau|^{-\frac{(4-d)}{2}}$  which is greater than  $C_P$  in the mean field approximation.

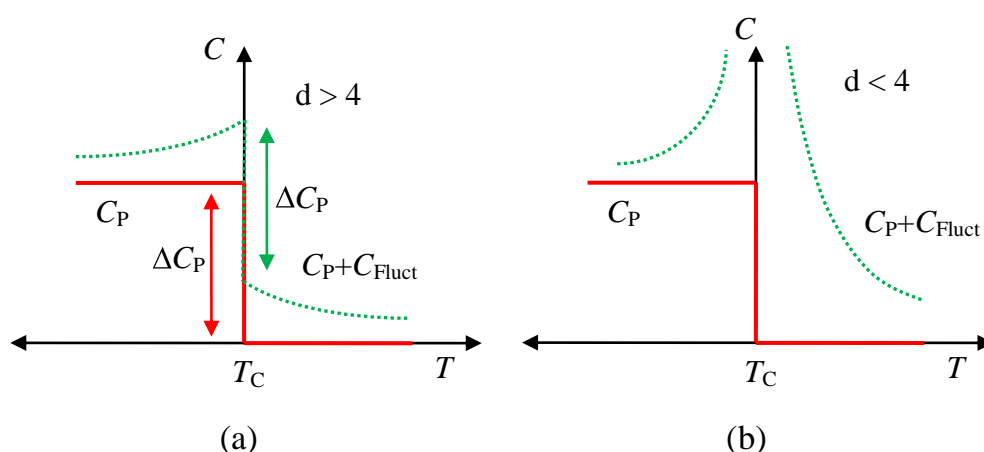


**Figure 2.11.** Schematic diagram of the heat capacity variation near the phase transition for the dimensions  $d > 4$  and  $d < 4$ . Red solid line is the mean field heat capacity and green dashed line corresponds to the same including the correction term appears due to the fluctuation of the correlation length.

Therefore, the fundamental expression of Ginzburg criterion can be written as

$$|\tau| \ll \tau_G \approx \frac{1}{[(\xi_0)^d (\Delta C_P)]^{2/(4-d)}} \quad (2.65)$$

where  $\Delta C_P$  is the discontinuity in heat capacity obtained from mean field approximation. However,  $\xi_0$  is the microscopic length scale which can be measured from scattering line shapes and  $\tau_G$  is the Ginzburg reduced temperature. The correlation length  $\xi_0$  is of the order of intermolecular spacing ( $a$ ) and  $\Delta C_P$  can be expressed as  $Nk_B$ . Thus the yielded value of the Ginzburg temperature in  $d = 3$  is  $\tau_G \approx \xi_0^{-5}$  [100]. In case of superconductor where  $\xi_0 = 10^3 a$ ,  $\tau_G$  demonstrates a value  $\sim 10^{-18}$  which is inaccessible by experimental techniques, while in superfluids it represents a value  $10^{-1} - 10^{-2}$ . Moreover, it has been observed that the region  $10^{-2} - 10^{-3}$  is hardly accessible by certain experimental techniques [95,102].

Based on the fundamental theories discussed above regarding the mesophase transition, it is clearly understood that the mean field theories are nothing but an approximation which omits the fluctuating order parameter and considers only the effect of the spatially uniform order parameter. Moreover, the mean field theory induces itself to its own self-consistency behavior and does not describe the dependency of transitional behavior upon the spatial dimension of the system. Practically, the mean field theory is only valid for the temperatures far away from the transition temperature. In case of the systems having a dimension less than 4 ( $d < 4$ ), the mean field approximations are inadequate to describe the transitional behavior close to the transition point due to the divergence nature of correlation length fluctuation. As a result, the response function (like specific heat capacity) describes a power law divergence nature in the vicinity of transition temperature. Now, due to the failure of mean field theory and leading to an introduction of correlation length fluctuation, experimental observation of scaling and universality is more interesting close to the transition point. Owing to the divergence behavior of

correlation length in the vicinity of critical point, all the thermodynamical functions (free energy, specific heat capacity, susceptibility etc.) diverges according to the correlation length. Furthermore, the singularity of a phase transition in any thermodynamical observables is characterized by a critical exponent like as  $\alpha$ ,  $\beta$ ,  $\gamma$  etc. which are not independent to each other. Hence, there must be a correlation to each other for the exponents as well as the thermodynamic functions which depend upon the temperature that is nailed as scaling behavior. This relationship between the observables and related exponents in the vicinity to a phase transition point can be well described by the power-law divergence near the transition temperature. The singularities of different physical properties can be estimated by the divergence behavior of  $\zeta$  at  $T_C$ . Moreover, the singularities or scaling condition in free energy expression can be described by a single generalized homogeneous function of temperature and conjugate field and represented as:

$$f(\tau, h) = |\tau|^2 g(h/|\tau|^\Delta) \quad (2.66)$$

where  $h$  is the externally applied field,  $\Delta$  is the gap exponent and  $g$  is the homogeneous function dependent upon  $h$  and  $\tau$ . However, considering the homogeneity, the singular form of free energy assumes an expression

$$f'(\tau, h) = |\tau|^{2-\alpha} g(h/|\tau|^\Delta) \quad (2.67)$$

Hence the singular form of the energy becomes

$$E'(\tau, h) \sim \frac{\partial f'}{\partial \tau} = |\tau|^{1-\alpha} g_E(h/|\tau|^\Delta) \quad (2.68)$$

and similarly, the singular form of heat capacity becomes

$$C'(\tau, h) \sim \frac{\partial^2 f'}{\partial \tau^2} = |\tau|^{-\alpha} g_C(h/|\tau|^\Delta) \quad (2.69)$$

or it may be expressed more generalized way as

$$C_\pm(\tau, h) = |\tau|^{-\alpha_\pm} g_{C_\pm}(h/|\tau|^{\Delta_\pm}) \quad (2.70)$$

with separate values of function and exponent for  $\tau < 0$  and  $\tau > 0$  that coincide at  $\tau = 0$ . However, at  $h = 0$ , Eq. (2.70) yields

$$C_{\pm}(\tau, 0) = A|\tau|^{-\alpha_{\pm}} \quad (2.71)$$

where  $A$  is the amplitude coefficient. On the other hand, the correlation length  $\xi$  is a homogeneous function that can be expressed as

$$\xi(\tau, h) = |\tau|^{-\nu} g(h/|\tau|^{\Delta}) \quad (2.72)$$

Thus the singular form of the free energy function reveals

$$f'(\tau, h) \sim \xi^{-d} \sim |\tau|^{d\nu} g(h/|\tau|^{\Delta}) \quad (2.73)$$

Comparing Eq. (2.67) and Eq. (2.73), one can get the relation  $2 - \alpha = d\nu$  or  $\alpha = 2 - d\nu$  which is named as Josephson's equality or identity. Similarly there are some other relations and these relations are a result of the homogeneity or scaling properties of correlation functions and thermodynamic quantities near  $T = T_c$  that can be derived using the renormalization group model introduced by Kenneth Wilson [103-105]. This procedure is based on the three concept- Coarse graining, Rescaling and Renormalization, explored that the critical exponents are dependent upon the spatial dimension, symmetry of the order parameter and symmetry as well as range of interactions. They belong to some universality classes in which the critical exponents for all the transitions is identical.

After the above theoretical discussions, it is obvious that the microscopic behavior at the critical point can be well reflected by the response functions such as specific heat capacity, susceptibility, magnetization etc. According to the mean field model the quantity  $(S-S_0)$  is proportional to  $\langle |\Psi|^2 \rangle$ , where  $S_0$  is the nematic order parameter in absence of any smectic ordering [91,106]. Moreover, the nematic order parameter ( $S$ ) is also proportional to optical birefringence ( $\Delta n$ ). Hence, by investigating the behavior of optical birefringence in the vicinity of transitions between liquid crystal mesophases, an identical power-law divergence behavior and hence a critical

exponent ( $\alpha'$ ) identical to specific heat critical exponent ( $\alpha$ ) can be established. Most of the experimental part in this dissertation is mainly concentrated on determining the mesophase transitional behavior and their order character by investigating the temperature dependent optical birefringence measurement.

---

---

## References:

- [1] D. Demus, and L. Richter, in *Textures of liquid crystals*, Verlag Chemie, New York (1978).
- [2] I. Dierking, in *Textures of liquid crystals*, Wiley-VCH Verlag GmbH & Co., Weinheim (2003).
- [3] P. Navard, and J. M. Haudin, *J. Therm. Anal.*, **30**, 61 (1985).
- [4] C.W. Garland, in *Liquid Crystals: Experimental Study of Physical Properties and Phase Transitions*, S. Kumar (Ed.), Cambridge University Press, Cambridge (2001).
- [5] J. Thoen, in *Heat Capacities Liquids, Solutions and Vapours*, E. Wilhelm, and T. M. Letcher (Eds.), RSC Publishing, Cambridge (2010).
- [6] R. Dabrowski, and K.C. Zuprynski, in *Advances in liquid crystal research and applications*, Pergamon press, Oxford (1980).
- [7] H. Stub, and W. Perron, *Anal. Chem.*, **46**, 128 (1974).
- [8] B. Das, A. Pramanik, M.K. Das, A. Bubnov, V. Hamplová, and M. Kašpar, *J. Mol. Struct.*, **1013**, 119 (2012).
- [9] B.R. Ratna, and S. Chandrasekhar, *Mol. Cryst. Liq. Cryst.*, **162**, 157 (1988).
- [10] A.K. Zeminder, S. Paul, and R. Paul, *Mol. Cryst. Liq. Cryst.*, **61**, 4191 (1980).
- [11] A. Prasad, and M.K. Das, *Phase Transitions*, **83**, 1072 (2010).
- [12] A. Saipa, and F. Giesselmann, *Liq. Cryst.*, **29**, 347 (2002).
- [13] T. Scharf, in *Polarized Light in Liquid Crystals and Polymers*, John Wiley and Sons, Hoboken (2007).
- [14] G. Sarkar, B. Das, M.K. Das, and W. Weissflog, *Phase Transitions*, **82**, 433 (2009).
- [15] A. Prasad, and M.K. Das, *J. Phys.: Condens. Matter*, **22**, 195106 (2010).
- [16] S.K. Sarkar, and M.K. Das, *RSC Adv.*, **4**, 19861 (2014).

- 
- 
- [17] G. Sarkar, M.K. Das, R. Paul, B. Das, and W. Weissflog, *Phase Transit.*, **82**, 433 (2009).
- [18] S.K. Sarkar, P.C. Barman, and M.K. Das, *Physica B*, **446**, 80 (2014).
- [19] S.K. Sarkar, and M.K. Das, *J. Mol. Liq.*, **199**, 415 (2014).
- [20] A. Chakraborty, S. Chakraborty, and M.K. Das, *Phys. Rev. E*, **91**, 032503 (2015).
- [21] M.K. Das, S. Chakraborty, R. Dabrowski, and M. Czerwinski, *Phys. Rev. E*, **95**, 012705 (2017).
- [22] A. Saipa, and F. Giesselmann, *Liq. Cryst.*, **29**, 347 (2002).
- [23] T. Scharf, in *Polarized Light in Liquid Crystals and Polymers*, John Wiley and Sons, Hoboken (2007).
- [24] A. Prasad, and M.K. Das, *Phys. Scr.*, **84**, 015603 (2011).
- [25] A. Chakraborty, M.K. Das, B. Das, U. Baumeister, and W. Weissflog, *J. Mater. Chem. C*, **1**, 7418 (2013).
- [26] S.K. Sarkar, and M.K. Das, *Fluid Phase Equilib.*, **365**, 41 (2014).
- [27] S.K. Sarkar, and M.K. Das, *Liq. Cryst.*, **41**, 1410 (2014).
- [28] P. Galatola, and C. Oldano, in *The Optics of Thermotropic Liquid Crystals*, S. Elston, and R. Sambles (Eds.), Taylor and Francis, London (1998).
- [29] P. Perkowski, M. Mrukiewicz, K. Garbat, M. Laska, U. Chodorow, W. Piecek, R. Dabrowski, and J. Parka, *Liq. Cryst.* **39**, 1237 (2012).
- [30] M. Mrukiewicz, P. Perkowski, K. Garbat, R. Dabrowski, and J. Parka, *Acta Physica Polonica A*, **124**, 940 (2013).
- [31] S. Havriliak, and S. Negami, *Polymer*, **8**, 161 (1967).
- [32] S. Havriliak, and S. Negami, *J. Poly. Sci.*, **14**, 99 (1966).
- [33] P. Nayek, S. Ghosh, S.K. Roy, T.P. Majumder, and R. Dabrowski, *J. Mol. Liq.* **175**, 91 (2012).
- [34] S. Ghosh, P. Nayek, S.K. Roy, T. P. Majumder, and R. Dabrowski, *Liq. Cryst.*, **37**, 369 (2010).
- [35] D.W. Davidson, and R. H. Cole, *J. Chem. Phys.* **19**, 1484 (1951).
- 
-

- 
- 
- [36] K.S. Cole, and R.H. Cole, *J. Chem. Phys.*, **9**, 341 (1941).
- [37] F.C. Frank, *Disc. Faraday Soc.*, **25**, 19 (1958).
- [38] C.W. Oseen, *Trans. Faraday Soc.*, **29**, 883 (1933).
- [39] H. Zocher, *Trans. Faraday Soc.*, **29**, 945 (1933).
- [40] W.H. de Jue, in *Physical Properties of Liquid Crystalline Materials*, Gordon and Breach, London (1980).
- [41] S. Chandrasekhar, in *Liquid Crystals*, Cambridge University Press, Cambridge (1992).
- [42] M. Kleman, in *Points, Lines and Walls*, Wiley, New York (1983).
- [43] P.G. de Gennes, and J. Prost, in *The Physics of Liquid Crystals*, Oxford University Press, Oxford (1993).
- [44] S. Singh, in *Liquid Crystals Fundamentals*, World Scientific, Singapore (2002).
- [45] V. Fréedericksz, and V. Zolina, *Trans. Faraday Soc.*, **29**, 919 (1933).
- [46] H.L. Ong, *Phys. Rev. A*, **33**, 3550 (1986).
- [47] M.J. Bradshaw, and E.P. Rayens, *Mol. Cryst. Liq. Cryst.*, **72**, 35 (1980).
- [48] H. Deuling, in *Liquid crystals, Solid state physics suppl. no. 14*, L Liebert, (Ed), Academic Press, New York (1978).
- [49] H. Gruler, T.J. Scheffer, and G. Meier, *Z. Naturforsch.*, **27a**, 966 (1972).
- [50] H. Gruler, and L. Cheung, *J. Appl. Phys.*, **46**, 5097 (1975).
- [51] L. Pohl, and U. Finkenzeller, in *Liquid Crystals – Applications and Uses*, B. Bahadur (Ed.), World Scientific, Singapore (1990).
- [52] P.P. Karat, and N.V. Madhusudana, *Mol. Cryst. Liq. Cryst.*, **40**, 239 (1977).
- [53] H.P. Schad, G. Baur, and G. Meier, *J. Chem. Phys.*, **70**, 2770 (1979).
- [54] M.J. Bradshaw, and E.P. Raynes, *Mol. Cryst. Liq. Cryst.*, **72**, 35 (1981).
- [55] H.P. Schad, and M.A. Osman, *J. Chem. Phys.*, **75**, 880 (1981).
- [56] F. Leenhouts, and A.J. Dekker, *J. Chem. Phys.*, **74**, 1956 (1981).
- [57] L. Csillag, I. Jánossy, V.F. Kitaeva, N. Kroó, N. Sobolev, and A.S. Zolotko, *Mol. Cryst. Liq. Cryst.*, **78**, 173 (1981).
- 
-

- 
- 
- [58] A. Chakraborty, M.K. Das, B. Das, A. Lehmann, and C. Tschierske, *Soft Matter*, **9**, 4273 (2013).
- [59] A. Prasad, and M.K. Das, *Liq. Cryst.*, **41**, 1261 (2014).
- [60] P. Sathyanarayana, T.A. Kumar, V.S.S. Sastry, M. Mathews, Q. Li, H. Takezoe, and S. Dhara, *Appl. Phys. Exp.*, **3**, 091702 (2010).
- [61] S. Das Gupta, P. Chattopadhyay, and S.K. Roy, *Phys. Rev. E.*, **63**, 041703 (2001).
- [62] S. Das Gupta, and S.K. Roy, *Liq. Cryst.*, **30**, 31 (2003).
- [63] E. Jakeman, and E.P. Raynes, *Physics Lett. A*, **39**, 69 (1972).
- [64] Hp. Schad, *J. Appl. Phys.*, **54**, 4994 (1983).
- [65] P. Martinot-lagarde, *J Phys. Lett. (Paris)*, **38**, 17 (1977).
- [66] K. Miyasato, S. Abe, H. Takezoe, A. Fukuda, and E. Kuze, *Jpn. J Appl. Phys.*, **22**, L661 (1983).
- [67] S.S. Bawa, A.M. Biradar, K. Saxena, and S. Chandra, *Rev. Sci. Instrum.*, **59**, 2023 (1988).
- [68] A. Pramanik, M.K. Das, B. Das, M. Żurowska, and R. Dabrowski, *Liq. Cryst.*, **42**, 412 (2015).
- [69] V.M. Vaksman, and Y.P. Panarin, *Mol. Mats.*, **1**, 147 (1992).
- [70] W. Maier, and A. Saupe, *Z. Natureforsch A*, **13a**, 564 (1958).
- [71] W. Maier, and A. Saupe, *Z. Natureforsch A*, **14a**, 882 (1959).
- [72] W. Maier, and A. Saupe, *Z. Natureforsch A*, **15a**, 287 (1960).
- [73] S. Chandrasekhar, in *Liquid crystals*, Cambridge University Press, Cambridge (1977).
- [74] G.R. Luckhurst, G.W. Gray (Eds), in *The molecular physics of liquid crystals*, Academic Press, London (1979).
- [75] W.L. McMillan, *Phys. Rev. A*, **4**, 1238 (1971).
- [76] W.L. McMillan, *Phys. Rev. A*, **6**, 936 (1972).
- [77] K. Kobayashi, *J. Phys. Soc. Jpn.*, **29**, 101 (1970).
- [78] K. Kobayashi, *Mol. Cryst. Liq. Cryst.*, **13**, 137 (1971).
- [79] K. Kobayashi, *Phys. Lett. A*, **31**, 125 (1970).
- 
-

- 
- 
- [80] P.J. Wojtowicz, in *Introduction to Liquid Crystals*, E. B. Priestley, P. J. Wojtowicz and P. Sheng (Eds.), Plenum Press (1976).
- [81] L.D. Landau, *Phys. Z Sowjetunion*, **11**, 26 (1937); in *Collected papers of L.D. Landau*, D. Ter Haar (2nd Ed.), Gordon and Breach, Science Publisher, New York (1967).
- [82] L.D. Landau, and E.M. Lifshitz, in *Statistical Physics* (Vol. 1, 3rd Ed.), Pergamon, Oxford (1980).
- [83] P.G. de Gennes, *Mol. Cryst. Liq. Cryst.*, **12**, 193 (1971).
- [84] E.B. Priestly, P.J. Wojtowicz, and P. Sheng (editors), in *Introduction to Liquid Crystals* (Ch. 10), Plenum Press, New York (1975).
- [85] S. Singh, *Phys. Rep.*, **324**, 107 (2000).
- [86] G. Vertogen, W.H. de Jeu, in *Thermotropic liquid crystals: Fundamentals*, Springer, Berlin (1988).
- [87] P.G. de Gennes, in *The Physics of Liquid Crystals*, Clarendon Press, Oxford (1974).
- [88] M.A. Anisimov, in *Critical phenomena in liquids and liquid crystals*, Gordon and Breach, New York (1991).
- [89] J.D. Litster, and R.J. Birgeneau, *Phys. Today*, **35**, 26 (1982).
- [90] P.G. de Gennes, *Solid State Comm.*, **10**, 753 (1972).
- [91] P.G. de Gennes, *Mol. Cryst. Liq. Cryst.*, **21**, 49 (1973).
- [92] P.G. de Gennes, *C. R. Acad. Sci. B*, **274**, 758 (1972).
- [93] M.J. Stephen, and J.P. Straley, *Rev. Mod. Phys.*, **46**, 617 (1974).
- [94] C.C Huang, and J.M. Viner, *Phys. Rev. A*, **25**, 3385 (1982).
- [95] S.C. Lien, and C.C. Huang, *Phys. Rev. A*, **30**, 624 (1984).
- [96] V. L. Ginzburg, *Sov. Phys. - Solid State*, **2**, 1824 (1961).
- [97] J. Als-Nielsen, and R.J. Birgeneau, *Am. J. Phys.*, **45**, 554 (1977).
- [98] N. Goldenfeld, in *Lectures on phase transitions and the renormalization group*, Talor & Francis group, NW (1992).
- [99] D.J. Amit, *J. Phys. C: Solid State Physics*, **7**, 3369 (1974).
- 
-

- [100] P.M. Chaikin, and T.C. Lubensky, in *Principles of condensed matter physics*, Cambridge University Press, New York (1995).
- [101] M. Kardar, in *Statistical physics of field*, Cambridge University Press, New York (2007).
- [102] G. Ahlers, A. Kornblit, and H.J. Guggenheim, *Phys. Rev. Lett.*, **34**, 1227 (1975).
- [103] K.G. Wilson, in *An investigation of the low equation and the Chew-Mandelstam equations*, Ph.D thesis, Cal. Tech. (1961).
- [104] K.G. Wilson, *Rev. Mod. Phys.*, **55**, 583 (1983).
- [105] K.G. Wilson, and J. Kogut, *Phys. Rep.*, **12**, 75 (1974).
- [106] K.-C. Lim, and J.T. Ho, *Phys. Rev. Lett.*, **40**, 944 (1978).

# CHAPTER 3

---

Effect of the hockey stick-shaped mesogen as an additive on the critical behavior at the isotropic to nematic and nematic to smectic-*A* phase transitions in octyloxy-cyano-biphenyl

---

---

### 3.1. Introduction

Fundamental mesogenic behavior of liquid crystalline compounds depends on their molecular structure and relative organization in mesophases. So far a number of mesogenic compounds displaying a variety of mesophases with diverse molecular ordering and phase structure have been synthesised and comprehensively studied. Some of them are of further interest due to their exclusive molecular behavior within such mesophases as well as at the transitions between them. In that sense, the bent-core or banana-shaped compounds have emerged as a field of significant interest in liquid crystal research. Apart from the interest on molecular behavior and appearance of different unique mesophases in bent-core liquid crystals, mixtures of such compounds with rod-like molecules, exhibiting exciting mesophase transitions including those usually appeared for only single calamitic compounds, are also much attractive for their unpredictable varying characteristics. Properties such as enhancement of chirality in cholesteric [1,2] and smectic- $C^*$  fluids [3], generation of antiferroelectric order in smectics [4-7], induction of novel smectic phases [8], inimitable temperature dependence of elastic constant [9-11] or nanophase segregations [12,13] of such mixtures of rod-like and bent-core liquid crystal brought them at the center of scientific attention and stimulates considerable research efforts regarding formulation and characterization of noble liquid crystalline mixtures.

In the past few decades, several experimental and theoretical efforts have been devoted to extract the exact order character of the isotropic to nematic ( $I-N$ ) phase transition. Considering the mean-field approach, Landau and de Gennes [14] explained the  $I-N$  phase transition by assuming the free energy density in powers of the nematic order parameter  $S(T)$ . However, the mean-field theory [15] cannot describe the critical phenomena at very close to the transition. A number of diverse experimental techniques have been reported so far to analyze this critical region as well as to disclose the unique aspects of

---

---

the  $I-N$  phase transition. However, none of the experimental techniques have been able to describe a complete picture regarding the nature of this transition. Besides a few disagreements, most of them reveal a tricritical nature [16–18] for the  $I-N$  phase transition which again can be explained in the context of Landau-de Gennes theory with the free energy density expanded up to sixth order in powers of the nematic order parameter  $S(T)$ .

Moreover, in case of nematic–smectic- $A$  ( $N-Sm-A$ ) phase transition a number of experimental attempts have been employed so far but it still remains only partially understood. On the basis of mean-field model, Kobayashi [19] and McMillan [20] suggested that depending upon the McMillan ratio ( $T_{NA}/T_{IN}$ , where  $T_{NA}$  and  $T_{IN}$  are the  $N-Sm-A$  and  $I-N$  phase transition temperatures respectively), the  $N-Sm-A$  phase transition can either be a first order or second order along with the existence of a tricritical point (TCP) where the transition undertakes a crossover from second order to first order in nature. With the introduction of a modified functional, de Gennes [14,21] further proposed a concept of coupling in between the nematic ( $S$ ) and smectic ( $\Psi$ ) order parameters, which predicts the transition to be in the 3D- $XY$  universality class. However, experimental evidences indicate a strong dependence of that transition on the width of the nematic range, which shows that a wide nematic width signifies a weak coupling between the nematic and smectic order parameter, thus making the  $N-Sm-A$  transition to be second order in nature, while for a sufficiently small nematic width, indicating a stronger coupling between  $S$  and  $\Psi$ , drives the transition to first order character. Although theoretically the tricritical limit is expected for a McMillan ratio of 0.87, experimental observations demonstrate somewhat higher values, ranging from 0.942 to 0.994 [22-28]. So the non-universal type behavior has been observed in a number of cases, *i.e.*, the 3D- $XY$  appearance can be feasible only when the nematic order is completely saturated [29-32]. Furthermore, Halperin, Lubensky and Ma (HLM) [33] by introducing a correction in the free energy

---

---

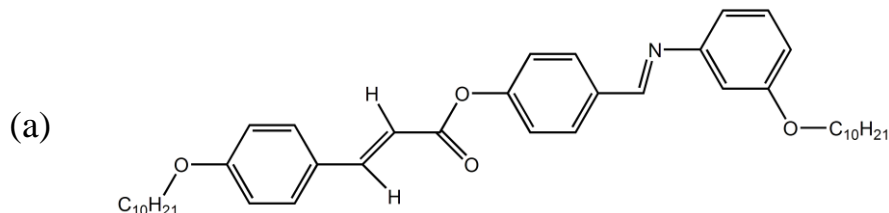
term  $\sim \Psi^3$ , have shown that the  $N$ -Sm-A transition is always weakly first order in nature because of the presence of the coupling between the nematic director fluctuations and smectic order parameter. Therefore, the concept of tricritical point (TCP) is ruled out in this case. So far, a number of experimental techniques such as specific heat capacity measurements, dielectric techniques, x-ray diffraction measurements *etc.*, have widely been used to study the nature of this phase transition in several rod-like liquid crystals having a variety of core structures as well as in their mixtures. However, transitional phenomena in mixtures involving rod-like and bent-core mesogens are relatively less investigated, even though they may prove to be helpful in extracting valuable information regarding transitional anomaly and order character of a transition.

In this chapter, a systematic investigation of the critical behavior in the vicinity of the  $I$ - $N$  and  $N$ -Sm-A phase transitions has been reported in a few binary liquid crystalline mixtures consisting of a hockey stick-shaped compound, 4-(3-decyloxyphenyliminomethyl) phenyl 4-decyloxybenzoate (SF7) and the calamitic compound, 4'-octyloxy-4-cyanobiphenyl (8OCB) from a quite high-resolution (in both the birefringence and temperature) measurement of optical birefringence ( $\Delta n$ ). An effective order parameter critical exponent ( $\beta$ ) value has been extracted by investigating the critical fluctuation near the  $I$ - $N$  phase transition. From an analysis of the temperature derivative of  $\Delta n$  data in the vicinity of  $N$ -Sm-A phase transitions, power-law behavior with a characteristic effective heat capacity critical exponent ( $\alpha'$ ) has been determined and compared with the available literature data. The effective critical exponent ( $\alpha'$ ) has also been investigated along the path of variation for the dopant concentration. The observed pretransitional behavior is discussed in the light of crossover behavior under the consideration of effect of the hockey stick-shaped molecules on the resultant molecular order in the host medium. Moreover, an order parameter critical exponent ( $\beta'$ ) has been extracted in the vicinity of  $N$ -Sm-A phase transition for all of the studied mixtures.

## 3.2. Materials

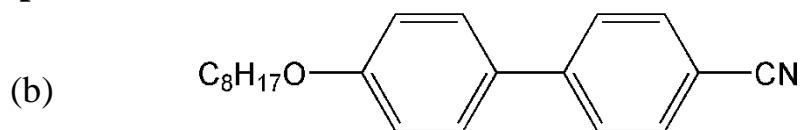
The hockey stick-shaped compound, 4-(3-decyloxyphenyliminomethyl) phenyl 4-decyloxy-cinnamate (SF7) was synthesized and purified at the Institute of Physical Chemistry, Martin Luther University, Halle, Germany and the compound 4'-octyloxy-4-cyanobiphenyl (8OCB) was purchased from E. Merck, UK (having purity higher than 99.9%) and were used without further purification. The structural formulae and transition scheme for both the pure compounds are given in Fig. 3.1. Several mixtures have been prepared with different molar concentrations ( $x_{\text{SF7}} = 0.012, 0.03, 0.05$  and  $0.065$ ) by adding small amounts of the hockey stick-shaped compound into the host rod-like mesogen. The textures of the samples were observed under a polarizing optical microscope (BANBROS) equipped with INSTEC HCS302 hot stage, controlled by INSTEC mK1000 thermo system.

### Compound 1



**Cr** (350 K) **Sm-C<sub>a</sub>** (361 K) **Sm-C<sub>s</sub>** (371.5 K) **Sm-A** (374 K) **I**

### Compound 2



**Cr** (327.5 K) **Sm-A<sub>d</sub>** (340 K) **N** (353 K) **I**

**Figure 3.1.** Chemical structure and phase behavior of (a) the hockey stick-shaped compound (SF7) and (b) the rod-like compound (8OCB).

## 3.3. Phase diagram

The phase diagram of the binary system consisting of SF7 and 8OCB for four different concentrations along with that of pure 8OCB, as obtained from

both the polarizing optical microscopy and the optical transmission technique has been illustrated in Fig. 3.2. The pure rod-like compound 8OCB shows the stable phase sequence  $I$ -Sm- $A_d$ - $N$ -Cr as being cooled from isotropic state. Here, Sm- $A_d$  refers to smectic- $A$  phase with partial bi-layer structure [the layer thickness ( $l$ ) is intermediate between the molecular length ( $d$ ) and twice the molecular length]. Conversely, the pure hockey stick-shaped compound (SF7) shows two polymorphic tilted smectic phases - the synclonic smectic- $C$  (Sm- $C_s$ ) as well as the anticlinic smectic- $C$  (Sm- $C_a$ ) phases along with a Sm- $A$  phase, appearing in a relatively small temperature range ( $\sim 2.5$  K) [34].

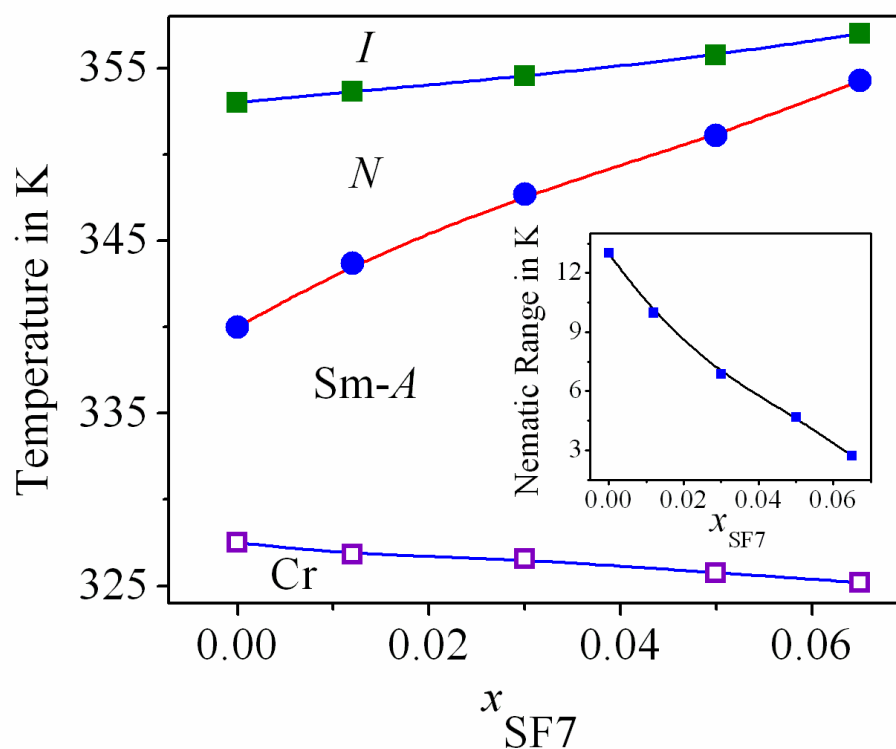


**Figure 3.2.** Phase diagram for the binary mixture consisting of SF7 and 8OCB.  $x_{SF7}$  denotes the mole fraction of SF7.  $I$  – isotropic phase,  $N$  – nematic phase and Sm- $A$  – smectic- $A$  phase. ■:  $I$ - $N$  transition temperature; ●:  $N$ -Sm- $A$  transition temperature; □: Melting temperatures measured during heating cycle. Inset depicts variation of nematic range with concentration for the present system. Solid lines are drawn for guidance to eye.

In these binary mixtures, particular focus has been taken on the region where the concentration of the guest compound, *i.e.*, hockey stick-shaped

---

---

compound (SF7) is less compared to that of the rod-like host compound (8OCB). It has been observed that by addition of a small amount of the hockey stick-shaped compound in the host mesogenic system has a significant influence on both the  $I-N$  ( $T_{IN}$ ) and  $N-Sm-A$  ( $T_{NA}$ ) transition temperatures. Further both  $T_{IN}$  and  $T_{NA}$  shows an increasing trend when plotted against concentration of SF7 with the phase boundary between the Sm-A and  $N$  phases being relatively steeper than that between the  $N$  and  $I$  phases and thus resulting a decrease in the nematic width. This again signifies a destabilization of the nematic phase in the host medium caused by the angular mesogenic compound. The variation of the nematic range against molar concentration is also presented in the inset of Fig. 3.2. The nematic range has been found to decrease from a value of 13 K to near about 3 K for the studied mixtures, where the shrinkage follows a nearly linear trend with the variation of molar concentration.

### 3.4. Optical birefringence measurements

#### 3.4.1. Optical transmission (OT) technique

The high-resolution optical birefringence ( $\Delta n = n_e - n_o$ ) data has been accomplished by measuring the optical phase retardation [35-38] of a laser beam ( $\lambda = 632.8$  nm) through a homogeneously aligned ITO-coated liquid crystal cell of all the binary mixtures along with pure 8OCB compound. The obtained experimental data for the investigated system has been represented in Fig. 3.3. At the  $I-N$  transition, the temperature dependence of birefringence ( $\Delta n$ ) demonstrates a sharp change, indicating a first-order nature of that transition. On further cooling, well within the nematic phase, the  $\Delta n$  value continues to increase with decrease in temperature which again follows a more or less identical pattern for all the mixtures under study. Such a change is in effect due to the enhancement of molecular ordering in the mesogenic medium with decreasing temperature. Moreover, it has been noticed that all the  $\Delta n$  vs. temperature curves are accompanied with a small but finite measurable

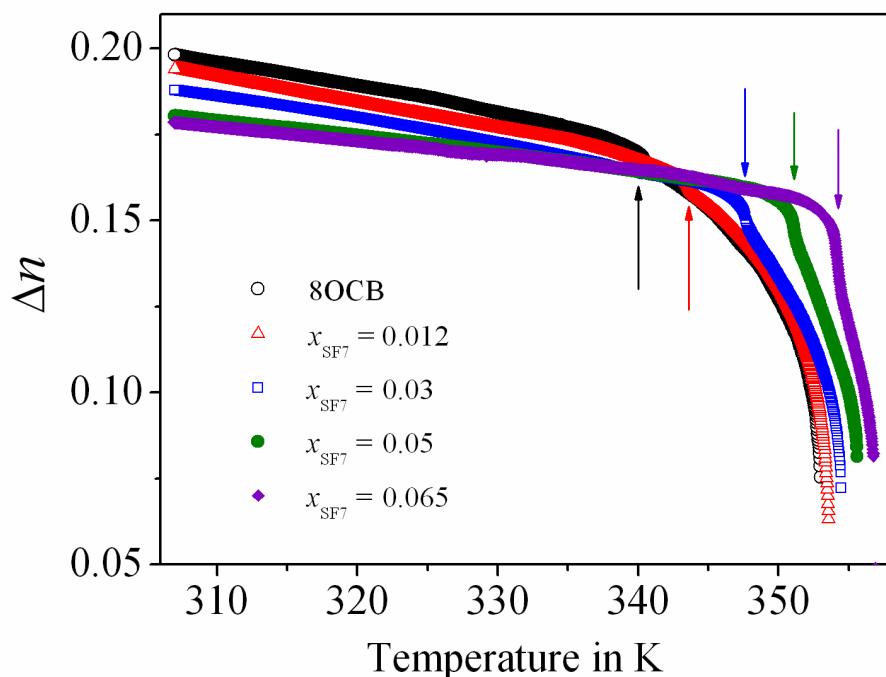
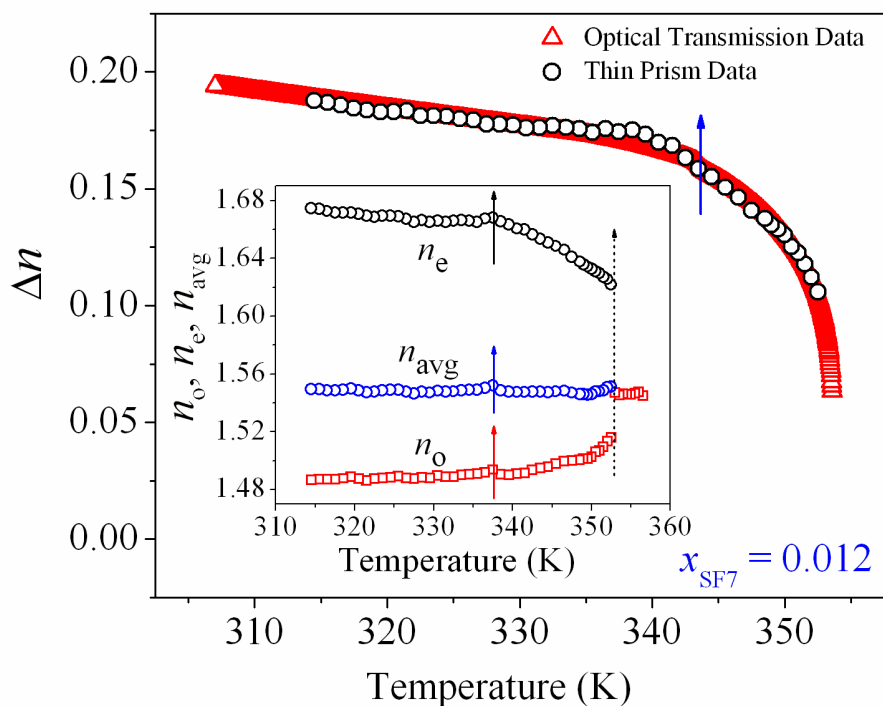


**Figure 3.3.** Temperature dependence of optical birefringence ( $\Delta n$ ) data for all the mixtures along with that for pure 8OCB. Vertical arrows show the  $N$ – $Sm-A$  phase transition for all the mixtures.

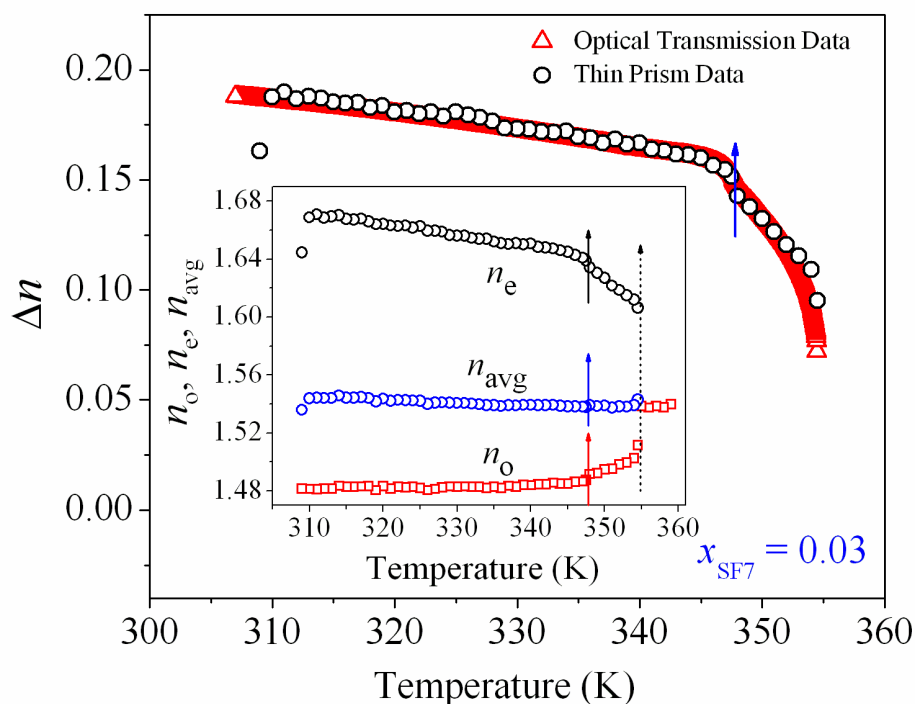
change in  $\Delta n$  on entering the low temperature  $Sm-A$  phase, which again is due to the development of additional translational ordering. A quite visible pretransitional behavior has been observed in the  $\Delta n$  curve within the nematic phase in the range of 2.2 K to 4.9 K, prior to the  $N$ – $Sm-A$  phase transition. Such an influence is owing to the coupling between the nematic and smectic- $A$  order parameters. Moreover, this coupling becomes stronger with shrinkage in the nematic width [39]. So in this case, by varying the concentration of SF7 in the host mesogen, the width of the nematic phase and hence the strength of the coupling between nematic and smectic- $A$  order parameter and therefore the resultant pretransitional behavior can be investigated.

### 3.4.2. Thin prism technique

The thin prism technique [40] has been used to measure the extraordinary ( $n_e$ ) and ordinary ( $n_o$ ) refractive indices for all of the mixtures under study by probing a laser beam of wavelength  $\lambda = 632.8$  nm. The variation

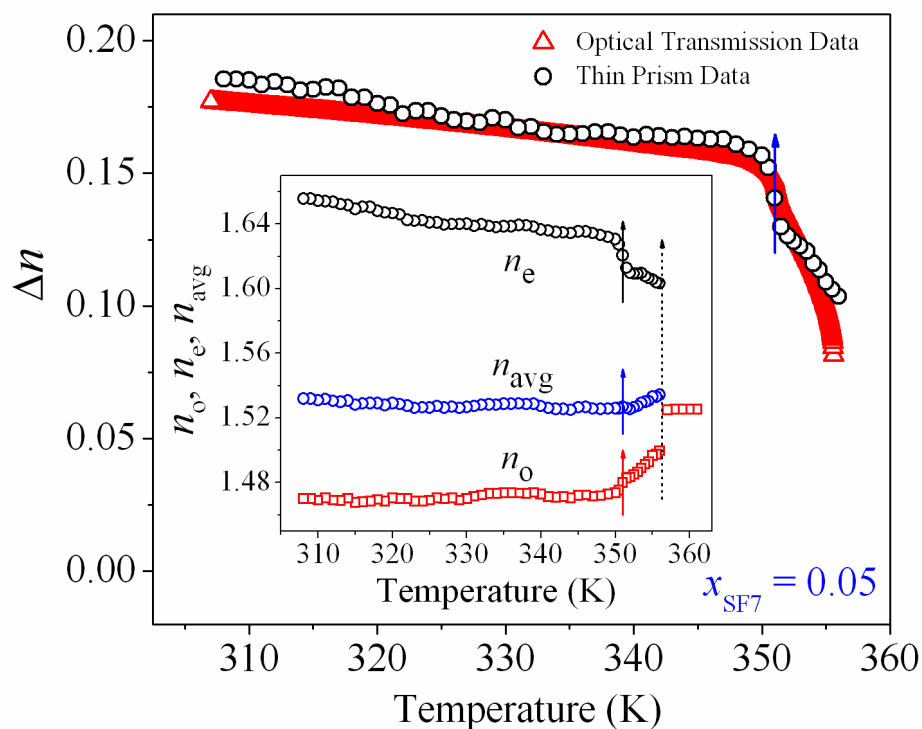


(a)

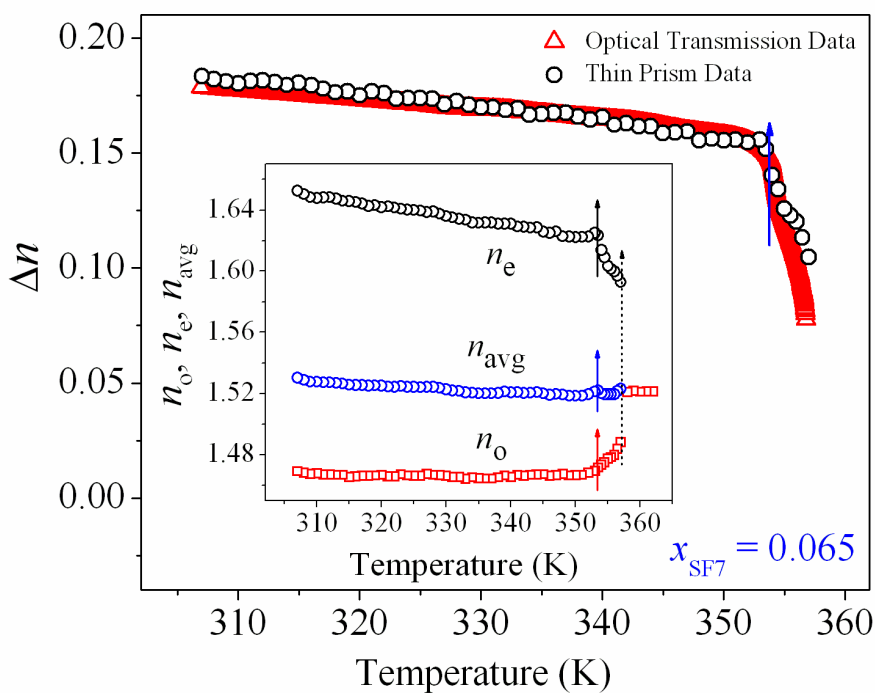


(b)

**Figure 3.4.** Refractive indices ( $n_e$ ,  $n_o$ ) and birefringence ( $\Delta n = n_e - n_o$ ) as a function of temperature for (a)  $x_{\text{SF7}} = 0.012$ , (b)  $x_{\text{SF7}} = 0.03$ . Dashed arrow and solid arrows denote the isotropic-nematic ( $T_{IN}$ ) and nematic-smectic-A ( $T_{NA}$ ) transition temperatures respectively.



(c)



(d)

**Figure 3.4 (cont'd).** Refractive indices ( $n_e$ ,  $n_o$ ) and birefringence ( $\Delta n = n_e - n_o$ ) as a function of temperature for (c)  $x_{\text{SF7}} = 0.05$ , (d)  $x_{\text{SF7}} = 0.065$ . Dashed arrow and solid arrows denote the isotropic–nematic ( $T_{IN}$ ) and nematic–smectic-A ( $T_{NA}$ ) transition temperatures respectively.

---

---

of two principal refractive indices ( $n_o$ ,  $n_e$ ) along with the average refractive index ( $n_{\text{avg}}$ ) with temperature for four different mixtures are shown in inset of Fig. 3.4(a-d). These figures clearly reveals that the measured refractive index ( $n_{\text{iso}}$ ) in the isotropic ( $I$ ) phase is nearly invariant with respect to the change in temperature. But at the  $I$ - $N$  phase transition, the refractive index splits into two parts, *i.e.*, one with higher and another with lower than the isotropic value correspond to the extraordinary ( $n_e$ ) and ordinary ( $n_o$ ) refractive indices respectively. The higher refractive index ( $n_e$ ) is found to be strongly temperature dependent within the whole mesomorphic range while the ordinary component ( $n_o$ ) is weakly dependent on temperature except in the vicinity of isotropic–nematic phase transition. Moreover, the  $n_o$ ,  $n_e$  data do not show any pronounced change near the  $N$ -Sm-A transition for all the investigated mixtures. The temperature dependent variation of the optical birefringence ( $\Delta n = n_e - n_o$ ) value for all of the investigated mixtures are also shown in the respective figures. It is quite evident that a relatively higher value of  $\Delta n$  in the Sm-A phase compared to  $N$  phase is due to the increase of molecular ordering, which results in an enhancement of the optical anisotropy. Nevertheless, the temperature variation of  $\Delta n$  in the Sm-A phase is comparatively sluggish compared to that in the nematic phase. Therefore, the measured  $\Delta n$  value reveals a quite well agreement obtained from both the optical transmission method and thin prism technique. In spite of such agreement, the  $\Delta n$  values obtained from high-resolution optical transmission technique are most efficient for further analysis owing to have small temperature interval between the successive data points.

### 3.5. Critical behavior at the $I$ - $N$ phase transition

In order to probe the critical behavior of the  $I$ - $N$  phase transition, proper understanding of the scalar order parameter  $S(T)$  [41] associated with the local field around a molecule is necessary. Two most widely accepted models are – (i) the isotropic internal field model, proposed by Vuks, Chandrasekhar and

Madhusudana (VCM model) [42,43], and (ii) the anisotropic internal field model of Neugebauer, Maier and Saupe (NMS model) [44-46].

According to VCM model, molecular polarizability ( $\alpha$ ) of a mesogenic medium is linked with the birefringence ( $\Delta n$ ) through the following relation:

$$\frac{\Delta\alpha}{\langle\alpha\rangle} S(T) = \frac{\Delta(n^2)}{\langle n^2 \rangle - 1} \quad (3.1)$$

where  $\Delta(n^2) = n_e^2 - n_o^2$  is the anisotropy of the square of the refractive index and  $\langle n^2 \rangle = (n_e^2 + 2n_o^2)/3$ , while  $n_e$  and  $n_o$  are the extraordinary and ordinary refractive indices respectively. The molecular polarizability anisotropy is termed as  $\Delta\alpha = \alpha_l - \alpha_t$  and the mean polarizability  $\langle\alpha\rangle = (\alpha_l + \alpha_t)/3$  where  $\alpha_l$  and  $\alpha_t$  are the longitudinal and transverse polarizabilities with respect to the long molecular axis, respectively. Moreover, to determine the temperature dependence of the nematic order parameter  $S(T)$ , the four-parameter power-law expression related to the mean-field theory for both the critical and tricritical character of a weakly first-order transition [18,47] has been used which can be expressed as:

$$S(T) = S^{**} + A \left| \left( 1 - \frac{T}{T^{**}} \right) \right|^\beta \quad (3.2)$$

where  $\beta$  represents the order parameter critical exponent,  $A$  is a constant,  $T^{**}$  is the effective second order transition temperature below the clearing temperature ( $T_{IN}$ ). This absolute limit of the superheating temperature in the nematic phase is found to be slightly higher than the observed  $I-N$  phase transition temperature ( $T_{IN}$ ). Hence, at  $T = T^{**}$ ,  $S(T^{**}) = S^{**}$ .

By introducing appropriate scaling condition and few approximations one can couple both the Eq. (3.1) and Eq. (3.2) together and modified to [48-50]:

$$\Delta n = \zeta \left[ S^{**} + (1 - S^{**}) \left| \left( 1 - \frac{T}{T^{**}} \right) \right|^\beta \right] \quad (3.3)$$

where,  $\zeta = (\Delta\alpha/\alpha)[(n_l^2 - 1)/2n_l]$  and  $n_l$  is the refractive index in the isotropic phase (just above  $T_{IN}$ ).

The critical anomaly near the  $I$ - $N$  phase transition has been evaluated by using a fitting procedure to the temperature dependence of high-resolution optical birefringence data with a simple power-law formula as expressed in Eq. (3.3) [51,52]. Fig. 3.5 illustrates the fitting curves of Eq. (3.3) with  $\Delta n$  for the pure compound 8OCB along with the investigated mixtures and the corresponding fit parameters are listed in Table 3.1.

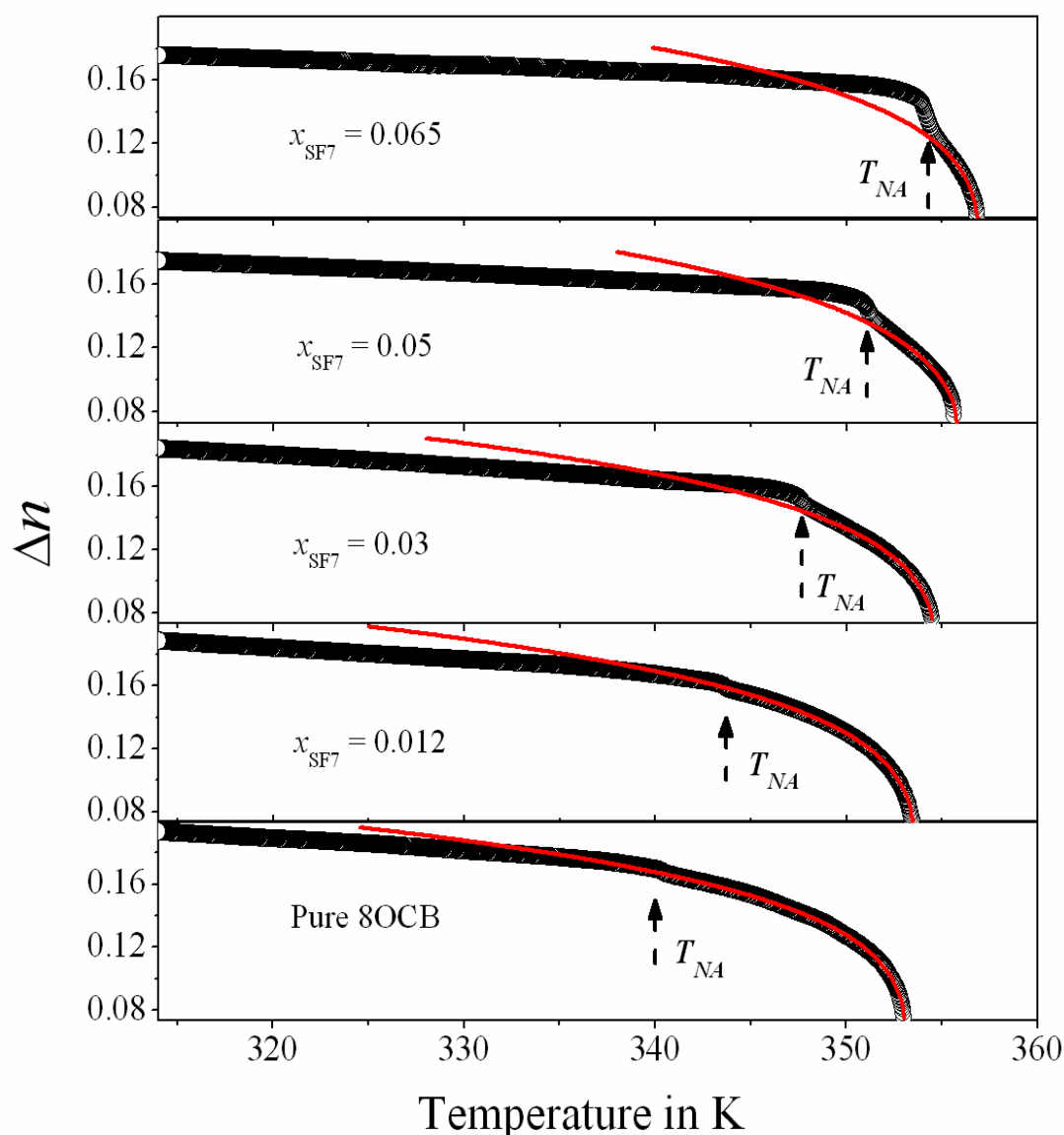


**Figure 3.5.** Variation of the temperature-dependent optical birefringence data for all the mixtures including pure 8OCB. Dashed arrow denotes the nematic–smectic-A ( $T_{NA}$ ) transition temperature. The solid line is a fit to Eq. (3.3).

**Table 3.1.** Values of the fit parameters obtained from the four-parameter fit of the temperature dependence of  $\Delta n$  to Eq. (3.3).

$x_{\text{SF7}}$	$\zeta$	$S^{**}$	$T^{**}$ in K	$\beta$	$\chi_v^2$
0	0.336±0.025	0.099±0.012	353.15±0.64	0.248±0.075	1.01
0.012	0.344±0.004	0.084±0.026	353.60±0.16	0.248±0.014	1.24
0.03	0.337±0.104	0.080±0.045	354.68±2.38	0.249±0.028	1.33
0.05	0.356±0.062	0.058±0.042	356.09±2.20	0.250±0.051	1.49
0.065	0.353±0.054	0.087±0.031	356.96±1.80	0.253±0.018	1.62

The quality of the fits has been tested with the aid of the reduced error function  $\chi_v^2$ , which is defined as the ratio of the variance of the fit ( $s^2$ ) data to the variance of the experimental data ( $\sigma^2$ ) [53],

$$\chi_v^2 = \frac{s^2}{\sigma^2} = \frac{1}{N-p} \sum_i \frac{1}{\sigma_i^2} (Q_i^{\text{obs}} - Q_i^{\text{fit}})^2 \quad (3.4)$$

Here  $N$  is the total number of data points,  $p$  is the number of adjustable parameters,  $Q_i^{\text{fit}}$  is the  $i^{\text{th}}$  fit value corresponding to the measurement  $Q_i^{\text{obs}}$ , and  $\sigma^i$  is the standard deviation corresponding to  $Q_i^{\text{obs}}$ . For an ideal fit,  $\chi_v^2$  is unity but in general values ranging between 1 and 1.5 corresponds to good fits.

Moreover, the fitting procedure have been performed only in the stable nematic range excluding the region very close to the transitions where the pretransitional effect of both the  $I-N$  and  $N-Sm-A$  are pronounced. Hence for the mixture with small nematic range ( $\sim 2.7$  K) provides only 2 K of usable nematic range for the fitting. The fitted curves are represented by red lines in Fig. 3.5 extrapolating into the smectic-A phase. In the present investigated system, the obtained order parameter critical exponent ( $\beta$ ) values lie in between 0.248 and 0.253 within a reasonable error limit. However, in case of three parameter Haller's method, reported  $\beta$  values are generally found less than 0.2, inconsistent with the nature of the weakly first-order character of the  $I-N$  phase transition [54]. Therefore, the four parameter power law expression approaches the theoretically predicted value better than the Haller's type expression as far

as the  $\beta$  value is concerned. According to tricritical hypothesis (TCH) of Keyes [16] and Anisimov *et al.* [17,18], the order parameter critical exponent endorse a value equal to 0.25 and hence the extracted  $\beta$  values in the present system are found to be concurred with the theoretically predicted tricritical value. Therefore, this study confirms the tricritical nature of the  $I$ - $N$  phase transition and discards the possibility of lower  $\beta$  values.

### 3.6. Critical behavior at the $N$ - $Sm$ - $A$ phase transition

The  $N$ - $Sm$ - $A$  phase transition is accompanied with an enhancement of orientational ordering, motivated by coupling between nematic and smectic order parameters. However, the temperature-dependent smectic- $A$  order parameter is related to specific heat capacity exponent  $\alpha$  as [21,55,56]:

$$\langle |\psi|^2 \rangle = U \pm V^\pm \left| \left( \frac{T}{T_{NA}} - 1 \right) \right|^\kappa \quad (3.5)$$

where  $\kappa = 1 - \alpha$ , and the  $\pm$  signs refer to quantities above and below the  $N$ - $Sm$ - $A$  phase transition temperature ( $T_{NA}$ ) respectively. According to mean field model, the quantity  $(S - S_0)$  is proportional to  $\langle |\Psi|^2 \rangle$ , where  $S_0$  is the nematic order parameter in absence of any smectic ordering [21,57]. Moreover, the nematic order parameter ( $S$ ) is also proportional to  $\Delta n$ . Hence, by investigating the behavior of optical birefringence in the vicinity of  $N$ - $Sm$ - $A$  phase transition, an identical power-law divergence behavior and a critical exponent ( $\alpha'$ ) identical to specific heat capacity critical exponent ( $\alpha$ ) can be established.

In an effort to investigate this critical region and as well as to reveal the unique aspects of the  $N$ - $Sm$ - $A$  phase transition the high-resolution optical birefringence ( $\Delta n$ ) data have been used to obtain an insight into the critical behavior at the  $N$ - $Sm$ - $A$  phase transition. Although the  $\Delta n$  curves do not accompanied by any visible discontinuity at the  $N$ - $Sm$ - $A$  phase transition, a quantity  $n' = -d(\Delta n)/dT$ , *i.e.*, the first order temperature derivative of  $\Delta n$  has been used to identify the exact transition temperature. The quantity  $n'$  has also been found to be related to specific heat capacity anomaly [58] and may be

utilized to investigate the critical fluctuations associated with that transition. But in this case, due to small temperature interval between the successive data points, the numerically obtained temperature derivative of  $\Delta n$  is significantly scattered. Hence, it is reasonable to introduce another differential quotient  $Q(T)$ , defined as [51,52,59]

$$Q(T) = -\frac{\Delta n(T) - \Delta n(T_{NA})}{T - T_{NA}} \quad (3.6)$$

where  $\Delta n(T_{NA})$  is the birefringence value at the  $N$ -Sm- $A$  phase transition temperature ( $T_{NA}$ ). The quantities  $n'$  and  $Q(T)$  share the identical power-law behavior and hence are characterized by the same critical exponent  $\alpha'$  describing the transitional fluctuations. In an attempt to obtain an impression of the limiting behavior of the quotient  $Q(T)$  at the  $N$ -Sm- $A$  phase transition, fits to the following renormalization group expression including the corrections to scaling term have been performed [59,60]:

$$Q(T) = A^\pm |\tau|^{-\alpha'} (1 + D^\pm |\tau|^\Delta) + E(T - T_{NA}) + B \quad (3.7)$$

where,  $\tau = (T - T_{NA})/T_{NA}$ ,  $\pm$  denote terms above and below  $T_{NA}$ ,  $A^\pm$  denotes the critical amplitudes,  $D^\pm$  are the coefficients of the first corrections-to-scaling terms,  $\alpha'$  is the effective critical exponent similar to specific heat capacity critical exponent,  $\Delta$  is the first corrections-to-scaling exponent and  $B$  represents the combined critical and regular backgrounds while the term  $E(T - T_{NA})$  stands for a temperature dependant part of the regular background contribution. The theoretically predicted value of  $\Delta$  is 0.524 for a 3D-XY case [61,62] and in this analysis it is set fixed at 0.5 without any further variation. The temperature dependence of the quotient  $Q(T)$  for four different mixtures under investigation along with that for pure 8OCB are shown in Fig. 3.6. Fits to Eq. (3.7) on either sides of the  $N$ -Sm- $A$  transition temperature are depicted as solid red lines in the same figure. The values of the fit parameters are listed in Table 3.2. During the fit process, few data points very close to the transition have been excluded to avoid the error resulting from the experimental uncertainty. Fits have been carried out for different temperature ranges and that interval for which the fit

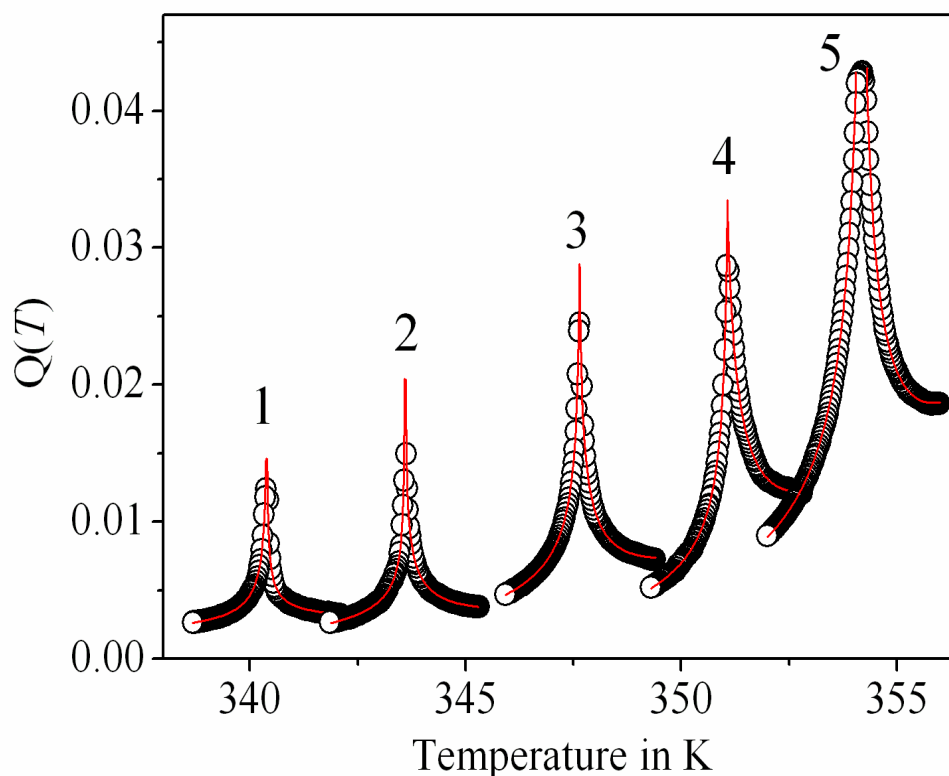


**Figure 3.6.** Temperature dependent variation of the quotient  $Q(T)$  in the vicinity of  $N$ - $Sm$ - $A$  phase transition for different mole fractions of SF7. Data are arranged in sequence of increasing mole fraction of SF7 from left to right with 1: 8OCB; 2:  $x_{SF7} = 0.012$ ; 3:  $x_{SF7} = 0.03$ ; 4:  $x_{SF7} = 0.05$ ; 5:  $x_{SF7} = 0.065$ . The solid lines are fit to Eq. (3.7).

**Table 3.2.** Results corresponding to the best fit for  $Q(T)$  near the  $N$ - $Sm$ - $A$  phase transition obtained in accordance with Eq. (3.7) and related  $\chi_v^2$  values associated with the fits.  $|\tau|_{\max}$  presents the upper limit of reduced temperature considered for these fits.

$x_{SF7}$	$\alpha'$	$A/A^+$	$D/D^+$	$ \tau _{\max}$	$\chi_v^2$
0.00	$0.201 \pm 0.005$	$0.87 \pm 0.005$	$0.83 \pm 0.002$	$5 \times 10^{-3}$	1.15
0.012	$0.278 \pm 0.003$	$0.97 \pm 0.001$	$0.98 \pm 0.003$	$5 \times 10^{-3}$	1.21
0.03	$0.379 \pm 0.006$	$1.00 \pm 0.004$	$1.00 \pm 0.015$	$5 \times 10^{-3}$	1.55
0.05	$0.440 \pm 0.010$	$0.88 \pm 0.032$	$0.99 \pm 0.024$	$5 \times 10^{-3}$	1.30
0.065	$0.485 \pm 0.019$	$1.01 \pm 0.066$	$0.99 \pm 0.056$	$5 \times 10^{-3}$	1.71

---

parameters remain practically stable for a small change in temperature range along with a minimum regular pattern in the residuals, have been considered [63]. The quality of the fits has been tested with the aid of the reduced error function  $\chi_v^2$ . In our present investigation,  $\chi_v^2$  values lie in the range between 1.15 and 1.71, which indicates a consistent fit of the temperature dependence of the quotient  $Q(T)$  to the model expression (3.7) considered. In each fit, from the temperature dependence of  $d(\Delta n)/dT$ , the transition temperature was first isolated and then kept fixed. This reduces the instability appearing in the least-squares minimization significantly.

The concentration dependence of the extracted effective critical exponent  $\alpha'$  values for the present investigated mixtures including that for the pure 8OCB is displayed in Fig. 3.7 while the variation of the same against the McMillan ratio (*i.e.*,  $T_{NA}/T_{IN}$ ) is illustrated in Fig. 3.8. The measured value of the critical exponent  $\alpha'$  for pure 8OCB has been found to be  $0.201 \pm 0.005$ , which again is consistent with those reported in literature [64-66]. It has been observed that with increasing hockey stick compound concentration,  $\alpha'$  increases monotonically from  $0.278 \pm 0.003$  for  $x_{SF7} = 0.012$  to  $0.485 \pm 0.019$  for  $x_{SF7} = 0.065$ , *i.e.*, the yielded values are in between those for a 3D-XY system (*i.e.*,  $\alpha_{3D-XY} = -0.007$ ) and for the tricritical case (*i.e.*,  $\alpha_{TCH} = 0.5$ ). Hence, non-universal values have been obtained for the effective critical exponent  $\alpha'$  and hence indicating a crossover character for the  $N$ -Sm- $A$  phase transitions in the present investigated mixtures. Moreover, throughout the concentration range, both the quotients  $A^-/A^+$  and  $D^-/D^+$  remain more or less equal to unity, indicating a symmetry of the  $Q(T)$  wings in both the Sm- $A$  and  $N$  phases.

Investigation of Fig. 3.7 and Fig. 3.8 reveals that an extrapolation of a quadratic fit to extracted  $\alpha'$  values results a crossover from second order to first order character for a composition  $x_{SF7} \sim 0.072$  with  $\alpha' = 0.5$ , with the associated McMillan ratio (*i.e.*,  $T_{NA}/T_{IN}$ ) being 0.994. Therefore, the tricritical point (TCP) for the investigated binary system is reached approximately at  $x_{SF7} \sim 0.072$ . It is

---

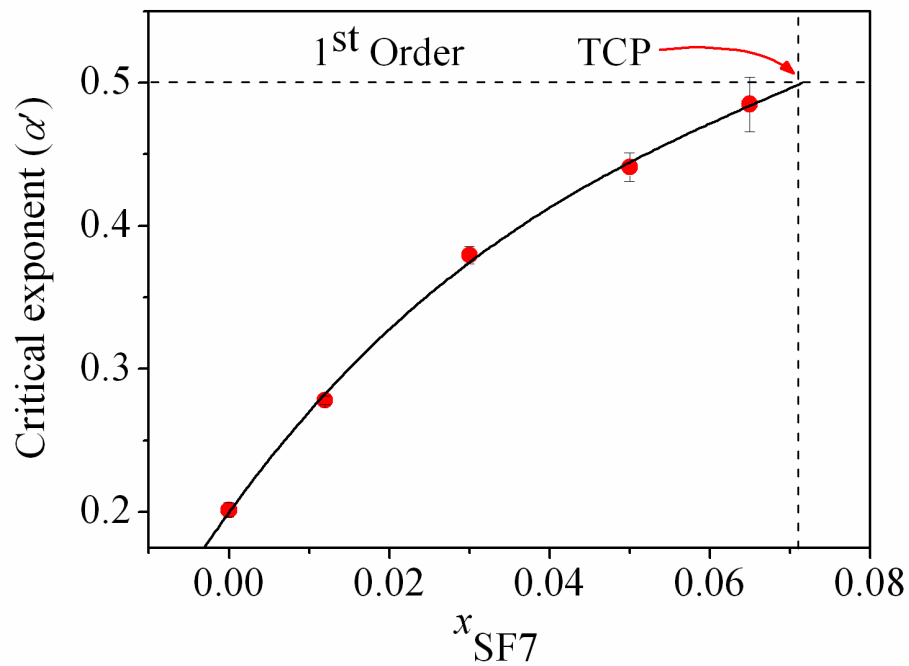


**Figure 3.7.** Concentration dependence of the effective critical exponent ( $\alpha'$ ) obtained by fitting  $Q(T)$  to Eq. (3.7). The vertical dashed line corresponds to the tricritical point (TCP). The solid line is a 2<sup>nd</sup> order polynomial fit to the data.

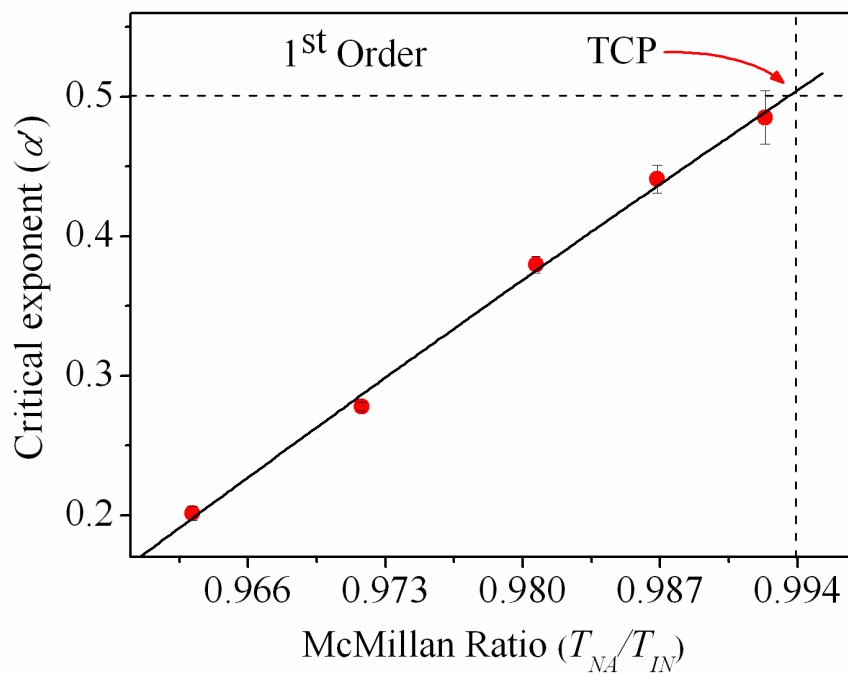


**Figure 3.8.** Variation of effective critical exponent ( $\alpha'$ ) with McMillan ratio ( $T_{\text{NA}}/T_{\text{IN}}$ ). The vertical dashed line corresponds to the tricritical point (TCP). The solid line is a linear fit to the data.

quite clear that addition of this angular mesogenic compound (SF7) in the calamitic medium (8OCB) strengthens the coupling between the nematic (S) and smectic ( $\Psi$ ) order parameters which again lead to a decrease in the nematic width. Additionally this coupling becomes considerably stronger for a relatively small increase in concentration of the angular mesogenic compound in the mixtures. Such an outcome is possibly due to modification in effective intermolecular interaction and the local molecular ordering in the host medium due to the introduction of the hockey stick-shaped dopant, which again drives the transition from second order to first order character [67].

Moreover, below the  $N$ -Sm- $A$  transition an analysis has also been carried out to characterize the critical behavior using an expression related to the reduced temperature ( $\tau'$ ) [67], as follows:

$$\Delta n = A|\tau'|^\lambda + B|\tau'| + C \quad (3.8)$$

where,  $|\tau'| = |1 - T/T_{NA}|$  is the reduced temperature,  $A$  is a constant and  $B|\tau'|$  presents the temperature-dependent part of the regular background, whereas  $C$  is the combined critical and regular background term and  $\lambda$  gives the critical coefficient. A representation of reduced temperature dependent value of  $\Delta n$  below the  $N$ -Sm- $A$  phase transition for all the mixtures has been presented in Fig. 3.9, while the fits to Eq. (3.8) has also been included on corresponding data points by red solid lines. The fit parameters so obtained are listed in Table 3.3. Range of  $\tau'$  has been taken to a value from 0 to 0.007 and this effectively made a temperature range 2.5 K below the  $N$ -Sm- $A$  phase transition. It has been observed from Table 3.3 that the exponent  $\lambda$  assumes a value of  $0.638 \pm 0.024$  for pure 8OCB and with increasing concentration of SF7 the  $\lambda$  value decreases to  $0.506 \pm 0.008$  for  $x_{SF7} = 0.065$ . Furthermore, for a long-range ordered system, scaling theory requires  $\lambda = 2\beta$ , where  $\beta$  is the critical exponent related to limiting behavior of order parameter at the  $N$ -Sm- $A$  phase transition. Additionally, by considering the Landau-de Gennes theory this exponent  $\lambda$  is

equal to  $(1-\alpha)$  for few mesogenic systems [56] and for a number of other mesogens it has been seen that  $\lambda < (1-\alpha)$  [56].

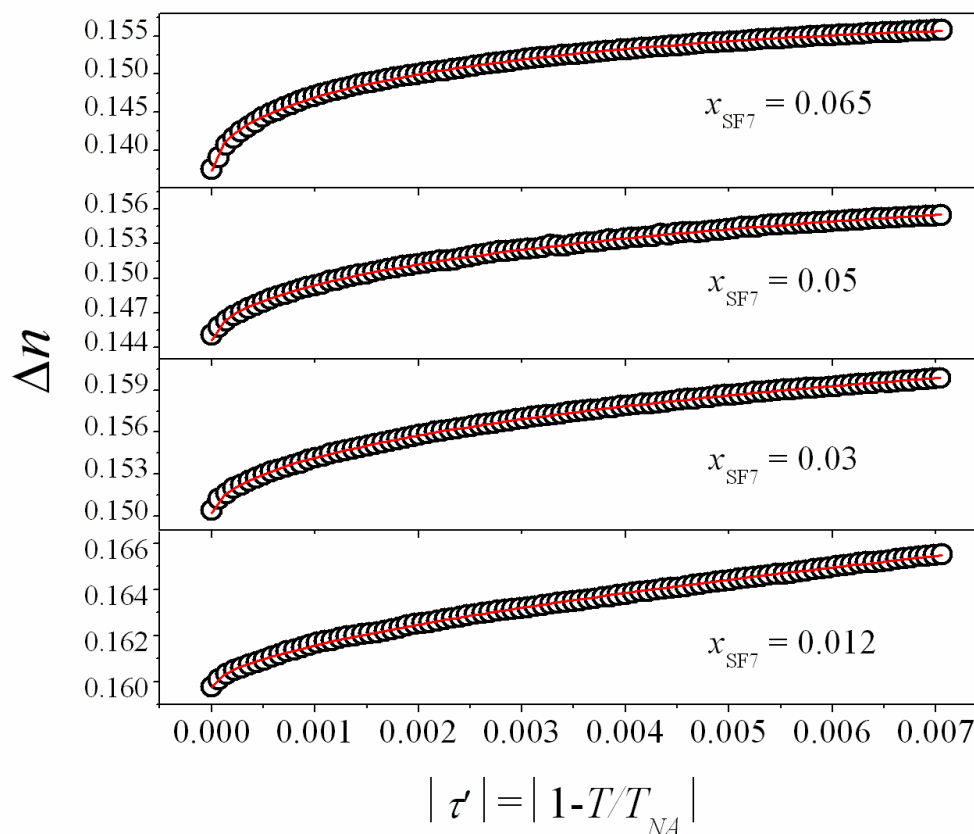


**Figure 3.9.** Plot of optical birefringence as a function of reduced temperature  $|\tau| = |1 - T/T_{NA}|$  for different mixtures. The solid lines are fit to Eq. (3.8).

**Table 3.3.** Values of the fit parameters obtained from the fit of the temperature dependence of  $\Delta n$  to Eq. (3.8).

$x_{SF7}$	$A$	$\lambda$	$\beta' (= \lambda/2)$	$B$	$C$	$\chi_v^2$
0	$0.094 \pm 0.043$	$0.638 \pm 0.024$	$0.319 \pm 0.012$	$0.202 \pm 0.094$	0.16818	1.6
0.012	$0.101 \pm 0.019$	$0.587 \pm 0.027$	$0.294 \pm 0.013$	$0.025 \pm 0.056$	0.15981	1.34
0.03	$0.218 \pm 0.015$	$0.562 \pm 0.009$	$0.281 \pm 0.005$	$-0.540 \pm 0.047$	0.15022	1.05
0.05	$0.223 \pm 0.022$	$0.537 \pm 0.014$	$0.268 \pm 0.007$	$-0.664 \pm 0.075$	0.14461	1.22
0.065	$0.373 \pm 0.172$	$0.506 \pm 0.008$	$0.253 \pm 0.004$	$-1.705 \pm 0.543$	0.1373	1.41

Combining all these conditions, it can be predicted that the  $\lambda$  values should lie in a range of  $2\beta \leq \lambda \leq (1-\alpha)$ . In the present system, it is clearly observed from Tables 3.2 and 3.3 that the extracted  $\lambda$  values are relatively smaller than the computed  $(1-\alpha)$  values, whereas  $\alpha$  is considered as  $\alpha'$  (Table 3.2). Again, if the extracted  $\lambda/2$  values are plotted against McMillan ratio, extrapolation to a quadratic fit of these values assigned a tricritical point at a McMillan ratio of  $\sim 0.994$ , which is almost equal value as obtained by the fit to  $\alpha'$  values, shown in Fig. 3.10. Therefore, it can be safe to assume  $\beta \cong \lambda/2 = \beta'$ . A comparison of the obtained values of  $\beta'$  for an another binary system [67] comprising a different hockey stick-shaped compound 4-(3-*n*-decyloxy-2-methyl phenyliminomethyl) phenyl 4-*n*-dodecyloxycinnamate (H-22.5) and the rod-like mesogen octylcyanobiphenyl (8CB) has been included in the present system on the same figure and reveals a close agreement of the obtained  $\beta'$

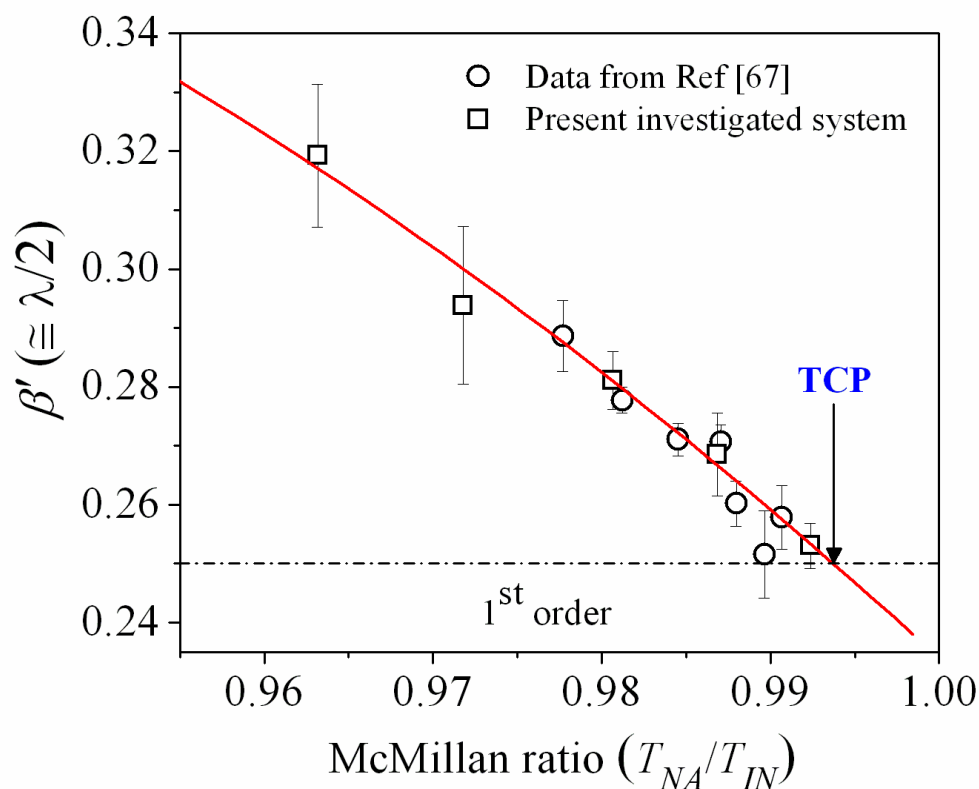


**Figure 3.10.** Variation of order parameter critical exponent ( $\beta'$ ) value with McMillan ratio ( $T_{NA}/T_{IN}$ ). The solid line is a second-order polynomial fit to the data.

---

---

values for both the systems. Hence, a crossover behavior of critical exponents ( $\alpha'$ ,  $\beta'$ ) within the limit of uncertainty has been established in the present investigated system.

In an earlier investigation [67] on an another binary system comprising of a different hockey stick-shaped mesogen H-22.5 with a lateral methyl group and the rod-like compound 8CB, the effective order parameter critical exponent ( $\beta$ ) for the  $I$ - $N$  phase transition has been found to be in agreement with the tricritical hypothesis. On the other hand, a crossover character has been revealed for the  $N$ - $Sm-A$  phase transition, with the related effective critical exponent ( $\alpha'$ ) being non-universal in nature. Furthermore, for the  $N$ - $Sm-A$  phase transition, the extracted critical character has usually been found to be sensitive to the width of the nematic phase range. The nematic width has also been found to be shrunk considerably with enhancing hockey stick molecule concentration along with the related effective critical exponent  $\alpha'$ , attaining a value of  $0.460 \pm 0.016$  for a mole-fraction 0.08 of the hockey stick-shaped compound. Due to a relatively small width of the nematic phase ( $\sim 7$  K) in the host 8CB, it became possible to investigate the critical exponent variation over a relatively narrow range (in between  $\alpha' = 0.319$  and  $0.46$ ). Now in the present study, the compound 8OCB possesses a comparatively larger nematic width ( $\sim 13$  K) and hence it is expected that the dependence of  $\alpha'$  on the McMillan ratio can be investigated on a relatively broad scale. However, in the present mixtures  $\alpha'$  has been found to vary between  $0.278 \pm 0.003$  and  $0.485 \pm 0.019$  depending on the dopant concentration and hence the variation range is marginally greater than that in the previous study. Furthermore, this variation is manifested over a relatively short range of concentration variation of the angular dopant in the host mesogen (*i.e.*,  $x_{SF7} = 0.012$  to  $0.065$ ) as compared to the earlier case. Such a strong augmentation in the exponent  $\alpha'$  certainly indicates a relatively rapid growth in the local molecular ordering and hence the coupling between the order parameters  $S$  and  $\Psi$ . A further indication

of such increase in coupling is the rather steep slope of the phase boundary, a measure of which again can be manifested by calculating related average  $d(T_{NA})/dx$  value. In the present case, the slope has been found to be  $\sim 212$  K which again is comparatively greater than the previous value  $\sim 169$  K. Furthermore, the concentration dependence of the nematic width has also been found to demonstrate a relatively sharp decrease (slope  $\sim 150$  K) compared to the former study (slope  $\sim 50$  K). Such an outcome is perhaps due to the fine structural dissimilarity between SF7 and H-22.5.

Both the hockey stick-shaped compounds possess a more or less identical molecular configuration except the presence of a lateral methyl group in the obtuse angle between the *meta*-alkyloxy chain attached to the terminal phenyl ring and the azomethine connecting group in H-22.5. Such a substitution has been observed to impart a dramatic influence on the phase behavior of H-22.5 causing the emergence of a nematic phase in a small temperature range [68]. Steric interactions between the methyl group and the

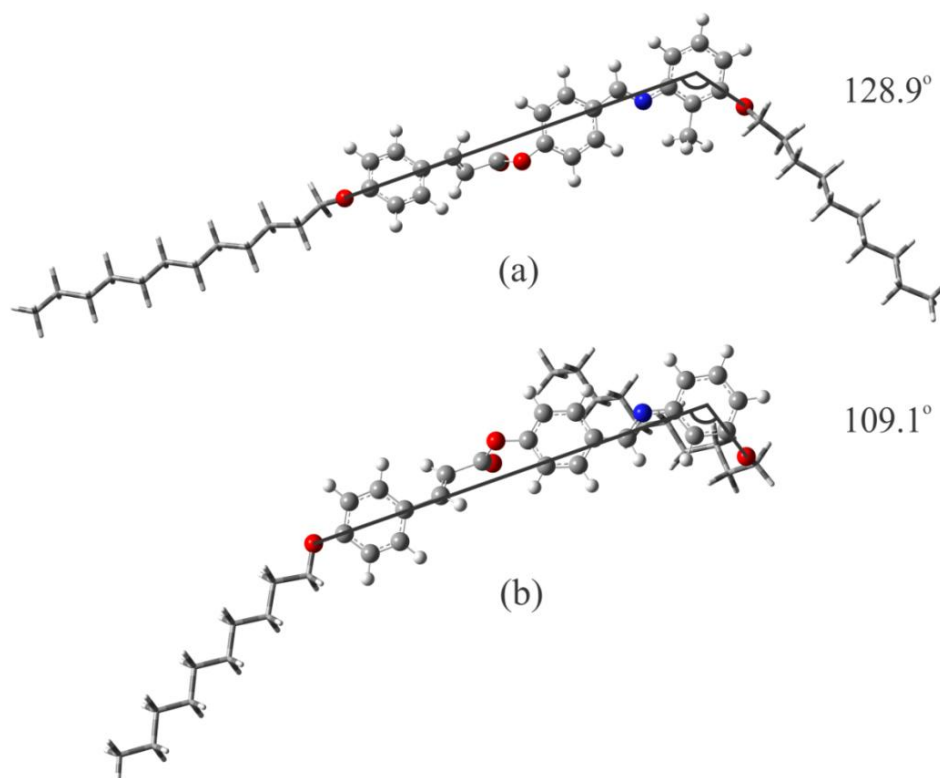


**Fig. 3.11.** Optimized molecular structure of (a) H-22.5, (b) SF7.

---

---

neighboring alkoxy chain in the *meta*-position in H-22.5 perhaps induce a more rod-like shape compared to SF7 which again is facilitated in a relatively less augmentation of the local molecular order and hence in a rather less strengthening of the coupling between S and  $\Psi$ . In an attempt to gain an idea, the molecular bend-angle of both the compounds has been calculated using Gauss View. The bend-angle appeared to be  $128.9^\circ$  and  $109.1^\circ$  for compounds H-22.5 and SF7 (as shown in Fig. 3.11) respectively which again certainly imply more rod-like appearance for H-22.5.

### 3.7. Conclusion

In this work, systematic measurements have been carried out on high-resolution temperature dependence of optical birefringence for a binary system, consisting of a hockey stick-shaped liquid crystal compound, 4-(3-decyloxyphenyliminomethyl) phenyl 4-decyloxycinnamate (SF7) and the rod like 4-cyano-4'-octyloxybiphenyl (8OCB). The measured optical birefringence ( $\Delta n$ ) values demonstrate a quite well consistency obtained from both the optical transmission method and thin prism technique. However, due to quite high resolution as well as large number of data points, the birefringence value obtained from optical transmission technique are found to be rather successful in describing the transitional behavior more precisely at the *I-N* and *N-Sm-A* phase transitions in all the investigated mixtures. The temperature dependence of birefringence exhibits a sharp change at the *I-N* phase transition for all of the investigated mixtures. The extracted order parameter critical coefficient  $\beta$  has found to be very close to the theoretically predicted tricritical value ( $\beta = 0.25$ ) for the *I-N* phase transition. Furthermore, a continuous change of  $\Delta n$  at the *N-Sm-A* transition has been observed, indicating a second order nature of that transition. An enhancement in hockey stick-shaped compound in the mixtures lead to a significant decrease in the nematic width, *i.e.*, it stabilizes the low temperature smectic phase. A noticeable pretransitional behavior has been observed in the temperature dependence of  $\Delta n$  in a certain temperature

range above and below the  $N$ -Sm-A transition. The differential quotient  $Q(T)$  exhibits a diverging character in the vicinity of  $N$ -Sm-A transition which reveals a good conformity with a renormalization-group model. The related effective critical exponent ( $\alpha'$ ), describing the critical fluctuations at that transition, has appeared to be non-universal in nature. The  $\alpha'$  values follow a monotonic enhancement against the concentration variation of the hockey stick-shaped compound, where an extension of fit to the exponents results a crossover to first order nature of the  $N$ -Sm-A phase transition for a McMillan ratio of 0.994 which again is in close agreement with the reported value for the mixtures of similar mesogenic systems. Moreover, a critical exponent ( $\beta'$ ) identical to the order parameter critical exponent  $\beta$  at the  $N$ -Sm-A phase transition has been found to be concentration dependent and reveals a good agreement with the same obtained from another binary system consisting of a hockey stick-shaped compound H-22.5 and a rod-like mesogen 8CB. One interesting fact emerging out from this study is that the molecular bend of the angular mesogenic dopant imparts an influence on the phase-character of the mixtures involving angular mesogenic dopant. From the observations, it is clear that an enhanced molecular bend leads to a relatively stronger  $S - \Psi$  coupling and a sharp decrease in the nematic width. This again manifest in a rapid approach towards the first order nature of the  $N$ -Sm-A phase transition. The exact description, portraying the dependence of order character of the  $N$ -Sm-A phase transition on the molecular bend of mesogenic dopant requires further investigations involving mesogenic systems with varied dopant-host combinations.

---

---

**References:**

- [1] J. Thisayukta, H. Niwano, H. Takezoe, and J. Watanabe, *J. Am. Chem. Soc.*, **124**, 3354 (2002).
- [2] M. Nakata, Y. Takanishi, J. Watanabe, and H. Takezoe, *Phys. Rev. E*, **68**, 041710 (2003).
- [3] E. Gorecka, M. Čepič, J. Mieczkowski, M. Nakata, H. Takezoe, and B. Žekš, *Phys. Rev. E*, **67**, 061704 (2003).
- [4] R.E. Gorecka, M. Nakata, J. Mieczkowski, Y. Takanashi, K. Ishikawa, J. Watanabe, H. Takezoe, S.H. Eichhorn, and T.M. Swager, *Phys. Rev. Lett.*, **85**, 2526 (2000).
- [5] K. Kishikawa, N. Muramatsu, S. Kohmoto, K. Yamaguchi, and M. Yamamoto, *Chem. Mater.*, **15**, 3443 (2003).
- [6] C.K. Lee, J.H. Kim, E.J. Choi, W.C. Zin, and L.C. Chien, *Liq. Cryst.*, **28**, 1749 (2001).
- [7] E.J. Choi, X. Cui, W.C. Zin, C.W. Ohk, T.K. Lim, and J.H. Lee, *Chem. Phys. Chem.*, **8**, 1919 (2007).
- [8] R. Prathibha, N.V. Madhusudana, and B.K. Sadashiva, *Science*, **288**, 2184 (2000).
- [9] B. Kundu, R. Pratibha, and N.V. Madhusudana, *Phys. Rev. Lett.*, **99**, 247802 (2007).
- [10] P. Sathyanarayana, M. Mathew, Q. Li, V.S.S. Sastry, B. Kundu, K.V. Le, H. Takezoe, and S. Dhara, *Phys. Rev. E*, **81**, 010702 (2010).
- [11] A. Chakraborty, M.K. Das, B. Das, A. Lehmann, and C. Tschierske, *Soft Matter*, **9**, 4273 (2013).
- [12] T. Otani, F. Araoka, K. Ishikawa, and H. Takezoe, *J. Am. Chem. Soc.*, **131**, 12368 (2009).
- [13] C. Zhu, D. Chen, Y. Shen, C.D. Jones, M.A. Glaser, J.E. MacLennan, and N.A. Clark, *Phys. Rev. E*, **81**, 011704 (2010).

- 
- 
- [14] P.G. de Gennes, and J. Prost, in *The Physics of Liquid Crystals*, Oxford University Press, Oxford (1993).
- [15] W. Maier, and A. Saupe, *Z. Naturforsch. A*, **13a**, 564 (1958); **14a**, 882 (1959).
- [16] P.H. Keyes, *Phys. Lett. A*, **67**, 132 (1978).
- [17] M.A. Anisimov, S.R. Garber, V.S. Esipov, V.M. Mamnitskii, G.I. Ovodov, L.A. Smolenko, and E.L. Sorkin, *Sov. Phys. JETP*, **45**, 1042 (1977).
- [18] M.A. Anisimov, *Mol. Cryst. Liq. Cryst. Inc. Nonlinear Opt.*, **162**, 1 (1988).
- [19] K.K. Kobayashi, *Phys. Lett. A*, **31**, 125 (1970); *J. Phys. Soc. Jpn.*, **29**, 101 (1970).
- [20] W.L. McMillan, *Phys. Rev. A*, **4**, 1238 (1971).
- [21] P.G. de Gennes, *Mol. Cryst. Liq. Cryst.*, **21**, 49 (1973).
- [22] H. Marynissen, J. Thoen, and W. vanDael, *Mol. Cryst. Liq. Cryst.*, **97**, 149 (1983).
- [23] M.E. Huster, K.J. Stine, and C.W. Garland, *Phys. Rev. A*, **36**, 2364 (1987).
- [24] H. Marynissen, J. Thoen, and W. vanDael, *Mol. Cryst. Liq. Cryst.*, **124**, 195 (1985).
- [25] K.J. Stine, and C.W. Garland, *Phys. Rev. A*, **39**, 3148 (1989).
- [26] S.K. Sarkar, and M.K. Das, *RSC Adv.*, **4**, 19861 (2014).
- [27] S.K. Sarkar, and M.K. Das, *J. Mol. Liq.*, **199**, 415 (2014).
- [28] P. Cusmin, M.R. de la Fuente, J. Salud, M.A. Pérez-Jubindo, S. Diez-Berart, and D.O. López, *J. Phys. Chem. B.*, **111**, 8974 (2007).
- [29] C.W. Garland, and G. Nounesis, *Phys. Rev. E*, **49**, 2964 (1994).
- [30] J. Thoen, H. Marynissen, and W. Van Dael, *Phys. Rev. A*, **26**, 2886 (1982).
- [31] J. Thoen, *Int. J. Mod. Phys. B*, **09**, 2157 (1995).
- 
-

- 
- 
- [32] P. Cusmin, J. Salud, D.O. López, M.R. de la Fuente, S. Diez, M.A. Pérez-Jubindo, M. Barrio, and J.L. Tamarit, *J. Phys. Chem. B.*, **110**, 26194 (2006).
- [33] B.I. Halperin, T.C. Lubenski, and S.K. Ma, *Phys. Rev. Lett.*, **32**, 292 (1974).
- [34] G. Sarkar, B. Das, M.K. Das, U. Baumeister, and W. Weissflog, *Mol. Cryst. Liq. Cryst.*, **540**, 188 (2011).
- [35] A. Saipa, and F. Giesselmann, *Liq. Cryst.*, **29**, 347 (2002).
- [36] G. Sarkar, M.K. Das, R. Paul, B. Das, and W. Weissflog, *Phase Transit.*, **82**, 433 (2009).
- [37] T. Scharf, in *Polarized Light in Liquid Crystals and Polymers*, Wiley, Hoboken, NJ, (2007).
- [38] A. Prasad, and M.K. Das, *J. Phys.: Condens. Matter*, **22**, 195106 (2010).
- [39] P.G. de Gennes, *Solid State Commun.*, **10**, 753 (1972).
- [40] A. Prasad, and M.K. Das, *Phase Transit.*, **83**, 1072 (2010).
- [41] W. Maier, and A. Saupe, *Z. Naturforsch. A*, **13a**, 564 (1958); **14a**, 882 (1959).
- [42] M. F. Vuks, *Opt. Spectrosc.*, **20**, 361 (1966).
- [43] S. Chandrasekhar, and N.V. Madhusudana, *J. Phys. (Paris)*, **30**, C4-24 (1969).
- [44] H.E.J. Neugebauer, *Can. J. Phys.*, **32**, 1 (1954).
- [45] A. Saupe, and W. Maier, *Z. Naturforsch. A*, **16a**, 816 (1961).
- [46] H.S. Subramhanyam, and D. Krishnamurthi, *Mol. Cryst. Liq. Cryst.*, **22**, 239 (1973).
- [47] J. Thoen, and G. Menu, *Mol. Cryst. Liq. Cryst.*, **97**, 163 (1983).
- [48] I. Chirtoc, M. Chirtoc, C. Glorieux, and J. Thoen, *Liq. Cryst.*, **31**, 229 (2004).
- [49] S. Yildiz, H. Özbek, C. Glorieux, and J. Thoen, *Liq. Cryst.*, **34**, 611 (2007).
- 
-

- [50] S. Erkan, M. Çetinkaya, S. Yildiz, and H. Özbek, *Phys. Rev. E*, **86**, 041705 (2012).
- [51] H.E. Stanley, in *Introduction to Phase Transitions and Critical Phenomena*, Clarendon, Oxford, (1971).
- [52] R. Brout, in *Phase Transitions*, Benjamin, New York, (1965).
- [53] P. R. Bevington, and D.K. Robinson, in *Data Reduction and Error Analysis for the Physical Sciences*, McGraw-Hill, New York (2003).
- [54] I. Haller, *Progr. Solid State Chem.*, **10**, 103 (1975).
- [55] M.E. Fisher, and A. Aharony, *Phys. Rev. Lett.*, **31**, 1238 (1973).
- [56] K.K. Chan, M. Deutsch, B.M. Ocko, P.S. Pershan, and L.B. Sorensen, *Phys. Rev. Lett.*, **54**, 920 (1985).
- [57] K.-C. Lim, and J.T. Ho, *Phys. Rev. Lett.*, **40**, 944 (1978).
- [58] A.V. Kityk, and P. Huber, *Appl. Phys. Lett.*, **97**, 153124 (2010).
- [59] M.C. Cetinkaya, S. Yildiz, H. Ozbek, P. Losada-Perez, J. Leys, and J. Thoen, *Phys. Rev. E*, **88**, 042502 (2013).
- [60] C.W. Garland, in *Liquid Crystals: Experimental Study of Physical Properties and Phase Transitions*, S. Kumar (Ed.), Cambridge University Press, Cambridge (2001).
- [61] C. Bagnuls, and C. Bervillier, *Phys. Rev. B*, **32**, 7209 (1985).
- [62] C. Bagnuls, C. Bervillier, D.I. Meiron, and B.G. Nickel, *Phys. Rev. B*, **35**, 3585 (1987).
- [63] J.A. Potton, and P.C. Lanchester, *Phase Transit.*, **6**, 43 (1985).
- [64] M.K. Das, P.C. Barman, and S.K. Sarkar, *Eur. Phys. J. B*, **88**, 175 (2015).
- [65] G.B. Kasting, K.J. Lushington, and C.W. Garland, *Phys. Rev. B*, **22**, 321 (1980).
- [66] G. Cordoyiannis, C.S.P. Tripathi, C. Glorieux, and J. Thoen, *Phys. Rev. E*, **82**, 031707 (2010).
- [67] A. Chakraborty, S. Chakraborty, and M.K. Das, *Phys. Rev. E*, **91**, 032503 (2015).

- [68] A. Chakraborty, B. Das, M.K. Das, S. Findeisen-Tandel, M.-G. Tamba, U. Baumeister, H. Kresse, and W. Weissflog, *Liq. Cryst.*, **38**, 1085 (2011).

# CHAPTER 4

---

Dielectric, elastic and viscous properties of  
some binary mixtures of hockey stick-  
shaped mesogen and octyloxy-cyano-  
biphenyl

---

---

## 4.1. Introduction

Investigation of different physical properties of liquid crystal (LC) mesophases is quite interesting from the application point of view in display as well as non-display photonic and electro-optic devices such as laser beam steering [1], phase modulator [2], optical shutter [3-5] etc. The advantageous feature of the nematic phase is to produce a mechanical distortion of the molecules in response to an external field, resulting in an electric polarization within the system [6]. The nematic liquid crystal compounds with desirable physical properties like high optical birefringence ( $\Delta n$ ), high dielectric anisotropy ( $\Delta\epsilon$ ), wide nematic phase range, low rotational viscosity ( $\gamma_1$ ), good thermal and photostability, greater response to the external field etc. are most efficient in many practical applications [7]. A highly conjugated liquid crystal compound with high optical birefringence also exhibits a high rotational viscosity due to the effect of moment of inertia. However, the most promising criterion to upgrade the nematic liquid crystal is to enhance its optical birefringence along with the reduction of the rotational viscosity [8,9]. Performance of the electro-optical devices is based on the molecular switching behavior which is associated with the relaxation or response time  $\tau_0$ . Till date several physical properties have been studied in pure nematic liquid crystal compounds having different molecular geometry such as rod-like, bent-core, hockey-stick shaped, disc-like etc. Different calamitic compounds has been found to exhibit high positive dielectric anisotropy [10,11], wide nematic mesophase stability [12] and low rotational viscosity etc. In addition to the principle director  $\hat{n}$  like the calamitic molecules, the bent-core (BC) molecules are found to exhibit a much faster switching behavior of the secondary director  $\hat{m}$ , perpendicular to  $\hat{n}$  [13,14]. Moreover, the BC nematogens have smectic-like small cybotactic clusters which further affects the physical properties of the system [15,16]. Due to the existence of such unusual characteristics in BC systems in their nematic phase, they reveal stable uniaxial and biaxial nematic

---

---

phases [17-20], different unusual smectic mesophases [21,22], giant flexoelectric response [23], dielectric anisotropy with a crossover nature [24,25] and atypical negative values of bend-splay anisotropy [26-28]. Moreover, the BC compounds also have large relaxation time ( $\tau_0$ ) and thereby greater value of the rotational viscosity ( $\gamma_1$ ) [29-31] which resists them in fast switching electro-optical devices. On the other hand, the hockey stick-shaped molecules possess a shape intermediate between the calamitic and conventional bent-core molecules exhibiting a lower value of  $\gamma_1$  relative to the symmetric bent-core molecules [25]. A number of efforts have been devoted to develop the physical properties of nematic LC compound and make an enormous use in display and non-display technological applications as per requirement [17,18,32-34]. However, any single mesogenic compound cannot fulfill all the desired properties for the multipurpose application. Therefore, the interest has grown to mix several components of liquid crystal compounds at a particular proportion and achieve the desired property. The mixture of LC compounds having divergent molecular structure has been found to critically optimize the properties of individual constituents.

In this chapter, the static dielectric permittivity ( $\epsilon_{||}$ ,  $\epsilon_{\perp}$ ) measurements have been carried out for four different binary mixtures ( $x_{SF7} = 0.012, 0.03, 0.05$  and  $0.065$ ) consisting of a hockey-stick shaped mesogen, 4-(3-decyloxyphenyliminomethyl) phenyl 4-decyloxybenzoate (SF7) and a calamitic compound 4'-octyloxy-4-cyanobiphenyl (8OCB). The molecular structures and transition scheme for both the compounds were discussed earlier in chapter 3. From the above measurement, different dielectric parameters such as temperature dependent dielectric anisotropy ( $\Delta\epsilon$ ) and average permittivity ( $\epsilon_{avg}$ ) have been determined for all the mixtures. Moreover, the critical exponent which defines the order nature of the *I-N* phase transition has also been extracted for all the studied mixtures by analyzing the pretransitional behavior of the average ( $\epsilon_{avg}$ ) and isotropic permittivity ( $\epsilon_{iso}$ ) data. In addition,

---

---

---

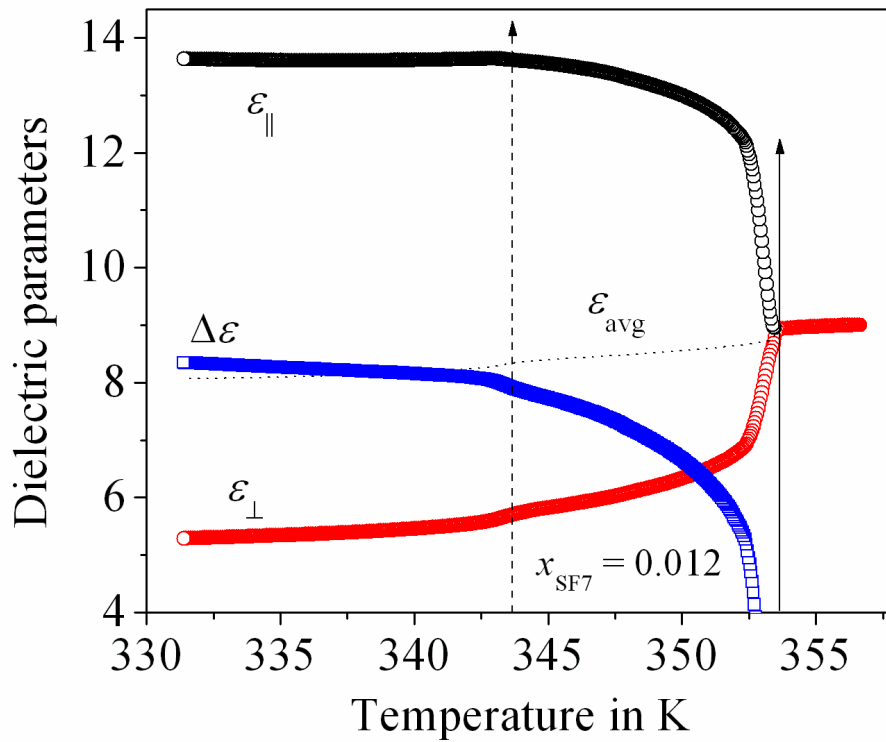


---

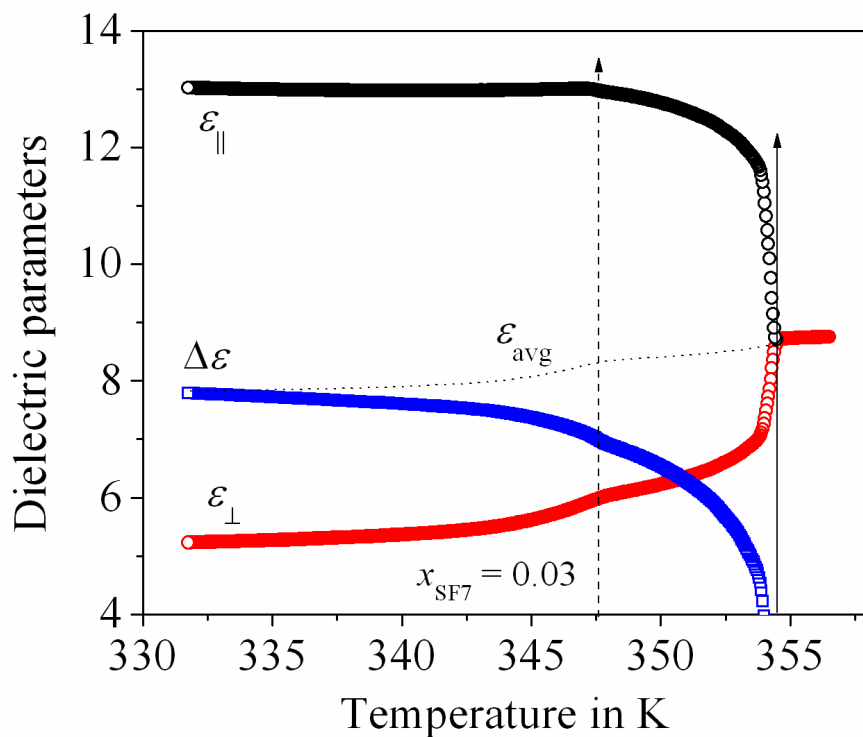
the critical behavior in the vicinity of  $N$ -Sm-A phase transition has also been investigated to assess the order nature of the transition by extracting the value of critical exponent from the dielectric anisotropy data and then compared it with the same obtained from the high-resolution optical birefringence measurement [35]. Furthermore, a detailed study of the temperature-dependent splay elastic constant ( $K_{11}$ ) [36-40], relaxation time ( $\tau_0$ ) as well as the rotational viscosity ( $\gamma_1$ ) in the nematic phase for all the mixtures has been performed by capacitive decay method [25,41]. Additionally, the activation energy ( $E_a$ ) has also been calculated with the help of rotational viscosity ( $\gamma_1$ ) and order parameter ( $\langle P_2 \rangle$ ) values, to make an idea about the intermolecular interaction.

## 4.2. Static dielectric parameter measurements

The temperature-dependent longitudinal and transverse component of the dielectric permittivity ( $\epsilon_{\parallel}$  and  $\epsilon_{\perp}$ ) has been measured in both planar and homeotropic configurations for four different mixtures by using Agilent 4294A LCR impedance analyzer. During cooling from a few degrees above the isotropic phase, the permittivity values have been acquired in the entire mesomorphic region. Additionally, the dielectric anisotropy ( $\Delta\epsilon = \epsilon_{\parallel} - \epsilon_{\perp}$ ) and also the average dielectric permittivity,  $\epsilon_{\text{avg}} = \{1/3(2\epsilon_{\perp} + \epsilon_{\parallel})\}$  values has been evaluated with the help of obtained parameters  $\epsilon_{\parallel}$  and  $\epsilon_{\perp}$ . The variation of  $\epsilon_{\parallel}$ ,  $\epsilon_{\perp}$ ,  $\epsilon_{\text{avg}}$  and  $\Delta\epsilon$  with respect to temperature at a constant frequency (10 kHz) are shown in Fig. 4.1(a-d) for all of the mixtures. It is evident from the figures that during cooling from the isotropic phase, the dielectric parameters  $\epsilon_{\parallel}$ ,  $\epsilon_{\perp}$  and  $\Delta\epsilon$  exhibit a sharp change on entering the  $N$  phase due to increase in orientational ordering. However, all the parameters reveal a small discontinuity in the vicinity of  $N$ -Sm-A phase transition which can be explained by considering a smectic-like short-range ordering developed within the nematic phase prior to the transition temperature. Interestingly, the value of longitudinal permittivity ( $\epsilon_{\parallel}$ ) at a specific temperature deep within the  $N$  or Sm-A phases has been found

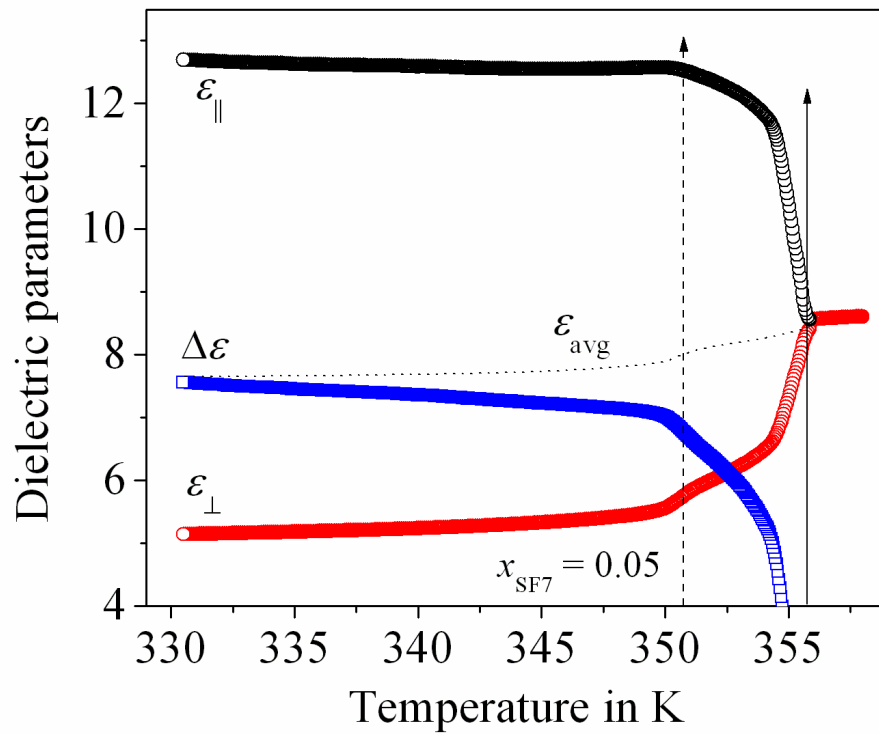


(a)

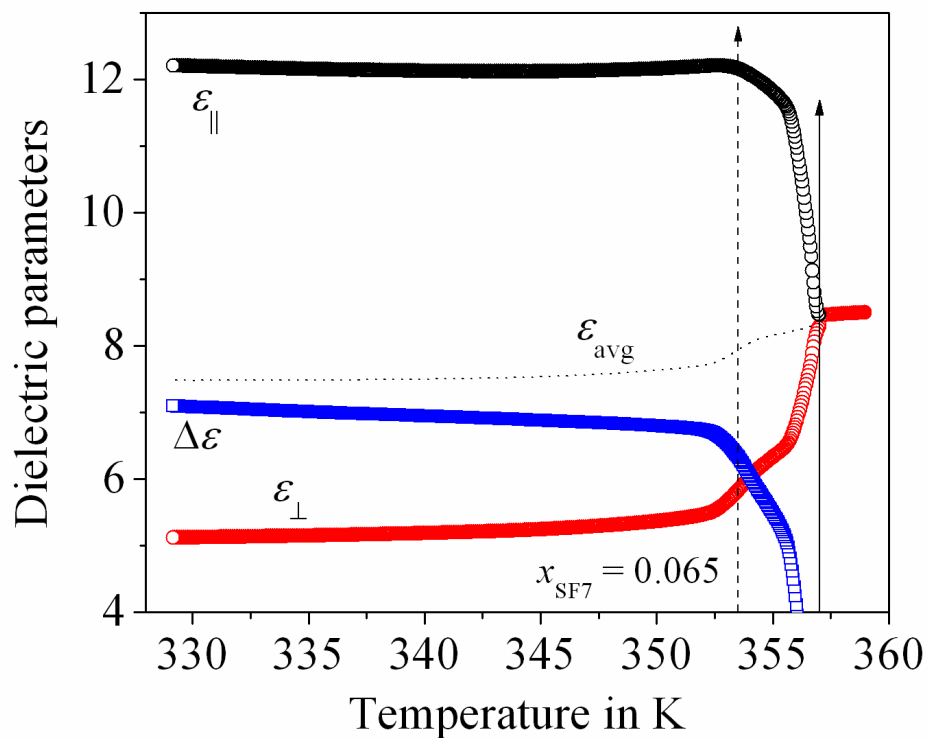


(b)

**Figure 4.1.** Temperature variation of the dielectric parameters for (a)  $x_{\text{SF7}} = 0.012$  and (b) 0.03. Solid arrow and dashed vertical arrow indicate the  $I$ - $N$  ( $T_{IN}$ ) and the  $N$ -Sm-A ( $T_{NA}$ ) phase transition temperatures respectively.



(c)



(d)

**Figure 4.1 (cont'd).** Temperature variation of the dielectric parameters for (c)  $x_{\text{SF7}} = 0.05$  and (d) 0.065. Solid arrow and dashed vertical arrow indicate the  $I-N$  ( $T_{IN}$ ) and the  $N$ -Sm-A ( $T_{NA}$ ) phase transition temperatures respectively.

to be decreased with increasing the dopant concentration. It should be noted that the molecular structure of the pure calamitic compound 8OCB is made-up of a polar CN group attached to one end originating a strong polar nature of the molecule. Hence the compound 8OCB exhibits a large positive dielectric anisotropy ( $\Delta\epsilon$ ) throughout the mesophase region [42]. Again all the mixtures also possess a large positive dielectric anisotropy value in the  $N$  and  $Sm-A$  phases. However, by increasing the concentration of the hockey stick-shaped mesogen in the mixtures, the  $\epsilon_{\parallel}$  value and hence the  $\Delta\epsilon$  value gradually decreases as seen in Fig. 4.2. This phenomenon may be considered to be related with the effective value of dipole moment within the mixtures for the organization of both the dissimilar molecules. It can be assumed that a strong anti-parallel interaction between the molecular dipoles persuading a small

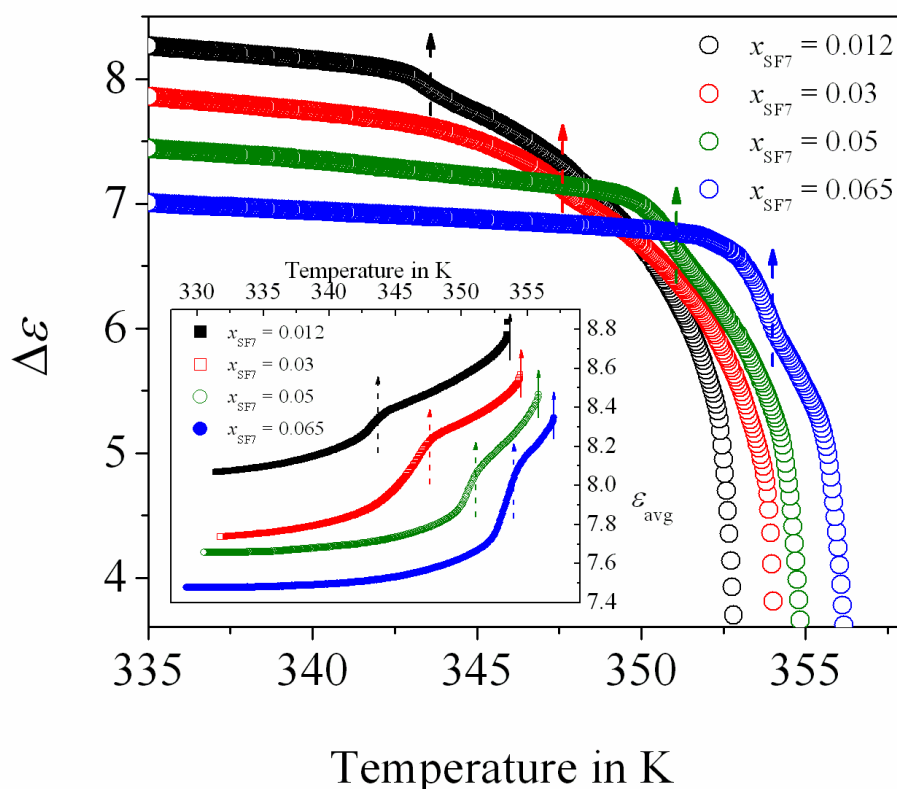


**Figure 4.2.** Temperature variation of the dielectric anisotropy ( $\Delta\epsilon$ ) for all the mixtures. Inset depicts the average permittivity ( $\epsilon_{avg}$ ) of the same. Solid arrow and dashed vertical arrow indicate the  $I-N$  ( $T_{IN}$ ) and the  $N-Sm-A$  ( $T_{NA}$ ) phase transition temperatures respectively.

reduction in the permittivity value [10,43] even for the presence of small amount of kink-shaped mesogen with 8OCB. Again this dipole-dipole interaction is quite strong in the nematic and smectic phases compared to that of the isotropic phase [44]. For this reason, the extrapolated value of isotropic permittivity ( $\epsilon_{\text{iso}}$ ) in the nematic and smectic phases found to be relatively greater than the average permittivity ( $\epsilon_{\text{avg}}$ ) for all the investigating mixtures. However, this difference ( $\epsilon_{\text{iso}} - \epsilon_{\text{avg}}$ ) increases as the concentration of the hockey stick-shaped compound increases which is clearly visible in the representative curves of  $\epsilon_{\text{avg}}$  (inset of Fig. 4.2) in both the nematic and smectic phases.

In order to investigate the pretransitional behavior in the vicinity of  $I-N$  phase transition and to extract the critical exponent related with the fluctuation at this transition, the temperature dependent permittivity data has been suitably used. The study of the pretransitional effect in the vicinity of  $I-N$  phase transition has been reported earlier in several pure calamitic compounds [45-49] as well as in some binary mixtures of calamitic compounds [44] and also has been described in the hockey stick-shaped compound [50]. Therefore, it is quite interesting to investigate the pretransitional phenomena in the mixtures of compounds having divergent molecular conformer. During the past few decades, the mean field model cannot describe the exact experimental observations based on the linear and non-linear dielectric permittivity studies. Therefore, a fluid-like model [51,52] has been considered to explain the pretransitional behavior at that transition. According to this model, the permittivity can be well described by the fluid like equation [52-56]:

$$\epsilon_{\text{iso}}(T) = \epsilon^* + A_1^+(T - T^*) + A_2^+(T - T^*)^{1-\alpha''} \quad (4.1)$$

$$\text{For } T > T_{IN} = T^* + \Delta T^*$$

$$\epsilon_{\text{avg}}(T) = \epsilon^{**} + A_1^-(T^{**} - T) + A_2^-(T^{**} - T)^{1-\alpha''} \quad (4.2)$$

$$\text{For } T < T_{IN} = T^{**} - \Delta T^{**}$$

where,  $\epsilon^*$  and  $\epsilon^{**}$  are the dielectric permittivity values ( $\epsilon_{\text{iso}}$  and  $\epsilon_{\text{avg}}$  respectively) at the critical temperatures  $T^*$  and  $T^{**}$  (extrapolated temperature of virtual

continuous phase transition) respectively. Here  $\alpha''$  is the critical exponent similar to the specific heat capacity critical exponent  $\alpha$  and  $A_1^+$ ,  $A_1^-$ ,  $A_2^+$  and  $A_2^-$  are the critical amplitudes.

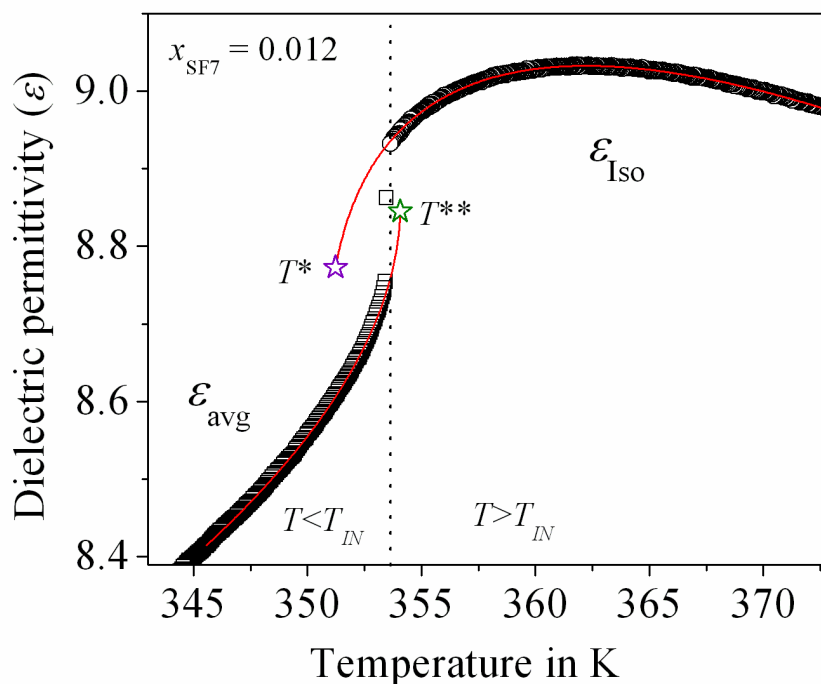


**Figure 4.3.** Variation of permittivities with temperature for the concentration  $x_{SF7} = 0.012$ . Solid lines are fit to Eq. (4.1) and (4.2). The critical temperatures  $T^*$  and  $T^{**}$  are indicated with star symbols ( $\star$ ) and the dotted vertical line represents the nematic-isotropic phase transition temperature ( $T_{IN}$ ).

In the present investigation, all the mixtures were heated up to 25-30 K above the clearing temperature and the permittivity values has been measured during cooling at a rate of 0.5 K per minute with a fixed frequency 10 kHz. The above mentioned Eq. (4.1) and Eq. (4.2) were fitted to the experimental data points of permittivity in the isotropic phase ( $\epsilon_{Iso}$ ) as well as in the nematic phase ( $\epsilon_{avg}$ ) individually, *i.e.*, above and below the clearing temperature ( $T_{IN}$ ). The best-fitted parameters are shown in Table 4.1. One of the fit representation is shown in Fig. 4.3 for the mixture  $x_{SF7} = 0.012$  in both the isotropic and nematic phases. Moreover, the temperature variations of  $\epsilon_{Iso}$  for all the studied mixtures are displayed in Fig. 4.4 in accordance with the fitted curve to Eq. (4.1).

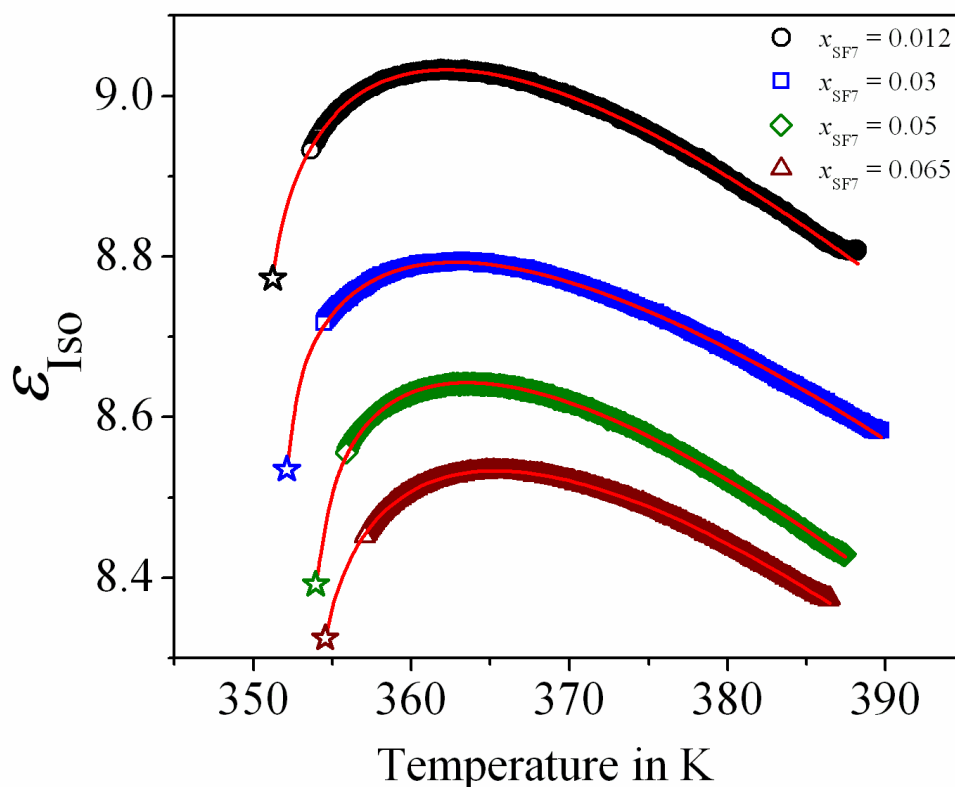


**Figure 4.4.** Variation of the isotropic permittivity ( $\epsilon_{\text{Iso}}$ ) with temperature for all of the mixtures. Solid lines are the fit to Eq. (4.1) and the star symbols ( $\star$ ) are representing the critical temperatures ( $T^*$ ).

The observation made from Fig. 4.3 and 4.4 that the isotropic permittivity ( $\epsilon_{\text{Iso}}$ ) follows a bending pattern after attaining a maximum value for all the mixtures and the value of  $\epsilon_{\text{Iso}}$  is greater than the value of  $\epsilon_{\text{avg}}$  in the neighborhood of the clearing temperature. However, at very close to the clearing temperature ( $T_{\text{IN}}$ ), the value of  $\epsilon_{\text{Iso}}$  sharply decreases as the temperature decreases, exhibiting a strong pretransitional behavior. This pretransitional behavior is originating due to the pre-nematic fluctuations of the pseudo nematic clusters developed within the isotropic phase. Moreover, the amount of bending decreases as the dopant concentration increases. It should be noted that the calamitic compound 8OCB has a greater dipole moment (6.3 D, along its long axis) in comparison to the dopant (4.48 D) having divergent molecular structure. The mutual anti-parallel interaction of the dipoles effectively

minimizes the resultant dipole moment in the mixture with a reduction in the pretransitional effect for the investigated systems. The observation of such pretransitional phenomena has also been confirmed by others in case of pure compound as well as in binary mixtures [44,56,57]. It has been claimed that owing to the existence of polar terminal groups, the adjacent molecules prefer to figure out an anti-parallel pair to reduce the effective dipole moment within the mesogenic system [58,59]. This anti-parallel packing originating the pseudo clusters within the medium. Thus the amount of bending and associated permittivity value in the isotropic phase decreases with increasing the hockey-stick shaped molecular concentration. Furthermore, a relative competition between the parallel and anti-parallel components of the dipole moment takes place near the  $I-N$  phase transition temperature. In the locality of  $T_{IN}$ , the anti-parallel component dominates and exhibiting a critical behavior.

**Table 4.1.** Results corresponding to the best fit for permittivity above and below the isotropic-nematic ( $T_{IN}$ ) phase transition temperatures obtained in accordance with Eq. (4.1) and Eq. (4.2).

$x_{SF7}$	Condition	$T^* / T^{**}$ (K)	$\varepsilon^*$ or $\varepsilon^{**}$	$A_I^+$ or $A_I^-$	$A_2^+$ or $A_2^-$	$\alpha''$
0.012	$T > T_{IN}$	351.230±0.230	8.721±0.009	-0.031±0.001	0.193±0.001	0.494±0.011
	$T < T_{IN}$	354.271±0.191	8.803±0.024	-0.029±0.010	-0.116±0.014	0.500±0.002
0.03	$T > T_{IN}$	353.103±0.078	8.511±0.019	-0.026±0.001	0.173±0.012	0.502±0.022
	$T < T_{IN}$	354.608±2.057	8.591±0.213	-0.025±0.007	-0.117±0.105	0.499±0.281
0.05	$T > T_{IN}$	354.184±0.002	8.374±0.004	-0.030±0.001	0.176±0.003	0.49±0.008
	$T < T_{IN}$	355.876±1.379	8.485±0.170	-0.031±0.004	-0.119±0.069	0.499±0.118
0.065	$T > T_{IN}$	354.000±0.085	8.190±0.022	-0.030±0.001	0.204±0.014	0.500±0.022
	$T < T_{IN}$	357.175±1.859	8.390±1.805	-0.029±0.020	-0.115±0.732	0.498±0.051

An inspection of Table 4.1 reveals that the extracted  $\alpha''$  values lie in between 0.49±0.008 and 0.502±0.022, indicating a tricritical nature of the  $I-N$  phase transition. These results agree well with the predicted critical exponent

value from tricritical hypothesis ( $\alpha_{TCH} = 0.5$ ) [60-62]. Furthermore, an insight into the other parameters shows that  $|A_2^+/A_2^-|$  value lies in a range from 1.47 to 1.77, whereas the  $|A_I^+/A_I^-|$  value is nearly or slightly greater than unity but have no systematic variation on increasing the molar concentration. A finite measurable difference between  $T^*$  and  $T^{**}$  has also been detected and both of them also differ from the value of  $T_{IN}$ . Therefore, the relative deviation for both of  $T^*$  and  $T^{**}$  with respect to the  $I-N$  phase transition temperature ( $\Delta T^* = T_{IN} - T^*$ ,  $\Delta T^{**} = T^{**} - T_{IN}$ ), along with the metastable region ( $T^{**} - T^*$ ) can be easily assumed from Table 4.1. However, no systematic variation has been recognized of them with the variation of dopant concentration.

### 4.3. Critical behavior at the $N-Sm-A$ phase transition

The anisotropy data of any physical parameter can be treated as an order parameter of the system, which is the elementary essence for analyzing the critical fluctuation associated with a transition. In chapter 3, the optical birefringence ( $\Delta n$ ) data has been successfully employed to investigate the critical behavior in the vicinity of  $N-Sm-A$  phase transition, while in the present case the dielectric anisotropy data ( $\Delta \epsilon$ ) is being used as another observable order parameter for the same LC binary system. Similar to the optical birefringence ( $\Delta n$ ) data, the dielectric anisotropy ( $\Delta \epsilon$ ) data also does not manifest any noticeable discontinuity at the  $N-Sm-A$  phase transition, but the main difference in both of  $\Delta n$  and  $\Delta \epsilon$  data for the pure compound and for the mixtures lie in the vicinity of the  $N-Sm-A$  phase transition as being observed from Fig. 4.2. Hence a quantity  $E(T)$  similar to  $Q(T)$  in chapter 3, has been considered in this case to study the critical anomaly associated with that transition and can be expressed as [63,64]:

$$E(T) = - \frac{\Delta \epsilon(T) - \Delta \epsilon(T_{NA})}{T - T_{NA}} \quad (4.3)$$

where  $\Delta\epsilon(T_{NA})$  is the dielectric anisotropy value at the  $N$ -Sm-A transition temperature ( $T_{NA}$ ). In order to characterize all the parameters,  $E(T)$  has been fitted with the power-law expression (similar to Eq. (3.7) in chapter 3):

$$E(T) = A^\pm |\tau|^{-\alpha'} (1 + D^\pm |\tau|^\Delta) + C(T - T_{NA}) + B \quad (4.4)$$

where,  $\tau = (T - T_{NA})/T_{NA}$  is the reduced temperature,  $\alpha'$  is the effective critical exponent similar to specific heat capacity critical exponent  $\alpha$ .

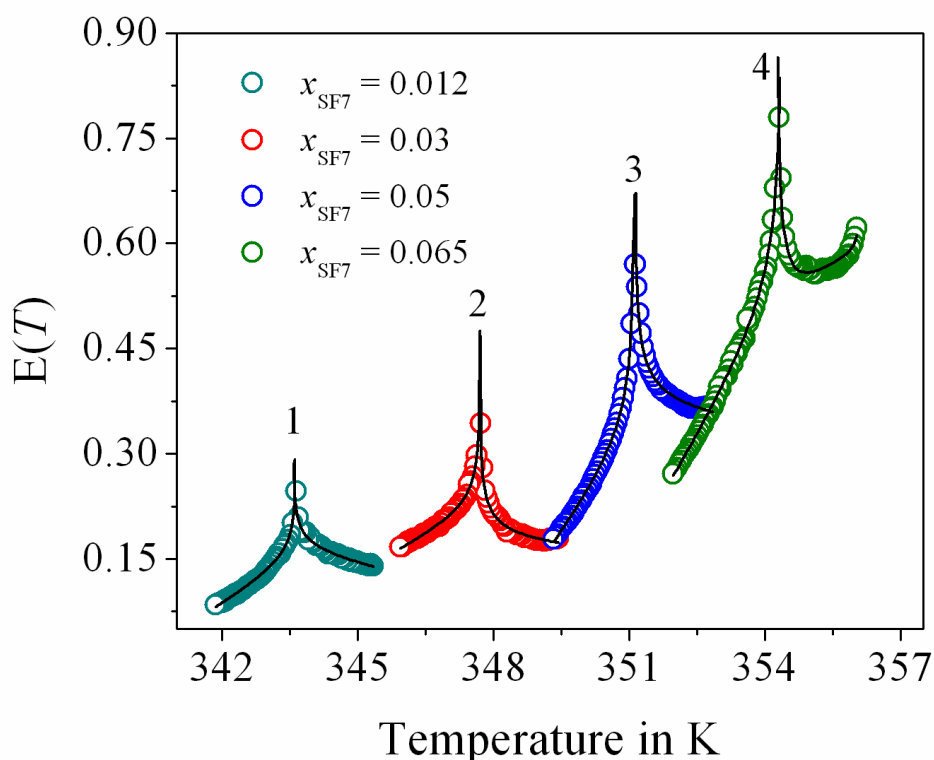


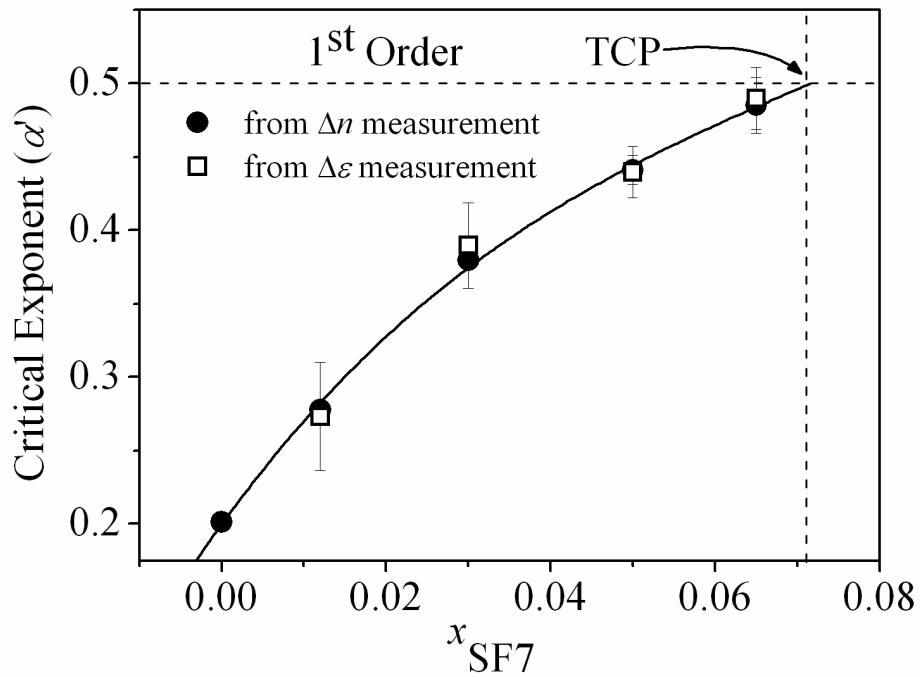
**Figure 4.5.** Temperature-dependent variation of the quotient  $E(T)$  in the vicinity of  $N$ -Sm-A phase transition at different mole fractions of SF7 in the binary mixtures. The solid lines are fit to Eq. (4.4).

In the present analysis, the reduced temperature ( $\tau$ ) value has been taken as fixed at  $5 \times 10^{-3}$  for all of the mixtures in both the  $N$  and Sm-A phases and  $\Delta$  value is also set fixed at 0.5 without any further variation. A representative variation of  $E(T)$  with temperature has been illustrated in Fig. 4.5 along with a fitting line of Eq. (4.4) for all the mixtures. The extracted parameter values are listed in Table 4.2 along with a reduced error function  $\chi_v^2$ .

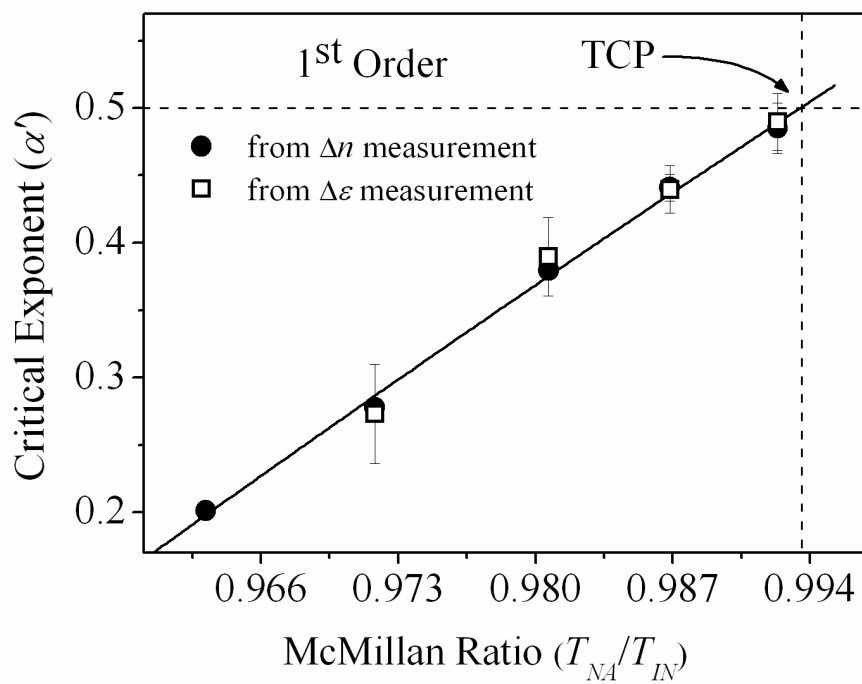
**Table 4.2.** Results corresponding to the best fit for  $E(T)$  near  $N$ -Sm- $A$  phase transition obtained in accordance with Eq. (4.4) and related  $\chi_v^2$  values associated with the fits.  $|\tau|_{\max}$  presents the upper limit of reduced temperature considered for these fits.

$x_{\text{SF7}}$	$\alpha'$	$A^-/A^+$	$D^-/D^+$	$ \tau _{\max}$	$\chi_v^2$
0.012	$0.273 \pm 0.037$	$0.972 \pm 0.112$	$0.988 \pm 0.003$	$5 \times 10^{-3}$	1.51
0.03	$0.389 \pm 0.029$	$1.010 \pm 0.071$	$1.003 \pm 0.023$	$5 \times 10^{-3}$	1.35
0.05	$0.439 \pm 0.017$	$1.184 \pm 0.028$	$1.008 \pm 0.091$	$5 \times 10^{-3}$	1.13
0.065	$0.489 \pm 0.021$	$1.475 \pm 0.374$	$1.182 \pm 0.049$	$5 \times 10^{-3}$	1.22

An inspection of Fig. 4.5 reveals that as the concentration increases, the peak height of  $E(T)$  in the vicinity of  $N$ -Sm- $A$  phase transition systematically increases and achieve a maximum value in the present investigating system for the mixture with the highest concentration ( $x_{\text{SF7}} = 0.065$ ). Moreover, the effective critical exponent  $\alpha'$  is found to lie in a range between  $0.273 \pm 0.037$  and  $0.489 \pm 0.021$  with a reasonable  $\chi_v^2$  value in between 1.13 and 1.51. Fig. 4.6(a-b) representing the variation of the effective critical exponent  $\alpha'$  against the concentration of hockey stick-shaped mesogen and also with the variation of McMillan ratio respectively. A comparison has also been done for the extracted  $\alpha'$  value with the same obtained from optical anisotropy ( $\Delta n$ ) data reported in chapter 3. Fig. 4.6(a-b) clearly shows that the yielded  $\alpha'$  values from both the experimental data of  $\Delta n$  and  $\Delta \varepsilon$  are almost identical. Moreover, they are limited in between the 3D-XY ( $\alpha' = -0.007$ ) and TCP (tricritical point;  $\alpha' = 0.5$ ) [35,65]. Additionally, the quotient  $A^-/A^+$  shows an increasing pattern from  $0.972 \pm 0.112$  for  $x_{\text{SF7}} = 0.012$  to  $1.475 \pm 0.374$  for  $x_{\text{SF7}} = 0.065$ , whereas  $D^-/D^+$  values remain more or less equal to unity which are also found to be in accordance with the theoretical hypothesis. Accordingly, a non-universal behavior of the effective critical exponent  $\alpha'$  has been observed and hence it defines a crossover character from second order to first order nature of the



(a)



(b)

**Figure 4.6.** The variation of the effective critical exponent ( $\alpha'$ ) with (a) molar concentration and (b) McMillan ratio ( $T_{\text{NA}}/T_{\text{IN}}$ ), obtained by fitting  $E(T)$  to Eq. (4.4). The vertical dashed line corresponds to the tricritical point (TCP). The solid lines are the polynomial fits to the data points.

---

---

$N$ -Sm-A phase transitions in the present investigated mixtures. Analytically this crossover point has been found for a composition  $x_{SF7} \sim 0.072$  with  $\alpha' = 0.5$  and the corresponding McMillan ratio (*i.e.*,  $T_{NA}/T_{IN}$ ) is being  $\sim 0.994$ . Therefore, as an additive, the role of the compound SF7 in the mixture is reflected by a substantial change in the width of the nematic phase which further drives the second order  $N$ -Sm-A phase transition towards the first order in nature. Indeed these results are found to be well consistency with the same obtained by investigating the high-resolution optical birefringence ( $\Delta n$ ) data in a quite identical procedure presented in chapter 3.

#### 4.4. Threshold voltage and splay elastic constant measurements

Due to the application of sufficient electric field to a planar aligned mesogenic medium in an orthogonal direction to the molecular long axis, the Freedericksz transition [36,37] takes place within the system, resulting a rotation of the molecular directors along the field direction. Beyond this Freedericksz threshold voltage ( $V_{th}$ ), the capacitance value ( $C_{\perp}$ ) for planar aligned sample sharply increases up to a saturation value ( $C_{\parallel}$ ). However, these  $V_{th}$  and  $C_{\parallel}$  both are depends upon the sample temperature. In the present investigated mixtures, the voltage-dependent capacitance value has been measured only in the nematic phase by using Agilent 4980A. A representative  $C$ - $V$  diagram is displayed in Fig. 4.7 for a mixture having molar concentration  $x_{SF7} = 0.012$  at different temperatures in the nematic phase and a few degrees below the  $N$ -Sm-A phase transition temperature. The value of  $V_{th}$ 's can be easily achieved from these curves. Fig. 4.8 depicts the temperature variation of  $V_{th}$  in the nematic phase for four different concentrations. It is clearly observed that by decreasing the temperature, the value of  $V_{th}$  gradually increases over the nematic phase due to an enhancement of orientational ordering as well as of molecular packing. All the mixtures follow more or less same variation by reducing the temperature. However, a noticeable increasing pattern has been

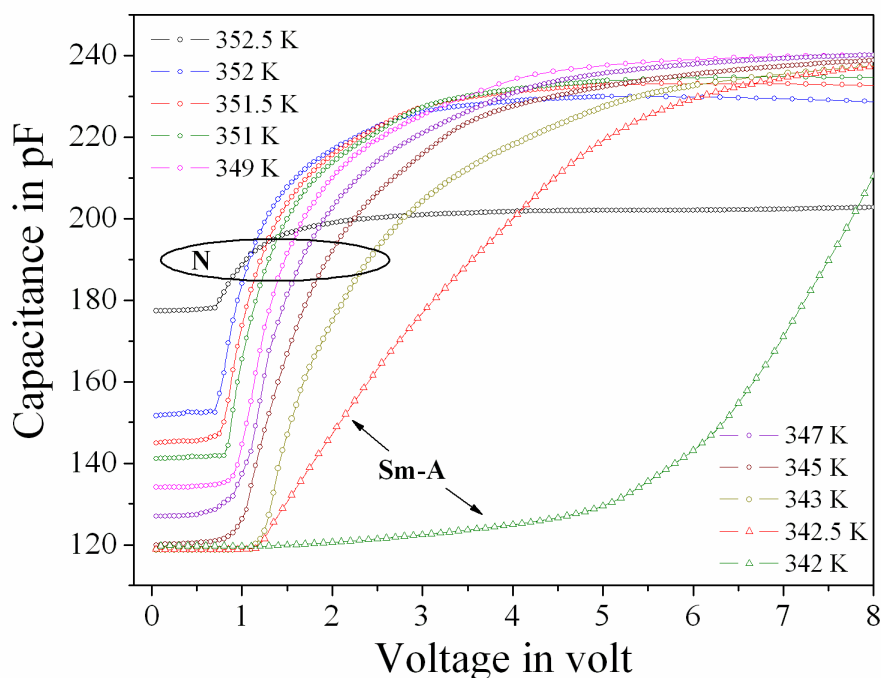


**Figure 4.7.** Variation of cell capacitance in planar configuration at different temperatures for  $x_{SF7} = 0.012$ . Different temperatures are mentioned in the figure in unit of Kelvin (K).

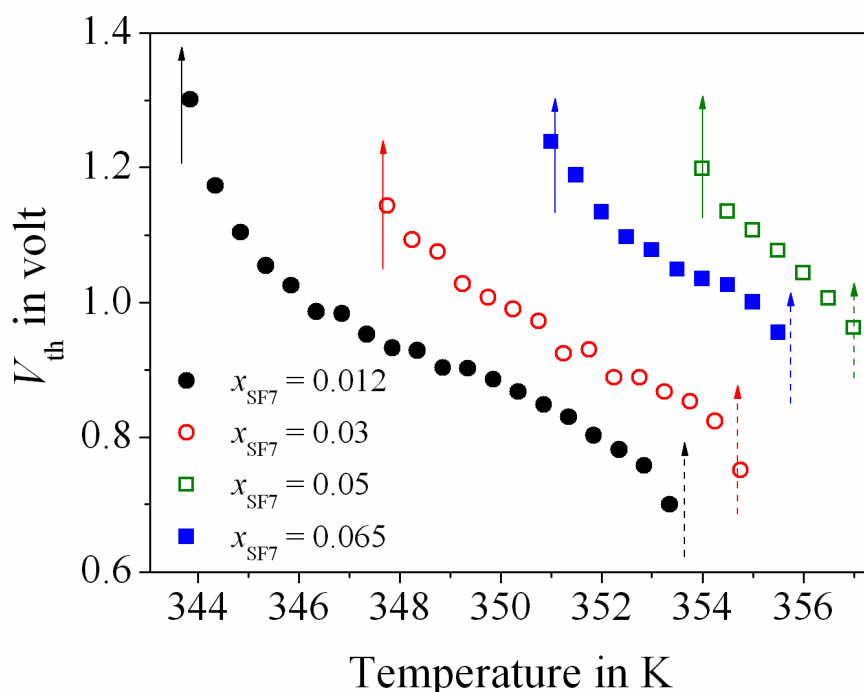


**Figure 4.8.** The variations of threshold voltage ( $V_{th}$ ) with temperature for all the mixtures only in nematic phase. The vertical dashed line and solid line corresponds to the  $T_{IN}$  and  $T_{NA}$  respectively for each of molar concentration.

---



---

found in the value of  $V_{th}$  with increasing the dopant concentration, implying that the strength of the electric field required to reorient the director axis becomes larger for the mixtures of higher concentrations. As an effect of increasing the kink-shaped mesogen, the molecular packing increases within the medium and an additional hindrance is developed to the molecular switching owing to the presence of bend-angle of the SF7 molecule. Additionally, the molecules have a tendency to lowering the orientational ordering within the nematic phase as well as for the stiffness of the molecules a short-range smectic-like ordering seems to be developed in higher concentrations which plays an important role in diminishing the nematic range and enhancing the value of  $V_{th}$ .

The splay elastic constant ( $K_{11}$ ) has been determined in the nematic phase for all the investigating binary mixtures with the help of obtained value of the threshold voltage ( $V_{th}$ ) and the dielectric anisotropy ( $\Delta\epsilon$ ) using the following relation [31,66-68]:

$$K_{11} = \frac{\epsilon_0 \Delta\epsilon V_{th}^2}{\pi^2} \quad (4.5)$$

where  $\epsilon_0$  is the free space permittivity. Fig. 4.9 represents the variation of  $K_{11}$  as a function of reduced temperature ( $T-T_{IN}$ ). In this figure,  $K_{11}$  demonstrates a gradual increase in magnitude from  $\sim 0.2$  pN to a maximum value  $\sim 10$  pN (for  $x_{SF7} = 0.012$ ) throughout the entire mesophase with lowering the temperature. This is the common phenomena seen for both rod-like and bent-core mesogens. All of the investigated mixtures possess the same increasing pattern but the slope of this variation gradually increases with increasing the amount of the hockey stick-shaped mesogen. However, each of these curves exhibits a pretransitional behavior on approaching the  $N$ - $Sm-A$  phase transition temperature. Probably some small domains with strong short-range smectic-like ordering of the molecules developed within the nematic phase which is being extended further during cooling, exhibiting such behavior at very close to

---



---

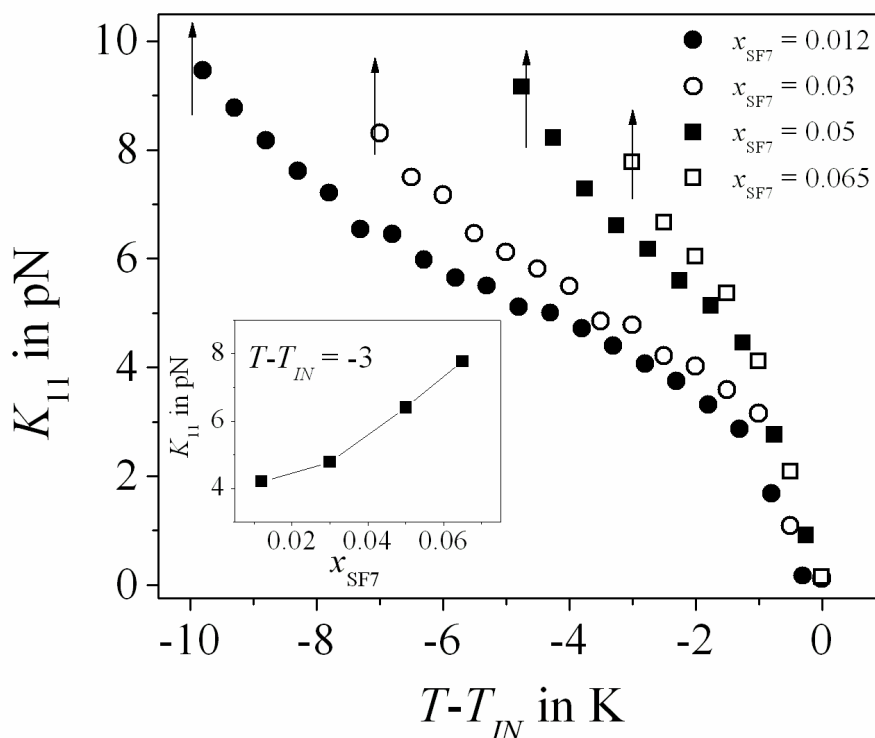


**Figure 4.9.** The variation of the splay elastic constant ( $K_{11}$ ) with reduced temperature for all the mixtures in the nematic phase. The vertical arrows correspond to  $T_{NA}$  for each of molar concentration.

the transition temperature. A number of pure calamitic compounds as well as their mixtures [67,69-71] also suggesting similar type of pretransitional phenomena. Conversely, some of the bent-core [72-74] and hockey stick-shaped compounds [29] were found not to demonstrate any pretransitional divergence of  $K_{11}$ . Here in this case also for the mixture  $x_{SF7} = 0.012$  in which the amount of hockey stick-shaped dopant is quite small, a prominent pretransitional effect is visible, while it is not so evident in mixtures of higher concentrations. The magnitude of the splay elastic constant for the lower concentration is very close to the reported value of the same for pure compound 8OCB [26,75]. Due to the combined effect of a relatively higher value of dielectric anisotropy ( $\Delta\epsilon$ ) and a lower value of threshold voltage ( $V_{th}$ ) leads to a smaller value of elastic constant for the mixture  $x_{SF7} = 0.012$  well within the nematic phase. Further increase in the dopant concentration,  $K_{11}$

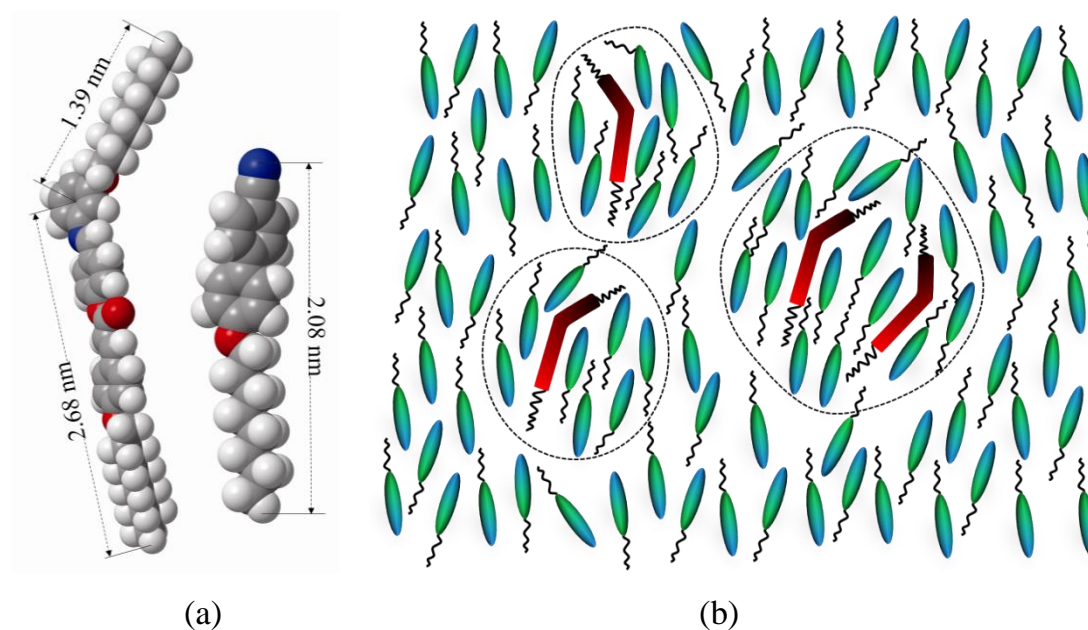


**Figure 4.10.** (a) Energy optimized molecular structure of SF7 and 8OCB. (b) Mutual alignment of both the hockey-stick shaped (SF7) and calamitic molecule (8OCB) in the nematic phase.

value reveals a monotonic enhancement at a particular temperature say  $|T_{IN} - T| = 3$  (inset of Fig. 4.9), although the value of  $K_{11}$  for all cases coalesces near the clearing temperature ( $T_{IN} - T = 0$ ). The above observation can be explained by considering the mutual orientation of the molecules in the mixture, creating a frustration in the molecular packing of calamitic mesogen (8OCB) by the hockey-stick shaped compound (SF7). The host calamitic molecule has a length 2.08 nm, while the longer part of the hockey stick-shaped mesogen (SF7) is about 2.68 nm along with a shorter arm of length 1.39 nm (see Fig. 4.10(a)). It is believed that owing to the affinity to form pair production of the polar groups, the calamitic molecules prefer to align themselves parallel to the longer arms of the hockey stick-shaped mesogen. As a result of such organization, a number of small sized temporary clusters (see Fig. 4.10(b)) are formed within the nematic phase and for the anti-parallel interactions of the dipoles effectively reduces the polar contribution along the director. Effect of such decrease in mutual dipole moment reflected by a relatively lower value of  $\Delta\epsilon$  compared to the pure compound. Moreover, the efficient packing of two

dissimilar molecules remarkably restricts the splay deformation. Earlier reports in binary mixtures of calamitic and bent-core compounds [58,59] also favor such type of molecular packing in the nematic phase representing a monotonic enhancement of  $K_{11}$  with increasing the bent-core mesogens within the mixture. Furthermore, the mutual alignment of both dissimilar molecules in the present system leads to a decrease in the nematic width. The smectic-like short range ordering developed within the clusters represents an intrinsic part of the nematic phase efficiently increases near the  $N$ - $Sm$ - $A$  phase transition which in turn rapidly enhances the value of the splay elastic constant.

#### 4.5. Relaxation time and rotational viscosity measurements

Using the capacitive decay technique [25,41], the molecular relaxation time ( $\tau_0$ ) has been determined for all the mixtures over the entire nematic phase. A systematic variation of relaxation time ( $\tau_0$ ) with reduced temperature

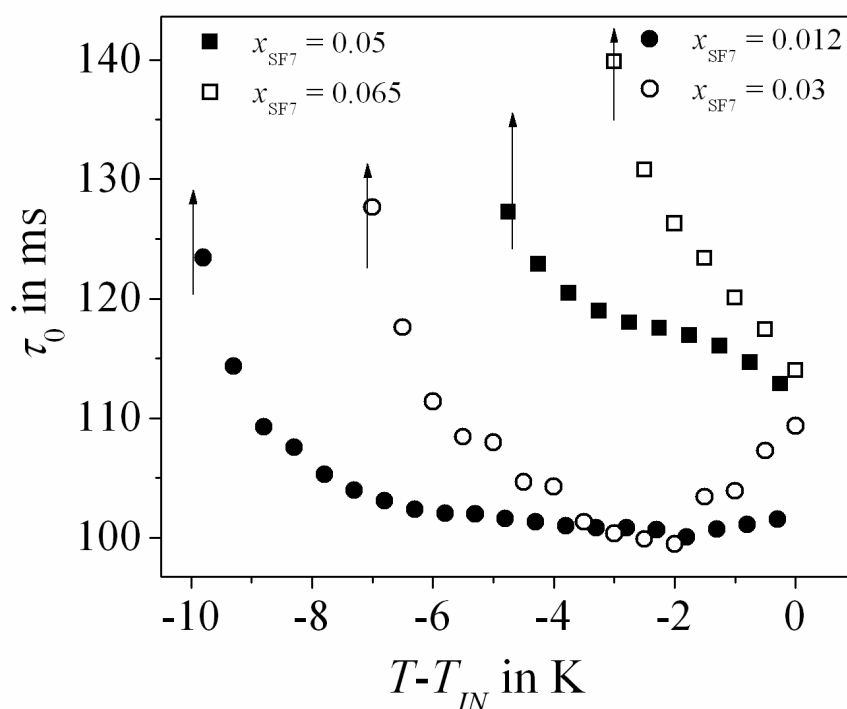


**Figure 4.11.** The variation of the relaxation time ( $\tau_0$ ) with reduced temperature for all the mixtures in the nematic phase. The vertical arrows correspond to  $T_{NA}$  for each of molar concentration.

is shown in Fig. 4.11. It is quite evident that during cooling from the isotropic phase,  $\tau_0$  value increases from  $\sim 100$  ms to a maximum value  $\sim 124$  ms for the lower concentration ( $x_{SF7} = 0.012$ ) which is possibly due to increase in the orientational ordering within the nematic phase. Moreover, in the vicinity of  $N$ - $Sm-A$  phase transition it exhibits a sharp augmentation. Further increase in the dopant angular mesogenic concentration,  $\tau_0$  values are also found to enhance progressively at a particular temperature ( $T_{IN}-T$ ) well within the nematic phase. A greater intermolecular packing of two dissimilar molecules existing in the mixtures and also for the influence of bending feature of SF7 molecule considerably hinders the rotational motion of the molecules within the system and renders an increasing trend of  $\tau_0$  value.

Rotational viscosity plays a significant role to determine the dynamical behavior of molecules within the LC system. In the present binary system, the value of rotational viscosity ( $\gamma_1$ ) has been measured using the following relation [25,31,41]:

$$\gamma_1 = \frac{\tau_0 K_{11} \pi^2}{d^2} \quad (4.6)$$

where  $d$  is the thickness of the planar-aligned LC cell and  $\tau_0$ ,  $K_{11}$  are the relaxation time and splay elastic constant respectively, those are already measured. The variation of rotational viscosity ( $\gamma_1$ ) with reduced temperature has been depicted in Fig. 4.12 for all the investigated mixture over the entire nematic phase. As the value of  $\gamma_1$  is directly proportional to the value of  $K_{11}$ , the divergence of  $\gamma_1$  has found to be in agreement with that of  $K_{11}$ , *i.e.*, the value of  $\gamma_1$  increases monotonically by reducing the temperature and finally assumes a maximum value on approaching the  $N$ - $Sm-A$  phase transition temperature. This is due to the gradual enhancement of the molecular orientational ordering throughout the nematic range. A quite similar type of observation has been reported in some pure bent-core systems [25,31] as well as in a mixture of bent-core and calamitic LC molecules [76,77]. However, all the mixtures exhibit a pretransitional behavior in the vicinity of  $N$ - $Sm-A$  phase transition

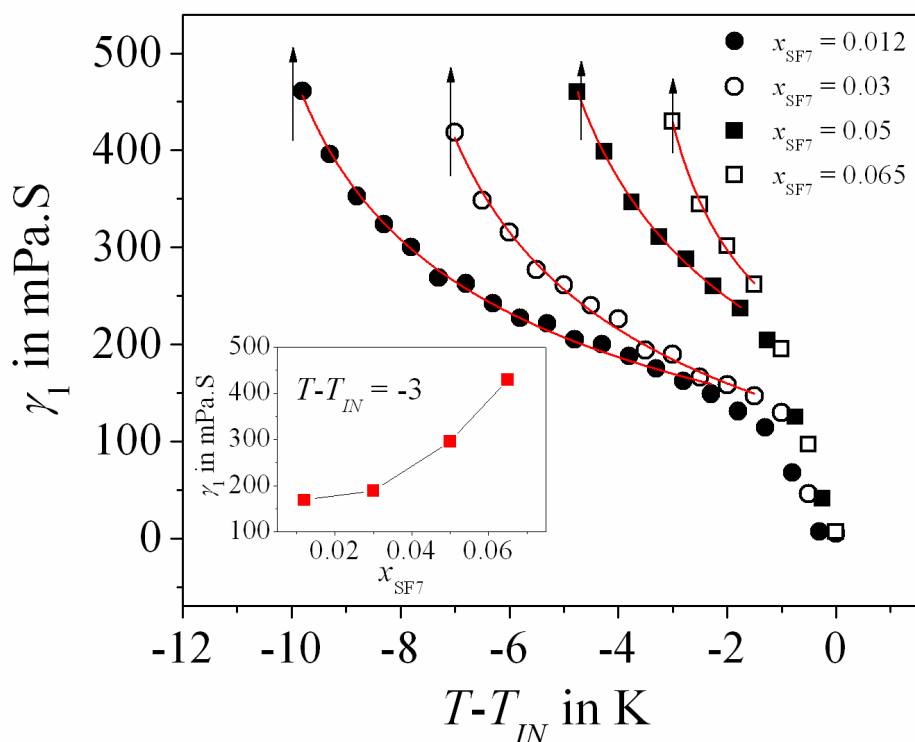


**Figure 4.12.** The variation of rotational viscosity ( $\gamma_1$ ) with reduced temperature for all the mixtures only in nematic phase. The vertical arrows correspond to  $T_{NA}$  for each of molar concentration. Solid lines are fit to Eq. (4.7).

because of the short-range smectic fluctuations in the nematic phase. Interestingly, the slope of the monotonic enhancement becomes higher by increasing the hockey stick-shaped compound within the mixtures. This implies that for a particular temperature say  $|T_{IN} - T| = 3$ , the value of  $\gamma_1$  increases with increase in concentration of hockey stick-shaped mesogen as depicted in inset of Fig. (4.12). In general the usual rod-like compounds possess a temperature dependent lower value of the rotational viscosity ( $\gamma_1$ ) in the nematic phase [78-80], while it has been reported to assume a relatively higher value in bent-core compounds [29-31]. Dorjgotov *et al.* [30] reported that the value of  $\gamma_1$  is much higher (10 times) for the bent-core LC compound having negative dielectric anisotropy than usual calamitic systems, whereas Satyanarayana *et al.* [31] has proposed slightly larger value of  $\gamma_1$  for a pure bent-core system having positive dielectric anisotropy. Therefore, it is expected and indeed experimentally proved that the present investigated binary system assumes a value of  $\gamma_1$

---



---

between that of a typical calamitic compounds (here 8OCB) and certain higher value of the bent-core mesogens. Such type of increasing character has also been reported earlier in some binary mixtures of calamitic and bent-core compounds [58,77]. The well-organized packing of dissimilar molecules within the temporary clusters (Fig. 4.10(b)) possesses a strong transverse polar interaction due to the presence of kink-shaped molecules and thereby represents a slightly higher value of  $\gamma_1$ . However, the yielded values of  $\gamma_1$  in the mixtures have found slightly higher than that of the pure 8OCB compound [80]. The hockey stick-shaped molecule (asymmetric bent-core) used in the present binary system (bending angle =  $109.1^\circ$ ) differs significantly from the typical bent-core compounds. Therefore, the effective values of rotational viscosity of the present binary system consisting of a hockey stick-shaped mesogen are found to be intermediate between the typical bent-core compounds and usual calamitic compounds. Moreover, due to the influence of smectic-like short-range fluctuation within the aggregates or clusters as well as for the increase of order parameter in the nematic phase, a rotational hindrance has been experienced by the molecules [81]. By lowering the temperature, the size of the temporary clusters rapidly grows up within the nematic phase which further causes a clear pretransitional behavior of the rotational viscosity ( $\gamma_1$ ) data (Fig. 4.12). In an attempt to investigate such pretransitional behavior associated with the rotational viscosity ( $\gamma_1$ ) data in the vicinity of  $N$ - $Sm$ - $A$  phase transition the critical exponent ( $\nu$ ) has been analyzed using the following relation [82,83]:

$$\gamma_1 = a(T - T_{NA})^{-\nu} + b \quad (4.7)$$

where  $a$  and  $b$  are two fit parameters and  $T_{NA}$  is the  $N$ - $Sm$ - $A$  phase transition temperature. Fit parameters are displayed in Table 4.3 and fitted lines are also displayed in the same figure as red lines for all the mixtures. According to mean field theoretical model of McMillan [84] the critical exponent ( $\nu$ ) assume a value 0.5, while by considering a local rotation of the director and the smectic

---



---

**Table 4.3.** Fit parameters obtained from the fitting of the temperature dependence of  $\gamma_1$  to Eq. (4.7) for different molar concentrations.

$x_{SF7}$	<b>a</b>	<b>b</b>	<b>v</b>
0.012	819.09±1.55	-234.95±2.33	0.33±0.01
0.03	856.57±3.85	-294.29±1.98	0.33±0.03
0.05	875.52±3.01	-272.76±2.52	0.34±0.19
0.065	550.65±1.15	-139.11±3.16	0.35±0.04

layers in the clusters, Jähnig *et al.* [82] have found this value nearly equal to 0.33. The extracted critical exponent ( $\nu$ ) value obtained by fitting the temperature dependent  $\gamma_1$  value with Eq. (4.7) is found to lie between 0.33 and 0.35 within the error limit for different concentrations studied here. Hence, the extracted critical exponent values are almost in agreement with ( $\nu = 0.33$ ) the value proposed by Jähnig *et al.* [82] and therefore excluding the higher possible mean field value ( $\nu = 0.5$ ).

## 4.6. Determination of activation energy

Activation energy ( $E_a$ ) makes an idea about the potential hindrance occurs due to the local field generated by other molecules in the system against which the director rotates. It suggests the knowledge about molecular mechanics, *i.e.*, inter-molecular packing and their interaction. The activation energy ( $E_a$ ) strongly depends upon molecular order parameter  $\langle P_2 \rangle$ , rotational viscosity ( $\gamma_1$ ) and can be obtained by the relation [85-88]:

$$\gamma_1 = \gamma_0 \langle P_2 \rangle \exp\left(\frac{E_a}{k_\beta T}\right) \quad (4.8)$$

where  $k_\beta$  is the Boltzmann's constant and  $\langle P_2 \rangle$  is the orientational order parameter which has been obtained for all of the above concentrations by analyzing optical birefringence data from high-resolution optical transmission measurement.

In an attempt to obtain the temperature variation of the orientational order parameter ( $\langle P_2 \rangle$ ), the high-resolution optical birefringence ( $\Delta n$ ) data as reported in Chapter 3 has been suitably used for all the mixtures under study. According to de Gennes [89], the anisotropy of any physical quantity can be a measure of orientational order parameter which provides a value in between 0 for a completely disordered phase and 1 for a completely ordered phase. As suggested by several workers [90-94], the optical anisotropy, *i.e.*, the birefringence ( $\Delta n$ ) value can be adopted for the determination of the order parameter because the thermal variation of  $\Delta n$  provides useful information regarding the order of the mesophases. However, the three parameter Haller's extrapolation method [95] has been considered in this investigation by which the value of  $\Delta n_0$  (birefringence value in the crystalline state) can be estimated.

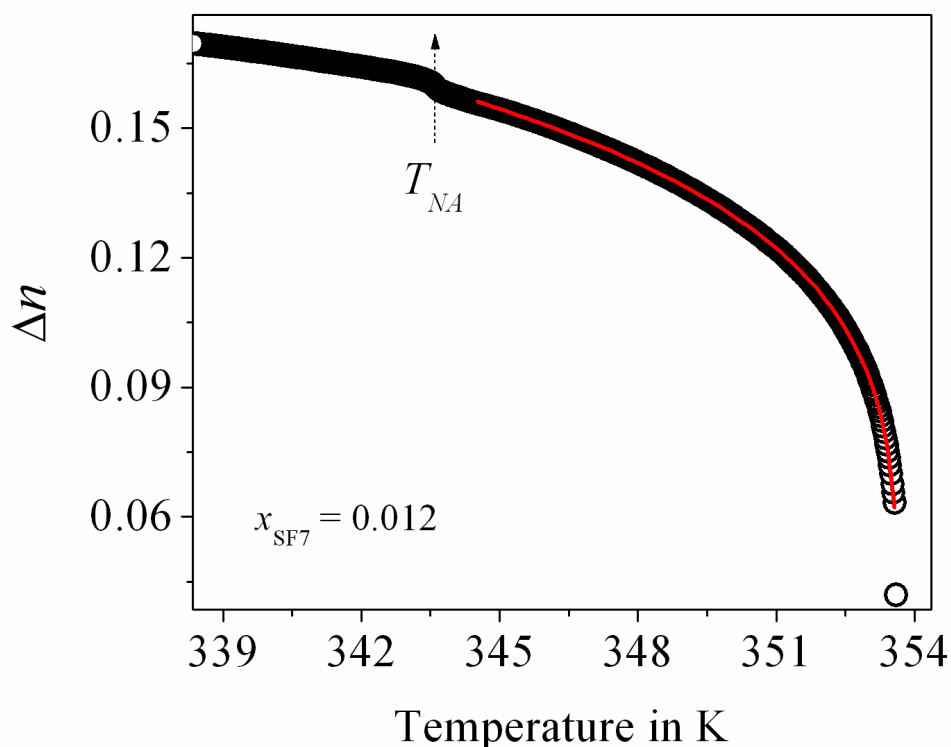


**Figure 4.13.** Temperature dependence of optical birefringence data for  $x_{SF7} = 0.012$ . Dashed arrow denotes the Nematic-Smectic-A transition temperature ( $T_{NA}$ ). The solid line is a fit to Eq. (4.9).

This method is convenient in this case because of the unavailability of density values and this procedure does not consider any local field to the LC molecule. Hence, the temperature dependence of optical birefringence data has been fitted with the expression:

$$\Delta n = \Delta n_0 \left(1 - \frac{T}{T_{IN}}\right)^\beta \quad (4.9)$$

where  $\Delta n_0$  is the extrapolated birefringence in the perfectly ordered state ( $T=0$  K) and  $\beta$  is the critical exponent which depends on the molecular structure. The value of the orientational order parameter  $\langle P_2 \rangle$  determined by the relation [88]:

$$\langle P_2 \rangle = \frac{\Delta n}{\Delta n_0} \quad (4.10)$$

The best fitted curve to Eq. (4.9) in the nematic phase has been represented in Fig. 4.13 for the investigated mixture  $x_{SF7} = 0.012$ , while the corresponding best fitted parameters  $\Delta n_0$  and  $\beta$  for all the mixtures are listed in Table 4.4.

**Table 4.4.** Values of the fitting parameters  $\Delta n_0$  and  $\beta$  obtained from Haller's fit.

$x_{SF7}$	$\Delta n_0$	$\beta$
0	0.319±0.001	0.195±0.001
0.012	0.323±0.001	0.198±0.001
0.03	0.336±0.003	0.214±0.003
0.05	0.344±0.013	0.215±0.006
0.065	0.365±0.011	0.220±0.006

The extracted critical exponent  $\beta$  is found to lie within a range from 0.195 to 0.220 for different mixtures. A discrepancy of critical exponent  $\beta$  value has also been arises with the theoretical values due to the incompatibility of Haller's technique with the weakly first-order character of the isotropic-nematic ( $I-N$ ) phase transition [96-100].

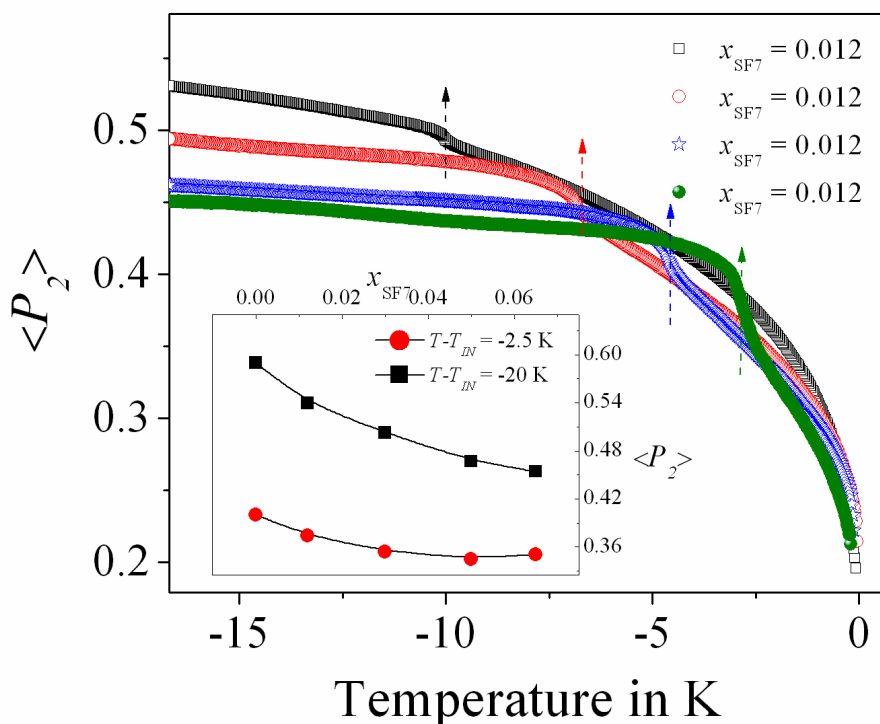


**Figure 4.14.** The temperature dependence of orientational order parameter ( $\langle P_2 \rangle$ ) for all the mixtures. Dashed arrow denotes the nematic–smectic-A ( $T_{NA}$ ) transition temperatures respectively. Inset represents the value of  $\langle P_2 \rangle$  at a particular temperature in both nematic and smectic phases for all the mixtures.

The temperature variation of the orientational order parameter ( $\langle P_2 \rangle$ ) for all the investigated mixtures is represented in Fig. 4.14. It has been observed that in the vicinity of isotropic–nematic phase transition the order parameter value sharply increases, exhibiting a first order nature of  $I$ – $N$  phase transition. Further decreasing the temperature,  $\langle P_2 \rangle$  value reveals a regular increase in the nematic phase due to development of the molecular orientational ordering within the medium. In the vicinity of nematic–smectic-A phase transition a continuous change has been identified in the order parameter data for all the mixtures under study. This continuous variation signaling a second order nature of the  $N$ – $Sm$ -A phase transition. However, by increasing the amount of hockey stick-shaped compound, the orientational order parameter value slightly decreases which is shown in inset of Fig. 4.14 both in the nematic and smectic phases. Moreover, due to the rapid enhancement of

cluster size at very close to the  $N$ -Sm-A phase transition produces a strong pretransitional fluctuation.

Consequently, a plot of  $\ln(\gamma_1/\langle P_2 \rangle)$  with the variation of  $(1/T)$  gives a straight line having a slope of  $(E_a/k_\beta)$ , from which  $E_a$  can easily be obtained. Fig. 4.15 illustrates a systematic variation of  $\ln(\gamma_1/\langle P_2 \rangle)$  with  $(1/T)$  for all the mixtures. Therefore, the activation energy  $E_a$  has been calculated from the slope of this Arrhenius plot and listed in Table 4.5.

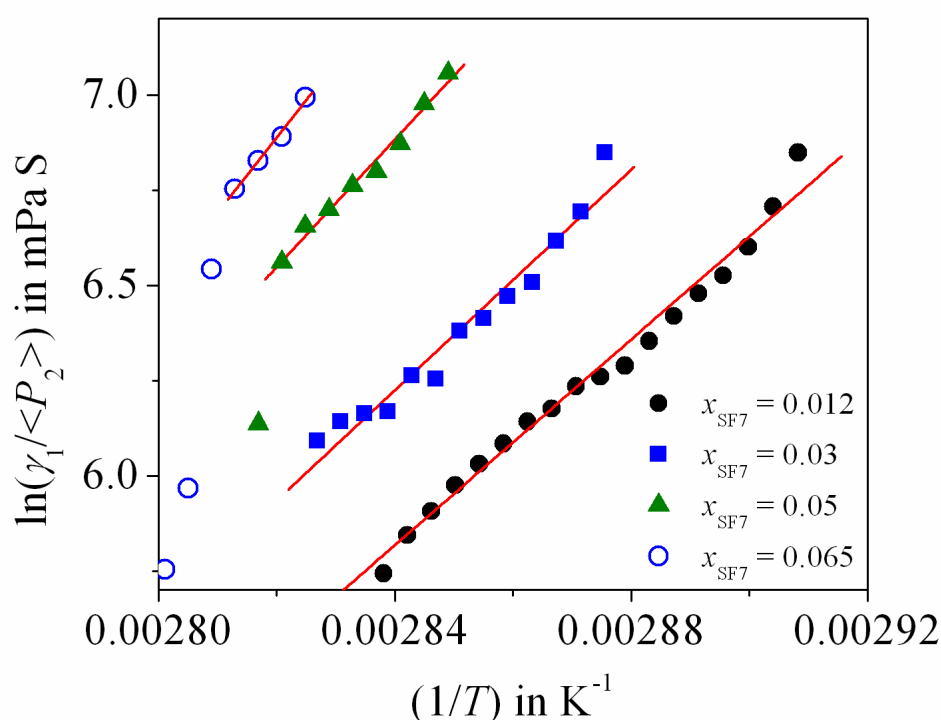


**Figure 4.15.** The variations of  $\ln(\gamma_1/\langle P_2 \rangle)$  with reciprocal of temperature  $(1/T)$  for all the concentrations only in nematic phase. Solid lines represent a linear fit to the data points.

**Table 4.5.** Activation energies for all the mixtures in the nematic phase.

$x_{\text{SF7}}$	Slope ( $E_a/k_\beta$ )	$E_a$ ( $\text{kJmol}^{-1}$ )
0.012	13505.26	112.29
0.03	14482.32	120.41
0.05	16729.87	139.10
0.065	19687.59	163.69

---

---

Table 4.5 reveals that the activation energy for the mixture having lowest concentration ( $x_{\text{SF7}} = 0.012$ ) is 112.29 kJ/mol which is quite large in comparison to that of usual calamitic compounds. Further increasing the hockey stick-shaped host compound, the activation energy monotonically increases up to a maximum value 163.69 kJ/mol for the highest concentration  $x_{\text{SF7}} = 0.065$ . These obtained results demonstrate that due to addition of SF7 compound, the intermolecular packing increases as well as a strong anti-parallel polar correlation is being developed within the rod-like environment which affects the molecular motion and thereby increases the activation energy.

## 4.7. Conclusion

The static dielectric and visco-elastic properties of some binary mixtures consisting of a hockey-stick shaped mesogen (SF7) with a calamitic mesogen (8OCB) have been carried out. Two different structural conformations play a significant role in the mixture leading to a noticeable shrinkage in the nematic width and impart an influence on the physical properties of the mixtures. All of the investigated mixtures possess a large positive dielectric anisotropy ( $\Delta\epsilon$ ), although the value of  $\epsilon_{\parallel}$  and  $\Delta\epsilon$  demonstrates a noticeable decrease by increasing the dopant concentration due to the strong polar interaction of anti-parallel aligned dipoles for both the diverse shaped mesogens. The extracted critical exponent value  $\alpha''$  obtained from the analysis of pretransitional behavior in  $\epsilon_{\text{iso}}$  as well as  $\epsilon_{\text{avg}}$  data in the vicinity of  $I$ - $N$  phase transition assumes a value nearly equal to 0.5 within a valid error limit which clearly implies a tricritical character of the  $I$ - $N$  phase transition for all the investigated mixtures. Moreover, by suitably employing the temperature-dependent dielectric anisotropy ( $\Delta\epsilon$ ) data in the vicinity of  $N$ - $\text{Sm-A}$  phase transition, the order character of this transition has been determined by a quite similar procedure used to obtain the same in high-resolution optical birefringence data. Based on the obtained results, the  $N$ - $\text{Sm-A}$  phase transition for all the mixtures signifying a second-order type of transitional nature and the extracted non-

---

---

---

---

universal values of the critical exponents divulges a systematic concentration variation. The critical exponents are found to reveal an excellent consistency obtained from the high-resolution optical birefringence measurements for the same binary system. Furthermore, the visco-elastic properties such as the splay elastic constant ( $K_{11}$ ) and the rotational viscosity ( $\gamma_1$ ) has been determined throughout the nematic phase for all the mixtures which also exhibit a systematic temperature and concentration dependency. By decreasing the temperature, both are found to increase gradually due to increases in molecular orientational ordering in the nematic phase. However, the efficient packing of these diverse molecules develops some temporary polar clusters within the rod-like environment having smectic-like strong short-range ordering. On increasing the amount of hockey stick-shaped mesogen, greater number of clusters developed within the system which is reflected by an increasing trend for the relative magnitude of both  $K_{11}$  and  $\gamma_1$ . Additionally, a pretransitional effect in the vicinity of  $N$ - $Sm$ - $A$  phase transition has also been observed in the experimental  $K_{11}$  and  $\gamma_1$  data due to rapid enhancement in size of the clusters by decreasing the temperature. The obtained values of  $\gamma_1$  for all of the investigated mixtures (consisting of hockey stick-shaped mesogen) have been found in between that of the usual calamitic compounds and that of the typical bent-core compounds. The activation energy ( $E_a$ ) reveals a smaller value for the lowest concentration and further increases with increasing the dopant concentration signifying an enhancement in intermolecular packing for the addition of dopant molecule which affects the molecular motion within the system. The entire observations made in the present system shows that due to the introduction of hockey stick-shaped mesogen effectively deteriorating the nematic phase range within the mixtures and depending upon the nematic range the  $N$ - $Sm$ - $A$  phase transition exhibit a crossover character from second order to first order in nature.

---

---

---

---

**References:**

- [1] P.F. McManamon, P.J. Boos, M.J. Escuti, J. Heikenfeld, S. Serati, H. Xie, and E.A. Watson, *Proc. IEEE*, **97**, 1078 (2009).
- [2] A. Liu, L. Liao, D. Rubin, H. Nguyen, B. Ciftcioglu, Y. Chetrit, N. Izhaky, and M. Paniccia, *Opt. Express*, **2**, 660 (2007).
- [3] V.A. Ezhov, in *Autostereoscopic display with full-screen 3D resolution (versions) and a method of controlling an active parallax barrier of the display*, Russian Federation Patent No. RU 2490818 (2012).
- [4] S.A. Studentsov, and V.A. Ezhov, in *Multistandard liquid-crystal stereo glasses*, Russian Federation Patent No. RU 2488150 (2011).
- [5] V.A. Ezhov, A.G. Sobolev, I.N. Kompanets, and A.L. Andreev, *Active liquid-crystal stereo glasses*, Russian Federation Patent No. RU 2456649 (2010).
- [6] J. Harden, B. Mbanda, N. Eber, K. Fodor-Csorba, S. Sprunt, J.T. Gleeson, and A. Jakli, *Phys. Rev. Lett.*, **97**, 157802 (2006).
- [7] A. Jakli, M. Chambers, J. Harden, M. Madhabi, R. Teeling, J. Kim, Q. Li, G.G. Nair, N. Eber, K. Fodor-Csorba, J.T. Gleeson, and S. Sprunt, *Proc. SPIE*, **6911**, 691105 (2008).
- [8] S.T. Wu, *Opt. Eng.*, **26**, 120 (1987).
- [9] B. Bahadur, in *Liquid crystals: applications and uses*, World Scientific, Singapore (1991).
- [10] B.R. Ratna, and R. Shashidhar, *Mol. Cryst. Liq. Cryst.*, **42**, 113 (1977).
- [11] M. Schadt, *The Journal of Chemical Physics*, **56**, 1494 (1972).
- [12] J. Li, M. Hu, J. Li, Z. An, X. Yang, Z. Yang, and Z. Che, *Liq. Cryst.*, **41**, 1783 (2014).
- [13] G.R. Luckhurst, *Thin Solid Films*, **393**, 40 (2001).
- [14] R. Berardi, L. Muccioli, and C. Zannoni, *J. Chem. Phys.*, **128**, 024905 (2008).

- 
- 
- [15] R. Balachandran, V. P. Panov, J. K. Vij, A. Lehmann, and C. Tschierske, *Phys. Rev. E*, **88**, 032503 (2013).
- [16] N. Avci, V. Borshch, D.D. Sarkar, R. Dev. G. Venkatesh, T. Turiv, S. J. Shiyakovskii, N.V.S. Rao, and O.D. Lavrentovich, *Soft Matter*, **9**, 1066 (2013).
- [17] B.R. Acharya, A. Primak, T.J. Dingemans, E.T. Samulski, and S. Kumar, *Pramana*, **61**, 231 (2003).
- [18] B.R. Acharya, A. Primak, and S. Kumar, *Phys. Rev. Lett.*, **92**, 145506 (2004).
- [19] L.A. Madsen, T.J. Dingemans, M. Nakata, and E.T. Samulski, *Phys. Rev. Lett.*, **92**, 145505 (2004).
- [20] R. Stannarius, A. Eremin, M.-G. Tamba, G. Pelzl, and W. Weissflog, *Phys. Rev. E*, **76**, 061704 (2007).
- [21] B. Das, S. Grande, W. Weissflog, A. Eremin, M.W. Schröder, G. Pelzl, S. Diele, and H. Kresse, *Liq. Cryst.*, **30**, 529 (2003).
- [22] R. Stannarius, L. Jianjun, and W. Weissflog, *Phys. Rev. Lett.*, **90**, 025502 (2003).
- [23] J. Harden, R. Teeling, J.T. Gleeson, S. Sprunt, and A. Jakli, *Phys. Rev. E*, **78**, 031702 (2008).
- [24] A. Chakraborty, M.K. Das, B. Das, A. Lehmann, and C. Tschierske, *Soft Matter*, **9**, 4273 (2013).
- [25] A. Chakraborty, M.K. Das, B. Das, U. Baumeister, and W. Weissflog, *J. Mater. Chem. C*, **1**, 7418 (2013).
- [26] B. Kundu, R. Pratibha, and N.V. Madhusudana, *Phys. Rev. Lett.*, **99**, 247802 (2007).
- [27] P. Sathyanarayana, M. Mathew, Q. Li, V.S.S. Sastry, B. Kundu, K.V. Le, H. Takezoe, and S. Dhara, *Phys. Rev. E*, **81**, 010702 (2010).
- [28] M. Majumdar, P. Salamon, A. Jákli, J.T. Gleeson, and S. Sprunt, *Phys. Rev. E*, **83**, 031701 (2011).
- 
-

- 
- 
- [29] P. Satyanarayana, S. Radhika, B.K. Sadashiva, and S. Dhara, *Soft Matter*, **8**, 2322 (2012).
- [30] E. Dorjgotov, K. Fodor-Csorba, J.T. Gleeson, S. Sprunt, and A. Jakli, *Liq. Cryst.*, **35**, 149 (2008).
- [31] P. Sathyanarayana, T. Arun Kumar, V.S.S. Sastry, M. Mathews, Q. Li, H. Takezoe, and S. Dhara, *Appl. Phys. Express*, **3**, 091702 (2010).
- [32] H. Takezoe, and Y. Takanishi, *Jpn. J. Appl. Phys.*, **45**(2A), 597 (2006).
- [33] O. Francescangeli, and E.T. Samulski, *Soft Matter*, **6**, 2413 (2010).
- [34] T. Niori, T. Sekine, J. Watanabe, T. Furukawa, and H. Takezoe, *J. Mater. Chem.*, **6**, 1231 (1996).
- [35] S. Chakraborty, A. Chakraborty, and M.K. Das, *J. Mol. Liq.*, **219**, 608 (2016).
- [36] V. Fréedericksz, and V. Zolina, *Trans. Faraday Soc.*, **29**, 919 (1933).
- [37] H.L. Ong, *Phys. Rev. A*, **33**, 3550 (1986).
- [38] H. Gruler, T.J. Schiffer, and G. Meier, *Z. Natureforsch.*, **27A**, 966 (1972).
- [39] H. Gruler, and L. Cheung, *J. Appl. Phys.*, **46**, 5097 (1975).
- [40] M.J. Bradshaw, and E.P. Rayens, *Mol. Cryst. Liq. Cryst.*, **72**, 35 (1981).
- [41] Hp. Schad, *J. Appl. Phys.*, **54**, 4994 (1983).
- [42] J. Jadzyn, and G. Czechowski, *Liq. Cryst.*, **4**, 157 (1989).
- [43] S. Sridevi, S.K. Prasad, D.S. Shankar Rao, C.V. Yelamaggad, *J. Phys.: Condens. Matter*, **20**, 465106 (2008).
- [44] S.K. Sarkar, and M.K. Das, *Fluid Phase Equilib.*, **365**, 41 (2014).
- [45] A. Drozd-Rzoska, S.J. Rzoska, and J. Ziolo, *Phys. Rev. E*, **55**, 2888 (1997).
- [46] M. Janik, S.J. Rzoska, A. Drozd-Rzoska, and J. Ziolo, *The Journal of Chemical Physics*, **124**, 144907 (2006).
- [47] S.J. Rzoska, J. Ziolo, W. Sulkoski, J. Jadzyn, and G. Czechowski, *Phys. Rev. E*, **64**, 052701 (2001).
- [48] M. Ginovska, H. Kresse, D. Bauman, G. Czechowski, and J. Jadzyn, *Phys. Rev. E*, **69**, 022701 (2004).
- 
-

- 
- 
- [49] J. Jadzyn, G. Czechowski, and J.-L. Déjardin, *J. Phys.: Condens. Matter*, **18**, 1839 (2006).
- [50] D. Wiant, S. Stojadinovic, K. Neupane, S. Sharma, K. Fodor-Csorba, A. Jákli, J. T. Gleeson, and S. Sprunt, *Phys. Rev. E*, **73**, 030703 (2006).
- [51] P.K. Mukherjee, and T.B. Mukherjee, *Phys. Rev. B*, **52**, 9964 (1995).
- [52] P.K. Mukherjee, *J. Phys. Condens. Matter*, **10**, 9191 (1998).
- [53] A. Drozd-Rzoska, *Phys. Rev. E*, **59**, 5556 (1999).
- [54] A. Drozd-Rzoska, S.J. Rzoska, J. Ziolo, *Phys. Rev. E*, **54**, 6452 (1996).
- [55] P. Cusmin, M.R. de la Fuente, J. Salud, M.A. Pérez-Jubindo, S. Diez-Berart, and D.O. López, *J. Phys. Chem. B*, **111**, 8974 (2007).
- [56] J. Jadzyn, G. Czechowski, and J.L. Déjardin, *J. Phys. Condens. Matter*, **18**, 1839 (2006).
- [57] A. Drozd-Rzoska, and S.J. Rzoska, in *Phase Transition: Application to liquid crystal, Organic Electronics and Optoelectronics Fields*, (Fifth Ed.) Popa-Nita, Trivandrum: Research Signpost (2006).
- [58] S. Parthasarathi, D.S. Shankar Rao, K.F. Csorba, and S.K. Prasad, *J. Phys. Chem. B*, **118**, 14526 (2014).
- [59] S. Parthasarathi, D.S. Shankar Rao, N.B. Palakurthi, C.V. Yelamagad, and S.K. Prasad, *J. Phys. Chem. B*, **120**, 5056 (2016).
- [60] P.H. Keyes, *Phys. Lett. A*, **67**, 132 (1978).
- [61] M.A. Anisimov, S.R. Garber, V.S. Episov, V.M. Mamnitskii, G.I. Ovodov, L.A. Smolenko, and E.L. Sorkin, *Sov. Phys. JETP*, **45**, 1042 (1977).
- [62] M.A. Anisimov, *Mol. Cryst. Liq. Cryst. Inc. Nonlinear Opt.*, **162**, 1 (1988).
- [63] S. Yildiz, H. Özbek, C. Glorieux, and J. Thoen, *Liq. Cryst.*, **34**, 611 (2007).
- [64] S. Erkan, M. Çetinkaya, S. Yildiz, and H. Özbek, *Phys. Rev. E*, **86**, 041705 (2012).
- 
-

- 
- 
- [65] A. Chakraborty, S. Chakraborty, and M.K. Das, *Phys. Rev. E*, **91**, 032503 (2015).
- [66] L.M. Blinov, and V.G. Chigrinov, in *Electro-optic effects in liquid crystal materials*, Springer-Verlag, New York (1994).
- [67] S. DasGupta, P. Chattopadhyay, and S.K. Roy, *Phys. Rev. E*, **63**, 041703 (2001).
- [68] S. DasGupta, and S.K. Roy, *Liq. Cryst.*, **30**, 31 (2003).
- [69] S. DasGupta, and S.K. Roy, *Phys. Lett. A*, **306**, 235 (2003).
- [70] S.W. Morris, P. Palffy-muhoray, and D.A. Balzarini, *Mol. Cryst. Liq. Cryst.*, **139**, 263 (1986).
- [71] D.V. Sai, K.P. Zuhail, R. Sarkar, and S. Dhara, *Liq. Cryst.*, **42**, 328 (2015).
- [72] P. Tadapatri, U.S. Hiremath, C.V. Yelamaggad, and K.S. Krishnamurthy, *J. Phys. Chem. B*, **114**, 1745 (2010).
- [73] P. Satyanarayana, M. Mathew, Q. Li, V.S.S. Sastry, B. Kundu, K.V. Le, H. Takezoe, and S. Dhara, *Phys. Rev. E*, **81**, 010702 (2010).
- [74] S. Kaur, J. Addis, C. Greco, A. Ferrarini, V. Görtz, J.W. Goodby, and H.F. Gleeson, *Phys. Rev. E*, **86**, 041703 (2012).
- [75] G. Czechowski, and J. Jadzyn, *Acta Physica Polonica A*, **106**, 475 (2004).
- [76] A. Chakraborty, S. Chakraborty, M.K. Das, and W. Weissflog, *J. Mol. Liq.*, **265**, 536 (2018).
- [77] P. Satyanarayana, B.K. Sadashiva, and S. Dhara, *Soft matter*, **7**, 8556 (2011).
- [78] S.T. Wu, and C.S. Wu, *Phys. Rev. A*, **42**, 2219 (1990).
- [79] M.L. Dark, M.H. Moore, D.K. Shenoy, and R. Shashidhar, *Liq. Cryst.*, **33**, 67 (2006).
- [80] A.V. Zakharov, and R.Y. Dong, *Eur. Phys. J. E*, **7**, 267 (2002).
- [81] P.G. de Gennes, *Solid State Commun.*, **10**, 753 (1972).
- [82] F. Jähnig, and F. Brochard, *J. Phys.*, **35**, 301 (1974).
- [83] D.R. Kim, *J. Korean Phys. Soc.*, **32**, 55 (1998).
- 
-

- 
- 
- [84] W.L. McMillan, *Phys. Rev. A*, **9**, 1720 (1974).
- [85] H. Knepe, F. Schneider, and N.K. Sharma, *J. Chem. Phys.*, **77**, 3203 (1982).
- [86] A. Pramanik, B. Das, M.K. Das, K. Garbat, S. Urban, and R. Dabrowski, *Liq. Cryst.*, **40**, 149 (2013).
- [87] G.W. Gray, V. Vill, H.W. Spiess, D. Demus, and J.W. Goodby, in *Physical properties of liquid crystals*, Wiley-VCH, Singapore (1999).
- [88] W.H. de Jeu, in *Physical properties of liquid crystalline materials*, Gordon and Breach, New York (1980).
- [89] P.G. de Gennes, in *The physics of liquid crystals*, Clarendon Press, Oxford (1974).
- [90] W. Kuczynski, B. Zywicki, and J. Malecki, *Mol. Cryst. Liq. Cryst.*, **381**, 1 (2002).
- [91] P. Pardhasaradhi , P.V.D. Prasad , D.M. Latha , V.G.K.M. Pisipati, and G.P. Rani, *Phase Transit.*, **85**, 1031 (2012).
- [92] K.D. Thingujama, P.R. Alapati, B. Choudhury and A. Bhattacharjee, *Phase Transit.*, **85**, 52 (2012).
- [93] A. Kumar, *Liq. Cryst.*, **40**, 203 (2013).
- [94] M. K. Das, G. Sarkar, B. Das, R. Rai, and N. Sinha, *J. Phys.: Condens. Matter*, **24**, 115101 (2012).
- [95] I. Haller, *Prog. Solid State Chem.*, **10**, 103 (1975).
- [96] A. Prasad, and M.K. Das, *Phase Transit.*, **83**, 1072 (2010).
- [97] M. Mitra, and R. Paul, *Mol. Cryst. Liq. Cryst.*, **148**, 185 (1987).
- [98] P.D. Roy, B. Das, and M.K. Das, *J. Phys.: Condens. Matter*, **21**, 335108 (2009).
- [99] P.D. Roy, A. Prasad, and M.K. Das, *J. Phys.: Condens. Matter*, **21**, 075106 (2009).
- [100] S.D. Sarkar, B. Choudhury, and M.K. Das, *Phase Transit.*, **85**, 85 (2012).
- 
-

# CHAPTER 5

---

Critical behavior at the smectic-*A* to smectic-*C*, nematic to smectic-*A* and isotropic to nematic phase transitions in a binary pyrimidine liquid crystal mixtures from high-resolution optical birefringence measurement

---

---

## 5.1. Introduction

Classical liquid crystal phases are characterized by broken symmetries and may be utilized to explore the complex and beautiful relationship in nature between symmetry and spatial dimensionality at phase transitions. The smectic layers are characterized by a quasi-long range one dimensional mass-density wave along the  $z$ -direction (*i.e.*, parallel to the layer-normal) and by a director (local orientational axis) which can either be parallel to the  $z$ -axis (Sm-A) or at an angle inclined to the  $z$ -axis (Sm-C). The transition between the Sm-A and Sm-C phases involves the breaking of a continuous rotational symmetry. Proposing the order parameter associated with the Sm-A–Sm-C transition to be  $\psi = \theta \exp(i\phi)$ , where  $\theta$  is the tilt angle of the director with respect to the smectic layer normal and  $\phi$  is an azimuthal angle, de Gennes has predicted that the Sm-A–Sm-C phase transition is continuous and should exhibit the same critical behavior as the superfluid transition in helium, *i.e.*, this transition should belong to the  $d = 3$ ,  $n = 2$  universality class (3D-XY model) [1]. However, the deviations from the helium-like behavior have often been observed in close vicinity of that transition [1-10]. A large number of experimental results from heat-capacity measurements have demonstrated classical mean-field behavior and can be described in the context of the extended mean-field model including the terms up to sixth-order in the tilt order parameters [2-8]. There are also several examples in which the heat capacity shows Landau behavior including tricritical appearance [9,10], while in some other cases, clear deviation from the mean field character has been observed, revealing either a 3D-XY or Gaussian tricritical behavior or a crossover from 3D-XY to tricritical nature [11-16]. The ultrasonic velocity and birefringence measurements have also been found to yield frequently non-Landau outcomes [17-20]. For butyloxy-benzylidene-heptylaniline (4O.7), it has been observed that the measurements of the tilt-angle variation face the difficulty of distinguishing critical behavior from mean field character on the

---

---

basis of order-parameter data alone, whereas the heat capacity and tilt-susceptibility data are uniquely described by the mean-field Landau model [4,5]. Therefore, the question that arises is why certain compounds show mean-field behavior while others critical behavior. Such a discrepancy is perhaps due to the fact that the bare correlation length describing the tilt fluctuations is usually much large so that the true critical region is unobservably small [21] and it may become inaccessible in certain experimental techniques. Later, Benguigui and Martinoty [22] tried to solve this issue using the Ginzburg criterion and proposed that the true critical behavior is expected only when  $|\tau| < \tau_G$ , where  $\tau$  is the reduced temperature and  $\tau_G$  is the Ginzburg temperature. They claimed that width of the critical region linked with the Sm-A–Sm-C phase transition is dependent on the physical properties studied, and consequently may lead to varying outcomes for the dissimilar observables probed. As in the ultrasonic velocity measurements, the elastic constants are found to exhibit non-Landau nature for their more sensitivity to fluctuation effects than the other measurement methods like heat capacity [22]. Safinya *et al.* showed that due to the large bare correlation lengths, as obtained from x-ray studies [21], the Ginzburg criterion yields  $\tau_G \sim 10^{-5}$ . Since the Sm-C ordering is apparently not driven by long-range interaction and the Sm-A–Sm-C transition is not at or above the upper critical dimensionality ( $d = 4$  for the XY universality class), mean-field theory is not applicable for the exact representation of this transition [23]. However, Huang and Lien [24] and Prasad *et al.* [25] indicated the possibility of observing a first-order or tricritical behavior of this transition by reduction of the Sm-A temperature range. Therefore, the absolute nature of the Sm-A–Sm-C phase transition (*i.e.*, its universality class) is still not properly been understood and necessitates further measurements, appropriate for studying the pretransitional fluctuation at this transition.

---

---

In chapter 3, the experimental verification of the crossover phenomena from 3D-XY to tricritical behavior by decreasing the nematic ( $N$ ) temperature range has been found to be quite successful in the  $N$ -Sm-A phase transition [26,27]. Therefore, it is quite plausible to expect that occurrence of such crossover from 3D-XY to tricritical and thereafter to first-order behavior seems to be related to the width of the Sm-A temperature range [24,25]. Thus the discovery of a suitable system that manifests critical fluctuations associated with the Sm-A-Sm-C transition is very important. Such a situation has been reported for a few phenyl pyrimidine compounds [28] and also in azoxy-4,4-biundecyl- $\alpha$ -methylcinnamate (AMC-11) [29] as well as some chiral systems [30]. As light is sensitive to the average molecular direction, probably optical measurements are accurate enough to allow for a discussion about the nature of the Sm-A-Sm-C phase transition. It has been well established in chapter 3 that the birefringence data can suitably be employed to study the critical anomaly at both the  $I$ - $N$  and the  $N$ -Sm-A phase transitions with a reasonably good accuracy. In fact, this method provides considerably precise data for  $\Delta n$  with a good reproducibility near the phase transition and hence facilitating a suitable interpretation of results – critical behavior, which in many cases become not possible in high resolution calorimetric or other measurements. Hence, the birefringence measurement is expected to supply further insights for clarifying whether or not the phase transition is of the Landau mean-field type.

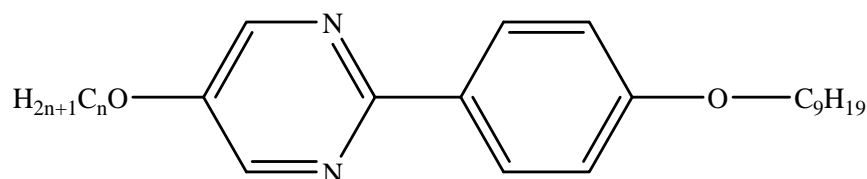
In this chapter, a high-resolution temperature scanning technique has been employed to determine the optical birefringence ( $\Delta n$ ) in a pure 5- $n$ -heptyloxy-2-(4- $n$ -nonyloxy-phenyl) pyrimidine (PhP2, the seventh homolog) liquid crystal as well as in some binary mixtures of the same with the second homologous compound 5- $n$ -ethyloxy-2-(4- $n$ -nonyloxy-phenyl) pyrimidine (PhP1) of the same series, to test the possibility of crossover behavior from nearly tricritical to 3D-XY critical nature near the Sm-A-Sm-C transition by reducing the temperature range of the Sm-A phase. Investigations have also

---

been carried out simultaneously at the nematic–smectic-A (*N*–*Sm*-A) phase transitions from which a comparative discussion has been established concerning the similarity and dissimilarity of order nature for both the transitions [31,32]. Additionally, the critical behavior in the vicinity of isotropic–nematic (*I*–*N*) phase transition has been reported for all of the studied mixtures including a pure compound.

## 5.2. Materials

The materials studied, were synthesized at the Institute of Chemistry, Military University of Technology, Warsaw, Poland (having purity higher than 99.9%), and were used without further purification. The structural formulae and the stable mesophase sequences for both the compounds are given below:



**Compound 1:** For **PhP1**,  $n = 2$ ; Phase sequence as follows,



**Compound 2:** For **PhP2**,  $n = 7$ ; Phase sequence as follows,



Eight mixtures of the binary system were prepared by adding small amounts of 5-*n*-ethyloxy-2-(4-nonyloxy-phenyl) pyrimidine (PhP1) compound into the host 5-*n*-heptyloxy-2-(4-*n*-nonyloxy-phenyl) pyrimidine (PhP2) compound having molar concentrations 0.05, 0.1, 0.15, 0.2, 0.3, 0.35, 0.4 and 0.45. The optical textures were observed under a polarizing optical microscope (BANBROS) equipped with HCS302 (INSTECH) hot stage, controlled by mK1000 (INSTECH) thermo system.

### 5.3. Phase diagram

The partial phase diagram of the binary system consisting of PhP2 with the second compound, PhP1 as obtained from polarizing optical microscopy and the optical transmission technique has been illustrated in Fig. 5.1. The pure compound PhP1 comprises a nematic ( $N$ ) phase appearing in a small range of  $\sim 3.8$  K, but the PhP2 compound exhibit a nematic phase with a temperature range of  $\sim 4$  K along with a Smectic-A (Sm-A) phase of range  $\sim 11$  K and a Smectic-C (Sm-C) phase of range  $\sim 22$  K.

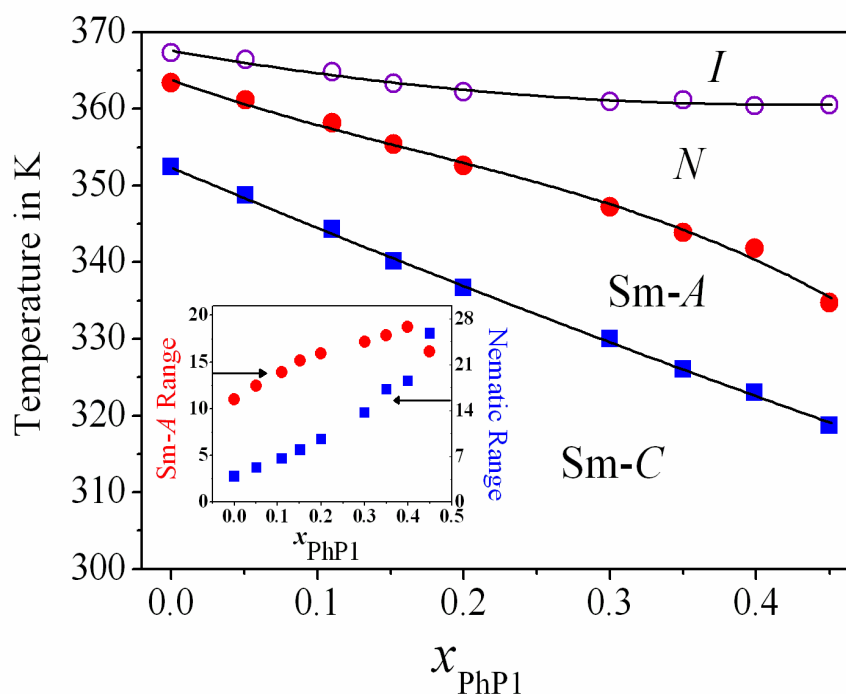


**Figure 5.1.** Partial phase diagram of the binary system comprising of PhP2 and PhP1.  $x_{\text{PhP1}}$  denotes the mole fraction of PhP1.  $I$ – isotropic phase,  $N$ – nematic phase, Sm-A–smectic-A phase, Sm-C–smectic-C phase,  $\circ$ : isotropic to nematic transition temperature;  $\bullet$ : nematic to smectic-A transition temperature;  $\blacksquare$ : smectic-A to smectic-C transition temperature; Inset shows the concentration dependence of the Sm-A and nematic ranges for the present system. Solid lines are drawn for guidance to eye.

It has been observed that a systematic variation in the  $N$  and Sm-A width has been accomplished by the addition of the second homologue (PhP1) of the same series. The nematic phase range has been found to increase from a value

---

---

of 4 K to 27 K whereas the Sm-A phase range lies between 11 K and 19 K for the studied mixtures. These variations of the  $N$  and Sm-A ranges against molar concentration is also presented in the inset of Fig. 5.1. The present binary system offers both the variation of  $N$  and Sm-A phase with reasonable ranges, which is very helpful to investigate the order character of the  $N$ -Sm-A and the Sm-A-Sm-C phase transition simultaneously. Therefore, it is expected that the dependence of the effective critical exponent ( $\alpha'$ ) on the temperature ratios  $T_{NA}/T_{IN}$  and  $T_{AC}/T_{NA}$  ( $T_{NA}$  :  $N$ -Sm-A phase transition temperature,  $T_{AC}$  : Sm-A-Sm-C phase transition temperature,  $T_{IN}$  : Isotropic to nematic phase transition temperature) can be investigated more rigorously, thus endowing with the insight on the nature of both the  $N$  to Sm-A and Sm-A to Sm-C phase transitions from the same binary system of rod-like liquid crystal molecules.

## 5.4. Optical birefringence measurements

A temperature scanning measurement of the optical birefringence during cooling from isotropic liquid (with the average scanning rate of  $0.5 \text{ K min}^{-1}$ ) to the room temperature have been accomplished by probing the phase retardation ( $\Delta\phi$ ) of a laser beam ( $\lambda = 532 \text{ nm}$ ) transmitted through a planar aligned ITO coated liquid crystal filled cell of thickness  $\sim 7.7 \mu\text{m}$  [31-37]. The birefringence in the nematic phase was calculated from the measured normalized intensity and this method was extended to the Sm-A and Sm-C mesophases as well. Moreover, to check the reproducibility of the data, measurements were also performed for several cooling and heating runs and reproducible results were obtained. The variation of optical birefringence ( $\Delta n$ ) against temperature ( $T$ ) for the pure compound (PhP2) and three of the binary mixture having molar concentration  $x_{\text{PhP1}} = 0.1, 0.2$  and  $0.3$  has been represented in Fig. 5.2(a-d). For all of the investigated systems, in the isotropic phase the birefringence value is equal to zero, which on entering the nematic phase increases rapidly following the  $I$ - $N$  phase transition, evidently due to the strong growth of the nematic order. The overall profile of the temperature dependence of  $\Delta n$  is in good

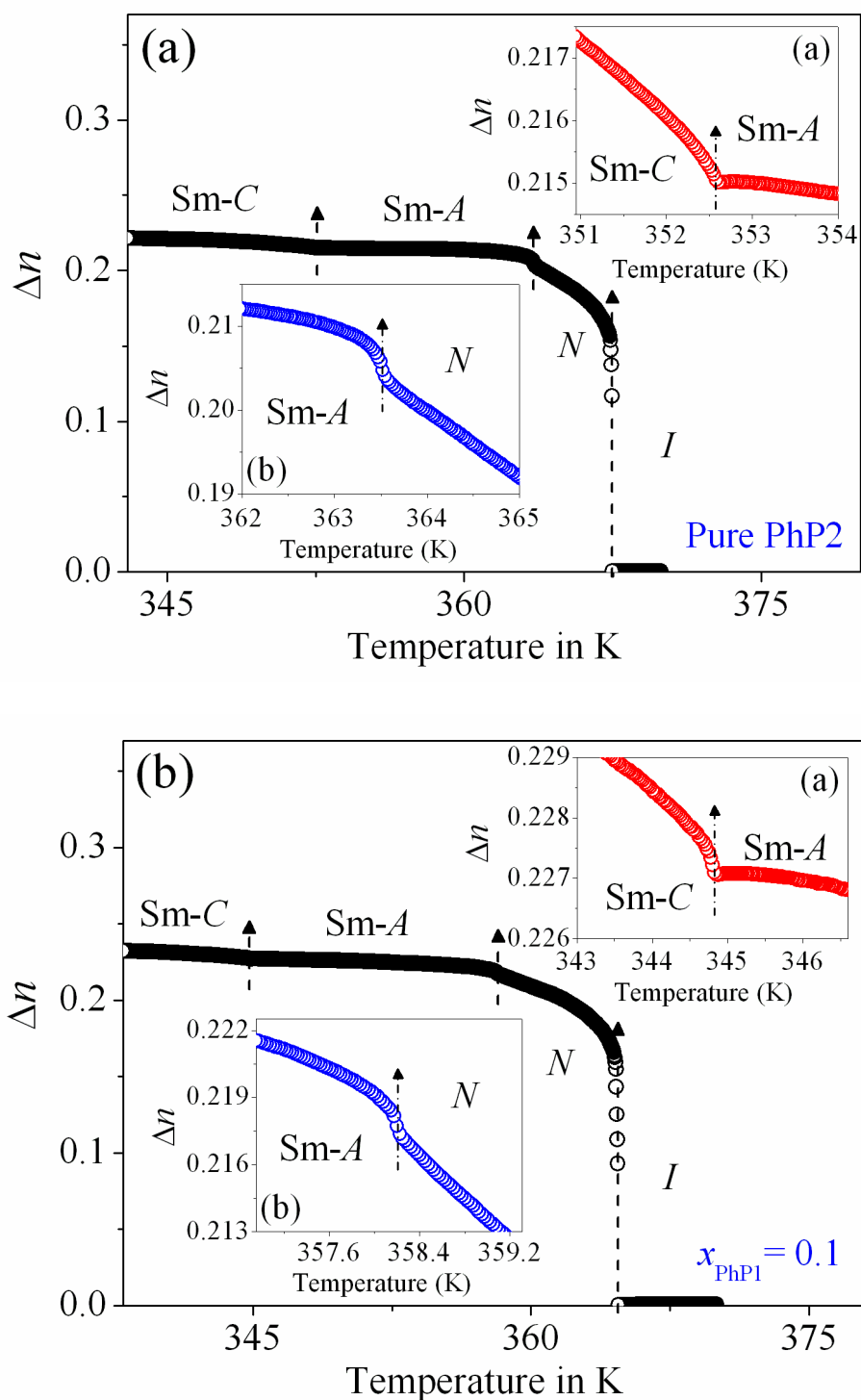


**Figure 5.2.** Temperature dependence of birefringence ( $\Delta n$ ) data for the (a) Pure PhP2 compound and (b) mixture  $x_{\text{PhPI}} = 0.1$ . Vertical arrows show the  $I$ - $N$ ,  $N$ - $\text{Sm-A}$  and  $\text{Sm-A}$ - $\text{Sm-C}$  phase transitions for the mixtures. In the insets variation of birefringence in the vicinity of  $\text{Sm-A}$ - $\text{Sm-C}$  transition [inset (a)] and  $N$ - $\text{Sm-A}$  transition [inset (b)] has been presented.

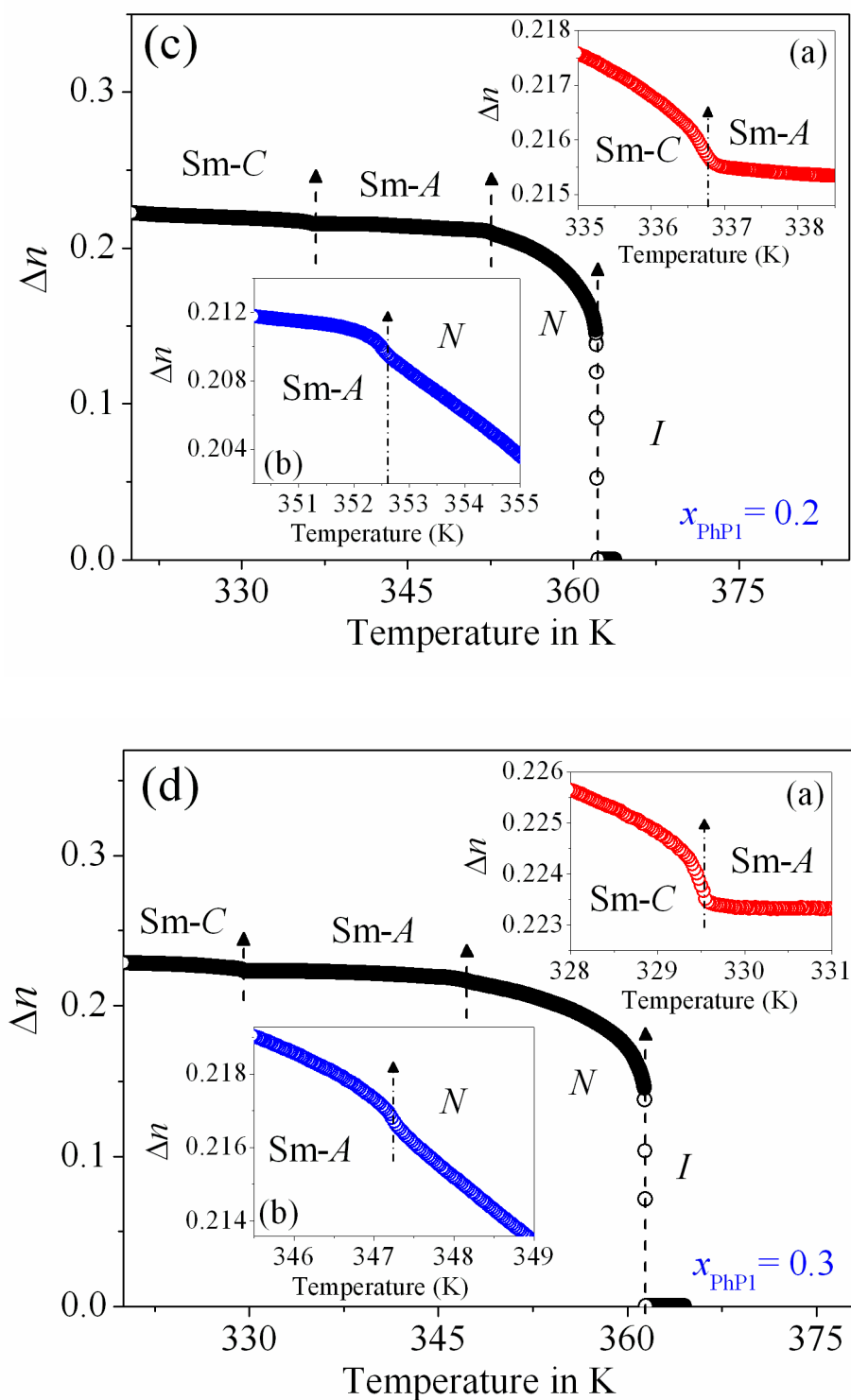


**Figure 5.2 (cont'd).** Temperature dependence of birefringence ( $\Delta n$ ) data for the mixture (c)  $x_{PhPI} = 0.2$  and (d)  $x_{PhPI} = 0.3$ . Vertical arrows show the  $I-N$ ,  $N-Sm-A$  and  $Sm-A-Sm-C$  phase transitions for the mixtures. In the insets variation of birefringence in the vicinity of  $Sm-A-Sm-C$  transition [inset (a)] and  $N-Sm-A$  transition [inset (b)] has been presented.

agreement with the reported various rod-like liquid crystals [38]. As seen in Fig. 5.2, upon lowering the temperature towards the Sm-A phase, an enhancement in  $\Delta n$  takes place at the  $N$ -Sm-A phase transition. Such augmentation is preferably owing to the smectic-like short-range order, building up within the nematic phase close to the  $N$ -Sm-A phase transition and consequently causing a further enhancement in the nematic (orientational) order. Moreover, on entering the low-temperature tilted Sm-C phase there is also a clear and overall increase in  $\Delta n$  due to the Sm-A-Sm-C phase transition. This may be due to the fact that the molecular long axis in the Sm-C phase of the surface aligned (planar cell of thickness  $7.7 \mu\text{m}$ ) bulk sample is oriented parallel to the aligning surface and the layers are tilted with respect to the surface alignment which causes an enhancement in the orientational order. Thus, a well-defined  $\Delta n$  curves in the vicinity of the transition temperatures has been obtained. In the present optical technique, the small transitional variation in birefringence and hence the related modification in the mesophase structure can suitably be used to precisely describe the nature of different phase transitions in liquid crystal media.

### 5.5. Critical behavior at the Sm-A-Sm-C phase transition

In this study, a sharp increasing nature in the temperature dependence of birefringence data has been observed in going from the Sm-A to the Sm-C phase. As no visible discontinuity is found in the temperature dependence of  $\Delta n$  at this transition, the exact transition temperature is identified by locating the minimum value of the temperature dependence quantity  $[-d(\Delta n)/dT]$ . Furthermore, a differential quotient  $Q(T)$  has been introduced following the same expression (Eq. 3.6) in Chapter 3 to take a proper look into the critical aspects of the Sm-A-Sm-C phase transition, defined as [39-41]:

$$Q(T) = -\frac{\Delta n(T) - \Delta n(T_{AC})}{T - T_{AC}} \quad (5.1)$$

where  $T_{NA}$  is changed to  $T_{AC}$ , and  $\Delta n(T_{AC})$  is the birefringence value at the Sm-A–Sm-C phase transition temperature ( $T_{AC}$ ). An overview of the temperature dependent variation of  $Q(T)$  for pure PhP2, close to the Sm-A–Sm-C phase transition is shown in Fig. 5.3. The  $Q(T)$  data exhibit a noticeable anomaly close to that transition, involving an asymmetry between the  $Q(T)$  wings in the Sm-A and Sm-C phases. Furthermore, in order to gain an impression of the critical fluctuation in  $Q(T)$ , appearing in the vicinity of the Sm-A–Sm-C phase transition, fit to the following renormalization group expression has also been performed [41],

$$Q(T) = \frac{A^\pm}{\alpha'} |\tau|^{-\alpha'} (1 + D^\pm |\tau|^\Delta) + E(T - T_{AC}) + B \quad (5.2)$$

where,  $\tau = (T - T_{AC})/T_{AC}$  is the reduced temperature,  $\alpha'$  is the critical exponent similar to the specific-heat capacity critical exponent  $\alpha$  and the other parameters are the same as appearing in Eq. (3.7) in Chapter 3, but now they corresponds to the Sm-A–Sm-C phase transition. The fit to Eq. (5.2) with the measured  $Q(T)$  data is displayed in Fig. 5.3 as solid line for the PhP2 compound.

In order to realize consistent fittings, few data points very close to the transition have been excluded from the fit process to avoid the error resulting from the experimental uncertainty and sample inhomogeneity. In each fit, the transition temperature was first isolated by identifying the minimum of the temperature dependence of  $-d(\Delta n)/dT$  and then was kept fixed. This helps in reducing the instability appearing in the least-squares minimization. The  $Q(T)$  data exhibit a noticeable divergent character on both side of the transition temperature, involving an asymmetry between the  $Q(T)$  wings in the Sm-A and Sm-C phases. In particular, the existence of such divergent behavior above the transition temperature clearly indicates that this transition is not of the mean-field type. It has been observed that the temperature dependence of  $Q(T)$  data close to  $T_{AC}$  is well described by Eq. (5.2), suggesting a good agreement between the experimental optical birefringence data and the theoretical power

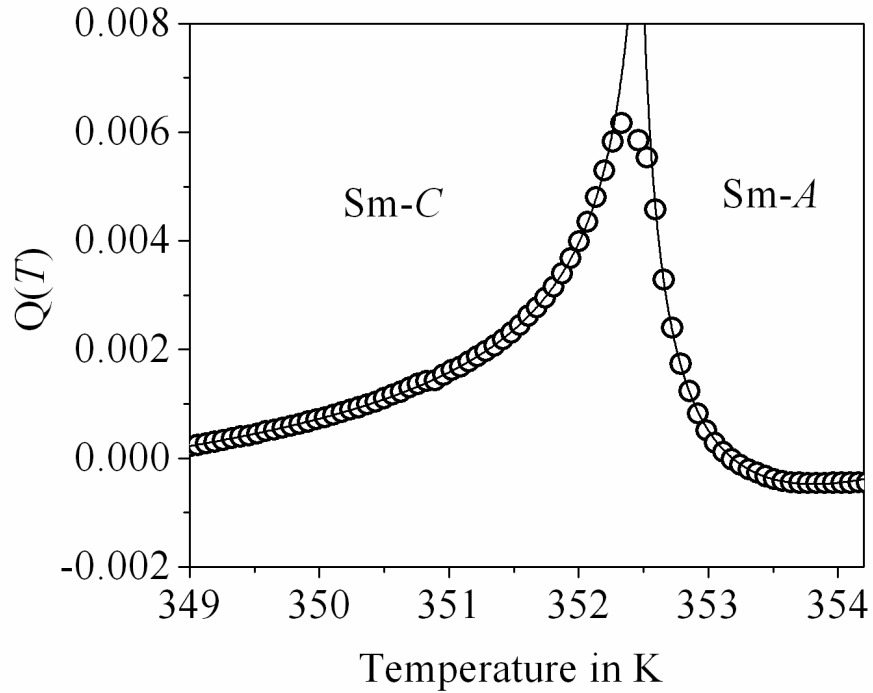


**Figure 5.3.** The temperature variation of the parameter  $Q(T)$  near the Sm-A–Sm-C phase transition. Solid lines are fit to Eq. (5.2) near the Sm-A–Sm-C phase transition.

**Table 5.1.** Results corresponding to the best fit for  $Q(T)$  of pure PhP2 compound near the Sm-A–Sm-C phase transition obtained in accordance with Eq. (5.2) and related  $\chi_v^2$  values associated with the fits. The Sm-A–Sm-C phase transition temperature  $T_{AC} = 352.45$  K was kept fixed in the fits.  $|\tau|_{\max}$  represents the upper limit of reduced temperature considered for these fits.

Phase	$\alpha'$	$A^-, A^+$	$D^-, D^+$	$ \tau _{\max}$	$\chi_v^2$
Smectic-C	$0.478 \pm 0.005$	$0.00031 \pm 0.00001$	$14.4 \pm 0.2$	$3 \times 10^{-3}$	1.1
Smectic-A	$0.474 \pm 0.008$	$0.00024 \pm 0.00001$	$14.2 \pm 0.6$	$3 \times 10^{-3}$	1.29
Smectic-C	$0.477 \pm 0.015$	$0.00016 \pm 0.00002$	$4.4 \pm 0.5$	$5 \times 10^{-3}$	1.09
Smectic-A	$0.483 \pm 0.024$	$0.00014 \pm 0.00002$	$11.4 \pm 0.7$	$5 \times 10^{-3}$	1.31
Smectic-C	$0.488 \pm 0.010$	$0.00013 \pm 0.00001$	$7.3 \pm 0.4$	$1 \times 10^{-2}$	1.14
Smectic-C	$0.502 \pm 0.008$	$0.00011 \pm 0.00001$	$5.7 \pm 0.2$	$1.5 \times 10^{-2}$	1.23

---



---

law behavior considered. Furthermore, the extracted critical character for the Sm-A–Sm-C phase transition has usually been found to be sensitive to the width of the temperature range, considered in the fit process. An investigation has been performed herewith to perceive the dependency of fit parameters on the fit range. In the vicinity of Sm-A–Sm-C transition, fit has been carried out for four different reduced temperature ranges:  $|\tau|_{\max} = 3 \times 10^{-3}$ ,  $5 \times 10^{-3}$ ,  $1 \times 10^{-2}$  and  $1.5 \times 10^{-2}$ . Corresponding fit parameters as obtained from the fit process are presented in Table 5.1 for the pure compound. The quality of the fits has been assessed by calculating the related reduced error function  $\chi_v^2$  value [42], have been found to be within 1.09 and 1.31 and thus signifying consistent fits. In these fits, the critical exponent ( $\alpha'$ ) for the Sm-A–Sm-C phase transition depends feebly on the fit range, appeared to be nearly 0.476 and 0.48 for the reduced temperature range  $|\tau|_{\max} = 3 \times 10^{-3}$  and  $5 \times 10^{-3}$  respectively, yielded slightly higher value for the relatively greater temperature ranges considered. The critical amplitude quotient ( $A^-/A^+$ ) has been found to be 1.301 and 1.14 for the reduced temperature range  $|\tau|_{\max} = 3 \times 10^{-3}$  and  $5 \times 10^{-3}$  respectively. However, the  $D^+$  value has been appeared to be comparatively greater than its counterpart in the Sm-C phase for  $|\tau|_{\max} = 5 \times 10^{-3}$  and other higher ranges, thus disagreeing with the theoretical prediction of  $D^-/D^+ \sim 1$ , while the  $D^-/D^+$  quotient assumes a value 1.01 for the fit range  $|\tau|_{\max} = 3 \times 10^{-3}$ , which reveals a well consistency with the theoretical value. Such a shortcoming of  $D^-$  for the greater fit ranges is perhaps owing to the strong correlation between  $D$  and  $B$  and also due to the nearly tricritical character of that transition [43].

Hence, nearly Gaussian (non-classical) tricritical behavior has been revealed for the Sm-A–Sm-C phase transition of the pure PhP2 compound. Moreover, in the pure compound as the Sm-A width is of only 11 K, the unsaturation of the Sm-A order parameter close to the Sm-A–Sm-C phase transition perhaps lead to a large Sm-C order correlation length, which also pushes the transition towards a mean-field like character. The dependence of

---

---

that transition on the size of the Sm-A phase has also been elucidated by others [24,25]. For another pyrimidine liquid crystal, 5-*n*-decyl-2-[4-*n*-(perfluoropentyl-metheleneoxy) phenyl] pyrimidine, with an almost identical Sm-A width as the present PhP2 compound, Reed *et al.* also reported a non-Landau, nearly tricritical nature is in line with the observed behavior [28]. However, it has also been observed that the exponent  $\alpha'$  demonstrates a weak decrease with the shrinkage of temperature range, considered in the fits. Furthermore, according to Safinya *et al.* as the large correlation length describing the tilt fluctuations results in a highly reduced critical region, experimentally it may not be possible to access the true critical region [21]. Thus there may be a possibility of crossover appearance of the Sm-A–Sm-C phase transition in this study as the true critical region may be much smaller than the present fit range so that it remains inaccessible. Yet, because of the well-consistency of parameter ratios with the theoretical values and also for revealing a reasonable range of reduced error function  $\chi_v^2$ , it seems more acceptable to investigate the critical behavior in a range  $|\tau|_{\max} = 3 \times 10^{-3}$ . However, it is apparent that the critical exponent  $\alpha'$  characterizing the critical fluctuations in  $Q(T)$  is in agreement with the theoretical description based on the renormalization-group method and hence reveal a disagreement of the nature of that transition with the extended Landau mean-field model.

Furthermore, investigation has been carried out for all of the mixtures to observe the dependency of critical exponent ( $\alpha'$ ) with the Sm-A phase range. An overview of the temperature-dependent variation of  $Q(T)$  in the vicinity of Sm-A–Sm-C phase transition for eight different mixtures including the pure compound is shown in Fig. 5.4 in a fit range  $|\tau|_{\max} = 3 \times 10^{-3}$ . All of the  $Q(T)$  data manifesting a divergent behavior on both side of the transition, involving an asymmetry between the  $Q(T)$  wings in the Sm-A and Sm-C phases. As both the compounds were chosen from the same homologous series, no Fisher renormalization [44] of the critical exponent has been observed even for nearly

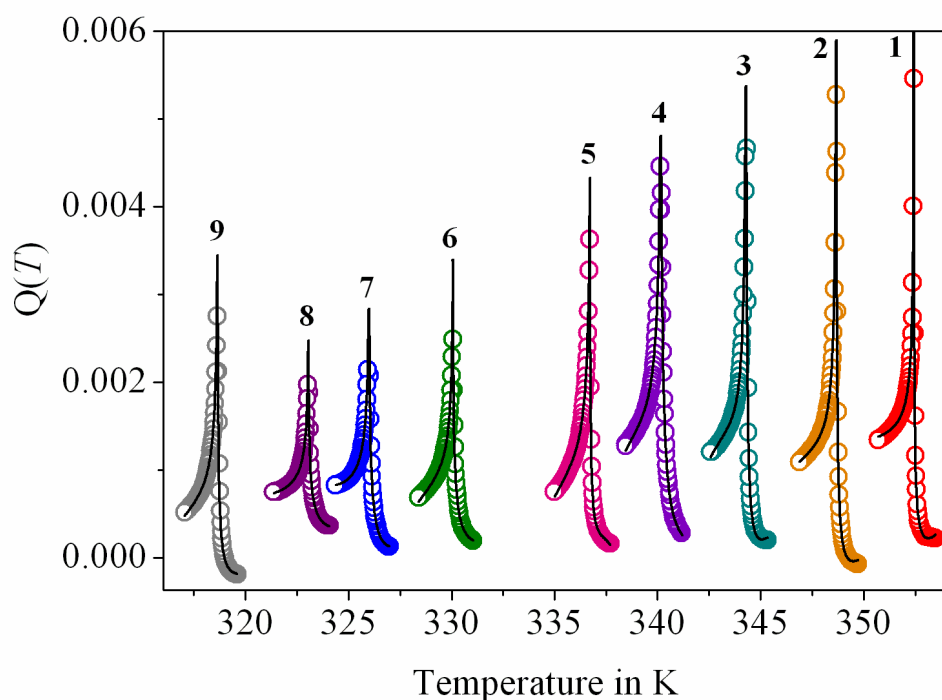


**Figure 5.4.** The temperature dependence of  $Q(T)$  in the vicinity of the Sm-A–Sm-C transition in mixtures of PhP1 and PhP2 for  $|\tau|_{\max} = 3 \times 10^{-3}$ . 1:  $x_{\text{PhP1}} = 0.0$ ; 2:  $x_{\text{PhP1}} = 0.05$ ; 3:  $x_{\text{PhP1}} = 0.1$ ; 4:  $x_{\text{PhP1}} = 0.15$ ; 5:  $x_{\text{PhP1}} = 0.2$ ; 6:  $x_{\text{PhP1}} = 0.3$ ; 7:  $x_{\text{PhP1}} = 0.35$ ; 8:  $x_{\text{PhP1}} = 0.4$ ; 9:  $x_{\text{PhP1}} = 0.45$ .

**Table 5.2.** Results corresponding to the best fit for  $Q(T)$  near Sm-A–Sm-C phase transition of all the mixtures obtained in accordance with Eq. (5.2) and related  $\chi_v^2$  values associated with the fits.

$x_{\text{PhP1}}$	$A^-/A^+$	$D^-/D^+$	$\alpha'$	$\chi_v^2$
0	$1.301 \pm 0.001$	$1.01 \pm 0.05$	$0.476 \pm 0.007$	1.19
0.05	$1.200 \pm 0.011$	$1.00 \pm 0.03$	$0.397 \pm 0.006$	1.24
0.10	$1.080 \pm 0.018$	$0.99 \pm 0.05$	$0.321 \pm 0.017$	1.17
0.15	$1.017 \pm 0.098$	$0.94 \pm 0.03$	$0.237 \pm 0.011$	1.19
0.20	$0.979 \pm 0.062$	$0.93 \pm 0.04$	$0.193 \pm 0.007$	1.25
0.30	$0.911 \pm 0.006$	$0.91 \pm 0.03$	$0.136 \pm 0.002$	1.13
0.35	$0.930 \pm 0.002$	$0.91 \pm 0.02$	$0.089 \pm 0.007$	1.17
0.40	$0.907 \pm 0.011$	$0.91 \pm 0.03$	$0.040 \pm 0.006$	1.15
0.45	$0.936 \pm 0.018$	$0.86 \pm 0.06$	$0.152 \pm 0.005$	1.08

tricritical compositions. The fits to Eq. (5.2) are displayed as solid lines, while the corresponding fit values are listed in Table 5.2. The reduced error functions  $\chi_v^2$ , which have been found to be within 1.08 and 1.25, signify consistent fits. However, with increasing the concentration of PhP1 compound, the measured value of critical exponent  $\alpha'$  in the vicinity of the Sm-A–Sm-C phase transition decreases monotonically from  $0.476 \pm 0.007$  for the pure PhP2 compound to  $0.04 \pm 0.006$  for the mixture  $x_{\text{PhP1}} = 0.40$ , *i.e.*, the yielded values of effective critical exponent  $\alpha'$ , characterizing the critical fluctuation at this transition, have appeared to be in between those predicted by the 3D-XY, *i.e.*,  $\alpha_{XY} = -0.007$  and tricritical, *i.e.*,  $\alpha_{\text{TCH}} = 0.5$  values. The variation of the extracted critical exponent ( $\alpha'$ ) values for the present investigated mixtures including pure PhP2 against the temperature ratio ( $T_{AC}/T_{NA}$ ) is illustrated in Fig. 5.5. Non-universal values have been observed for the critical exponent  $\alpha'$  and hence indicate a

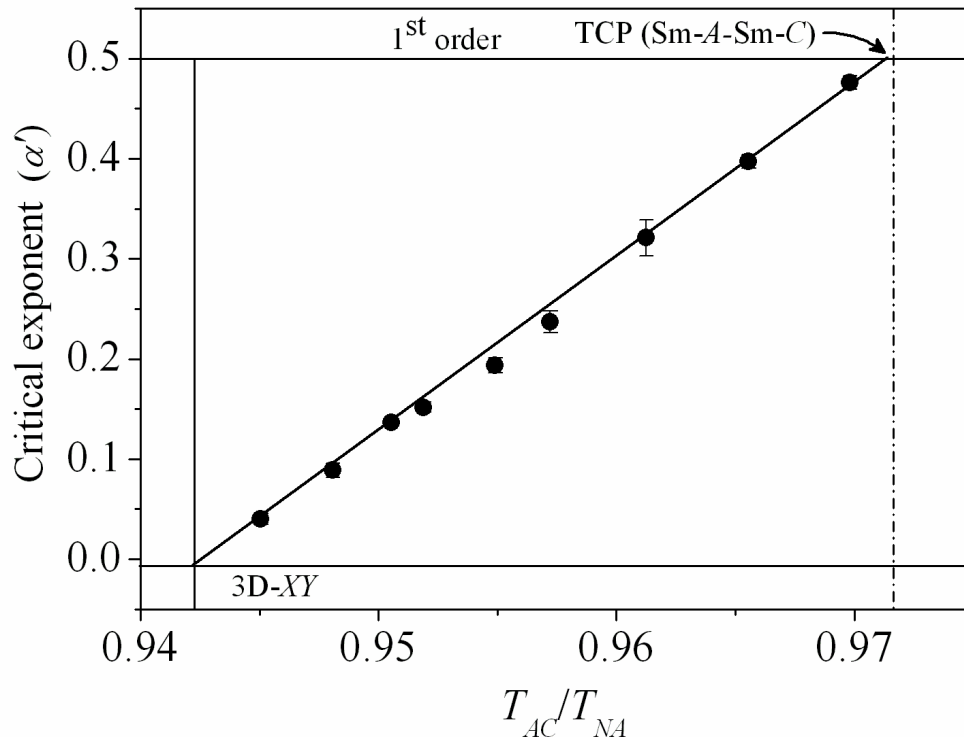


**Figure 5.5.** Variation of the effective critical exponent ( $\alpha'$ ) with  $T_{AC}/T_{NA}$  for Sm-A–Sm-C phase transition. The vertical dashed line and solid line corresponds to the tricritical point (TCP) and 3D-XY limit respectively. The solid line is a linear fit to the data points.

---

crossover character for the Sm-A–Sm-C phase transition. An extrapolation of the linear fit to the extracted  $\alpha'$  values yield a tricritical point for the  $T_{AC}/T_{NA}$  ratio of 0.972 and reveal a  $T_{AC}/T_{NA}$  value of 0.942 corresponding to the 3D-XY point. It should also be mentioned here that this crossover of  $\alpha'$  gives rise to the characteristic behavior regarding amplitude ratio ( $A^-/A^+$ ) and the magnitude of the first-order corrections-to-scaling terms ( $D^-/D^+$ ). In that case, the  $A^-/A^+$  values are in the range between 1.301 and 0.907 (from the extrapolation of the linear fit it yields about 1.39 for the tricritical point (TCP) and 0.954 for the 3D-XY point) and the first-order corrections-to-scaling ratio is between 1.01 to 0.86 (from the extrapolation of the linear fit it yields about 1.05 for the TCP and 0.89 for the 3D-XY point). The theory for the 3D-XY universality class predicts an amplitude ratio  $A^-/A^+ = 0.971$  and  $D^-/D^+ \approx 1$  while for TCP the theoretical amplitude ratio  $A^-/A^+ = 1.6$  and  $D^-/D^+ \approx 1$ . Therefore, from this observation, it is clear that the studied mixtures exhibit non-universal behaviors with effective critical exponents lying between the 3D-XY and tricritical limits.

## 5.6. Critical behavior at the $N$ –Sm-A phase transition

Following the same procedure as discussed in chapter 3 the critical anomaly associated with the  $N$ –Sm-A phase transition has been explored to the present system as well from the precise  $\Delta n$  data. In this study, similar renormalization group expression including the corrections to scaling term have been reused, in an attempt to obtain an insight into the limiting behavior of the quotient  $Q(T)$  near the  $N$ –Sm-A phase transition.

The temperature dependence of  $Q(T)$  for the pure compound PhP2 in the vicinity of  $N$ –Sm-A phase transition is depicted in Fig. 5.6. The fit to the equation is displayed as solid lines in the same figure, while the corresponding fit parameters are presented in Table 5.3. Although the fits have been performed for two different temperature ranges ( $|\tau|_{\max} = 5 \times 10^{-3}, 7.7 \times 10^{-3}$ ), the fit

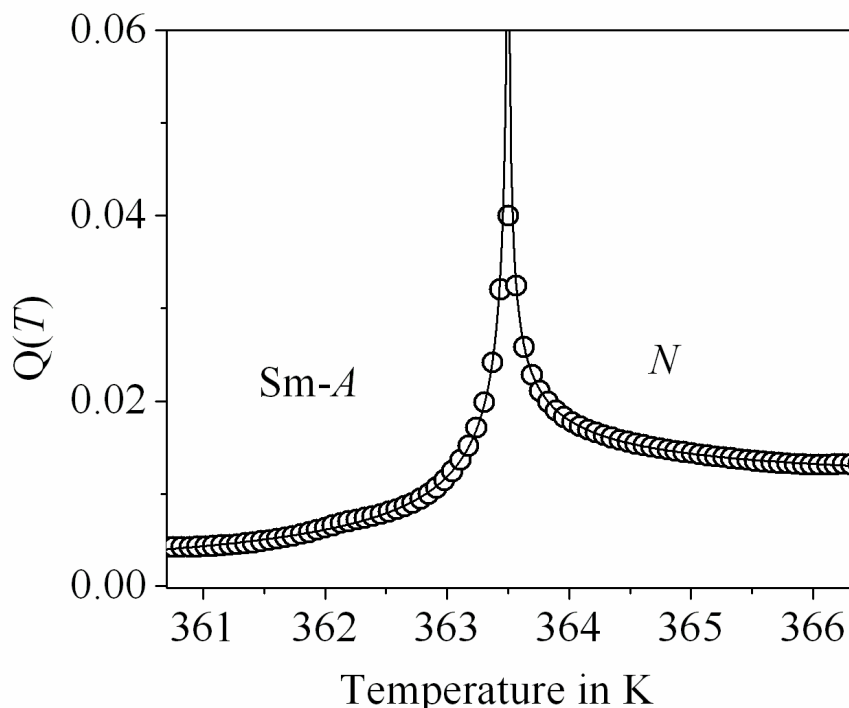


**Figure 5.6.** Temperature variation of the parameter  $Q(T)$  near the  $N$ - $Sm-A$  phase transition for sample PhP2. Solid lines are fit to Eq. (5.2) near the  $N$ - $Sm-A$  phase transition.

**Table 5.3.** Results corresponding to the best fit for  $Q(T)$  of pure PhP2 compound near the  $N$ - $Sm-A$  phase transition and related  $\chi_v^2$  values associated with the fits. The  $N$ - $Sm-A$  phase transition temperature  $T_{NA} = 363.5$  K was kept fixed in the fits.  $|\tau|_{\max}$  represents the upper limit of reduced temperature considered for these fits.

Phase	$\alpha'$	$A^-, A^+$	$D^-, D^+$	$ \tau _{\max}$	$\chi_v^2$
Smectic-A	$0.463 \pm 0.014$	$0.00057 \pm 0.00007$	$9.26 \pm 0.36$	$5 \times 10^{-3}$	1.35
Nematic	$0.462 \pm 0.008$	$0.00035 \pm 0.00003$	$9.35 \pm 0.87$	$5 \times 10^{-3}$	1.07
Smectic-A	$0.463 \pm 0.015$	$0.00073 \pm 0.00003$	$8.41 \pm 0.72$	$7.9 \times 10^{-3}$	1.06
Nematic	$0.465 \pm 0.007$	$0.00044 \pm 0.00001$	$8.22 \pm 0.34$	$7.7 \times 10^{-3}$	1.18

range  $\tau = 5 \times 10^{-3}$  have been accepted because the fit parameters remain practically stable for a small change in temperature range along with a minimum regular pattern in the residuals [45]. The goodness of the fits has

been tested with the help of reduced error function  $\chi_v^2$ . In this study, the  $\chi_v^2$  values related to fits to the  $Q(T)$  wings are found within 1.06 and 1.35, indicating a satisfactory fit of the  $Q(T)$  data to the model expression considered. In this fits, the critical exponent  $\alpha'$  has come out to be close to 0.462 for the pure compound PhP2 and hence indicates a nearly tricritical nature of the  $N$ -Sm-A phase transition. According to theoretical predictions, the 3D-XY universality class requires the occurrence of a critical amplitude ratio ( $A^-/A^+$ ) equal to 0.971, a critical exponent ( $\alpha'$ ) of -0.007 and ( $D^-/D^+$ )  $\sim 1$  while for a tricritical point the critical amplitude ratio ( $A^-/A^+$ ) is close to 1.6, critical exponent ( $\alpha'$ ) takes on a value 0.5 and ( $D^-/D^+$ ) is close to unity. Here in this case, the values of the quotients, ( $A^-/A^+$ ) and ( $D^-/D^+$ ) have been appeared to be  $1.630 \pm 0.029$  and  $0.99 \pm 0.04$  respectively for the fit range  $\tau = 5 \times 10^{-3}$ ; both of which are also close to the tricritical values.

Investigation of the critical anomaly associated with the  $N$ -Sm-A phase transition has also been extended to the binary mixtures as well. The temperature-dependent variation of  $Q(T)$  for eight different mixtures including the pure compound PhP2 in the vicinity of  $N$ -Sm-A phase transition are depicted in Fig. 5.7 over the range  $\tau = 5 \times 10^{-3}$ . Corresponding best fitted parameters are listed in Table 5.4. The magnitude of the anomaly in  $Q(T)$  decreases significantly as the  $N$  ranges grows, showing that thermal fluctuations associated with the  $Q(T)$  anomaly are very sensitive to the saturation of nematic order parameter.

The result of fits represents the  $Q(T)$  data quite well, as indicated by the  $\chi_v^2$  values ranging between 1.02 and 1.46. However, the critical region for each mixture at the Sm-A-Sm-C phase transition is quite small compared to that for the  $N$ -Sm-A phase transition. In this study, the values of critical exponent  $\alpha'$  has been found within 0.053 and 0.462, consequently indicating a crossover character for the  $N$ -Sm-A phase transition. Furthermore, the values of the quotients, ( $A^-/A^+$ ) and ( $D^-/D^+$ ) also have been appeared within a range from 1.63

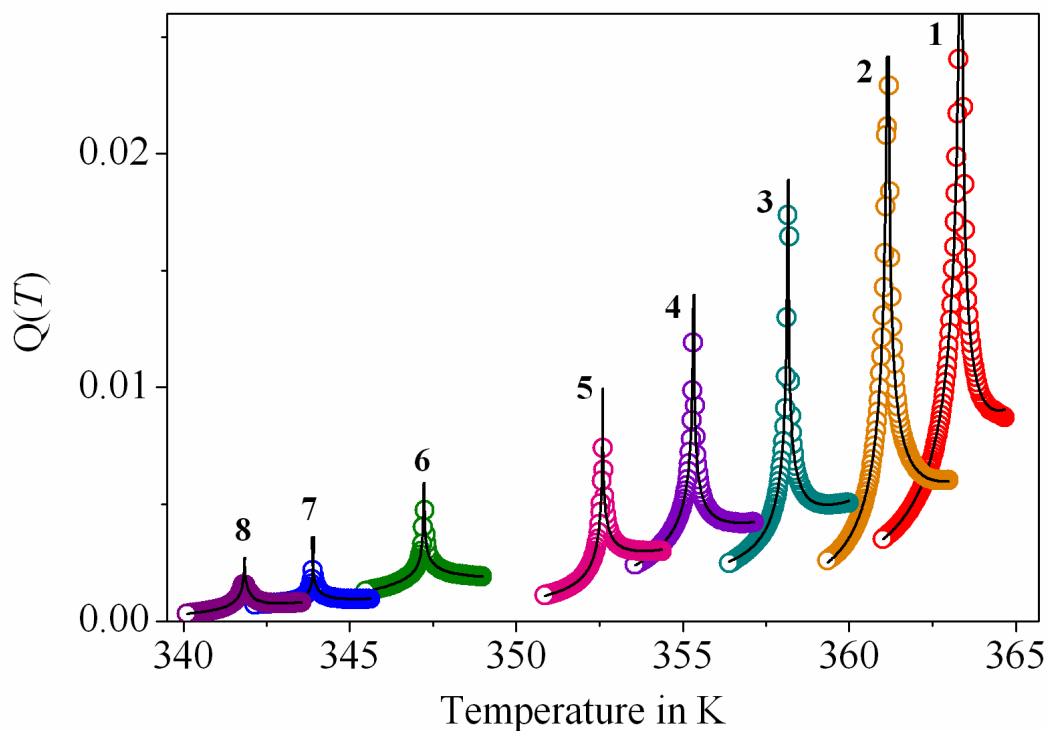


**Figure 5.7.** The temperature dependence of  $Q(T)$  in the vicinity of the  $N$ – $Sm$ – $A$  transition in mixtures of PhP1 and PhP2. 1:  $x_{\text{PhP1}} = 0.0$ ; 2:  $x_{\text{PhP1}} = 0.05$ ; 3:  $x_{\text{PhP1}} = 0.1$ ; 4:  $x_{\text{PhP1}} = 0.15$ ; 5:  $x_{\text{PhP1}} = 0.2$ ; 6:  $x_{\text{PhP1}} = 0.3$ ; 7:  $x_{\text{PhP1}} = 0.35$ ; 8:  $x_{\text{PhP1}} = 0.4$ .

**Table 5.4.** Results corresponding to the best fit for  $Q(T)$  near  $N$ – $Sm$ – $A$  phase transition of all the mixtures obtained in accordance with Eq. (5.2) and related  $\chi_v^2$  values associated with the fits.

$x_{\text{PhP1}}$	$A^-/A^+$	$D^-/D^+$	$\alpha'$	$\chi_v^2$
0	$1.630 \pm 0.029$	$0.99 \pm 0.04$	$0.462 \pm 0.002$	1.29
0.05	$1.521 \pm 0.052$	$0.99 \pm 0.01$	$0.425 \pm 0.007$	1.11
0.1	$1.417 \pm 0.036$	$1.00 \pm 0.01$	$0.387 \pm 0.011$	1.36
0.15	$1.368 \pm 0.107$	$1.00 \pm 0.01$	$0.345 \pm 0.005$	1.02
0.2	$1.450 \pm 0.088$	$1.00 \pm 0.01$	$0.303 \pm 0.004$	1.12
0.3	$1.053 \pm 0.038$	$1.01 \pm 0.01$	$0.188 \pm 0.003$	1.21
0.35	$0.970 \pm 0.017$	$1.00 \pm 0.01$	$0.084 \pm 0.001$	1.18
0.4	$0.983 \pm 0.010$	$1.01 \pm 0.03$	$0.053 \pm 0.001$	1.46

to 0.97 and from 0.99 to 1.01 respectively, which reveals a well consistency with the theoretical values in between 3D-XY and tricritical limit. Moreover, the critical exponent  $\alpha'$  is found to be sensitive to the temperature width of the nematic phase and exhibits a systematic variation depending on it. The variation of the critical exponent  $\alpha'$  values for the present investigated mixtures including that for the pure PhP2 compound against the McMillan ratio ( $R_M = T_{NA}/T_{IN}$ ) is illustrated in Fig. 5.8. Simultaneous comparison has also been displayed by placing the critical exponent values of the same mixture obtained at the Sm-A–Sm-C phase transition. It is quite evident that the theoretical value for tricritical limit is expected for a temperature ratio ( $R_M$ ) of 0.87 in the vicinity of  $N$ –Sm-A phase transition, although experimental observations yields relatively higher values, ranging between 0.942 and 0.994, while for 3D-XY

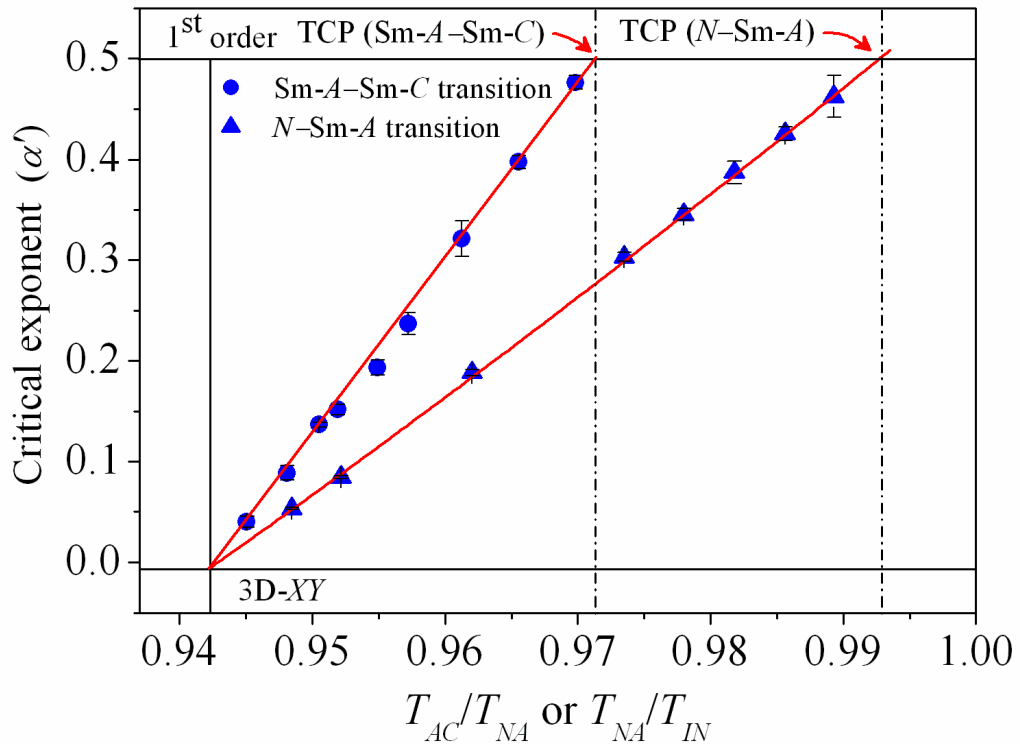


**Figure 5.8.** The variation of effective critical exponent ( $\alpha'$ ) with  $T_{NA}/T_{IN}$  for the  $N$ –Sm-A phase transition and  $T_{AC}/T_{NA}$  for the Sm-A–Sm-C phase transition. The vertical dashed lines and solid line corresponds to the tricritical point (TCP) and 3D-XY limit respectively. The solid lines (red) are linear fit to the data.

limit, it is expected for a value of 0.94. In this binary system, an extrapolation of the linear fit to the extracted  $\alpha'$  values yield a tricritical behavior (*i.e.*,  $\alpha' = 0.5$ ) for the McMillan ratio ( $R_M$ ) of 0.992, which is somewhat greater in comparison to that obtained for a similar temperature ratio  $T_{AC}/T_{NA} = 0.972$  at the Sm-A–Sm-C phase transition. However, the linear fit to the  $\alpha'$  data yields a McMillan ratio ( $T_{NA}/T_{IN}$ ) value of 0.942 corresponding to the 3D-XY point which is found to be very close to the temperature ratio  $T_{AC}/T_{NA}$ , for the Sm-A–Sm-C phase transition. The overall behavior between  $\alpha'$  and McMillan ratio ( $T_{NA}/T_{IN}$ ) from the tricritical point (TCP) towards approaching the 3D-XY value is in good agreement with the previous reports on the *N*–Sm-A phase transitions [37,46-51]. Therefore, the origin of such critical behavior is a unique feature for the both the *N*–Sm-A and the Sm-A–Sm-C phase transitions for all of the compounds and they are seen to follow two distinctly different linear curves as shown in Fig. 5.8.

Based on the obtained results in present binary system confirms that the width of the *N* and Sm-A temperature ranges plays an important role in deciding the nature of both the *N*–Sm-A and the Sm-A–Sm-C phase transitions. For the appearance of a tricritical point of the *N*–Sm-A phase transition, it requires a nematic width around 2.5 K, while for the Sm-A–Sm-C phase transition the same can be obtained for a Sm-A range around 10.5 K. Likewise for the manifestation of 3D-XY limit, it requires a *N* range about 21 K for the *N*–Sm-A phase transition, which is nearly equal to the Sm-A range for the Sm-A–Sm-C phase transition.

## 5.7. Critical behavior at the *I*–*N* phase transition

The high resolution optical birefringence ( $\Delta n$ ) data have also been employed to investigate the critical fluctuation appearing in vicinity of the *I*–*N* phase transition. In the investigated system, recourse of a four parameter power-law model [38,52,53] consistent with the mean-field theory for both critical and tricritical points of weakly first-order transitions as discussed

earlier in chapter 3, has been adopted. According to the model, the temperature dependence of optical birefringence ( $\Delta n$ ) in the nematic phase may be approximated as [38,54],

$$\Delta n = \zeta [S^{**} + (1 - S^{**}) \left| 1 - \frac{T}{T^{**}} \right|^{\beta}] \quad (5.3)$$

without considering any local field influence. Here,  $T^{**}$  is the temperature corresponding to the effective second order transition point and  $\zeta = (\Delta\alpha/\alpha)[(n_i^2 - 1)/2n_i]$ , where  $n_i$  is the refractive index in the isotropic phase (just above  $T_{IN}$ ). Thus at  $T = T^{**}$ ,  $S(T^{**}) = S^{**}$ .  $\beta$  represents the order parameter critical exponent. This method has been appeared to be superior to the earlier attempts to fit the temperature dependence of  $\Delta n$  using Haller's procedure which contains a relatively smaller number of fit parameters [55]. Furthermore, the Haller's method frequently leads to relatively lower values of

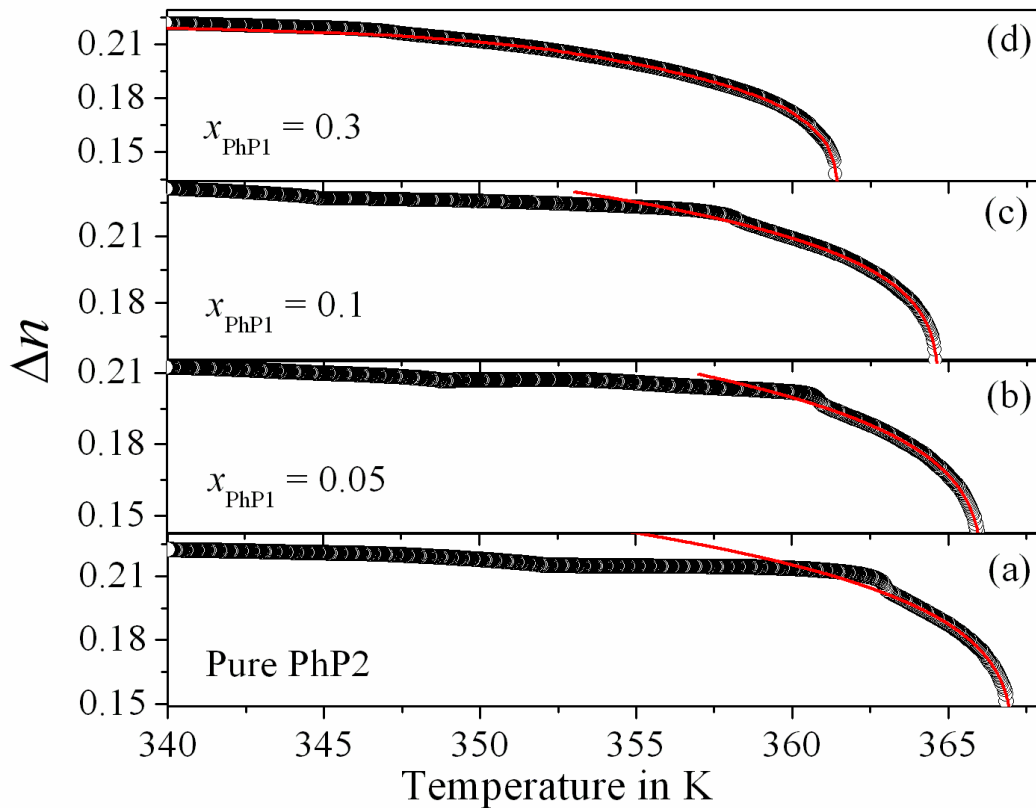


**Figure 5.9.** Experimental values of birefringence ( $\Delta n = n_e - n_o$ ) as a function of temperature for (a) PhP2, (b)  $x_{\text{PhP1}} = 0.05$ , (c)  $x_{\text{PhP1}} = 0.1$  and (d)  $x_{\text{PhP1}} = 0.3$ . Solid lines (Red) represent the fit to Eq. (5.3) and extrapolated to the Sm-A phase.

**Table 5.5.** Values of the fit parameters obtained from the four-parameter fit of the temperature dependence of  $\Delta n$  to Eq. (5.3).

$x_{\text{PhP1}}$	$\zeta$	$S^{**}$	$T^{**}$ in K	$\beta$	$T^{**}-T_{IN}$	$\chi_v^2$
0	0.390±0.071	0.28±0.22	367.07±1.77	0.248±0.208	0.24	1.04
0.05	0.364±0.049	0.29±0.16	366.09±1.37	0.248±0.161	0.35	1.09
0.1	0.368±0.025	0.34±0.08	364.65±0.81	0.249±0.091	0.18	1.13
0.15	0.391±0.142	0.29±0.43	363.66±3.64	0.251±0.428	0.32	1.11
0.2	0.372±0.049	0.27±0.16	362.31±1.34	0.251±0.156	0.22	1.27
0.3	0.349±0.005	0.32±0.02	361.46±0.21	0.251±0.023	0.33	1.01
0.35	0.367±0.007	0.33±0.02	361.21±0.25	0.251±0.027	0.25	1.40
0.4	0.308±0.009	0.42±0.04	361.01±0.51	0.251±0.052	0.21	1.39

$\beta$  with  $\beta \leq 0.2$  and also does not suit for its incompatibility with the weakly first-order nature of the  $I-N$  phase transition [56]. In the temperature dependence of birefringence a clearly distinguishable pretransitional smectic influence has been observed in a region up to few temperatures above the  $N-Sm-A$  phase transition temperature. The fits to Eq. (5.3) with the birefringence data are represented as solid line for four different mixtures in Fig. 5.9(a–d). The best fit values for the quantities  $\Delta n_0$ ,  $S^{**}$ ,  $T^{**}$  and  $\beta$  are listed in Table 5.5 for all of the mixtures including the pure compound PhP2. From an inspection of the extracted data it is obvious that the  $\beta$  value, obtained from the four parameter model expression, is clearly in line with the tricritical hypothesis (TCH) ( $\beta_{\text{TCH}} = 0.25$ ) of Keyes [57] and Anisimov *et al.* [58,59] and thus discard the possibility of other higher theoretical values. Similar outcome has also been reported for a number of compounds with different molecular structures and also for their mixtures obtained from various experimental techniques like the specific heat capacity, birefringence, dielectric and volumetric measurements [37,38,52,53,60-66]. Hence, the present experimental outcomes once more confirm the validity of the tricritical nature for the  $I-N$  phase transition. Furthermore, the temperature difference ( $T^{**}-T_{IN}$ ) for the pure compound PhP2

---

---

as obtained from the extracted  $T^{**}$  value is come out to be 0.24 K, which reveals a good agreement with those reported for distinct smectogenic compounds from high resolution rotating-analyzer technique [38] and refractometer measurements [52]. However, the obtained  $(T^{**}-T_{IN})$  values for the mixtures are found to lie in a range between 0.18 to 0.35, those are comparatively higher than the reported values measured from the specific heat capacity, dielectric and molar volume measurements [61,66]. Recently from the study of the profile of the order parameter  $S(T)$  derived from various anisotropic quantities, Simoes *et al.* showed that all experimental data coalesce along a common line over the entire range of the nematic phase signaling a global universal behavior [67-69]. They also obtained the critical exponent  $\beta = 0.25$  together with the temperature difference  $(T^{**}-T_{IN})$  close to 0.3. Such outcomes relating  $\beta$  and  $(T^{**}-T_{IN})$  is also fairly in agreement with the present observation.

## 5.8. Conclusion

Precise optical birefringence measurement has been undertaken to study the Sm-A–Sm-C, N–Sm-A and I–N phase transitions in a phenyl pyrimidine (seventh homolog) liquid crystal as well as in eight binary mixtures of the same with the second homologous compound (PhP1). The precise  $\Delta n$  data are quite successful in probing the transitional anomaly accompanying all the phase transitions in the investigated system. No visible discontinuity appears in the temperature dependence of  $\Delta n$  at both the N–Sm-A and Sm-A–Sm-C phase transitions. The order character of these smectic transitions has also been explored and compared with the available theoretical models. Divergences in the quotient  $Q(T)$  in the vicinity of phase transitions has been well described in terms of the renormalization-group model. For the Sm-A–Sm-C transition, a weak dependence of critical exponent  $\alpha'$  on fit ranges has been observed for the pure compound. It is quite evident that the transitional behavior of this phase transition is really critical over the reduced temperature range  $3 \times 10^{-3}$ , estimated

in the range about 2 K on both side from the transition. Moreover, the non-universal values have been observed for the critical exponent  $\alpha'$  for both the  $N$ -Sm-A and Sm-A-Sm-C phase transitions and hence indicate a crossover character from second order to the first order transition. The non-universal behavior of this transition with either very weak first-order or second-order transitions with Gaussian tricritical or crossover from 3D-XY critical to tricritical behavior has been clearly explained on the basis of the width of the Sm-A temperature range linked with the Sm-A-Sm-C phase transition, which in effect may close the controversy on the nature of the Sm-A-Sm-C transition. However, mean-field tricritical or mean-field 3D-XY is only an approximation where the true critical region remains inaccessible. Moreover, the origin of such critical behavior is a unique feature for the both the  $N$ -Sm-A and the Sm-A-Sm-C phase transitions for all of the compounds and they are seen to follow two distinctly different linear curves as shown in Fig. 5.8. Furthermore, for the  $I$ - $N$  phase transition, the critical exponent  $\beta$ , characterizing the limiting behavior of the nematic order parameter close to that transition, has come out to be close to 0.25 and hence in agreement with the tricritical hypothesis. The work presented in this chapter can be useful for other temperature-driven phase transitions which include binary alloys, superconductors, ferromagnetic and ferroelectric materials, classical fluids as well as thermal phase transitions in subatomic particles [70]. Moreover, the work can also be extended to encompass all such phase transition phenomena which are not driven by temperature but also by some other parameters such as pressure, composition, or magnetic field, *i.e.*, the so-called quantum phase transitions. Particularly the recently observed phases within strongly correlated materials (*viz.* quantum liquid crystals) exhibiting the same symmetry breaking transitions as in classical liquid crystals which are now being intensively studied [71] and are expected to unveil a wealth of new and absorbing physics in future.

---

---

## References:

- [1] P.G. de Gennes, *Mol. Cryst. Liq. Cryst.*, **21**, 49 (1973).
- [2] C.A. Shantz, and D.L. Johnson, *Phys. Rev. A*, **17**, 1504 (1978).
- [3] C.C. Huang, and J.M. Viner, *Phys. Rev. A*, **25**, 3385 (1982).
- [4] R.J. Birgeneau, C.W. Garland, A.R. Kortan, J.D. Litster, M. Meichle, B.M. Ocko, C. Rosenblatt, L.J. Yu, and J. Goodby, *Phys. Rev. A*, **27**, 1251 (1983).
- [5] M. Meichle, and C.W. Garland, *Phys. Rev. A*, **27**, 2624 (1983).
- [6] S.C. Lien, C.C. Huang, T. Carlsson, I. Dahl, and S.T. Lagerwall, *Mol. Cryst. Liq. Cryst.*, **108**, 149 (1984).
- [7] S. Dumrongrattana, C.C. Huang, G. Nounesis, S.C. Lien, and J.M. Viner, *Phys. Rev. A*, **34**, 5010 (1986).
- [8] P. Das, K. Ema, and C.W. Garland, *Liq. Cryst.*, **4**, 205 (1989).
- [9] H.Y. Liu, C.C. Huang, Ch. Bahr, and G. Heppke, *Phys. Rev. Lett.*, **61**, 345 (1988).
- [10] T. Chan, Ch. Bahr, G. Heppke, and C.W. Garland, *Liq. Cryst.*, **13**, 667 (1993).
- [11] K. Ema, J. Watanabe, A. Takagi, and H. Yao, *Phys. Rev. E*, **52**, 1216 (1995).
- [12] L. Reed, T. Stoebe, and C.C. Huang, *Phys. Rev. E*, **52**, R2157 (1995).
- [13] K. Ema, A. Takagi, and H. Yao, *Phys. Rev. E*, **53**, R3036 (1996).
- [14] K. Ema, M. Ogawa, A. Takagi, and H. Yao, *Phys. Rev. E*, **54**, R25 (1996).
- [15] K. Ema, H. Yao, A. Fukuda, Y. Takanishi, and H. Takezoe, *Phys. Rev. E*, **54**, 4450 (1996).
- [16] K. Ema, and H. Yao, *Phys. Rev. E*, **57**, 6677 (1998).
- [17] D. Collin, J.L. Gallani, and P. Martinoty, *Phys. Rev. Lett.*, **61**, 102 (1988).
- [18] D. Collin, S. Moyses, M.E. Neubert, and P. Martinoty, *Phys. Rev. Lett.*, **73**, 983 (1994).

- 
- 
- [19] M. Škarabot, K. Kočevar, R. Blinc, G. Heppke, and I. Muševič, *Phys. Rev. E*, **59**, R1323 (1999).
- [20] J. Fernsler, D. Wicks, D. Staines, A. Havens, and N. Paszek, *Liq. Cryst.*, **39**, 1204 (2012).
- [21] C.R. Safinya, M. Kaplan, J. Als-Nielsen, R.J. Birgeneau, D. Davidov, J.D. Litster, D.L. Johnson, and M.E. Neubert, *Phys. Rev. B*, **21**, 4149 (1980).
- [22] L. Benguigui, and P. Martinoty, *Phys. Rev. Lett.*, **63**, 774 (1989); *J. Phys. II France*, **7**, 225 (1997).
- [23] A. Altland, and B. Simons, in *Condensed Matter Field Theory*, Cambridge University Press, Cambridge (2010).
- [24] C.C. Huang, and S.C. Lien, *Phys. Rev. A*, **31**, 2621 (1985).
- [25] S.K. Prasad, V.N. Raja, D.S. Rao, G.G. Nair, and M.E. Neubert, *Phys. Rev. A*, **42**, 2479 (1990).
- [26] K.J. Stine, and C.W. Garland, *Phys. Rev. A*, **39**, 3148 (1989).
- [27] A. Chakraborty, S. Chakraborty, and M.K. Das, *Phys. Rev. E*, **1**, 032503 (2015).
- [28] L. Reed, T. Stoebe, and C.C. Huang, *Phys. Rev. E*, **52**, R2157 (1995); G.S. Iannacchione, C.W. Garland, P.M. Johnson, and C.C. Huang, *Liq. Cryst.*, **26**, 51 (1999).
- [29] Y. Galerne, *Phys. Rev. A*, **24**, 2284 (1981).
- [30] K. Ema, and H. Yao, *Phys. Rev. E*, **57**, 6677 (1998), and reference therein.
- [31] A. Chakraborty, S. Chakraborty, and M.K. Das, *Physica B*, **479**, 90 (2015).
- [32] M.K. Das, S. Chakraborty, R. Dabrowski, and M. Czerwinski, *Phys. Rev. E*, **95**, 012705 (2017).
- [33] A. Saipa, and F. Giesselmann, *Liq. Cryst.*, **29**, 347 (2002).
- [34] G. Sarkar, M.K. Das, R. Paul, B. Das, and W. Weissflog, *Phase Transit.*, **82**, 433 (2009).
- [35] T. Scharf, in *Polarized Light in Liquid Crystals and Polymers*, Wiley, Hoboken, NJ (2007).
- 
-

- 
- 
- [36] A. Prasad, and M.K. Das, *J. Phys.: Condens. Matter*, **22**, 195106 (2010).
- [37] A. Chakraborty, S. Chakraborty, and M.K. Das, *Phys. Rev. E*, **91**, 032503 (2015).
- [38] S. Erkan, M. Çetinkaya, S. Yildiz, and H. Özbek, *Phys. Rev. E*, **86**, 041705 (2012); and references therein.
- [39] H.E. Stanley, in *Introduction to Phase Transitions and Critical Phenomena*, Clarendon, Oxford (1971).
- [40] R. Brout, in *Phase Transitions*, Benjamin, New York, (1965).
- [41] M.C. Cetinkaya, S. Yildiz, H. Ozbek, P. Losada-Perez, J. Leys, and J. Thoen, *Phys. Rev. E*, **88**, 042502 (2013).
- [42] P.R. Bevington, and D.K. Robinson, in *Data Reduction and Error Analysis for the Physical Sciences (3rd ed.)*, McGraw-Hill, New York (2003).
- [43] K. Ema, H. Yao, T. Matsumoto, and A. Fukuda, *Mol. Cryst. Liq. Cryst.*, **364**, 335 (2001).
- [44] M. E. Fisher, *Phys. Rev.*, **176**, 257 (1968).
- [45] J.A. Potton, and P.C. Lanchester, *Phase Transit.*, **6**, 43 (1985).
- [46] S.K. Sarkar, and M.K. Das, *J. Mol. Liq.*, **199**, 415 (2014).
- [47] S.K. Sarkar, A. Chakraborty, and M.K. Das, *Liq. Cryst.*, **43**, 22 (2016).
- [48] S. Chakraborty, A. Chakraborty, and M.K. Das, *J. Mol. Liq.*, **219**, 608 (2016).
- [49] G. Cordoyiannis, C.S.P. Tripathi, C. Glorieux, and J. Thoen, *Phys. Rev. E*, **82**, 031707 (2010).
- [50] C.W. Garland, and G. Nounesis, *Phys. Rev. E*, **49**, 2964 (1994).
- [51] Y. Sasaki, K. Ema, K.V. Le, H. Takezoe, S. Dhara, and B.K. Sadashiva, *Phys. Rev. E*, **83**, 061701 (2011).
- [52] I. Chirtoc, M. Chirtoc, C. Glorieux, and J. Thoen, *Liq. Cryst.*, **31**, 229 (2004).
- [53] S. Yildiz, H. Özbek, C. Glorieux, and J. Thoen, *Liq. Cryst.*, **34**, 611 (2007).
- 
-

- 
- 
- [54] H. Ozbek, S. Ustunel, E. Kutlu, and M.C. Cetinkaya, *J. Mol. Liq.*, **199**, 275 (2014).
- [55] I. Haller, *Progr. Solid State Chem.*, **10**, 103 (1975).
- [56] J. Thoen, and G. Menu, *Mol. Cryst. Liq. Cryst.*, **97**, 163 (1983).
- [57] P.H. Keyes, *Phys. Lett. A*, **67**, 132 (1978).
- [58] M.A. Anisimov, S.R. Garber, V.S. Esipov, V.M. Mamnitskii, G.I. Ovodov, L.A. Smolenko, and E.L. Sorkin, *Sov. Phys. JETP*, **45**, 1042 (1977).
- [59] M.A. Anisimov, *Mol. Cryst. Liq. Cryst.*, **162A**, 1 (1988).
- [60] S.K. Sarkar, P.C. Barman, and M.K. Das, *Physica B*, **446**, 80 (2014).
- [61] P. Cusmin, M.R. de la Fuente, J. Salud, M.A. Pérez-Jubindo, S. Diez-Berart, and D.O. López, *J. Phys. Chem. B*, **111**, 8974 (2007).
- [62] J. Salud, P. Cusmin, M.R. de la Fuente, M.A. Pérez-Jubindo, D.O. López, and S. Diez-Berart, *J. Phys. Chem. B*, **113**, 15967 (2009).
- [63] A. Drozd-Rzoska, S.J. Rzoska, and J. Ziolo, *Phys. Rev. E.*, **54**, 6452 (1996).
- [64] S.J. Rzoska, J. Ziolo, W. Sulkowski, J. Jadzyn, and G. Czechowski, *Phys. Rev. E.*, **64**, 052701 (2001).
- [65] A. Prasad, and M.K. Das, *Phys. Scr.*, **84**, 015603 (2011).
- [66] A. Żywociński, *J. Phys. Chem. B.*, **107**, 9491 (2003).
- [67] M. Simões, and D.S. Simeão, *Phys. Rev. E.*, **74**, 051701 (2006).
- [68] M. Simões, D.S. Simeão, and K.E. Yamaguti, *Liq. Cryst.*, **38**, 935 (2011).
- [69] M. Simões, D.S. Simeão, and S.M. Domiciano, *Mol. Cryst. Liq. Cryst.*, **576**, 76 (2013).
- [70] Y. Hidaka, and S. Kai, *Forum Forma*, **24**, 123 (2009).
- [71] P. Romanczuk, H. Chaté, L. Chen, S. Ngo, and J. Toner, *New J. Phys.*, **18**, 063015 (2016).
- 
-

# CHAPTER 6

---

Evidence of broad tricritical range for the  
smectic-*A* to smectic-*C* phase transition

---

---

## 6.1. Introduction

Liquid crystals formed by bent-shaped molecules have been a subject of intense experimental and theoretical investigations due to their unique properties and potential applications in the field of fast switching displays [1-5]. In spite of usual bent-shaped molecules, delicate modifications in molecular structure may yield calamitic like polymorphisms involving smectic-*C* (Sm-*C*), smectic-*A* (Sm-*A*) and even nematic (*N*) phases [6-10]. However, the interest on molecular behavior and appearance of different exceptional mesophases in pure bent-core liquid crystals, binary mixtures composed of bent-shaped and rod-like molecules have shown various interesting phenomena [11–13] and novel phase transitions [3,14], which brought them at the center of scientific interest and stimulates considerable research efforts regarding formulation and characterization of noble liquid crystalline mixtures. The effect of mixing on the mesophase sequence and transitional behavior in such doped system is of unparalleled advantage for obtaining a deeper understanding of the unresolved issues regarding transitional phenomena in soft matter systems.

Over the past few decades, the nature of the smectic-*A*–smectic-*C* (Sm-*A*–Sm-*C*) transition has been a topic of great interest in an effort to determine the order of the transition and the universality class to which it belongs [15-29]. Despite considerable progress, the critical characteristics and universality class of the Sm-*A*–Sm-*C* phase transition remains only partially unveiled and till now has been treated as a controversial issue in the field of equilibrium statistical mechanics of soft condensed matter [17,22-29].

In the previous chapter (chapter 5), a high-resolution temperature scanning technique was successfully used in determining the optical birefringence ( $\Delta n$ ) precisely throughout the mesomorphic range and discusses the possibility of crossover behavior from tricritical to 3D-*XY* critical nature near the Sm-*A*–Sm-*C* transition in a binary system belonging to the same homologous series of phenyl pyrimidine compounds [30,31]. It has been shown

---

---

---

---

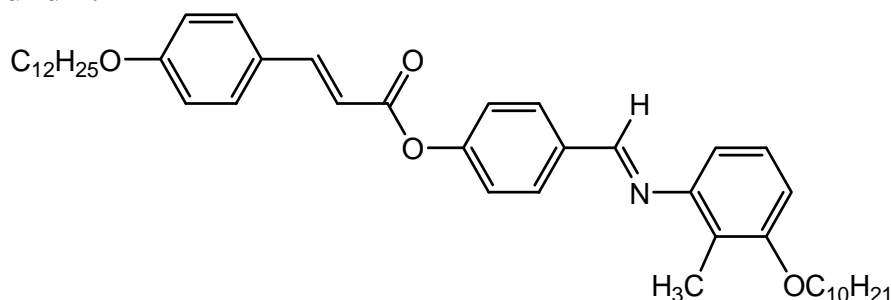
that the character of the Sm-A–Sm-C transition is really critical over the reduced temperature range  $3 \times 10^{-3}$ , estimated in the range of 2 K from the transition. The non-universal behavior of this transition with either very weak first-order or second-order transitions was explained on the basis of the Sm-A temperature range linked with the Sm-A–Sm-C phase transition. It should be noted that, these binary mixtures of rod-like compounds was found to demonstrate a variation of the Sm-A phase range from 11 K to 19 K. However, the extrapolation of the linear fit yields a crossover from second order to first order nature at the Sm-A range  $\sim 10.5$  K. Therefore, it is of great interest to investigate how does further reduction of the Sm-A range influences the transitional behavior of the Sm-A–Sm-C phase transition. On the other hand, it is also interesting to characterize the critical fluctuations near the Sm-A–Sm-C transition for the mixtures of compounds having complex and varied molecular structure rather than the mixtures of homologous compounds.

The present chapter is mainly dedicated to focus on an extensive optical investigation in a binary system comprising of a laterally methyl substituted hockey stick-shaped compound (H-22.5) and a calamitic compound (7OCB). The temperature-dependent optical birefringence ( $\Delta n$ ) value has been measured from the high-resolution temperature scanning technique and hence employed to take a deeper insight into the critical behavior associated with the Sm-A–Sm-C phase transition. The values of the effective critical exponent  $\alpha'$  have been explored with the variation of Sm-A temperature range and the observed outcomes are discussed in light of the crossover behavior. However, an attempt has also been made to test the plausibility of tricriticality nature of the Sm-A–Sm-C phase transition by modifying the renormalization group expression with additional correction terms. Interestingly, in spite of the steep phase boundary, no sign of the Fisher renormalization of the critical exponent has been found, even for the tricritical mixtures.

## 6.2. Materials

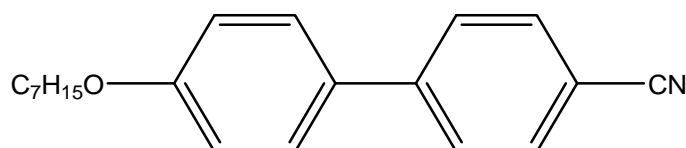
The hockey stick-shaped compound, 4-(3-n-decyloxy-2-methylphenyliminomethyl) phenyl 4-n-dodecyloxy cinnamate (H-22.5) was obtained from the Institute of Physical Chemistry, Martin Luther University, Halle, Germany and the compound 4-cyano-4'-heptyloxybiphenyl (7OCB) was purchased from E. Merck, UK (having a purity higher than 99.9%) and were used to prepare the mixtures without further purification. The structural formulae and transition scheme for both the pure compounds are given in Fig. 6.1.

### Compound 1:



**Cr** (347.2 K) **Sm-C<sub>a</sub>** (374.4 K) **Sm-C<sub>s</sub>** (382.8 K) **N** (383.1 K) **I**

### Compound 2:



**Cr** (327 K) **N** (347 K) **I**

**Figure. 6.1.** Chemical structure and phase behavior of the hockey-stick-shaped compound (Compound 1: H-22.5) and the rod-like compound (Compound 2: 7OCB).

Nine different mixtures with molar concentrations of  $x_{7OCB} = 0.211, 0.2, 0.184, 0.174, 0.167, 0.158, 0.15, 0.1$  and  $0.05$  have been prepared by adding small amounts of the rod-like compound (7OCB) into the host hockey stick-shaped mesogen. The phase transition temperatures were determined from polarizing optical microscopy and optical transmission technique.

---

---

### 6.3. Texture observation

The optical textures of different mesophases of the studied mixtures were observed under a polarizing optical microscope (BANBROS) equipped with INSTEC HCS302 hot stage, controlled by INSTEC mK1000 thermo system. Three distinct mesophases have been detected by polarized light optical microscopy for all of the investigated mixtures, out of them optical textures for the mixture  $x_{7\text{OCB}} = 0.184$  is presented in Fig. 6.2. The high-temperature mesophase behaves like the conventional Sm-A phase, characterized by a typical fan-shaped texture in planar alignment cell (Fig. 6.2(a)). The homeotropically aligned areas are found optically isotropic and appears completely dark between the crossed polarizers (Fig. 6.2(d)). Such an appearance indicates the presence of the Sm-A phase. On further cooling in planar oriented samples, a broken fan-like texture emerges with a significant change in the birefringence near the phase transition (Fig. 6.2(b)). However, the color change from green to yellow indicates an increase in the effective birefringence of the sample. On the other hand, the appearance of schlieren texture has also been seen in homeotropic alignment which indicates a transition to a new optically biaxial mesophase (Fig. 6.2(e)). These textural features are in general a gesture for Sm- $C_s$  phases [6] where the direction of the molecular tilt is the same in adjacent smectic layers. Similar types of textures were often observed experimentally in pure hockey stick-shaped compounds [6,8]. The transition to the third lower temperature mesophase has been ascertained by a clear change in the optical textures. On cooling the sample, the broken fan-shaped texture of the Sm- $C_s$  phase modified with irregular stripes [Fig. 6.2(c)], arises sharply across the fans and this optical feature sustains further to some definite range of temperature below the transition. This is the indication of the transition to an anticlinic Sm-C phase, namely Sm- $C_a$  phase in which the direction of the molecular tilt alternates between the smectic layers [6,8]. Fig. 6.2(b) displayed the growth of irregular stripes over the texture of

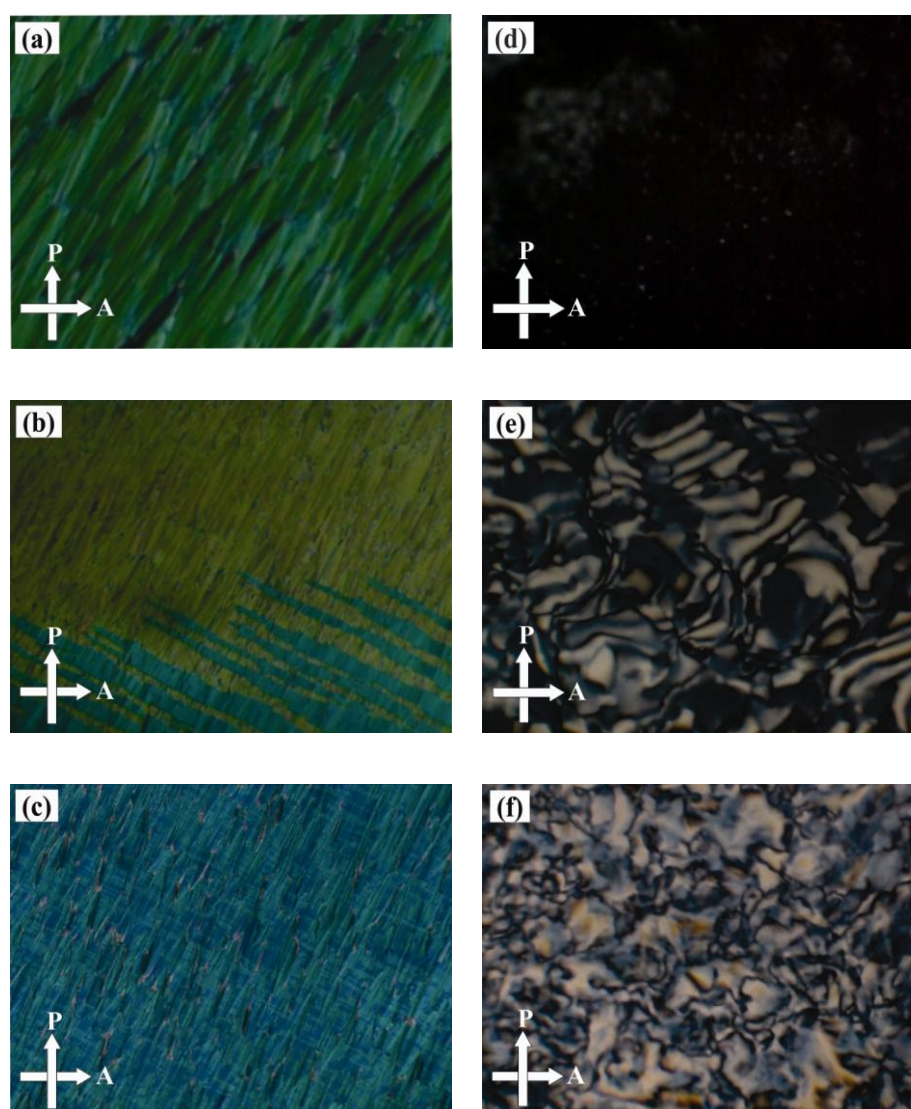


**Figure 6.2.** Optical texture observed for a mixture with mol fraction  $x_{7\text{OCB}} = 0.184$  in homogeneous alignment (a-c) and homeotropic alignment (d-f). (a) Sm-A phase at 380 K, (b) Sm- $C_s$  phase at 369 K, (c) Sm- $C_a$  phase at 360 K, (d) Sm-A phase at 378 K, (e) Sm- $C_s$  phase at 371 K, (f) Sm- $C_a$  phase at 365 K. Arrows indicates the direction of the polarizers.

the Sm- $C_s$  phase. Again in homeotropic alignment the Sm- $C_a$  phase exhibits the schlieren texture which strongly differs from that of the Sm- $C_s$  phase. This type of schlieren texture is accompanied by some disclination points with two brushes ( $S = 1/2$ ) in addition to four brushes ( $S = 1$ ). Therefore, it indicates a Sm- $C$  like organization in which the layer planes are tilted with respect to the molecules and it confirms its anticlinic structure [6]. Moreover, the Schlieren

---

---

texture strongly fluctuates near the  $\text{Sm-C}_s\text{-Sm-C}_a$  transition which is a characteristic behavior at the synclinic–anticlinic transitions. The reason for such typical change in texture is due to the fact that the reorientation of the molecular tilt proceeds step by step in every second layer [32]. Interestingly, the birefringence value decreases at that transition which is also verified by the textural color change from yellow to blue in accordance with Michel Levy interference color chart [33].

## 6.4. Phase diagram

In this work, a rod-like compound (7OCB) was used as a dopant in the host hockey-stick-shaped compound (H-22.5). Particular focus has been taken in the region where the concentration of 7OCB is less compared to the host mesogen. Several mixtures were prepared by adding small amounts of the calamitic compound (having molar concentrations ranging between 0.05 and 0.211) into the hockey stick-shaped molecule H-22.5.

The partial phase diagram of the binary system consisting of 7OCB and H-22.5 for nine different mixtures is depicted in Fig. 6.3 which includes the  $I\text{-Sm-A}$ ,  $\text{Sm-A-Sm-C}_s$  and  $\text{Sm-C}_s\text{-Sm-C}_a$  transitions as obtained from polarizing optical microscopy. The pure calamitic compound shows a stable  $I\text{-N-Cr}$  phase sequence as being cooled from the isotropic state. Conversely, the pure hockey stick-shaped compound comprises of a nematic phase, appearing in a quite small temperature range ( $\sim 0.3$  K) and two polymorphic tilted smectic phases, the synclinic smectic- $C$  ( $\text{Sm-C}_s$ ) as well as the anticlinic smectic- $C$  ( $\text{Sm-C}_a$ ) phases. In the  $\text{Sm-C}_s$  phase, the direction of the molecular tilt is the same in adjacent smectic layers, whereas it alternates between the layers of the  $\text{Sm-C}_a$  phase [6,8].

The addition of calamitic molecules imparts a dramatic influence on the phase behavior of the mixtures involving angular mesogenic host. Although, the hockey stick-shaped host H-22.5 possesses a small nematic temperature

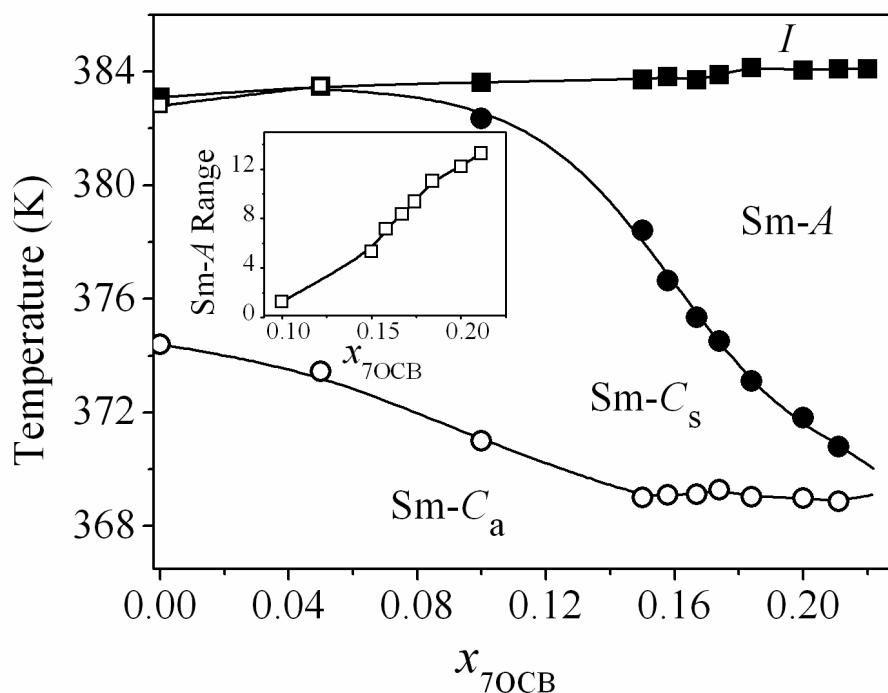


**Figure 6.3.** Partial phase diagram of the binary system comprising of 7OCB and H-22.5.  $x_{7OCB}$  denotes the mole fraction of 7OCB. *I* – isotropic phase, Sm-A – smectic-A phase, Sm- $C_s$  – smectic- $C_s$  phase, Sm- $C_a$  – smectic- $C_a$  phase □: *N*–Sm- $C_s$  phase transition; ■: *I*–Sm-A phase transition; ●: Sm-A–Sm- $C_s$  phase transition; ○: Sm- $C_s$ –Sm- $C_a$  phase transition temperatures. The inset shows the concentration dependence of the Sm-A range for the present system. Solid lines are drawn for guidance to the eye.

range, introduction of a small quantity of the nematogenic rod-like compound initially decreases the width of the nematic phase. Further increasing the quantity of the rod-like mesogenic molecules leads to completely destabilization of the nematic phase of the host compound and gives rise to an induction of Sm-A phase in certain molar concentration range of the binary system. Therefore, the presence of hockey-stick-shaped molecule plays a decisive role for induction of Sm-A phase of the studied mixtures at the Sm-A–Sm- $C$  transition. Moreover, the Sm-A width increases further with the increase in the molar concentration of 7OCB, resulting a sharp reduction of Sm- $C_s$  phase range of the bent mesogenic compound. This may be due to the fact that the addition of 7OCB in the angular mesogenic medium (H-22.5) weakens the coupling between the smectic-A ( $\Psi$ ) and smectic- $C$  ( $\theta$ ) order parameters and

---

---

corresponding sharp enhancement of the Sm-A width finally eliminates both the Sm-C<sub>s</sub> and Sm-C<sub>a</sub> phases. In the present binary system, both the Sm-C<sub>s</sub> and Sm-C<sub>a</sub> phases are found to disappear for the mixtures having molar concentration  $x_{7\text{OCB}} > 0.211$  and only the Sm-A phase predominantly appears in the phase diagram. The variation of the Sm-A phase range against the molar concentrations has also been presented in the inset of Fig. 6.3. However, an augmentation of the Sm-A temperature range has been observed from a value 1.2 K to 13.5 K.

## 6.5. Optical birefringence measurements

The optical birefringence ( $\Delta n$ ) measurement was carried out by high-resolution optical transmission [34-37] as well as thin prism techniques [38] for all of the binary mixtures. Fig. 6.4(a-b) illustrates the temperature dependence of optical birefringence data for the two representative mixtures  $x_{7\text{OCB}} = 0.184$  and 0.167 obtained from both the methods, measured at a wavelength of  $\lambda = 532$  nm. Such a dual measuring process enables one to get a rather precise description of  $\Delta n$  within the mesophases. As expected, upon cooling from the isotropic phase, a significant increase of the birefringence (obtained from both the measurement techniques) has been observed within the Sm-A phase. This is due to the rapid increase of short-range positional ordering via a significant growth of the cybotactic clusters from the disordered fluid state and their alignment by strong surface anchoring, which in turn facilitates in the rapid growth of the optical anisotropy of the media. On further cooling, well within the Sm-A phase, the  $\Delta n$  value increases and attains a maximum saturation value. All the studied mixtures follow the almost identical pattern. Such a change is in effect due to the enhancement of molecular ordering to a certain level in the mesogenic medium. Moreover, on entering the low-temperature Sm-C<sub>s</sub> phase, a further sharp augmentation in birefringence value has also been observed at the Sm-A–Sm-C<sub>s</sub> phase transition, which again is caused due to enhancement of the positional ordering in the tilted phase. This can be

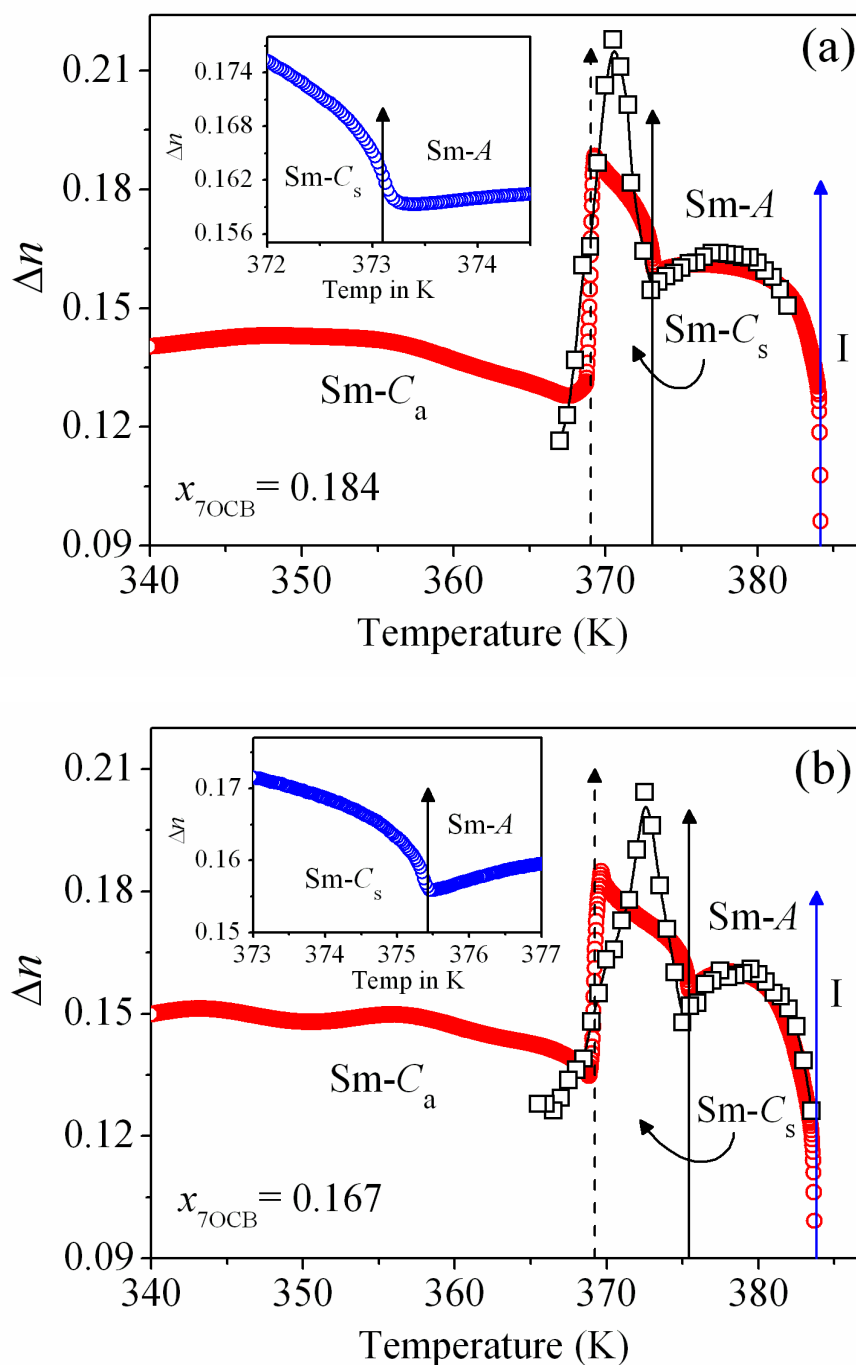


**Figure 6.4.** Temperature dependence of birefringence ( $\Delta n$ ) data for (a)  $x_{7OCB} = 0.184$  and (b)  $x_{7OCB} = 0.167$ .  $\circ$ : Birefringence data from optical transmission method,  $\square$ : Birefringence data from thin prism technique. Blue solid arrows indicate isotropic to smectic-A ( $I$ - $Sm-A$ ) phase transition temperatures ( $T_{IA}$ ), black solid arrows indicate the smectic-A to smectic-C ( $Sm-A$ - $Sm-C_s$ ) phase transition temperatures ( $T_{AC}$ ) and dashed arrows indicate the smectic- $C_s$  to smectic- $C_a$  phase transition temperatures ( $T_{CC}$ ). Insets show the variation of birefringence in the vicinity of  $Sm-A$ - $Sm-C_s$  transition temperature ( $T_{AC}$ ).

---

---

explained due to the fact that the molecular long axes in the Sm- $C_s$  phase of the surface aligned planar cell (of thickness 7.7  $\mu\text{m}$  bulk sample) are oriented parallel to the aligning surface and the layers are tilted with respect to the surface alignment [6]. However, the temperature variation of  $\Delta n$  in the Sm- $C_s$  phase is quite rapid with respect to that in the Sm-A phase. Again the birefringence value sharply decreases at the Sm- $C_s$ –Sm- $C_a$  phase transition and remains more or less constant throughout the Sm- $C_a$  phase for all the mixtures under study. Since the transition to the Sm- $C_a$  phase leads to an effective reorientation of the molecules to form an anticlinic arrangement, the molecules in this phase are now tilted with respect to the surface, causes a drop in the parallel component of the polarizability, *i.e.*, along the molecular long axis, thereby reducing the polarizability anisotropy and hence the birefringence of the material. Such a lowering of birefringence has also been observed from the color change of the optical texture during the phase transition. It is evident that the sharp change of the optical birefringence at the Sm- $C_s$ –Sm- $C_a$  phase transition clearly indicates a first order nature of that transition. The overall profile of the birefringence data is in close agreement with the findings for the pure hockey stick-shaped compounds as well as their multi-component mixtures [6,39] and also for few other bent-shaped mesogens [40]. A quite fair conformity between the values of  $\Delta n$  obtained from both the methods has been found within the temperature range of the Sm-A phase, but they differ in the lower temperature Sm-C phases due to the weak surface anchoring effect of the bulk sample within the prism. However, both the sets of data clearly exhibit a significant enhancement in the vicinity of Sm-A–Sm- $C_s$  phase transition along with a sharp decrease at the Sm- $C_s$ –Sm- $C_a$  phase transition.

## 6.6. Critical behavior at the Sm-A–Sm-C phase transition

The high-resolution optical birefringence data has been used to obtain an insight into the critical behavior at the Sm-A–Sm- $C_s$  phase transition. Following

the same procedure as discussed in chapter 5, the present system is also deals with the critical fluctuation in the vicinity of the transition point by investigating the precise  $\Delta n$  data. As the optical birefringence data exhibit no significant discontinuity at the Sm-A–Sm-C phase transition, a differential quotient  $Q(T)$  has been introduced with the following form [41,42]

$$Q(T) = -\frac{\Delta n(T) - \Delta n(T_{AC})}{T - T_{AC}} \quad (6.1)$$

where  $\Delta n(T_{AC})$  is the birefringence value at the Sm-A–Sm-C transition temperature ( $T_{AC}$ ) and this temperature was obtained by locating the minimum value of temperature derivative of  $\Delta n$  at that transition. The temperature-dependent variation of  $Q(T)$  for all of the mixtures is represented in Fig. 6.5. All of the  $Q(T)$  data exhibit a noticeable divergent character on both sides of the transition temperature and demonstrate an asymmetry between the  $Q(T)$  wings in the Sm-A and Sm-C phases. Moreover, the peak height of  $Q(T)$  monotonically decreases as the concentration of rod-like compound increases. In an attempt to describe the limiting behavior of the quotient  $Q(T)$  at that transition, the following renormalization group expression including the first order corrections-to-scaling term has been used to fit the experimental data [42,43].

$$Q(T) = \frac{A^\pm}{\alpha'} |\tau|^{-\alpha'} (1 + D^\pm |\tau|^\Delta) + E(T - T_{AC}) + B^\pm \quad (6.2)$$

where  $\tau = (T - T_{AC})/T_{AC}$ ,  $\pm$  denote terms above and below  $T_{AC}$ ,  $A^\pm$  denotes the critical amplitudes,  $D^\pm$  are the coefficients of the first corrections-to-scaling terms,  $\alpha'$  is the critical exponent similar to specific heat capacity critical exponent  $\alpha$ ,  $\Delta$  is the first corrections-to-scaling exponent and  $B^\pm$  presents the constant combined critical and regular background term while  $E(T - T_{AC})$  corresponds to a temperature-dependent part of the regular background contribution. Moreover, the value of  $\Delta$  is kept fixed at a value 0.5 without any further variation. The values of the parameters as extracted from the fit process are tabulated in Table 6.1, while the corresponding fits are presented as solid

lines in Fig. 6.5 at a reduced temperature range  $|\tau|_{\max} = 4 \times 10^{-3}$ . In the region above and below the Sm-A–Sm- $C_s$  transition, fits have also been carried out for two other reduced temperature ranges of  $|\tau|_{\max} = 2 \times 10^{-3}$  and  $6 \times 10^{-3}$ . Corresponding best-fit parameter values are also summarized in the Table 6.1.

It is quite evident that the temperature dependence of  $Q(T)$  for all the binary mixtures close to  $T_{AC}$  have been well described by Eq. (6.2), suggesting a good agreement between the experimental optical birefringence data and the theoretical power-law behavior considered here. The quality of the fits have been tested with the aid of the reduced error function  $\chi_v^2$  [44,45], ranging between 1.01 to 1.44 which represents a good fit to the model expression

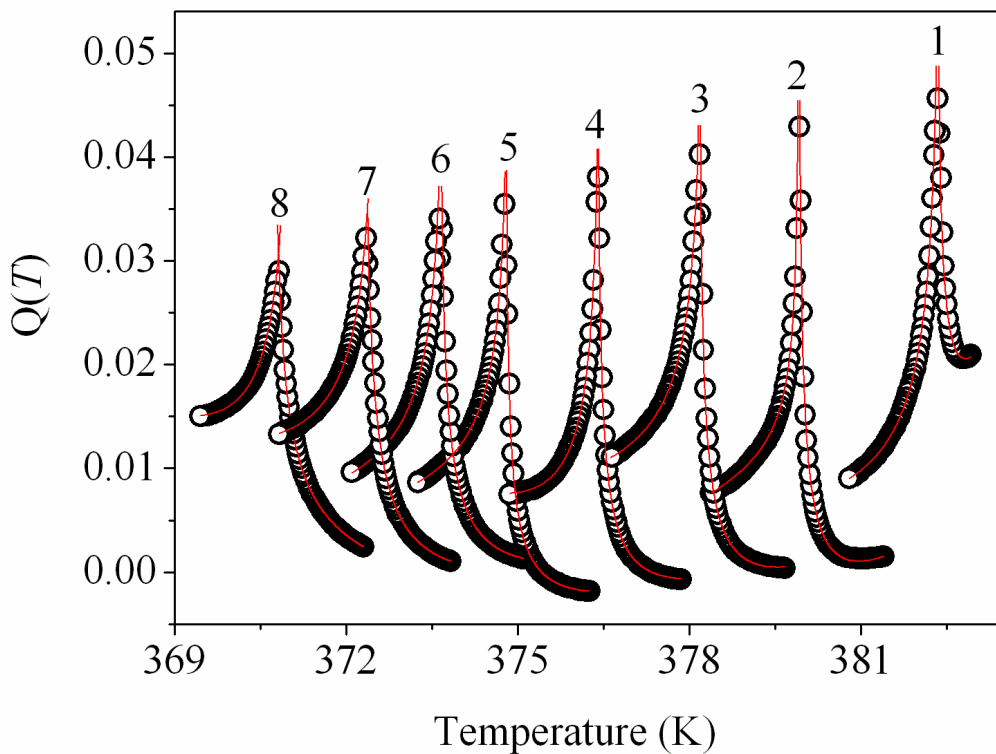


**Figure 6.5.** The temperature dependence of  $Q(T)$  in the vicinity of Sm-A–Sm- $C_s$  transition in mixtures of H-22.5 and 7OCB for  $|\tau|_{\max} = 4 \times 10^{-3}$ . 8:  $x_{7OCB} = 0.211$ ; 7:  $x_{7OCB} = 0.2$ ; 6:  $x_{7OCB} = 0.184$ ; 5:  $x_{7OCB} = 0.174$ ; 4:  $x_{7OCB} = 0.167$ ; 3:  $x_{7OCB} = 0.158$ ; 2:  $x_{7OCB} = 0.15$ ; 1:  $x_{7OCB} = 0.1$ . All of these  $Q(T)$  data have been shifted in temperature axis for the guidance of eye as follows: curve 7 by +0.5 K, curve 6 by +0.5 K, curve 4 by +1 K, curve 3 by +1.5 K, curve 2 by +1.5 K. Solid lines representing the fits to Eq. (6.2).

**Table 6.1.** Results corresponding to the best fit for  $Q(T)$  near Sm-A–Sm-C phase transition obtained in accordance with Eq. (6.2) and related  $\chi^2_{\nu}$  values associated with the fits.  $|\tau|_{\max}$  presents the upper limit of reduced temperature considered for these fits.

$x_{7\text{OCB}}$	$ \tau _{\max}$	$\alpha'$	$A^-/A^+$	$D^-/D^+$	$\chi^2_{\nu}$
0.211	0.006	$0.399 \pm 0.013$	$1.292 \pm 0.012$	$1.001 \pm 0.020$	1.35
	0.004	$0.394 \pm 0.006$	$1.292 \pm 0.041$	$0.999 \pm 0.054$	1.13
	0.002	$0.399 \pm 0.013$	$1.428 \pm 0.634$	$1.010 \pm 0.445$	1.12
0.200	0.006	$0.437 \pm 0.013$	$1.328 \pm 0.027$	$1.000 \pm 0.082$	1.13
	0.004	$0.437 \pm 0.009$	$1.328 \pm 0.062$	$1.000 \pm 0.042$	1.16
	0.002	$0.443 \pm 0.019$	$1.327 \pm 0.591$	$0.999 \pm 0.399$	1.15
0.184	0.006	$0.487 \pm 0.004$	$1.379 \pm 0.084$	$1.002 \pm 0.050$	1.08
	0.004	$0.488 \pm 0.007$	$1.379 \pm 0.101$	$1.004 \pm 0.075$	1.38
	0.002	$0.483 \pm 0.025$	$1.250 \pm 0.431$	$1.004 \pm 0.302$	1.29
0.174	0.006	$0.501 \pm 0.010$	$1.579 \pm 0.098$	$0.994 \pm 0.050$	1.06
	0.004	$0.501 \pm 0.006$	$1.579 \pm 0.071$	$1.009 \pm 0.084$	1.03
	0.002	$0.501 \pm 0.008$	$1.500 \pm 0.213$	$0.984 \pm 0.111$	1.13
0.167	0.006	$0.501 \pm 0.003$	$1.522 \pm 0.069$	$1.001 \pm 0.040$	1.21
	0.004	$0.499 \pm 0.011$	$1.591 \pm 0.068$	$0.995 \pm 0.039$	1.44
	0.002	$0.504 \pm 0.018$	$1.579 \pm 0.492$	$0.984 \pm 0.222$	1.23
0.158	0.006	$0.502 \pm 0.004$	$1.440 \pm 0.070$	$0.999 \pm 0.058$	1.17
	0.004	$0.501 \pm 0.006$	$1.440 \pm 0.081$	$0.999 \pm 0.074$	1.10
	0.002	$0.498 \pm 0.022$	$1.591 \pm 0.555$	$0.998 \pm 0.281$	1.18
0.15	0.006	$0.500 \pm 0.007$	$1.583 \pm 0.086$	$1.007 \pm 0.037$	1.42
	0.004	$0.499 \pm 0.018$	$1.577 \pm 0.046$	$1.012 \pm 0.023$	1.37
	0.002	$0.503 \pm 0.029$	$1.650 \pm 0.757$	$1.011 \pm 0.157$	1.32
0.1	0.006	$0.501 \pm 0.012$	$1.571 \pm 0.091$	$1.001 \pm 0.044$	1.36
	0.004	$0.500 \pm 0.012$	$1.571 \pm 0.108$	$1.015 \pm 0.078$	1.01
	0.002	$0.499 \pm 0.018$	$1.591 \pm 0.639$	$1.024 \pm 0.171$	1.17

considered. Moreover, in each of the mixtures, the critical exponent  $\alpha'$  values are found to be practically constant for all of the three fit ranges. However, among the three fit ranges, the fitted curve over the reduced temperature range

---



---

$|\tau|_{\max} = 4 \times 10^{-3}$  has found to be quite satisfactory with the experimental data throughout the analysis for the Sm-A–Sm-C transition.

In the present investigated system, the effective critical exponent  $\alpha'$  assumes a value almost equal to 0.5 for the mixture concentration  $x_{7\text{OCB}} = 0.1, 0.15, 0.158, 0.167$  and  $0.174$ , indicating non-classical tricritical behavior of the Sm-A–Sm-C phase transition. Despite the sharp change of the transition temperatures with the mixing ratio, no feature of the Fisher renormalization [46] of the critical exponent has been observed in these mixtures. With increasing the concentration of 7OCB, the values of  $\alpha'$  monotonically decreases from the tricritical value  $0.501 \pm 0.006$  for the mixture  $x_{7\text{OCB}} = 0.174$  to  $0.394 \pm 0.006$  for the mixture  $x_{7\text{OCB}} = 0.211$ . Therefore, the coupling between the smectic-A ( $\Psi$ ) and smectic-C ( $\theta$ ) order parameter becomes considerably weaker for a relatively small increase in the concentration of the calamitic nematogen within the mixtures. Such an outcome is possibly due to the modification in effective intermolecular interaction and the local molecular ordering in the host medium, which drives the transition from first order to second order character. Thus, the non-universal values have been obtained for the effective critical exponent  $\alpha'$  and hence indicating a crossover character for the Sm-A–Sm-C phase transitions in the present investigated binary system. The variation of extracted critical exponent values with the temperature ratio ( $T_{NA}/T_{IN}$ ) is illustrated in Fig. 6.6 (a). An extrapolation of a quadratic fit to the  $\alpha'$  values results a crossover from second order to first order for a composition  $x_{7\text{OCB}} = 0.179$  with  $\alpha' = 0.5$  and the corresponding temperature ratio (*i.e.*,  $T_{AC}/T_{AI}$ ) is being 0.972. This temperature ratio has been found to be almost identical with that obtained from previously discussed calamitic homologous system (*i.e.*, chapter 5) in the vicinity of Sm-A–Sm-C phase transition [31]. Moreover, the observed quotient  $A^-/A^+$  reveals a value nearly equal to 1.6 for the tricritical compositions which fairly agrees with the theoretical prediction for the tricritical appearance and for rest of the mixtures it varies between 1.250 and

---



---

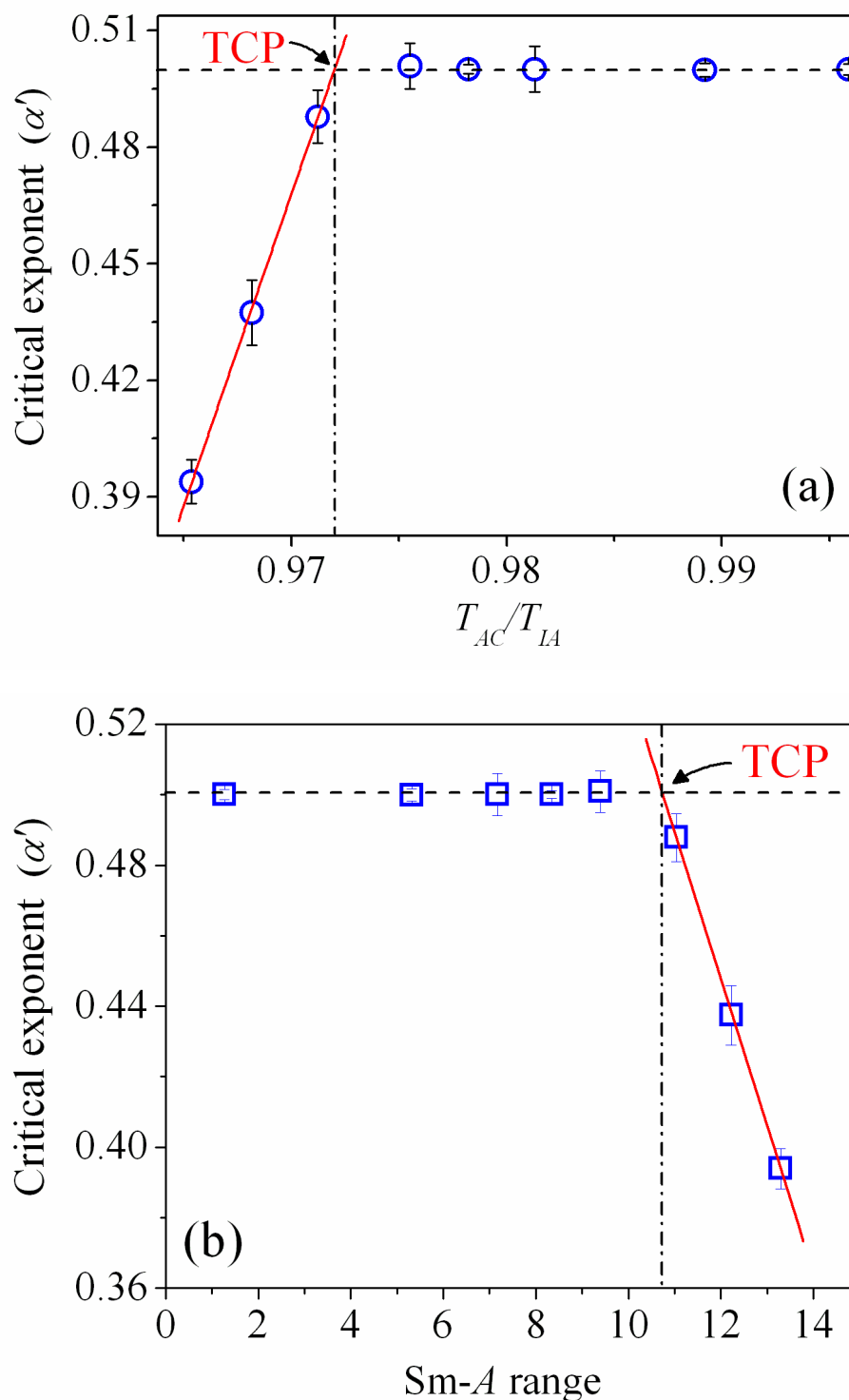


**Figure 6.6.** Variation of the effective critical exponent against (a) the temperature ratio  $T_{AC}/T_{IA}$  and (b) the temperature width of Sm-A phase at the Sm-A–Sm-C phase transition in the present investigated binary mixtures. The vertical dashed lines correspond to the tricritical point (TCP). The solid lines (red) are the 2<sup>nd</sup> order fit to the data points.

1.428. Conversely, the value of parameter ratio  $D^-/D^+$  is nearly equal to 1 for all of the investigated mixtures, divulging a close agreement to the theoretical prediction. Additionally, a variation of effective critical exponent  $\alpha'$  with the temperature width of the Sm-A phase has been explored which is depicted in Fig. 6.6(b). The present binary system indicates that the  $\alpha'$  value lies on the tricritical limit ( $\alpha' \cong 0.5$ ) for the five mixtures having the dopant concentration  $x_{7\text{OCB}} \leq 0.174$ . Accordingly, the tricritical behavior of the Sm-A–Sm-C phase transition has also been observed up to the Sm-A temperature range  $\sim 9.2$  K and further increase of the Sm-A width (greater than 11 K) drives the transition to second order in nature. Therefore, the critical exponent  $\alpha'$  demonstrates a crossover from the tricritical limit toward the XY-like value with increase in the Sm-A temperature range. An extrapolation of these extracted critical exponent values exhibit a crossover point (first order to second order in nature) for a Sm-A temperature range  $\sim 10.6$  K, which also agrees well with the finding observed in previous chapter.

## 6.7. Tricritical fitting

Based on the magnitude of the effective  $\alpha'$  values discussed in the previous section, it has been observed that the mixtures having concentration  $x_{7\text{OCB}} < 0.179$  are close to or above the tricritical composition. To test the possibility of first order character of the Sm-A–Sm-C phase transition and to validate the yielded values of the critical exponent in the tricritical limit, an extensive analysis has been performed on the mixtures those are found to exhibit tricritical value of  $\alpha'$ . The analysis has been carried out using a more general form for  $Q(T)$ , including the first and second order correction terms which are required in describing the present data [47] and can be expressed as:

$$Q(T) = \frac{A^\pm}{\alpha'} |\tau|^{-\alpha'} (1 + D_1^\pm |\tau|^{\Delta_1} + D_2^\pm |\tau|^{2\Delta_1}) + E(T - T_{AC}) + B^\pm \quad (6.3)$$

where  $D_2$  is the coefficients of the second corrections-to-scaling terms and other parameters are same as said for Eq. (6.2).

In this case,  $\Delta_1$  assumes a value 0.5 and the investigation has been performed for the tricritical compositions by fixing the effective  $\alpha'$  value at 0.5. Ema *et al.* have also shown that for the tricritical fit,  $\Delta_1$  value lies close to 0.5 [48]. As a consequence of imposing the values in Eq. (6.3), the first corrections-to-scaling term merges with  $B$  and a new constant term  $F$  is introduced. Therefore, Eq. (6.3) is now simplified to [49]:

$$Q(T) = \frac{A^\pm}{\alpha'} |\tau|^{-1/2} (1 + D_2^\pm |\tau|) + E(T - T_{AC}) + F^\pm \quad (6.4)$$

Moreover, the stability of the fits to Eq. (6.4) has also been tested over three different ranges of reduced temperature: range-**A** ( $|\tau|_{\max} = 2 \times 10^{-3}$ ), range-**B** ( $|\tau|_{\max} = 4 \times 10^{-3}$ ) and range-**C** ( $|\tau|_{\max} = 6 \times 10^{-3}$ ). Corresponding fits to the experimental data with Eq. (6.4) have been illustrated by the solid lines for all the compositions  $x_{7\text{OCB}} < 0.179$  in Fig. 6.7(a-b) for range-**B** and range-**A** respectively, while the fitted parameters are tabulated in Table 6.2. The quality of these fits has been assessed by calculating the related reduced error function  $\chi_v^2$  value [44,45] and found to be limited within 1.08 and 1.62 and thus signifying consistent fits. In the present analysis, it has been found that the parameter  $D_2^\pm$  emerging a negative value, suggesting a qualitative agreement with those previously obtained for the tricritical  $N$ -Sm- $A$  phase transition [50-52]. However, the quotient  $D_2^-/D_2^+$  has been found to be  $D_2^-/D_2^+ < 1$  for the range-**A** and range-**C** as observed from Table 6.2, while the parameter  $D_2^-$  is more or less equal to its counterpart  $D_2^+$  (*i.e.*,  $D_2^- \approx D_2^+$ ) for the range-**B**, indicating a close agreement with the theoretical prediction  $D_2^- = D_2^+$  for the  $N$ -Sm- $A$  phase transition [49,52]. On the other hand, a small systematic variation has been observed for the quotient  $A^-/A^+$  over the influence of dopant concentration. Additionally, the extracted values of that quotient appear in a range between 0.85 and 1.062 for the fit range-**A** and **B**, while it exhibits some higher values for the fit range-**C**. However, it is expected to be 1.6 at the tricritical point in accordance with the theoretical prediction for the  $N$ -Sm- $A$

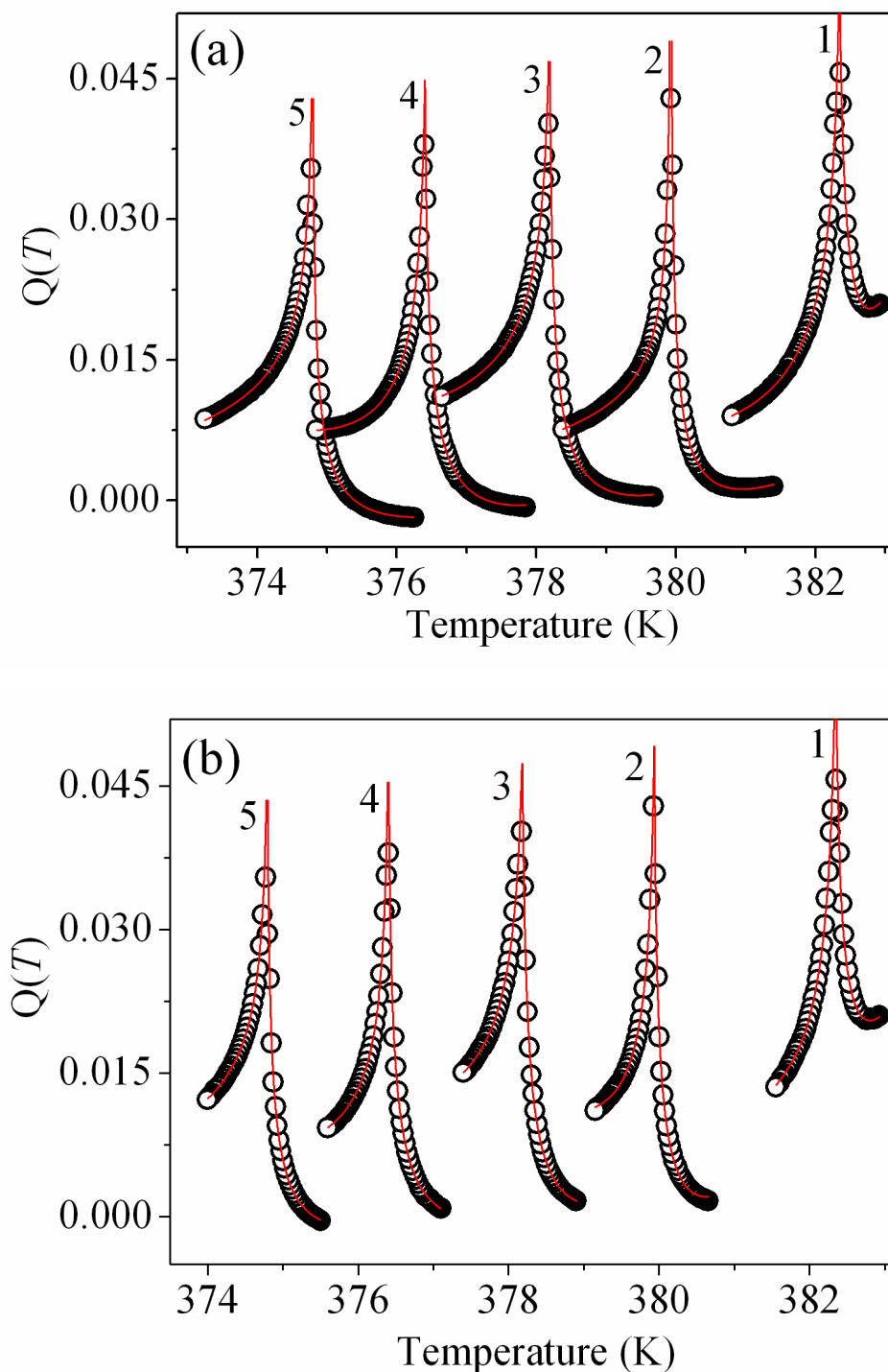


**Figure 6.7.** The temperature dependent variation of  $Q(T)$  in the vicinity of Sm-A–Sm-C transition in mixtures of H-22.5 and 7OCB for (a) fit range-**B** ( $|\tau|_{\max} = 4 \times 10^{-3}$ ), and (b) fit range-**A** ( $|\tau|_{\max} = 2 \times 10^{-3}$ ). 5:  $x_{7\text{OCB}} = 0.174$ ; 4:  $x_{7\text{OCB}} = 0.167$ ; 3:  $x_{7\text{OCB}} = 0.158$ ; 2:  $x_{7\text{OCB}} = 0.15$ ; 1:  $x_{7\text{OCB}} = 0.1$ . These  $Q(T)$  data has been shifted in temperature axis for the guidance of eye as follows: curve 7 by +0.5 K, curve 6 by +0.5 K, curve 4 by +1 K, curve 3 by +1.5 K, curve 2 by +1.5 K.

**Table 6.2.** Results corresponding to the best fit for  $Q(T)$  near Sm-A–Sm-C phase transition obtained in accordance with Eq. (6.4) and related  $\chi_v^2$  values associated with the fits.  $|\tau|_{\max}$  presents the upper limit of reduced temperature considered for these fits.

$x_{70CB}$	$ \tau _{\max}$	$10^4 A^+$	$A^-/A^+$	$z$	$D_2^+$	$D_2^-/D_2^+$	$\chi_v^2$
0.174	0.006	1.7±0.024	1.353±0.019	0.59437	-165.46±1.56	0.459±0.011	1.08
	0.004	1.8±0.035	0.966±0.034	0.71839	-160.81±2.15	1.002±0.018	1.12
	0.002	2.0±0.018	1.019±0.016	0.70061	-166.50±1.04	0.429±0.020	1.10
0.167	0.006	2.1±0.038	1.347±0.024	0.59608	-166.20±1.73	0.758±0.011	1.37
	0.004	2.4±0.035	1.011±0.023	0.70278	-169.58±1.78	1.000±0.014	1.13
	0.002	2.3±0.030	1.042±0.022	0.69229	-166.99±1.47	0.462±0.009	1.32
0.158	0.006	2.2±0.036	1.344±0.022	0.59694	-167.49±1.39	0.814±0.010	1.08
	0.004	2.3±0.051	1.052±0.032	0.68832	-180.35±1.21	1.001±0.011	1.45
	0.002	2.8±0.035	1.062±0.016	0.68505	-167.35±2.89	0.500±0.013	1.25
0.15	0.006	2.3±0.014	1.348±0.008	0.5958	-177.00±1.38	0.853±0.013	1.62
	0.004	2.0±0.032	0.850±0.020	0.76194	-203.24±2.99	0.995±0.017	1.23
	0.002	2.6±0.043	0.986±0.019	0.71194	-168.00±2.70	0.500±0.021	1.45
0.1	0.006	2.5±0.074	1.320±0.039	0.60386	-179.37±2.13	0.836±0.013	1.14
	0.004	3.7±0.017	0.946±0.026	0.72645	-221.86±1.90	0.991±0.010	1.30
	0.002	3.1±0.017	0.973±0.015	0.71659	-186.53±3.70	0.499±0.015	1.12

phase transition [50-52]. Therefore, in the present system the extracted values of the quotient  $A^-/A^+$  are non-universal over the variation of fit ranges. According to Fisher and Sarbach [53,54], this type of amplitude ratios at the tricritical point can be well described by an exactly solvable spherical ( $n = \infty$ ) model, where  $A^-/A^+$  is a function of the single variable  $z = (a/R_0)^3$ , and can be expressed as  $A^-/A^+ = (1 - z^2)^{1/2}/z$ . Here  $a$  is the lattice spacing and  $R_0$  is the range of interaction. Furthermore, while  $z$  goes to zero, the range of interaction becomes infinitely large and then  $A^-/A^+$  approaches to infinity, recovering the Landau behavior. In the present analysis, the extracted  $z$  values are found to be very close to 0.7 for fit range-**A** and **B** (Table 6.2). Conversely, the parameter  $z$  reveals a relatively smaller value for the fit range-**C**. The representation of these  $z$  values with the variation of the amplitude ratio

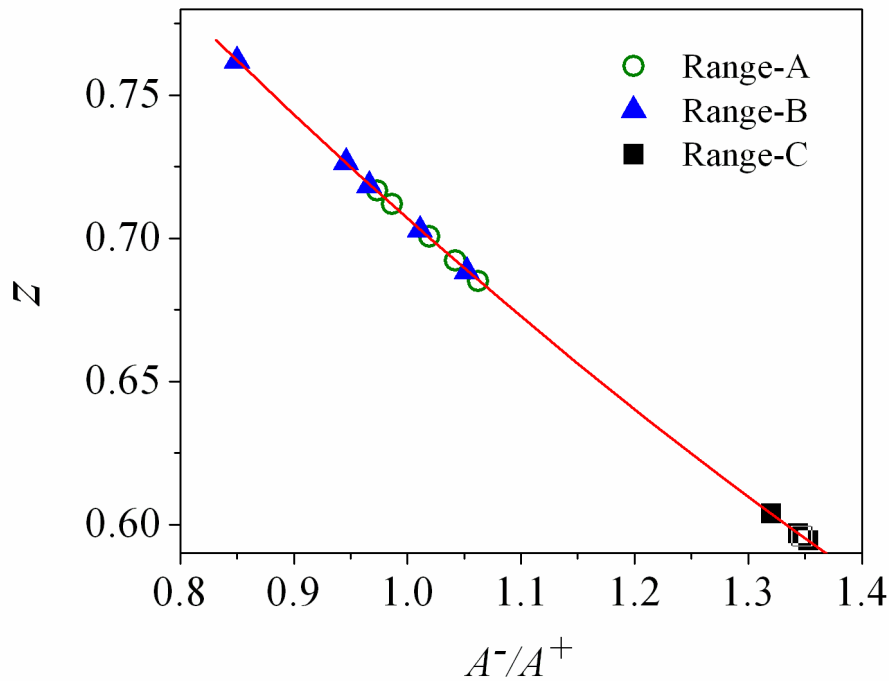


**Figure 6.8.** The representation of extracted  $z$  values with the variation of the amplitude ratio  $A^-/A^+$  over three fit ranges in the vicinity of Sm-A–Sm-C transition. Solid line is a 2<sup>nd</sup> order polynomial to the data points.

$A^-/A^+$  is given in Fig. 6.8. The extracted  $z$  values for the smaller fit ranges in the present system reveals a well agreement with the reported values at the tricritical  $N$ –Sm-A phase transition for polar cyanobiphenyls [50], while they are found to be quite higher than the reported values of  $z = 0.12$  for  $^3\text{He}$ – $^4\text{He}$  mixtures and  $z = 0.21$  for the metamagnet  $\text{Dy}_3\text{Al}_5\text{O}_{12}$  [Dysprosium Aluminum Garnet (DAG)] [53,54]. Therefore, it can be concluded that the order character of the Sm-A–Sm-C transition for the mixtures  $x_{7\text{OCB}} = 0.1, 0.15, 0.158, 0.167$  and  $0.174$  are truly tricritical in nature. The fitting results in Table 6.2 especially over the fit range-**A** and **B** demonstrates a well-consistency with the renormalization group expression considered here, in which the first and second order correction terms plays a crucial role for the tricritical nature of the Sm-A–Sm-C phase transition. Moreover the agreement between the observed data and the fitted curve to Eq. (6.4) is quite well over the region  $2 \times 10^{-3}$  and  $4 \times 10^{-3}$ .

A qualitative comparison has been made for the values of effective critical exponent ( $\alpha'$ ) in the vicinity of Sm-A–Sm-C phase transition in the present binary system with the same obtained from the homologous calamitic binary mixtures reported in previous chapter. All the values of  $\alpha'$  extracted from both the binary systems are plotted against related temperature ratios (similar to McMillan ratio) in Fig. 6.9. For the binary system reported here, three mixtures have the temperature ratios ( $T_{AC}/T_{IA}$ ) less than 0.972 and the extracted value of  $\alpha'$  has been found to demonstrate a non-universal behavior lying in between the tricritical and 3D-XY limit. However, they follow the same curve as indicated by red solid line in Fig. 6.9 obtained from the study of binary mixtures consisting of the homologous rod-like compounds.

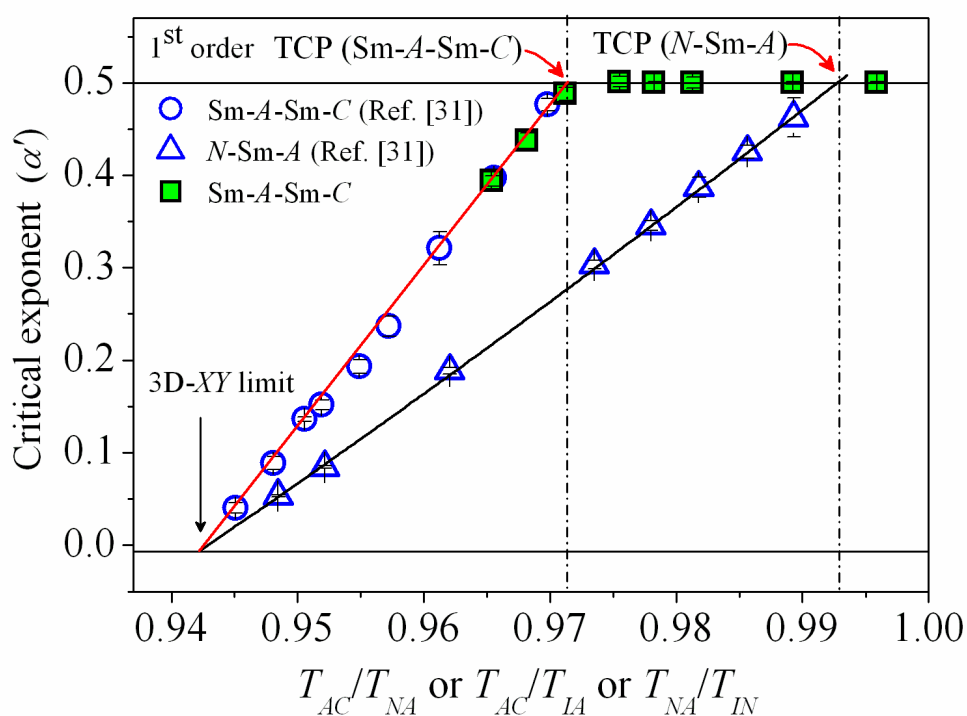


**Figure 6.9.** Variation of the effective critical exponent ( $\alpha'$ ) with the temperature ratio  $T_{AC}/T_{IA}$  for Sm-A–Sm-C<sub>s</sub> phase transitions of the present binary system. ○: Values of  $\alpha'$  for Sm-A–Sm-C transition from chapter 5; □: Values of  $\alpha'$  for N–Sm-A transition from chapter 5. The vertical dashed-dot lines are corresponding to the tricritical point (TCP). The solid lines (red) are the linear fit to the data points.

---

---

On the other hand, the mixtures having temperature ratio ( $T_{AC}/T_{IA}$ ) greater than 0.972 exhibit the value of  $\alpha'$  almost equal to 0.5 signifying a Gaussian tricritical nature of the Sm-A–Sm-C phase transition. Thus the observed phenomena reveal a crossover point at a temperature ratio of 0.972, which is quite low in comparison to the McMillan ratio ( $T_{NA}/T_{IN}$ ) 0.994 for the N–Sm-A phase transition [31]. Additionally, in light of the tricritical nature yielded in the N–Sm-A phase transition at a nematic phase range  $\sim 2.5$  K, the Sm-A–Sm-C transition emphasizes the crossover point (second order to first order) at a temperature range of Sm-A phase of about  $\sim 10.5$  K. Conversely, the linear fit to the  $\alpha'$  data yields a temperature ratio ( $T_{AC}/T_{IA}$  or  $T_{AC}/T_{NA}$ ) of 0.942 corresponding to the 3D-XY point which is found to be very close to the McMillan ratio ( $T_{NA}/T_{IN}$ ), for the N–Sm-A phase transition [31,52,55]. As a result, the values of  $\alpha'$  follows two distinctly different straight lines for the Sm-A–Sm-C and N–Sm-A phase transitions with the variation of the temperature width of the Sm-A and N phases respectively [31]. Therefore, a broad tricritical region for the Sm-A–Sm-C phase transition is experimentally revealed in the present binary system.

## 6.8. Conclusion

In this work, a systematic study has been performed on the high-resolution temperature-dependent optical birefringence for a binary system, consisting of a methyl group substituted hockey-stick-shaped compound, 4-(3-n-decyloxy-2-methyl-phenyliminomethyl) phenyl 4-n-dodecyloxycinnamate (H-22.5) and a calamitic heptyloxy-cyanobiphenyl (7OCB). A significant destabilization of the nematic phase along with an emergence of the Sm-A phase is observed in the phase diagram due to the increase in the concentration of the calamitic nematogen. The birefringence data are found to be rather successful in describing the transitional anomaly at the Sm-A–Sm-C phase transition for all the investigated mixtures. The temperature dependence of birefringence data exhibits a sharp enhancement at the Sm-A–Sm-C transition.

---

---

---

---

By analyzing the temperature derivative of optical birefringence, the power-law divergence behavior has been observed in the vicinity of the Sm-A–Sm-C transition. The related effective critical exponent ( $\alpha'$ ), describing the critical fluctuations at that transition, has appeared to be non-universal in nature. The present outcomes again confirm that the width of the Sm-A phase range plays an important role in determining the nature of the Sm-A–Sm-C phase transition as observed in previous chapter. Interestingly, the values of  $\alpha'$  lie in between 3D-XY and tricritical point (TCP) by decreasing the Sm-A phase range of about  $\sim 10.5$  K and further decrease in Sm-A range the critical exponent ( $\alpha'$ ) values remain in the tricritical limit ( $\alpha' = 0.5$ ). The manifestation of such tricritical nature has also been confirmed by analyzing the experimental data in an extended procedure with the aid of modified renormalization group expression. Consequently, the present system divulges a crossover point at a temperature ratio (similar to McMillan ratio,  $T_{NA}/T_{IN}$ ) of about 0.972 for the Sm-A–Sm-C phase transition. In spite of the binary system formed by divergent molecular structure, the crossover point in the present system is in a good agreement with that obtained from the binary mixtures of the homologous compounds as reported in previous chapter (chapter 5). Interestingly, the critical exponent ( $\alpha'$ ) values observed in the present system suggesting a broad tricritical range for the Sm-A–Sm-C phase transition over a wide scale of temperature ratio (from 0.972 to 0.996), which is quite unusual and probably being reported for the first time.

---

---

**References:**

- [1] S. Chandrasekhar, in *Liquid Crystals*, 2nd ed., Cambridge University Press, New York (1992).
- [2] T. Niori, F. Sekine, J. Watanabe, T. Furukawa, and H. Takezoe, *J. Mater. Chem.*, **6**, 1231 (1996).
- [3] R. Pratibha, N.V. Madhusudana, and B.K. Sadashiva, *Science*, **288**, 2184 (2000).
- [4] G. Pelzl, S. Diele, and W. Weissflog, *Adv. Mater.*, **11**, 707 (1999).
- [5] A. Chakraborty, M.K. Das, B. Das, A. Lehmann, and C. Tschierske, *Soft Matter*, **9**, 4273 (2013).
- [6] B. Das, S. Grande, W. Weissflog, A. Eremin, M.W. Schröder, G. Pelzl, S. Diele, and H. Kresse, *Liq. Cryst.*, **30**, 529 (2003).
- [7] G. Sarkar, B. Das, M.K. Das, U. Baumeister, and W. Weissflog, *Mol. Cryst. Liq. Cryst.*, **540**, 188 (2011).
- [8] A. Chakraborty, B. Das, M.K. Das, S. Findeisen-Tandel, M.-G. Tamba, U. Baumeister, H. Kresse, and W. Weissflog, *Liq. Cryst.*, **38**, 1085 (2011).
- [9] X.F. Han, S.T. Wang, A. Cady, Z.Q. Liu, S. Findeisen, W. Weissflog, and C.C. Huang, *Phys. Rev. E*, **68**, 060701 (2003).
- [10] A. Chakraborty, M.K. Das, B. Das, U. Baumeister, and W. Weissflog, *J. Mater. Chem. C*, **1**, 7418 (2013).
- [11] T. Otani, F. Araoka, K. Ishikawa, and H. Takezoe, *J. Am. Chem. Soc.*, **131**, 12368 (2009).
- [12] C. Zhu, D. Chen, Y. Shen, C.D. Jones, M.A. Glaser, J.E. Maclennan, and N.A. Clark, *Phys. Rev. E*, **81**, 011704 (2010).
- [13] Y. Takanishi, Y. Ohtsuka, Y. Takahashi, and A. Iida, *Phys. Rev. E*, **81**, 011701 (2010).
- [14] R. Pratibha, N.V. Madhusudana, and B.K. Sadashiva, *Phys. Rev. E*, **71**, 011701 (2005).

- 
- 
- [15] C.A. Shantz, and D.L. Johnson, *Phys. Rev. A*, **17**, 1504 (1978).
- [16] C.C. Huang, and J.M. Viner, *Phys. Rev. A*, **25**, 3385 (1982).
- [17] R.J. Birgeneau, C.W. Garland, A.R. Kortan, J.D. Litster, M. Meichle, B.M. Ocko, C. Rosenblatt, L.J. Yu, and J. Goodby, *Phys. Rev. A*, **27**, 1251 (1983).
- [18] M. Meichle, and C.W. Garland, *Phys. Rev. A*, **27**, 2624 (1983).
- [19] S.C. Lien, C.C. Huang, T. Carlsson, I. Dahl, and S.T. Lagerwall, *Mol. Cryst. Liq. Cryst.*, **108**, 149 (1984).
- [20] S. Dumrongrattana, C.C. Huang, G. Nounesis, S.C. Lien, and J.M. Viner, *Phys. Rev. A*, **34**, 5010 (1986).
- [21] P. Das, K. Ema, and C.W. Garland, *Liq. Cryst.*, **4**, 205 (1989).
- [22] H.Y. Liu, C.C. Huang, Ch. Bahr, and G. Heppke, *Phys. Rev. Lett.*, **61**, 345 (1988).
- [23] T. Chan, Ch. Bahr, G. Heppke, and C.W. Garland, *Liq. Cryst.*, **13**, 667 (1993).
- [24] K. Ema, J. Watanabe, A. Takagi, and H. Yao, *Phys. Rev. E*, **52**, 1216 (1995).
- [25] L. Reed, T. Stoebe, and C.C. Huang, *Phys. Rev. E*, **52**, R2157 (1995).
- [26] K. Ema, A. Takagi, and H. Yao, *Phys. Rev. E*, **53**, R3036 (1996).
- [27] K. Ema, M. Ogawa, A. Takagi, and H. Yao, *Phys. Rev. E*, **54**, R25 (1996).
- [28] K. Ema, H. Yao, A. Fukuda, Y. Takanishi, and H. Takezoe, *Phys. Rev. E*, **54**, 4450 (1996).
- [29] K. Ema, and H. Yao, *Phys. Rev. E*, **57**, 6677 (1998).
- [30] A. Chakraborty, S. Chakraborty, and M.K. Das, *Physica B*, **479**, 90 (2015).
- [31] M.K. Das, S. Chakraborty, R. Dabrowski, and M. Czerwinski, *Phys. Rev. E*, **95**, 012705 (2017).
- [32] R. Stannarius, J. Li, and W. Weissflog, *Phys. Rev. Lett.*, **90**, 025502-1-4 (2003).
- 
-

- 
- 
- [33] [https://applications.zeiss.com/C125792900358A3F/0/E037A9841E664961C1257906004802D6/\\$FILE/70\\_2\\_0110\\_e\\_michel\\_levy.pdf](https://applications.zeiss.com/C125792900358A3F/0/E037A9841E664961C1257906004802D6/$FILE/70_2_0110_e_michel_levy.pdf)
- [34] A. Saipa, and F. Giesselmann, *Liq. Cryst.*, **29**, 347 (2002).
- [35] G. Sarkar, M.K. Das, R. Paul, B. Das, and W. Weissflog, *Phase Transit.*, **82**, 433 (2009).
- [36] T. Scharf, in *Polarized Light in Liquid Crystals and Polymers*, Wiley, Hoboken, NJ, (2007).
- [37] A. Prasad, and M.K. Das, *J. Phys.: Condens. Matter*, **22**, 195106 (2010).
- [38] A. Prasad, and M.K. Das, *Phase Transit.*, **83**, 1072 (2010).
- [39] A. Chakraborty, S. Chakraborty, M.K. Das, and W. Weissflog, *J. Mol. Liq.*, **265**, 536 (2018).
- [40] J.A. Olivares, S. Stojadinovic, T. Dingemans, S. Sprunt, and A. Jákli, *Phys. Rev. E*, **68**, 041704 (2003).
- [41] M.C. Çetinkaya, S. Yildiz, H. Özbek, P. Losada-Pérez, J. Leys, and J. Thoen, *Phys. Rev. E*, **88**, 042502 (2013).
- [42] S. Erkan, M. Cetinkaya, S. Yildiz, and H. Ozbek, *Phys. Rev. E*, **86**, 041705 (2012).
- [43] C.W. Garland, in *Liquid Crystals: Experimental Study of Physical Properties and Phase Transitions*, edited by S. Kumar, Cambridge University Press, Cambridge (2001).
- [44] P.R. Bevington, and D.K. Robinson, in *Data Reduction and Error Analysis for the Physical Sciences*, 3rd ed., McGraw-Hill, New York (2003).
- [45] A. Żywociński, and J. Phys. Chem. B, **107**, 9491 (2003).
- [46] M. E. Fisher, *Phys. Rev.*, **176**, 257 (1968).
- [47] A. Aharony, and M.E. Fisher, *Phys. Rev.B*, **27**, 4394 (1983).
- [48] K. Ema, A. Takagi, and H. Yao, *Phys. Rev. E*, **55**, 508 (1997).
- [49] K. Ema, A. Takagi, and H. Yao, *Phys. Rev. E*, **53**, R3036 (1996).
- [50] K. Stine, and C.W. Garland, *Phys. Rev. A*, **39**, 3148 (1989).
- 
-

- [51] G. Nounesis, C.W. Garland, and R. Shashidhar, *Phys. Rev. A*, **43**, 1849 (1991).
- [52] A. Chakraborty, S. Chakraborty, and M.K. Das, *Phys. Rev. E*, **91**, 032503 (2015).
- [53] M. E. Fisher, and S. Sarbach, *Phys. Rev. Lett.*, **41**, 1127 (1978).
- [54] S. Sarbach, and M. E. Fisher, *Phys. Rev. B*, **20**, 2797 (1979).
- [55] S. Chakraborty, A. Chakraborty, and M.K. Das, *J. Mol. Liq.*, **219**, 608 (2016).

# CHAPTER 7

---

Induced TGB phases in binary mixtures of achiral hockey stick-shaped and chiral rod-like mesogen

---

---

## 7.1. Introduction

Chirality, *i.e.*, the lack of mirror symmetry is the inherent self-organized property of chiral molecules in liquid crystal (LC) system. Physical properties of nematic and smectic phases formed by chiral molecules differs from the mesophases formed by usual calamitic molecules [1,2]. In addition to normal orientational ordering of LC molecules in the nematic phase, the precessional motion of local director around a helical axis is present in the chiral nematic ( $N^*$ ) or cholesteric phase. On the other hand, the chirality endorsed in smectic-A (Sm-A) and smectic-C (Sm-C) phases are known as smectic-A\* (Sm-A\*) and smectic-C\* (Sm-C\*) [3] phases. Such a combined molecular organization acts as an external field to the system and hence establishes some typical paraelectric, ferroelectric and anti-ferroelectric mesophases in LC compounds. Due to the presence of supramolecular helicity, development of several novel thermodynamic phases along with beneficial electro-optic effects of such materials make them advantageous in smart display devices [4-12] and electro-optic technological appliances [13-17].

In chiral LC system, variety of new mesophases such as blue phase (BP) [18,19], chiral line liquid ( $N_L^*$ ) phase [20,21], twist grain boundary (TGB) [22,23] phase etc. have drawn the attention of the researchers in the last few decades. All these phases are thermodynamically distinct phases of highly chiral compounds, arises in a small temperature range. TGB phases are developed due to competition between helical superstructure of molecular director and positional ordering of smectic layers. The reason for the existence of different TGB phases is that the direct transformation from highly twisted  $N^*$  to smectic phases cannot occur in a continuous way as the cholesteric twist of the director is incompatible to form the smectic layer structure. Therefore, encompassing both the structural features reveals a frustrated TGB phase in which locally ordered smectic slabs are separated by grain boundaries which in turn consist of a lattice of screw dislocations and the corresponding helix axis

---

---

is perpendicular to the smectic layer normal (Fig. 1.11 in chapter 1). It was theoretically predicted by Renn and Lubensky [1,24] that the TGB phases are identical to the Abrikosov's triangular flux vortex lattice phase of type-II superconductors in an external magnetic field. In case of TGBA phase, the orientation of the molecules within each slab is similar to regular Sm-A phase, first observed by Goodby *et al.*[2,25], while the molecular orientation within the slabs of the TGBC phase is tilted as like Sm-C phase [24,26]. On the other hand, TGBC\* phase comprises of smectic slabs with Sm-C\* orientation of the molecules thereby possess two orthogonal helix axis. Although the TGB phases are generally found in some pure compound having lower pitch length or high chirality in nature, some binary LC mixtures also exhibit the same [27-31]. Notably, the stability of these TGB phases is generally observed in a small temperature range.

The structural features of the molecule have a crucial role to favor the complex orientation in TGB phases. Apart from the typical rod-like molecules, TGB phases has also been found in some pure bent-core mesogens with chiral chain [32,33] and also in some mixtures of chiral compounds with achiral bent-core mesogens [34,35]. The bent-core mesogens have shown global interest in LC community, as they exhibit exceptional structure-induced mesomorphic behavior and unconventional mesophase sequences. Some of the bent-core mesogens are found to possess both spontaneous polarization and biaxiality in orthogonal (Sm-A) [36,37] and tilted smectic (Sm-C) [38,39] phases. Additionally, the bent-core mesogens reveal some intriguing properties such as giant flexoelectricity [40,41], unique rheological properties [42,43], a considerable Kerr effect [44], unprecedented behavior of electroconvection patterns [45-47], polar switching behavior and structural layer chirality [48-50] due to the presence of bent-shaped unit in the molecular conformation. On the other hand, the asymmetrically configured hockey-stick shaped liquid crystals possess a variety of combinational properties of both symmetric bent-core and

---

---

calamitic compounds. For several hockey stick-shaped compounds, no feasible polar character has been found from the electro-optical measurements [51,52]. However, there are also contradictory evidences of low, but clearly measurable value of spontaneous polarization in freestanding films formed by hockey stick-shaped liquid crystals [53,54]. Therefore, the polar character of such compounds is still under investigation. It can be assumed that mixtures of bent-core compounds with the chiral mesogenic system may either influence the polar property of the mixture or may induce atypical mesophases like BP, TGB phases. Till date, a number of chiral-achiral mixtures have been reported to exhibit induced frustrated mesophases. Several physical properties have also been determined in these phases to understand the proper molecular architecture and associated behavior [19,55-58]. The actual process of formation of frustrated structure in such complicated system is still not been properly understood which necessitates further experimental investigations.

In this chapter, two wide temperature ranged TGB phases – TGBA and TGBC\* have been observed in a binary system consisting of highly tilted chiral ferroelectric rod-like compound, (S)-(+)-4'-( $\omega$ -alkanoyloxy) alkoxybiphenyl-4-yl 4-(1-methylheptyloxy) benzoates ( $nHmR$ ), with  $n = 2$ ,  $m = 6$  and an achiral hockey stick-shaped compound, namely 4-(3- $n$ -decyloxy-2-methylphenyliminomethyl) phenyl 4- $n$ -dodecyloxy cinnamate (H-22.5). Different optical, dielectric and electro-optical investigations have been performed for these binary chiral-achiral mixtures and discussed the possible outcomes in the viewpoint of perturbation introduced by the achiral hockey stick-shaped compound.

## 7.2. Materials

The investigated host chiral ferroelectric liquid crystal belongs to the homologous series of (S)-(+)-4'-( $\omega$ -alkanoyloxy) alkoxybiphenyl-4-yl 4-(1-methylheptyloxy) benzoates ( $nHmR$ ) with  $n = 2$ ,  $m = 6$  [59], obtained from the Institute of Chemistry, Military University of Technology, Warsaw, Poland and

the guest hockey stick-shaped liquid crystal compound, 4-(3-n-decyloxy-2-methyl-phenyliminomethyl) phenyl 4-n-dodecyloxy cinnamate (H-22.5) [60], discussed earlier in chapter 6, has been used to formulate the investigated mixtures. The structural formulae and transition scheme for the compound 2H6R is given in Fig. 7.1.

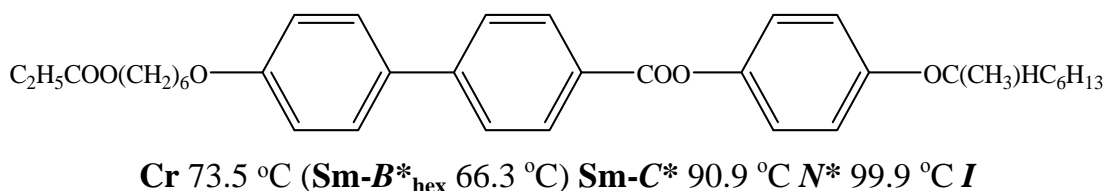


**Figure 7.1.** Chemical structure and phase behavior of the chiral ferroelectric compound (2H6R).

The rod-like chiral compound (2H6R) possesses a cholesteric or  $N^*$  phase ( $\sim 9$  °C) along with a Sm-C\* phase. However, a hexatic Sm-B\*<sub>hex</sub> phase is also found during cooling cycle [59]. In Sm-C\* phase, the obtained value of the tilt angle is about 33° and spontaneous polarization of about 110 nC/cm<sup>2</sup> with a helical pitch 400–600 nm. Whereas the asymmetrical hockey stick shaped compound (H-22.5) exhibits the stable phase sequence  $I-N-Sm-C_s-Sm-C_a-Cr$  as being cooled from the isotropic state [60,61], where Sm-C<sub>s</sub> and Sm-C<sub>a</sub> refer to Smectic-C phases having synclinic and anticlinic alignment of the molecules in the adjacent layers. Hence the mixtures of such chiral and achiral, rod-like and hockey stick-shaped compounds with nearly equal clearing temperature are of significant interest to study the resultant mesophase behavior and their physical properties. Three concentrations have been prepared by adding guest hockey stick-shaped compound (H-22.5) in the host chiral ferroelectric compound (2H6R), having mole fractions of H-22.5:  $x_{H-22.5} = 0.101, 0.202, 0.306$ .

### 7.3. Optical texture and DSC studies

Identification of different liquid crystalline mesophases and corresponding temperature scheme for all the studied mixtures have been

---

---

carried out by polarizing optical microscopy and DSC study. The optical textures were observed during cooling cycle of the samples, filled in commercially available ITO coated planar and homeotropically aligned cells of thickness  $\sim 9 \mu\text{m}$ .

During cooling from the isotropic phase, all the investigated mixtures exhibit four distinct mesophases. The  $N^*$  or cholesteric phase emerges as a first high-temperature mesophase similar to the pure chiral compound 2H6R. Fig. 7.2 represents the optical micrographs for the concentration  $x_{\text{H-22.5}} = 0.202$  in the  $N^*$  phase. The appearance of nematic droplets has been noticed at the isotropic to  $N^*$  phase transition (Fig. 7.2(a)). However, the cholesteric Grandjean texture (Fig. 7.2(b)) is also observed for the 2H6R compound as well as for the mixture concentration  $x_{\text{H-22.5}} = 0.306$  just after the transition from the isotropic phase. Generally this texture defines a pitch length of the order of a few  $\mu\text{m}$ . With lowering of temperature, different types of cholesteric textures appears *viz.* the broken fan-like texture of the short pitch depicted in Fig. 7.2(c), oily streaks texture in Fig. 7.2(d,e), fluctuating color domain cholesteric textures in Fig. 7.2(f,g), a sharp appearance of cholesteric finger in Fig. 7.2(h) and reappearance of oily streaks textures at a lower temperature as illustrated in Fig. 7.2(i) [23,62]. Different color domains in Fig. 7.2(f,g) correspond to different twist states and the “black” domain in Fig. 7.2(g) stands for a quasi-nematic director configuration that can be brought into an extinction position by rotating the sample between crossed polarizers. Specifically, this state is named as the twist inversion state [23] where the nucleation and quickly grown up of some color domains can be visualized in all the mixtures. Different chiral compounds and even some binary mixtures are reported to reveal this twist inversion phenomenon [62-67]. Due to existence of the helical superstructure of the  $N^*$  phase, its textural appearance and optical properties are quite different from those of usual nematic phases. All these textures in Fig. 7.2(a-i) have been observed in the planar configuration of the sample. In case

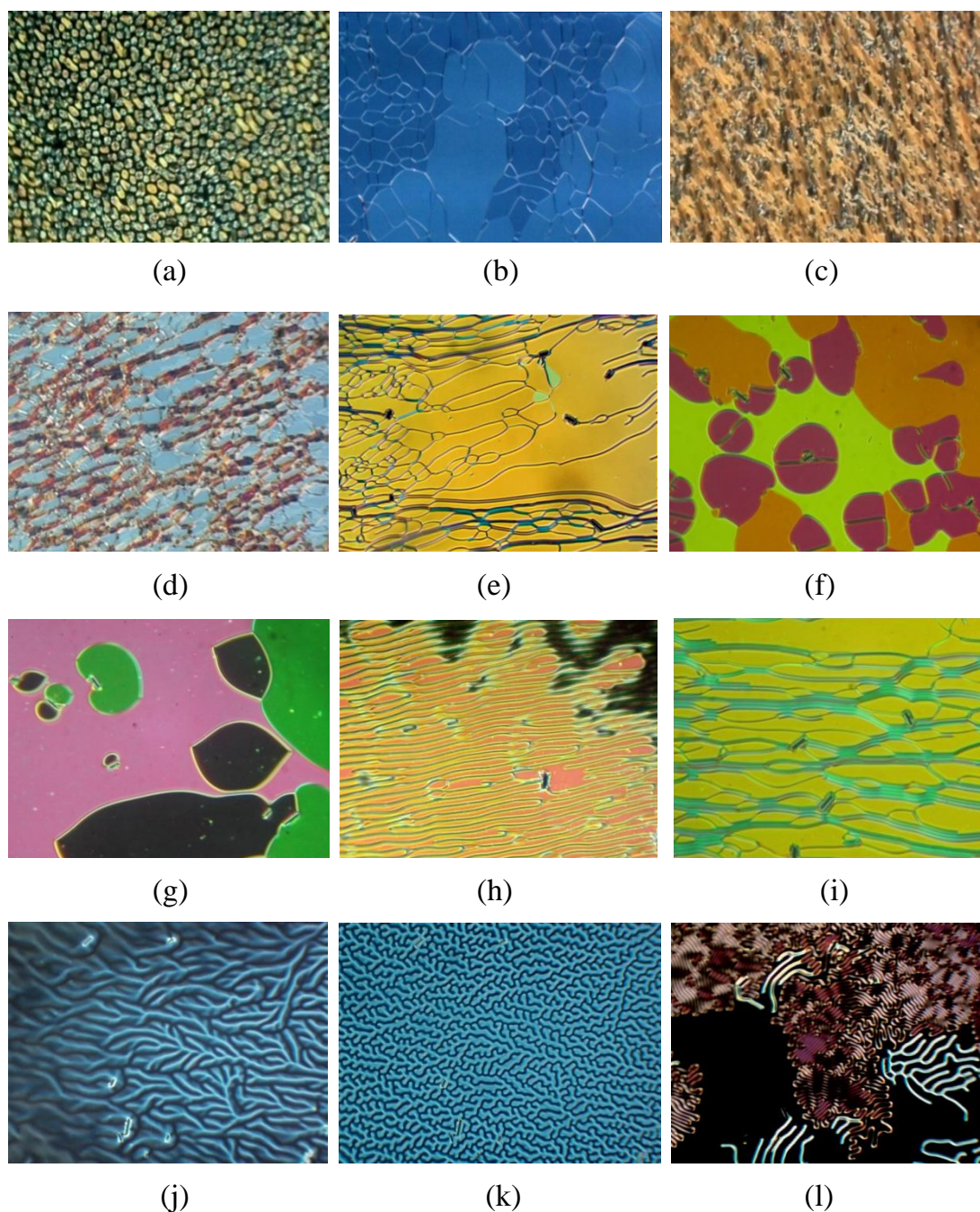


**Figure 7.2.** Optical textures of  $N^*$  phase by lowering the temperature as: (a) nematic droplets at 98.5 °C, (b) cholesteric Grandjean texture of 2H6R at 98.3 °C, (c) cholesteric fan-like texture at 98 °C, (d-e) oily streaks texture at 97.6 °C and 97.2 °C, (f-g) color domain texture of different twist and twist-inversion states at 96.8 °C and 96.6 °C, (h) texture with cholesteric finger at 96.2 °C, (i) oily streaks textures appears again at 95.5 °C, (j-k) texture with cholesteric finger in homeotropic cell at 96.5 °C, 96 °C respectively, (l) coexisting of fingerprint texture with cholesteric finger at 94.3 °C for  $x_{H-22.5} = 0.306$ .

---

---

of homeotropic anchoring condition, an optical texture with typical cholesteric fingers has appeared close to the twist inversion temperature of the  $N^*$  phase as shown in Fig. 7.2(j,k). The dark areas representing a pseudo-isotropic twisted state for a strong homeotropically aligned sample. A coexistence of fingerprint texture with cholesteric fingers has also been observed for  $x_{H-22.5} = 0.306$  (Fig. 7.2(l)). Black regions of this texture specifying the unwound, non-helical state where the director tends to align parallel to the optic axis in the homeotropic configuration of the sample [23]. Hence, it is an indication of a transition to a mesophase where the molecular director is parallel to the direction of light propagation. All the texture confirms that the cholesteric pitch length of the twisted  $N^*$  phase is increasing by lowering the temperature and thereby exhibiting a continuous change of several optical textures with different colors.

The transition from the  $N^*$  phase to low-temperature mesophase is characterized by Grandjean type optical textures in planar aligned sample as shown in Fig. 7.3(a-c), while the homeotropically anchoring sample leads to filament type textures as shown in Fig. 7.3(d-f). The optical textures observed in the homeotropic alignment are mostly covered by black (optically isotropic) region. Here the molecular director is oriented in a parallel direction to the optic axis as like homeotropically aligned Sm-A phase. However, all of these textures appearing in the present system are the characteristics of the TGBA phase [32,68,69]. Moreover, the theoretical prediction suggesting that the transition from cholesteric to chiral smectic-C (Sm-C\*) phases can occur either by first order untwisting of molecular director or by inducing both the TGBA and TGBC\* phases [1,26]. Therefore, the presence of higher order pitch length of helix axis and an affinity to form layer structure with the orthogonal Sm-A ordering of the molecules gives rise to such frustrated TGBA phase by decreasing the temperature from the  $N^*$  phase. Although, this type of frustrated phases is mostly found in a small temperature ranges, but the stability of the present TGBA phase is observed in a broad temperature range (around 5-8 °C).

---

---

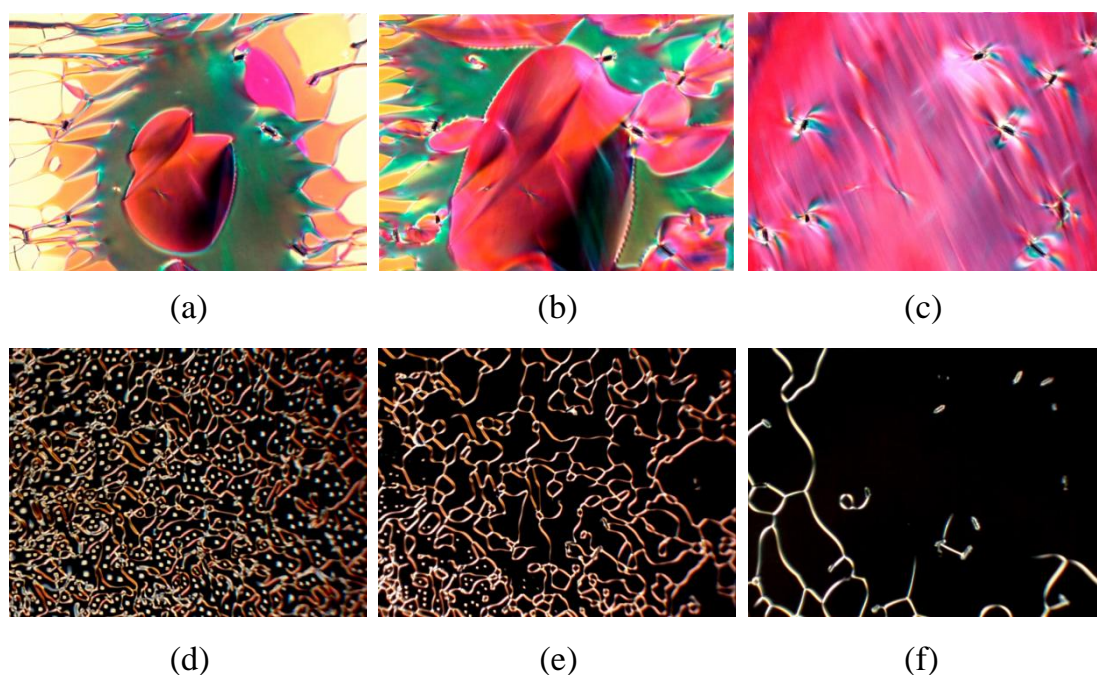


**Figure 7.3.** Optical textures of TGBA phase by lowering the temperature as follows: (a-b) transition from  $N^*$  to TGBA phase in planar configuration at 93.3 °C and 93.25 °C, (c) Grandjean texture of TGBA phase at 92.1 °C, (d-e) filament texture at the transition from  $N^*$  to TGBA phase in homeotropic configuration at 93.25 °C and 93.2 °C, (f) appearance of black domain for TGBA phase at 93 °C.

Further lowering the temperature, optical textures of the TGBA phase modifies to a square grid pattern across the Grandjean texture in planar boundary condition. The manifestation of such square grid texture is the characteristic features of TGBC\* phase [70,71]. Fig. 7.4(a-c) illustrates the micrographs in the TGBC\* phase in planar configuration and Fig. 7.4(d-e) represents the same in homeotropic alignment. The appearance of such square grid pattern in the TGBC\* phase may be a consequence of the undulation of the smectic slabs [72]. However, according to the model of Galerne [73], which is an extended model of Renn *et al.* [26], this type of cross grid structure develops due to the separation of helislabs by disclination lines. Since the pure compound 2H6R possess Sm- $C^*$  phase, a significant influence of the molecular tilt as well as precessional approach is responsible to develop this frustrated undulated TGBC\* phase in the mixtures in which the TGB helix is oriented

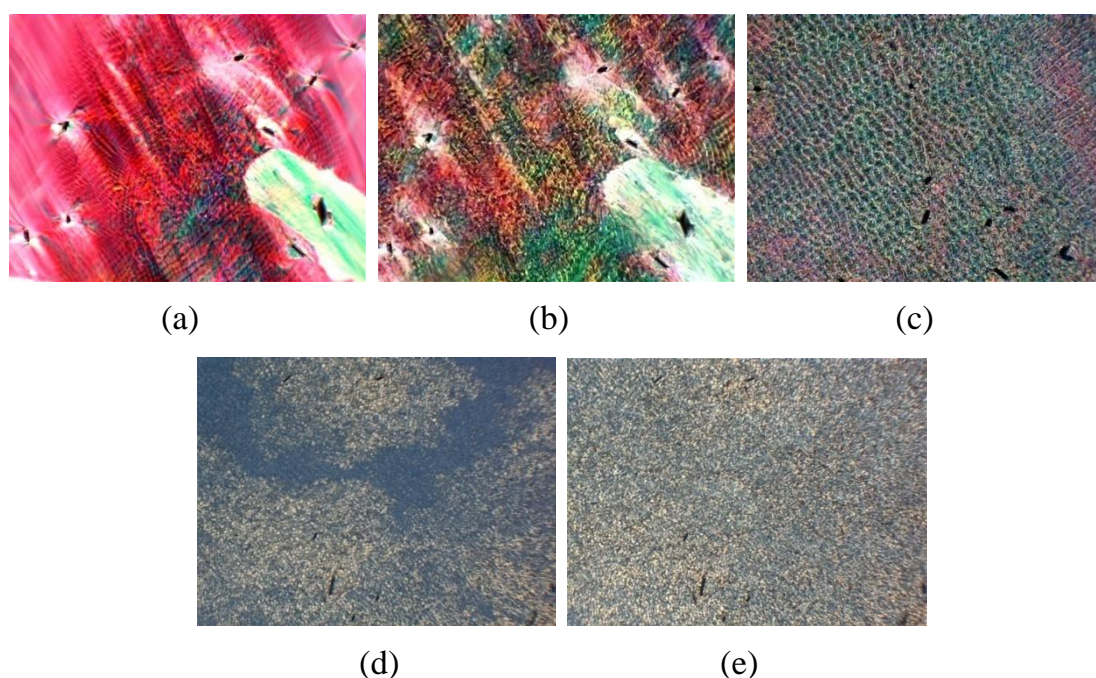


**Figure 7.4.** Optical textures of TGBC\* phase by lowering the temperature: (a) appearance of cross-grid pattern in planar aligned Grandjean texture of TGBA phase at 84.6 °C, (b) well-formed texture of TGBC\* phase at 84.5 °C, (c) appearance of modulated texture of TGBC\* phase at 80 °C for  $x_{H-22.5} = 0.306$ , (d) transition to TGBA–TGBC\* phase at 84.8 °C in homeotropic cell, (e) well-formed TGBC\* phase texture at 82 °C in homeotropic cell.

perpendicular to the bounding plates, *i.e.*, parallel to the direction of the light propagation. Therefore, the square grid structure is the result of the mutual configuration of the helical director within the individual Sm- $C^*$  blocks where the helix axis of all the slabs being in the plane of the substrate and mutually perpendicular in adjacent smectic blocks [32,74-76]. The temperature stability of this mesophase has found to be quite large (maximum 37.5 °C for  $x_{H-22.5} = 0.202$ ) compared to that of the TGBA phase.

The fourth mesophase, *i.e.*, the Sm- $B^*_{hex}$  phase has been observed with the appearance of a mosaic texture in planar anchoring cell at a low temperature for all the investigated mixtures. In both the configurations, almost similar textures are found in the mixtures and pure compound 2H6R. Fig. 7.5 (a) and Fig. 7.5(b) illustrate the textures of Sm- $B^*_{hex}$  phase in planar anchoring condition for the pure compound and the homeotropic anchoring texture for the

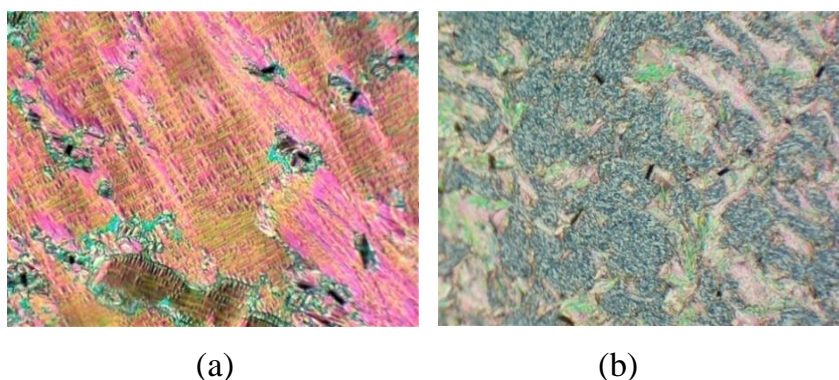


**Figure 7.5.** Optical textures of lower temperature  $\text{Sm-}B^*_{\text{hex}}$  phase at (a) 50 °C for pure 2H6R compound in planar cell, (b) 48.6 °C for  $x_{\text{H-22.5}} = 0.202$  in homeotropic alignment.

mixture concentration  $x_{\text{H-22.5}} = 0.202$ . This type of mosaic texture demonstrates a smectic phase with hexatic order in a most stable configuration. Moreover, the optical textures reveal some small domains with uniform optical appearance, separated by domain boundaries. In this case, the smectic layers are oriented in a perpendicular direction to the substrate plane and the director in each domain is oriented along a particular direction, which varies from domain to domain. This causes a uniform optical appearance within a single domain.

Furthermore, the phase transition temperatures associated with all the mesophases were determined by investigating the differential scanning calorimetry (DSC) using Pyris Diamond Perkin-Elmer 7. Measurements were carried out by taking the sample ( $\sim 4$  mg) in a hermetically sealed aluminium pan in a nitrogen atmosphere. The representative thermogram for the mixture  $x_{\text{H-22.5}} = 0.202$  during heating and cooling cycles (at a rate  $10 \text{ }^\circ\text{C min}^{-1}$ ) is presented in Fig. 7.6. DSC thermogram shows sharp peaks at the transitions of the investigated mixtures and the corresponding amount of enthalpy change  $[\Delta H]$  (kJ/g) has been calculated from the experimental curve. The phase transition scheme obtained from DSC study is summarized in Table 7.1 for the mixture  $x_{\text{H-22.5}} = 0.202$ . All the phase transition temperatures were easily detected (except the  $N^*-\text{TGBA}$  transition) from the DSC study and found to

reveal a good agreement with the same obtained from polarizing optical microscopy. Therefore, all the mixtures exhibit the following phase sequence:  $I-N^*-TGBA-TGBC^*-Sm-B^*_{hex}$ . Among all the mesophases,  $TGBC^*$  phase sustains in a quite large temperature range which is very rare and the bend-shaped molecular structure of hockey stick-shaped compound is assumed to be responsible for the induction of these ( $TGBA$  and  $TGBC^*$ ) frustrated mesophases.

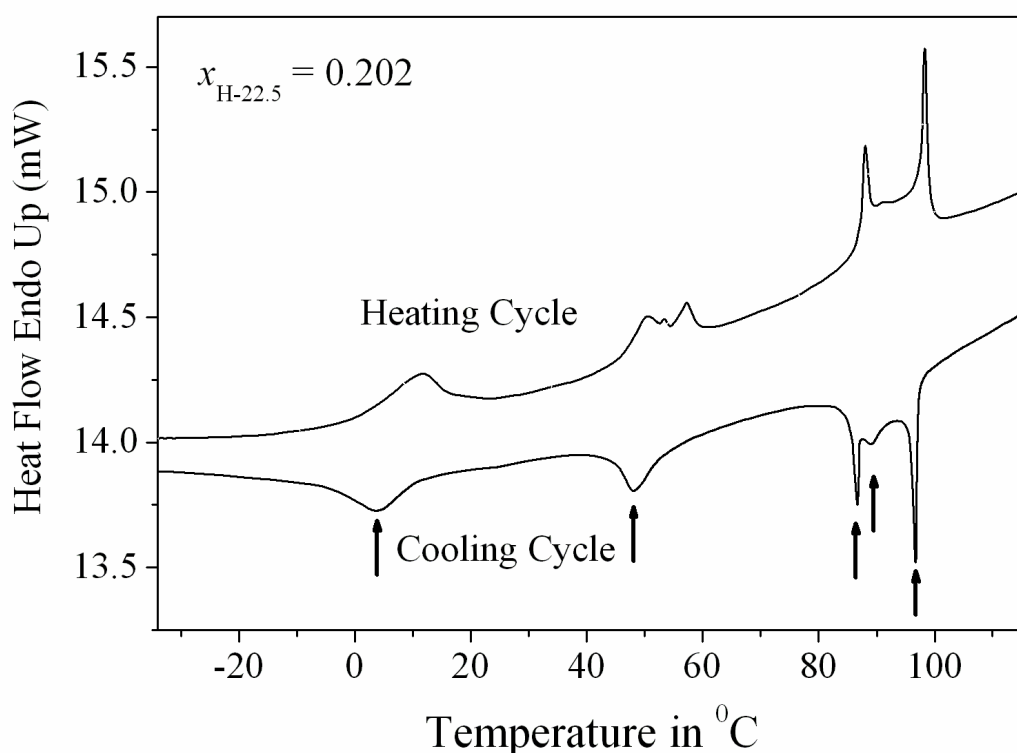


**Figure 7.6.** DSC thermograms on both heating and cooling cycle for the mixture concentration  $x_{H-22.5} = 0.202$ .

**Table 7.1.** Sequence of phases, temperature schemes ( $^{\circ}C$ ) and transition enthalpies [ $\Delta H$  (J/g)] during cooling cycle for the mixture  $x_{H-22.5} = 0.202$ .

Cr	←	$Sm-B^*_{hex}$	←	$TGBC^*$	←	$TGBA$	←	$N^*$	←	$I$
•	4.2	•	49.1	•	86.6	•	90.5	•	96.4	•
	[-4.5]		[-2.2]		[-1.5]		[-0.4]		[-1.4]	

---

---

## 7.4. Phase diagram

The partial phase diagram of the binary system consisting of H-22.5 and 2H6R for three different concentrations along with the pure compound 2H6R has been illustrated in Fig. 7.7(a). The transition temperatures are based on the values obtained from the polarizing optical microscopy and DSC study. The pure hockey stick-shaped compound H-22.5 shows the stable phase sequence  $I-N-Sm-C_s-Sm-C_a-Cr$  as being cooled from the isotropic state [60], where  $Sm-C_s$  and  $Sm-C_a$  refer to Smectic- $C$  phases having synclinic and anticlinic alignment of the molecules in the adjacent layers. On the other hand, the pure chiral ferroelectric compound (2H6R) exhibits the  $N^*$  and  $Sm-C^*$  phases in conjunction with hexatic smectic ( $Sm-B^*_{hex}$ ) phase [59].

A small amount of guest H-22.5 compound has been added to the host mesogenic chiral ferroelectric compound to prepare the mixtures. In these binary mixtures, significant focus has been taken on the region where the concentration of the guest compound (H-22.5) is much less compared to that of the chiral compound (2H6R). In this regard, the presence of the bent-shaped mesogenic compound highly interrupts the chiral environment of the host mesogen and responsible to develop a couple of TGB phases. Noticeably, the suppression of  $Sm-C^*$  phase of the pure compound has been found along with a significant induction of TGBA and TGBC\* phases in all the mixtures. However, the estimated temperature range of the  $N^*$  phase monotonically decreases by increasing the amount of hockey stick-shaped compound in the host mesogenic system. The variation of the  $N^*$ , TGBA and TGBC\* phase ranges against molar concentration is also presented in Fig. 7.7(b). By increasing the amount of H-22.5 compound enhances the width of TGBC\* phase with a relatively small change in the width of  $N^*$  and TGBA phases. The width of  $N^*$  phase decreases from a value 9 °C (for pure 2H6R) to a value of 5 °C for the mixture concentration  $x_{H-22.5} = 0.306$ , while the temperature ranges of TGBA and TGBC\* phases follow a non-linear trend opposite to each other

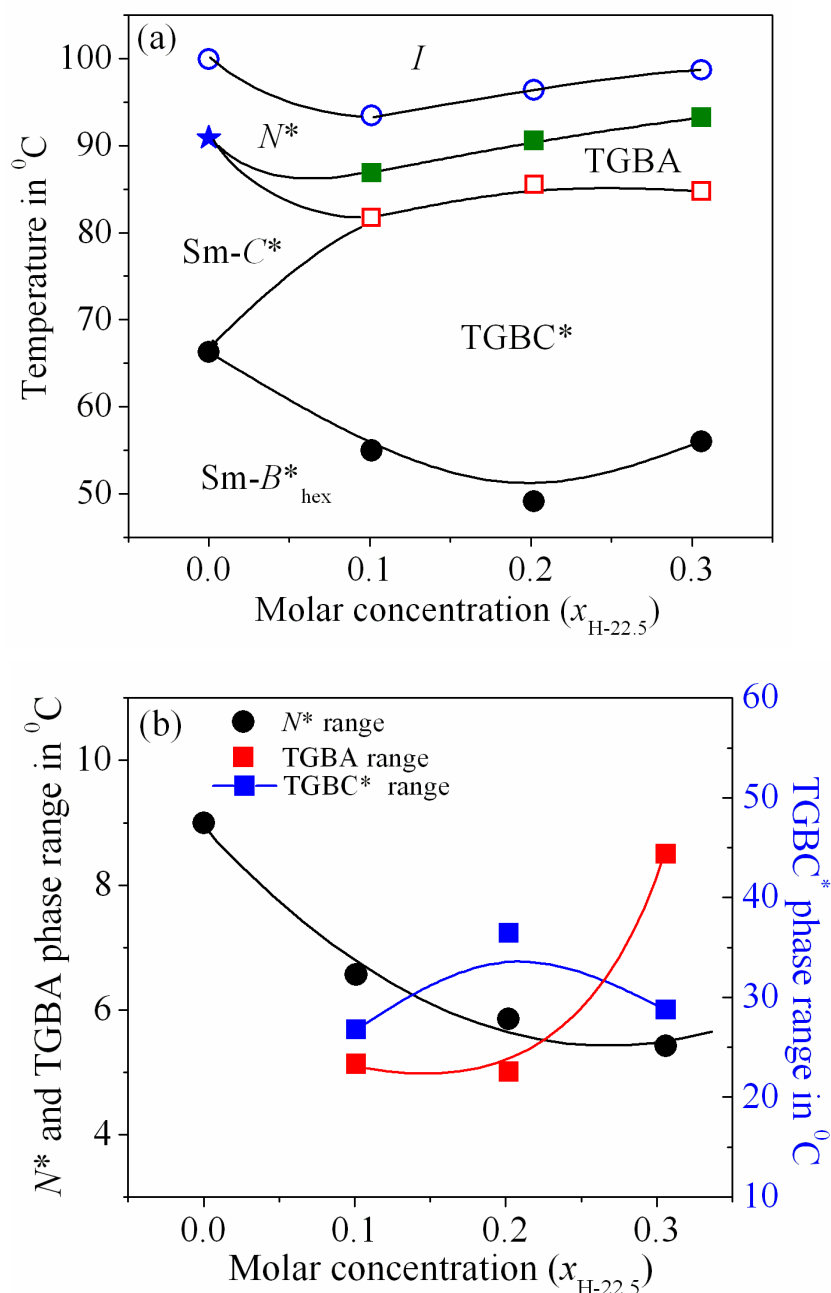


**Figure 7.7.** (a) Phase diagram for the composite mixture consisting of H-22.5 and 2H6R.  $x_{H-22.5}$  denotes the mole fraction of H-22.5.  $I$  - isotropic phase,  $N^*$  - chiral nematic phase,  $\text{Sm-C}^*$ - chiral Sm-C phase,  $\text{TGBA}$ - frustrated smectic-A phase and  $\text{TGBC}^*$ - frustrated smectic-C phase.  $\circ$ :  $I-N^*$  transition temperature;  $\square$ :  $N^*\text{-TGBA}$  transition temperature;  $\square$ :  $\text{TGBA-TGBC}^*$  transition temperature;  $\star$ :  $N^*\text{-Sm-C}^*$  transition temperature;  $\bullet$ :  $\text{TGBC}^*\text{-Sm-B}_{\text{hex}}^*$  phase transition temperature. (b) Variation of  $N^*$ ,  $\text{TGBA}$  and  $\text{TGBC}^*$  phase range with concentration for the present system. Solid lines are drawn for guidance to the eye.

---

---

with the variation of molar concentration. However, the temperature stability of the TGBA phase is quite smaller in comparison to the TGBC\* phase, although it increases by increasing the concentration of the hockey stick-shaped mesogen. Besides, the maximum range of TGBC\* phase has been found around 37 °C for  $x_{H-22.5} = 0.202$  which is quite large for frustrated phases.

## 7.5. Optical transmission intensity study

The temperature-dependent optical transmission intensity, measured by the high-resolution optical transmission (OT) technique [77-80] are depicted in Fig. 7.8(a-d) for all of the studied mixtures including the pure chiral compound (2H6R). The measurement has been carried out by taking the samples in ITO coated commercial cells of thickness 9  $\mu\text{m}$  in both the planar (HG) and homeotropic (HT) configurations. In this study all the phase transition temperatures are clearly been detected for both the cell configurations.

The obtained results reveal that the transmitted intensity value increases at the  $I-N^*$  phase transition for all the investigated samples in both the planar and homeotropic cell configurations due to the increase of order parameter. For the pure compound (2H6R), the intensity value has been found to decrease sharply at the  $N^*-Sm-C^*$  phase transition. However, at the  $N^*-TGBA$  phase transition a pronounce change in the transmission intensity is observed for all the studied mixtures. On entering the TGBA phase, the intensity data exhibit a sharp enhancement followed by a decrease just before the phase transition and this change is well recognized in HT configuration compare to that of the planar alignment. Noticeably, this minimum intensity value close to the  $N^*-TGBA$  phase transition has also been observed in optical texture which appears as black in HT cell at the twist inversion temperature as shown in Fig. 7.2 (l). As the pitch length of the cholesteric phase monotonically increases by decreasing the temperature, helix is continuously unwinding in this mesophase. Probably, due to the occurrence of twist inversion phenomena in the present

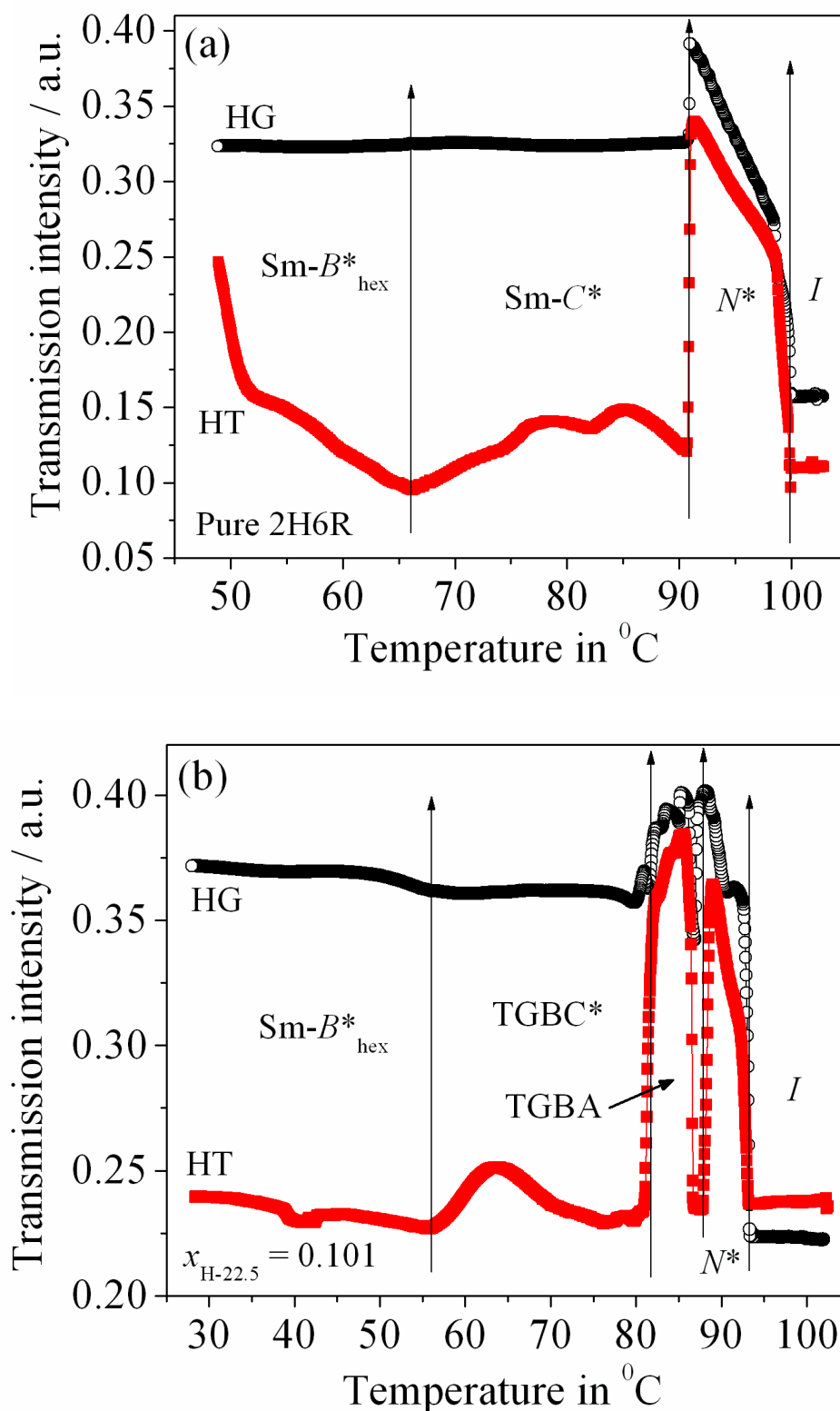


**Figure 7.8.** Temperature-dependent measured optical transmission intensity for compound (a) 2H6R, and (b)  $x_{\text{H-22.5}} = 0.101$  respectively in planar (open circle) cell and also homeotropic (closed square) cell configuration. Vertical arrows represent the corresponding phase transition.

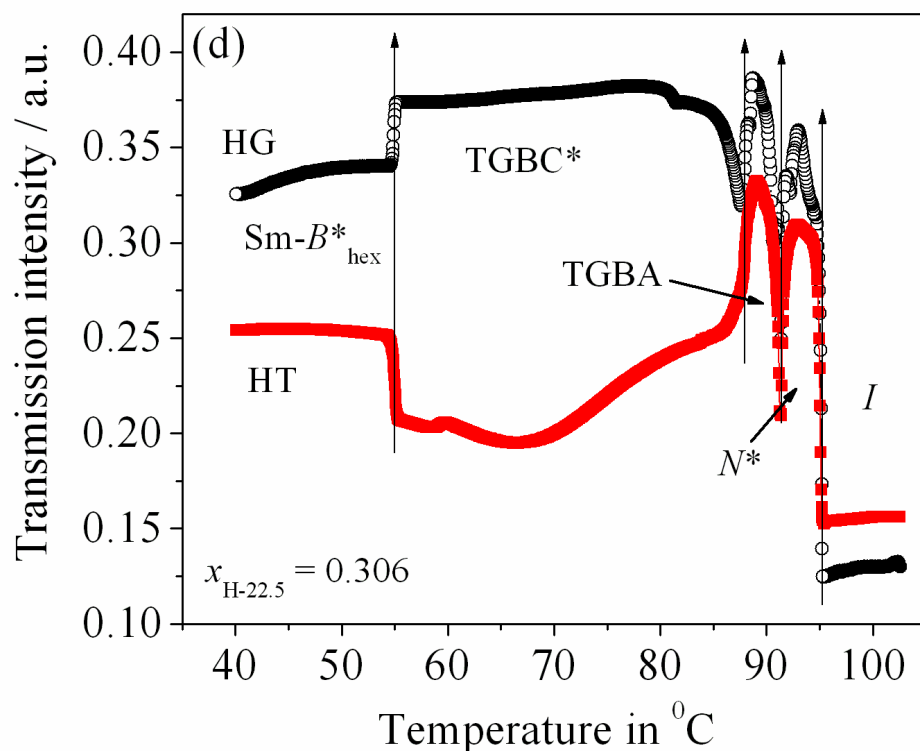
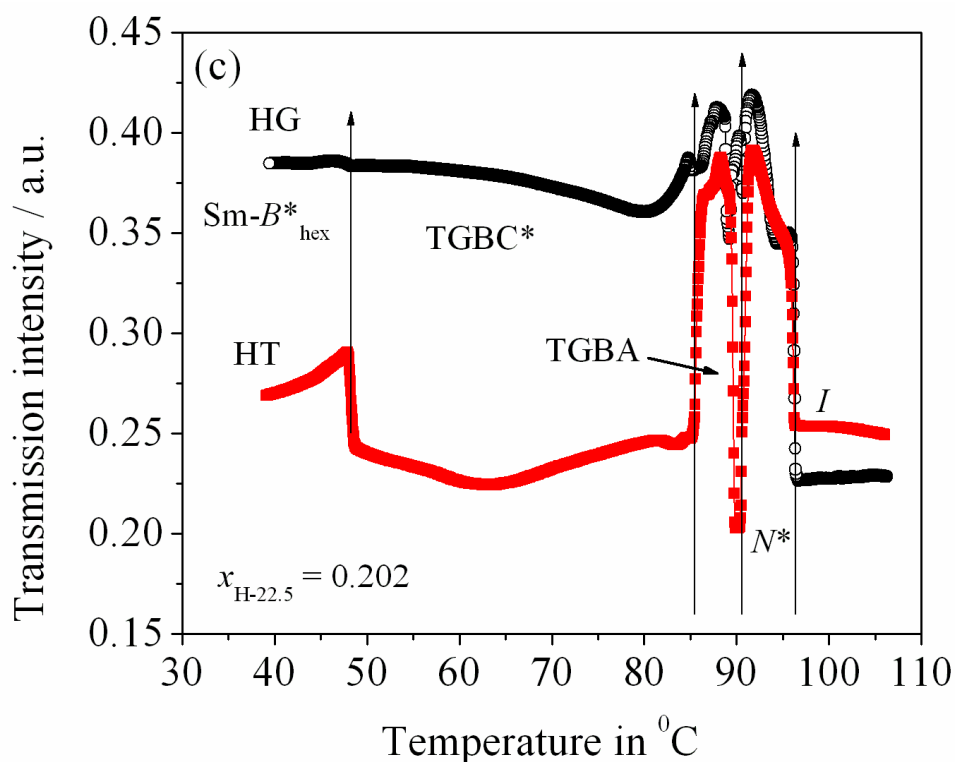


**Figure 7.8 (cont'd).** Temperature-dependent measured optical transmission intensity for mixture component (c)  $x_{\text{H-22.5}} = 0.202$ , and (d)  $x_{\text{H-22.5}} = 0.306$  respectively in planar (open circle) cell and also homeotropic (closed square) cell configuration. Vertical arrows represent the corresponding phase transition.

---

---

system, the optical intensity value rapidly decreases prior to the transition to TGBA phase. However, it increases on entering the TGBA phase. On further cooling, the intensity drops down to a lower value at the transition to TGBC\* phase for the mixtures except for the mixture  $x_{H-22.5} = 0.306$  in planar cell. This reduction in intensity is due to the mutual orientation of two orthogonal helix axes within the smectic blocks of this frustrated phase. Finally, the TGBC\*–Sm- $B^*_{hex}$  phase transition has been identified by a relatively small but continuous change in intensity for the mixture  $x_{H-22.5} = 0.101$  and also for the pure compound. However, it exhibit an abrupt change for the mixture  $x_{H-22.5} = 0.202$  and  $0.306$ . The overall intensity for HG configuration has been found to be quite high than HT configuration for all of the investigated mixtures as well as for the pure compound. Hence, all of the phase transitions in the mixtures including the pure compound have clearly been detected and the related temperatures reveal a close agreement in accordance with the polarizing optical microscopy and DSC study.

## 7.6. Static dielectric parameters measurement

The temperature dependent parallel and perpendicular components of dielectric permittivity ( $\epsilon_{\parallel}$  and  $\epsilon_{\perp}$ ) have been measured by using Agilent 4294A impedance analyzer for the pure rod-like chiral compound along with all mixtures. By applying a signal voltage of 500 mV with a fixed frequency 10 kHz the dielectric parameters were recorded in both the HG and HT cell configurations. Following the values of both  $\epsilon_{\parallel}$  and  $\epsilon_{\perp}$ , the average dielectric permittivity ( $\epsilon_{avg}$ ) along with the dielectric anisotropy ( $\Delta\epsilon = \epsilon_{\parallel} - \epsilon_{\perp}$ ) values have been determined throughout the whole mesomorphic region. Fig. 7.9(a) shows the dielectric parameters for the pure compound (2H6R) while Fig. 7.9(b-d) represents the same for mixtures  $x_{H-22.5} = 0.101, 0.202,$  and  $0.306$  respectively.

It has been observed that the parallel component of permittivity ( $\epsilon_{\parallel}$ ) is higher than the perpendicular component ( $\epsilon_{\perp}$ ) in the vicinity of isotropic to  $N^*$

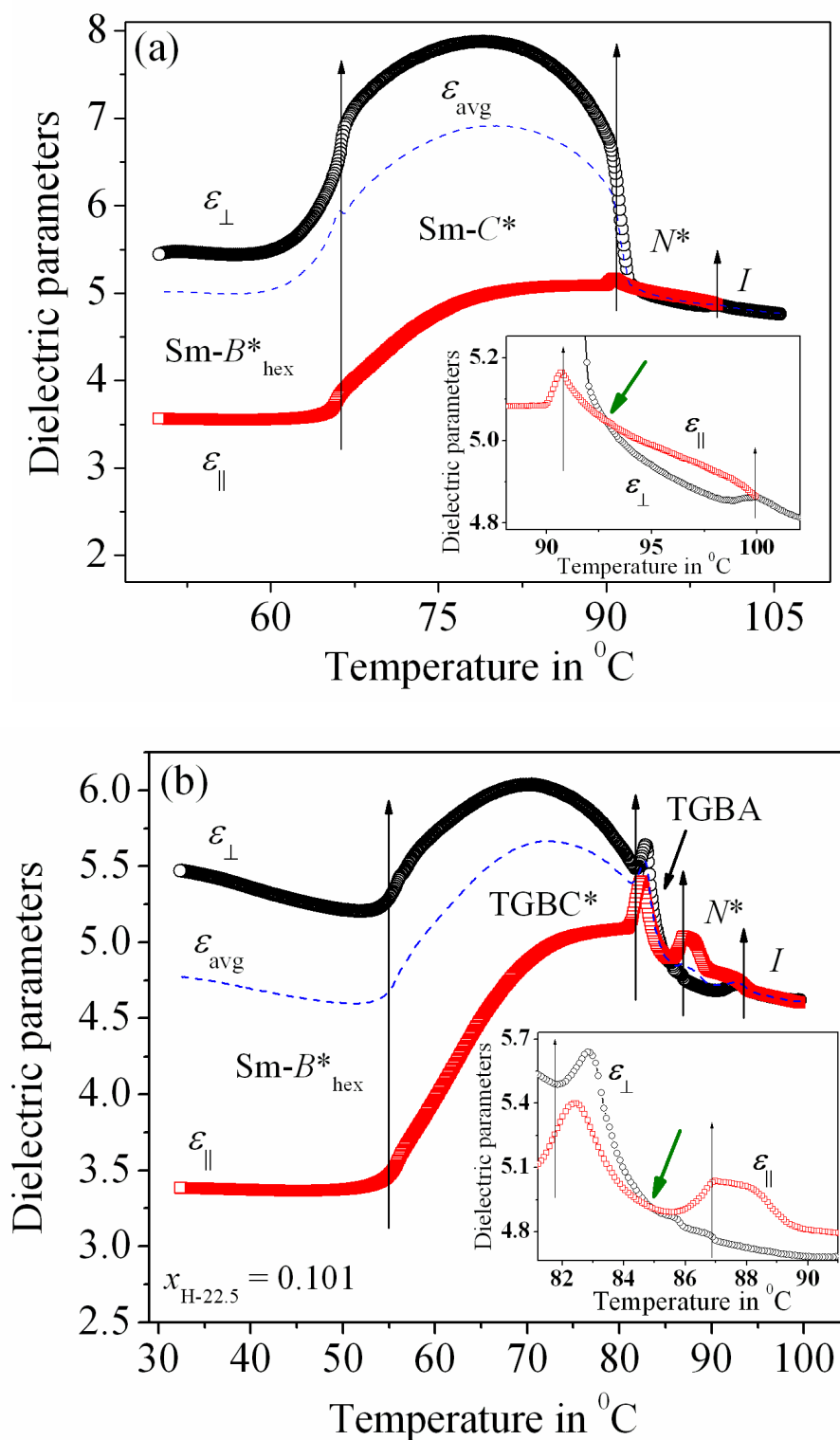


**Figure 7.9.** Temperature-dependent dielectric parameters ( $\epsilon_{\parallel}$ ,  $\epsilon_{\perp}$ ,  $\epsilon_{\text{avg}}$ ) for compound (a) 2H6R, (b)  $x_{H-22.5} = 0.101$  in planar or HG (open circle) cell and also homeotropic or HT (open square) cell configuration. Inset depicts the magnified version of permittivity inversion region. Vertical arrows represent the corresponding phase transition.

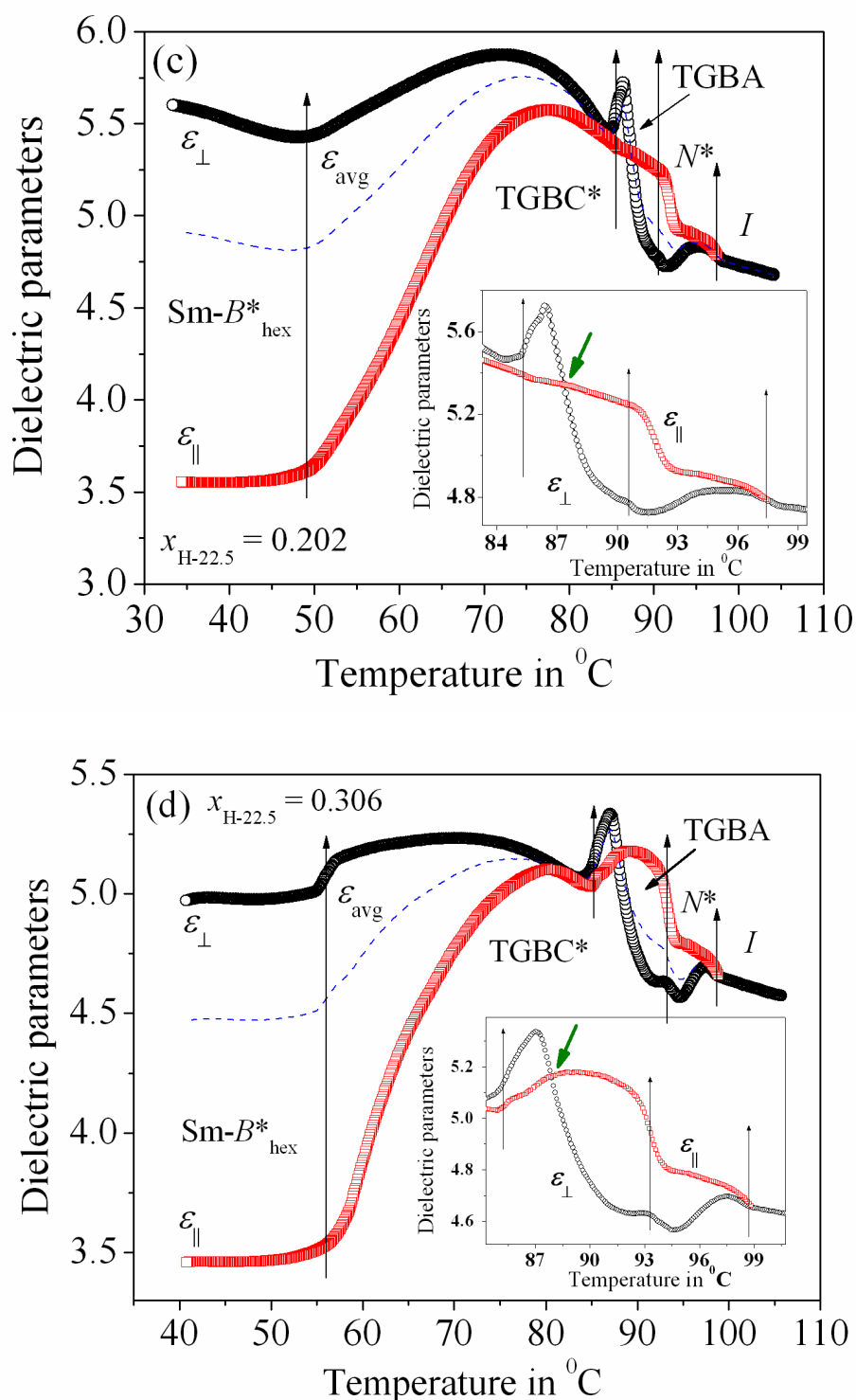


**Figure 7.9 (cont'd).** Temperature-dependent dielectric parameters ( $\epsilon_{\parallel}$ ,  $\epsilon_{\perp}$ ,  $\epsilon_{\text{avg}}$ ) for compound (c)  $x_{\text{H-22.5}} = 0.202$ , (d)  $x_{\text{H-22.5}} = 0.306$  in planar or HG (open circle) cell and also homeotropic or HT (open square) cell configuration. Inset depicts the magnified version of permittivity inversion region. Vertical arrows represent the corresponding phase transition.

phase transition for all the investigated samples, specifying a positive value of the dielectric anisotropy ( $\Delta\varepsilon$ ). On further cooling, the perpendicular component ( $\varepsilon_{\perp}$ ) of permittivity in compound 2H6R represents a sharp augmentation in comparison to the parallel component ( $\varepsilon_{\parallel}$ ) just prior to the transition from  $N^*$  to  $Sm-C^*$  phase. This type of quick enhancement of permittivity value at the transition is a characteristic gesture of  $Sm-C^*$  phase and it follows the temperature dependent Curie-Weiss law:

$$\varepsilon = \frac{C}{T_C - T} \quad (7.1)$$

where  $C$  is the Curie constant and  $T_C$  is the transition temperature. Consequently, the dielectric anisotropy data reveals a crossover from positive to negative value close to the  $N^*$ - $Sm-C^*$  phase transition temperature and this particular inversion temperature ( $T_i$ ) is marked with a green arrow in the inset of Fig. 7.9(a). Further decreasing the temperature, both the  $\varepsilon_{\parallel}$  and  $\varepsilon_{\perp}$  are initially found to increase gradually leading to the formation of a broad maximum within the  $Sm-C^*$  phase and then decreases slowly on approaching the low temperature  $Sm-B^*_{\text{hex}}$  phase, *i.e.*, it follows a convex type pattern in the  $Sm-C^*$  phase. Furthermore, a small but pronounce change in both the dielectric components has been observed at the transition to  $Sm-B^*_{\text{hex}}$  phase and remains more or less constant up to certain lower temperatures. Investigation on the dielectric parameters for the studied mixtures describes a similar kind of appearance for positive dielectric anisotropy in the cholesteric phase as shown in Fig. 7.9(b-d) and the sign inversion of the dielectric anisotropy ( $\Delta\varepsilon$ ) value occurs in the TGBA phase. However, the variation of all the dielectric parameters with temperature in TGBC\* phase has found to be almost identical as observed in the  $Sm-C^*$  phase for 2H6R compound. Moreover, in the  $Sm-B^*_{\text{hex}}$  phase, the magnitude of permittivity accomplishes a lower value in comparison to TGBC\* phase and remains almost constant or slightly increases by lowering the temperature. The thermal variation of the dielectric anisotropy ( $\Delta\varepsilon$ ) data for all the mixtures including the pure compound (2H6R) is depicted

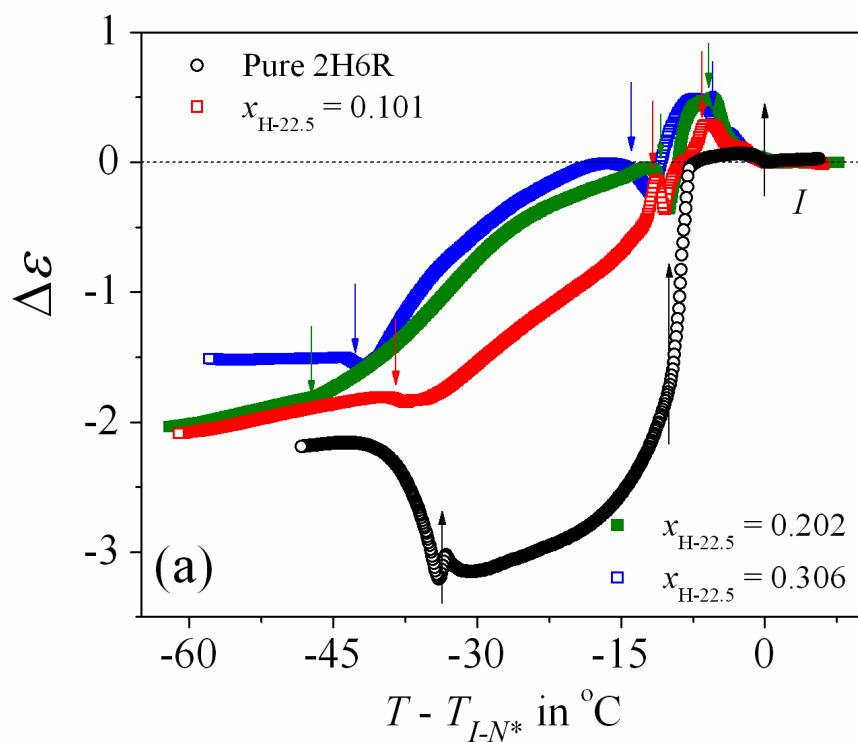


**Figure 7.10.** (a) Variation of dielectric anisotropy ( $\Delta\varepsilon$ ) against the reduced temperature ( $T - T_{I-N^*}$ ). Vertical arrows represent the corresponding phase transition temperatures.

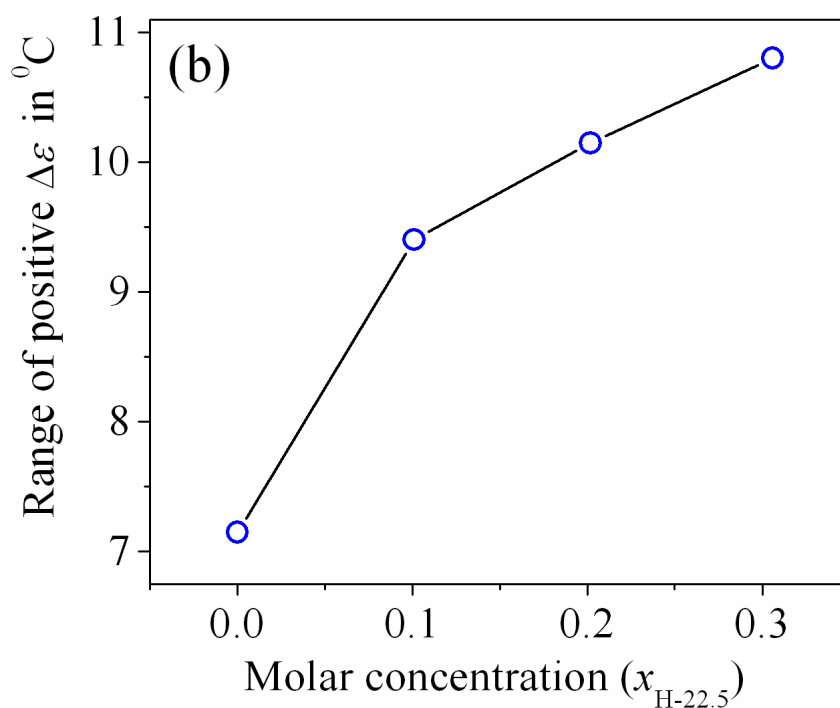


**Figure 7.10.** (b) The concentration variation of positive anisotropy ( $\Delta\varepsilon$ ) range for all the mixture including the pure chiral 2H6R mesogen.

in Fig. 7.10(a). It is quite evident that the  $\Delta\varepsilon$  always assumes a small positive value within the  $N^*$  phase and extend up to a certain temperature range of the TGBA phase. Although, the studied mixtures possess a negative value of the dielectric anisotropy in the TGBC\* phase, the magnitude has found to increase by increasing the amount of bend-shaped compound. However, the  $\Delta\varepsilon$  value is very low in the Sm-C\* phase for the pure compound. Surprisingly, the inversion temperature ( $T_i$ ) of the dielectric anisotropy has a greater influence on the dopant concentration. In the present binary system, the inversion temperature reveals a large difference from the clearing temperature in accordance with the enhancement of the dopant concentration. As a result, the temperature range of the positive dielectric anisotropy region monotonically increases from a value of 7.15 °C for 2H6R to 10.44 °C for the mixture concentration  $x_{H-22.5} = 0.306$  as depicted in Fig. 7.10(b).

## 7.7. Spontaneous polarization study

The field induced spontaneous polarization ( $P_s$ ) value for all the studied samples has been measured by field reversal polarization technique [81-83] in planar aligned ITO coated cell of thickness  $\sim 9 \mu\text{m}$  using a square wave as well as triangular wave AC input voltage ( $V_{pp} = 38\text{V}$ ,  $f = 20\text{Hz}$ ). In case of TGBC\* phase, a single polarization peak has been detected in response to a triangular wave signal voltage and a current response hump appears in the square wave output voltage, indicating the TGBC\* phase as a ferroelectric phase. Fig. 7.11 represents the measured value of  $P_s$  as a function of reduced temperature ( $T/T_C$ ), where  $T_C$  is the corresponding TGBA–TGBC\* phase transition temperature.

Investigation of Fig. 7.11 reveals that the value of  $P_s$  increases with decreasing the temperature and attains a maximum saturation value  $\sim 100 \text{ nC/Cm}^2$  at the Sm-C\* phase of the pure compound 2H6R, divulging a quite good agreement with the obtained value by Węglowska *et al.*[59]. Such high value of polarization is due to the presence of the high tilt angle and strong

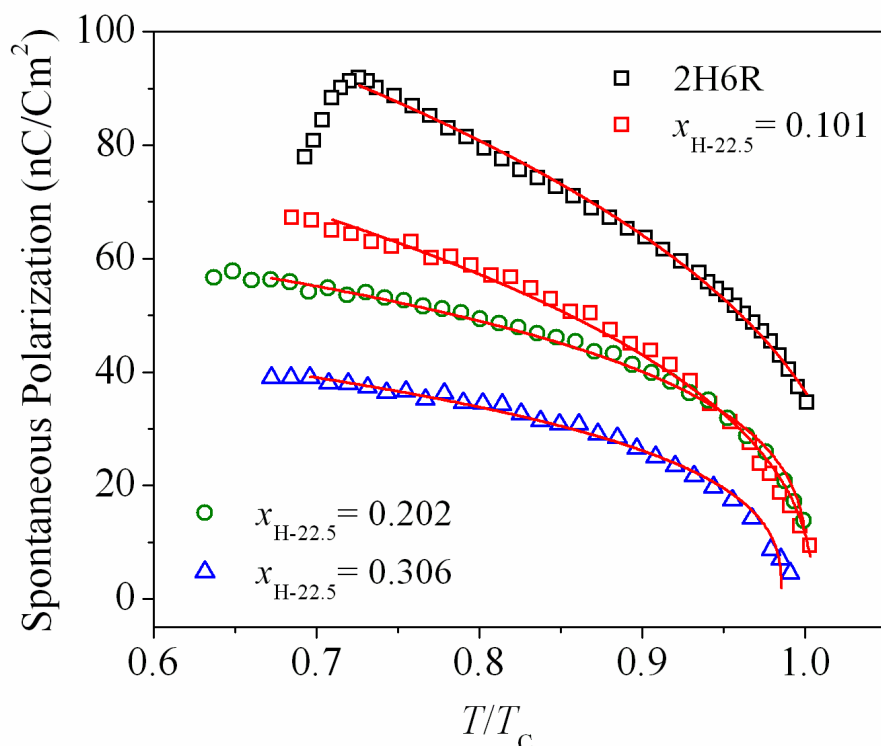


**Figure 7.11.** Value of spontaneous polarization ( $P_s$ ) as a function of reduced temperature for pure compound (2H6R) and all the mixture components. The solid line is a fitting curve of Eq. (7.2).

alignment of the transverse dipole moments in the Sm-C\* phase. The increasing trend of spontaneous polarization values with decreasing temperature may be explained in terms of the reorientation of the dipoles and electrostatic interaction between the neighboring molecules. The induced TGBC\* phases for the mixtures also exhibit a similar variation of polarization with decreasing temperature, having magnitude relatively smaller than that of the pure compound. The maximum value of  $P_s$  has found to be 68.4 nC/Cm<sup>2</sup>, 57 nC/Cm<sup>2</sup> and 40 nC/Cm<sup>2</sup> for the mixture concentrations  $x_{\text{H-22.5}} = 0.101$ , 0.202 and 0.306 respectively. Therefore, the effective value of  $P_s$  is reduced due to the introduction of achiral hockey stick-shaped compound in chiral mesogenic environment. It can be assumed that the mutual orientation of dipole moments for both the molecules is not favorable to each other in the mixtures and hence it reduces the value of spontaneous polarization. However, further increase in the dopant concentration, progressively suppresses the polarization value. The

weakening of core-core correlation between the dissimilar mesogenic compounds may affect the value of  $P_s$  [84-86]. Again the significant disparity in terminal chain length between the guest and host molecules may give rise to an influence on such decrease in  $P_s$  [87,88]. A similar type of decrease in spontaneous polarization value for a number of binary mixtures has been reported earlier [87].

In an attempt to verify the order nature of the TGBA–TGBC\* phase transition the reduced temperature dependent polarization curves have been fitted with following expression [89,90]:

$$P_s = P_0(T_C - T)^\beta \quad (7.2)$$

where  $\beta$  is the critical exponent, both the  $P_0$  and  $\beta$  are adjustable parameters and  $T_C$  represents the TGBA–TGBC\* phase transition temperature. Fitted curves of Eq. (7.2) to the data points are shown in Fig. 7.11 as red lines whereas the fitted parameters are listed in Table 7.2. The extracted critical exponent  $\beta$  assumes a value  $0.26 \pm 0.01$  for the pure compound at the  $N^*$ –Sm- $C^*$  phase transition. This value is very close to the tricritical mean field value ( $\beta = 0.25$ ) indicating a weakly first order nature of the  $N^*$ –Sm- $C^*$  phase transition [91]. Such type of first order transition from the  $N^*$  to Sm- $C^*$  phase has also been reported in literature [92]. Furthermore, the value of  $\beta$  at the TGBA–TGBC\* phase transition has found to be  $\beta = 0.28 \pm 0.02$ ,  $0.30 \pm 0.01$  and

**Table 7.2.** Obtained fit parameter values from the fit to experimental  $P_s$  value with Eq. (7.2) for all of the mixtures including 2H6R compound.

$x_{H-22.5}$	$P_0$ in nC cm <sup>-2</sup>	$T_C$ in °C	$\beta$
0	22.61±0.52	90.09±0.37	0.26±0.01
0.101	17.28±0.89	82.14±0.14	0.28±0.02
0.202	21.31±0.81	85.67±0.13	0.30±0.01
0.306	13.55±0.75	83.55±0.16	0.33±0.02

$0.33 \pm 0.02$  for the mixture concentration  $x_{\text{H-22.5}} = 0.101, 0.202$  and  $0.306$  which shows an increasing pattern. Nevertheless, the related critical exponent  $\beta$  assumes a value  $0.3125$  predicted by the three-dimensional Ising model [91]. Here the critical exponent  $\beta$  for the mixtures  $x_{\text{H-22.5}} = 0.202$  and  $0.306$  are very close to the theoretically predicted value in 3-D Ising model, representing a second order nature of the TGBA–TGBC\* phase transition. Accordingly, the obtained  $\beta$  values demonstrates that by increasing the hockey stick-shaped mesogen in the mixture, drives the weakly first order character of the  $N^*$ –Sm- $C^*$  phase transition to the second order nature of the TGBA–TGBC\* phase transition.

## 7.8. Response time and effective torsional bulk viscosity measurement

The response time ( $\tau$ ) for all the investigated mixtures along with the pure compound (2H6R) are portrayed in Fig. 7.12 against reduced temperature ( $T/T_C$ ). In this system, the value of  $\tau$  describes a monotonic enhancement

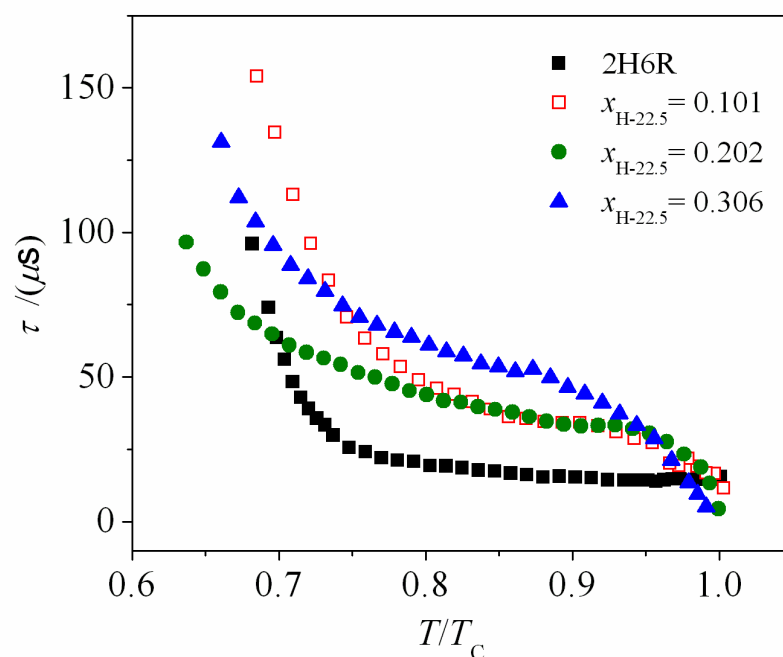


**Figure 7.12.** Reduced temperature dependent value of response time ( $\tau$ ) for pure compound (2H6R) including all the mixture components.

---

---

throughout the TGBC\* phase by lowering the temperature. At a particular reduced temperature, all the mixtures possess a higher value of response time in comparison to that of the pure compound 2H6R. It signifies that due to the introduction of kink-shaped mesogen, effectively hinders the motion of the chiral center. Moreover, the mixture having molar concentration  $x_{\text{H-22.5}} = 0.202$  divulges a slightly lower value ranging between 22–96  $\mu\text{s}$  relative to other mixtures at lower temperature of the TGBC\* phase. Probably the mutual interaction of divergent molecules is responsible to exhibit moderate  $\tau$  value. Therefore, the studied mixtures having negative dielectric anisotropy in the TGBC\* phase, exhibit a response time maximum up to  $\tau_{\text{max}} \sim 152 \mu\text{s}$  are useful for the application in electro-optical devices.

The effective torsional bulk viscosity ( $\eta$ ) is the necessary parameter to investigate the dynamical behavior of chiral LC compound, which is related to the rotational motion of the molecules around the twisted cone of the TGBC\* or Sm-C\* phase. The variation of the effective torsional bulk viscosity with respect to reduced temperature ( $T/T_C$ ) for all the mixtures including 2H6R compound are illustrated in Fig. 7.13 (a). A significant increasing pattern of the effective torsional bulk viscosity ( $\eta$ ) has been observed by lowering the temperature and this trend is almost identical for all the mixtures including the pure compound as depicted in Figure 7.13(a). As the value of  $\eta$  is mostly depends upon the value of  $\tau$ , the thermal variation exhibits almost similar pattern. However, all the investigated mixtures demonstrate slightly higher values of  $\eta$  relative to that of the pure chiral compound. Interestingly, although the value of  $\eta$  does not indicate any systematic variation with increasing achiral dopant concentration in the investigated mixtures, the magnitude of  $\eta$  achieve a maximum value of about 360 mPa S for the mixture concentration  $x_{\text{H-22.5}} = 0.101$ . As a result of the addition of the hockey stick-shaped mesogen into the chiral environment, such a variation of response time as well as torsional bulk viscosity can be described by Boulder model [93,94], according to which, the

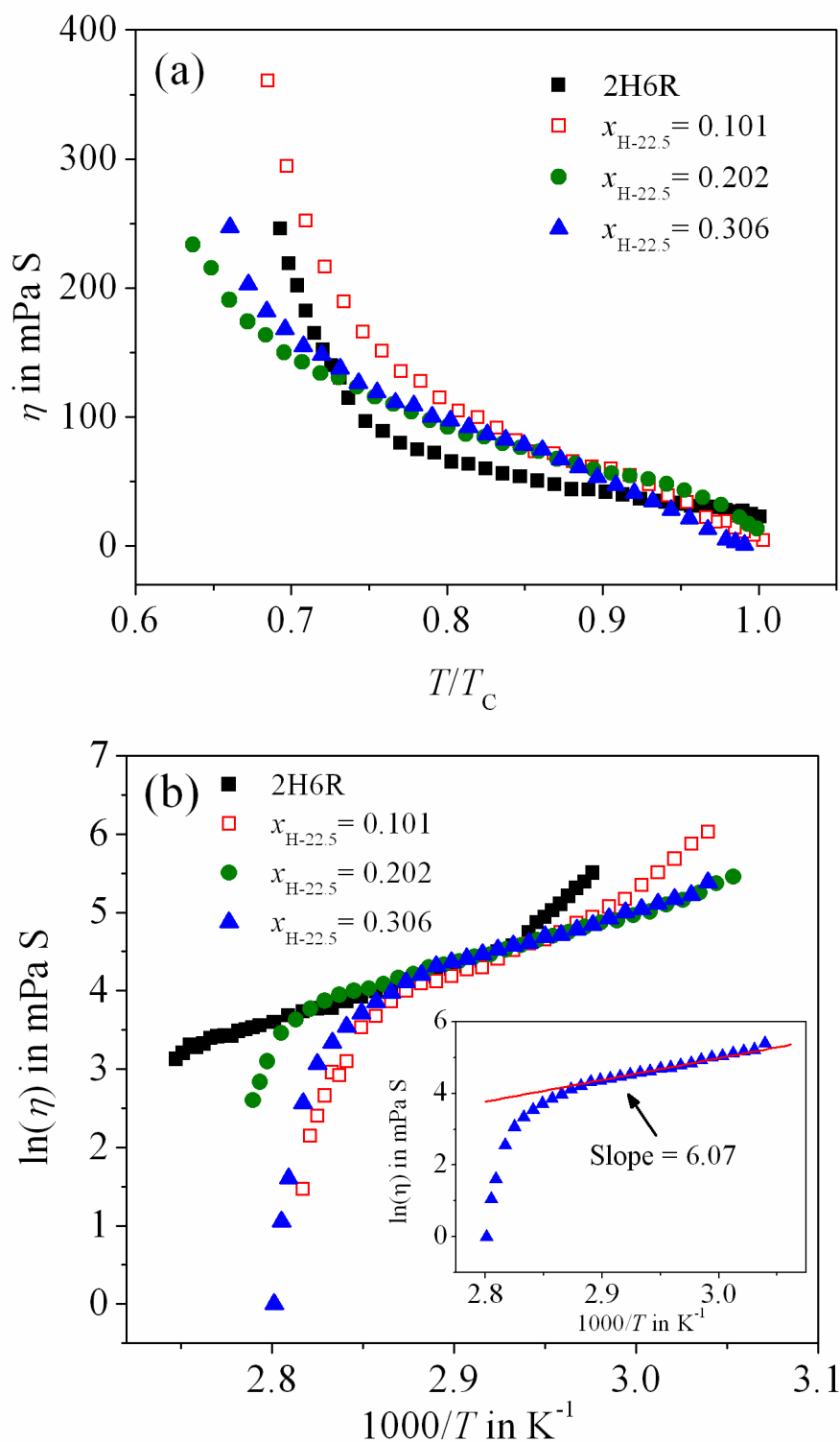


**Figure 7.13.** (a) Reduced temperature dependent value of effective torsional bulk viscosity ( $\eta$ ) for all of the mixtures including the pure compound (2H6R). (b) Arrhenius plot of effective torsional bulk viscosity vs.  $(1000/T)$ . Inset represents the linear fit to Eq. (7.3) to experimental data of  $x_{\text{H-22.5}} = 0.306$ .

chiral molecules in the chiral-achiral system causes a modification in the orientational distributions of the transverse dipole moment of achiral molecules with regard to the polar  $C_2$  axis. In fact, mutual core-core interactions of chiral and achiral components present in the mixtures may favor or oppose the orientation of the transverse dipole moment along the polar  $C_2$  axis [84].

In an effort to determine the associated activation energy ( $E_a$ ), the Arrhenius plot of effective torsional bulk viscosity has been plotted in Fig 7.13(b) for all of the mixtures along with the 2H6R compound and fitted with the following expression [95]:

$$\eta = \eta_0 \exp\left(\frac{E_a}{k_\beta T}\right) \quad (7.3)$$

where  $T$  is the absolute temperature and  $k_\beta$  is the Boltzmann's constant. A representative fit has been shown in the inset of Fig. 7.13(b) for the mixture concentration  $x_{H-22.5} = 0.306$ . The slope of the linear region is calculated and further utilized to estimate the associated activation energy ( $E_a$ ). The obtained values of  $E_a$  are found to be about 58 kJ/mole for pure 2H6R compound in Sm- $C^*$  phase and 68.15 kJ/mole, 52.61 kJ/mole and 50.46 kJ/mole for the mixture concentrations  $x_{H-22.5} = 0.101, 0.202$  and  $0.306$  respectively in TGBC\* phase. These experimental values of  $E_a$  are relatively higher than that of the reported values in mixtures having dissimilar molecular architectures [95].

## 7.9. Dielectric spectroscopy measurement

To recognize the frequency dependent molecular dynamics and their bulk properties associated with chiral phases (especially in frustrated TGB phases), the dielectric spectroscopy measurement has been performed in ITO coated HG (planar) cell for all the mixtures including the pure chiral compound. The frequency dependent real and imaginary parts ( $\epsilon'$  and  $\epsilon''$ ) of the complex permittivity are shown in Fig. 7.14 (a-b) for the mixture component  $x_{H-22.5} = 0.202$  throughout the entire mesophase. In order to determine the relaxation frequency ( $f_R$ ) and other dielectric parameters, the real and imaginary

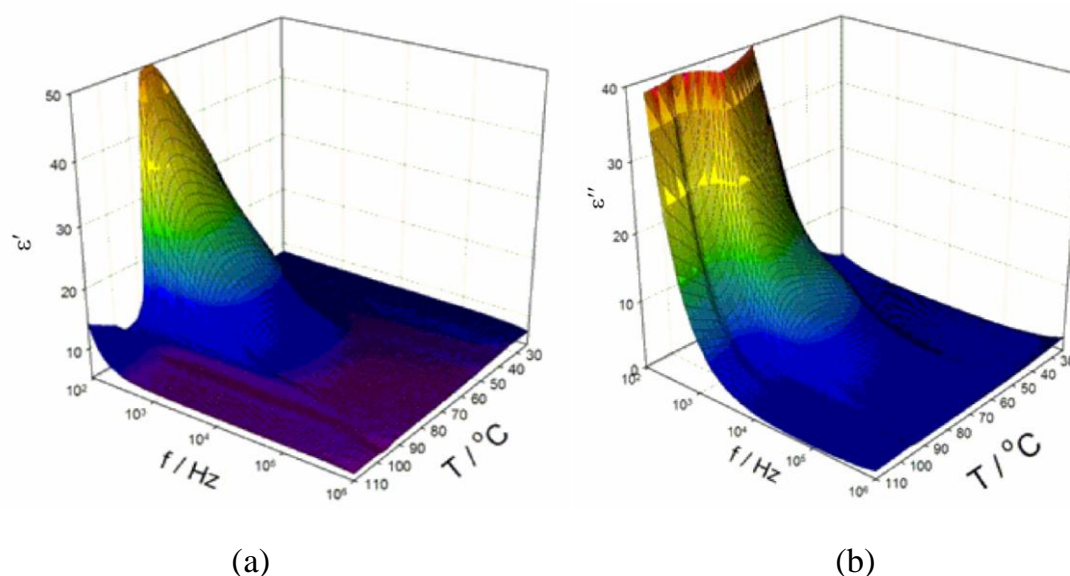
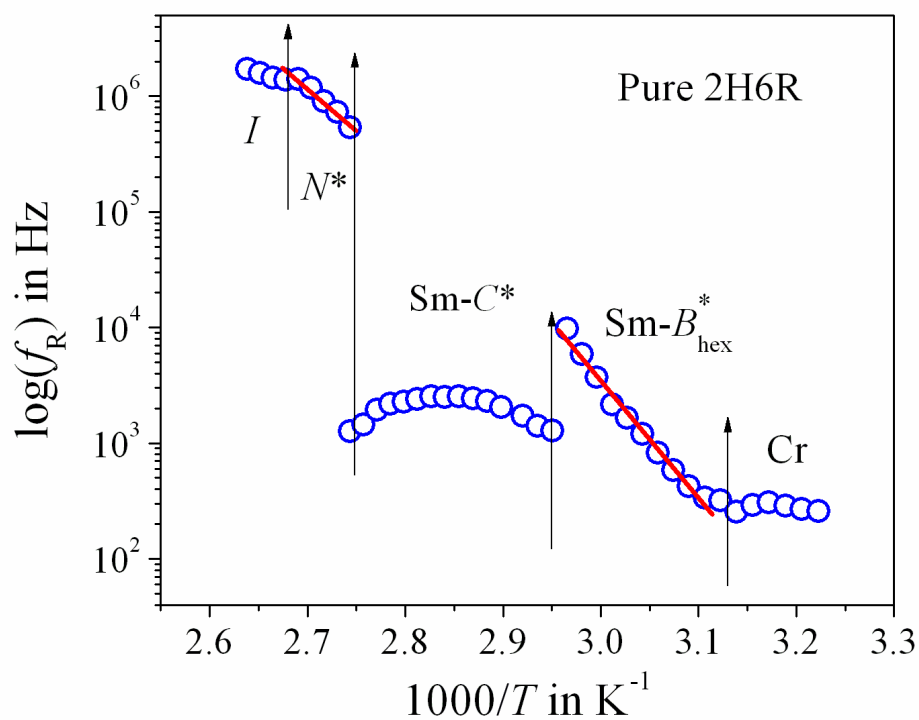


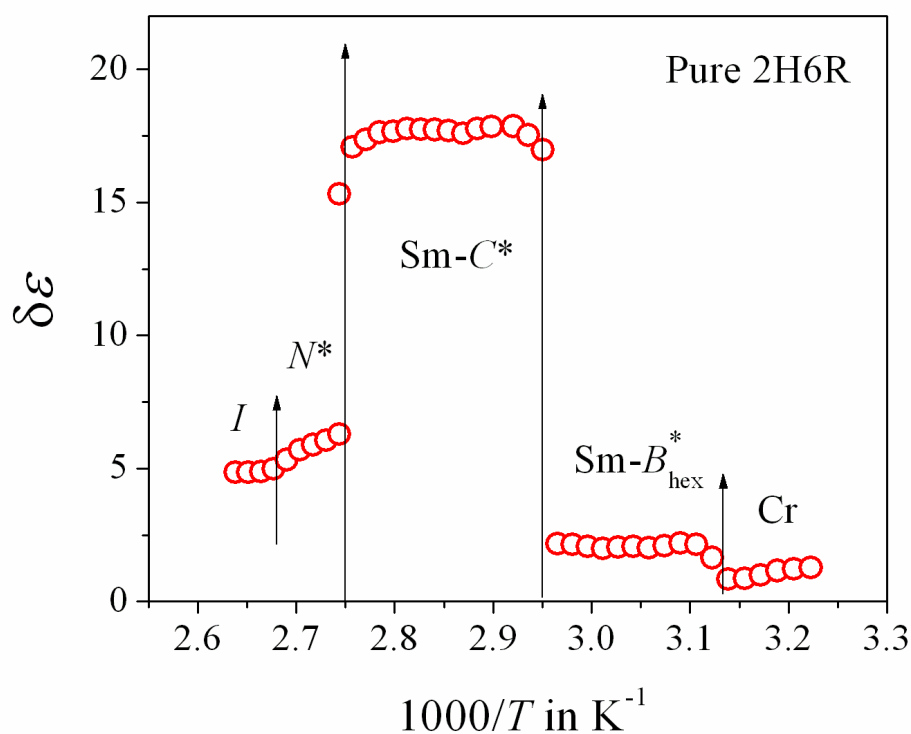
**Figure 7.14.** 3D plot of (a) real (left side) and (b) imaginary (right-side) parts of complex permittivity versus temperature and frequency measured on cooling from the isotropic phase for the mixture component  $x_{\text{H-22.5}} = 0.202$ .

parts of the complex dielectric permittivity were fitted with the Havriliak-Negami (H-N) fitting functions [96-99] as described in chapter 2. The Arrhenius plots of relaxation frequency ( $f_{\text{R}}$ ) and the variation of the dielectric strength ( $\delta\epsilon$ ) have been presented in Fig. 7.15(a,b) for pure 2H6R and one of the binary mixture  $x_{\text{H-22.5}} = 0.202$  in Fig. 7.16(a,b) respectively.

Investigation on the relaxation parameters for pure compound (2H6R) (see Fig. 7.15) clearly describes a single characteristic relaxation mode in the  $N^*$  phase having a higher value of relaxation frequency of about  $\sim 1.2$  MHz with a lower value of dielectric strength  $\delta\epsilon \sim 6$ , though it increases by lowering the temperature at the  $N^*$ -Sm- $C^*$  phase transition. However, the activation energy of this mode is 65.05 kJ/mole, which is a typical range for the  $N^*$  phase. As a consequence, this mode can be recognized as a soft mode of relaxation arises due to amplitude fluctuation of the polarization vector [100]. In case of Sm- $C^*$  phase, another relaxation mode has appeared at the low-frequency region ( $\sim 2.5$  kHz) with a quite higher value of the dielectric strength  $\sim 18$  compared to that of the  $N^*$  phase. Corresponding values of  $f_{\text{R}}$  and  $\delta\epsilon$  remains

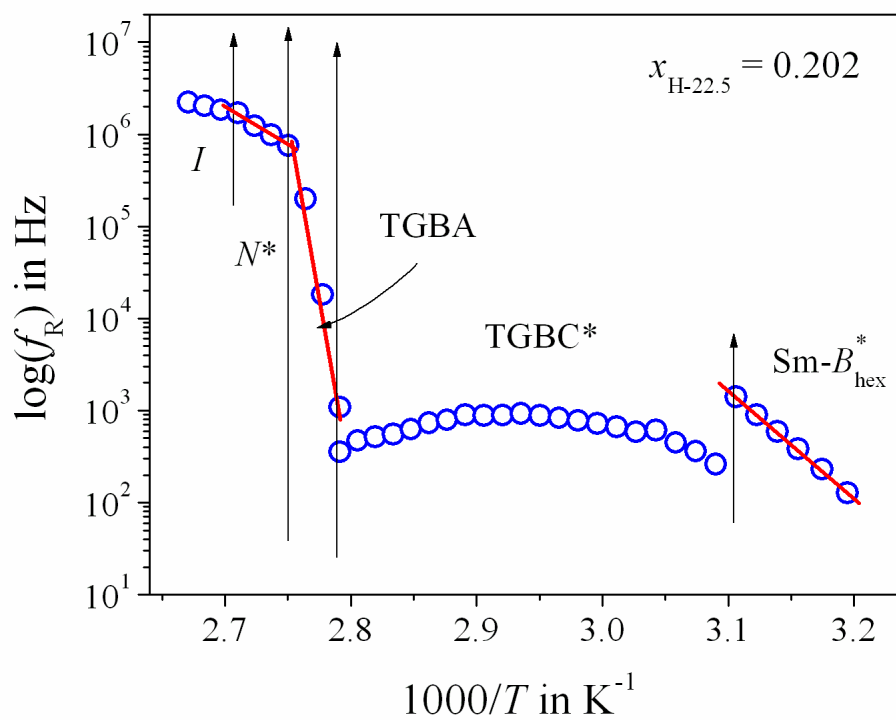


(a)

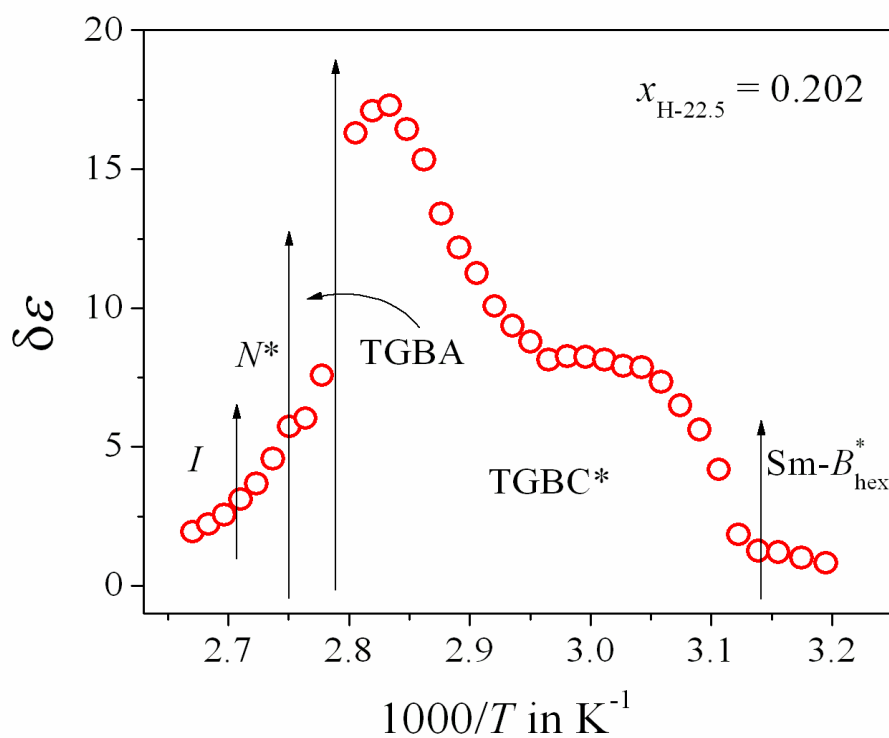


(b)

**Figure 7.15.** (a) Arrhenius plot of the relaxation frequency ( $f_R$ ) and (b) the variation of dielectric strength ( $\delta\epsilon$ ) at different mesophases for the pure compound 2H6R.



(a)



(b)

**Figure 7.16.** (a) Arrhenius plot of the relaxation frequency ( $f_R$ ) and (b) the variation of dielectric strength ( $\delta\epsilon$ ) at different mesophases for the mixture concentration  $x_{H-22.5} = 0.202$ .

---

---

almost constant throughout this mesophase region. Such a low-frequency relaxation phenomena manifests the phase fluctuations of the molecular director around the azimuthal orientation [101-104]. For the sake of convenience, this mode is ascribed as the Goldstone mode. Furthermore, it has been noticed that dielectric strength sharply increases near the  $N^*$ - $Sm-C^*$  phase transition, which is the characteristics behavior of  $Sm-C^*$  phase and this enhancement follows the Curie-Weiss law (Eq. (7.1)). Furthermore, on entering to the  $Sm-B^*_{hex}$  phase, another relaxation mode appears at a moderate frequency of about  $\sim 10$  KHz and monotonically decreases to lower frequency region by decreasing the temperature. Additionally, the dielectric strength is too low about 2.5 and remains constant throughout the mesophase. The activation energy of this mode is 85.52 kJ/mole. Consequently it can be assumed that this mode arises due to collective rotation of molecular director about their short axis [105]. Such weak relaxation mode can be expected for a hard type of smectic phase ( $Sm-B^*_{hex}$ ) in which a rotational hinderence of the molecular director takes place around the long-axis due to the viscosity of the medium. A similar type of observations for the soft mode in  $N^*$  phase and Goldstone mode in  $Sm-C^*$  phase has been reported by Mishra *et al.* [106] and Wojciechoeski *et al.* [107] for two other chiral homologous compounds 4H3R and 1H3R respectively. Therefore our investigated results agreed well with the reported observations, but the only difference is to observe a higher value of dielectric strength in  $Sm-C^*$  phase. Relevance to this, the investigation of the dielectric modes in the binary mixtures demonstrates a similar type of soft mode relaxation in the  $N^*$  phase for all the concentrations (see Fig. 7.16 for  $x_{H-22.5} = 0.202$ ). Corresponding relaxation frequency ( $f_R$ ) and the dielectric strength ( $\delta\epsilon$ ) of this mode are almost identical to that of pure 2H6R. The activation energy of this mode is about 71.59 kJ/mole, demonstrates a slightly higher value than that of the pure compound. However, all the mixtures reveals a similar kind of Goldstone mode in the TGBC\* phase but have a relatively smaller value of relaxation frequency ( $\sim 1.5$  kHz) than the pure compound in

---

---

---

---

the Sm-C\* phase. The magnitude of the dielectric strength has found to be almost identical to that of the pure compound. On the other hand, the relaxation frequency in TGBA phase lies in between the soft mode and Goldstone mode, that seems like a transition from soft mode to Goldstone mode having greater activation energy of about 559.12 kJ/mole for the mixture  $x_{H-22.5} = 0.202$ . Several experimental results on dielectric spectroscopy in TGBA [108-110] and TGBC\* [111,112] phases have been reported earlier. It is anticipated that an electric field induces amplitude fluctuation of the tilt angle and hence a soft mode is visible in the TGBA phase. While in case of TGBC\* phase, the phase fluctuation of the tilt angle leads to a Goldstone mode similar to the Sm-C\* phase. However, the present system divulges an Arrhenius type of relaxation mode in the TGBA phase, leading to a value of  $f_R$  which lies in between that of the soft mode and Goldstone mode. On the basis of spontaneous polarization measurement in the pure compound, the N\*-Sm-C\* phase transition exhibits a weakly first order nature, while due to the influence of hockey stick-shaped compound in the mixtures induces two intermediate TGB phases and drives the TGBA-TGBC\* phase transition to a second order in nature. Moreover, the results from the investigation of relaxation phenomena suggest that the TGBA phase representing an intermediate state which defines a transition from a soft mode of N\* phase to a Goldstone mode of TGBC\* phase. Furthermore, the low temperature Sm-B\*<sub>hex</sub> phase exhibit the similar type of Arrhenius behavior of relaxation frequency for all the mixtures. This is due to the rotational hindrance of the molecular director around the long-axis. However, the activation energy for the low temperature Sm-B\*<sub>hex</sub> phase is about 97.01 kJ/mole which is slightly higher than that of the pure compound.

## 7.10. Conclusion

The optical, dielectric and electro-optical properties have been carried out in the mesophases of a highly tilted ferroelectric chiral liquid crystal compound as well as in three binary mixtures with achiral hockey stick-shaped

---

---

compound H-22.5. Although the pure chiral 2H6R compound possess the phase sequence  $I-N^*-Sm-C^*-Sm-B^*_{hex}$ , two frustrated TGB phases (TGBA and TGBC\*) have found to induced in between cholesteric ( $N^*$ ) and  $Sm-B^*_{hex}$  phases for all of the investigated mixtures. Both the TGB phases preliminary identified by optical textures as well as DSC study. Introduction of small quantity of hockey stick-shaped compound in binary mixtures is sufficient to perturb the helix of chiral compound and produces chiral twisted states (frustrated TGB phases) of higher pitch length. However, the temperature stability of such TGB phases has found to be a quite large range, but exhibit a non-linear dependency on the dopant concentration. Moreover, a sign inversion (positive to negative) of the dielectric anisotropy has been observed for all of the investigated mixtures including the pure compound and the corresponding inversion temperature signifies a remarkable influence on the dopant concentration. The obtained temperature range of the positive dielectric anisotropy region increases progressively by increasing the achiral hockey stick-shaped compound. Additionally, a significant decrease in the field induced spontaneous polarization value has been observed in the mixtures while the response time and effective torsional bulk viscosity exhibit a higher value than that of the pure compound. This is due to the influence of rotational hindrance of the molecules caused by the introduction of kink-shaped mesogen. Additionally, the obtained value of the exponent  $\beta$  suggesting that the mutual interaction between the two divergent molecules drives the weakly first order nature of the  $N^*-Sm-C^*$  phase in pure compound towards the second order nature of the TGBA–TGBC\* phase transition. Investigation on dielectric spectroscopy reveals that the relaxation frequency and associated dielectric strength of the Goldstone mode in TGBC\* phase slightly decreases with increasing the dopant concentration. However, the intermediate TGBA phase represents a transition from soft mode in  $N^*$  phase to a Goldstone mode in TGBC\* phase with a greater value of activation energy. All such integral properties differing from the pure compound is due to the perturbation made by

---

---

the kink-shaped achiral molecule in the chiral-achiral system which opposes the inherent self-organized chiral properties of the pure ferroelectric compound. Consequently, the addition of bent-core molecule within a chiral environment essentially induces the TGB phases with negative dielectric anisotropy, reduces the spontaneous polarization value, and enhances the response time as well as the pitch length. Therefore, the appearances of such experimental results in the present binary system may facilitate clear understanding regarding the formation of quite stable TGB phases.

---

---

## References:

- [1] S.R. Renn, and T.C. Lubensky, *Phys. Rev. A*, **38**, 2132 (1988).
- [2] J.W. Goodby, M.A. Waugh, S.M. Stein, E. Chin, R. Pindak, and J.S. Patel, *Nature*, **337**, 449 (1989).
- [3] P.H. Martinot-Lagarde, *J. Phys.*, **37**, 129 (1976).
- [4] M. Schadt, and W. Helfrich, *Appl. Phys. Lett.*, **18**, 127 (1971).
- [5] G.W. Gray, and S.M. Kelly, *J. Mater. Chem.*, **9**, 2037 (1999).
- [6] M. Klasen, M. Bremer, and K. Tarumi, *Jpn. J. Appl. Phys.*, **39**, L1180 (2000).
- [7] Y. Ouchi, H. Takezoe, and A. Fukuda, *Jpn. J. Appl. Phys.*, **26**, 1 (1987).
- [8] S.T. Lagerwall, in *Ferroelectric and antiferroelectric liquid crystals*, Wiley-VCH, New York (1999).
- [9] N.A. Clark, and S.T. Lagerwall, *Appl. Phys. Lett.*, **36**, 899 (1980).
- [10] H. Kawamoto, *The history of liquid crystal displays, Proc. IEEE.*, **90**, 460 (2002).
- [11] J.A. Castellano, *Liquid Crystals Today*, **1**, 1 (1991).
- [12] D.M. Walba, E. Korblova, L. Eshdat, M. C. Biewer, H. Yang, C. Jones, M. Nakata, M. Talarico, R. Shao, and N. A. Clark, *Journal of the SID*, **15**, 585 (2007).
- [13] D.K. Yang, and S.T. Wu, in *Fundamentals of liquid crystal devices*, John Wiley & Sons Ltd., England (2006).
- [14] B. Bahadur, in *Liquid crystals: applications and uses*, World Scientific, Singapore (1991).
- [15] I. Inoi, in *Organofluorine chemistry, principles and commercial applications*, Plenum Press, New York (1994).
- [16] S.M. Kelly, and M. O'Neill, in *Handbook of advanced electronic and photonic materials and devices*, Academic Press, London (2000).
- [17] J.A. Castellano, in *Liquid gold: the story of liquid crystal displays and the creation of an industry*, World Scientific, Singapore (2005).

- 
- 
- [18] P.P. Crooker, in *Blue Phases. Chirality in Liquid Crystals*, H.S. Kitzerow, C. Bahr, (Eds.), Springer, New York (2001).
- [19] M. Nakata, Y. Takanashi, J. Watanabe, and H. Takezoe, *Phys. Rev. E*, **68**, 041710 (2003).
- [20] T. Chan, C.W. Garland, and H.T. Nguyen, *Phys. Rev. E*, **52**, 5000 (1995).
- [21] C. Ybert, L. Navailles, B. Pansu, F.Rieutord, H.T. Nguyen, and P. Barois, *Europhys. Lett.*, **63**, 840 (2003).
- [22] H.-S. Kitzerow, in *Twist Grain Boundary Phases. Chirality in Liquid Crystals*; H.-S. Kitzerow, C. Bahr, (Eds.), Springer, New York (2001).
- [23] I. Dierking, in *Textures of Liquid Crystals*, Wiley, Germany (2003).
- [24] S.R. Renn, and T.C. Lubensky, *Mol. Cryst. Liq. Cryst.*, **209**, 349 (1991).
- [25] J.W. Goodby, M.A. Waugh, S.M. Stein, E. Chin, R. Pindak, and J.S. Patel *J. Am. Chem. Soc.*, **111**, 8119 (1989).
- [26] S.R. Renn, *Phys. Rev. A*, **45**, 953 (1992).
- [27] W. Kuczynski, and H. Stegemeyer, *Mol. Cryst. Liq. Cryst.*, **260**, 377 (1995).
- [28] O.D. Lavrentovich, Y.A. Nastishin, V.I. Kulishov, Y.S. Narkevich, and A.S. Tolochko, *Europhys. Lett.*, **13**, 313 (1990).
- [29] S.K. Prasad, V.N. Raja, G.G. Nair, and J.W. Goodby, *Mol. Cryst. Liq. Cryst.*, **250**, 239 (1994).
- [30] C.J. Booth, J.W. Goodby, J.P. Hardy, and K.J. Toyne, *Liq. Cryst.*, **16**, 43 (1994).
- [31] Y. Sah, *Mol. Cryst. Liq. Cryst.*, **302**, 207 (1997).
- [32] H. Ocak, B. Bilgin-Eran, D. Guzeller, M. Prehm, and C. Tschierske, *Chem. Commun.*, **51**, 7512 (2015).
- [33] V. Punjani, G. Mohiuddin, S. Kaur, R.K. Khan, S. Ghosh, and S.K. Pal, *Chem. Commun.*, **54**, 3452 (2018).
- [34] T. Seikine, T. Niori, M. Sone, J. Watanabe, S.W. Choi, Y. Takanashi, and H. Takezoe, *Jpn. J. Appl. Phys.*, **36**, 6455 (1997).
- [35] G. Pelzl, S. Diele, and W. Weissflog, *Adv. Mater.*, **11**, 707 (1999).
- 
-

- 
- 
- [36] K.J.K. Semmler, T.J. Dingemans, and E.T. Samulski, *Liq. Cryst.*, **24**, 799 (1998).
- [37] A. Eremin, S. Diele, G. Pelzl, H. Nádas, W. Weissflog, J. Salfetnikova, and H. Kresse, *Phys. Rev. E*, **64**, 051707 (2001).
- [38] T. Sekine, T. Takanishi, T. Niori, J. Watanabe, and H. Takezoe, *Jpn. J. Appl. Phys.*, **36**, 1201 (1997).
- [39] D. Link, G. Natale, R. Shao, J.E. MacLennan, N.A. Clark, E. Korblova, and D.M. Walba, *Science*, **278**, 1924 (1997).
- [40] J. Harden, B. Mbanda, N. Éber, K. Fodor-Csorba, S. Sprunt, J.T. Gleeson, and A. Jákli, *Phys. Rev. Lett.*, **97**, 157802 (2006).
- [41] J. Harden, R. Teeling, J.T. Gleeson, S. Sprunt, and A. Jákli, *Phys. Rev. E*, **78**, 031702 (2008).
- [42] C. Bailey, K. Fodor-Csorba, J.T. Gleeson, S.N. Sprunt, and A. Jákli, *Soft Matter*, **5**, 3618 (2009).
- [43] E. Dorjgotov, K. Fodor-Csorba, J.T. Gleeson, S. Sprunt, and A. Jákli, *Liq. Cryst.*, **35**, 149 (2008).
- [44] S. Dhara, F. Araoka, M. Lee, K.V. Le, L. Guo, B.K. Sadashiva, K. Song, K. Ishikawa, and H. Takezoe, *Phys. Rev. E*, **78**, 050701 (2008).
- [45] D. Wiant, J. T. Gleeson, N. Éber, K. Fodor-Csorba, A. Jákli, and T. Tóth-Katona, *Phys. Rev. E*, **72**, 041712 (2005).
- [46] S. Tanaka, S. Dhara, B.K. Sadashiva, Y. Shimbo, Y. Takanishi, F. Araoka, K. Ishikawa, and H. Takezoe, *Phys. Rev. E*, **77**, 041708 (2008).
- [47] S. Tanaka, H. Takezoe, N. Éber, K. Fodor-Csorba, A. Vajda, and A. Buka, *Phys. Rev. E*, **80**, 021702 (2009).
- [48] M. Alaasar, M. Prehm, S. Poppe, and C. Tschierske, *Chem. Eur. J.*, **23**, 5541 (2017).
- [49] N. Sebastian, S. Belau, A. Eremin, M. Alaasar, M. Prehm, and C. Tschierske, *Phys. Chem. Chem. Phys.*, **19**, 5895 (2017).
- [50] D. Guzeller, H. Ocak, B.B. -Eran, M. Prehm, and C. Tschierske, *J. Mater. Chem. C*, **3**, 4269 (2015).
- 
-

- 
- 
- [51] F.C. Yu, and L.J. Yu, *Chem. Mater.*, **18**, 5410 (2006).
- [52] F.C. Yu, and L.J. Yu, *Liq. Cryst.*, **35**, 799 (2008).
- [53] R. Stannarius, J. Li, and W. Weissflog, *Phys. Rev. Lett.*, **90**, 025502 (2003).
- [54] S.T. Wang, S.L. Wang, X.F. Han, Z.Q. Liu, S. Findeisen, W. Weissflog, and C.C. Huang, *Liq. Cryst.*, **32**, 609 (2005).
- [55] B. Das, A. Pramanik, M.K. Das, A. Bubnov, V. Hamplova, and M. Kašpar, *J. Mol. Struct.*, **1013**, 119 (2012).
- [56] M. Nakata, Y. Takanishi, J. Watanabe, and H. Takezoe, *Phys. Rev. E*, **68**, 041710 (2003).
- [57] S. Taushanoff, K. Van Le, J. Williams, R.J. Twieg, B. K. Sadashiva, H. Takezoe, and A. Jakli, *J. Mater. Chem.*, **20**, 5893 (2010).
- [58] V. Novotná, M. Glogarová, V. Kozmík, J. Svoboda, V. Hamplová, M. Kašpar, and D. Pocięcha, *Soft Matter*, **9**, 647 (2013).
- [59] D. Węłowska, and R. Dąbrowski, *Liq. Cryst.*, **41**, 1116 (2014).
- [60] A. Chakraborty, B. Das, M.K. Das, S. Findeisen-Tandel, M. -G. Tamba, U. Baumeister, H. Kresse, and W. Weissflog, *Liq. Cryst.*, **38**, 1085 (2011).
- [61] A. Chakraborty, M.K. Das, B. Das, U. Baumeister, and W. Weissflog, *J. Mater. Chem. C*, **1**, 7418 (2013).
- [62] I. Dierking, F. Giesselmann, P. Zugenmaier, W. Kuczynskit, S.T. Lagerwall, and B. Stebler, *Liq. Cryst.*, **13**, 45 (1993).
- [63] E. Sackmann, S. Meiboom, L.C. Snyder, A.E. Meixner, and R.E. Dietz, *J. Am. Chem. Soc.*, **90**, 3567 (1968).
- [64] F.D. Saeva, and J. Wysocki, *J. Am. Chem Soc.*, **93**, 5928 (1971).
- [65] H. Finkelmann, and H. Stegemeyer, *Z. Naturforsch.*, **28a**, 799 (1973).
- [66] A. J. Slaney, I. Nishiyama, P. Styring, and J.W. Goodby, *J. Mater. Chem.*, **2**, 805 (1992).
- [67] I. Dierking, F. Giesselmann, P. Zugenmaier, K. Mohr, H. Zschke, and W. Kuczynski, *Z. Naturforsch.*, **49a**, 1081 (1994).
- [68] I. Dierking, and S.T. Lagerwall, *Liq. Cryst.*, **26**, 83 (1999).
- 
-

- 
- 
- [69] P. Archer, and I. Dierking, *Liq. Cryst.*, **33**, 257 (2006).
- [70] W. Kuczynski, and H. Stegemeyer, *SPIE*, **3318**, 90 (1997).
- [71] W. Kuczynski, in *Self-organization in Chiral Liquid Crystals*, W. Kuczynski (ed.), Scientific, Poznan (1997).
- [72] P.A. Pramod, R. Pratibha, and N.V. Madhusudana, *Current Science*, **73**, 761 (1997).
- [73] Y. Galerne, *J. Phys. France II*, **4**, 1699 (1994).
- [74] V. Novotná, M. Glogarová, V. Kozmik, J. Svoboda, V. Hamplová, M. Kašpar, and D. Pociecha, *Soft Matter*, **9**, 647 (2013).
- [75] R. Dhar, *Phase Transit.*, **79**, 175 (2006).
- [76] I. Dierking, *Liq. Cryst.*, **28**, 165 (2001).
- [77] A. Saipa, and F. Giesselmann, *Liq. Cryst.*, **29**, 347 (2002).
- [78] G. Sarkar, M.K. Das, R. Paul, B. Das, and W. Weissflog, *Phase Transit.*, **82**, 433 (2009).
- [79] T. Scharf, in *Polarized Light in Liquid Crystals and Polymers*, Wiley, Hoboken, NJ, (2007).
- [80] A. Prasad, and M.K. Das, *J. Phys.: Condens. Matter*, **22**, 195106 (2010).
- [81] K. Miyasato, S. Abe, H. Takezoe, A. Fukuda, and E. Kuze, *Jpn. J Appl. Phys.*, **22**, L661 (1983).
- [82] A. Pramanik, M.K. Das, B. Das, M. Źurowska, and R. Dabrowski, *Liq. Cryst.*, **42**, 412 (2015).
- [83] S.S. Bawa, A.M. Biradar, K. Saxena, and S. Chandra, *Rev. Sci. Instrum.*, **59**, 2023 (1988).
- [84] R.P. Lemieux, *Chem. Soc. Rev.*, **36**, 2033 (2007).
- [85] R.P. Lemieux, *Acc. Chem. Res.*, **34**, 845 (2001).
- [86] D. Vizitiu, C. Lazar, B.J. Halden, and R.P. Lemieux, *J. Am. Chem. Soc.*, **121**, 8229 (1999).
- [87] S. Jaradat, N.W. Roberts, Y. Wang, L.S. Hirst, and H.F. Gleeson, *J. Mater. Chem.*, **16**, 3753 (2006).
- [88] M.P. Thompson, and R.P. Lemieux, *J. Mater. Chem.*, **17**, 5068 (2007).
- 
-

- 
- 
- [89] J.W. Goodby, J.S. Patel, and E. Chin, *J. Phys. Chem.*, **91**, 5151 (1987).
- [90] A.D.L. Chandani, T. Hagiwara, Y. Suzuki, Y. Ouchi, H. Takezoe, and A. Fukuda, *Jpn. J. Appl. Phys.*, **27**, L729 (1988).
- [91] H. Yurtseven, and D. Kavruk, *Ferroelectrics*, **367**, 190 (2008).
- [92] A. Mikułko, M. Marzec, M.D. Ossowska-Chruściel, J. Chruściel, and S. Wróbel, *Ferroelectrics*, **343**, 209 (2006).
- [93] D.M. Walba, in *Advances in the Synthesis and Reactivity of Solids*, T.E. Mallouk (Ed.), Vol.1, JAI Press Ltd. Greenwich (1991).
- [94] D.M. Walba, and N.A. Clark, *Proc. SPIE, Spatial Light Modulators and Applications II*, **0825**, 81 (1988).
- [95] J. Hemine, A. Daoudi, M. Zazoui, C. Legrand, N. Isaert, A. Elkaaouachi, and H.T. Nguyen, *Spectrosc. Lett.*, **41**, 285 (2008).
- [96] S. Havriliak, and S. Negami, *Polymer* **8**, 161 (1967).
- [97] S. Havriliak, and S. Negami, *J. Poly. Sci.* **14**, 99 (1966).
- [98] P. Nayek, S. Ghosh, S. Roy, T. P. Majumder, and R. Dabrowski, *J. Mol. Liq.*, **175**, 91 (2012).
- [99] S. Ghosh, P. Nayek, S. K. Roy, T. P. Majumder, and R. Dabrowski, *Liq. Cryst.*, **37**, 369 (2010).
- [100] R. Dabrowski, *Liq. Cryst.*, **42**, 783 (2015).
- [101] A. Mishra, M. Zurowska, R. Dabrowski, and R. Dhar, *Phase Transit.*, **87**, 746 (2014).
- [102] A. Levstik, T. Carlsson, C. Filipič, I. Levstik, and B. Žekš, *Phys. Rev. A*, **35**, 3527 (1987).
- [103] P.K. Mandal, B.R. Jaishi, W. Hasse, R. Dabrowski, M. Tykarska, and P. Kula, *Phase Transit.*, **79**, 223 (2006).
- [104] S. Haldar, K.C. Dey, D. Sinha, P.K. Mandal, W. Hasse, and P. Kula, *Liq. Cryst.*, **39**, 1196 (2012).
- [105] M.B. Pandey, S.K. Pandey, U.B. Singh, R. Dhar, M. Tykarska, and R. Dabrowski, *Liq. Cryst.*, **41**, 1879 (2014).
- 
-

- [106] A. Mishra, D. Węglowska, R. Dąbrowski, and R. Dhar, *Liq. Cryst.*, **42**, 1543 (2015).
- [107] M. Wojciechoeski, G. W. Bak, and M. Tykarska, *Scientific Bulletin of the Lodz University of Technology*, **36**, 77 (2015).
- [108] C. Girold, C. Legrand, N. Isaert, P. Pochat, J.P. Parneix, H.T. Nguyen, and C. Destrade, *Ferroelectrics*, **147**, 171 (1993).
- [109] H. Xu, Y.P. Panarin, J.K. Vij, A.J. Seed, M. Hird, and J.W. Goodby, *J. Phys.: Condens. Matter*, **7**, 7443 (1995).
- [110] S. Wrobel, S. Hiller, M. Pfeiffer, M. Marzec, and W. Haase, *Liq. Cryst.*, **18**, 21 (1995).
- [111] F. Bougrioua, N. Isaert, C. Legrand, A. Bouchta, P. Barois, and H.T. Nguyen, *Ferroelectrics*, **180**, 35 (1996).
- [112] M. Ismaili, F. Bougrioua, N. Isaert, C. Legrand, and H.T. Nguyen, *Phys. Rev. E*, **65**, 11701 (2001).

# CHAPTER 8

---

Dielectric spectroscopy and electro-optical  
studies of three homologous bent-core  
mesogens

## 8.1. Introduction

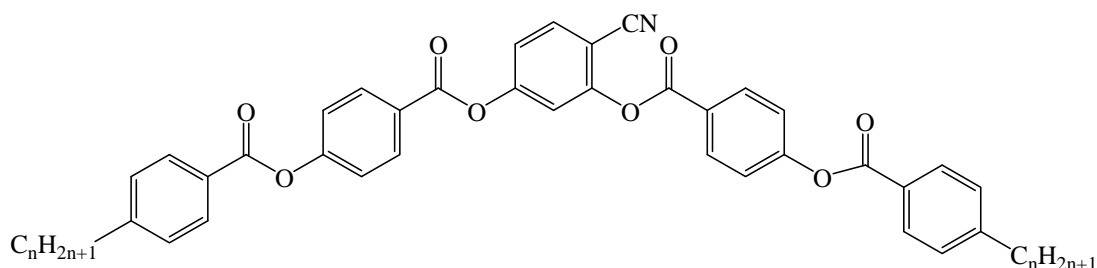
The dielectric spectroscopy study is based on determining the frequency dependent complex permittivity of a substance and is an essential tool for investigating the dielectric and molecular properties of liquid crystals (LC). It deals with the intermolecular interactions and explores different cooperative relaxation processes at the molecular level [1]. Possible experimental outcomes provide the information about the material properties, molecular dynamics as well as macroscopic phase behavior of the system. The contribution of different relaxation processes to the orientational and distortion polarizations in the complex permittivity can be investigated by monitoring the reorientation of polar and non-polar molecules respectively in response to an oscillating electric field. Different LC phases possess one or more relaxation modes, precisely defines several valuable physical properties of that particular mesophase. Investigation of several relaxation processes by dielectric spectroscopy measurement has been found to be a convenient tool for distinguishing different atypical mesophases such as de Vries [2,3], TGBA [4], several sub-phases of AFLCs [5] etc. and also classifying their molecular structure. Over the past few decades, enormous efforts have been devoted to characterize the relaxation modes in different LC systems comprising of calamitic [6-11], discotic [12], T-shaped [13], chiral [14-16] molecules etc. and also some LC system doped with nanoparticles and porous media [17-20]. Usually, the calamitic nematogens are found to exhibit three dielectric relaxation modes at the high-frequency range [7]. So far from the conventional calamitic compounds, the more exciting behavior is expected to observe in bent-core compounds due to steric hindrance induced by the bent geometry which distorts the symmetry of these molecules. Eventually, in recent years, a number of relaxation modes at the lower frequency region have been discovered in those bent-core systems in comparison to that of calamitic compounds [21,22]. Investigation has also been extended to some binary mixtures consisting of

calamitic and bent-core compounds with different concentrations in order to recognize the possible gradual changes of dielectric parameters from the usual bent-core system to that of the regular calamitic LCs [21,22].

In bent-core compounds, different mesophases exhibit unusual and quite rare characteristics depending on the magnitude and position of bend-angle, the size of the molecules as well as the influence of the terminal chain, linking groups, number of aromatic rings, transverse molecular polarity etc. [23,25]. Although the nematic phase is quite rare in the bent-core compounds, the smectic-like strong short-range local ordering in the nematic phase (namely cybotactic nematic mesophase) has been reported in a number of cases [26-34]. Torgova *et al.* recently synthesized a bent-core molecule based on 1,2,4-oxadiazole as a central unit which exhibits the ferroelectric-like response in the nematic phase due to the existence of smectic-like polar cybotactic clusters [35]. Furthermore, Keith *et al.* have reported a homologous series of the bent-core compounds having a broad range of cybotactic nematic phase along with the higher ordered smectic phases and put forward an idea about the molecular orientations within these phases [36]. More surprisingly, Link *et al.* [37] observed the chirality in layers for the bent-core mesogens due to the combined existence of opposite molecular tilt in adjacent layers and polar vector of the molecules, though they are achiral in nature [38]. Investigation of relaxation modes in such mesophases is an attractive issue because the integrating behavior of the molecules in these phases is much deviating from the usual mesophase behavior. Till now several experimental verifications affirm that the presence of Sm-C type polar nano-clusters is responsible for the occurrence of such unusual behavior [39]. Moreover, the macroscopic ferroelectricity has also been observed in these phases [39,40]. Therefore, the presence of these types of unusual mesophases in bent-core compounds is quite encouraging to perform the dielectric spectroscopy study in a broad sense.

In this chapter, the dielectric spectroscopy measurement and the electro-optical investigation has been carried out in detail for three pure achiral bent-core compounds of a homologous series derived from 4-cyanoresorcinol bisbenzoates. The manifestation of the relaxation modes throughout the entire mesomorphic regions has been discussed in light of the molecular associative behavior both in planar and homeotropic alignments. Moreover, a relative comparison of the relaxation modes has been conferred for all of the homologs in accordance with the variation of temperature and chain length as well as the strength of the dipole moments in respective mesophases. To verify the correlation of polar ordering on the relaxation modes, the response to an externally applied DC bias has been measured in these phases. Additionally, the field reversal switching behavior has also been studied to validate the polar ordering of the molecular dipoles and their associative orientation in adjacent layers of the respective mesophases.

## 8.2. Materials



For Compound **1/7**, ( $n = 7$ ): **I** 383 K  $N_{\text{CybC}}$  313.3 K **CybC**

For Compound **1/9**, ( $n = 9$ ): **I** 378.6 K  $N_{\text{CybC}}$  333.5 K **CybC** 325.4 K **Sm-C<sub>(I)</sub>**

For Compound **1/10**, ( $n = 10$ ): **I** 377.6 K  $N_{\text{CybC}}$  351.6 K **CybC** 341.6 K **Sm-C<sub>(I)</sub>**  
330.1 K **Sm-C<sub>(II)</sub>**

Investigation on the dielectric spectroscopy has been carried out for three symmetric bent-core compounds of a homologous series of 4-cyanoresorcinol bisbenzoates having terminally substituted alkyl chains

[36,41], synthesized at the Institute of Organic Chemistry, Martine-Luther-University, Halle, Germany. The structural formulae and phase transition scheme of these homologs (**1/7**, **1/9** and **1/10**) are shown above. All three compounds exhibit a highly correlated nematic phase ( $N_{\text{cybC}}$ ) over a wide temperature range followed by a phase (CybC) comprising of elongated but not completely fused strings of cybotactic clusters. In addition, the higher homologs (**1/9** and **1/10**) exhibit one or more tilted smectic phases ( $\text{Sm-C}_{(\text{I})}$ ,  $\text{Sm-C}_{(\text{II})}$ ). The higher homologous compounds **1/9** and **1/10** exhibits a negative value of dielectric anisotropy, while the compound **1/7** reveals an inversion from positive to negative dielectric anisotropy in the  $N_{\text{cybC}}$  phase [41].

### 8.3. Dielectric spectroscopy study

Different dielectric parameters have been explored for the investigated compounds by using an impedance analyzer Agilent 4294A, in the frequency range 40 Hz-15 MHz with a maximum AC voltage of 0.5 V (RMS) to avoid nonlinear responses. Samples were filled into ITO coated LC cells of thickness  $\sim 9 \mu\text{m}$  having both the planar (HG) and homeotropic (HT) configuration. During cooling from the isotropic phase, the real ( $\epsilon'$ ) and the imaginary ( $\epsilon''$ ) parts of complex dielectric permittivity have been measured in each temperature throughout the entire mesomorphic range at an interval of 1 K, using the well-known procedures as discussed in chapter 2 [42,43]. Obtained dielectric spectrums ( $\epsilon'$  and  $\epsilon''$ ) were fitted with the Havriliak-Negami (H-N) fitting functions [44-47] given below:

$$\epsilon' = \epsilon_{\infty} + \sum_{k=1}^N \frac{\delta\epsilon_k [1 + (2\pi f\tau_k)^{\alpha_k} \cos(\alpha_k\pi/2)]}{[1 + (2\pi f\tau_k)^{2\alpha_k} + 2(2\pi f\tau_k)^{\alpha_k} \cos(\alpha_k\pi/2)]} \quad (8.1)$$

$$\epsilon'' = \frac{\sigma_0}{(2\pi f)^S} + \sum_{k=1}^N \frac{\delta\epsilon_k [1 + (2\pi f\tau_k)^{\alpha_k} \sin(\alpha_k\pi/2)]}{[1 + (2\pi f\tau_k)^{2\alpha_k} + 2(2\pi f\tau_k)^{\alpha_k} \cos(\alpha_k\pi/2)]} \quad (8.2)$$

where  $\delta\epsilon_k$  is the dielectric strength,  $\epsilon_{\infty}$  is the high-frequency limit of the permittivity,  $\tau_k$  ( $= 1/2\pi f_k$ ) is the relaxation time,  $f$  is the corresponding

---

---

relaxation frequency,  $\alpha_k$  and  $\beta_k$  are shape parameters describing the symmetric and non-symmetric broadness of the dielectric dispersion curve respectively, ranging between 0 and 1, and  $k$  is the number of relaxation processes. However,  $\sigma_0$  is related to the DC conductivity, and  $S$  is a fitting parameter responsible for the slope of the conductivity.

The frequency-dependent real ( $\epsilon'$ ) and imaginary ( $\epsilon''$ ) parts of the complex permittivity for the compound **1/7** (at a particular temperature 348 K) have been displayed in Fig. 8.1(a) and Fig. 8.1(b) for the planar (HG) and homeotropic (HT) alignments respectively. Corresponding temperature dependence of the relaxation frequency ( $f_R$ ) for different relaxation processes are presented in Fig. 8.2(a,b) for both cell configurations, while the obtained dielectric strengths ( $\delta\epsilon$ ) are shown in Fig. 8.2(c,d).

The dielectric spectra in Fig. 8.1(a) for HG cell configuration clearly indicates two relaxation peaks, one is marked as  $P_1$ , appeared in a few kHz ranges and a high-frequency peak marked as  $P_{ITO}$  which is independent of temperature and arises due to the influence of ITO resistance in series with the cell capacitance. Conversely, in the case of HT cell, corresponding relaxation modes are depicted in Fig. 8.1(b), representing a high-frequency peak  $H_{ITO}$  along with two temperature-dependent peaks ( $H_1$ ,  $H_2$ ) appeared at the lower frequency side of the  $H_{ITO}$ . Noticeably, the  $P_1$  mode in HG cell has a smaller value of dielectric strength ( $\delta\epsilon$ ) throughout the whole cybotactic nematic ( $N_{CybC}$ ) phase. On the other hand, the  $H_1$  mode in HT cell has appeared at a lower frequency range with a smaller value of dielectric strength which is weakly sensitive to the externally applied bias field. Thus, the reason behind the appearance of  $P_1$  and  $H_1$  modes may be regarded as the rotation of the molecules around their long and short axes respectively [48]. Hence, in case of transverse component (HG cell), the effect of the molecular rotation around the long axis leads to a high-frequency relaxation peak, while in longitudinal

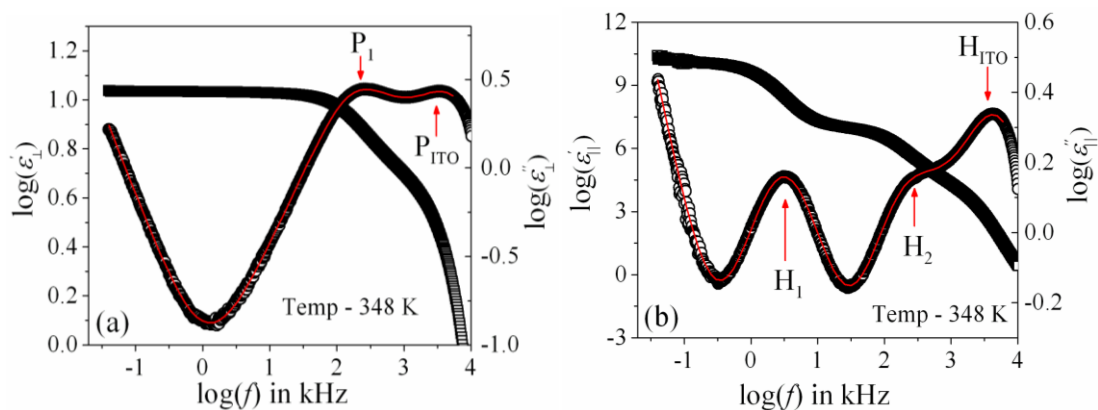


**Figure 8.1.** Frequency dependence of the real ( $\epsilon'$ ) and imaginary ( $\epsilon''$ ) parts of the permittivity for compound **1/7** in (a) HG or planar and (b) HT or homeotropic cell configurations. Red solid lines represent the fitting curve to data points with Eq. (8.2).

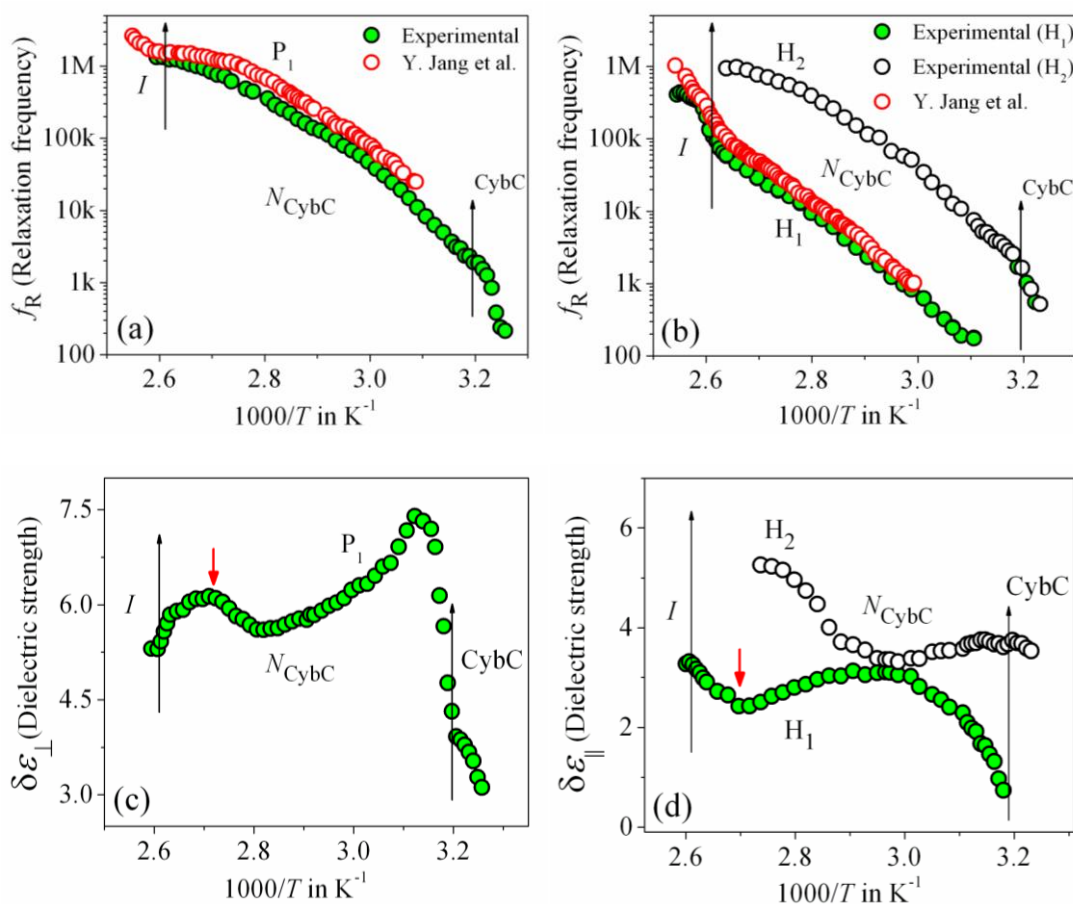


**Figure 8.2.** Temperature dependence of relaxation frequency ( $f_R$ ) and dielectric strength ( $\delta\epsilon$ ) for compound **1/7** in (a,c) planar and (b,d) homeotropic cells respectively. Vertical arrows define corresponding phase transition temperatures.

---

---

component (HT cell) the same about short axis leads to a low-frequency relaxation peak. Similar observation has been reported by Jang *et al.* [48] in planar and homeotropic orientations. The extracted experimental values for the relaxation frequency ( $f_R$ ) in the present system agrees quite well with others in both the cell alignments as represented in Fig. 8.2(a,b). However, in addition to  $H_1$  relaxation mode in HT cell, the present system offers a second mode ( $H_2$ ) at higher frequency region. By lowering the temperature, the value of relaxation frequency ( $f_R$ ) for this mode progressively decreases towards the lower frequency region throughout the  $N_{CybC}$  phase. However, the value of  $f_R$  is found to be nearly equal to that of the  $P_1$  mode in the planar configuration and also reveals a weak dependence upon the applied biasing field. Hence, it can be assumed that due to the superposition of different independent rotation of polar molecules around their long axis or around the principle director implements this relaxation mode. Earlier investigations of Tadapatri *et al.* for a similar type of molecule with alkoxy terminal chain, also support the present outcomes [49,50]. This type of high-frequency relaxation mode in longitudinal component appears in GHz range for usual calamitics but downshift of this mode in the bent-core compound may be assigned due to molecular size and very high viscosity of the sample. Moreover, a quite analogous identification of three relaxation peaks ( $H_1$ ,  $H_2$  in HT cell, and  $P_1$  in HG cell) has also been observed in some bent-core nematic as well as in mixtures with calamitics [51-53]. Furthermore, in the present investigation, the dielectric strength ( $\delta\varepsilon$ ) for the  $P_1$  and  $H_1$  modes has found to demonstrate an anomalous behavior at a region below  $\sim 15$  K from the isotropic–nematic ( $I-N_{CybC}$ ) phase transition as shown in Fig. 8.2(c,d). The value of  $\delta\varepsilon$  is found to initially increase in HG cell while it reduces in HT cell followed by the  $I-N_{CybC}$  phase transition. Surprisingly, near the temperature 365 K (marked with red arrow) both of the data for  $\delta\varepsilon$  has been observed to reveal a kink and follow the opposite pattern thereafter. The previous investigation of this compound also unveils an

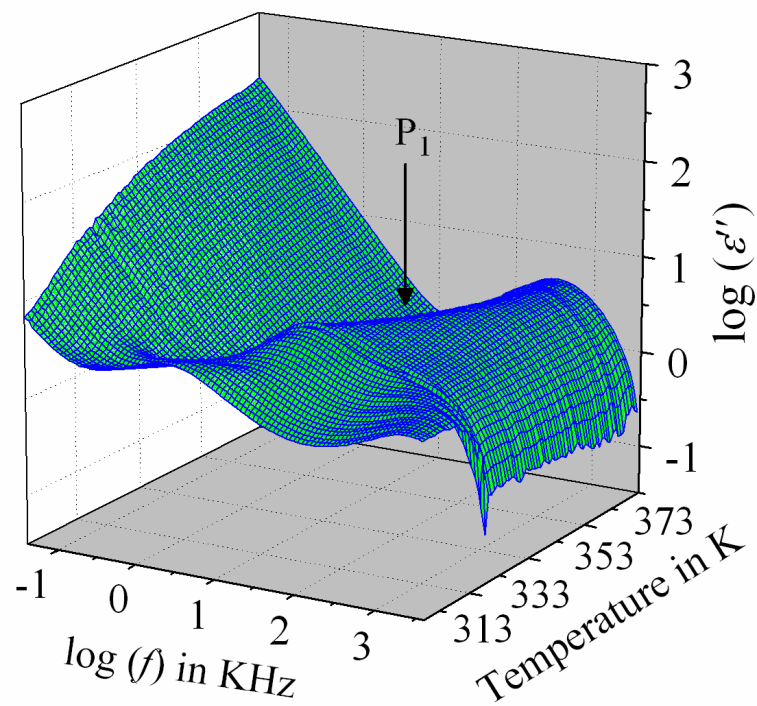
---

---

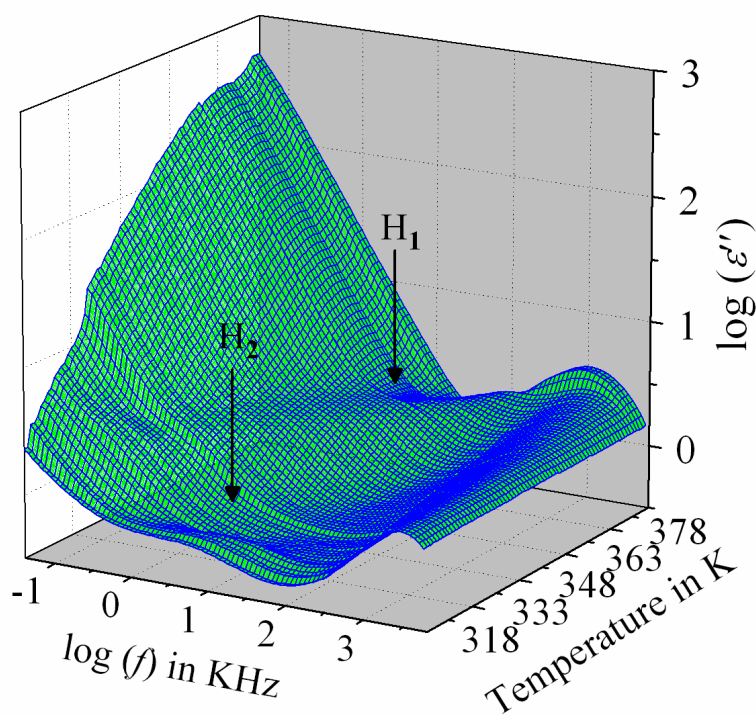
inversion in positive to negative dielectric anisotropy at  $\sim 18$  K below the  $I-N_{\text{CybC}}$  phase transition temperature [41]. Due to the presence of Sm-C type polar nano-clusters in the nematic phase and the mutual alignment of these clusters leads to such a behavior. However, it has been reported that this inversion of dielectric anisotropy is also dependent on frequency and the nature of corresponding crossover frequency is highly non-Arrhenius type at lower temperature [48,54]. Recently, Jang *et al.* explained that inversion by assuming the value of anisotropic Kirkwood correlation factors ( $g_{\parallel}$  and  $g_{\perp}$ ) not equal to 1, rather  $g_{\parallel}$  decreases and  $g_{\perp}$  increases than unity, *i.e.*,  $g_{\parallel} < 1$  and  $g_{\perp} > 1$  [54].

The frequency-dependent imaginary ( $\epsilon''$ ) part of the complex permittivity for the second homologous compound **1/9** is shown in Fig. 8.3(a,b) for both the HG and HT cell alignments respectively. Corresponding temperature-dependent relaxation frequencies ( $f_{\text{R}}$ ) and the dielectric strengths ( $\delta\epsilon$ ) are plotted in Fig. 8.4(a,b) and Fig. 8.4(c,d) respectively, as a function of  $1000/T$ .

In this case, the frequency dependent imaginary component of permittivity ( $\epsilon''$ ) for HG cell is characterized by a single relaxation peak ( $P_1$ ). On the other hand in HT cell, the dielectric modes are portrayed by two relaxation peaks-  $H_1$  and  $H_2$ . The  $H_1$  mode appears at a frequency about 100 kHz and found to decrease throughout in  $N_{\text{CybC}}$  phase by lowering the temperature. However, the other mode ( $H_2$ ) arises near the  $N_{\text{CybC}}-C_{\text{ybC}}$  phase transition but at relatively high-frequency region than  $H_1$  mode. On a close look to the temperature variation of relaxation frequency for  $P_1$  mode, it reveals an almost same variation as observed in the planar-aligned compound **1/7**. Moreover, it has been found that the dielectric strength ( $\delta\epsilon$ ) of this peak is strongly dependent on temperature, *i.e.*, it gradually increases its magnitude in the nematic phase with decreasing the temperature. Further lowering the temperature, the value of  $\delta\epsilon$  decreases sharply in the Sm- $C_{(I)}$  phase via the



(a)



(b)

**Figure 8.3.** Frequency dependence of the imaginary ( $\epsilon''$ ) parts of the permittivity for compound **19** in (a) HG or planar and (b) HT or homeotropic cell configurations.

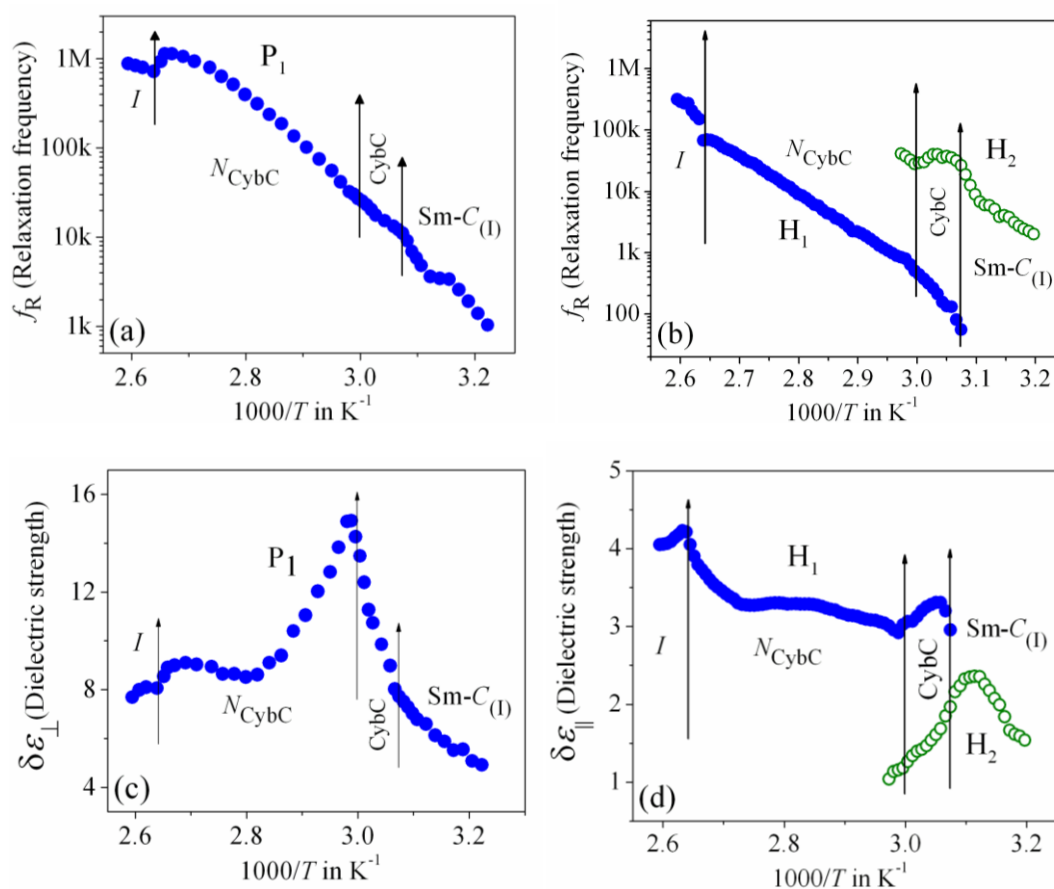


**Figure 8.4.** Temperature dependence of relaxation frequency ( $f_R$ ) and dielectric strength ( $\delta\epsilon$ ) for compound **1/9** in (a,c) planar and (b,d) homeotropic cells respectively. Vertical arrows define the corresponding phase transition temperatures.

$CybC$  phase. A similar type of observation for the dielectric strength has been reported by Eremin *et al.* at the transition to a para-electric to anti-ferroelectric  $Sm-C$  phase transition for a bent-core compound [55]. In the  $N_{CybC}$  phase there exist a number of small-sized cybotactic clusters with  $Sm-C$  type layer structure which correspond to a strong short-range correlation among the molecules and the cluster size is being elongated by lowering the temperature [36]. Thus, the appearance of this mode can be assigned due to rotation of molecules within the clusters around the long axis of the director in the nematic phase. However, it can be considered that the anti-parallel correlation of the molecular dipoles along the long axis essentially affecting this mode in  $Sm-C_{(I)}$  phase. The  $CybC$  phase is a phase comprising elongated but not completely

---

---

fused strings of cybotactic clusters, the anti-parallel dipolar alignments are observed to be initiated from the  $N_{\text{CybC}}$ –CybC phase transition. Although, the compound **1/9** possesses a larger molecular size and dimension of the cluster in comparison to that of the compound **1/7**, the temperature-dependent variation of the cluster size as well as the molecular tilt plays a significant role in the entire  $N_{\text{CybC}}$  mesophase. The tilt angles of these molecules enhance from  $15^\circ$  in  $N_{\text{CybC}}$  phase to  $32^\circ$  in a perfectly aligned Sm- $C_{(I)}$  phase through the CybC phase in which molecular tilt angle is  $28^\circ$  [36]. Therefore, it can be assumed that in the  $N_{\text{CybC}}$  phase the assembly of molecular dipole moments associated with Sm- $C$  type polar clusters forms a ferroelectric type of alignment in neighboring layers and thereby increases the strength of the relaxation modes by decreasing the temperature followed by the elongation of the cluster size. Consequently, the value of  $\delta\varepsilon$  enhances gradually in the  $N_{\text{CybC}}$  phase. Further lowering the temperature, the clusters are fused into elongated ribbon-like aggregates in the CybC phase and orient the dipole moments in such a way that an anti-ferroelectric type of ordering of the dipoles develops in adjacent layers. The strong dipole-dipole interaction favors to align the molecular dipole moments in adjacent layers with an anti-parallel ordering. This anti-ferroelectric type of orientation has been observed to continue throughout the Sm- $C_{(I)}$  phase which causes an effective decrease in  $\delta\varepsilon$  value in the CybC and Sm- $C_{(I)}$  phases. Almost identical type of behavior has been observed by Guo *et al.* for a bent-core compound at the transition from Sm- $AP_R$  phase to anti-ferroelectric Sm- $AP_A$  phase [56]. Again, this mode is sensitive to the external bias field. From the Fig. 8.5(a) it is clearly evident that the strength of the mode  $P_1$  is further increases by increasing the bias field without any change of  $f_R$ . This indicates that this mode ( $P_1$ ) develops due to the molecular rotation about the long axis and additionally influenced by the local anti-ferroelectric ordering of the molecular dipoles in adjacent layers. A complete realization of this issue has been drawn from the field-induced polarization technique as described later. Further increasing the field strength, the trivial appearance of an additional

---

---

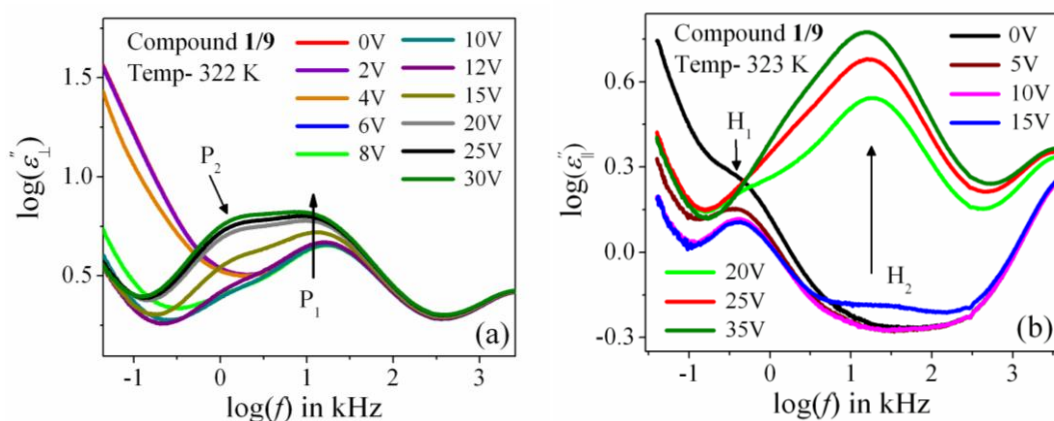


**Figure 8.5.** The variation of frequency-dependent imaginary ( $\epsilon''$ ) part of permittivity with the bias voltage for compound **1/9** in (a) planar and (b) the homeotropic alignment cells.

peak ( $P_2$ ) has been observed in the  $Sm-C_{(I)}$  phase at a lower frequency side. This suggests that there also exist an additional rotational motion of the molecules around the short axis or bow axis, as well as it has an effect of local polar ordering that has been apparently recognized after the application of external voltage. Nevertheless, in case of HT cell, both  $H_1$  and  $H_2$  peaks have a relatively smaller dielectric strength than  $P_1$  mode and having a weak temperature dependency. However, a noticeable change in  $\delta\epsilon$  has been found in the CybC and  $Sm-C_{(I)}$  phases. The relaxation frequency for  $H_1$  mode is quite similar to that of the compound **1/7** in  $N_{CybC}$  phase. Therefore, this mode is also assigned to the molecular relaxation, appearing due to the end-over-end rotation of molecules around their short axis or bow axis. An identical observation has been reported in a bent-core compound having similar molecular core structure but with alkoxy terminal chain [50]. Moreover, the signature of the mode  $H_2$  has found from the CybC mesophase relatively at higher frequency region than  $H_1$  and it extends to the entire  $Sm-C_{(I)}$  phase. Interestingly, the strength of this mode is highly sensitive to the external bias field, *i.e.*, the value of  $\delta\epsilon$  increases with increasing the bias voltage, while it is very small in absence of the field as observed from Fig. 8.5(b). Hence, this mode can be attributed to a collective mode of relaxation in which anti-

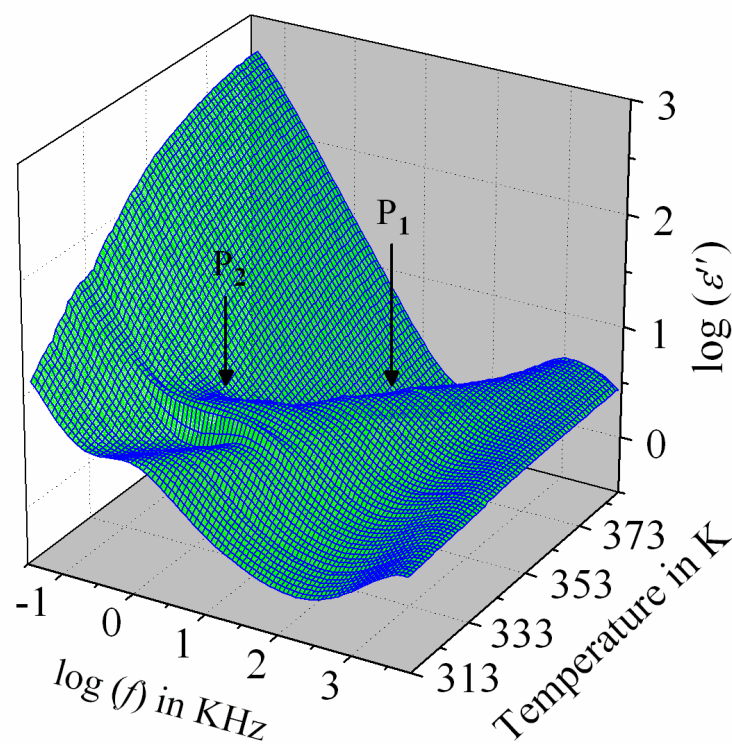
---

---

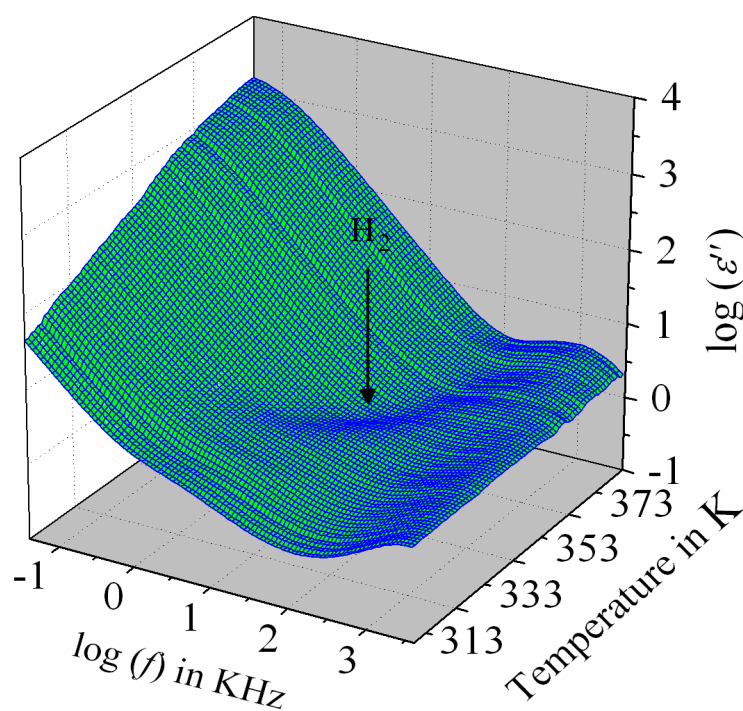
ferroelectric domains of polar molecules in Sm- $C_{(I)}$  phase transforms to ferroelectric domains by inducing external DC field, thereby effectively increases the strength. It has been observed from Fig. 8.5 that the electric field response of relaxation modes is too much strong in HT cell than that of the HG cell. It demonstrates that the contribution of effective molecular dipole moments in HT cell is greater compare to HG cell subsequent to the application of bias voltage. Hence, due to the anti-parallel alignment of the molecular dipoles, the effective dielectric strength initially shows much smaller value in absence of the field. On increasing the external field, the dipolar groups tend to reorient progressively parallel to the field direction, while the long molecular axes remain randomly distributed around the field direction. This results an enhancement of the dielectric strength along the field direction with increasing the field strength. However, in case of HG cell, the component of the dipole moment parallel to the field direction is too weak compared to that in HT cell and therefore, not so sensitive to the external bias field.

The frequency-dependent imaginary ( $\epsilon''$ ) part of the dielectric permittivity for the higher homologue **1/10** at different temperature is shown in Fig. 8.6(a,b) for both the HG and HT cells respectively. Corresponding temperature-dependent relaxation frequencies ( $f_R$ ) and the dielectric strengths ( $\delta\epsilon$ ) are plotted in Fig. 8.7(a,b) and Fig. 8.7(c,d) respectively, as a function of  $1000/T$ .

In planar configuration, a high-frequency peak ( $P_1$ ) appeared in a frequency range identical to the lower homologous compounds, with a relatively large value of  $\delta\epsilon$ . During cooling from the isotropic phase, the value of  $\delta\epsilon$  gradually increases in  $N_{CybC}$  phase and found to decrease in the CybC and Sm- $C_{(I)}$  phases. This observation is quite similar to the compound **1/9** in HG cell. Moreover, in the Sm- $C_{(I)}$  phase, an additional relaxation mode ( $P_2$ ) with a very close value of  $f_R$  has been observed. By applying an external bias field,



(a)



(b)

**Figure 8.6.** Frequency dependence of the imaginary ( $\epsilon''$ ) parts of the complex permittivity for compound 1/10 in (a) HG or planar and (b) HT or homeotropic configuration cells.

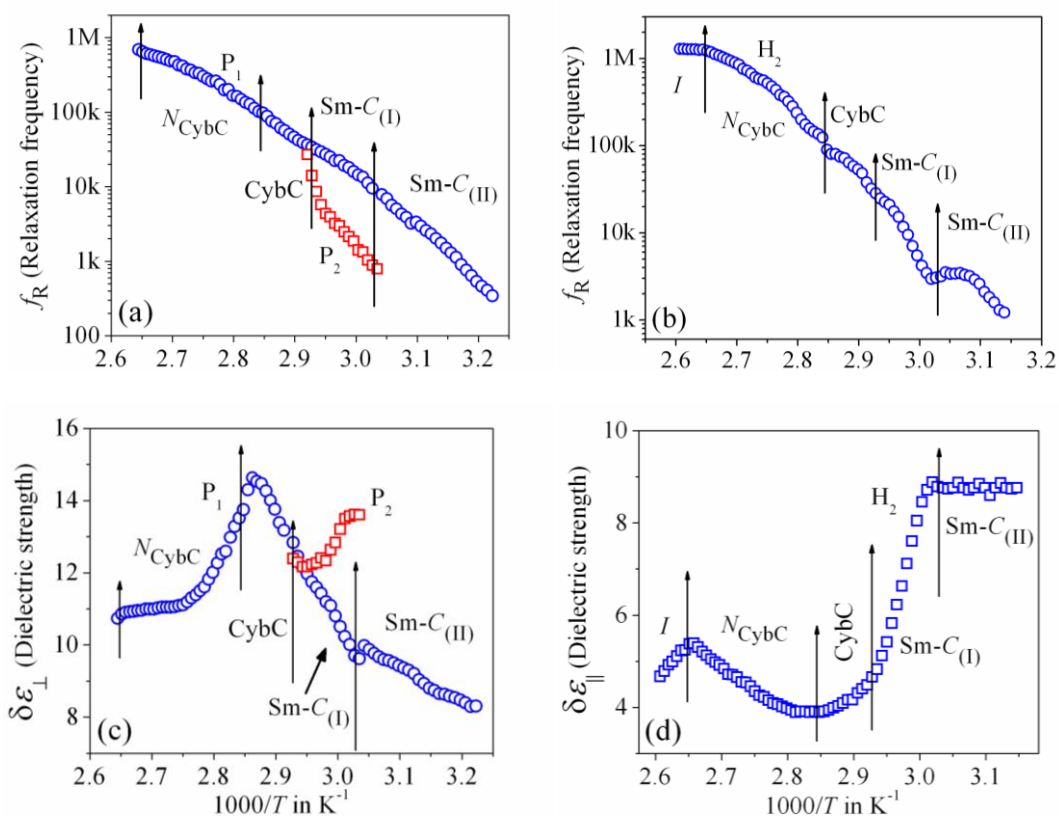


**Figure 8.7.** Temperature dependence of relaxation frequency ( $f_R$ ) and dielectric strength ( $\delta\epsilon$ ) for the compound 1/10 in (a,c) planar and (b,d) homeotropic cells respectively. Vertical arrows define the corresponding phase transition temperatures.

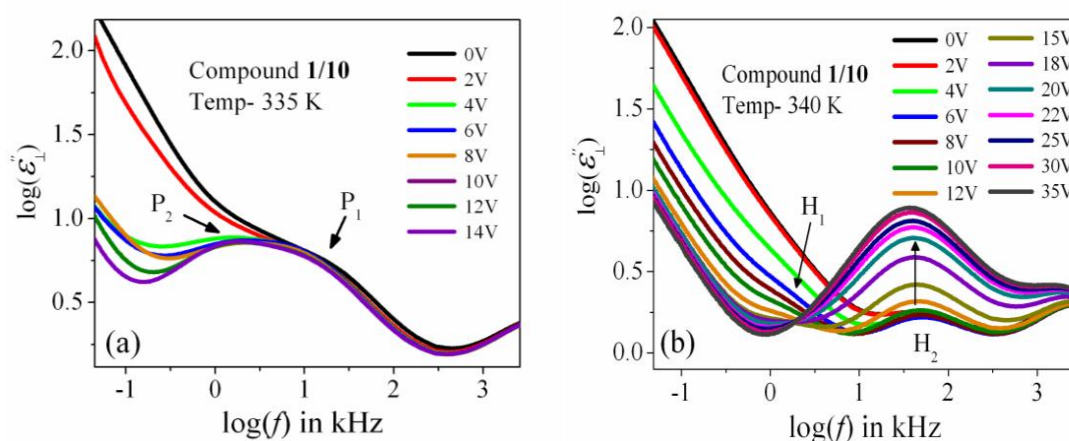


**Figure 8.8.** The variation of frequency-dependent imaginary ( $\epsilon''$ ) part of the complex permittivity with the bias voltage for compound 1/10 in (a) planar and (b) the homeotropic alignment cells.

---

---

these two modes can be resolved clearly (See Fig. 8.8(a)). On further cooling, the  $P_1$  mode persists to the lower temperature  $Sm-C_{(II)}$  phase. Therefore, similar to the compound **1/9**, the  $P_1$  mode in the compound **1/10** can be ascribed as the molecular mode in the  $N_{CybC}$  phase, while in tilted  $Sm-C_{(I)}$  phase, the orientation of the molecules in anti-parallel fashion with a greater tilt angle, describing a collective process of relaxation. Conversely, in the homeotropic cell, a single relaxation mode ( $H_2$ ) has been observed throughout the whole mesomorphic range rather than the two relaxation modes ( $H_1$  and  $H_2$ ) as observed in lower homologous compounds (**1/7** and **1/9**). However, the strength of this mode is comparatively lower than that of the HG cell. Although, during cooling, the value of the dielectric strength slightly decreases in  $N_{CybC}$  phase, it enhances further in the  $CybC$  and  $Sm-C_{(I)}$  phases. Furthermore, the  $\delta\epsilon$  value remains almost constant at the  $Sm-C_{(II)}$  phase, in which the molecules are considered to be organized in a quite close-packed structure. Interestingly, the strength of this mode in the  $Sm-C_{(I)}$  phase sharply increases with the applied biasing field as shown in Fig. 8.8(b). Notably, on applying the bias voltage, the first longitudinal mode ( $H_1$ ) is observed minutely at a lower frequency region than  $H_2$ , which has been found to appear predominantly in the lower homologous compounds without any bias voltage. It can be explained that due to the enhancement of the molecular length in compound **1/10**, the terminal chains easily escaped into the surface boundary and produce the aliphatic excrescences around the cluster [36]. Moreover, combination of the steric interaction and dipole-dipole interaction favors to orient the terminal chains parallel to the layer boundary, which allows the interdigitation of the terminal chains [57]. As a result, the rotation of the molecules about its short axis is hindered in HT cell, but imparts a significant influence in HG cell. Owing to the enhancement of the molecular size, the emergence of the  $P_2$  mode has been observed in HG cell without bias field. By applying an external field, both of the compounds **1/9** and **1/10** clearly resolve the relaxation peak ( $P_2$ ) in the planar anchoring  $Sm-C_{(I)}$  phase as seen from Fig.

---

---

---

---

8.5(a) and Fig. 8.8(a). This mode is basically referred to a molecular mode arises due to rotation of molecules around their short axis. Additionally, this mode has an effect of the anti-ferroelectric organization of molecular dipoles. It has been observed that the mode  $P_2$  is definitively absent in the compound **1/7**, while it appears in compound **1/9** after the application of external field and predominantly been found in the compound **1/10** without any bias field. This implies that by increasing the chain length, the molecular rotation is facilitating gradually about the short axis in case of HG cell. Therefore, it can be predicted that further increase of chain length should exhibit a noticeable appearance of this mode with a greater value of dielectric strength [56,58]. However, in case of HT cell, the direction of the effective dipole moment diverges from the field direction by increasing the chain length. In addition to this molecular rotation about the short axis is inhibiting by the enhancement of the chain length. As a result, prominently appearance of the mode  $H_1$  in lower homologue turns out to an insignificant peak in the compound **1/10** which is clearly visible in the spectrum by the application of bias voltage (Fig. 8.8(b)). Therefore, the molecular motion becomes collective in the  $Sm-C_{(I)}$  phase, *i.e.*, the relaxation process can be assumed due to the cooperative fluctuation of the dipoles. The associative arrangement of the molecules results an anti-ferroelectric ordering in adjacent layers which has also been found in other bent core-molecules [58,59]. However, the  $Sm-C_{(II)}$  phase is like a glassy state or solid-like state which does not respond in external bias field. For deeper understanding of polar ordering for these smectic phases, the field induced switching behavior has also been studied which is described below.

## 8.4. Electro-optical investigation

The electro-optical investigation for the three investigated bent-core compounds has been carried out in combination with the field reversal polarization technique [60] by applying a triangular wave AC input voltage (amplified by 20 times) and simultaneous observation of the optical textures

---

---

(by using square wave) under a crossed polarizing optical microscope. An absolute voltage of  $180 V_{pp}$ , 20 Hz has been applied with a proper resistive circuit to the sample filled ITO coated cells both in the planar and homeotropic orientations. Hence, an effective voltage of about  $\pm 20$  V acts per  $\mu\text{m}$  on the cell which drives a current through the material. The output current spectrums have been acquired in Agilent DSOX2000A and the optical textures were observed by using a polarizing optical microscope (BANBROS) at a temperature interval of 1 K.

Out of the three investigated compounds, the lower homolog **1/7** has  $N_{CybC}$  and CybC phases where no prominent polarization peak has been detected throughout the mesomorphic range. On the other hand, the higher homologous compounds (**1/9** and **1/10**) exhibit two significant polarization peaks in the lower temperature smectic phases and a single polarization peak in the  $N_{CybC}$  phase, which exist also in the isotropic phase. The obtained current response spectrums along with the applied AC triangular wave voltage for the compounds **1/9** and **1/10** are depicted in Fig. 8.9(a-e) for both of the cell alignments. The corresponding temperature dependence values of the spontaneous polarization ( $P_s$ ) are illustrated in Fig. 8.9(f,g). Simultaneous observations of optical textures in response to the applied square wave AC field are also represented in Fig. 8.10.

The output current spectrum for the planar-aligned compound **1/9** exhibits a broad asymmetrical current peak in the  $N_{CybC}$  phase even also in the isotropic phase as represented in Fig. 8.9(a) at different temperature above and below the  $I-N_{CybC}$  phase transition. However, an appearance of a sharp current peak has been observed in the HT configuration which is shown in the inset of Fig. 8.9(a). Similar observation has also been noticed in case of the compound **1/10** in the  $N_{CybC}$  phase for both the cell configurations. The area covered by the peak for both the compounds is sufficiently large near the isotropic phase

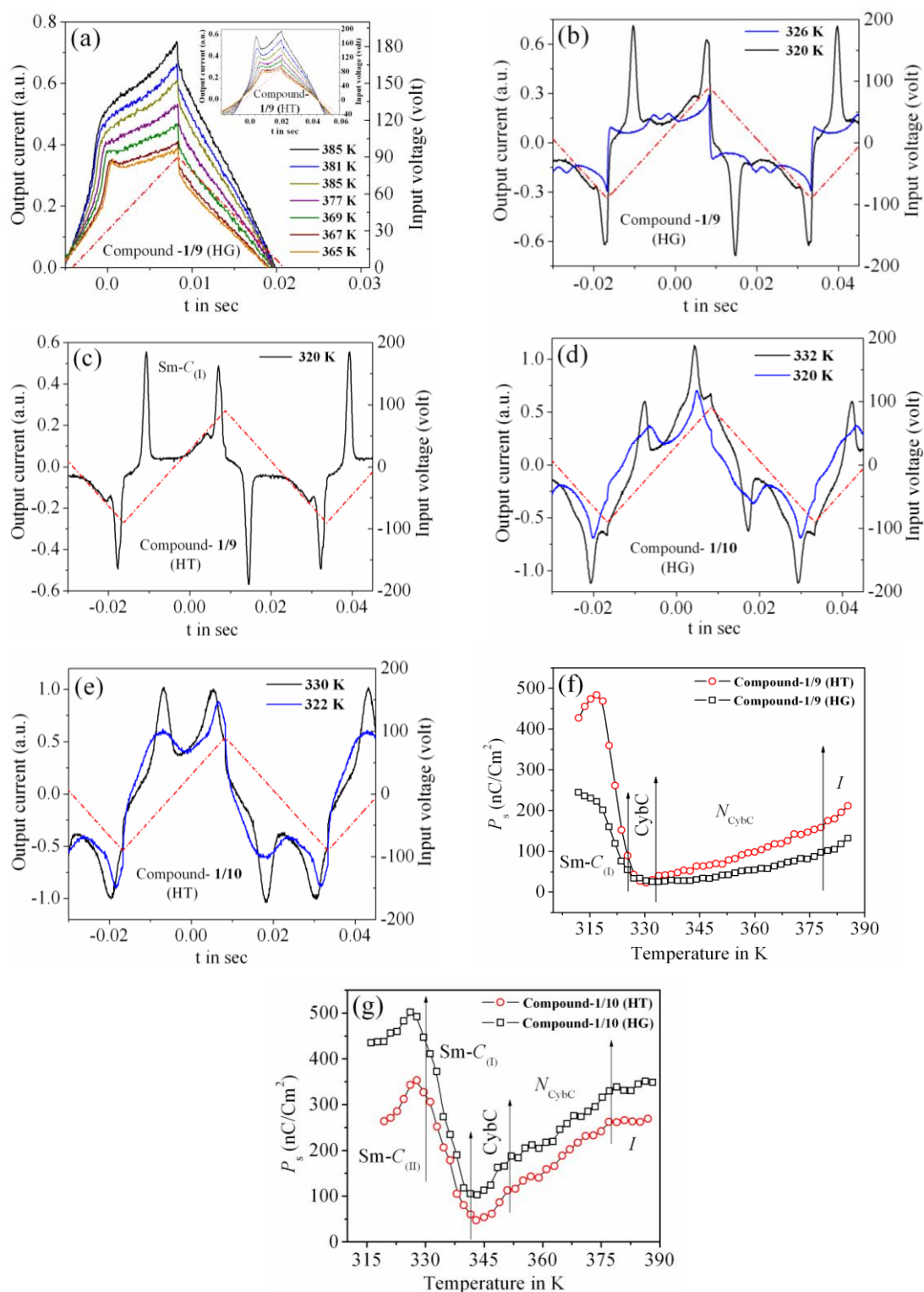


**Figure 8.9.** Switching current response curves of compound 1/9 and 1/10 for a triangular wave voltage (Red dashed line) at different temperatures; (a-c) Compound 1/9 in HG cell, (d) Compound 1/10 in HG cell, (e) Compound 1/10 in HT cell, (f-g) Temperature-dependent polarization value for the compound 1/9 and 1/10 respectively.

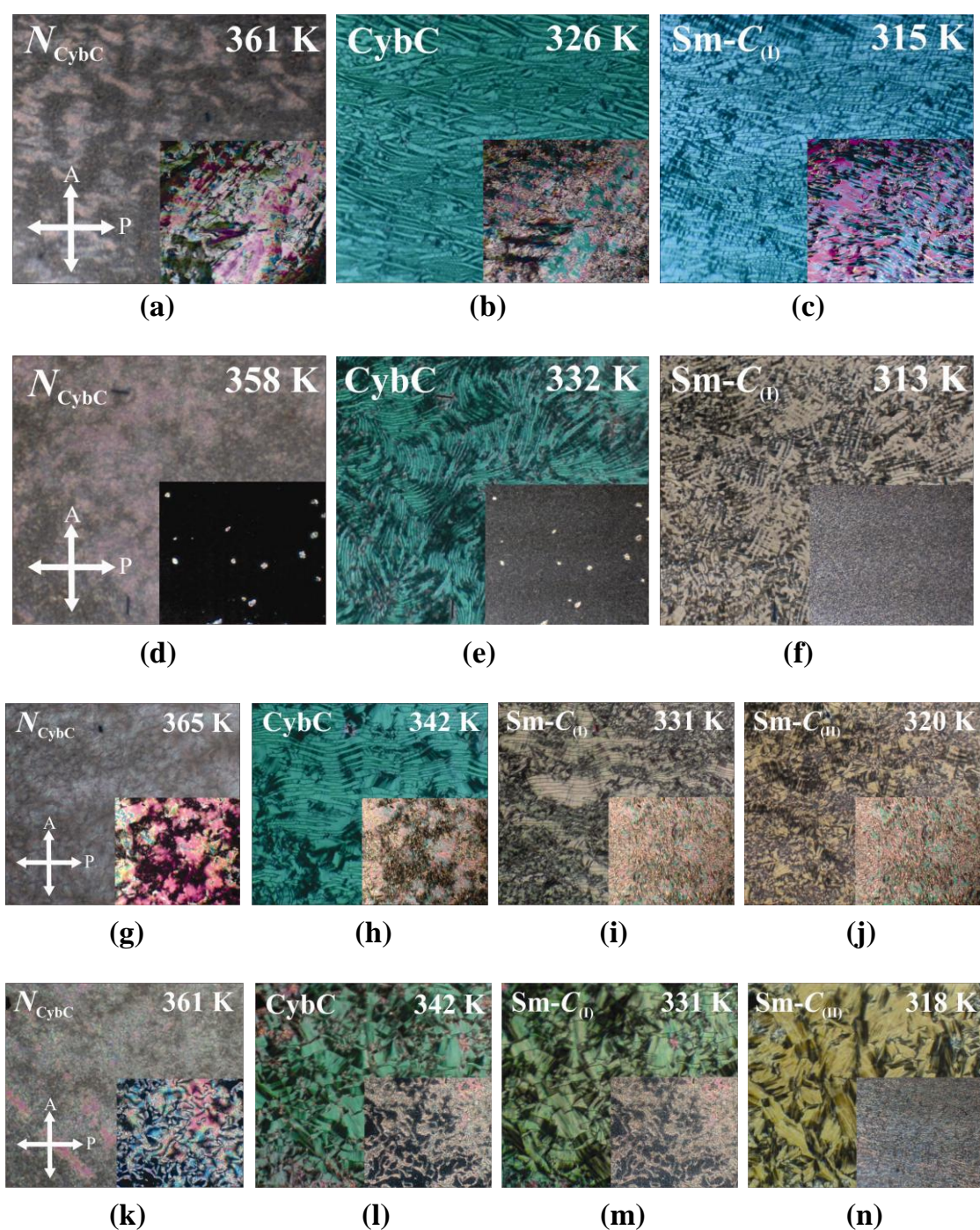


**Figure 8.10.** Optical textures of the compound **1/9** and **1/10** for an applied square wave AC voltage at different mesophases; (a-c): compound **1/9** in HG cell, (d-f): compound **1/9** in HT cell, (g-j): compound **1/10** in HG cell, (k-n): compound **1/10** in HT cell. Corresponding insets are the textures before the application of the field and arrows indicate the direction of the analyzer and polarizer.

---

---

and slowly diminishes in the  $N_{\text{CybC}}$  phase by lowering the temperature. Thus, the corresponding value of polarization ( $P_s$ ) has been found to be about 210 nC/cm<sup>2</sup> in HT cell and about 140 nC/cm<sup>2</sup> in case of HG cell in the isotropic phase for the compound **1/9** (see Fig. 8.9(f)). On the other hand, the compound **1/10** reveals a quite higher value of about 320 nC/cm<sup>2</sup> in HG cell and about 260 nC/cm<sup>2</sup> in HT cell as represented in Fig. 8.9(g). Further lowering the temperature, the value of  $P_s$  gradually decreases throughout the entire  $N_{\text{CybC}}$  phase. Moreover, the application of a square wave input voltage (at different frequencies) also produces a hump in the output spectrum which eventually ruled out the emergence of this peak as ionic contribution. Rather it may be concluded that due to the existence of small clusters consisting of Sm-C type polar molecules in the  $N_{\text{CybC}}$  phase and even also in the isotropic phase induces such polarization peak. Quite similar type of observation has been reported in four-ring bent-core samples [61] and in the Sm-A phase of three-ring bent-core compound [62]. Therefore, the single peak observed in the switching current indicates that the fluctuation of the polarization vector of these polar cybotactic clusters is induced by the application of an external field, resulting in a ferroelectric-like polar switching [61,63,64] both in the isotropic and  $N_{\text{CybC}}$  phases. However, the average size of the polar clusters is very small near the isotropic phase which makes the reorientation of the dipolar axes quite easier and hence demonstrates a high value of polarization [30]. Moreover, as the temperature decreases the polar clusters grow up in size resulting in an effective increase of viscosity which also restricts the reorientation of the clusters within the  $N_{\text{CybC}}$  phase and hence the polarization value decreases by lowering the temperature. Subsequently, a sharp change of the planar-aligned schlieren nematic texture (inset of Fig. 8.10(a,g)) has been observed as shown in Fig. 8.10 (a,g) due to the application of an AC square wave field (180 V<sub>pp</sub>, 5 Hz) in the  $N_{\text{CybC}}$  phase for both of the compounds. When the field is removed, the texture switches back into the initial state within a few milliseconds. Similar observation has also been found in HT cell as depicted in Fig.

---

---

---

---

8.10(d,k). Such ferroelectric nature in the nematic phase reveals a good consistency with several experimental reports [30,61,65] and often a quite higher value of polarization has also been reported in bent-core nematic phase [66]. As the polar clusters of the nematic phase are fused into elongated aggregates in the CybC phase, a ribbon-like optical texture arises in the CybC phase as a result of applied field which is depicted in Fig. 8.10(b,h) for HG cell and in Fig. 8.10(e,l) for the HT cell. Additionally, an appearance of two insignificant peaks in switching current has been found in this phase (blue curve in Fig. 8.9(b)). Further decreasing the temperature, two well distinct sharp peaks developed in the current response spectrum at the Sm- $C_{(1)}$  phase as shown in Fig. 8.9(b,c) for both the cell configurations. This is the signature of weak anti-ferroelectric ordering of the dipoles in adjacent layers. Nevertheless, the optical texture also shows a considerable change at the field-on state in the Sm- $C_{(1)}$  phase as represented in Fig. 8.10(c,i) for HG cell and Fig. 8.10(f,m) for the HT cell. Although the texture patterns are almost identical in the CybC and Sm- $C_{(1)}$  phases, a considerable change in the birefringence has been observed between these two phases. However, as the anti-parallel organization of the molecules in the neighboring layers is initiating from the CybC phase, the dual insignificant polarization peaks has found to appear from the CybC phase. On lowering the temperature, the obtained polarization value sharply increases to 250 nC/cm<sup>2</sup> for the HG configuration and 498 nC/cm<sup>2</sup> for the HT configuration in the Sm- $C_{(1)}$  phase as described in Fig. 8.9(f). Similar type of enhancement for the polarization value has also been reported in some bent-core anti-ferroelectric smectic phases [51,55,67-71]. Possibly, the steric interaction between the molecules reorients the terminal chains parallel to the layer boundary, which allows partial interlayer diffusion (interdigitation) of terminal chains [72]. Moreover, the strong dipole-dipole interaction also favors to align the molecular dipole moments in adjacent layers in an anti-parallel fashion. Combination of both the interaction stabilizes the anti-ferroelectric phase [72]. In addition, two well distinct sharp peaks of the compound **1/10** become

---

---

---

---

initially distorted in Sm- $C_{(II)}$  phase and finally disappears at a lower temperature as represented in Fig. 8.9(d,e) for the HG and HT cell configurations respectively. Moreover, the field-on optical texture in the Sm- $C_{(II)}$  phase eventually does not return to its initial state when the bias field is switched off as shown in Fig. 8.10(j,n) for the HG and HT cells respectively. This is essentially due to the effect of a more viscous medium with closely packed nature of the molecules in Sm- $C_{(II)}$  phase. Thus the Sm- $C_{(II)}$  phase corresponds to a more solid-like Sm- $C$  phase or a glassy state. The value of the polarization increases with decrease in temperature having a maximum up to 520 nC/cm<sup>2</sup> for the HG configuration and 370 nC/cm<sup>2</sup> for the HT configuration in Sm- $C_{(I)}$  phase, while it decreases in the Sm- $C_{(II)}$  phase (see Fig. 8.9(g)). Surprisingly, the value of polarization for the compound **1/10** has found to be comparatively greater in case of HG cell than that of the HT cell in the lower temperature smectic phases, while the opposite nature has been observed in case of the second homologous compound **1/9**, *i.e.*, the value of polarization is greater for the HT cell than that of the HG cell. This unusual behavior can be explained by considering the deviation of resultant dipolar contribution with the variation of chain length in both the cell configurations. The magnitude of dipole moment for both the compounds are nearly equal, but owing to the elongation of chain length a strong component of the effective dipole moment is being oriented towards the direction of the field in the HG cell while it becomes weak in the HT cell. The obtained results in dielectric spectroscopy also support this behavior in which the first longitudinal peak ( $H_1$ ) is absent in higher homologous compound (**1/10**), while a distinct appearance of second transverse mode ( $P_2$ ) is observed in HG cell which is also observed in the planar-aligned compound **1/9**. Recently, a similar type of bent-core molecules ( $n = 6,8,12,14,16,18$ ) has been synthesized from 4-cyanoresorcinol aromatic core [69,73-76] with the reversal of ester linking groups in which the higher homologous compounds ( $n = 16,18$ ) possess a non-tilted and non-polar uniaxial Sm-A phase in addition to two uniform tilted Sm- $C$  phases (Sm- $C_S P_F$  and Sm-

---

---

---

---

$C_S P_A$ ) those are also exhibiting similar type of bulk polarization behavior. The field induced polarization study of present compounds (**1/9** and **1/10**) indicate that both lower temperature Sm-C phases are polar in nature with the anti-ferroelectric ordering of the dipoles and have a sufficiently high value of polarization ( $P_S$ ). All these observations are found to be supportive with the conclusions made from the dielectric spectroscopy measurements. Finally, it appears that the Sm- $C_{(I)}$  phase should be designated as Sm- $C_S P_A$  phase ( $C_S$  stands for synclinic-type of molecular organization and  $P_A$  corresponds to anti-ferroelectric ordering of polar orientation in neighboring layers) while Sm- $C_{(II)}$  phase is nothing but a quite solid-like state or close-packed Sm-C phase having another version of synclinic - anti-ferroelectric ordering (Sm- $C'_S P_A$  phase).

## 8.5. Conclusion

Precise dielectric spectroscopy and electro-optical measurements have been performed to investigate the molecular dynamics for three homologous compounds (**1/7**, **1/9** and **1/10**) derived from 4-cyanoresorcinol bisbenzoates with terminally substituted varying alkyl chains ( $n = 7, 9, 10$ ). All the compounds possess almost equal magnitude of dipole moment ( $\sim 5.1$  D). The lower homolog (**1/7**) comprises of a stable  $N_{CybC}$  phase in a broad temperature range, while the higher homologue (**1/9** and **1/10**) exhibit a  $N_{CybC}$  phase, in addition to tilted Sm-C phases- Sm- $C_{(I)}$  and Sm- $C_{(II)}$  followed by a CybC phase. The molecular conformations and their association impart a significant role in the mesomorphic behavior of the investigated compounds. Investigation on the dielectric spectroscopy for all of the compounds reveals that the compound **1/7** exhibits only one relaxation mode ( $P_1$ ) in the planar-aligned  $N_{CybC}$  phase and ascribed as the molecular mode, arising due to the rotation of polar molecules around the long axis of the director within the Sm-C type tiny clusters. Besides, in HT cell, a couple of distinct relaxation modes has been found in which the low-frequency relaxation peak ( $H_1$ ) appears due to the rotation of the molecules around their short axis and the higher frequency relaxation peak ( $H_2$ )

---

---

corresponds to the molecular mode associated with the local polar ordering of the molecules. However, the relaxation modes in  $N_{\text{CybC}}$  phase of the compound **1/9** have been found to be of similar nature as the relaxation modes ( $P_1$ ,  $H_1$  and  $H_2$ ) of the lower homolog **1/7**. Interestingly, the dielectric strengths of these modes are too much sensitive to the externally applied bias field, indicating an influence of the effective dipole moment of the molecules on these modes. On the other hand, the higher homologous compound **1/10** exhibit only one longitudinal relaxation mode ( $H_2$ ) throughout the mesomorphic region, which is also very sensitive to the applied bias field. Additionally, this compound exhibits two relaxation modes ( $P_1$ ,  $P_2$ ) in planar aligned  $\text{Sm-C}_{(I)}$  phase. Due to the presence of a long terminal chain of the compound **1/10**, the steric interaction between the molecules reorients the terminal chains parallel to the layer boundary and forms an interdigitation of the terminal chains. This in effect restricts the rotational motion of the molecules around the short axis in HT cell and found to be gradually facilitating about the short axis in HG cell. More specifically it can be stated that due to the elongation of chain length a strong component of the effective dipole moment is being oriented towards the direction of the field in the HG cell while it becomes weaken in the HT cell. In order to investigate the polar contribution of these mesophases, the field reversal switching polarization has been measured in the investigated compounds over the whole mesomorphic range both in the HG and HT cell configurations. On the basis of all investigated results, it can be concluded that the  $N_{\text{CybC}}$  phase of these compounds mostly differ from the usual nematics, where a switchable macroscopic bulk polarization has been found in the direction of the applied electric field and defines a ferroelectric type of polar ordering. The molecules in the  $N_{\text{CybC}}$  phase are organized themselves in such a way that their individual dipoles suitably pile up to produce a large ferroelectric polarization within the medium. Moreover, the lower temperature  $\text{Sm-C}$  phases ( $\text{Sm-C}_{(I)}$  and  $\text{Sm-C}_{(II)}$ ) exhibit two well distinct peaks in current response curve, indicating an anti-ferroelectric type of ordering of the molecular dipoles in

---

---

---

---

adjacent layers. Due to this reason, the effective cancellation of the dipole moments reduces the dielectric strength ( $\delta\epsilon$ ) of the relaxation modes, but an application of an external bias voltage principally switches the dipoles along the field direction and hence significantly enhances the dielectric strength. The intermediate CybC phase endorsed the transition from the ferroelectric-type  $N_{\text{CybC}}$  phase to the anti-ferroelectric type of  $\text{Sm-C}_{(\text{I})}$  phase where the cybotactic clusters are being elongated. However, the  $\text{Sm-C}_{(\text{II})}$  phase is nothing but a  $\text{Sm-C}$  phase with enhanced packing density in comparison to  $\text{Sm-C}_{(\text{I})}$  phase, that seems like more solid-like state or glassy state. For this reason, even the field-on optical texture in the  $\text{Sm-C}_{(\text{II})}$  phase eventually does not return to its initial state as the field is completely switched off. Therefore, the development of polar order of the molecules in layers has been discussed in accordance with the variation of temperature and chain length. Considering all experimental findings it is concluded that the  $\text{Sm-C}_{(\text{I})}$  phase can be designated as  $\text{Sm-C}_S\text{P}_A$  (synclinic- anti-ferroelectric ordering) while the  $\text{Sm-C}_{(\text{II})}$  phase a quite solid-like state or close-packed  $\text{Sm-C}$  phase with similar type of synclinic - anti-ferroelectric ordering. This type of transition character from a rare ferroelectric  $N_{\text{CybC}}$  phase to anti-ferroelectric  $\text{Sm-C}$  phase is quite interesting among the bent-core molecules. All of the obtained outcomes emphasizes that these compounds may be used to formulate mixtures having improved material parameters like induced biaxiality, effective dipole moment, switching time etc. for practical applications.

---

---

**References:**

- [1] F. Kremer, *J. Non-Cryst. Solids*, **305**, 1 (2002).
- [2] O.E. Panarin, Y.P. Panarin, F. Antonelli, J.K. Vij, M. Reihmann, and G. Galli, *J. Matter. Chem.*, **16**, 842 (2006).
- [3] U. Manna, J.-K. Song, Y.P. Panarin, A. Fukuda, and J.K. Vij, *Phys. Rev. E*, **77**, 041707 (2006).
- [4] H. Xu, Y.P. Panarin, J.K. Vij, A.J. Seed, M. Hird, and J.W. Goodby, *J. Phys.: Condens. Mater*, **7**, 7443 (1995).
- [5] Y.P. Panarin, H. Xu, S.T. MacLughadha, J.K. Vij, A.J. Seed, M. Hird, and J.W. Goodby, *J. Phys.: Condens. Matter*, **7**, L351 (1995).
- [6] A. H. Price, and Á. Buka, in *Advances in Liquid Crystal Research and Applications*, edited by L. Bata, Pergamon Press, New York, Budapest (1980).
- [7] H. Kresse, in *Physical Properties of Liquid Crystals: Nematics*, edited by D.A. Dunmur, A. Fukuda, and G. R. Luckhurst, Inspec, London (2001).
- [8] L. Bata, and Á. Buka, *Acta Phys. Pol. A*, **54**, 635 (1978).
- [9] Á. Buka, P.G. Owen, and A.H. Price, *Mol. Cryst. Liq. Cryst.*, **51**, 295 (1979).
- [10] J. McConnell, in *Rotational Brownian motion and dielectric theory*, Academic Press, New York (1980).
- [11] W.T. Coffey, and Y. P. Kalmykov, *Adv. Chem. Phys.*, **113**, 487 (2000).
- [12] C. Krause, H. Yin, C. Cerclier, D. Morineau, A. Wurm, C. Schick, F. Emmerling, and A. Schonhals, *Soft Matter*, **8**, 11115 (2012).
- [13] M. Marik, A. Mukherjee, D. Jana, A. Yoshizawa, and B.K. Chaudhuri, *Phys. Rev. E*, **88**, 012502 (2013).
- [14] M.B. Pandey, R. Dhar, V.K. Agrawal, R.P. Khare, and R. Dabrowski, *Phase transit.*, **76**, 845 (2003).

- 
- 
- [15] H. Takezoe, and Y. Takanishi, in *Smectic Liquid Crystals: antiferroelectric and ferroelectric phases*, H.S. Kitzerow, and C. Bahr (Eds.) in *Chirality in Liquid Crystals*, Springer-Verlag, Berlin (2001).
- [16] R. Dabrowski, J.M. Oton, V. Urruchi, J.L. Gayo, K. Czuprynski, and S. Gauza, *Polish J. Chem.*, **76**, 331 (2002).
- [17] M. Rajnak, P. Kopcansky, V. Gdovinova, V. Zavisova, I. Antal, J. Kurimsky, B. Dolnik, J. Jadzyn, N. Tomasovicova, M. Koneracka, and M. Timko, *Mol. Cryst. Liq. Cryst.*, **611**, 40 (2015).
- [18] S. Kobayashi, T. Miyama, N. Nishida, Y. Sakai, H. Shiraki, Y. Shiraishi, and N. Toshima, *J. Disp. Technol.*, **2**, 121 (2006).
- [19] G.P. Sinha, and F.M. Aliev, *Phys. Rev. E*, **58**, 2001 (1998).
- [20] X.-L. Wu, W.I. Goldberg, M.X. Liu, and J.Z. Xue, *Phys. Rev. Lett.*, **69**, 470 (1992).
- [21] Á. Buka, N. Éber, K. Fodor-Csorba, A. Jákli, and P. Salamon, *Phase Transit.*, **85**, 872 (2012).
- [22] P. Salamon, N. Éber, Á. Buka, J.T. Gleeson, S. Sprunt, and A. Jákli, *Phys. Rev. E*, **81**, 031711 (2010).
- [23] G. Pelzl, S. Diele, and W. Weissflog, *Adv. Mater.*, **11**, 707 (1999).
- [24] S.K. Lee, S. Heo, J.G. Lee, K.-T. Kang, K. Kumazawa, K. Nishida, Y. Shimbo, Y. Takanishi, J. Watanabe, T. Doi, T. Takahashi, and H. Takezoe, *J. Am. Chem. Soc.*, **127**, 11085 (2005).
- [25] S. Kumar, and A.N. Gowda, *Liq. Cryst. Rev.*, **3**, 99 (2015).
- [26] O. Francescangeli, V. Stanic, S.I. Torgova, A. Strigazzi, N. Scaramuzza, C. Ferrero, I.P. Dolbnya, T.M. Weiss, R. Berardi, L. Muccioli, S. Orlandi, and C. Zannoni, *Adv. Funct. Mater.*, **19**, 2592 (2009).
- [27] E. Dorjgotov, K. Fodor-Csorba, J.T. Gleeson, S. Sprunt, and A. Jakli, *Liq. Cryst.*, **35**, 149 (2008).
- [28] S. Stojadinovic, A. Adorjan, S. Sprunt, H. Sawade, and A. Jákli, *Phys. Rev. E*, **66**, 060701 (2002).
- 
-

- 
- 
- [29] D. Wiant, S. Stojadinovic, K. Neupane, S. Sharma, K. Fodor-Csorba, A. Jakli, J.T. Gleeson, and S. Sprunt, *Phys. Rev. E*, **73**, 030703 (2006).
- [30] O. Francescangeli, V. Stanic, S. Torgova, A. Strigazzi, N. Scaramuzza, C. Ferrero, I.P. Dolbnya, T.M. Weiss, R. Berardi, L. Muccioli, S. Orlandi, and C. Zannoni, *Adv. Funct. Mater.*, **19**, 2592 (2009).
- [31] O. Francescangeli, and E.T. Samulski, *Soft Matter*, **6**, 2413 (2010).
- [32] O. Francescangeli, F. Vita, C. Ferrero, T. Dingemans, and E.T. Samulski, *Soft Matter*, **7**, 895 (2011).
- [33] S. Chakraborty, J.T. Gleeson, A. Jákli, and S. Sprunt, *Soft Matter*, **9**, 1817 (2013).
- [34] C. Zhang, M. Gao, N. Diorio, W. Weissflog, U. Baumeister, S. Sprunt, J.T. Gleeson, and A. Jákli, *Phys. Rev. Lett.*, **109**, 107802 (2012).
- [35] S. Torgova, S.P. Sreenilayam, Y.P. Panarin, O. Francescangeli, F. Vita, J.K. Vij, E. Pozhidaev, M. Minchenko, C. Ferrero, and A. Strigazzi, *Phys. Chem. Chem. Phys.*, **19**, 22946 (2017).
- [36] C. Keith, A. Lehmann, U. Baumeister, M. Prehm, and C. Tschierske, *Soft Matter*, **6**, 1704 (2010).
- [37] D.R. Link, G. Natale, R. Shao, J.E. Maclennan, N.A. Clark, E. Körblova, and D.M. Walba, *Science*, **278**, 1924 (1997).
- [38] G. Pelzl, S. Diele, and W. Weissflog, *Adv. Mater.*, **11**, 707 (1999).
- [39] G. Shanker, M. Prehm, M. Nagaraj, J.K. Vij, M. Weyland, A. Eremin, and C. Tschierske, *Chem. Phys. Chem.*, **15**, 1323 (2014).
- [40] G. Shanker, M. Nagaraj, A. Kocot, J.K. Vij, M. Prehm, and C. Tschierske, *Adv. Funct. Mater.*, **22**, 1671 (2012).
- [41] A. Chakraborty, M.K. Das, B. Das, A. Lehmann, and C. Tschierske, *Soft Matter*, **9**, 4273 (2013).
- [42] P. Perkowski, M. Mrukiewicz, K. Garbat, M. Laska, U. Chodorow, W. Piecek, R. Dabrowski, and J. Parka, *Liq. Cryst.*, **39**, 1237 (2012).
- [43] M. Mrukiewicz, P. Perkowski, K. Garbat, R. Dabrowski, and J. Parka, *Acta Physica Polonica A*, **124**, 940 (2013).
- 
-

- 
- 
- [44] S. Havriliak, and S. Negami, *Polymer*, **8**, 161 (1967).
- [45] S. Havriliak, and S. Negami, *J. Poly. Sci.*, **14**, 99 (1966).
- [46] P. Nayek, S. Ghosh, S. Roy, T.P. Majumder, and R. Dabrowski, *J. Mol. Liq.*, **175**, 91 (2012).
- [47] S. Ghosh, P. Nayek, S.K. Roy, T.P. Majumder, and R. Dabrowski, *Liq. Cryst.*, **37**, 369 (2010).
- [48] Y. Jang, V.P. Panov, C. Keith, C. Tschierske, and J.K. Vij, *App. Phys. Lett.*, **97**, 152903 (2010).
- [49] P. Tadapatri, U.M. Hiremath, C.V. Yelamaggad, and K.S. Krishnamurthy, *J. Phys. Chem. B*, **114**, 1745 (2010).
- [50] P. Tadapatri, K.S. Krishnamurthy, and W. Weissflog, *Phys. Rev. E*, **82**, 031706 (2010).
- [51] L. Kovalenko, M.W. Schröder, R.A. Reddy, S. Diele, G. Pelzl, and W. Weissflog, *Liq. Cryst.*, **32**, 857 (2005).
- [52] P. Salamon, N. Eber, A. Buka, J.T. Gleeson, S. Sprunt, and A. Jákli, *Phys. Rev. E*, **81**, 031711 (2010).
- [53] R. Balachandran, V.P. Panov, J.K. Vij, G. Shankar, C. Tschierske, K. Merkel, and A. Kocot, *Phys. Rev. E*, **90**, 032506 (2014).
- [54] Y. Jang, V.P. Panov, A. Kocot, A. Lehmann, C. Tschierske, and J.K. Vij, *Phys. Rev. E*, **84**, 060701 (2011).
- [55] A. Eremin, H. Nádasi, G. Pelzl, S. Diele, H. Kresse, W. Weissflog, and S. Grande, *Phys. Chem. Phys.*, **6**, 1290 (2004).
- [56] L. Guo, K. Gomola, E. Grecka, D. Pocięcha, S. Dhara, F. Araoka, K. Ishikawa, and H. Takezoe, *Soft Matter*, **7**, 2895 (2011).
- [57] R.A. Reddy, and C. Tschierske, *J. Matter. Chem.*, **16**, 907 (2006).
- [58] Y.P. Panarin, S.P. Sreenilayam, J.K. Vij, A. Lehmann, and C. Tschierske, *Beilstein J. Nanotechnol.*, **9**, 1288 (2018).
- [59] H. Schlacken, P. Schiller, and H. Kresse, *Liq. Cryst.*, **28**, 1235 (2001).
- [60] A. Pramanik, M.K. Das, B. Das, M. Żurowska, and R. Dabrowski, *Liq. Cryst.*, **42**, 412 (2015).
- 
-

- 
- 
- [61] S. Ghosh, N. Begum, S. Turlapati, S.K. Roy, A.K. Das, and N.V.S. Rao, *J. Mater. Chem. C*, **2**, 425 (2014).
- [62] W. Weissflog, U. Baumeister, M.–G. Tamba, G. Pelzl, H. Kresse, R. Friedmann, G. Hempel, R. Kurz, M. Roos, K. Merzweiler, A. Jakli, C. Zhang, N. Diorio, R. Stannarius, A. Eremin, and U. Kornek, *Soft Matter*, **8**, 2671 (2012).
- [63] G. Shanker, M. Prehm, M. Nagaraj, J.K. Vij, M. Weyland, A. Eremin, and C. Tschierske, *Chem. Phys. Chem.*, **15**, 1323 (2014).
- [64] G. Shanker, M. Nagaraj, A. Kocot, J.K. Vij, M. Prehm, and C. Tschierske, *Adv. Funct. Mater.*, **22**, 1671 (2012).
- [65] S. Turlapati, R.K. Khan, S. Ghosh, P. Tadapatri, R. Pratibha, and N.V.S. Rao, *Journal of Applied Physics*, **120**, 174101 (2016).
- [66] O. Francescangeli, F. Vita, and E.T. Samulski, *Soft Matter*, **10**, 7685 (2014).
- [67] N. Sebastian, S. Belau, A. Eremin, M. Alasar, M. Prehm, and C. Tschierske, *Phys. Chem. Chem. Phys.*, **19**, 5895 (2017).
- [68] S. Sreenilayam, M. Nagaraj, Y.P. Panarin, J.K. Vij, A. Lehmann, and C. Tschierske, *Mol. Cryst. Liq. Cryst.*, **553**, 140 (2012).
- [69] C. Keith, M. Prehm, Y.P. Panarin, J.K. Vij, and C. Tschierske, *Chem. Commun.*, **46**, 3702 (2010).
- [70] M. Alaasar, M. Prehm, S. Poppe, and C. Tschierske, *Chem. Eur. J.*, **23**, 5541 (2017).
- [71] S.P. Sreenilayam, Y.P. Panarin, J.K. Vij, A. Lehmann, M. Poppe, and C. Tschierske, *Phys. Rev. Materials*, **1**, 035604 (2017).
- [72] K. Nishida, M. Čepič, W.J. Kim, S.K. Lee, S. Heo, J.G. Lee, Y. Takanishi, K. Ishikawa, K.-T. Kang, J. Watanabe, and H. Takezoe, *Phys. Rev. E*, **74**, 021704 (2006).
- [73] M. Nagaraj, Y.P. Panarin, J.K. Vij, C. Keith, and C. Tschierske, *App. Phys. Lett.*, **97**, 213505 (2010).
- 
-

- [74] S. Sreenilayam, Y.P. Panarin, J.K. Vij, M. Osipov, A. Lehmann, and C. Tschierske, *Phys. Rev. E*, **88**, 012504 (2013).
- [75] Y.P. Panarin, M. Nagaraj, J.K. Vij, C. Keith, and C. Tschierske, *Europhys. Lett.*, **92**, 26002 (2010).
- [76] S.P. Sreenilayam, Y.P. Panarin, J.K. Vij, P. Panov, A. Lehmann, M. Poppe, M. Prehm, and C. Tschierske, *Nature Comm.*, **7**, 11369 (2016).

# CHAPTER 9

---

## Summary and conclusions

The dissertation entitled “*Phase transitions in binary mixtures of calamitic and bent-core mesogens*” submitted for the degree of Doctor of Philosophy (Physics) of the University of North Bengal is principally devoted to comprehensive study and understanding of several phase transitions in binary liquid crystal mixtures consisting of calamitic and bent-core mesogens using different experimental techniques. The investigation of various physical parameters influenced by variation of temperature provides precious information about mesophase properties. The detailed investigation of these mesophase behavior and their transitions emerged a field of significant interest in liquid crystal (LC) research. Since extensive research works have been utilized so far to describe the nature of mesophase transition involving isotropic (*I*), nematic (*N*), smectic-*A* (*Sm-A*) phases in a number of pure calamitic compounds and their mixtures, it should be an appropriate formalism for the study of phase transition in liquid crystalline mixtures involving bent-core mesogens exhibiting a number of exotic mesomorphic features, finding no trace in classic calamitic compounds. Despite the success of qualitative explanations about the nature of transitions among these mesophases, an unsolved controversy still persists in ascertaining the exact nature of the smectic-*A* to smectic-*C* (*Sm-A–Sm-C*) phase transition. The bulk of this dissertation is mainly representing a clear scenario about the phase behavior and experimentally characterization of the order character for the isotropic–nematic (*I–N*), nematic–smectic-*A* (*N–Sm-A*) phase transitions and most importantly the smectic-*A* to smectic-*C* (*Sm-A–Sm-C*) phase transition in some binary mixtures comprising of calamitic and bent-core compounds. The influence of bent-core molecules on the phase character of rod-like and chiral mesogenic environment has also been discussed from the experimental point of view. Additionally, the molecular dynamics and the nature of the mesophases have been studied in some homologous symmetrical pure bent-core liquid crystal compounds. A brief summary and conclusions of eight various chapters are described as follows:

Chapter 1 deals with a brief introduction and basic concept of liquid crystal materials as well as their basic classification scheme, particularly the thermotropic liquid crystals. Associated molecular arrangements and general behavior of different mesophases for both the calamitic and bent-core LC system have been discussed. The importance regarding formulation of liquid crystal mixtures and appearance of the induced phase has also been described. The chapter also includes a concise discussion about the phase transition along with the critical phenomena and critical exponents.

Chapter 2 describes the experimental techniques and relevant procedures employed to investigate pure LC compounds and binary mixtures. Moreover, the basic theories of the  $I-N$  and  $N-Sm-A$  phase transitions along with an extension to the  $Sm-A-Sm-C$  phase transition in liquid crystal system have also been discussed in brief.

In chapter 3, an extensive optical investigation has been carried out in a binary system, consisting of a hockey stick-shaped liquid crystal, 4-(3-decyloxyphenyliminomethyl) phenyl 4-decyloxybenzoate (SF7) and the rod-like 4-cyano-4'-octyloxybiphenyl (8OCB). An enhancement of the concentration of hockey stick-shaped compound within the mixtures leads to a significant decrease in the nematic width of the rod-like sample, *i.e.*, it stabilizes the lower temperature smectic phase. The molecular bend of the angular mesogenic dopant reflects a stronger influence on the phase-character of mixtures and leads to a relatively stronger coupling between nematic and smectic order parameter. The temperature-dependent variation of optical birefringence ( $\Delta n$ ) demonstrates a quite well consistency obtained from both the high-resolution optical transmission method and thin prism technique. The birefringence data has been found to be rather successful in describing the transitional behavior more precisely associated with both the  $I-N$  and the  $N-Sm-A$  phase transitions in all the investigated mixtures. The experimental  $\Delta n$  data demonstrates a clearly distinguishable pretransitional phenomenon near

---

---

the  $I-N$  phase transition. The extracted order parameter critical coefficient  $\beta$  related to this transition has found to reveal a good conformity with the theoretically predicted tricritical value ( $\beta = 0.25$ ) for all of the studied mixtures. Furthermore, a noticeable pretransitional behavior has been observed in  $\Delta n$  data at the  $N-Sm-A$  transition. The divergence character of the differential quotient  $Q(T)$  in the vicinity of that transition has found to be well described by a power-law expression including the scaling terms. The related effective critical exponent ( $\alpha', \beta'$ ), describing the critical fluctuations at that transition has appeared to be non-universal in nature representing the values in between the 3D-XY and tricritical limit. The obtained  $\alpha'$  values demonstrates a strong dependency on the width of the nematic phase, while a crossover character of the  $N-Sm-A$  phase transition from second order to first order nature for a McMillan ratio of 0.994 and an approximate nematic width of about 2.5 K which again reveals a close agreement with the reported value for the mixtures of similar mesogenic systems. Therefore, the modification in effective intermolecular interactions in the host medium demonstrates a sharp decrease in the nematic width and drives the  $N-Sm-A$  phase transition towards the first order in nature.

Chapter 4 embraces the static dielectric and visco-elastic properties of the binary system reported in chapter 3. The value of longitudinal component of the dielectric permittivity exhibits a noticeable decrease with increase in dopant concentration due to a stronger dipole-dipole interaction within the mixture. All the investigated mixtures possess a large positive dielectric anisotropy ( $\Delta\epsilon$ ), but found to diminish monotonically by increasing the hockey stick-shaped dopant concentration. The obtained values of the parameters  $\epsilon_{avg}$  and  $\Delta\epsilon$  exhibits a systematic temperature and concentration dependency. By analyzing the pretransitional fluctuation in the vicinity of  $I-N$  phase transition, yielded critical coefficient assumes a value nearly equal to 0.5 within a valid error limit and independent of the concentration variation which clearly implies

---

---

a first-order character of the  $I$ - $N$  phase transition. By the similar procedure as used in chapter 3, the critical anomaly in the vicinity of  $N$ - $Sm$ - $A$  phase transition has been investigated from the temperature-dependent dielectric anisotropy ( $\Delta\epsilon$ ) data. The extracted critical exponent ( $\alpha'$ ) divulges a systematic concentration variation and found to reveal a quite good consistency obtained from both the high-resolution optical birefringence and dielectric anisotropy measurements. Furthermore, the temperature-dependent value of the splay elastic constant ( $K_{11}$ ) and the rotational viscosity ( $\gamma_1$ ) in the nematic phase has been observed to enhance gradually by lowering the temperature due to increase in molecular ordering, while the slope of the increasing pattern for both the  $K_{11}$  and  $\gamma_1$  becomes steeper with increasing the hockey stick-shaped mesogen. The obtained values of  $\gamma_1$  for all of the mixtures have been found to be slightly higher than that of the usual calamitic compounds as well as comparatively lower value than the reported values of the bent-core compounds. The calculated activation energy ( $E_a$ ) increases with the dopant concentration signifying an enhancement in intermolecular packing which affects the molecular motion within the system. Moreover, the strong dipolar correlation between dissimilar molecules within the mixture significantly affects the molecular motion.

Chapter 5 focuses on the investigations of the critical behavior at the nematic–smectic- $A$  ( $N$ - $Sm$ - $A$ ) and smectic- $A$ –smectic- $C$  ( $Sm$ - $A$ - $Sm$ - $C$ ) phase transitions from the optical investigation in a pure pyrimidine (PhP2) liquid crystal compound as well as in some binary mixtures of PhP2 with another homologous compound (PhP1) of the same series. The order character of these transitions has been explored by varying the temperature range of the  $Sm$ - $A$  and  $N$  phases. However, an inspection carried out in this system concerning the dependency of critical exponent  $\alpha'$  on the reduced temperature and observed that the transitional behavior of the  $Sm$ - $A$ - $Sm$ - $C$  phase transition is really critical over the range  $3 \times 10^{-3}$ . The obtained values of the critical exponent  $\alpha'$

---

---

have been found to be non-universal in nature for both the  $N$ -Sm-A and Sm-A-Sm-C phase transitions and hence indicate a crossover character from second order to the first order transition. Moreover, the crossover character of these phase transitions from the second-order to weakly first-order in nature has been clearly explained on the basis of the width of the  $N$  and Sm-A temperature range linked with the  $N$ -Sm-A and Sm-A-Sm-C phase transitions respectively. Moreover, a comparative discussion has been accomplished concerning the similarity and dissimilarity of order nature for both the transitions. It has been seen that the origin of such critical behavior is a unique feature for both the  $N$ -Sm-A and the Sm-A-Sm-C phase transitions for all the studied compounds and they are seen to follow two distinctly different linear curves. Additionally, the critical behavior in the vicinity of isotropic-nematic ( $I$ - $N$ ) phase transition has been reported for all the studied mixtures including a pure compound. The critical exponent  $\beta$ , characterizing the limiting behavior of the nematic order parameter close to that transition, has come out to be close to 0.25 and hence in agreement with the tricritical hypothesis.

In chapter 6, an extensive investigation has been carried out for the endorsement of tricriticality nature of the Sm-A-Sm-C phase transition in a binary system comprising of hockey-stick-shaped compound (H-22.5) and the calamitic compound (7OCB) from a high-resolution temperature scanning measurement of optical birefringence ( $\Delta n$ ). A significant destabilization of the nematic phase along with an emergence of the Sm-A phase has been observed in the phase diagram due to the increase in the concentration of the calamitic nematogen. From a precise investigation on the temperature derivative of optical birefringence in the vicinity of the Sm-A-Sm-C phase transition, the yielded values of the effective critical exponent ( $\alpha'$ ) have found to be non-universal in nature and exhibit a variation in accordance with the change of the Sm-A phase range. The values of  $\alpha'$  are found to follow the same pattern in between 3D-XY and tricritical (TCP) limit as observed in chapter 5 for the

---

---

lower limit of Sm-A phase range of about  $\sim 10.5$  K and further decrease in the Sm-A range drives the  $\alpha'$  values to the tricritical limit ( $\alpha' = 0.5$ ). The justification of such tricritical nature has been reanalyzed more elaborately with the aid of renormalization group expression including some precise modification. Interestingly, the extracted critical exponent ( $\alpha'$ ) values suggesting a broad tricritical range for the Sm-A–Sm-C phase transition over a wide range of temperature ratio (from 0.972 to 0.994). Considering all experimental findings it has been ascertained that the order character of the Sm-A–Sm-C phase transition is strictly depends upon the Sm-A phase range and simultaneously it is independent on the molecular conformer of the mixture constituents. Based on the results obtained from both the chapter 5 and chapter 6, a conclusive discussion has been incorporated about the relative disparity between the *N*–Sm-A and Sm-A–Sm-C phase transitions.

Chapter 7 deals with optical, dielectric and electro-optical investigations in some binary mixtures of chiral ferroelectric compound (2H6R) with an achiral hockey stick-shaped compound (H-22.5). Noticeably, two stable TGB phases - TGBA and TGBC\* with wide range of temperature have found to induce in these binary chiral-achiral mixtures. Introduction of small quantity of hockey stick-shaped compound in binary mixtures is sufficient to perturb the direction of the helical axis which can produce higher pitch length chiral twisted state, leading to the formation of such frustrated TGB phases. Several physical properties in these mesophases and related transitional phenomena have been discussed from the viewpoint of perturbation introduced by the achiral hockey stick-shaped compound. Dielectric studies reveal a sign inversion (positive to negative) of the dielectric anisotropy ( $\Delta\epsilon$ ) for all of the investigated mixtures including the pure compound. However, the obtained temperature range of the positive dielectric anisotropy region has found to increase successively by increasing the achiral hockey stick-shaped compound. On the other hand, the field induced spontaneous polarization ( $P_S$ ) value

---

---

decreases in TGBC\* phase of the mixtures than the Sm-C\* phase of the pure compound, while the response time ( $\tau$ ) and effective torsional bulk viscosity ( $\eta$ ) exhibit a higher value than that of the pure compound. Moreover, the values of critical exponent  $\beta$  extracted from polarization data affirm that the weakly first order character of the  $N^*$ -Sm-C\* phase transition transform towards the second order nature of TGBA-TGBC\* phase transition by introduction of hockey stick-shaped mesogen in the mixtures. Additionally, the frequency-dependent dielectric spectroscopy measurement reveals that the relaxation frequency ( $f_R$ ) and associated dielectric strength ( $\delta\epsilon$ ) of the Goldstone mode in TGBC\* phase slightly decreases with increasing the dopant concentration. However, the intermediate TGBA phase represents a transition from soft mode in  $N^*$  phase to a Goldstone mode in TGBC\* phase with a greater value of activation energy.

Chapter 8 presents a comparative study based on the dielectric spectroscopy measurement and the electro-optical investigation of three pure homologous bent-core compounds (**1/7**, **1/9** and **1/10**) derived from 4-cyanoresorcinol bisbenzoates as a central core unit. The molecular conformations and their association impart a significant role in the mesomorphic behavior of the investigated compounds. The compounds **1/7** and **1/9**, exhibit a single molecular relaxation mode ( $P_1$ ) in the planar-aligned  $N_{CyBC}$  phase and a couple of distinct relaxation modes ( $H_1$ ,  $H_2$ ) in homeotropic (HT) cell. Both  $P_1$  and  $H_1$  modes are ascribed as molecular relaxation mode appeared due to molecular rotation around their short axis and long axis respectively within the tiny clusters of  $N_{CyBC}$  phase. Besides, the high frequency longitudinal relaxation peak ( $H_2$ ) corresponds to the molecular mode, while it is associated with the influence of the anti-ferroelectric ordering of the molecular dipoles in adjacent layers of Sm-C<sub>(1)</sub> phase for compound **1/9**. The dielectric strength of the relaxation modes for the compound **1/9** is much sensitive to the externally applied bias field, confirms the influence of the effective dipole moment of the

---

---

molecules on these modes. Moreover, the higher homologous compound **1/10** exhibit only one longitudinal relaxation mode ( $H_2$ ) and a transverse mode ( $P_1$ ) throughout the mesomorphic region along with an additional relaxation mode ( $P_2$ ) in planar aligned Sm- $C_{(I)}$  phase. This is due to the presence of a long terminal chain in compound **1/10**, the steric interaction between the molecules reorients the terminal chains parallel to the layer boundary and forms an interdigitation of the terminal chains. This in effect restricts the rotational motion of the molecules around the short axis in HT cell and found to be intensifies in planar (HG) cell. Moreover, owing to the elongation of chain length, a strong component of the effective dipole moment is being emphasized towards the direction of the field in the HG cell while it becomes weakened in the HT cell. The observed polarity of these mesophases has been confirmed by field reversal polarization technique and simultaneous observation of optical textures in polarizing optical microscope. On the basis of all investigated results, it is concluded that the  $N_{CybC}$  phase much differs from the usual nematics and consisting of tiny polar cluster which in effect reveals a ferroelectric polarization within the medium. Moreover, the lower temperature Sm- $C$  phases (Sm- $C_{(I)}$  and Sm- $C_{(II)}$ ) representing an anti-ferroelectric type of ordering of the molecular dipoles in adjacent layers. The intermediate CybC phase accomplished the transition from the ferroelectric-type  $N_{CybC}$  phase to the anti-ferroelectric type of Sm- $C_{(I)}$  phase where the cybotactic clusters are being elongated. The Sm- $C_{(II)}$  phase is nothing but a Sm- $C$  phase with enhanced packing density in comparison to Sm- $C_{(I)}$  phase, that seems like a more solid-like state or glassy state. Considering all the experimental findings it has been concluded that the Sm- $C_{(I)}$  phase should be designated as Sm- $C_S P_A$  phase ( $C_S$  stands for synclitic-type of molecular organization and  $P_A$  corresponds to anti-ferroelectric ordering of polar orientation in neighboring layers) where Sm- $C_{(II)}$  phase is nothing but a quite solid-like state or close-packed Sm- $C$  phase with similar type of synclitic - anti-ferroelectric ordering (Sm- $C'_S P_A$  phase).

---

---

All of these findings presented in this dissertation demonstrate a basis for further qualitative research on transitional order and the universality class of the associated critical exponents for other liquid crystalline mesophases such as  $N$ - $Sm-C$ ,  $Sm-A^*$ - $Sm-C^*$ , transition between higher ordered smectic phases, transition to smectic mesophases from cybotactic nematic phase in bent-core mesogens etc. Investigation on these mesophase transitions necessitates further confirmation encompassing both the theoretical and experimental approaches by analyzing the heat capacity data (DSC study), tilt-angle measurement, dielectric study etc. Despite the success of proper explanation about phase transitional critical phenomena in binary mixtures, there exist several motivating investigations in multi-component mixtures involving bent-core compounds. In addition, continuous research efforts are required to increase the temperature stability of noble mesophases (blue phase, TGB phases etc.) by incorporating some achiral perturbation or nano-particle segregation in chiral environment. Moreover, the interest has grown up to extend the investigation towards the LC systems doped by polar or non-polar, conductive or non-conductive nano-particles which also contribute important information regarding the applicability of LC systems in several enhanced devices. Further work in this direction may be carried out to deal with the above mentioned problems.

# List of publications

## Referred Journals

1. A. Chakraborty, **S. Chakraborty**, and M. K. Das, “Effect of hockey-stick-shaped molecules on the critical behavior at the nematic to isotropic and smectic-A to nematic phase transitions in octylcyanobiphenyl”, *Phys. Rev. E*, **91**, 032503 (2015).
2. A. Chakraborty, **S. Chakraborty**, and M. K. Das, “Critical behavior at the isotropic to nematic, nematic to smectic-A and smectic-A to smectic-C phase transitions in a pyrimidine liquid crystal compound”, *Physica B*, **479**, 90-95 (2015).
3. **S. Chakraborty**, A. Chakraborty, M. K. Das, and W. Weissflog, “Effect of the hockey-shaped mesogen as an additive on the critical behaviour at the smectic A to nematic phase transition”, *J. Mol. Liq.*, **219**, 608-613 (2016).
4. M. K. Das, **S. Chakraborty**, R. Dabrowski, and M. Czerwiński, “Birefringence in the vicinity of the smectic-A to smectic-C phase transition: Crossover from XY critical to tricritical behavior”, *Phys. Rev. E*, **95**, 012705 (2017).
5. A. Chakraborty, **S. Chakraborty**, M. K. Das, and W. Weissflog, “Visco-elastic properties of multi-component mixtures of hockey stick-shaped liquid crystal compounds”, *J. Mol. Liq.*, **265**, 536-543 (2018).

## Paper Presented in Conferences

1. A. Chakraborty, **S. Chakraborty**, M. K. Das and W. Weissflog, “Optical, Dielectric and Elastic Properties of a few Multi-Component Liquid Crystal Mixtures of Hockey Stick-Shaped Molecules”, *Proceedings of the 21<sup>st</sup> National Conference on Liquid Crystals*, **P107**, Kanpur (2014).
2. **S. Chakraborty** and M. K. Das, “Effect of Nano Particle Doping on Liquid Crystal Medium”, *Proceedings of the 22<sup>nd</sup> West Bengal State Science and Technology Congress-2015*, **Phy 24**, Siliguri (2015).
3. **S. Chakraborty** and M. K. Das, “Mesomorphic behavior in the nematic and smectic mesophases of a few liquid crystalline mixtures involving rod-like and hockey stick-shaped molecules”, *Proceedings of the National Conference on Modern Trends in Material Science-2015*, **P29**, Siliguri (2015).
4. **S. Chakraborty** and M. K. Das, “Nature of Smectic-A to Smectic-C Transition in a binary Liquid Crystal Mixture Consisting of Hockey Stick-Shaped and Rod-Like Molecules”, *Proceedings of the 23<sup>rd</sup> National Conference on Liquid Crystals*, **P110**, IIT (ISM) Dhanbad (2016).
5. **S. Chakraborty** and M. K. Das, “Dielectric behavior in the cybotactic nematic and smectic mesophases of a homologous series of bent-core liquid crystal”, *Proceedings of the 24<sup>th</sup> National Conference on Liquid Crystals*, **P63**, IISER Mohali, Chandigarh (2017).
6. **S. Chakraborty** and M. K. Das, “Induced TGB phases in binary mixtures of achiral hockey stick-shaped and chiral rod-like mesogen”, *Proceedings of the 25<sup>th</sup> National Conference on Liquid Crystals*, **P125**, University of Allahabad (2018)\*.

\*Adjudged the best poster paper presentation in physics section for the year 2018 by the Indian Liquid Crystal Society.

# Index

## A

Activation energy	156, 161, 255, 259
Abrikosov flux	18,229
Average permittivity	61, 135, 244

## B

Bent-core liquid crystals	19, 22, 273
Biaxial nematic phase	6, 22, 133
Blue phase	16, 228

## C

Calamitic liquid crystals	5, 105
Cholesteric or chiral nematic ( $N^*$ ) phase	13, 231
Chiral Smectic A ( $Sm-A^*$ ) phase	14
Chiral Smectic C ( $Sm-C^*$ ) phase	14, 231
Critical behavior	32, 111, 115, 143,178, 209
Critical amplitude	116, 140, 181,187, 210
Critical exponents	34, 92, 115, 145,181, 210, 218
Cybotactic clusters	30, 133, 207, 272, 280

## D

Dielectric anisotropy	62, 135, 244
Dielectric spectroscopy measurement	62, 255, 274
Differential Scanning Calorimetry	54, 238

## E

Elastic constant	64, 149
Electro-optical measurement	68, 287

## F

Freedericksz transition	66
-------------------------	----

## G

Ginzburg criterion	91, 171
--------------------	---------

## H

Hockey stick-shaped liquid crystals	31, 105, 202, 231
Hexatic Smectic phase	10, 231

## L

Layer spacing	9, 26
Liquid crystals	2
Liquid crystals mixture	32, 53, 105
Lyotropic liquid crystals	4

## M

McMillan's theory for smectic A phase	75
Maier-Saupe theory	71
McMillan ratio	78, 85, 118, 190, 220

## N

Nematic ( $N$ ) phase	5
Nematic phase of bent-core liquid crystals	29

**O**

Optical birefringence measurement	55, 107, 175, 207
Optical transmission method	57, 107, 207
Orientational order parameter	6, 73, 157

**P**

Phase diagram	105, 174, 205, 239
Phase transition	33, 78, 86

**R**

Rotational viscosity measurement	67, 152
Reduced temperature	88, 120, 179, 211
Refractive index	55, 108,
Relaxation time	64, 67, 152
Relaxation frequency	274

**S**

Smectic (Sm) phase	7, 22
Smectic A (Sm-A) phase	8
Smectic C (Sm-C) phase	9
Spontaneous polarization	71, 249
Smectic phases of bent-core liquid crystals	22
Splay elastic constant	64, 149
Static permittivity measurement	60, 135, 244

**T**

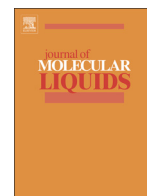
Thin prism technique	56, 108, 207
Texture observation	53, 203, 232
Tricritical point	78, 85, 118, 185, 213, 215
TGB phases	18, 229
Torsional bulk viscosity	71, 253

**V**

Vuks, Chandrasekhar and Madhusudana model	112
---	-----

**X**

X-ray diffraction study	23
-------------------------	----



# Effect of the hockey-shaped mesogen as an additive on the critical behaviour at the smectic A to nematic phase transition



Susanta Chakraborty<sup>a</sup>, Anish Chakraborty<sup>a</sup>, Malay Kumar Das<sup>a,\*</sup>, Wolfgang Weissflog<sup>b</sup>

<sup>a</sup> Department of Physics, North Bengal University, Siliguri 734013, India

<sup>b</sup> Martin-Luther-Universität Halle-Wittenberg, Institut für Chemie, Physikalische Chemie, Halle, Germany

## ARTICLE INFO

### Article history:

Received 19 January 2016

Received in revised form 1 April 2016

Accepted 2 April 2016

Available online xxxx

### Keywords:

Hockey stick-shaped mesogen

Optical birefringence

Phase transition

Pretransitional fluctuation

Critical exponent

## ABSTRACT

We present systematic experimental data on high resolution measurements of temperature dependence of optical birefringence ( $\Delta n$ ) in a binary liquid crystalline system comprising calamitic 4-cyano-4'-octyloxybiphenyl (8OCB) and a hockey stick-shaped compound, 4-(3-decyloxyphenyliminomethyl) phenyl 4-decyloxybenzoate (SF7). The hockey stick-shaped mesogen shows a smectic A (SmA) phase in addition to two polymorphic tilted smectic phases. From an analysis of the  $\Delta n$  data, a quotient  $Q(T)$  has been derived which exhibits power law divergences both above and below the smectic A-nematic (SmA-N) phase transition. A noticeable shrinkage in width of the nematic range has been observed for a small increase in concentration of the angular mesogenic dopant. In the vicinity of the SmA-N phase transition, the values of effective critical exponent ( $\alpha'$ ), characterizing the critical fluctuation at this transition, have appeared to be in between those predicted by the 3D-XY and tricritical hypothesis. Furthermore, with increasing hockey stick-shaped molecular concentration, the SmA-N transition shows a tendency to be driven towards a first order nature.

© 2016 Elsevier B.V. All rights reserved.

## 1. Introduction

Fundamental mesogenic behaviour of liquid crystalline compounds is dependent on their molecular structure and organization in mesophases. So far a number of mesogenic compounds displaying a variety of mesophases with diverse molecular ordering and phase structure have been synthesised and studied thoroughly. Some of them are of further interest due to their exclusive molecular behaviour within such mesophases as well as at the transitions between them. In that sense, the bent-core or banana-shaped compounds have emerged as a field of significant interest in liquid crystal research. Aside from the interest on molecular behaviour and appearance of different unique mesophases in single bent-core liquid crystals, mixtures of such compounds with rod-like molecules, exhibiting exciting mesophase transitions including those usually appeared for only single calamitic compounds, are also much attractive for their unpredictable varying characteristics. Properties such as enhancement of chirality in cholesteric [1,2] and smectic C\* fluids [3], generation of antiferroelectric order in smectics [4–7], induction of novel smectic phases [8], inimitable temperature dependence of elastic constant [9–11] or nanophase segregations [12,13] of such mixtures of rod-like and bent-core liquid crystal brought them at the center of scientific attention and stimulates considerable research efforts regarding formulation and characterization of noble liquid crystalline mixtures.

Furthermore, in the past few decades, several experimental and theoretical efforts have been given to extract the exact order character of the smecticA-nematic (SmA-N) phase transition but it still remains only partially understood. On the basis of mean-field model, Kobayashi [14] and McMillan [15] suggested that depending upon the McMillan ratio ( $T_{SN}/T_{NI}$ , where  $T_{SN}$  and  $T_{NI}$  are the smecticA-nematic (SmA-N) and nematic-isotropic (N-I) transition temperatures respectively), the SmA-N phase transition can either be of first order or second order along with the presence of a tricritical point (TCP) where the transition undertakes a crossover from second order to first order nature. With the introduction of a modified functional, de Gennes [16,17] further proposed a concept of coupling in between the nematic (S) and smectic ( $\Psi$ ) order parameters, which predicts the transition to be in the 3D-XY universality class. However, experimental evidences indicate a strong dependence of that transition on width of the nematic range, which shows that a wide nematic width signifies a weak coupling between the nematic and smectic order parameter, thus making the SmA-N transition to be second order in nature, while for a sufficiently small nematic width, indicating a stronger coupling between S and  $\Psi$ , drives the transition to first order character. Although theoretically the tricritical limit is expected for a McMillan ratio of 0.87, experimental observations demonstrates somewhat higher values, ranging from 0.942 to 0.994 [18–24]. So non-universal type behaviour has been obtained in a number of cases i.e., the 3D-XY appearance can be feasible only when the nematic order is completely saturated [25–28]. Furthermore, Halperin, Lubensky and Ma (HLM) [29] by introducing a correction in the free energy term  $\sim \Psi^3$ , have shown that the SmA-N transition is

\* Corresponding author.

E-mail address: [mkdnbu@yahoo.com](mailto:mkdnbu@yahoo.com) (M.K. Das).

always weakly first order in nature because of the presence of the coupling between the nematic director fluctuations and smectic order parameter. Therefore, the concept of tricritical point (TCP) is ruled out in this case. So far, a number of experimental techniques such as specific heat measurements, dielectric techniques, and X-ray diffraction measurements have widely been used to study the nature of phase transition in several rod-like liquid crystals having a variety of core structures as well as in their mixtures. However, transitional phenomena in mixtures involving rod-like and bent-core mesogens are relatively less investigated, even though they may prove to be helpful in extracting valuable information regarding transitional anomaly and order character of a transition.

In this work, we have reported a systematic investigation of the critical behaviour in the vicinity of the SmA-N phase transition in a few binary liquid crystalline mixtures consisting of a hockey stick-shaped compound, 4-(3-decyloxyphenyliminomethyl) phenyl 4-decyloxybenzoate (SF7) and the calamitic 4-cyano-4'-octyloxybiphenyl (8OCB) from a quite high resolution (in both the birefringence and temperature) measurement of optical birefringence ( $\Delta n$ ). From an analysis of the temperature derivative of  $\Delta n$  data at both above and below the SmA-N phase transition, power-law behaviour with a characteristic effective critical exponent ( $\alpha'$ ) has been observed. The effective critical exponent ( $\alpha'$ ) has been investigated along the path of variation of the hockey stick molecule concentration. The observed pretransitional behaviour is discussed in the light of crossover behaviour under the consideration of effect of the hockey stick-shaped molecules on the resultant molecular order in the host medium. In earlier investigation on an another binary system comprising a different hockey stick-shaped mesogen involving a lateral methyl group and the rod-like octylcyanobiphenyl (8CB), a crossover character has been revealed for the SmA-N phase transition, with the related effective critical exponent ( $\alpha'$ ) being nonuniversal in nature [30]. However, for the relatively small width of the nematic phase ( $\sim 7$  K) in the host 8CB, in that case, it was possible to study the variation of the effective critical exponent ( $\alpha'$ ) only over a limited range. In that sense, in the present study, due to the occurrence of a comparatively wider nematic range ( $\sim 13$  K), it is expected that the dependence of the effective critical exponent ( $\alpha'$ ) on the McMillan ratio can be investigated more rigorously on a rather broad scale, thus endowing us with further insight on the nature of influence of angular mesogenic entity on the mesophase structures and phase transitions in rod-like liquid crystals.

## 2. Experimental

### 2.1. Materials

The hockey stick-shaped compound, 4-(3-decyloxyphenyliminomethyl) phenyl 4-decyloxybenzoate (SF7) was synthesized and purified at the Institute of Physical Chemistry, Martin Luther University, Halle, Germany and the compound 4-cyano-4'-octyloxybiphenyl (8OCB) was purchased from E. Merck, UK (having purity higher than 99.9%) and were used without further purification. The structural formulae and transition scheme for both the pure compounds are given below:

We have prepared several mixtures having different molar concentration ( $x_{SF7} = 0.012, 0.03, 0.05$  and  $0.065$ ) by adding small amounts of the hockey stick-shaped compound into the host rod-like mesogen. The textures of the samples were observed under a polarizing optical microscope (BANBROS) equipped with INSTEC HCS302 hot stage, controlled by INSTEC mK1000 thermo system.

### 2.2. Optical transmission (OT) method

The high resolution measurement of optical birefringence ( $\Delta n$ ) has been performed by directing a He-Ne laser beam ( $\lambda = 632.8$  nm) through a homogeneously aligned liquid crystal filled ITO-coated cell

(purchased from INSTEC Co. Ltd., USA) of thickness  $5 \mu\text{m}$  held between two crossed polarizers (Glan-Thomson) and hence probing the related phase retardation ( $\Delta\phi$ ) of the transmitted beam. The LC filled cell was kept inside a brass thermostat, the temperature of which was controlled and measured by a temperature controller (Eurotherm PID 2404). A two-stage heating arrangement was used by putting the heater inside another hollow cylindrical oven, to obtain a better thermal stability [30]. During the experiment, temperature was varied at a rate of  $\pm 0.5 \text{ }^\circ\text{C min}^{-1}$  and the transmitted light intensity was measured by a photodiode at an interval of 3 s. This results in a temperature difference of  $0.025 \text{ }^\circ\text{C}$  between two successive readings.

The normalized intensity ( $I_t$ ) of the transmitted laser light can be written as [31]

$$I_t = \frac{\sin^2 \theta}{2} (1 - \cos \Delta\phi) \quad (1)$$

where,  $\theta$  is the angle made by the polarizer with the optical axis and the phase retardation,

$$\Delta\phi = \frac{2\pi}{\lambda} d \Delta n \quad (2)$$

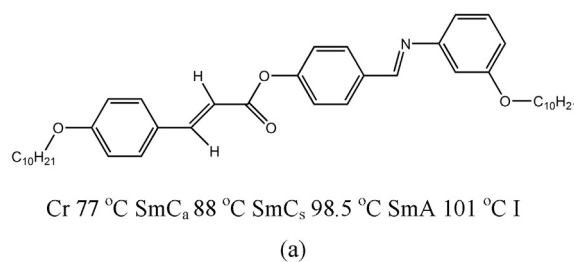
$\Delta n = n_e - n_o$ , where  $n_e$  and  $n_o$  are the extraordinary and ordinary refractive indices of the liquid crystal medium and  $d$  is the cell thickness. The angle  $\theta$  was set at  $\pm 45^\circ$  to optimize the measurements. The birefringence was calculated from the measured intensity [32,33]. The detail of the measuring procedure has already been reported in our earlier publications [32,34].

## 3. Results and discussions

### 3.1. Phase diagram

Fig. 2 illustrates the phase diagram of the binary system consisting of SF7 and 8OCB for four different concentrations along with that of pure 8OCB, as obtained from polarizing optical microscopy and the optical transmission technique. The pure rod-like compound 8OCB shows the stable phase sequence I-SmA<sub>d</sub>-N-Cr as being cooled from isotropic state (See Fig. 1). Here, SmA<sub>d</sub> refers to smectic phase with partial bilayer structure (the layer thickness ( $l$ ) is intermediate between the molecular length ( $d$ ) and twice the molecular length). Conversely, the pure hockey

Compound 1



Compound 2

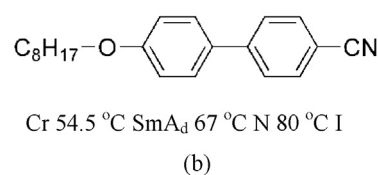
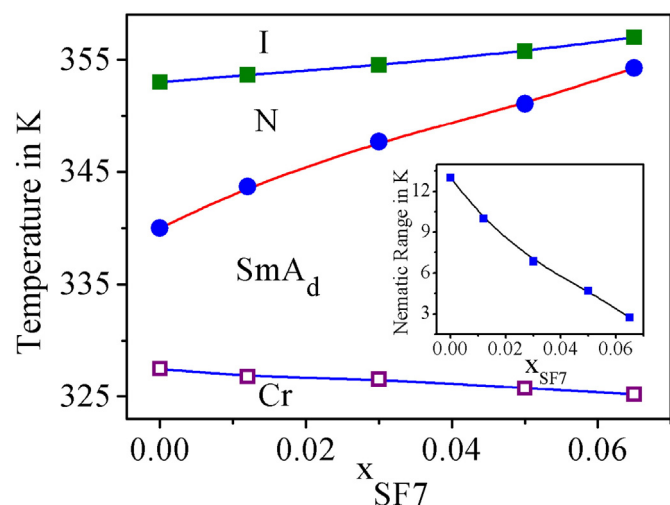


Fig. 1. Chemical structure and phase behaviour of (a) the hockey stick-shaped compound (SF7) and (b) the rod-like compound (8OCB).



**Fig. 2.** Phase diagram for the binary mixture consisting SF7 and 80CB.  $x_{SF7}$  denotes the mole fraction of SF7. I - isotropic phase, N - nematic phase and  $SmA_d$  - partially bilayered smectic A phase. ■: N-I transition temperature; ●:  $SmA_d$ -N transition temperature; □: Melting temperatures measured during heating cycle. Inset depicts variation of nematic range with concentration for the present system. Solid lines are drawn for guidance to eye.

stick-shaped compound (SF7) shows two polymorphic tilted smectic phases - the synclincic smectic C ( $SmC_s$ ) as well as the anticlincic smectic C ( $SmC_a$ ) phases along with a  $SmA$  phase, appearing in a relatively small temperature range ( $\sim 2.5$  K) (See Fig. 1) [35]. In these binary mixtures, we have particularly focused on the region where the concentration of the guest compound i.e. hockey stick-shaped compound (SF7) is much less compared to that of the rod-like host compound (80CB). It has been observed that addition of a small amount of the hockey stick-shaped compound in the host mesogenic system has a significant influence on both the N-I ( $T_{NI}$ ) and  $SmA$ -N ( $T_{SN}$ ) transition temperatures. Further both  $T_{NI}$  and  $T_{SN}$  show increasing trend when plotted against concentration of SF7 with the phase boundary between the  $SmA$  and N phases being relatively steeper than that between the N and I phases and thus resulting a decrease in the nematic width. This again signifies a destabilization of the nematic phase in the host medium caused by the angular mesogen. The variation of the nematic range against molar concentration is also presented in the inset of Fig. 2. Nematic range has been found to decrease from a value of 13 K to near about 3 K for the studied mixtures, where the shrinkage follows a nearly linear trend with the variation of molar concentration.

### 3.2. Optical birefringence measurements

The optical birefringence ( $\Delta n = n_e - n_o$ ) data for all the binary mixtures along with that for pure 80CB, in both nematic and  $SmA$  phases, for  $\lambda = 632.8$  nm is shown in Fig. 3. At the N-I transition, the temperature dependence of birefringence ( $\Delta n$ ) demonstrates a sharp change, indicating first order nature of that transition. On further cooling, well within the nematic phase, the  $\Delta n$  value continues to increase with decrease in temperature which again follows a more or less identical pattern for all the mixtures under study. Such a change is in effect due to the enhancement of molecular ordering in the mesogenic medium with falling temperature. Moreover, it has been noticed that all the  $\Delta n$  vs.  $T$  curves are accompanied with a small but finite measurable change in  $\Delta n$  on entering the low temperature  $SmA$  phase, which again is due to the development of translational ordering. A pretransitional behaviour has been detected in the  $\Delta n$  curve within the nematic phase in a range 2.2 K to 4.9 K prior the  $SmA$ -N phase transition. Such an influence is owing to the coupling between nematic and smectic order parameters. Moreover, this coupling becomes stronger with shrinkage in the nematic width [36]. So in this case, by varying the concentration of

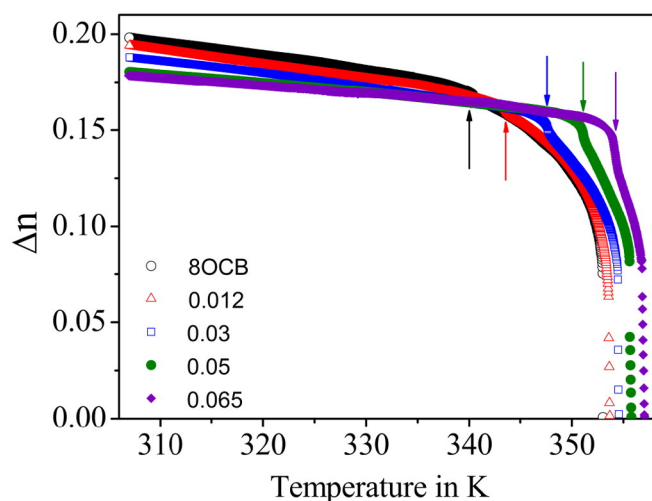


**Fig. 3.** Temperature dependence of birefringence data for all the mixtures along with that for pure 80CB. Vertical arrows show the  $SmA$ -N phase transition for all the mixtures.

SF7 in the host mesogen, the width of the nematic phase and hence the strength of the coupling between nematic and smectic order parameter and the resultant pretransitional behaviour is investigated.

### 3.3. Critical behaviour at the $SmA$ -N phase transition

The high resolution optical birefringence data have been used to obtain an insight into the critical behaviour at the  $SmA$ -N phase transition. As the  $\Delta n$  curves are not accompanied by any visible discontinuity at the  $SmA$ -N phase transition, to identify transition temperatures, the quantity  $n' = -d(\Delta n)/dT$  i.e., first order temperature derivative of  $\Delta n$ , has been used. The quantity  $n'$  has also been found to be related to specific heat capacity anomaly [37] and may be utilized to investigate the critical fluctuations associated with that transition. But in this case, due to the small temperature interval between the successive data points, the numerically obtained temperature derivative of  $\Delta n$  is significantly scattered. Hence, it is reasonable to introduce another differential quotient  $Q(T)$ , defined as [38–40]

$$Q(T) = -\frac{\Delta n(T) - \Delta n(T_{SN})}{T - T_{SN}} \quad (3)$$

where  $\Delta n(T_{SN})$  is the birefringence value at the  $SmA$ -N transition temperature ( $T_{SN}$ ). The quantities  $n'$  and  $Q(T)$  share identical power-law behaviour and hence are characterized by the same critical exponent  $\alpha$  describing the transitional fluctuations. In an attempt to obtain an impression of the limiting behaviour of the quotient  $Q(T)$  at the  $SmA$ -N phase transition, fits to the following renormalization group expression including the corrections to scaling have been performed:

$$Q(T) = A^\pm |\tau|^{-\alpha'} \left( 1 + D^\pm |\tau|^\Delta \right) + E(T - T_{SN}) + B \quad (4)$$

where,  $\tau = (T - T_{SN})/T_{SN}$ ,  $\pm$  denote terms above and below  $T_{SN}$ ,  $A^\pm$  denotes the critical amplitudes,  $D^\pm$  are the coefficients of the first corrections-to-scaling terms,  $\alpha'$  is the effective critical exponent similar to specific heat capacity critical exponent,  $\Delta$  is the first corrections-to-scaling exponent and  $B$  represents the combined critical and regular backgrounds while the term  $E(T - T_{SN})$  corresponds to a temperature dependant part of the regular background contribution. The theoretically predicted value for  $\Delta$  is 0.524 for a 3D-XY case [41,42] and in this analysis it is set fixed at 0.5 without any further variation.

The temperature dependence of quotient  $Q(T)$  for the four mixtures under investigation along with that for pure 80CB are shown in Fig. 4. The fits to Eq. (4) on either side of the  $SmA$ -N transition temperature

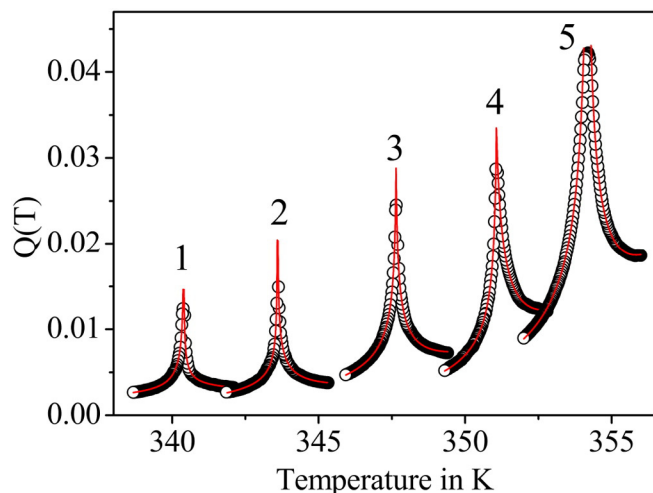


**Fig. 4.** Temperature dependent variation of the quotient  $Q(T)$  in the vicinity of SmA-N phase transition at different mole fractions of SF7 in the mixtures of SF7 and 8OCB. Data are arranged in sequence of increasing mole fraction of SF7 from left to right with 1: 8OCB; 2:  $x_{SF7} = 0.012$ ; 3:  $x_{SF7} = 0.03$ ; 4:  $x_{SF7} = 0.05$ ; 5:  $x_{SF7} = 0.065$ . The solid lines are fit to Eq. (4).

are depicted as solid lines in the same figure. The values of the fit parameters are listed in Table 1. During fit process, few data points very close to the transition have been excluded to avoid the error resulting from the experimental uncertainty. Fits have been carried out for different temperature ranges and that interval for which the fit parameters remain practically stable for a small change in temperature range along with a minimum regular pattern in the residuals, have been considered [43]. The quality of the fits has been tested with the aid of the reduced error function  $\chi_v^2$ , which is defined as the ratio of the variance of the fit ( $s^2$ ) to the variance of the experimental data ( $\sigma^2$ ) [44],

$$\chi_v^2 = \frac{s^2}{\sigma^2} = \frac{1}{N-p} \sum_i \frac{1}{\sigma_i^2} (Q_i^{obs} - Q_i^{fit})^2 \quad (5)$$

where  $N$  is the total number of data points,  $p$  is the number of adjustable parameters,  $Q_i^{fit}$  is the  $i$ th fit value corresponding to the measurement  $Q_i^{obs}$ , and  $\sigma_i$  is the standard deviation corresponding to  $Q_i^{obs}$ . For an ideal fit,  $\chi_v^2$  is unity but in general values ranging between 1 and 1.5 corresponds to good fits. In our present investigation,  $\chi_v^2$  values lie in the range between 1.2 and 1.7, which indicates a consistent fit of the temperature dependence of the quotient  $Q(T)$  to the model expression (4) considered. In each fit, from the temperature dependence of  $d(\Delta n)/dT$ , the transition temperature was first isolated and then kept fixed. This reduces the instability appearing in the least-squares minimization significantly. The concentration dependence of the extracted effective critical exponent  $\alpha'$  values for the present investigated mixtures including that for the pure 8OCB is displayed in Fig. 5 while the variation of the same against the McMillan ratio (i.e.  $T_{SN}/T_{NI}$ ) is illustrated in Fig. 6. The measured value of effective critical exponent  $\alpha'$  for pure 8OCB has been found to be  $0.201 \pm 0.005$ , which again is consistent with those reported in literature [45–47]. It has been observed that with increasing

**Table 1**

Results corresponding to the best fit for  $Q(T)$  near SmA-N phase transition obtained in accordance with Eq. (4) and related  $\chi_v^2$  values associated with the fits.  $|\tau|_{max}$  presents the upper limit of reduced temperature considered for these fits.

$x_{SF7}$	$\alpha'$	$A^-/A^+$	$D^-/D^+$	$ \tau _{max}$	$\chi_v^2$
0.00	$0.201 \pm 0.005$	$0.87 \pm 0.005$	$0.83 \pm 0.002$	$5 \times 10^{-3}$	1.15
0.012	$0.278 \pm 0.003$	$0.97 \pm 0.001$	$0.98 \pm 0.003$	$5 \times 10^{-3}$	1.21
0.03	$0.379 \pm 0.006$	$1.00 \pm 0.004$	$1.00 \pm 0.015$	$5 \times 10^{-3}$	1.55
0.05	$0.440 \pm 0.010$	$0.88 \pm 0.032$	$0.99 \pm 0.024$	$5 \times 10^{-3}$	1.3
0.065	$0.485 \pm 0.019$	$1.01 \pm 0.066$	$0.99 \pm 0.056$	$5 \times 10^{-3}$	1.71

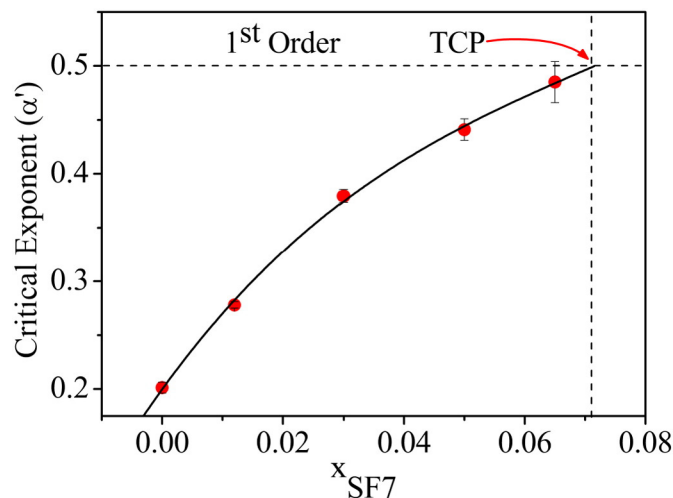


**Fig. 5.** Concentration dependence of the effective critical exponent ( $\alpha'$ ) obtained by fitting  $Q(T)$  to Eq. (4). The vertical dashed line corresponds to the tricritical point (TCP). The solid line is a 2nd order polynomial fit to the data.

hockey stick compound concentration,  $\alpha'$  increases monotonically from  $0.278 \pm 0.003$  for  $x_{SF7} = 0.012$  to  $0.485 \pm 0.019$  for  $x_{SF7} = 0.065$  i.e., the yielded values are in between those for a 3D-XY system (i.e.  $\alpha_{3D-XY} = -0.007$ ) and for the tricritical case (i.e.  $\alpha_{TCH} = 0.5$ ). Hence, non-universal values have been obtained for the effective critical exponent  $\alpha'$  and hence indicating a crossover character for the SmA-N phase transitions in the present investigated mixtures. Moreover, throughout the concentration range, both the quotients  $A^-/A^+$  and  $D^-/D^+$  remain more or less equal to unity, indicating a symmetry of the  $Q(T)$  wings in both the SmA and N phases.

Investigation of Fig. 5 and Fig. 6 reveals that an extrapolation of a quadratic fit to our extracted  $\alpha'$  values results a crossover from second order to first order character for a composition  $x_{SF7} \sim 0.072$  with  $\alpha' = 0.5$ , with the corresponding McMillan ratio (i.e.  $T_{SN}/T_{NI}$ ) being 0.994. Therefore, the tricritical point (TCP) for the investigated binary system is reached approximately at  $x_{SF7} \sim 0.072$ . It is quite clear that addition of this angular mesogenic compound (SF7) in the calamitic medium (8OCB) strengthens the coupling between the nematic (S) and smectic ( $\Psi$ ) order parameters which again lead to a decrease in the nematic width. Also this coupling becomes considerably stronger for a relatively small increase in concentration of the angular mesogenic compound in

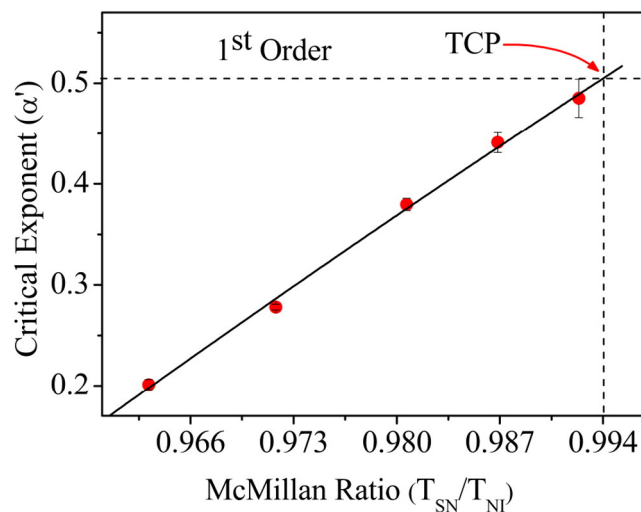


**Fig. 6.** Variation of effective critical exponent ( $\alpha'$ ) with McMillan ratio ( $T_{SN}/T_{NI}$ ). The vertical dashed line corresponds to the tricritical point (TCP). The solid line is a linear fit to the data.

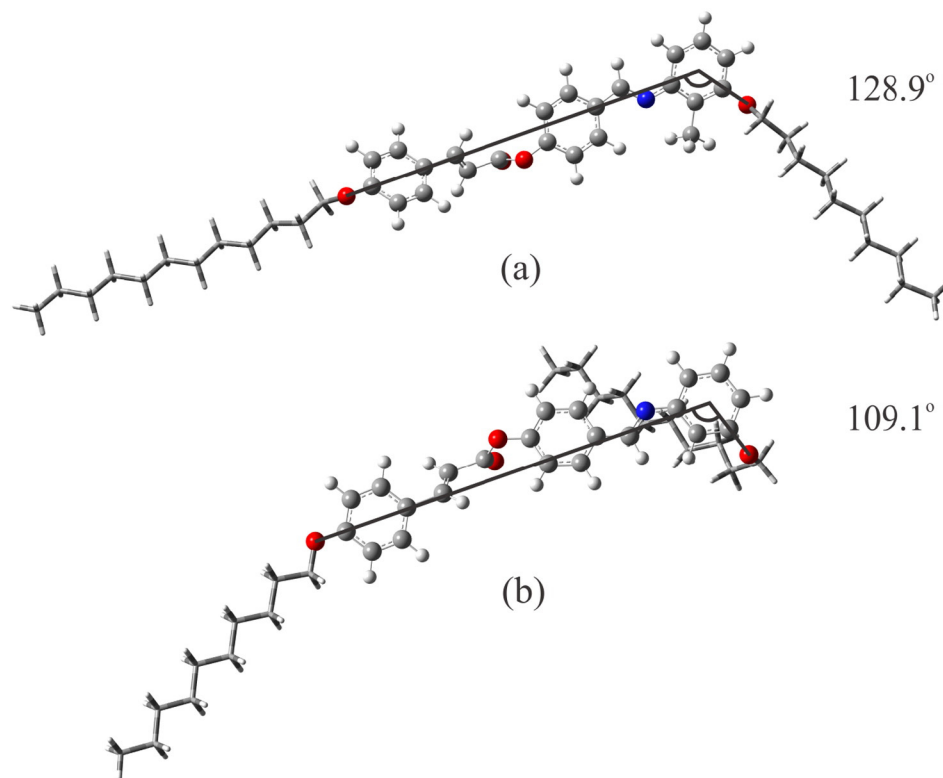


Fig. 7. Optimized molecular structure of (a) H-22.5, (b) SF7.

the mixtures. Such an outcome is possibly due to modification in effective intermolecular interaction and the local molecular ordering in the host medium due to the introduction of the hockey stick-shaped dopant, which again drives the transition from second order to first order character [30].

As stated earlier, in our previous publication [30], we have analyzed the critical behaviour at the N-I and SmA-N phase transitions in mixtures consisting of another hockey stick-shaped compound 4-(3-*n*-decyloxy-2-methylphenyliminomethyl)phenyl 4-*n*-dodecyloxycinnamate (H-22.5), with a lateral methyl group and a rod-like mesogen, octylcyanobiphenyl (8CB). In that case as well a crossover character has been revealed by the SmA-N phase transition. The nematic width has also been found to be shrunk considerably with enhancing hockey stick molecule concentration along with the related effective critical exponent  $\alpha'$ , reaching a value of  $0.460 \pm 0.016$  for a mole-fraction of 0.08 of hockey stick-shaped compound. Due to a relatively small width of the nematic phase ( $\sim 7$  K) in the host 8CB, it became possible to investigate the critical exponent variation over a relatively narrow range (in between  $\alpha' = 0.319$  and  $0.46$ ). Now in this case, the compound 8OCB possesses a comparatively larger nematic width ( $\sim 13$  K) and hence it is expected that the dependence of  $\alpha'$  on the McMillan ratio can be investigated on a relatively broad scale. However, in the present mixtures  $\alpha'$  has been found to vary between  $0.278 \pm 0.003$  and  $0.485 \pm 0.019$  depending on the dopant concentration and hence the variation range is marginally greater than that in the previous study. Furthermore, this variation is manifested over a relatively short range of concentration variation of the angular dopant in the host mesogen (i.e.  $x_{SF7} = 0.012$  to  $0.065$ ) as compared to the earlier case. Such a strong augmentation in the exponent  $\alpha'$  certainly indicates a relatively rapid growth in the local molecular ordering and hence the coupling between the order parameters  $S$  and  $\Psi$ . A further indication of such increase in coupling is the rather steep slope of the phase boundary, a measure of which again can be manifested by calculating related average  $d(T_{SN})/dx$  value. In the present case, the slope has been found to be  $\sim 212$  K which again is comparatively greater than the previous

value  $\sim 169$  K. Furthermore, the concentration dependence of the nematic width has also been found to demonstrate a relatively sharp decrease (slope  $\sim 150$  K) compared to the former study (slope  $\sim 50$  K). Such an outcome is perhaps due to the fine structural dissimilarity between SF7 and H-22.5.

Both the hockey stick-shaped compounds possess a more or less identical molecular configuration except the presence of a lateral methyl group in the obtuse angle between the *meta*-alkoxy chain attached to the terminal phenyl ring and the azomethine connecting group in H-22.5. Such a substitution has been observed to impart a dramatic influence on the phase behaviour of H-22.5 causing the emergence of a nematic phase in a small temperature range [48]. Steric interactions between the methyl group and the neighboring alkoxy chain in the *meta*-position in H-22.5 perhaps induce a more rod-like shape compared to SF7 which again is facilitated in a relatively less augmentation of the local molecular order and hence in a rather less strengthening of the coupling between  $S$  and  $\Psi$ . In an attempt to gain an idea, the molecular bend-angle of both the compounds has been calculated using Gauss View (See Fig. 7). The bend-angle appeared to be  $128.9^\circ$  and  $109.1^\circ$  for compounds H-22.5 and SF7 respectively which again certainly imply more rod-like appearance for H-22.5.

#### 4. Summary and conclusions

In this work, we have undertaken systematic measurements on high resolution temperature dependence of optical birefringence for a binary system, consisting of a hockey stick-shaped liquid crystal, 4-(3-decyloxyphenyliminomethyl) phenyl 4-decyloxycinnamate (SF7) and the rod like 4-cyano-4'-octyloxybiphenyl (8OCB). The birefringence data are found to be rather successful in describing the transitional behaviour at the SmA-N phase transition in all of the investigated mixtures. The temperature dependence of birefringence exhibits no discontinuous change at the SmA-N transition, indicating a second order nature of that transition. An enhancement in hockey stick-shaped compound concentration leads to a significant decrease in the

nematic width, i.e., stabilizes the lower smectic phase. A strong pretransitional behaviour has been observed in the temperature dependence of  $\Delta n$  in a certain temperature range above and below the SmA-N transition. The differential quotient  $Q(T)$  exhibits a diverging character in vicinity of the SmA-N transition which again has found to be in agreement with a renormalization-group model. The related effective critical exponent ( $\alpha'$ ), describing the critical fluctuations at that transition, has appeared to be non-universal in nature. The  $\alpha'$  values follow a monotonic enhancement against the concentration variation of the hockey stick-shaped compound, where an extension of fit to it leads to a crossover to first order nature of the SmA-N phase transition for a McMillan ratio of 0.994 which again is in agreement with the reports for similar mesogenic systems. One interesting fact emerging out from this study is the influence of the extent of molecular bend on the phase-character of mixtures involving angular mesogenic dopant. From the observations, it is clear that an enhanced molecular bend leads to a relatively stronger  $S - \Psi$  coupling and a corresponding sharp decrease in the nematic width. This again is manifested in a rapid approach towards first order nature of the SmA-N phase transition. However, the situation is not clear yet. The exact description, portraying the dependence of order character of the SmA-N phase transition on the molecular bend of mesogenic dopant, requires further investigations involving mesogenic systems with varied dopant-host combinations.

### Acknowledgment

Financial support from the Department of Science and Technology, New Delhi (Project No: SB/EMEQ-290/2013) is gratefully acknowledged. We are grateful to Prof. A. Misra, Department of Chemistry, North Bengal University, Siliguri, India for his active contribution in analysis of bend-angle using Gauss view.

### References

- [1] J. Thisayukta, H. Niwano, H. Takezoe, J. Watanabe, *J. Am. Chem. Soc.* 124 (2002) 3354.
- [2] M. Nakata, Y. Takanashi, J. Watanabe, H. Takezoe, *Phys. Rev. E* 68 (2003) 041710.
- [3] E. Gorecka, M. C'epic', J. Mieczkowski, M. Nakata, H. Takezoe, B. Z'eks', *Phys. Rev. E* 67 (2003) 061704.
- [4] R.E. Gorecka, M. Nakata, J. Mieczkowski, Y. Takanashi, K. Ishikawa, J. Watanabe, H. Takezoe, S.H. Eichhorn, T.M. Swager, *Phys. Rev. Lett.* 85 (2000) 2526.
- [5] K. Kishikawa, N. Muramatsu, S. Kohmoto, K. Yamaguchi, M. Yamamoto, *Chem. Mater.* 15 (2003) 3443.
- [6] C.K. Lee, J.H. Kim, E.J. Choi, W.C. Zin, L.C. Chien, *Liq. Cryst.* 28 (2001) 1749.
- [7] E.J. Choi, X. Cui, W.C. Zin, C.W. Ohk, T.K. Lim, J.H. Lee, *Chem. Phys. Chem.* 8 (2007) 1919.
- [8] R. Prathibha, N.V. Madhusudana, B.K. Sadashiva, *Science* 288 (2000) 2184.
- [9] B. Kundu, R. Prathibha, N.V. Madhusudana, *Phys. Rev. Lett.* 99 (2007) 247802.
- [10] P. Sathyanarayana, M. Mathew, Q. Li, V.S.S. Sastry, B. Kundu, K.V. Le, H. Takezoe, S. Dhara, *Phys. Rev. E* 81 (2010) 010702.
- [11] A. Chakraborty, M.K. Das, B. Das, A. Lehmann, C. Tschierske, *Soft Matter* 9 (2013) 4273.
- [12] T. Otani, F. Araoka, K. Ishikawa, H. Takezoe, *J. Am. Chem. Soc.* 131 (2009) 12368.
- [13] C. Zhu, D. Chen, Y. Shen, C.D. Jones, M.A. Glaser, J.E. MacLennan, N.A. Clark, *Phys. Rev. E* 81 (2010) 011704.
- [14] K.K. Kobayashi, *Phys. Lett. A* 31 (125) (1970) 125; *J. Phys. Soc. Jpn.* 29, 1970, 101.
- [15] W.L. McMillan, *Phys. Rev. A* 4 (1971) 1238.
- [16] P.G. de Gennes, J. Prost, *The Physics of Liquid Crystals*, second ed. Clarendon, Oxford, 1993.
- [17] P.G. de Gennes, *Mol. Cryst. Liq. Cryst.* 21 (1973) 49.
- [18] H. Marynissen, J. Thoen, W. van Dael, *Mol. Cryst. Liq. Cryst.* 97 (1983) 149.
- [19] M.E. Huster, K.J. Stine, C.W. Garland, *Phys. Rev. A* 36 (1987) 2364.
- [20] H. Marynissen, J. Thoen, W. van Dael, *Mol. Cryst. Liq. Cryst.* 124 (1985) 195.
- [21] K.J. Stine, C.W. Garland, *Phys. Rev. A* 39 (1989) 3148.
- [22] S.K. Sarkar, M.K. Das, *RSC Adv.* 4 (2014) 19861.
- [23] S.K. Sarkar, M.K. Das, *J. Mol. Liq.* 199 (2014) 415.
- [24] P. Cusmin, M.R. de la Fuente, J. Salud, M.A. Pérez-Jubindo, S. Diez-Berart, D.O. López, *J. Phys. Chem. B* 111 (2007) 8974.
- [25] C.W. Garland, G. Nounesis, *Phys. Rev. E* 49 (1994) 2964.
- [26] J. Thoen, H. Marynissen, W. Van Dael, *Phys. Rev. A* 26 (1982) 2886.
- [27] J. Thoen, *Int. J. Mod. Phys. B* 09 (1995) 2157.
- [28] P. Cusmin, J. Salud, D.O. López, M.R. de la Fuente, S. Diez, M.A. Pérez-Jubindo, M. Barrio, J. L.Tamarit, *J. Phys. Chem. B* 110 (2006) 26194.
- [29] B.I. Halperin, T.C. Lubenski, S.K. Ma, *Phys. Rev. Lett.* 32 (1974) 292.
- [30] A. Chakraborty, S. Chakraborty, M.K. Das, *Phys. Rev. E* 91 (2015) 032503.
- [31] A. Saipa, F. Giesselmann, *Liq. Cryst.* 29 (2002) 347.
- [32] G. Sarkar, M.K. Das, R. Paul, B. Das, W. Weissflog, *Phase Transit.* 82 (2009) 433.
- [33] T. Scharf, *Polarized Light in Liquid Crystals and Polymers* (Hoboken, NJ: Wiley), 2007.
- [34] A. Prasad, M.K. Das, *J. Phys. Condens. Matter* 22 (2010) 195106.
- [35] G. Sarkar, B. Das, M.K. Das, U. Baumeister, W. Weissflog, *Mol. Cryst. Liq. Cryst.* 540 (2011) 188.
- [36] P.G. de Gennes, *Solid State Commun.* 10 (1972) 753.
- [37] A.V. Kityk, P. Huber, *Appl. Phys. Lett.* 97 (2010) 153124.
- [38] S. Erkan, M. Cetinkaya, S. Yildiz, H. Ozbek, *Phys. Rev. E* 86 (2012) 041705.
- [39] S. Yildiz, H. Ozbek, C. Glorieux, J. Thoen, *Liq. Cryst.* 34 (2007) 611.
- [40] M.C. Cetinkaya, S. Yildiz, H. Ozbek, P. Losada-Perez, J. Leys, J. Thoen, *Phys. Rev. E* 88 (2013) 042502.
- [41] C. Bagnuls, C. Bervillier, *Phys. Rev. B* 32 (1985) 7209.
- [42] C. Bagnuls, C. Bervillier, D.I. Meiron, B.G. Nickel, *Phys. Rev. B* 35 (1987) 3585.
- [43] J.A. Potton, P.C. Lanchester, *Phase Transit.* 6 (1985) 43.
- [44] P.R. Bevington, D.K. Robinson, *Data Reduction and Error Analysis for the Physical Sciences*, third ed. McGraw-Hill, New York, 2003.
- [45] M.K. Das, P.C. Barman, S.K. Sarkar, *Eur. Phys. J. B* 88 (2015) 175.
- [46] G.B. Kasting, K.J. Lushington, C.W. Garland, *Phys. Rev. B* 22 (1980) 321.
- [47] G. Cordoyiannis, C.S.P. Tripathi, C. Glorieux, J. Thoen, *Phys. Rev. E* 82 (2010) 031707.
- [48] A. Chakraborty, B. Das, M.K. Das, S. Findeisen-Tandel, M.-G. Tamba, U. Baumeister, H. Kresse, W. Weissflog, *Liq. Cryst.* 38 (2011) 1085.

## Birefringence in the vicinity of the smectic-*A* to smectic-*C* phase transition: Crossover from *XY* critical to tricritical behavior

Malay Kumar Das,<sup>1,\*</sup> Susanta Chakraborty,<sup>1</sup> Roman Dabrowski,<sup>2</sup> and Michał Czerwiński<sup>2</sup>

<sup>1</sup>*Department of Physics, University of North Bengal, Siliguri, Darjeeling 734 013, India*

<sup>2</sup>*Faculty of Advanced Technologies and Chemistry, Military University of Technology, Kaliskiego Street 2, 00-908 Warsaw, Poland*

(Received 2 September 2016; published 19 January 2017)

High-resolution birefringence ( $\Delta n$ ) measurements are carried out to probe the critical behavior at the smectic-*A*–smectic-*C* (Sm-*A*–Sm-*C*) phase transition in a binary system. The critical behavior of this transition is explored with the aid of a differential quotient extracted from the  $\Delta n$  values. The results obtained reveal that the Sm-*A*–Sm-*C* and nematic–smectic-*A* (*N*–Sm-*A*) transitions exhibit nonuniversal behaviors with effective exponents lying between the tricritical and three-dimensional *XY* values and follow two distinctly different curves with decreasing width of the Sm-*A* and *N* phases, respectively. The origin of such critical behavior is a unique feature for the respective phase transitions.

DOI: [10.1103/PhysRevE.95.012705](https://doi.org/10.1103/PhysRevE.95.012705)

Classical liquid crystal phases are characterized by broken symmetries and may be utilized to explore the complex and beautiful relationship in nature between symmetry and spatial dimensionality at phase transitions. The smectic-*A* (Sm-*A*) and smectic-*C* (Sm-*C*) phases can be described as orientationally ordered fluids with quasi-long-range one-dimensional mass density waves either parallel (Sm-*A*) or inclined (Sm-*C*) to the unique orientational axis. The transition between the Sm-*A* and Sm-*C* phases involves the breaking of a continuous rotational symmetry. Proposing the order parameter associated with the Sm-*A*–Sm-*C* transition to be  $\Psi = \theta \exp(i\phi)$ , where  $\theta$  is the tilt angle of the director with respect to the smectic layer normal and  $\phi$  is an azimuthal angle, de Gennes has predicted that this transition can be continuous and is expected to belong to the three-dimensional (3D) *XY* universality class ( $d = 3$  and  $n = 2$ ) [1].

Early experimental studies reveal classical mean-field behavior and can be well described by the extended mean-field model [2]. There are also several examples in which the heat capacity shows Landau behavior including tricritical appearance [3], while in some other cases, clear deviation from the mean-field character has also been observed, exhibiting either a 3D *XY* [4] or Gaussian tricritical [5] nature. Therefore, the question that arises is why certain compounds show mean-field behavior while others critical behavior. The justification for the absence of critical fluctuation for most of the Sm-*A*–Sm-*C* transition can be explained in terms of the Ginzburg criterion, i.e., true critical behavior is expected only when  $|\tau| < \tau_G$ , where  $\tau$  is the reduced temperature and  $\tau_G$  is the Ginzburg temperature. Safinya *et al.* showed that due to the large bare correlation lengths, as obtained from x-ray studies [6], the Ginzburg criterion yields  $\tau_G \sim 10^{-5}$ . Since the Sm-*C* ordering is apparently not driven by long-range interaction and the Sm-*A*–Sm-*C* transition is not at or above the upper critical dimensionality ( $d = 4$  for the *XY* universality class), mean-field theory is not applicable for the exact nature of this transition [7]. However, Huang and Lien [8] and Prasad *et al.* [9] indicated the possibility of observing a first-order or

tricritical behavior of this transition by reduction of the Sm-*A* temperature range.

Recently, experimental verification of the crossover phenomena from 3D *XY* to tricritical behavior by decreasing the nematic (*N*) temperature range has been found to be quite successful in the *N*–Sm-*A* phase transition [10,11]. Therefore, it is quite plausible to expect that occurrence of such crossover from 3D *XY* to tricritical and thereafter to first-order behavior seems to be related to the width of the Sm-*A* temperature range [8,9]. Thus the discovery of a suitable system that manifests critical fluctuations associated with the Sm-*A*–Sm-*C* transition is very important. Such a situation has been reported for a few phenyl pyrimidine compounds [12] and also in azoxy-4,4'-bi-undecyl- $\alpha$ -methyl cinnamate [13] as well as some chiral systems [14]. As light is sensitive to the average molecular direction, probably optical measurements are accurate enough to allow for a discussion about the nature of the Sm-*A*–Sm-*C* phase transition. In fact, a nearly tricritical behavior has recently been reported by analyzing the  $\Delta n$  data near the Sm-*A*–Sm-*C* transition in a phenyl pyrimidine compound [15]. We have therefore undertaken high-resolution birefringence measurements to test the possibility of crossover behavior from nearly tricritical to 3D *XY* critical nature near the Sm-*A*–Sm-*C* transition by reducing the Sm-*A* temperature range. In this paper it is shown that the transitional behavior is really critical over the reduced temperature range  $2 \times 10^{-4} - 3 \times 10^{-3}$  estimated within 1 K from the transition.

In the present work we report the results on a high-resolution temperature scanning measurement of  $\Delta n$  in a binary system consisting of the second and seventh homologs of the 5-alkyloxy-2-(4-nonyloxy-phenyl) pyrimidine series. A temperature scanning measurement of the optical birefringence has been accomplished by probing the phase retardation  $\Delta\phi$  of a laser beam ( $\lambda = 532$  nm) transmitted through a planar aligned liquid-crystal-filled cell. The birefringence was calculated from the measured normalized intensity and has been described in detail in Ref. [11].

The phase diagram presented in Fig. 1 has been constructed by optical microscopy. Eight mixtures of the binary system (PhP1 + PhP2) were prepared having molar concentrations

\*Corresponding author: [mkdnbu@yahoo.com](mailto:mkdnbu@yahoo.com)

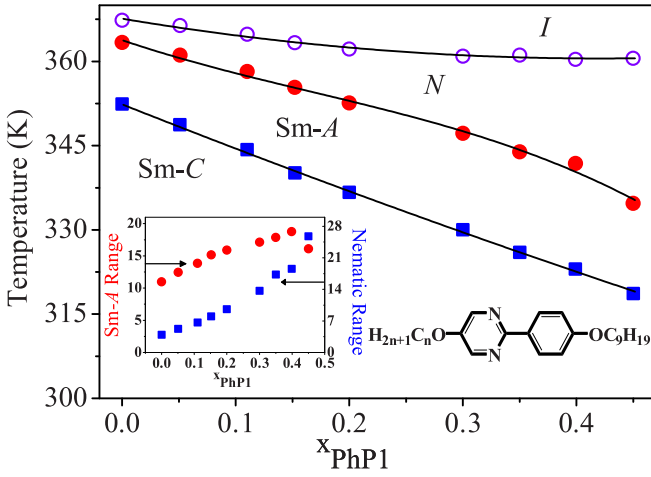


FIG. 1. Partial phase diagram of the binary system comprised of PhP2 and PhP1. Here  $x_{\text{PhP1}}$  denotes the mole fraction of PhP1;  $I$ : isotropic phase;  $N$ : nematic phase; Sm-A: smectic-A phase; Sm-C: smectic-C phase;  $\circ$ : isotropic to nematic transition temperature;  $\bullet$ : nematic to smectic-A transition temperature;  $\blacksquare$ : smectic-A to smectic-C transition temperature; The structure of the PhP compound is shown. For PhP1,  $n = 2$ ; Crystal (359.7 K)  $N$  (363.5 K)  $I$ ; For PhP2,  $n = 7$ ; Crystal (330 K) Sm-C (352.45 K) Sm-A (363.5 K)  $N$  (367.55 K)  $I$ . The Inset shows the concentration dependence of the Sm-A and nematic ranges for the present system. Solid lines are drawn to guide the eye.

ranging between 0.05 and 0.45 of PhP1. The variation of the nematic and Sm-A ranges against molar concentration is also presented in the inset of Fig. 1.

Systematic variations in the  $N$  and Sm-A widths have been accomplished by the addition of the second homolog (PhP1) of the same series. The nematic range is found to increase from a value of 4–27 K, whereas the Sm-A range lies between 11 and 19 K for the studied mixtures. Therefore, it is expected that the dependence of the effective critical exponent  $\alpha'$  on the temperature ratios  $T_{AC}/T_{NA}$  and  $T_{NA}/T_{IN}$  (where  $T_{AC}$  is the Sm-A–Sm-C phase transition temperature,  $T_{NA}$  is the  $N$ –Sm-A phase transition temperature, and  $T_{IN}$  is the isotropic to nematic phase transition temperature) can be investigated more rigorously on a rather broad scale, thus endowing us with the insight into the nature of both the Sm-A to Sm-C and  $N$  to Sm-A phase transitions from the same binary system of rodlike liquid crystal molecules. The temperature dependence of the  $\Delta n$  for one representative mixture ( $x_{\text{PhP1}} = 0.2$ ) is shown in Fig. 2. After a discontinuity at the weakly first-order transition from the isotropic phase, the birefringence increases rapidly with decreasing temperature due to the increase of the nematic order parameter. Upon lowering the temperature, an enhancement in  $\Delta n$  takes place at the  $N$ –Sm-A phase transition. Such augmentation is possibly due to the smectic like short-range order, building up within the nematic phase close to the  $N$ –Sm-A phase transition and consequently causing a further enhancement in the nematic orientational order. Moreover, on entering the low-temperature Sm-C phase there is also a clear and overall increase in  $\Delta n$  due to the Sm-A–Sm-C phase transition. This may be due to the fact that the molecular long axis in the Sm-C phase

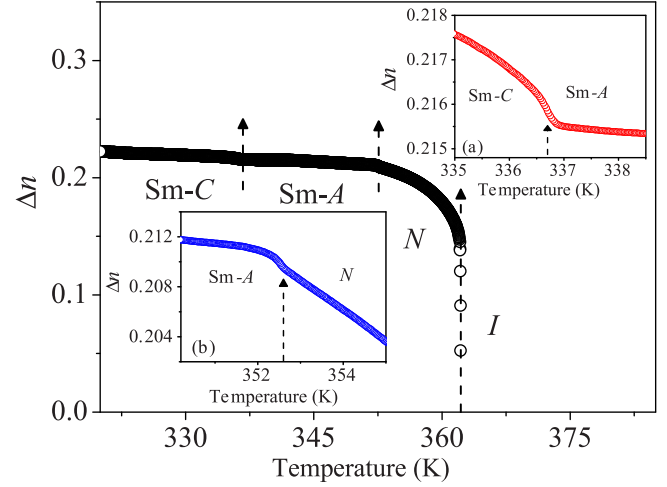


FIG. 2. Temperature dependence of birefringence data for the mixture  $x_{\text{PhP1}} = 0.2$ . Vertical arrows show the  $I$ – $N$ ,  $N$ –Sm-A, and Sm-A–Sm-C phase transitions for the mixtures. In the insets variation of birefringence in the vicinity of the Sm-A–Sm-C transition [inset (a)] and  $N$ –Sm-A transition [inset (b)] has been presented.

of the surface aligned (planar cell of thickness  $7.7 \mu\text{m}$ ) bulk sample is oriented parallel to the aligning surface and the layers are tilted with respect to the surface alignment, which causes an enhancement in the orientational order. We have obtained very well defined  $\Delta n$  curves in the near vicinity of the transition temperatures. It has been found that the quantity  $-d(\Delta n)/dT$  is related to a specific-heat capacity anomaly [16] and may be utilized to investigate the critical fluctuation associated with a phase transition. Due to the small temperature interval between the successive data points, the numerically determined temperature derivative of  $\Delta n$  is rather scattered. Therefore, it is reasonable to introduce the differential quotient  $Q(T)$ , defined as [16,17]

$$Q(T) = -\frac{\Delta n(T) - \Delta n(T_{AC})}{T - T_{AC}}, \quad (1)$$

where  $\Delta n(T_{AC})$  is the birefringence value at  $T_{AC}$ , as obtained by differentiating the temperature dependence of  $\Delta n$ . The  $Q(T)$  data as obtained have been analyzed in detail with the following renormalization-group expression including the correction-to-scaling terms [17,18]:

$$Q(T) = A^{\pm} |\tau|^{-\alpha'} (1 + D^{\pm} |\tau|^{\Delta}) + E(T - T_{AC}) + B, \quad (2)$$

where  $\tau = (T - T_{AC})/T_{AC}$  is the reduced temperature and the superscripts  $\pm$  denote those above and below  $T_{AC}$ ,  $A^{\pm}$  presents the critical amplitudes,  $\alpha'$  is the critical exponent similar to the specific-heat critical exponent  $\alpha$ ,  $D^{\pm}$  are the coefficients of the first correction-to-scaling terms, and the correction-to-scaling exponent  $\Delta$  has been taken to be fixed at 0.5 [18]. The term  $E(T - T_{AC})$  corresponds to a temperature-dependent part of the regular background, while  $B$  is a constant giving the combined critical and regular backgrounds. Data very close to the transition are excluded from the fitting due to experimental uncertainty and sample inhomogeneity. An overview of the temperature-dependent variation of  $Q(T)$  for pure PhP2 and eight different mixtures in the vicinity of the

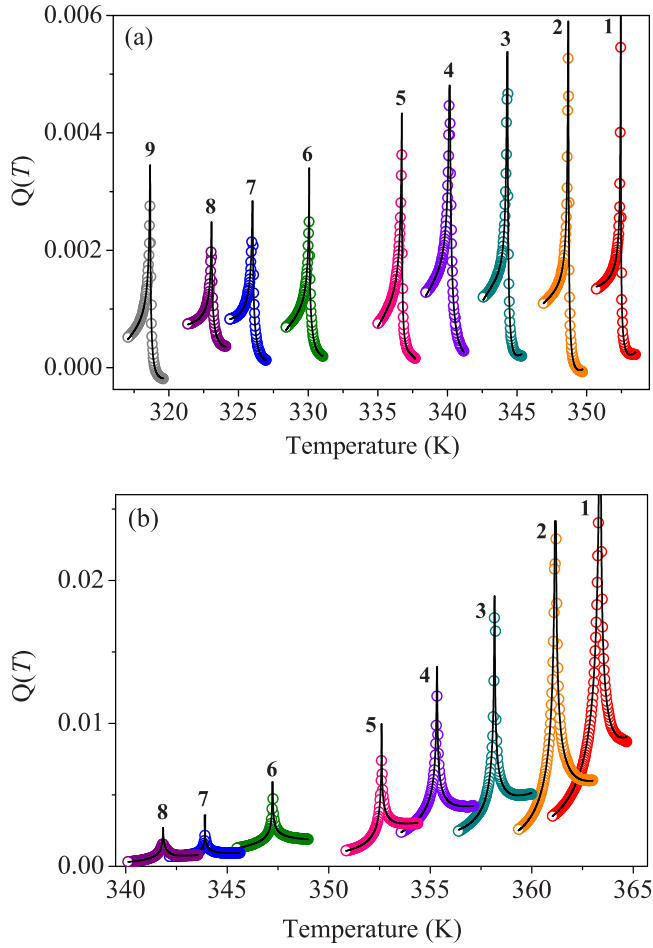


FIG. 3. Temperature dependence of  $Q(T)$  in the vicinity of the (a) Sm-A-Sm-C transition and (b) N-Sm-A transition in mixtures of PhP1 + PhP2. 1:  $x_{\text{PhP1}} = 0.0$ ; 2:  $x_{\text{PhP1}} = 0.05$ ; 3:  $x_{\text{PhP1}} = 0.1$ ; 4:  $x_{\text{PhP1}} = 0.15$ ; 5:  $x_{\text{PhP1}} = 0.2$ ; 6:  $x_{\text{PhP1}} = 0.3$ ; 7:  $x_{\text{PhP1}} = 0.35$ ; 8:  $x_{\text{PhP1}} = 0.4$ ; 9:  $x_{\text{PhP1}} = 0.45$ .

Sm-A-Sm-C phase transition is shown in Fig. 3(a). The  $Q(T)$  data exhibit a noticeable divergent character on both sides of the transition temperature, involving an asymmetry between the  $Q(T)$  wings in the Sm-A and Sm-C phases. In particular, the existence of such divergent behavior above the transition temperature clearly indicates that this transition is not of the mean-field type. As both the compounds were chosen from the same homologous series, no Fisher renormalization [19] of the critical exponent has been observed even for nearly tricritical compositions. The fits to Eq. (2) over the range  $\tau = 3 \times 10^{-3}$  are displayed as solid lines, while the corresponding fit values are presented in Table I. The reduced error functions  $\chi_v^2$ , which have been found to be within 1.08–1.25, signify consistent fits.

In an attempt to analyze the critical anomaly associated with the N-Sm-A phase transition the above-discussed procedure has also been used [11]. Here  $\Delta n(T_{AC})$  is replaced by  $\Delta n(T_{NA})$ , while  $T_{AC}$  is changed to  $T_{NA}$ . The values of the fit parameters as extracted from the fit process are gathered in Table II. The results of fits over the range  $\tau = 5 \times 10^{-3}$  represent the  $Q(T)$  data well [Fig. 3(b)], as indicated by the  $\chi_v^2$  values. Moreover, the critical region for each mixture at the

TABLE I. Results corresponding to the best fit for  $Q(T)$  near the Sm-A-Sm-C phase transition obtained in accordance with Eq. (2) and related  $\chi_v^2$  values associated with the fits.

$x_{\text{PhP1}}$	$A^-/A^+$	$D^-/D^+$	$\alpha'$	$\chi_v^2$
0	$1.301 \pm 0.014$	$1.01 \pm 0.05$	$0.476 \pm 0.007$	1.19
0.05	$1.200 \pm 0.011$	$1.00 \pm 0.03$	$0.397 \pm 0.006$	1.24
0.10	$1.080 \pm 0.018$	$0.99 \pm 0.05$	$0.321 \pm 0.017$	1.17
0.15	$1.017 \pm 0.098$	$0.94 \pm 0.03$	$0.237 \pm 0.011$	1.19
0.20	$0.979 \pm 0.062$	$0.93 \pm 0.04$	$0.193 \pm 0.007$	1.25
0.30	$0.911 \pm 0.006$	$0.91 \pm 0.03$	$0.136 \pm 0.002$	1.13
0.35	$0.930 \pm 0.002$	$0.91 \pm 0.02$	$0.089 \pm 0.007$	1.17
0.40	$0.907 \pm 0.011$	$0.91 \pm 0.03$	$0.040 \pm 0.006$	1.15
0.45	$0.936 \pm 0.018$	$0.86 \pm 0.06$	$0.152 \pm 0.005$	1.08

Sm-A-Sm-C phase transition is quite small compared to that for the N-Sm-A phase transition.

The variation of the extracted critical exponent  $\alpha'$  values for the present investigated mixtures including that for the pure PhP2 against the temperature ratios (i.e.,  $T_{NA}/T_{IN}$  and  $T_{AC}/T_{NA}$ ) is illustrated in Fig. 4. Nonuniversal values have been observed for the critical exponent  $\alpha'$  and hence indicate a crossover character for both the N-Sm-A and Sm-A-Sm-C phase transitions. The present results confirm that the width of the N and Sm-A temperature ranges plays an important role in deciding the nature of both the N-Sm-A and the Sm-A-Sm-C phase transitions.

The magnitude of the anomaly in  $Q(T)$  decreases significantly as the N and Sm-A ranges grows, showing that thermal fluctuations associated with the  $Q(T)$  anomaly are very sensitive to the saturation of both the N and the Sm-A order. The overall behavior between  $\alpha'$  and  $T_{NA}/T_{IN}$  from the tricritical point (TCP) towards approaching the 3D XY value is in good agreement with the previous reports on the N-Sm-A phase transitions [11,20–25], which are also included in Fig. 4.

In the vicinity of the Sm-A-Sm-C phase transition, the measured value of critical exponent  $\alpha'$  for pure PhP2 as reported by Chakraborty *et al.* [15] was  $0.48 \pm 0.02$  and the repeated measurement for different cell thickness yielded  $0.476 \pm 0.007$ . With increasing PhP1 concentration,  $\alpha'$  decreases monotonically from  $0.476 \pm 0.007$  for PhP2 to  $0.04 \pm 0.006$  for  $x_{\text{PhP1}} = 0.40$ , i.e., the yielded values of the effective critical exponent  $\alpha'$ , characterizing the critical fluctuation at this transition, have appeared to be in between those predicted

TABLE II. Results corresponding to the best fit for  $Q(T)$  near the N-Sm-A phase transition obtained in accordance with Eq. (2) and related  $\chi_v^2$  values associated with the fits.

$x_{\text{PhP1}}$	$A^-/A^+$	$D^-/D^+$	$\alpha'$	$\chi_v^2$
0	$1.630 \pm 0.029$	$0.99 \pm 0.04$	$0.462 \pm 0.002$	1.29
0.05	$1.521 \pm 0.052$	$0.99 \pm 0.01$	$0.425 \pm 0.007$	1.11
0.10	$1.417 \pm 0.036$	$1.00 \pm 0.01$	$0.387 \pm 0.011$	1.36
0.15	$1.368 \pm 0.107$	$1.00 \pm 0.01$	$0.345 \pm 0.005$	1.02
0.20	$1.450 \pm 0.088$	$1.00 \pm 0.01$	$0.303 \pm 0.004$	1.12
0.30	$1.053 \pm 0.038$	$1.01 \pm 0.01$	$0.188 \pm 0.003$	1.21
0.35	$0.970 \pm 0.017$	$1.00 \pm 0.01$	$0.084 \pm 0.001$	1.18
0.40	$0.983 \pm 0.010$	$1.01 \pm 0.03$	$0.053 \pm 0.001$	1.46

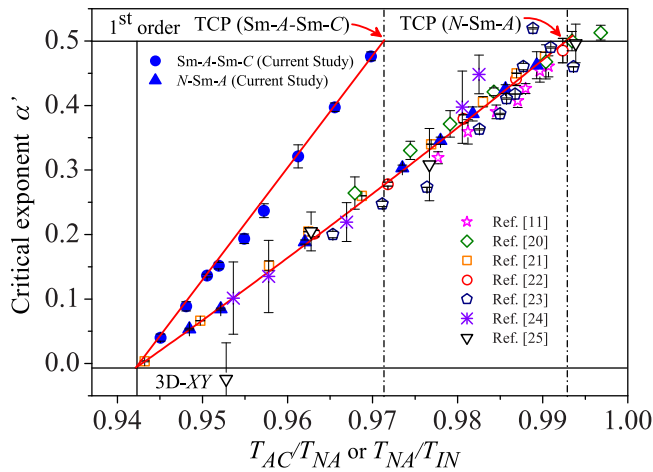


FIG. 4. Variation of effective critical exponent  $\alpha'$  with  $T_{NA}/T_{IN}$  for the  $N$ -Sm- $A$  transition and  $T_{AC}/T_{NA}$  for the Sm- $A$ -Sm- $C$  transition. The vertical dash-dotted lines and solid line correspond to the TCP and 3D  $XY$  limit, respectively. The solid (red) lines are linear fit to the data.

by the 3D  $XY$ , i.e.,  $\alpha_{XY} = -0.007$ , and tricritical, i.e.,  $\alpha = 0.5$ , values. The dependence of this transition on the Sm- $A$  range has also qualitatively been observed by others [8,9].

An extrapolation of the linear fit to the extracted  $\alpha'$  values yield a tricritical behavior (i.e.,  $\alpha' = 0.5$ ) for the  $T_{AC}/T_{NA}$  ratio of 0.972, which is quite low in comparison to that obtained for a similar temperature ratio ( $T_{NA}/T_{IN} = 0.992$ ) at the  $N$ -Sm- $A$  phase transition. However, the linear fit to the  $\alpha'$  data yields a  $T_{AC}/T_{NA}$  value of 0.942 corresponding to the 3D  $XY$  point, which is found to be very close to the McMillan ratio ( $T_{NA}/T_{IN}$ ) for the  $N$ -Sm- $A$  phase transition.

It should be mentioned here that this crossover of  $\alpha'$  gives rise to characteristic behavior regarding the amplitude ratio ( $A^-/A^+$ ) and the magnitude of the first-order correction-to-scaling terms ( $D^-/D^+$ ). In the case of the Sm- $A$ -Sm- $C$  phase transition the  $A^-/A^+$  values are in the range between 1.301 and 0.907 (from the extrapolation 1.39 for the TCP and

0.954 for the 3D  $XY$  point) and the first-order correction-to-scaling ratio is between 1.01 and 0.86 (from the extrapolation 1.05 for the TCP and 0.89 for the 3D  $XY$  point), while for the  $N$ -Sm- $A$  phase transition, although  $A^-/A^+$  varies from 1.63 to 0.97 (from the extrapolation 1.67 for the TCP and 0.99 for the 3D  $XY$  point),  $D^-/D^+$  remains nearly unity. The theory for the 3D  $XY$  universality class predicts an amplitude ratio  $A^-/A^+ = 0.971$  and  $D^-/D^+ \approx 1$ , while for the TCP the theoretical amplitude ratio  $A^-/A^+ = 1.6$  and  $D^-/D^+ \approx 1$ . Therefore, from our observation, it is clear that the studied mixtures exhibit nonuniversal behaviors with effective exponents lying between the 3D  $XY$  and tricritical limits.

It may be worth mentioning that recently, another binary mixture of the rodlike 4'-heptyloxy-4-cyanobiphenyl and the hockey-stick-shaped compound [4-(3-*n*-decyloxy-2-methylphenyliminomethyl) phenyl 4-*n*-dodecyloxy cinnamate] exhibit critical behavior and has also been found to show a tricritical point around  $T_{AC}/T_{NA} = 0.97$  with a quite broad tricritical range [26].

In conclusion, we believe that our result may close the controversy on the nature of the Sm- $A$ -Sm- $C$  transition. The nonuniversal behavior of this transition with either very weak first-order or second-order nature with Gaussian tricritical or crossover from 3D  $XY$  critical to tricritical behavior can now be clearly explained on the basis of the width of the Sm- $A$  temperature range linked with the Sm- $A$ -Sm- $C$  phase transition. However, mean-field tricritical or mean-field 3D  $XY$  behavior is only an approximation where the true critical region remains inaccessible. Moreover, it seems that the origin of such critical behavior is perhaps a unique feature for both the  $N$ -Sm- $A$  and the Sm- $A$ -Sm- $C$  phase transitions for all the compounds since they are observed to follow two distinctly different linear curves as shown in Fig. 4.

We gratefully acknowledge financial support from the Department of Science and Technology, New Delhi (Project No. SB/EMEQ-290/2013). S.C. is grateful to the DST, New Delhi for support through the award of a project assistantship.

- [1] P. G. de Gennes, *Mol. Cryst. Liq. Cryst.* **21**, 49 (1973).
- [2] C. C. Huang and J. M. Viner, *Phys. Rev. A* **25**, 3385 (1982); M. Meichle and C. W. Garland, *ibid.* **27**, 2624 (1983); P. Das, K. Ema, and C. W. Garland, *Liq. Cryst.* **4**, 205 (1989).
- [3] H. Y. Liu, C. C. Huang, C. Bahr, and G. Heppke, *Phys. Rev. Lett.* **61**, 345 (1988); T. Chan, C. Bahr, G. Heppke, and C. W. Garland, *Liq. Cryst.* **13**, 667 (1993); R. J. Birgeneau, C. W. Garland, A. R. Kortan, J. D. Litster, M. Meichle, B. M. Ocko, C. Rosenblatt, L. J. Yu, and J. Goodby, *Phys. Rev. A* **27**, 1251 (1983).
- [4] K. Ema, J. Watanabe, A. Takagi, and H. Yao, *Phys. Rev. E* **52**, 1216 (1995).
- [5] K. Ema, A. Takagi, and H. Yao, *Phys. Rev. E* **55**, 508 (1997); T. Stoebe, L. Reed, M. Veum, and C. C. Huang, *ibid.* **54**, 1584 (1996).
- [6] C. R. Safinya, M. Kaplan, J. Als-Nielsen, R. J. Birgeneau, D. Davidov, J. D. Litster, D. L. Johnson, and M. E. Neubert, *Phys. Rev. B* **21**, 4149 (1980).
- [7] A. Altland and B. Simons, *Condensed Matter Field Theory* (Cambridge University Press, Cambridge, 2010).
- [8] C. C. Huang and S. C. Lien, *Phys. Rev. A* **31**, 2621 (1985).
- [9] S. K. Prasad, V. N. Raja, D. S. Rao, G. G. Nair, and M. E. Neubert, *Phys. Rev. A* **42**, 2479 (1990).
- [10] K. J. Stine and C. W. Garland, *Phys. Rev. A* **39**, 3148 (1989).
- [11] A. Chakraborty, S. Chakraborty, and M. K. Das, *Phys. Rev. E* **91**, 032503 (2015).
- [12] L. Reed, T. Stoebe, and C. C. Huang, *Phys. Rev. E* **52**, R2157 (1995); G. S. Iannacchione, C. W. Garland, P. M. Johnson, and C. C. Huang, *Liq. Cryst.* **26**, 51 (1999).
- [13] Y. Galerne, *Phys. Rev. A* **24**, 2284 (1981).
- [14] K. Ema and H. Yao, *Phys. Rev. E* **57**, 6677 (1998), and references therein.
- [15] A. Chakraborty, S. Chakraborty, and M. K. Das, *Physica B* **479**, 90 (2015).

- [16] M. C. Çetinkaya, S. Yıldız, H. Özbek, P. Losada-Pérez, J. Leys, and J. Thoen, *Phys. Rev. E* **88**, 042502 (2013).
- [17] S. Erkan, M. Çetinkaya, S. Yıldız, and H. Özbek, *Phys. Rev. E* **86**, 041705 (2012).
- [18] C. W. Garland, in *Liquid Crystals: Experimental Study of Physical Properties and Phase Transitions*, edited by S. Kumar (Cambridge University Press, Cambridge, 2001).
- [19] M. E. Fisher, *Phys. Rev.* **176**, 257 (1968).
- [20] S. K. Sarkar and M. K. Das, *J. Mol. Liq.* **199**, 415 (2014).
- [21] S. K. Sarkar, A. Chakraborty, and M. K. Das, *Liq. Cryst.* **43**, 22 (2016).
- [22] S. Chakraborty, A. Chakraborty, and M. K. Das, *J. Mol. Liq.* **219**, 608 (2016).
- [23] G. Cordoyiannis, C. S. P. Tripathi, C. Glorieux, and J. Thoen, *Phys. Rev. E* **82**, 031707 (2010).
- [24] C. W. Garland and G. Nounesis, *Phys. Rev. E* **49**, 2964 (1994).
- [25] Y. Sasaki, K. Ema, K. V. Le, H. Takezoe, S. Dhara, and B. K. Sadashiva, *Phys. Rev. E* **83**, 061701 (2011).
- [26] S. Chakraborty and M. K. Das (unpublished).